

National Academy of Sciences of Ukraine
Bogolyubov Institute for Theoretical Physics

Has the rights of a manuscript

Bugaev Kyrill Alekseevich

UDC: 532.51; 533.77; 539.125/126; 544.586.6

Equation of State and Phase Transitions in the Nuclear and Hadronic Systems

Speciality 01.04.02 - theoretical physics

DISSERTATION

to receive a scientific degree of
the Doctor of Science in physics and mathematics

Kiev - 2009

arXiv:1012.3400v1 [nucl-th] 15 Dec 2010

Abstract

An investigation of strongly interacting matter equation of state remains one of the major tasks of modern high energy nuclear physics for almost a quarter of century. The present work is my doctor of science thesis which contains my contribution (42 works) to this field made between 1993 and 2008.

Inhere I mainly discuss the common physical and mathematical features of several exactly solvable statistical models which describe the nuclear liquid-gas phase transition and the deconfinement phase transition. Luckily, in some cases it was possible to rigorously extend the solutions found in thermodynamic limit to finite volumes and to formulate the finite volume analogs of phases directly from the grand canonical partition. It turns out that finite volume (surface) of a system generates also the temporal constraints, i.e. the finite formation/decay time of possible states in this finite system.

Among other results I would like to mention the calculation of upper and lower bounds for the surface entropy of physical clusters within the Hills and Dales model; evaluation of the second virial coefficient which accounts for the Lorentz contraction of the hard core repulsing potential between hadrons; inclusion of large width of heavy quark-gluon bags into statistical description.

I believe that the suggested mathematical solution of the freeze-out problem in relativistic hydrodynamic model and in hydro-cascade model has not only an academic interest, but also has some practical value. In addition I hope that the experience gained in working out some partly successful signals of deconfinement transition can be useful for other researchers to go further in this direction.

CONTENTS

Abbreviations	7
Introduction	9
1 Nuclear Matter in Thermodynamic Limit	30
1.1. A Self-consistent Mean-Field EOS for Nuclear Matter	33
1.2. Statistical Multifragmentation Model in Thermodynamic Limit	39
1.3. Singularities of Isobaric Partition and the Mechanism of Phase Transitions	43
1.4. The Critical Indices and Scaling Relations of the SMM	52
1.5. Major Conclusions	57
2 Exactly Solvable Statistical Models for Finite Nuclear Systems	60
2.1. The Complement Method for Finite Drop	63
2.2. Constrained SMM in Finite Volumes	71
2.2.1. Isobaric Partition Singularities at Finite Volumes.	73
2.2.2. No Phase Transition Case.	75
2.2.3. Finite Volume Analogs of Phases.	78
2.3. Gas of Bags in Finite Volumes	81
2.4. Hills and Dales Model and Source of Surface Entropy	84
2.4.1. Grand Canonical Surface Partition.	85
2.4.2. Special Ensembles for Surface Partition.	88
2.4.3. The Lower Bounds for the Surface Entropy Coefficients.	92
2.5. Conclusions	96
3 Virial Expansion for the Lorentz Contracted Rigid Spheres and Relativistic VdW EOS for Hadronic Binary Mixtures.	99

3.1.	The Van der Waals EOS for the Lorentz Contracted Hard Spheres	102
3.2.	Hadronic Binary Mixtures in Canonical Ensemble	109
3.2.1.	The Van der Waals Excluded Volume Model.	111
3.2.2.	Generalization to the Two-component Case.	113
3.2.3.	Comparison of Two-component VdW Approximations.	116
3.3.	Grand Canonical Treatment of Binary Mixtures	118
3.3.1.	The Two VdW Approximations.	119
3.3.2.	Relativistic Excluded Volumes.	122
3.3.3.	Hard-core Radii from Particle Yield Ratios.	126
3.3.4.	Intermediate Conclusions.	131
3.4.	Relativization of the VdW EOS	133
3.4.1.	Proof of Causality in the High Pressure Limit.	138
3.4.2.	A Few Remarks on Possible Observables.	143
3.5.	Conclusions	144
4	Exactly Solvable Phenomenological EOS of the Deconfinement PT	147
4.1.	Microcanonical Analysis of the Hagedorn Model	149
4.1.1.	Harmonic Oscillator Coupled to \mathcal{H}	154
4.1.2.	An Ideal Vapor Coupled to \mathcal{H}	154
4.1.3.	\mathcal{H} as a Radiant Bag.	156
4.1.4.	Fragmentation of \mathcal{H}	158
4.2.	Hagedorn Thermostat Model	159
4.2.1.	A Single Hagedorn Thermostat Case.	160
4.2.2.	The Role of the Mass Cut-off.	162
4.2.3.	Concluding Remarks on the HTM.	165
4.3.	Mott-Hagedorn Model for QGP	167
4.3.1.	Resonance Width Model: Mott Transition.	169
4.3.2.	Applications to Lattice Quantum Chromodynamics and Heavy-Ion Collisions.	172
4.3.3.	Anomalous J/ψ Suppression.	174

4.4.	Quark Gluon Bags with Surface Tension	178
4.4.1.	The Role of Surface Tension.	181
4.4.2.	Generalization to Non-Zero Baryonic Densities.	187
4.4.3.	Surface Tension Induced Phase Transition.	190
4.5.	Conclusions and Perspectives	194
5	Freeze-out Problem of Relativistic Hydrodynamics and Hydrokinetics	200
5.1.	Freeze-out Problem in Relativistic Hydrodynamics	206
5.1.1.	Decay of Perfect Fluid into the Gas of Free Particles.	206
5.1.2.	Conservation Laws at the Freeze-out Hypersurface.	212
5.1.3.	Consistency Theorem.	217
5.2.	Equations for the Freeze-out Hypersurface	220
5.2.1.	Freeze-out Calculus: General Scheme.	220
5.2.2.	Freeze-out in 1 + 1 Dimensional Hydrodynamics.	224
5.2.3.	Entropy Production in the Freeze-out Shock.	228
5.2.4.	Freeze-out of the Simple Wave.	231
5.3.	Relativistic Kinetic Equations for Finite Domains	241
5.3.1.	Drift Term for Semi-Infinite Domain.	244
5.3.2.	Collision Term for Semi-Infinite Domain.	247
5.4.	Derivation of Conservation Laws for Hydrokinetics	250
5.4.1.	Boundary Conditions at Σ^* for a Single Degree of Freedom.	254
5.4.2.	Boundary Conditions at Σ^* for Many Degrees of Freedom.	258
5.5.	Concluding Remarks	262
6	Experimental Signals of the Deconfinement Transition	267
6.1.	Statistical Production of Particles.	269
6.1.1.	Particle Spectra and Apparent Temperature.	271
6.1.2.	Freeze-out of J/ψ Meson.	273
6.1.3.	Ω , J/ψ and ψ' Early Hadronization at SPS Energies.	275

6.2. Hadron Spectra and QGP Hadronization in Au+Au Collisions at RHIC	281
6.3. Transverse Caloric Curves of Kaons as the Signal of Deconfinement Transition in A+A Collisions	288
6.4. Concluding Remarks	293
Conclusions	295
Appendices	301
Appendix A	301
The Canonical Treatment of the Relativistic VdW EOS.	301
Stability of the Non-linear Approximation.	304
Appendix B	305
Derivation of the Lorentz Contracted Excluded Volumes	305
The List of Used Sources	311

Abbreviations

1. PT phase transition
2. A+A nuclear heavy-ion (collision; reaction)
3. QGP quark-gluon plasma
4. EOS equation of state
5. HS hypersurface
6. FO freeze-out
7. SMM Statistical Multifragmentation Model
8. FDM Fisher Droplet Model
9. GBM Gas of Bags Model
10. QGBST Quark-Gluon Bags with Surface Tension
11. GCE grand canonical ensemble
12. HDM Hills and Dales Model
13. VdW Van der Waals
14. GCSP grand canonical surface partition
15. CCSP canonically constrained surface partition
16. SGCSP semi-grand canonical surface partition
17. CSMM constrained Statistical Multifragmentation Model
18. GSMM generalized Statistical Multifragmentation Model

19. SBM	Statistical Bootstrap Model
20. HTM	Hagedorn Thermostat Model
21. BD	Bass-Dumitru
22. TLS	Teaney-Lauret-Shuryak
23. t.l.	time-like
24. s.l.	space-like
25. RFG	reference frame of gas
26. RFF	rest frame of fluid
27. AT	apparent temperature

Introduction

In this dissertation, the author investigates the equation of state of strongly interacting matter. The main attention is devoted to theoretical research of two major phase transitions (PT), which are accessible for the experimental studies in the nuclear heavy-ion (A+A) collisions. They are the liquid-gas PT in nuclear media observed in A+A reactions at intermediate energies known as nuclear multifragmentation, and the deconfinement PT from usual hadrons to quark-gluon plasma (QGP).

The major difficulties of experimental and theoretical studies of these PTs are determined by the spatial and temporal finiteness of strongly interacting systems created during the A+A collision process. Thus, the characteristic number of particles at the beginning of a collision is about a few hundred nucleons which collide in practically vanishing volume due to the Lorentz contraction of original nuclei. After a complicated evolution during 10 to 20 fm/c, which includes thermalization of highly excited hadronic/nuclear matter, its expansion accompanied by a possible PT and cooling down to free streaming particles, the system typically stops its nontrivial evolution in the volume of about a few thousand fm³ which is filled up with a few thousand secondary hadrons. Therefore, theoretical investigations of these PTs in the course of A+A collision inevitably combine three relatively independent elements:

I) Development of the statistical description of the PT which accounts for some specific features of the interaction between the corresponding constituents and normalization of the model parameters on the available data;

II) Modeling the PT dynamics in the collision process and transformation of strongly interacting constituents into the free moving particles;

III) Analysis of the experimental signatures of PT and their comparison with the data.

These elements form the phenomenological basis to study the strongly interacting matter properties and its phase diagram, i.e. equation of state (EOS), in the nuclear laboratories. On one

hand, they allow one to make a bridge between the results obtained within the modern theory of strong interaction, the quantum chromodynamics and its lattice formulation, and, on the other hand, they provide the experimentalists with explanations of the observed phenomena and give recommendations for future measurements.

The author's motivation to study the EOS of nuclear and hadronic matter is based on the following three reasons. First, despite the recent progress, the lattice quantum chromodynamics provides us with a very limited information for non-zero baryonic densities. Also the present and planned experimental measurements cannot cover the full range of thermodynamic parameters of the strongly interacting matter EOS. Therefore, for practical purposes, including even understanding of the experimental results, it is necessary to develop the phenomenological models of EOS which can be compared with the existing data and extended to the terra incognita regions on the phase diagram.

Second, since the system under investigation is not a macroscopically large one, the theoretical studies of phase transformations are extremely difficult. Therefore, it is necessary to develop the approaches that would allow one to rigorously describe the phases and PTs of strongly interacting matter in finite systems. Such approaches are important from the academic point of view and their results can be, in principle, used in other branches of physics to study the PTs in systems with long range interaction which may not have a thermodynamic limit. In this dissertation, the author presents several exactly solvable models for finite volume EOS along with the new methods and ideas which allow to rigorously define the finite volume analogs of phases for some classes of models.

Third, since the PTs occur dynamically in the course of a collision, their modeling requires a reliable theoretical apparatus to describe the expansion, cooling down, phase transformation(s), and emission of secondary particles at the same time. This is a real challenge for theoreticians. One of the most promising approaches of this type is relativistic hydrodynamics, which is best suited to study the strongly interacting matter EOS. However, despite an essential progress achieved in hydrodynamic simulations, as shown below, the internal problems of the approach require an important modification and inclusion of the elements of relativistic kinetic theory to correctly describe

the particle emission of the perfect fluid. Also, the discussion covers the necessary modifications of relativistic kinetic equations for two domains separated by an arbitrary hypersurface (HS) and their possible consequences for the hydrocascade description of the collision process with several observables.

Overall, the present dissertation is devoted to the development of statistical mechanics for the static and dynamic processes occurring during A+A collisions at relativistic energies.

Relevance of the theme. Investigation of the properties of strongly interacting matter under extreme conditions is one of the most important subjects of modern physics. The experimental programs operating at CERN SPS and BNL RHIC colliders have opened a principal possibility to test the modern theory of strong interaction at high temperatures and high energy densities against a vast amount of data as well as to find a new state of matter, the QGP, and study its properties in the laboratory. Other experimental programs for studying the strongly interacting matter EOS may open soon. Thus, the low energy BNL RHIC, Darmstadt's FAIR and, perhaps, Dubna's Nuclotron experimental programs will search for the (tri)critical endpoint of the deconfinement PT diagram, whereas the present CERN SPS program will study the size and energy dependence of existing signatures of the deconfinement PT. On the other hand, the CERN LHC experiments will probe the quantum chromodynamics at high energy densities. In all these cases, the QGP, created during the collision, will hadronize either via cross-over or via PT and, hence, the description and interpretation of the measurements will inevitably require the knowledge of realistic EOS and adequate dynamic models for the collision process.

Besides the tantalizing technical difficulties, there exist some unresolved scientific problems which make these investigations quite hard. Thus, the main theoretical difficulties are due to highly nonlinear structure and complexity of the quantum chromodynamics. Since these difficulties are not yet resolved, the theoretical description of the collision process, in principle, cannot be achieved without the phenomenological EOS models. Furthermore, the only known way to dynamically model PTs in the collision process is through relativistic hydrodynamics because, unfortunately, the microscopic kinetic theory of PTs even for infinite systems has not been developed so far. The same is valid for the hydrokinetic or hydrocascade model, where the hydrodynamic equations are

used just to describe the PT. The hydrodynamic description, however, has to be interrupted at the HS, where it becomes irrelevant. This procedure, the freeze-out (FO) of momentum distribution functions of particles, cannot be done arbitrarily, but requires a mathematically correct boundary conditions for relativistic hydrodynamics. The correct formulation of these boundary conditions, that does not lead to the recoil paradox, had been a long standing (over 40 years) problems which found its solution in the author's works.

Another principal problem of the theoretical modeling of relativistic A+A collisions is a necessity to study the PT in a finite system. Originally the theory of critical phenomena was formulated for infinite systems only. However, the A+A collision experiments are dealing with finite and, sometimes, small systems and, hence, they require the development of theoretical approaches which can rigorously define the PT in a finite system. On the other hand, there exist systems with the long range interaction which do not have thermodynamic limit at all (namely, charged systems with Coulomb interaction). The nuclear liquid-gas PT is a typical example of such a system, which requires the correct and rigorous extension of the critical phenomena theory to finite systems. Such approaches are under extensive discussion in the nuclear multifragmentation community during last 15 years. Fortunately, recently in this field there were obtained several rigorous results, based on the exact analytical solutions for specific statistical model EOS in finite systems.

Therefore, the relevance and importance of the theme of this dissertation is based on three facts. First, the description and understanding of the measurements require the development of phenomenological models of the strongly interacting matter EOS in a wide range of parameters. Second, to study the strongly interacting matter PTs in A+A collisions, it is necessary to rigorously define the finite volume analogs of phases. Finally, to investigate the many-body reactions with phase transformation(s), it is vitally necessary to have an appropriate theoretical apparatus to describe the collective dynamics of a PT in the course of a collision.

Relation to other research programs. The present work was done at the Department of High Energy Densities of the Bogolyubov Institute for Theoretical Physics of the National Academy of Sciences of Ukraine. The major part of this dissertation is a constituent element of the investigations of the strongly interacting matter properties under extreme conditions, i.e. at

high temperatures and/or high densities, which are conducted at the Department of High Energy Densities within the state program. During last 15 years the Department of High Energy Densities was working on the following state programs:

1994-1998: Studies of strongly interacting matter in particle and nuclear collisions. The number of state registration is 0194U025942, code is 1.4.7.5.

1999-2001: Research of strongly interacting matter at high energy densities and high baryonic densities. The number of state registration is 0100U000215, code is 1.4.7.7.

2002-2004: Research of strongly interacting matter at high energy densities and high baryonic densities. The number of state registration is 0101U006428, code is 1.4.7.13.

2005-2007: Studies of strongly interacting matter in particle and nuclear collisions at high energies. The number of state registration 0105U000431, code is 1.3.1.

The aim and tasks of the research. The major aim of the present dissertation is the development of statistical methods to rigorously study the EOS of finite strongly interacting matter, its PTs, and their dynamics in the relativistic A+A collisions. The spatial and temporal finiteness of the system, created during the collision, are unavoidable elements of the experimental and theoretical analysis and have to be incorporated into the statistical description of the deconfinement and nuclear liquid-gas PTs.

To reach this goal, it was necessary to resolve the following tasks:

1. To study the EOS and phase diagram of strongly interacting matter on the basis of exactly solvable statistical models which have PT(s) in thermodynamic limit. They include: a simplified version of the Statistical Multifragmentation Model (SMM), the Fisher Droplet Model (FDM), the Gas of Bags Model (GBM), the Mott-Hagedorn resonance gas model, and the Quark Gluon Bags with Surface Tension (QGBST) model.
2. To develop the methods of solving various statistical models with PT in finite volumes and define the finite volume analogs of phases from the first principles of statistical mechanics.
3. To account for important features of strong interaction (the mass spectrum, surface tension, the short range repulsion with multi hard core radii, the Lorentz contraction of hadronic hard core radii e.t.c.) into statistical description, and to derive the model EOS.

4. To include the correct boundary conditions into hydrodynamic equations of finite perfect fluid, and to account for the emission of free streaming particles from the surface and/or volume of the fluid.
5. To generalize the relativistic Boltzmann equation for finite domains of different kinetics which are separated by the arbitrary HS, and to derive the hydrokinetic equations from the first principles of statistical mechanics.
6. To apply the statistical and hydrodynamic models to the description of particle yields and hadronic transverse momentum spectra, and to extract from the data an information about the hadronization stage of QGP in central A+A collisions.

The object of the research. The object of the research of this dissertation is highly excited strongly interacting matter that is created during the relativistic A+A collision. At intermediate colliding energies, this can be highly compressed nuclear matter which breaks up into some amount of fragments depending on its phase state. At high and very high energies (per nucleon) of collision, this can be hot and dense hadronic matter, QGP, or their mixture.

The subject of the research. The subject of the research of the present dissertation is the statistical mechanics of PTs, which occur in finite nuclear/hadronic matter during the A+A collisions at intermediate and high energies. The main attention is paid to finding the exact analytical solutions of a variety of statistical models and to analyzing the PTs in these models for infinite and finite volume. However, an essential part of the dissertation is also devoted to the development of hydrodynamic and hydrokinetic approaches to study the space-time dynamics of PTs during the expansion of highly excited, strongly interacting matter created in the A+A collision. Also, a comparison with the experimental data has been made whenever possible, in order to fix the model parameters, on one hand, and to extract information about the system evolution, on the other hand. Therefore, the author concentrates on the following problems:

1. The phase structure of nuclear matter. It includes an exact analytical solution of a simplified SMM and the analysis of the dependence of the phase diagram and (tri)critical point properties on the model parameters. Also, the mechanism of PT in statistical models, that

are similar to the SMM, is discussed in detail. A special attention is paid to the calculations of critical indices of the model and their dependence on the Fisher index τ .

2. Exactly solvable statistical models for finite nuclear systems. Here the author focuses on a simplified SMM and three ensembles of the Hills and Dales Model (HDM), proposed to study the surface deformations of physical clusters. The main attention is devoted to the rigorous definitions of the finite volume analogs of phases of nuclear matter within the finite volume SMM. The latter is solved analytically by a newly developed method, the Laplace-Fourier transform. Such a solution allows one, in principle, to study the statistical mechanics of nuclear systems with Coulomb interaction without taking the thermodynamic limit. The HDM is formulated to study the degeneracy factor of large, but finite, physical clusters of fixed volume. It allows one to find out the supremum and infimum for the surface entropy of such systems like the usual nuclei, 2- and 3-dimensional Ising model clusters, and so on.
3. The virial expansion for the Lorentz contracted rigid spheres and the EOS for hadronic binary mixtures. The hard core repulsion for hadron gas is necessary, but at high pressures existing at the deconfinement PT and/or above the deconfinement cross-over regions the relativistic effects for the hard core interaction of light hadrons become important and have to be accounted for. For this purpose, the author proposes and analyzes the relativistic analog of the VdW EOS for the Lorentz contracted hard spheres.
4. The exactly solvable phenomenological EOS for the deconfinement PT. This is the problem of a correct statistical description of the exponential mass spectrum of hadrons, suggested by Hagedorn. The author critically analyzes the Hagedorn model in the microcanonical ensemble. This analysis allows to explain why the statistical ensembles are not equivalent for the exponential mass spectrum, and to study the thermostatic properties of the Hagedorn-like systems. Then the two extensions of the Hagedorn model, the Mott-Hagedorn resonance gas model and the QGBST model, are analyzed. In the Mott-Hagedorn resonance gas model, the singular properties of the thermodynamic functions above the Hagedorn temperature are removed by the assumption that, due to the Mott transition, the discrete hadronic mass

spectrum becomes continuous with the width of hadrons being exponentially dependent on their mass. In another generalization of the Hagedorn model, the QGBST model, which is also solved analytically, the usual problems are avoided because of the hard core repulsion between the quark-gluon bags. It turns out that the null line of the surface tension coefficient of quark-gluon bags plays a crucial role in the deconfinement cross-over existence at high temperatures and low baryonic densities.

5. The FO problem of relativistic hydrodynamics and hydrokinetics. This is a fundamental problem of the correct formulation of the boundary conditions for the system of nonlinear partial differential equations of relativistic hydrodynamics at the FO HS where they become irrelevant. It was unresolved for almost 45 years. One of the difficulties was related to the fact that, while for the space-like parts of the FO HS the Cooper-Frye prescription works well, for the time-like parts of the FO HS it generates the unphysical negative particle numbers. However, it turns out that, to avoid the recoil problem and negative numbers of particles due to the emission of free streaming particles from the time-like parts of the FO HS, it is necessary to modify the original hydrodynamic equations. Therefore, a self-consistent formulation of relativistic hydrodynamics is considered. Then this problem is studied at the kinetic theory level, where the finiteness of the domains with two, generally different, kinetics requires modification of the relativistic Boltzmann equation.
6. The signatures of the deconfinement transition. An essential progress was achieved recently in solving this problem. The author discusses the idea of early statistical hadronization of charmonia (J/ψ , ψ' mesons), charmed particles and multistrange hadrons (ϕ meson, Ω hyperon e.t.c.) along with the experimental consequences. Also, the transverse momentum spectra of K-mesons are analyzed, and it is argued that the plateau of the inverse slopes of K^\pm mesons as the function of the colliding energy evidences for the onset of the deconfinement transition.

The methods of research. To solve the above formulated problems, the author uses the standard methods of statistical mechanics, like the Laplace transform, cluster and virial expansions, the maximum term method of Lee-Yang, Van der Waals approximation e.t.c., as well as the newly

proposed ones. The new methods are discussed in this dissertation in detail. The main essence of the latter methods is related to accounting for the spatial and temporal finiteness of highly excited strongly interacting systems created in the A+A collisions.

The simplified SMM is solved analytically by the standard Laplace transform method. However, to analyze the divergent sums, which define the critical indices of this model, the author has proposed a rigorous method based on the Newton-Leibnitz definition of the integral. The application of this method to the well known FDM shows that the previously stated range of the τ index, $2 < \tau < 3$, must, in fact, be changed to $2 < \tau < 2\frac{2}{3}$. With the help of this method, a principal correction is made to Fisher's derivation of the Fisher-Rushbrooke and Fisher-Griffiths inequalities for the critical exponents. This finding indicates fundamental problems in defining some critical indices of statistical systems, in particular, the α index.

The Complement method to analyze the chemical equilibrium in finite systems is also proposed. It is based on the evaluation of the free energy change occurring when a cluster moves from one phase to another. For a finite liquid drop in equilibrium with its vapor, this is done by virtually transferring a cluster from the liquid drop to the vapor and evaluating the energy and entropy changes associated with both the vapor cluster and the residual liquid drop (complement). The method is applied to the description of the clusters in 2- and 3-dimensional Ising models. It allows one to account for the finite size effects associated with the the largest (but mesoscopic) drop representing the liquid in equilibrium with the vapor and derive the Gibbs-Thomson correction for pressure and cluster density. This method can be generalized to incorporate energy terms common in the nuclear case: symmetry, Coulomb and angular momentum energies.

The author has developed the Laplace-Fourier method as a generalization of the usual Laplace technique. It is based on the integral representation of the Dirac δ -function which allows one to rewrite any complicated dependence as an exponential of a corresponding parameter. The resulting exponential can be dealt with the usual Laplace transformation. Such an approach allows to exactly solve a simplified SMM for finite volumes. It is shown that, for finite volumes, the grand canonical ensemble (GCE) partition can be identically represented via the simple poles singularities of the isobaric partition. The behavior of these simple poles in the complex free energy

density plane as function of the system's volume allows one to distinguish the model with PT from the model without it. The analysis of the real part of the effective chemical potential allows one to unambiguously define the finite volume analog of the phase diagram and the corresponding phases. These results are also generalized to define the finite volume analogs of phases for the deconfinement PT in the GBM.

Also, using this method, the author has exactly solved three ensembles of HDM for the clusters of finite size. This is the statistical model of surface deformations of physical clusters with the constraint of the fixed cluster volume. This method, for the first time, allows one to estimate the upper and lower bounds on the degeneracy of different physical clusters consisting of the finite size constituents. In order to elucidate the influence of the volume conservation condition on the surface entropy, the author has introduced and studied two new isochoric ensembles, semigrand canonical and specially constrained canonical ensembles, of the surface partition.

The usual cluster and virial expansion methods are generalized to the momentum dependent interparticle potentials. This generalization is necessary to account for the Lorentz contraction of the hard core repulsion of light hadrons at the deconfinement PT region and/or above the deconfinement cross-over. It is shown that, in contrast with the previous unsuccessful attempts, the obtained relativistic analog of the Van der Waals (VdW) EOS obeys causality.

To solve the FO problem in relativistic hydrodynamics, the author has extended the equations of motion of the perfect fluid with the help of generalized functions to the system consisting of two subsystems, the fluid and the gas of free particles emitted by the fluid, which are separated by a FO HS. Then the extended equations of motion generate the equations of motion of each subsystem and the boundary conditions between them which have to be solved consistently with the equations of the perfect fluid. Such an approach allows to avoid the problems and paradoxes faced by the previous researches of this problem, and to build up the paradox-free, self-consistent relativistic hydrodynamics.

This method was refined further and applied to derive the kinetic and hydrokinetic equations for two domains of generally different kinetics separated by an arbitrary HS. Using this method, the author has accounted for the exchange of particles via the boundary HS and has derived the

source terms in the relativistic Boltzmann equations for both domains. Such an approach has allowed for the first time to self-consistently derive the boundary conditions for the hydrocascade model and to discover a discontinuity of the most general form, the three flux discontinuity. The latter generates all previously known kinds of hydrodynamic discontinuities as limiting cases.

Scientific novelty of the obtained results. Applications of all these methods to the statistical mechanics of strongly interacting matter and to solving specific problems, discussed above, have led to multiple new and original results. The most important and new of these results are the following:

1. An exact analytical solution of a simplified SMM is found in the thermodynamic limit. A rigorous mathematical proof of the 1-st order nuclear liquid-gas PT has been given and the possibility of the existence of a 2-nd order PT has been found. The critical indices $\alpha', \beta, \gamma', \delta$ as functions of the Fisher parameter τ are calculated for this analytical solution of the SMM. For the first time, it is found that these indices differ from those of the FDM. It is also shown that, in contrast to general expectations, the scaling relations for the SMM critical indices differ from the corresponding relations of the FDM. In contrast to the FDM, the SMM predicts a narrow range of values for index τ , $1.799 < \tau < 1.846$, which is consistent with both the ISiS Collaboration data and EOS Collaboration data. As shown in the dissertation, such a range of τ index is of a principal importance because it gives a direct evidence that nuclear matter has a tricritical rather than a critical point.
2. For the first time the cluster and virial expansions are derived for the momentum dependent inter-particle potentials. Using these results, the two models of the relativistic EOS of the VdW gas are proposed and analyzed. In both of these EOS the Lorentz contraction of the sphere's volume is taken into account. The first EOS, which does not obey causality in the limit of high densities, is generalized to the two-component excluded volume model and applied to describe the hadron yield ratios for BNL AGS and CERN SPS data. The first EOS is refined further to obey the causality at high densities, i.e., the sound velocity of this model is subluminal. As shown for the high values of chemical potential, the pressure in the second EOS has an interesting kinetic interpretation. The second EOS indicates that

for high densities the most probable configuration corresponds to the smallest value of the relativistic excluded volume. In other words, for high densities the configurations with the collinear velocities of the neighboring hard core particles are the most probable ones. This, perhaps, may shed light on the coalescence process of any relativistic hard core constituents.

3. A novel powerful mathematical method, the Laplace-Fourier transform, is proposed. It has allowed to find an analytical solution of a simplified version of the SMM with the restriction that the largest fragment size cannot exceed the finite volume of the system. A complete analysis of the singularities of the isobaric partition function is done for the finite volumes. The finite size effects for large fragments and the role of metastable (unstable) states are discussed. These results allowed the author, for the first time, to rigorously define the finite volume analogs of nuclear liquid phase, gaseous phase, and the mixed phase. Also these findings explicitly demonstrate that the famous T. Hill approach to define the PT in finite systems is based on a wrong assumption.
4. To elucidate the origin of surface entropy of large physical clusters the HDM for their surface deformations is proposed. It is solved analytically for large finite clusters by the Laplace-Fourier transformation method. The requirement of volume conservation of the deformed cluster is automatically accounted for. In the limit of small amplitude of deformations, the HDM reproduces the leading term of the famous Fisher result for the surface entropy within a few percent. In other words, in this limit the HDM generates a linear temperature dependence of surface tension coefficient of large clusters. Also, the model gives the degeneracy prefactor of large fragments which was unknown to Fisher. The surface entropy coefficient of two other surface partitions with the different volume conservation constraints are exactly solved and compared with the surface entropy coefficients of 2- and 3-dimensional Ising models.
5. The effects of the finite size of a liquid drop undergoing a PT are described in terms of the complement, the largest (while still mesoscopic) drop representing liquid in equilibrium with vapor. Vapor cluster concentrations, pressure and density from fixed mean density lattice gas (Ising) model calculations are explained in terms of the complement. The complement

approach generalizes the FDM and SMM by accounting for generic features of chemical equilibrium in finite systems. Accounting for this finite size effect is a key element in constructing the infinite nuclear matter phase diagram from experimental data.

6. A microcanonical treatment of Hagedorn systems, i.e. finite mass hadronic resonances with an exponential mass spectrum controlled by the Hagedorn temperature T_H , is performed. For the first time it is shown that, in the absence of any restrictions, a Hagedorn system is a perfect thermostat, i.e. it imparts its temperature T_H to any other system in thermal contact with it. It is found that, if the particles of different masses are generated by a Hagedorn system, then they are in chemical equilibrium with each other. Thus, a Hagedorn system is a perfect particle reservoir. The thermodynamic effects of the lower mass cut-off in the Hagedorn mass spectrum is analyzed. By a direct calculation of the microcanonical partition, it is found that in the presence of a single Hagedorn resonance the temperature of any number of N_B Boltzmann particles only slightly differs from T_H up to the kinematically allowed limit N_B^{kin} . For $N_B > N_B^{kin}$ however, the low mass cut-off leads to a decrease of the temperature as N_B grows. The properties of Hagedorn thermostats naturally explain a single value of hadronization temperature observed in elementary particle collisions at high energies which is a consequence of a finite volume PT.
7. The statistical bootstrap model is critically revised in order to include a medium-dependent resonance width into it. It is shown that a thermodynamic model with a vanishing width below the Hagedorn temperature T_H and a Hagedorn spectrum-like width above T_H not only eliminates the divergence of the thermodynamic functions above T_H , but also gives a satisfactory description of lattice quantum chromodynamics data on the energy density above the chiral/deconfinement transition. The proposed model allows one to explain the absence of heavy resonance contributions in the fit of the experimentally measured particle ratios at SPS and RHIC energies. This approach is applied to the description of the NA50 experiment and the analysis suggests that the anomalous suppression of J/ψ production can be explained by the increase of the effective number of degrees of freedom at the Hagedorn temperature.

8. The temperature and chemical potential dependent surface tension of bags is introduced into the gas of quark-gluon bags model. This resolves a long standing problem of a unified description of the first and second order PT with the cross-over. Such an approach is necessary to model the complicated properties of the QGP and hadronic matter from the first principles of statistical mechanics. As shown in this dissertation, the proposed model has an exact analytical solution and allows one to rigorously study the vicinity of the critical endpoint of the deconfinement PT. The existence of higher order PT at the critical endpoint is discussed. In addition, it is found that, at the curve of a zero surface tension coefficient, there must exist a surface induced PT of the 2^{nd} or higher order, which separates the pure QGP from the cross-over states, that are the mixed states of hadrons and QGP bags. Thus, the suggested model predicts that for $\tau \leq 2$ the critical endpoint of quantum chromodynamics is the tricritical endpoint. Using the other results of the dissertation, one can extend this analytical solution to finite volumes.

9. The FO problem of relativistic hydrodynamics is solved in the zero width approximation. For the solution, the author has derived the correct generalization of the Cooper-Frye formula, the cut-off distribution, for the invariant momentum spectra of secondary particles emitted from the time-like HSs. Then, for the first time, the conservation laws are formulated not just for a perfect fluid alone, but for a perfect fluid and the gas of emitted particles. The conservation laws at the boundary of the fluid and gas of free particles are analyzed, and the new kind of a discontinuity in relativistic hydrodynamics, the FO shock, is discovered. It is shown that the FO condition in relativistic hydrodynamics has to be formulated not for a fluid, but exclusively for a gas of free particles. For a wide class of EOS it is proven that the FO shock resolves the recoil problem. Thus, a self-consistent, paradox-free relativistic hydrodynamics with particle emission is formulated for the first time.

10. The relativistic kinetic equations for two domains, separated by the HS with both the space- and time-like parts, are derived for the first time. The particle exchange between these domains, occuring at the time-like boundaries, generates the source terms and modifies the collision term of the kinetic equations. By integrating the derived set of transport equations,

the correct boundary conditions between the hydro and cascade domains are obtained. Remarkably, the conservation laws at the boundary between these domains conserve both the incoming and outgoing components of energy, momentum and baryonic charge separately. Thus, the relativistic kinetic theory generates twice the number of conservation laws compared to traditional hydrodynamics. Further analysis shows that these boundary conditions between domains, the three flux discontinuity, can be satisfied only by a special superposition of two cut-off distribution functions for the “out” domain. All these results are applied to the case of the PT between the QGP and hadronic matter. The possible consequences for an improved hydrocascade description of the relativistic nuclear collisions are discussed. The unique properties of the three flux discontinuity and their effect on the space-time evolution of the transverse expansion are also analyzed. The possible modifications of both transversal radii of pion correlations, generated by a correct hydrocascade approach, are discussed.

11. A hypothesis of early hadronization of charmonia and multistrange hadrons is formulated for the first time. In this dissertation, it is shown that this hypothesis naturally explains the data on the apparent temperature (inverse slope) of the transverse mass spectra of J/ψ and ψ' mesons at SPS energies. The transverse mass spectra of Ω , J/ψ and ψ' (Pb+Pb at 158 AGeV) and ϕ , Ω (Au+Au at $\sqrt{s_{NN}} = 130$ GeV) particles are perfectly reproduced within the hypothesis of simultaneous kinetic and chemical FO of those particles from the hadronizing QGP and predictions for the J/ψ and ψ' spectra at RHIC are made. Also it is shown that the RHIC data for (anti) Λ and (anti)proton transverse momentum spectra are in contradiction with the predictions of a popular Single Freeze-out Model.
12. The analysis of the experimental values of the inverse slopes of transverse momentum spectra of kaons produced in central Pb+Pb (Au+Au) interactions shows an anomalous dependence on the collision energy. The inverse slopes of the spectra increase with energy in the low (AGS) and high (RHIC) energy domains, whereas they are constant in the intermediate (SPS) energy range. It is shown that this anomaly is caused by a modification of the EOS in the transition region between confined and deconfined matter, and is similar to the usual caloric curves. Therefore, such a behavior of the transverse caloric curves can be considered

as a new signature of the onset of deconfinement located in the low SPS energy domain. Nowadays this signature is known to the relativistic heavy ion community as a Step.

Practical value of the obtained results. The results obtained in the present dissertation give a principally new understanding of the strongly interacting matter EOS and its PTs. Thus, the new scaling relations between critical exponents, found for a simplified SMM, predict a very narrow range of the τ index which, in contrast to the FDM, is perfectly consistent with the experimental findings of the ISiS and EOS collaborations. Such a finding is of principal importance because it gives a direct evidence that nuclear matter has a tricritical point rather than the critical one.

A hypothesis of statistical production of charmonia at hadronization of QGP has not only helped to explain the inverse momentum spectra of early hadronized particles, measured by NA50 and WA97 experiments performed at CERN SPS, and by STAR Collaboration at BNL RHIC, but also to predict the inverse slopes of J/ψ and Ψ' mesons which are to be measured at BNL RHIC at the center of mass energy 130 GeV·A.

Despite almost three decades of searches for the QGP signals, the transverse caloric curves (the inverse slopes of transverse momentum spectra) of K^\pm mesons as the function of the collision energy is one of the only three experimentally established signals of the deconfinement transition.

Besides the practical importance of these results for understanding the experiments, the results obtained in this dissertation have a principal theoretical importance. Thus, the theoretical description of PTs in finite system is, on one hand, demanded by the experiments on A+A collisions, in which the finite or even small number of particles is produced. On the other hand, it is necessary to study the critical phenomena in the systems with the Coulomb-like interaction which, in principle, do not have the thermodynamic limit. The analysis of several exactly solvable models of realistic EOS of strongly interacting matter, for instance, shows that in finite systems the GCE partition is defined by a set of states having (in general) the complex values of free energy, and that these states are not in a true chemical equilibrium for the same value of the chemical potential due to the interaction of the constituents. Such a feature cannot be obtained within a famous FDM due to lack of the hard core repulsion between the constituents.

Also the obtained results indicate that, in contrast to Hill's expectations, the mixed phase at

finite volumes is not just a composition of two pure phases. It is rigorously shown that a finite volume analog of the mixed phase is a superposition of three and more collective states, each of them is characterized by its own value of (complex) free energy, and, consequently, the difference between the free energies of these states is not a surface-like, as Hill argued in his many works and several books on statistical mechanics of small systems, but volume-like. It is necessary to stress that such results cannot be, in principle, obtained either numerically or by the mean-field models, which are not truly statistical. Since there are only a few statistical models with PT which are exactly solved for finite systems, the results of the present dissertation are indispensable for building up the theory of critical phenomena in finite systems.

The solution of such a long standing problem as the FO of relativistic hydrodynamics is also of a great theoretical significance because it completes the relativistic hydrodynamics for the fluid emitting the gas of free particles and converts the relativistic hydrodynamics into a powerful and reliable tool of research of the strongly interacting matter EOS and/or the collective phenomena associated with the matter under extreme conditions (nuclear A+A collisions, the Big Bang, the supernova explosions e.t.c.). The results, obtained in solving the FO problem, have initiated the ten-year long activity of the Bergen and San Paulo hydro groups on further refinement of this approach. Also these results were used by U. Heinz and collaborators to study the FO effects in pion interferometry and by E. Shuryak and collaborators for their hydrocascade model.

Furthermore, this activity had increased the author's personal interest in the hydrokinetic (hydrocascade) approach which has led to the rigorous formulation of such a model based on the firm theoretical ground. As discussed in the present dissertation, the hydrokinetic approach is based on the generalized relativistic Boltzmann equations which are rigorously derived for the finite domains separated by an arbitrary HS. The derived equations include the boundary conditions at this HS, and it is shown that the relativistic kinetics generates, in general, twice the number of conservation laws compared to the usual relativistic hydrodynamics. The analysis of these boundary conditions shows that they could be important for understanding the source of turbulence which up to now remains a true challenge for theoreticians. Also, the developed hydrokinetic approach can be used to model the dynamics of PTs in the inhomogeneous media which is rather

hard to describe by the usual hydrodynamic equations.

The personal contribution of the candidate. The personal contribution of the candidate in obtaining the results 1-12, listed above, is decisive for the development of major ideas, main approaches and strategic lines of the research. In particular:

1. In analyzing the thermodynamic limit of a simplified SMM (a series of works in collaboration with M. I. Gorenstein, W. Greiner and I. N. Mishustin), the candidate suggested to apply the Laplace transform technique to solve this model, made all the analytical and numerical calculations, and gave a correct physical interpretation of the obtained results.
2. During the studies of the GCE partition of the relativistic gas of Lorentz contracted rigid spheres (in collaboration with M. I. Gorenstein, H. Stöcker and W. Greiner), the candidate suggested to generalize the cluster and virial expansions for the momentum dependent potentials, derived the analytical formulas, and performed their numerical analysis. Later on a candidate alone has reformulated the acausal EOS, obtained with his collaborators, and made it causal.
3. To study the problem of surface entropy (one paper in collaboration with J. B. Elliott and L. Phair and another in collaboration with J. B. Elliott) the candidate formulated the HDM and solved it analytically by the Laplace-Fourier methods which he proposed earlier.
4. An analytic analysis of magnetization of the 2- and 3-dimensional Ising models with the help of a Complement method (in collaboration with L.G. Moretto, J. B. Elliott, R. Ghetti, J. Helgesson and L. Phair) was done by the candidate. Also he found the derivation of the Gibbs-Thomson correction of the system's free energy due to the presence of a finite liquid drop.
5. An analytic treatment of the microcanonical systems with a Hagedorn mass spectrum (a series of works in collaboration with L.G. Moretto, J. B. Elliott, and L. Phair) was proposed and performed by the candidate. Using these results, the candidate also showed that such an analysis justifies the Statistical Hadronization Model of Becattini and explains the con-

stant value of hadronization temperature, observed in elementary particle collisions at high energies.

6. A modification of the EOS of the Mott-Hagedorn model above T_H (a series of works in collaboration with D. B. Blaschke) was proposed by the candidate. He also fitted the data of lattice quantum chromodynamics, and, using this model, he suggested an explanation of the absence of heavy resonances (heavier than 5 GeV) in the relativistic A+A collisions. The latter occurs due to a very short life time of heavy resonances in the media with the temperature higher than that one of the Mott-Hagedorn transition.
7. The solution of the FO problem was proposed by the candidate alone and is published in his paper without coauthors. In the subsequent papers on this subject, written in collaboration with M. I. Gorenstein and W. Greiner, the candidate developed his original ideas further. All the analytical and numerical results of these subsequent publications were obtained by a candidate himself.
8. The hypothesis of early kinetic FO of charmonia at the QGP hadronization was suggested by the candidate. He derived the necessary expressions and fitted the experimental data to describe the transverse momentum spectra of early hadronized particles (a series of works in collaboration with M. I. Gorenstein and M. Gazdzicki). He also predicted the results of the future measurements of the transverse momentum spectra of J/ψ and ψ' mesons at the center of mass energy $\sqrt{s_{NN}} = 130$ GeV.
9. The argumentation based on the mixed phase softest point to justify the plateau in the dependence of the inverse slopes of the soft kaons transverse momentum spectra on the colliding energy per nucleon as a signal of the deconfinement was suggested by a candidate.

Approbation of the dissertation results. All the results of this dissertation were presented at more than 20 international conferences and schools on phenomenology of A+A collisions and close themes, at the seminars of the Bogolyubov Institute for Theoretical Physics of the National Academy of Sciences of Ukraine and many leading scientific centers in this field of research.

The latter include: Brookhaven National Laboratory (New York, USA), Lawrence Berkeley National Laboratory (California, USA), Columbia University (New York, USA), Institute for Nuclear Physics (Seattle, Washington, USA), GSI Darmstadt, University of Regensburg (Germany), University of Bielefeld (Germany), University of Frankfurt (Germany), University of Hannover (Germany), University of Giessen (Germany), ECT Trento (Italy), University of Salamanca (Spain), etc. The most important presentations were made at the following conferences and schools:

- International conference “Structure of the Nucleus at the Dawn of the Century”, Bologna, Italy, May 29 - June 3, 2000,
- Int. conference “Nucleus Nucleus Collisions 2000”, Strasbourg, France, July 3-7, 2000,
- International conference “Quark Matter in Astro- and Particle Physics”, Rostock, Germany, November 27–29, 2000,
- International conference “Dynamical Aspects of the QCD Phase Transition”, Trento, Italy, March 12 - 15, 2001,
- “International Conference on Nucleus and Particle Collisions (INPC) 2001”, Berkeley, California, USA, July 30 – August 3, 2001,
- Conference “Strange Quarks in Matter 2001”, Frankfurt, Germany, September 24–29, 2001,
- 50-th Gordon Research Conference “Nuclear Chemistry”, New London, New Hampshire, USA, June 16-22, 2002,
- International Program INT-03 “Three Years of RHIC Physics”, Seattle, Washington, USA, April 15 - October 15, 2003,
- International workshop “Aspects of Nonperturbative QCD - Hadrons and Thermodynamics”, Rostock, Germany, July 14-16, 2003,
- International workshop “Modern Methods in Relativistic Nuclear Physics”, Dubna, Russia, August 19-20, 2003,

- International Workshop on Progress in Particle and Nuclear Physics: “Heavy Ion Reactions from Nuclear to Quark Matter”, Erice, Italy, September 16-23, 2003,
- International conference “Tracing the Onset of Deconfinement in Nucleus-Nucleus Collisions”, Trento, Italy, April 23-30, 2004,
- Gordon Research Conference “Nuclear Chemistry”, New London, New Hampshire, USA, June 13-18, 2004,
- International conference “World Consensus Initiative III”, Texas A & M University, College Station, Texas, USA, February 11-17, 2005,
- “School of Collective Dynamics in High-Energy Collisions”, Berkeley, USA, May 19-27, 2005,
- International school-seminar “New Physics and Quantum Chromodynamics at External Conditions”, Dnepropetrovsk, Ukraine, May 3-6, 2007,
- International Workshop “Relativistic Nuclear Physics: from Nuclotron to LHC Energies”, Kiev, Ukraine, June 18-22, 2007.

Using the results obtained in the present dissertation, the candidate gave a series of lectures for the advanced students at the Center for Physics of Ultra-relativistic Nuclear Collisions at the Faculty of Nuclear Sciences and Physical Engineering of the Czech Technical University in Prague, Czech Republic, April 15-26, 2007.

Publications. The results of this dissertation are published in 42 works, including the articles in the leading scientific journals, conference proceedings and preprints. In particular, 30 papers are published in scientific journals, Refs. [47, 48, 50, 56, 106, 110, 111, 113, 114, 115, 140, 154, 155, 156, 173, 200, 205, 206, 207, 208, 209, 225, 226, 240, 242, 258, 260, 263, 264, 265], 6 works are published as conference proceedings, Refs. [49, 51, 52, 57, 241, 259], and 6 works are preprints, Refs. [57, 58, 112, 141, 142, 257]. 12 publications are prepared by K. A. Bugaev alone.

The structure and volume of the dissertation. The dissertation consists of an introduction, six chapters, conclusions, two appendices and bibliography which contains 358 references. The dissertation has 55 figures and 8 tables. The volume is 341 pages of the printed text.

CHAPTER 1

NUCLEAR MATTER IN THERMODYNAMIC LIMIT

It was noted long ago that statistical methods could be applied to nuclear processes, if the energies involved are large when compared to the lowest excitation energies of nuclei [1]. Assuming this, Weisskopf was able to formulate expressions for the probability of neutron (or charged particle) emission from excited nuclei.

Following Bohr, Weisskopf divided process initiated by nuclear collisions into two stages: the first stage was the formation of a compound and the second one was the disintegration of the compound nucleus. Both stages could be treated independently. The energy of compound nucleus is similar to the heat energy in a solid or liquid and the emission of particles from the compound nucleus is analogous to an evaporation process. Exploiting this idea, Weisskopf derived a general statistical formula for evaporation of particles from an excited nucleus accounting for finiteness of the nucleus and for the fact that the evaporation of a particle takes away significant energy from the compound nucleus. In that regard, Weisskopf worked out the formulas to describe the evaporation neutrons from a hot nucleus, i.e. he was describing a 1st order PT with a neutron leaving (or evaporating from) the condensed phase (the hot nucleus) and entering the dilute phase (a very low density neutron vapor).

Already this example of neutron evaporation shows that for some processes the Coulomb interaction can be neglected at leading order because of its weakness compared to strong interaction. Such a view was refined further in a concept of infinite nuclear matter. This is a helpful mathematical construct which corresponds to the nucleons without electrical charge. In nuclear physics such a concept is very similar to the concept of idea gas: like in many applications the dilute real gases behave similarly to the ideal gas, in many respects the hot compound nucleus reminds a finite piece of nuclear matter.

Historically this was the first concept allowing one to study the nuclear liquid-gas PT in nuclear reactions. Like in Weisskopf's treatment the compound nucleus represent a nuclear matter, whereas the emitted fragments of different masses (charges) correspond to a nuclear vapor. Then, studying the fragment distributions at different excitation energies one can learn the information about the emission stage of the reaction and probe the nuclear matter EOS. This was exactly the case: for excitation energy below 4-5 MeV per nucleon the fission probability W_A of compound nucleus emitting a A-nucleon fragment shows an exponential behavior of as the function of inverse square root of excitation energy $E^* = \varepsilon/\rho - M$, i.e. $W_A \sim \exp(-B_A/\sqrt{E^*})$, where B_A is a fission barrier for a fragment A , ε is the energy density of a nucleus and ρ is its particle density. Such a behavior of the compound nucleus temperature $T \sim \sqrt{E^*}$ is typical for a Fermi liquid with the EOS (caloric curve) $E^* = aT^2$ [2, 3, 4, 6]. If, however, the excitation energy per nucleon is increased by a few MeVs only, the nucleus breaks down into several fragments and its EOS, $E^* = \frac{3}{2}T$ [2, 3, 4, 6], corresponds to the nonrelativistic gas of massive Boltzmann particles. Also the mass distribution of fragments is similar to that one of the molecule clusters in the vapor of real liquids.

The change of the caloric curve behavior from a Fermi liquid regime to the nonrelativistic massive Boltzmann gas can be naturally explained [7, 8, 9] by a PT from the nuclear liquid phase representative to the vapor of nuclear fragments. The multi particle nature of this phenomenon is reflected in its name - nuclear multifragmentation.

The early theoretical arguments on the nuclear liquid-gas PT [7, 8, 9] initiated the theoretical and experimental efforts to study the nuclear matter EOS which are going on over the two decades. The theoretical approaches can be divided into two different categories: analytical/semi-analytical models [10, 11, 12, 13, 14, 15, 16, 17, 18] and computational models: both on a lattice [19, 20, 21, 22, 23, 24, 25, 26, 27, 28, 29, 30, 31, 32] and off it [33, 34, 35, 36, 37, 38, 39, 40, 41, 42, 43].

The analytical/semi-analytical theories employed various methods (e.g. particles interacting through a Skyrme force, finite temperature Hartree-Fock theory and various nuclear extensions of the FDM) to determine the critical point of bulk (i.e. infinite, uncharged and symmetric) nuclear matter and the liquid-vapor phase boundary. This lead to estimates of the critical temperature in the range of 12.6 MeV to 28.9 MeV depending on the theoretical techniques employed. Once

estimates were made for bulk nuclear matter, the effects of a finite number of nucleons and a fluid made up of two components (one which carries an electric charge) were studied. Those effects generally lead to a lower critical temperature with estimates between 8.1 MeV and 20.5 MeV. Computational models on the lattice attempted to study the process of nuclear cluster formation from “the bottom up” by modeling in a simple way the short range interaction of the nucleons. This was done both geometrically with percolation models [19, 20, 21, 22, 23, 24, 25, 26] and thermally with lattice gas (Ising) models [27, 28, 29, 30, 31, 32].

Despite a great variety of the theoretical models they can be divided into two groups: the mean-field models and the statistical models. The vast majority of these models are mean-fielded ones, whereas there are only two successful statistical models, and both of them are the cluster models. The latter are the extensions of the FDM [44, 45] and SMM [46]. These cluster models are used to study the nuclear liquid-gas PT both in finite and infinite nuclear matter. In this chapter I consider the infinite nuclear matter. It is investigated by a mean-fielded model, which is a phenomenological generalization [47] of a famous Walecka model [10], and by an exact solution [48, 49, 50, 51, 52] of a simplified SMM [53, 54] for symmetric (i.e. with equal number of protons and neutrons) nuclear matter.

The suggested mean-fielded model [47] has three parameters only which are fixed to reproduce three major properties of the nuclear matter (for details see below). However, surprisingly this model simultaneously reproduces the value of the nucleon effective mass and the incompressibility factor at the normal nuclear density. The suggested model belongs to the class of self-consistent EOS of nuclear matter. Since its partition does not obey the first Van Hove axiom [55], it is necessary to assume some additional conditions on the EOS which will provide the validity of thermodynamic identities.

In contrast to the mean-field models an exact analytical solution of statistical models [48, 49, 50, 51, 52] are much more valuable because they allow one not only to study the nuclear matter phase diagram, but also to study the properties of the (tri)critical point of the PT diagram, which, as we know from the theory of critical phenomena, depend only on the most general characteristics of short range interaction and the dimensionality of the system. Therefore, investigation of a

statistical model with somewhat simplified interaction can provide us with the results valid for the (tri)critical point of more realistic models and/or some substances. The found critical exponents of the SMM [56, 57] allow one to verify the scaling relations for the SMM critical indices and compare them with the experimental findings. Such a comparison enables us to determine the universality class of the SMM and that one of nuclear matter.

This chapter is based on the results obtained in [47, 48, 49, 50, 51, 52, 56, 57, 58].

1.1. A Self-consistent Mean-Field EOS for Nuclear Matter

The determination of the nuclear matter EOS is one of the foremost goals in today's heavy-ion physics. Up to now our knowledge of the the nuclear EOS is restricted to one point in the plane of the independent thermodynamical variables temperature T and net baryon density ρ . This point is the so-called ground state of nuclear matter: at $T = 0$ nuclear matter saturates (i.e. the pressure $p = p_0 = 0$) at a density $\rho_0 \approx 0.16 \text{ fm}^{-3}$. From nuclear physics data one derives the following value for the energy per particle $W(\rho) \equiv (\varepsilon/\rho)_{T=0} - M$ (ε is the energy density, M is the nucleon mass) of infinite nuclear matter:

$$W(\rho = \rho_0) \equiv W_0 \approx -16 \text{ MeV}. \quad (1.1)$$

It is just bulk part in a Bethe-Weitzsäcker formula for nuclear binding energy.

An analysis of the incompressibility [59]

$$K_0 \equiv 9 \frac{\partial p}{\partial \rho} \Big|_{T=0, \rho=\rho_0} \equiv 9 \rho_0^2 \frac{\partial^2 W}{\partial \rho^2} \Big|_{T=0, \rho=\rho_0} \quad (1.2)$$

shows that a large value of K_0 ($\approx 300 \text{ MeV}$, with considerable error) may be more compatible with the data than the previously reported low one, $K_0 = 180 - 240 \text{ MeV}$ [60, 61]. The recent analysis shows that the situation is still not very clear. Thus, the simulations of the sideward anisotropy observed in the A+A collisions at low and intermediate energies require $K_0 \approx 210 \text{ MeV}$, whereas the the elliptic flow anisotropy observed in the same experiment requires $K_0 \approx 300 \text{ MeV}$ [62, 63]. The present situation is hoped to be clarified soon at the GSI accelerator FAIR.

However, to fix the coupling constants of the phenomenological model it is possible to use the estimations of the effective nucleon mass M_0^* at $T = 0$ and $\rho = \rho_0$ which can be found in the

literature [64, 65] are $M_o^* = (0.7 \pm 0.15)M$. Therefore, keeping in mind that K_o data are not too conclusive, we will pay more attention to the M_o^* value.

Any reasonable model for the nuclear matter EOS must be thermodynamically self-consistent and reproduce the above quantities ρ_o , W_o , K_o and M_o^* . These properties have clear meaning: at normal nuclear density the binding energy (1.1) is defined, but it must be a minimum (then the system is mechanically stable because of vanishing pressure $p = p_o = 0$) and the width of this minimum is defined by the incompressibility factor (1.2). Once the model is worked out in the vicinity of normal nuclear matter, its behavior in other regions of the n-T plane can be then probed via heavy-ion collisions. The aim of this section is to formulate a phenomenological generalization of the mean-field theory approach and obtain a class of nuclear matter equations of state. This EOS is compared with the non-relativistic many-body theory of [65] and various relativistic equations of state.

Following early theoretical suggestions [66], experiments which measure the π -meson multiplicity in heavy-ion collisions [7] have been performed in order to extract the nuclear EOS directly from data. For this purpose the following decomposition for the energy per baryon

$$\frac{\varepsilon}{\rho} = M + W_{th} + W_c, \quad (1.3)$$

was introduced with some phenomenological anzätzen for the thermal energy W_{th} , and the compression energy W_c . The whole construction was, however, not physically self-consistent: for the calculation of W_{th} the momentum distribution of an ideal nucleon gas was used, but when introducing, in addition, the ‘compression energy’ one took into account the interaction between nucleons. The interaction, however, modifies the ideal-gas momentum distribution, and one faces the problem of adjusting the relativistic Fermi distribution of the nucleons to the functional form of the ‘compression energy’.

To find a solution of this problem we remember that in the relativistic mean-field theory of Walecka [10] (see also [11]) the interaction is described by scalar ϕ and vector U^μ mesonic fields with baryon-meson interaction terms in the Lagrangian: $g_s \bar{\psi} \psi \phi$ and $g_v \bar{\psi} \gamma^\mu \psi U_\mu$. For nuclear matter in thermodynamical equilibrium these meson fields are considered to be constant classical quantities. The scalar field describes the attraction between nucleons and changes the nucleon

mass $M \rightarrow M^* = M - g_s \phi$. The nucleon repulsion is described by a zero component (the spatial components must vanish due to the translational invariance) of a vector field which adds $U(\rho) = C_v^2 \rho$ ($C_v = \text{const}$) to the nucleon energy ($-U(\rho)$ for the antinucleon). Following [67] it is possible to formulate a generalized nuclear matter EOS which includes the mean-field theory and pure phenomenological models as special cases. Restricting ourself at the moment to nucleonic degrees of freedom we suggest the following general form for the nuclear EOS in GCE:

$$p(T, \mu) = \frac{\gamma_N}{3} \int \frac{d^3k}{(2\pi)^3} \frac{k^2}{\sqrt{k^2 + M^{*2}}} (f_+ + f_-) + \rho U(\rho) - \int_0^\rho dn U(n) + P(M^*), \quad (1.4)$$

where f_+ and f_- are the distribution functions of nucleons and antinucleons

$$f_\pm \equiv \left[\exp \left(\frac{\sqrt{k^2 + M^{*2}} \mp \mu \pm U(\rho)}{T} \right) + 1 \right]^{-1}, \quad (1.5)$$

μ is the baryonic chemical potential and γ_N is the number of spin-isospin nucleon states, which equals four for symmetric nuclear matter. The dependence of the effective nucleon mass M^* on T and μ is defined by extremizing the thermodynamical potential (maximum of the pressure):

$$\left(\frac{\delta p(T, \mu)}{\delta M^*} \right)_{T, \mu} \equiv \frac{d P(M^*)}{d M^*} - \gamma_N \int \frac{d^3k}{(2\pi)^3} \frac{M^*}{\sqrt{k^2 + M^{*2}}} (f_+ + f_-) = 0. \quad (1.6)$$

The baryonic number density and energy density can be found from (1.4)-(1.6) using the well-known thermodynamical relations:

$$\rho(T, \mu) \equiv \left(\frac{\partial p}{\partial \mu} \right)_T = \gamma_N \int \frac{d^3k}{(2\pi)^3} (f_+ - f_-), \quad (1.7)$$

$$\begin{aligned} \varepsilon(T, \mu) &\equiv T \left(\frac{\partial p}{\partial T} \right)_\mu + \mu \left(\frac{\partial p}{\partial \mu} \right)_T \\ &= \gamma_N \int \frac{d^3k}{(2\pi)^3} \sqrt{k^2 + M^{*2}} (f_+ - f_-) + \int_0^\rho dn U(n) - P(M^*). \end{aligned} \quad (1.8)$$

It follows from (1.5) that the nucleon (antinucleon) momentum distribution has the form of the ideal Fermi distribution in ‘external fields’: the scalar field changes the nucleon (antinucleon) mass M to the effective mass M^* and the vector field adds the energy $U(\rho)$ ($-U(\rho)$ for the antinucleon). It is important, however, that additional terms in (1.4) and (1.8) appear and represent thermodynamically self-consistent ‘field’ contributions to the pressure and the energy density. The form of these additional contributions to the pressure (1.4) is adjusted to the Fermi distributions

(1.5) through the general thermodynamical relation (1.6)! Formulas (1.4)-(1.8) define, therefore, a special class of thermodynamically self-consistent equations of state for nuclear matter. It is a phenomenological extension of the mean-field theory. Models of this class are fixed by specifying the two functions $U(\rho)$ and $P(M^*)$. General physical restrictions on these functions have the form:

$$\begin{aligned} U(-\rho) &= -U(\rho), & U(\rho)_{\rho \rightarrow \infty} &\sim \rho^a \quad \text{for } 0 \leq a \leq 1, \\ U(\rho)_{\rho \rightarrow 0} &\sim \rho^b, & &\text{for } 0 \leq b \\ P(M^*) &= \sum_{k \geq 2} a_k (M - M^*)^k \quad \text{with } a_2 < 0. \end{aligned} \quad (1.9)$$

For instance, the upper bound $a \leq 1$ for the power a provides the causality condition at high baryonic densities, i.e. that speed of sound does not exceed that of light.

Particular choices of $U(\rho)$ and $P(M^*)$ satisfying (1.9) reproduce a great variety of nuclear EOS models known from the literature. The models of [68, 69] correspond to $M^* = M$ ($P(M^*) \equiv 0$) in (1.4) and special forms of $U(\rho)$. For the mean-field theory models [10, 11, 64, 70, 71] $U(\rho) = C_V^2 \rho$. The choice $a_2 = -1/2 C_s^2$, $a_k = 0$ ($k > 3$) corresponds to the linear mean-field theory (in the following also referred to as ‘Walecka model’) [10], while considering $a_2 = -1/2 C_s^2$, $a_3 = 0$, $a_4 \neq 0$, $a_k = 0$ ($k \geq 5$) the model reproduces the non-linear mean-field theory [64, 70, 71].

At $T = 0$ we find the general relation for the models (1.4)-(1.8):

$$U(\rho) + \sqrt{\left[\frac{3}{2}\pi^2 \rho\right]^{\frac{2}{3}} + M^{*2}} = M + W(\rho) + \rho \frac{dW}{dn} \quad (1.10)$$

which corresponds to the Hugenholtz-Van Hove theorem [68] for an interacting Fermi gas at zero temperature. As $\left(\frac{dW}{dn}\right)_{\rho=\rho_0} = 0$, at saturation density we obtain the original Weisskopf relation [69] between Fermi energy and the energy per particle

$$U(\rho_0) + \sqrt{\left[\frac{3}{2}\pi^2 \rho_0\right]^{\frac{2}{3}} + M_o^{*2}} = M + W_o \approx 922 \text{ MeV}. \quad (1.11)$$

Equation (1.11) gives us the relation between $U(\rho_0)$ and M_o^* , therefore only one of these quantities (e.g. M_o^*) is free.

I consider now one new example for the nuclear matter EOS from the generalized mean-field theory class (1.4)-(1.8). One can choose

$$P(M^*) = -\frac{1}{2} C_s^2 (M - M^*)^2 \quad U(\rho) = C_v^2 \rho - C_d^2 \rho^{\frac{1}{3}}. \quad (1.12)$$

Thus, the Walecka model is extended by an attractive term in the potential $U(\rho)$. Such a modification of $U(\rho)$ is to some extent similar to the approach of the models [72, 73]. However, unlike to these models we now account for the fact that $M^* \neq M$ in the nuclear medium. The introduction to the third parameter C_d allows us to choose M_o^* freely in addition to the required values of ρ_o and $W(\rho_o)$. It is necessary to stress that, if one requires that our ‘coupling constant’ has the dimension of an integer power of the fundamental units, only the power $\frac{1}{3}$ of ρ in the new attractive term of $U(\rho)$ has the property to satisfy the constraints (1.9). The additional term in the potential $U(\rho)$ could be derived (in mean-field approximation) from a Lagrangian containing an additional nucleon-nucleon self-interaction term of the form

$$\frac{3}{4} C_d^2 (\bar{\psi} \gamma^\mu \psi \bar{\psi} \gamma_\mu \psi)^{\frac{2}{3}}. \quad (1.13)$$

Of course, there is no immediate physical motivation for such a term on field-theoretical grounds. However, such a motivation is certainly not strictly required for a phenomenological EOS. As justification, it is sufficient that the equation of state has physically reasonable properties. This can be shown in the following.

Although the incompressibility K_o cannot be chosen independently from M_o^* , one finds that reasonable values of M_o^* lead to values of K_o which lie in the experimentally found range (see Table 1.1.). The first line in the Table 1.1. corresponds to the Walecka model for which we have a too small value of M , and a too large value of K_o .

Table 1.1. Different sets of ‘coupling constants’ for fixed $\rho_o = 0.15891 \text{ fm}^{-3}$ [65] and $W_o = -16 \text{ MeV}$.

M^*/M	$C_v^2 \text{ (GeV}^{-2}\text{)}$	$C_s^2 \text{ (GeV}^{-2}\text{)}$	C_d^2	$K_o \text{ (MeV)}$
0.543	285.90	377.56	0	553
0.600	257.40	326.40	0.124	380
0.635	238.08	296.05	0.183	300
0.688	206.79	251.14	0.254	210
0.720	186.94	244.52	0.288	170

The surprisingly good correlation between M_o^* and K_o implies that the above model accounts

for four ground-state properties of nuclear matter with only three independent parameters. The energy density in present model [47] has the form

$$\varepsilon(T, \mu) = \gamma_N \int \frac{d^3k}{(2\pi)^3} \sqrt{k^2 + M^{*2}} (f_+ - f_-) + \frac{1}{2} C_v^2 \rho^2 - \frac{3}{4} C_d^2 \rho^{\frac{4}{3}} + \frac{1}{2} C_s^2 (M - M^*)^2. \quad (1.14)$$

For further analysis we fix $K_o = 300$ MeV (cf [59]). Note that for this value of K_o the effective mass M_o^* is in very good agreement with that obtained in the non-relativistic many-body calculations of Friedman and Pandharipande [65]. In Fig. 1.1 I compare the free energy per baryon in their calculations [65] with that of the present model. One finds rather good agreement at small ρ and systematic deviations from the non-relativistic results at large ρ . This happens at $\rho \geq 3\rho_o$ where the nucleon Fermi momentum is large, $k_F \geq M$ and, therefore, relativistic effects become important. At low temperatures and densities our EOS exhibits a liquid-vapour nuclear phase transition, as shown in Fig. 1.2. The critical temperature beyond which there is no two-phase equilibrium is ~ 14 MeV. This value is somewhat by a few MeVs lower than the expected value, however, one should remember that the present model is rather simple and does not take into account any clustering effects (e.g. deuterons, tritons and α -particles) which are necessary. Nevertheless, since the present model correctly accounts for the fact that the domination of the internucleon attraction at around normal nuclear density changes to the domination of short range repulsion at high baryonic densities. As a consequence the model predicts a PT existence.

The non-linear mean-field theory [64, 70] with four parameters C_v^2 , C_s^2 , α_3 , α_4 allows one to choose M_o^* and K_o at will. However, the value of α_4 is positive for experimentally reasonable sets of M_o^* and K_o (see [71]). This means that the energy density of the system is not bounded from below (because of the term $-P(M^*)$) with respect to variations of M^* : such a theory is unstable, since its energetic minimum is $-\infty$ which demands an infinite value of the scalar field, i.e. $\phi \rightarrow \pm\infty$.

Thus, the above results generalize the mean-field theory approach to the nuclear matter EOS. They give us the rules (1.4)-(1.8) to construct a class of thermo- dynamically self-consistent phenomenological models. As an example, a simple version of the nuclear EOS from this class is suggested and investigated. It allows for a reasonable value of the nucleon effective mass M_o^* and simultaneously allows from an incompressibility K_o in the range of the experimental values. The non-relativistic many-body calculations of [65] coincide with the suggested EOS up to a few

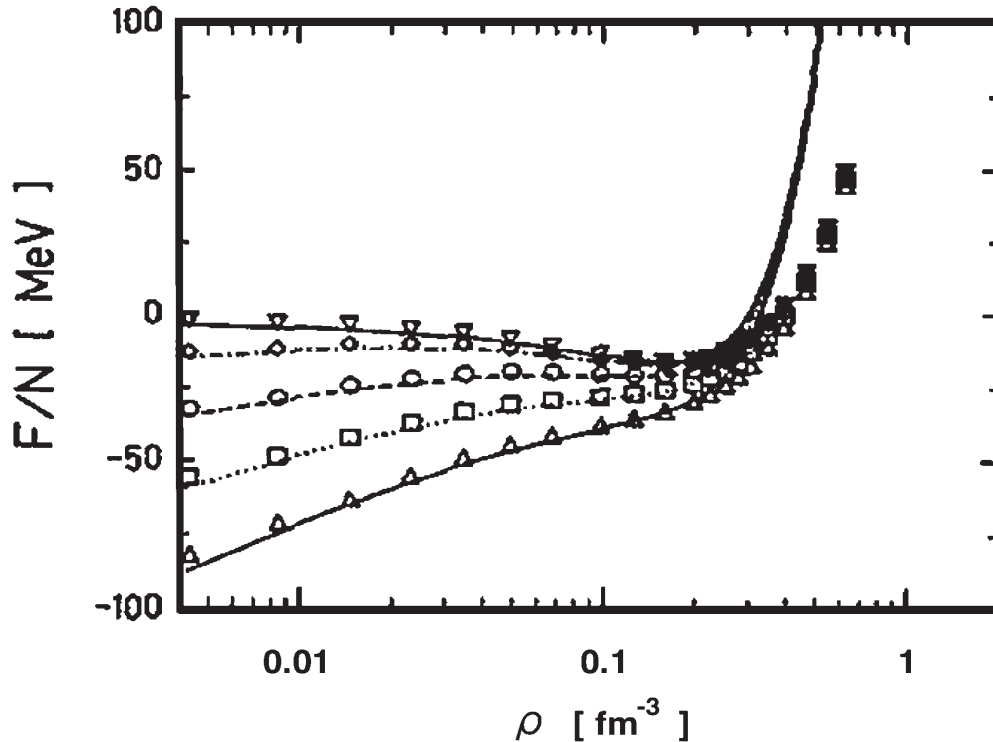


Figure 1.1. The free energy per baryon as a function of ρ for constant T is shown for the new EOS with $M_0^* = 0.635M$, $K_0 = 300$ MeV (lines) in comparison to the calculations of [5] (symbols). The upper full line (and symbol ∇) corresponds to $T = 0$, the lower full line (and Δ) to $T = 20$ MeV. Dashed-dotted (and \diamond): $T = 5$ MeV; dashed (and \circ): $T = 10$ MeV; dotted (and \square): $T = 15$ MeV.

percent in the low-density and low-temperature region. Its agreement with known nuclear matter properties is better than for either the phenomenological models with $M^* = M$, or the Walecka model as well as stable versions ($a_4 \leq 0$) of the non-linear mean-field theory.

1.2. Statistical Multifragmentation Model in Thermodynamic Limit

Here I present a more specialized and profound model of the nuclear EOS. During more than two decades it was playing a guiding role in the research of nuclear liquid-gas PT. This success is based on two facts: first, since it is a cluster model, the short range attraction between fragments

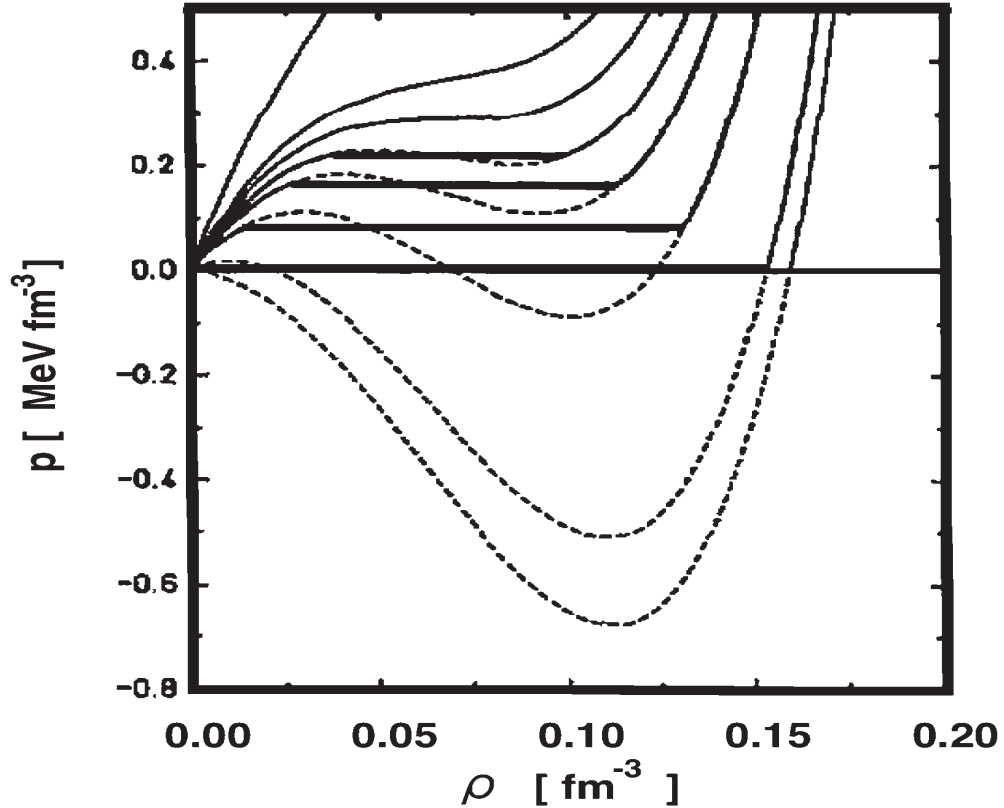


Figure 1.2. $\rho - p$ diagram showing the liquid-vapour phase transition in the self-consistent EOS. The curves are isotherms for $T = 0, 5, 10, 12, 13, 14, 15, 20$ MeV (from below to above). Dashed lines mark the unstable part of the isotherms in the phase coexistence region, which are replaced by the full horizontal lines according to Maxwell's construction.

is accounted by the reactions between all fragments, and, second, the hard-core repulsion is an essential improvement compared to the FDM [44] which, as will be shown below, leads to very different scaling relations in the SMM compared to the FDM. The infinite number of the degrees of freedom results in a qualitatively different PT mechanism compared to the mean-field models, whereas the different scaling relations of the SMM signals about another universality class compared to the FDM. However, despite the great success the proof of a PT existence in SMM and the SMM critical indices were missing until recently.

The system states in the SMM are specified by the multiplicity sets $\{n_k\}$ ($n_k = 0, 1, 2, \dots$) of k -nucleon fragments. The partition function of a single fragment with k nucleons is [46]: $V\phi_k(T) =$

$V (mTk/2\pi)^{3/2} z_k$, where $k = 1, 2, \dots, A$ (A is the total number of nucleons in the system), V and T are, respectively, the volume and the temperature of the system, m is the nucleon mass. The first two factors on the right hand side (r.h.s.) of the single fragment partition originate from the non-relativistic thermal motion and the last factor, z_k , represents the intrinsic partition function of the k -nucleon fragment. Therefore, the function $\phi_k(T)$ is a phase space density of the k -nucleon fragment. For $k = 1$ (nucleon) we take $z_1 = 4$ (4 internal spin-isospin states) and for fragments with $k > 1$ we use the expression motivated by the liquid drop model (see details in Ref. [46]): $z_k = \exp(-f_k/T)$, with fragment free energy

$$f_k = -W(T) k + \sigma(T) k^{2/3} + (\tau + 3/2)T \ln k, \quad (1.15)$$

with $W(T) = W_o + T^2/\epsilon_o$. Here $W_o = 16$ MeV is the bulk binding energy per nucleon. T^2/ϵ_o is the contribution of the excited states taken in the Fermi-gas approximation ($\epsilon_o = 16$ MeV). $\sigma(T)$ is the temperature dependent surface tension parameterized in the following relation: $\sigma(T) = \sigma(T)|_{SMM} \equiv \sigma_o[(T_c^2 - T^2)/(T_c^2 + T^2)]^{5/4}$, with $\sigma_o = 18$ MeV and $T_c = 18$ MeV ($\sigma = 0$ at $T \geq T_c$). The last contribution in Eq. (1.15) involves the famous Fisher's term with dimensionless parameter τ . As will be shown below, at the critical (tricritical) point the fragment mass distribution will lose its exponential form and will become a power law $k^{-\tau}$.

It is necessary to stress that the SMM parametrization of the surface tension coefficient is not a unique one. For instance, the FDM successfully employs another one $\sigma(T)|_{FDM} = \sigma_o[1 - T/T_c]$. As we shall see later the temperature dependence of the surface tension coefficient in the vicinity of the critical point will define the critical indices of the model, but the following mathematical analysis of the SMM is general and is valid for an arbitrary $\sigma(T)$ function.

The canonical partition function (CPF) of nuclear fragments in the SMM has the following form:

$$Z_A^{id}(V, T) = \sum_{\{n_k\}} \left[\prod_{k=1}^A \frac{[V \phi_k(T)]^{n_k}}{n_k!} \right] \delta(A - \sum_k k n_k). \quad (1.16)$$

In Eq. (1.16) the nuclear fragments are treated as point-like objects. However, these fragments have non-zero proper volumes and they should not overlap in the coordinate space. In the excluded volume (Van der Waals) approximation this is achieved by substituting the total volume V in Eq. (1.16) by the free (available) volume $V_f \equiv V - b \sum_k k n_k$, where $b = 1/\rho_o$ ($\rho_o = 0.16 \text{ fm}^{-3}$ is the

normal nuclear density). Therefore, the corrected CPF becomes: $Z_A(V, T) = Z_A^{id}(V - bA, T)$. The SMM defined by Eq. (1.16) was studied numerically in Refs. [53, 54]. This is a simplified version of the SMM, since the symmetry and Coulomb contributions are neglected. However, its investigation appears to be of principal importance for studies of the nuclear liquid-gas phase transition.

The calculation of $Z_A(V, T)$ is difficult due to the constraint $\sum_k kn_k = A$. This difficulty can be partly avoided by evaluating the GCE partition)

$$\mathcal{Z}(V, T, \mu) \equiv \sum_{A=0}^{\infty} \exp\left(\frac{\mu A}{T}\right) Z_A(V, T) \Theta(V - bA), \quad (1.17)$$

where μ denotes a chemical potential. The calculation of \mathcal{Z} is still rather difficult. The summation over $\{n_k\}$ sets in Z_A cannot be performed analytically because of additional A -dependence in the free volume V_f and the restriction $V_f > 0$. The presence of the theta-function in the GCE partition (1.17) guarantees that only configurations with positive value of the free volume are counted. However, similarly to the delta function restriction in Eq. (1.16), it makes again the calculation of $\mathcal{Z}(V, T, \mu)$ (1.17) to be rather difficult. This problem was resolved [48, 50] by performing the Laplace transformation of $\mathcal{Z}(V, T, \mu)$. This introduces the so-called isobaric partition function (IP) [134]:

$$\begin{aligned} \hat{\mathcal{Z}}(s, T, \mu) &\equiv \int_0^{\infty} dV e^{-sV} \mathcal{Z}(V, T, \mu) = \int_0^{\infty} dV' e^{-sV'} \sum_{\{n_k\}} \prod_k \frac{1}{n_k!} \left\{ V' \phi_k(T) e^{\frac{(\mu - sbT)k}{T}} \right\}^{n_k} \\ &= \int_0^{\infty} dV' e^{-sV'} \exp \left\{ V' \sum_{k=1}^{\infty} \phi_k e^{\frac{(\mu - sbT)k}{T}} \right\}. \end{aligned} \quad (1.18)$$

After changing the integration variable $V \rightarrow V'$, the constraint of Θ -function has disappeared. Then all n_k were summed independently leading to the exponential function. Now the integration over V' in Eq. (1.18) can be done resulting in

$$\hat{\mathcal{Z}}(s, T, \mu) = \frac{1}{s - \mathcal{F}(s, T, \mu)}, \quad (1.19)$$

where

$$\begin{aligned} \mathcal{F}(s, T, \mu) &= \sum_{k=1}^{\infty} \phi_k \exp \left[\frac{(\mu - sbT)k}{T} \right] \\ &= \left(\frac{mT}{2\pi} \right)^{\frac{3}{2}} \left[z_1 \exp \left(\frac{\mu - sbT}{T} \right) + \sum_{k=2}^{\infty} k^{-\tau} \exp \left(\frac{(\tilde{\mu} - sbT)k - \sigma k^{2/3}}{T} \right) \right]. \end{aligned} \quad (1.20)$$

Here we have introduced the shifted chemical potential $\tilde{\mu} \equiv \mu + W(T)$. From the definition of pressure in the grand canonical ensemble it follows that, in the thermodynamic limit, the GCE partition of the system behaves as

$$p(T, \mu) \equiv T \lim_{V \rightarrow \infty} \frac{\ln \mathcal{Z}(V, T, \mu)}{V} \Rightarrow \mathcal{Z}(V, T, \mu) \Big|_{V \rightarrow \infty} \sim \exp \left[\frac{p(T, \mu)V}{T} \right]. \quad (1.21)$$

An exponentially over V increasing part of $\mathcal{Z}(V, T, \mu)$ on the right-hand side of Eq. (1.21) generates the rightmost singularity s^* of the function $\hat{\mathcal{Z}}(s, T, \mu)$, because for $s < p(T, \mu)/T$ the V -integral for $\hat{\mathcal{Z}}(s, T, \mu)$ (1.18) diverges at its upper limit. Therefore, in the thermodynamic limit, $V \rightarrow \infty$ the system pressure is defined by this rightmost singularity, $s^*(T, \mu)$, of IP $\hat{\mathcal{Z}}(s, T, \mu)$ (1.18):

$$p(T, \mu) = T s^*(T, \mu). \quad (1.22)$$

Note that this simple connection of the rightmost s -singularity of $\hat{\mathcal{Z}}$, Eq. (1.18), to the asymptotic, $V \rightarrow \infty$, behavior of \mathcal{Z} , Eq. (1.21), is a general mathematical property of the Laplace transform. Due to this property the study of the system behavior in the thermodynamic limit $V \rightarrow \infty$ can be reduced to the investigation of the singularities of $\hat{\mathcal{Z}}$.

1.3. Singularities of Isobaric Partition and the Mechanism of Phase Transitions

The IP, Eq. (1.18), has two types of singularities: 1) the simple pole singularity defined by the equation

$$s_g(T, \mu) = \mathcal{F}(s_g, T, \mu), \quad (1.23)$$

2) the singularity of the function $\mathcal{F}(s, T, \mu)$ it-self at the point s_l where the coefficient in linear over k terms in the exponent is equal to zero,

$$s_l(T, \mu) = \frac{\tilde{\mu}}{Tb}. \quad (1.24)$$

The simple pole singularity corresponds to the gaseous phase where pressure is determined by the equation

$$p_g(T, \mu) = \left(\frac{mT}{2\pi} \right)^{3/2} T \left[z_1 \exp \left(\frac{\mu - bp_g}{T} \right) + \sum_{k=2}^{\infty} k^{-\tau} \exp \left(\frac{(\tilde{\mu} - bp_g)k - \sigma k^{2/3}}{T} \right) \right]. \quad (1.25)$$

The singularity $s_l(T, \mu)$ of the function $\mathcal{F}(s, T, \mu)$ (1.20) defines the liquid pressure

$$p_l(T, \mu) \equiv T s_l(T, \mu) = \frac{\tilde{\mu}}{b}. \quad (1.26)$$

In the considered model the liquid phase is represented by an infinite fragment, i.e. it corresponds to the macroscopic population of the single mode $k = \infty$. Here one can see the analogy with the Bose condensation where the macroscopic population of a single mode occurs in the momentum space.

In the (T, μ) -regions where $\tilde{\mu} < bp_g(T, \mu)$ the gas phase dominates ($p_g > p_l$), while the liquid phase corresponds to $\tilde{\mu} > bp_g(T, \mu)$. The liquid-gas phase transition occurs when two singularities coincide, i.e. $s_g(T, \mu) = s_l(T, \mu)$. A schematic view of singular points is shown in Fig. 1.3a for $T < T_c$, i.e. when $\sigma > 0$. The two-phase coexistence region is therefore defined by the equation

$$p_l(T, \mu) = p_g(T, \mu), \quad \text{i.e., } \tilde{\mu} = b p_g(T, \mu). \quad (1.27)$$

One can easily see that $\mathcal{F}(s, T, \mu)$ is monotonously decreasing function of s . The necessary condition for the phase transition is that this function remains finite in its singular point $s_l = \tilde{\mu}/Tb$:

$$\mathcal{F}(s_l, T, \mu) < \infty. \quad (1.28)$$

The convergence of \mathcal{F} is determined by τ and σ . At $\tau = 0$ the condition (1.28) requires $\sigma(T) > 0$. Otherwise, $\mathcal{F}(s_l, T, \mu) = \infty$ and the simple pole singularity $s_g(T, \mu)$ (1.23) is always the rightmost s -singularity of $\hat{\mathcal{Z}}$ (1.18) (see Fig. 1.3b). At $T > T_c$, where $\sigma(T)|_{SMM} = 0$, the considered system can exist only in the one-phase state. It will be shown below that for $\tau > 1$ the condition (1.28) can be satisfied even at $\sigma(T) = 0$.

It is possible to generalize the SMM with its specific parameterization for the liquid phase pressure to more general expressions [112]. Indeed, if in the SMM equations above one substitutes $W(T) \rightarrow bp_{lg}(\mu, T) - \mu$ and $\tilde{\mu} \rightarrow bp_{lg}(\mu, T)$, where some general expression is used for the liquid phase pressure $p_{lg}(\mu, T)$, then it can be checked that all the SMM remain valid. Therefore, the resulting exactly solvable model can be called the generalized SMM, or GSMM hereafter. As was discussed at the beginning of this chapter, to be realistic the generalized SMM should reproduce the properties of normal nuclear matter. The usual SMM was formulated in such a way that these

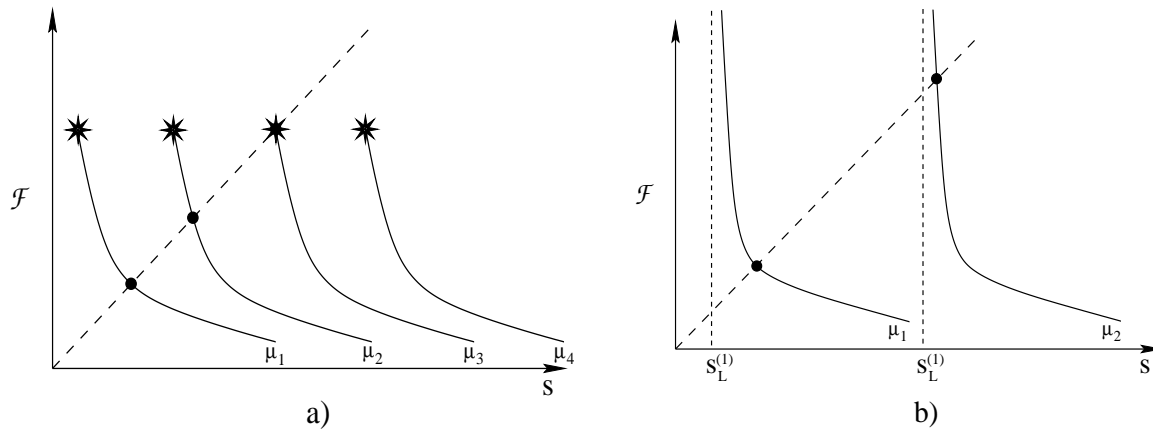


Figure 1.3. Schematic view of singular points of the Isobaric Partition, Eq. (1.19), at $T < T_c$ (a) and $T > T_c$ (b). Full lines show $\mathcal{F}(s, T, \mu)$ as a function of s at fixed T and μ , $\mu_1 < \mu_2 < \mu_3 < \mu_4$. Dots and asterisks indicate the simple poles (s_g) and the singularity of function \mathcal{F} it-self (s_l), respectively. At $\mu_3 = \mu^*(T)$ the two singular points coincide signaling a phase transition.

properties are reproduced automatically. This choice is, however, not a unique one. Moreover, it turns out that by a proper choice of the liquid phase pressure the GSMM can account for the compressibility of the nuclear matter. In particular, for $p_{lg}(\mu, T)$ it is possible to use either the self-consistent mean-field EOS discussed at the beginning of this chapter or the hadronic matter EOS which will be considered in the chapter 3.

At $T < T_c$ the system undergoes the 1-st order phase transition across the line $\mu^* = \mu^*(T)$ defined by Eq.(1.27). Its explicit form is given by the expression:

$$\mu^*(T) = -W(T) + \left(\frac{mT}{2\pi}\right)^{3/2} Tb \left[z_1 \exp\left(-\frac{W(T)}{T}\right) + \sum_{k=2}^{\infty} k^{-\tau} \exp\left(-\frac{\sigma k^{2/3}}{T}\right) \right]. \quad (1.29)$$

The points on the line $\mu^*(T)$ correspond to the mixed phase states. First we consider the case $\tau = -1.5$ because it is the standard SMM choice.

The baryonic density is found as $(\partial p / \partial \mu)_T$ and is given by the following formulae in the liquid and gas phases

$$\rho_l \equiv \left(\frac{\partial p_l}{\partial \mu}\right)_T = \frac{1}{b}, \quad \rho_g \equiv \left(\frac{\partial p_g}{\partial \mu}\right)_T = \frac{\rho_{id}}{1 + b \rho_{id}}, \quad (1.30)$$

respectively. Here the function ρ_{id} is defined as

$$\rho_{id}(T, \mu) = \left(\frac{mT}{2\pi}\right)^{3/2} \left[z_1 \exp\left(\frac{\mu - bp_g}{T}\right) + \sum_{k=2}^{\infty} k^{1-\tau} \exp\left(\frac{(\tilde{\mu} - bp_g)k - \sigma k^{2/3}}{T}\right) \right]. \quad (1.31)$$

Due to the condition (1.27) this expression is simplified in the mixed phase:

$$\rho_{id}^{mix}(T) \equiv \rho_{id}(T, \mu^*(T)) = \left(\frac{mT}{2\pi}\right)^{3/2} \left[z_1 \exp\left(-\frac{W(T)}{T}\right) + \sum_{k=2}^{\infty} k^{1-\tau} \exp\left(-\frac{\sigma k^{2/3}}{T}\right) \right] \quad (1.32)$$

This formula clearly shows that the bulk (free) energy acts in favor of the composite fragments, but the surface term favors single nucleons.

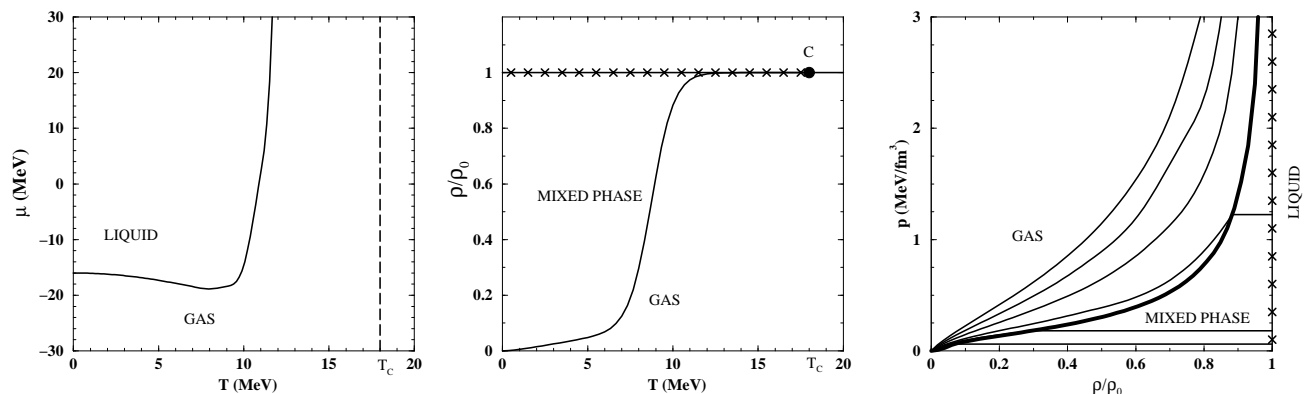


Figure 1.4. Phase diagram in $T - \mu$ (left panel), $T - \rho$ (middle panel) and $\rho/\rho_o - p$ (right panel) planes for $\tau = -1.5$. The mixed phase is represented by the line $\mu^*(T)$ in the left panel and by the extended region in the middle panel. Liquid phase (shown by crosses) exists at density $\rho = \rho_o$. Point C is the critical point. In the right pane the isotherms (thin solid lines) are shown for $T = 4, 8, 10, 14, 18$ and 22 MeV from bottom to top. The boundary of the mixed and gaseous phases is shown by the thick solid line. Liquid phase is indicated by crosses. The critical point $T = T_c = 18$ MeV, $\rho = \rho_o$ corresponds to infinite pressure.

Since at $\sigma > 0$ the sum in Eq. (1.32) converges at any τ , ρ_{id} is finite and according to Eq. (1.30) $\rho_g < 1/b$. Therefore, the baryonic density has a discontinuity $\Delta\rho = \rho_l - \rho_g > 0$ across the line $\mu^*(T)$ (1.29) for any τ . The discontinuities take place also for the energy and entropy densities. The phase diagram of the system in the (T, ρ) -plane is shown in the middle panel of Fig. 1.4 The line

$\mu^*(T)$ (1.29) (see the left panel of Fig. 1.4) corresponding to the mixed phase states is transformed into the finite region in the (T, ρ) -plane. As usual, in this mixed phase region of the phase diagram the baryonic density ρ and the energy density are superpositions of the corresponding densities of liquid and gas:

$$\rho = \lambda \rho_l + (1 - \lambda) \rho_g, \quad \varepsilon = \lambda \varepsilon_l + (1 - \lambda) \varepsilon_g. \quad (1.33)$$

Here λ ($0 < \lambda < 1$) is a fraction of the system volume occupied by the liquid inside the mixed phase, and the partial energy densities for ($i = l, g$) can be found from the thermodynamic identity [48]:

$$\varepsilon_i \equiv T \frac{\partial p_i}{\partial T} + \mu \frac{\partial p_i}{\partial \mu} - p_i. \quad (1.34)$$

One finds

$$\varepsilon_l = \frac{T^2/\epsilon_o - W_o}{b}, \quad (1.35)$$

$$\varepsilon_g = \frac{1}{1 + b\rho_{id}} \left\{ \frac{3}{2} p_g + (T^2/\epsilon_o - W_o) \rho_{id} + \left(\frac{mT}{2\pi} \right)^{3/2} \left(\sigma - T \frac{d\sigma}{dT} \right) \left[z_1 \exp\left(\frac{\mu - bp_g}{T} \right) + \sum_{k=2}^{\infty} k^{\frac{2}{3}-\tau} \exp\left(\frac{(\nu - bp_g)k - \sigma k^{2/3}}{T} \right) \right] \right\}. \quad (1.36)$$

The pressure on the phase transition line $\mu^*(T)$ (1.29) is a monotonically increasing function of T

$$p^*(T) \equiv p_g(T, \mu^*(T)) = \left(\frac{mT}{2\pi} \right)^{3/2} T \left[z_1 \exp\left(-\frac{W}{T} \right) + \sum_{k=2}^{\infty} k^{-\tau} \exp\left(-\frac{\sigma k^{2/3}}{T} \right) \right]. \quad (1.37)$$

The right panel of Fig. 1.4 shows the pressure isotherms as functions of the reduced density ρ/ρ_o for $\tau = -1.5$. Inside the mixed phase the obtained pressure isotherms are horizontal straight lines in accordance with the Gibbs criterion. These straight lines go up to infinity when $T \rightarrow T_c - 0$. This formally corresponds to the critical point, $T = T_c$, $\rho = \rho_c = 1/b$ and $p_c = \infty$, in the considered case of $\tau = -1.5$. For $T > T_c$ the pressure isotherms never enter into the mixed phase region. Note that, if $\sigma(T)$ would never vanish, the mixed phase would extend up to infinite temperatures.

Inside the mixed phase at constant density ρ the parameter λ has a specific temperature dependence shown in the left panel of Fig. 1.5: from an approximately constant value ρ/ρ_o at small T the function $\lambda(T)$ drops to zero in a narrow vicinity of the boundary separating the mixed phase and the pure gaseous phase. This corresponds to a fast change of the configurations from the state which is dominated by one infinite liquid fragment to the gaseous multifragment

configurations. It happens inside the mixed phase without discontinuities in the thermodynamical functions.

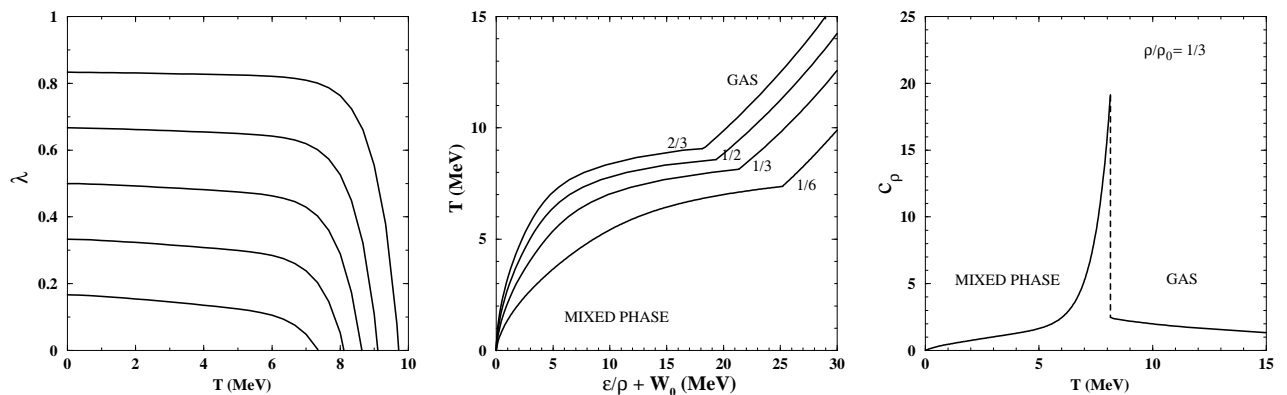


Figure 1.5. **Left panel:** Volume fraction $\lambda(T)$ of the liquid inside the mixed phase is shown as a function of temperature for fixed nucleon densities $\rho/\rho_0 = 1/6, 1/3, 1/2, 2/3, 5/6$ (from bottom to top) and $\tau = -1.5$.

Middle panel: Temperature as a function of energy per nucleon (caloric curve) is shown for fixed nucleon densities $\rho/\rho_0 = 1/6, 1/3, 1/2, 2/3$ and $\tau = -1.5$. Note that the shape of the model caloric curves is very similar to the experimental finding [6], although our estimates for the excitation energy is somewhat larger due to oversimplified interaction. For a quantitative comparison between the simplified SMM the full SMM interaction should be accounted for.

Right panel: Specific heat per nucleon as a function of temperature at fixed nucleon density $\rho/\rho_0 = 1/3$. The dashed line shows the finite discontinuity of $c_\rho(T)$ at the boundary of the mixed and gaseous phases for $\tau = -1.5$.

An abrupt decrease of $\lambda(T)$ near this boundary causes a strong increase of the energy density as a function of temperature. This is evident from the middle panel of Fig. 1.5 which shows the caloric curves at different baryonic densities. One can clearly see a leveling of temperature at energies per nucleon between 10 and 20 MeV. As a consequence this leads to a sharp peak in the specific heat per nucleon at constant density, $c_\rho(T) \equiv (\partial\varepsilon/\partial T)_{\rho/\rho}$, presented in Fig. 1.5. A finite discontinuity of $c_\rho(T)$ arises at the boundary between the mixed phase and the gaseous phase.

This finite discontinuity is caused by the fact that $\lambda(T) = 0$, but $(\partial\lambda/\partial T)_\rho \neq 0$ at this boundary (see Fig. 1.5).

It should be emphasized that the energy density is continuous at the boundary of the mixed phase and the gaseous phase, hence the sharpness of the peak in c_ρ is entirely due to the strong temperature dependence of $\lambda(T)$ near this boundary. Moreover, at any $\rho < \rho_o$ the maximum value of c_ρ remains finite and the peak width in $c_\rho(T)$ is nonzero in the thermodynamic limit considered in our study. This is in contradiction with the expectation of Refs. [53, 54] that an infinite peak of zero width will appear in $c_\rho(T)$ in this limit. Also a comment about the so-called “boiling point” is appropriate here. This is a discontinuity in the energy density $\varepsilon(T)$ or, equivalently, a plateau in the temperature as a function of the excitation energy. Our analysis shows that this type of behavior indeed happens at constant pressure, but not at constant density! This is similar to the usual picture of a liquid-gas phase transition. In Refs. [53, 54] a rapid increase of the energy density as a function of temperature at fixed ρ near the boundary of the mixed and gaseous phases (see the middle panel of Fig. 1.5) was misinterpreted as a manifestation of the “boiling point”.

New possibilities appear at non-zero values of the parameter τ . At $0 < \tau \leq 1$ the qualitative picture remains the same as discussed above, although there are some quantitative changes. For $\tau > 1$ the condition (1.28) is also satisfied at $T > T_c$ where $\sigma(T)|_{SMM} = 0$. Therefore, the liquid-gas phase transition extends now to all temperatures. Its properties are, however, different for $\tau > 2$ and for $\tau \leq 2$. If $\tau > 2$ the gas density is always lower than $1/b$ as ρ_{id} is finite (see Fig. 1.6). Therefore, the liquid-gas transition at $T > T_c$ remains the 1-st order phase transition with discontinuities of baryonic density, entropy and energy densities. The pressure isotherms as functions of the reduced density ρ/ρ_o are shown for this case in Fig. 1.6

At $1 < \tau \leq 2$ the baryonic density of the gas in the mixed phase, see Eqs. (1.30), (1.32), becomes equal to that of the liquid at $T > T_c$, since $\rho_{id} \rightarrow \infty$ and $\rho_g^{mix} = 1/b \equiv \rho_o$ (see also Fig. fig:five). It is easy to prove that the entropy and energy densities for the liquid and gas phases are also equal to each other. There are discontinuities only in the derivatives of these densities over T and μ , i.e., $p(T, \mu)$ has discontinuities of its second derivatives. Therefore, the liquid-gas transition at $T > T_c$ for $1 < \tau \leq 2$ becomes the 2-nd order phase transition. According to standard definition,

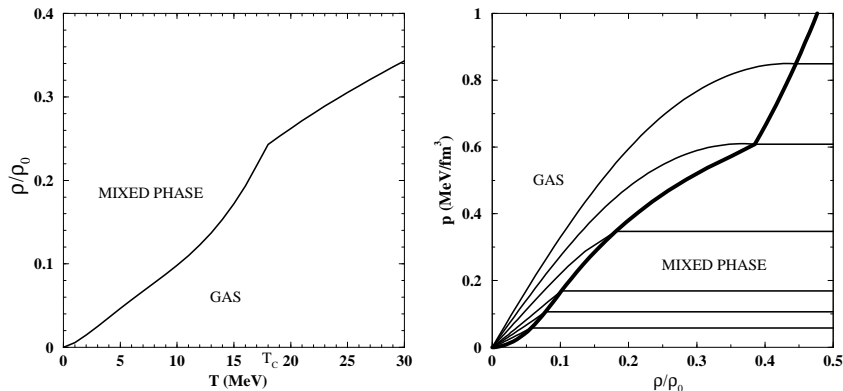


Figure 1.6. Phase diagram in $T - \rho$ (left panel) and $\rho/\rho_0 - p$ (right panel) planes for $\tau = 2.1$. The isotherms in the right panel are the same as in Fig. 1.4. There is no critical point in this case. For $\tau > 2$ the PT exists for all temperatures $T \geq 0$.

the point $T = T_c$, $\rho = 1/b$ separating the first and second order transitions is the tricritical point. One can see that this point is now at a finite pressure. Fig. 1.7 shows the pressure isotherms as functions of the reduced density ρ/ρ_0 .

It is interesting to note that at $\tau > 0$ the mixed phase boundary in $T - \rho$ plane shown in Figs. 1.6 and 1.7 is not so steep function of T as in the case $\tau = -1.5$ presented in Fig. 1.5. Therefore, the peak in the specific heat discussed above becomes less pronounced.

The density of fragments with k nucleons can be obtained by differentiating the gas pressure (1.25) with respect to the k -fragment chemical potential $\mu_k = k\mu$. This leads to the fragment mass distribution $P(k)$ in the gas phase

$$P_g(k) = a_o k^{-\tau} \exp(-a_1 k - a_2 k^{2/3}), \quad (1.38)$$

where $a_1 \equiv (bp_g - \nu)/T \geq 0$, $a_2 \equiv \sigma/T$ and a_o is the normalization constant. Since the coefficients a_o, a_1, a_2 depend on T and μ the distribution $P(k)$ (1.38) has different shapes in different points of the phase diagram. In the mixed phase the condition (1.27) leads to $a_1 = 0$ and Eq. (1.38) is transformed into

$$P_g^{mix}(k) = a_o k^{-\tau} \exp(-a_2 k^{2/3}). \quad (1.39)$$

The liquid inside the mixed phase is one infinite fragment which occupies a fraction λ of the

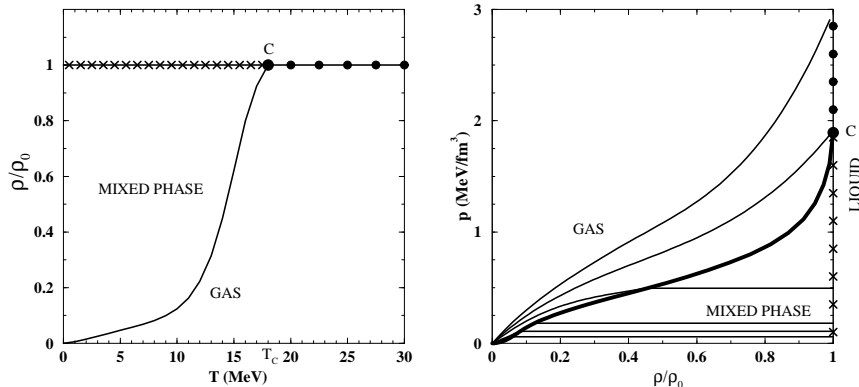


Figure 1.7. Phase diagram in $T - \rho$ (left panel) and $\rho/\rho_0 - p$ (right panel) planes for $\tau = 1.1$. The isotherms in the right panel are the same as in Fig. 1.4. The mixed phase is represented by the extended region. Liquid phase (shown by crosses) exists at density $\rho = \rho_0$. The 2-nd order PT line is shown by circles. Point C in the left panel is the tricritical point.

total system volume. Therefore, in a large system with A nucleons in volume V ($A/V = \rho$) the mixed phase consists of one big fragment with $\lambda V \rho_0$ nucleons (liquid) and $(1 - \lambda)V \rho_g$ nucleons distributed in different k -fragments according to Eq. (1.39) (gas). At low T most nucleons are inside one big liquid-fragment with only few small gas-fragments distributed according to Eq. (1.39) with large a_2 . At increasing temperature the fraction of the gas fragments increases and their mass distribution becomes broader since $a_2(T)$ in Eq. (1.39) decreases. Outside the mixed phase region the liquid disappears and the fragment mass distribution acquires an exponential falloff, Eq.(1.38). Therefore, the fragment mass distribution is widest at the boundary of the mixed phase. At even higher temperatures, $T > T_c$, the coefficient a_2 vanishes.

Details of the fragment mass distribution depend on the parameter τ . At $\tau < 1$ one observes a sudden transformation of the large liquid fragment into light and intermediate mass fragments in the narrow vicinity of the mixed phase boundary. This sudden change of the fragment composition has the same origin as a narrow peak in the specific heat, i.e. a sharp drop of $\lambda(T)$ near the mixed phase boundary (see Fig. 1.7). For larger τ all these changes are getting smoother.

An interesting possibility opens when $1 < \tau \leq 2$. As shown in Fig. 1.6 the mixed phase in

this case ends at the tricritical point $T = T_c$, $\rho = \rho_o$. In this point both the coefficients a_1 and a_2 vanish and the mass distribution becomes a pure power law

$$P_g(k) = a_o k^{-\tau} . \quad (1.40)$$

At $\tau > 2$ the mixed phase exists at all T (see Fig1.6). Thus the mass distribution of gaseous fragments inside the mixed phase fulfills a power-law (1.40) at all $T > T_c$.

1.4. The Critical Indices and Scaling Relations of the SMM

Scaling has been called a pillar of modern critical phenomena [117]. The scaling hypothesis used in the study of critical phenomena was independently developed by several scientists, including Widom, Domb, Hunter, Kadanoff, Fisher, Patashinskii and Pokrovskii (see reference [118] for an authoritative review). Much of scaling is contained in the renormalization group work of Wilson [119]. The most important prediction of scaling hypothesis, which have been verified experimentally for a variety of physical systems, is a set of relations called scaling laws. These scaling laws relate the critical exponents α' , β and γ' which describe, for instance, the behavior of the specific heat, density differences of the phases (order parameter) and isothermal compressibility for fluid systems; specific heat, magnetization and isothermal susceptibility for magnetic systems or the singular part of the zeroth, first and second moment of the cluster distribution percolating systems near a critical point ($\varepsilon = \frac{T_c - T}{T_c}$ for physical systems and $\varepsilon = \frac{p_c - p}{p_c}$ for percolating systems). In all the systems mentioned here, and more, these exponents are related via the scaling laws. The FDM, which is often used to describe the nuclear multifragmentation data, belongs to the universality class of 3-dimensional Ising model. Since the SMM is also used for the same purpose it would be interesting, first, to determine its critical exponents and, second, to compare them with the available experimental data.

The exact results described above allow one to find the critical exponents α' , β and γ' of the simplified SMM. These exponents describe the temperature dependence of the system near the critical point on the coexistence curve $\mu^* = \mu^*(T)$ (1.27), where the effective chemical potential

$\nu \equiv \mu^*(T) + W(T) - bp(T, \mu^*(T)) = 0$ vanishes

$$c_\rho \sim \begin{cases} |\varepsilon|^{-\alpha}, & \text{for } \varepsilon < 0, \\ \varepsilon^{-\alpha'}, & \text{for } \varepsilon \geq 0, \end{cases} \quad (1.41)$$

$$\Delta\rho \sim \varepsilon^\beta, \quad \text{for } \varepsilon \geq 0, \quad (1.42)$$

$$\kappa_T \sim \varepsilon^{-\gamma'}, \quad \text{for } \varepsilon \geq 0, \quad (1.43)$$

where $\Delta\rho \equiv \rho_l - \rho_g$ defines the order parameter, $c_\rho \equiv \frac{T}{\rho} \left(\frac{\partial s}{\partial T} \right)_\rho$ denotes the specific heat at fixed particle density and $\kappa_T \equiv \frac{1}{\rho} \left(\frac{\partial \rho}{\partial p} \right)_T$ is the isothermal compressibility. The shape of the critical isotherm for $\rho \leq \rho_c$ is given by the critical index δ (the tilde indicates $\varepsilon = 0$ hereafter)

$$p_c - \tilde{p} \sim (\rho_c - \tilde{\rho})^\delta \quad \text{for } \varepsilon = 0. \quad (1.44)$$

The calculation of α and α' requires the specific heat c_ρ . With the formula [74]

$$\frac{c_\rho(T, \mu)}{T} = \frac{1}{\rho} \left(\frac{\partial^2 p}{\partial T^2} \right)_\rho - \left(\frac{\partial^2 \mu}{\partial T^2} \right)_\rho \quad (1.45)$$

one obtains the specific heat on the PT curve by replacing the partial derivatives by the total ones [75]. The latter can be done for every state inside or on the boundary of the mixed phase region. For the chemical potential $\mu^*(T) = bp^*(T) - W(T)$ one gets $\frac{c_{\rho_l}^*(T)}{T} = \left(\frac{1}{\rho} - b \right) \frac{d^2 p^*(T)}{dT^2} + \frac{d^2 W(T)}{dT^2}$. Here the asterisk indicates the condensation line ($\nu = 0$) hereafter. Fixing $\rho = \rho_c = \rho_l = 1/b$ one finds $c_{\rho_l}^*(T) = T \frac{d^2 W(T)}{dT^2}$ and, hence, obtains $\alpha = \alpha' = 0$. To calculate β , γ' and δ the behavior of the series

$$\Sigma_{\mathbf{q}}(\varepsilon, \nu) \equiv \sum_{k=2}^{\infty} k^{q-\tau} e^{\frac{\nu}{T_c} k} - A\varepsilon^\zeta k^\sigma \quad (1.46)$$

should be analyzed for small positive values of ε and $-\nu$ ($A \equiv a_o/T_c$). In the limit $\varepsilon \rightarrow 0$ the function $\Sigma_{\mathbf{q}}(\varepsilon, 0)$ remains finite, if $\tau > q + 1$, and diverges otherwise. For $\tau = q + 1$ this divergence is logarithmic. The case $\tau < q + 1$ is analyzed in some details, since even in Fisher's papers it was performed incorrectly.

With the substitution $z_k \equiv k [A\varepsilon^\zeta]^{1/\sigma}$ one can prove [56] that in the limit $\varepsilon \rightarrow 0$ the series on the r. h. s. of (1.46) converges to an integral

$$\Sigma_{\mathbf{q}}(\varepsilon, 0) = [A\varepsilon^\zeta]^{\frac{\tau-q}{\sigma}} \sum_{k=2}^{\infty} z_k^{q-\tau} e^{-z_k^\sigma} \rightarrow [A\varepsilon^\zeta]^{\frac{\tau-q-1}{\sigma}} \int_{2[A\varepsilon^\zeta]^{\frac{1}{\sigma}}}^{\infty} dz z^{q-\tau} e^{-z^\sigma}. \quad (1.47)$$

The assumption $q - \tau > -1$ is sufficient to guarantee the convergence of the integral at its lower limit. Using this representation, one finds the following general results [56]

$$\Sigma_{\mathbf{q}}(\varepsilon, 0) \sim \begin{cases} \varepsilon^{\frac{\zeta}{\sigma}(\tau - q - 1)}, & \text{if } \tau < q + 1, \\ \ln |\varepsilon|, & \text{if } \tau = q + 1, \\ \varepsilon^0, & \text{if } \tau > q + 1. \end{cases} \quad \text{and} \quad \Sigma_{\mathbf{q}}(0, \tilde{\nu}) \sim \begin{cases} \tilde{\nu}^{\tau - q - 1}, & \text{if } \tau < q + 1, \\ \ln |\tilde{\nu}|, & \text{if } \tau = q + 1, \\ \tilde{\nu}^0, & \text{if } \tau > q + 1, \end{cases} \quad (1.48)$$

which allowed us to find out the critical indices of the SMM (see Table 1.2).

Table 1.2. Critical exponents of the SMM and FDM as functions of Fisher index τ for the general parametrization of the surface free energy $\sigma(T)k^{\frac{2}{3}} \rightarrow \varepsilon^{\zeta}k^{\sigma}$ with $\varepsilon = (T_c - T)/T_c$.

	α'	α'_s	β	γ'	δ
SMM for $\tau < 1 + \sigma$	0	$2 - \frac{\zeta}{\sigma}$	$\frac{\zeta}{\sigma}(2 - \tau)$	$\frac{2\zeta}{\sigma} \left(\tau - \frac{3}{2} \right)$	$\frac{\tau-1}{2-\tau}$
SMM for $\tau \geq 1 + \sigma$	0	$2 - \frac{\zeta}{\sigma}(\sigma + 2 - \tau)$	$\frac{\zeta}{\sigma}(2 - \tau)$	$\frac{2\zeta}{\sigma} \left(\tau - \frac{3}{2} \right)$	$\frac{\tau-1}{2-\tau}$
FDM	$2 - \frac{\zeta}{\sigma}(\tau - 1)$	N/A	$\frac{\zeta}{\sigma}(\tau - 2)$	$\frac{\zeta}{\sigma}(3 - \tau)$	$\frac{1}{\tau-2}$

In the special case $\zeta = 2\sigma$ the well-known exponent inequalities proven for real gases by

$$\text{Fisher[76]} : \quad \alpha' + 2\beta + \gamma' \geq 2, \quad (1.49)$$

$$\text{Griffiths[77]} : \quad \alpha' + \beta(1 + \delta) \geq 2, \quad (1.50)$$

$$\text{Liberman[78]} : \quad \gamma' + \beta(1 - \delta) \geq 0, \quad (1.51)$$

are fulfilled exactly for any τ . (The corresponding exponent inequalities for magnetic systems are often called Rushbrooke's, Griffiths' and Widom's inequalities, respectively.) For $\zeta > 2\sigma$, Fisher's and Griffiths' exponent inequalities are fulfilled as inequalities and for $\zeta < 2\sigma$ they are not fulfilled. The contradiction to Fisher's and Griffiths' exponent inequalities in this last case is not surprising. This is due to the fact that in the present version of the SMM the critical isochore $\rho = \rho_c = \rho_l$ lies on the boundary of the mixed phase to the liquid. Therefore, in expression (2.13) in Ref.

[76] for the specific heat only the liquid phase contributes and, therefore, Fisher's proof of Ref. [76] following (2.13) cannot be applied for the SMM. Thus, the exponent inequalities (1.49) and (1.50) have to be modified for the SMM. Using results of Table 1.2, one finds the following scaling relations

$$\alpha' + 2\beta + \gamma' = \frac{\zeta}{\sigma} \quad \text{and} \quad \alpha' + \beta(1 + \delta) = \frac{\zeta}{\sigma}. \quad (1.52)$$

Liberman's exponent inequality (1.51) is fulfilled exactly for any choice of ζ and σ .

Since the coexistence curve of the SMM is not symmetric with respect to $\rho = \rho_c$, it is interesting with regard to the specific heat to consider the difference $\Delta c_\rho(T) \equiv c_{\rho_g}^*(T) - c_{\rho_l}^*(T)$, following the suggestion of Ref. [75]. Using Eq. (1.45) for gas and liquid and noting that $1/\rho_g^* - b = 1/\rho_{id}^*$, one obtains a specially defined index α'_s from the most divergent term for $\zeta > 1$

$$\Delta c_\rho(T) = \frac{T}{\rho_{id}^*(T)} \frac{d^2 p^*(T)}{dT^2} \quad \Rightarrow \quad \alpha'_s = \begin{cases} 2 - \frac{\zeta}{\sigma}, & \text{if } \tau < \sigma + 1, \\ 2 - \frac{\zeta}{\sigma}(\sigma + 2 - \tau), & \text{if } \tau \geq \sigma + 1. \end{cases} \quad (1.53)$$

Then it is $\alpha'_s > 0$ for $\zeta/\sigma < 2$. Thus, approaching the critical point along any isochore within the mixed phase region except for $\rho = \rho_c = 1/b$ the specific heat diverges for $\zeta/\sigma < 2$ as defined by α'_s and remains finite for the isochore $\rho = \rho_c = 1/b$. This demonstrates the exceptional character of the critical isochore in this model.

In the special case that $\zeta = 1$ one finds $\alpha'_s = 2 - 1/\sigma$ for $\tau \leq 1 + 2\sigma$ and $\alpha'_s = -\beta$ for $\tau > 1 + 2\sigma$. Therefore, using α'_s instead of α' , the exponent inequalities (1.49) and (1.50) are fulfilled exactly if $\zeta > 1$ and $\tau \leq \sigma + 1$ or if $\zeta = 1$ and $\tau \leq 2\sigma + 1$. In all other cases (1.49) and (1.50) are fulfilled as inequalities. Moreover, it can be shown that the SMM belongs to the universality class of real gases for $\zeta > 1$ and $\tau \geq \sigma + 1$.

The comparison of the above derived formulae for the critical exponents of the SMM for $\zeta = 1$ with those obtained within the FDM (Eqs. 51-56 in [44]) shows that these models belong to different universality classes (except for the singular case $\tau = 2$).

Furthermore, one has to note that for $\zeta = 1$, $\sigma \leq 1/2$ and $1 + \sigma < \tau \leq 1 + 2\sigma$ the critical exponents of the SMM coincide with those of the exactly solved one-dimensional FDM with non-zero droplet-volumes [75].

For the usual parameterization of the SMM [46] one obtains with $\zeta = 5/4$ and $\sigma = 2/3$ the exponents

$$\alpha'_s = \begin{cases} \frac{1}{8}, & \text{if } \tau < \frac{5}{3} \\ \frac{15}{8}\tau - 3, & \text{if } \tau \geq \frac{5}{3} \end{cases}, \quad \beta = \frac{15}{8}(2 - \tau), \quad \gamma' = \frac{15}{4}\left(\tau - \frac{3}{2}\right), \quad \delta = \frac{\tau - 1}{2 - \tau}. \quad (1.54)$$

Thus, Fisher suggestion to use α'_s instead of α' allows one to “save” the exponential inequalities, however, it is not a final solution of the problem.

The critical indices of the nuclear liquid-gas PT were determined from the multifragmentation of gold nuclei [79] and found to be close to those ones of real gases. The method used to extract the critical exponents β and γ' in Ref. [79] was, however, found to have large uncertainties of about 25 per cents [80]. Nevertheless, those results allow us to estimate the value of τ from the experimental values of the critical exponents of real gases taken with large error bars. Using the above results we generalized [56] the exponent relations of Ref. [75]

$$\tau = 2 - \frac{\beta}{\gamma' + 2\beta} \quad \text{and} \quad \tau = 2 - \frac{1}{1 + \delta} \quad (1.55)$$

for arbitrary σ and ζ . Then, one obtains with [81] $\beta = 0.32 - 0.39$, $\gamma' = 1.3 - 1.4$ and $\delta = 4 - 5$ the estimate $\tau = 1.799 - 1.846$. This demonstrates also that the value of τ is rather insensitive to the special choice of β , γ' and δ , which leads to $\alpha'_s \cong 0.373 - 0.461$ for the SMM. Theoretical values for β , γ' and δ for Ising-like systems within the renormalized ϕ^4 theory [82] lead to the narrow range $\tau = 1.828 \pm 0.001$. The values of β , γ' and δ indices for nuclear matter and percolation of two- and three-dimensional clusters are reviewed in [58].

This finding is not only of a principal theoretical importance, since it allows one to find out the universality class of the nuclear liquid-gas phase transition, if τ index can be determined from experimental mass distribution of fragments, but also it enhanced a great activity in extracting the value of τ exponent from the data [86, 87] and by a full SMM. The latter numerical analysis agrees with our estimate for a reasonable values of T_c .

There was a decent try to study the critical indices of the SMM numerically [83]. The version V2 of Ref. [83] corresponds precisely to our model with $\tau = 0$, $\zeta = 5/4$ and $\sigma = 2/3$, but their results contradict our analysis. Their results for version V3 of Ref. [83] are in contradiction with

our proof presented in Ref. [48]. There it was shown that for non-vanishing surface energy (as in version V3) the critical point does not exist at all. The latter was found in [83] for the finite system and the critical indices were analyzed. Such a strange result, on the one hand, indicates that the numerical methods used in Ref. [83] are not self-consistent, and, on the other hand, it shows an indispensable value of the analytical calculations, which can be used as a test problem for numerical algorithms.

It is widely believed that the effective value of τ defined as $\tau_{\text{eff}} \equiv -\partial \ln n_k(\varepsilon) / \partial \ln k$ attains its minimum at the critical point (see references in [85]). This can be easily shown for the SMM. Indeed, taking the SMM fragment distribution $n_k(\varepsilon) = g(T)k^{-\tau} \exp[\frac{\nu}{T}k - \frac{a(\varepsilon)}{T}k^\sigma] \sim k^{-\tau_{\text{eff}}}$ one finds

$$\tau_{\text{eff}} = \tau - \frac{\nu}{T}k + \frac{\sigma a(\varepsilon)}{T}k^\sigma \quad \Rightarrow \quad \tau = \min(\tau_{\text{eff}}) , \quad (1.56)$$

where the last step follows from the fact that the inequalities $a(\varepsilon) \geq 0$, $\nu \leq 0$ become equalities at the critical point $\nu = a(0) = 0$. Therefore, the SMM predicts that the minimal value of τ_{eff} corresponds to the critical point, where, as we see now, the mass distribution of fragments is power-like.

In the E900 $\pi^- + \text{Au}$ multifragmentation experiment [84] the ISiS collaboration measured the dependence of τ_{eff} upon the excitation energy and found the minimum value $\min(\tau_{\text{eff}}) \cong 1.9$ (Fig. 5 of Ref. [84]). Also the EOS collaboration [85] performed an analysis of the minimum of τ_{eff} on $\text{Au} + \text{C}$ multifragmentation data. The fitted τ_{eff} , plotted in Fig. 11.b of Ref. [85] versus the fragment multiplicity, exhibits a minimum in the range $\min(\tau_{\text{eff}}) \cong 1.8 - 1.9$. Both results contradict the original FDM [44], but agree well with the above estimate of τ for real gases and for Ising-like systems in general. The main consequence of such a comparison is the fact the nuclear matter EOS has a tricritical point rather than the critical one.

1.5. Major Conclusions

In this chapter I presented a mean-field model based on a concept of nuclear matter. In nuclear physics this concept plays a role which is comparable to the ideal gas concept in statistical mechanics. From the discussed model [47] which is a phenomenological generalization of the

Walecka model [10] it is seen that in the absence of the Coulomb interaction between nucleons even a model inspired by a simple field theory predicts the existence of the nuclear liquid-gas PT, although its critical temperature is somewhat lower than expected. A suggested model [47] correctly reproduces the four known properties of nuclear matter with three parameters only and even the low density results of numerical simulations based on a realistic internuclear interaction [65]. Also this model simultaneously reproduces the value of effective mass of the nucleon in the normal nuclear matter and its compressibility of about $K_o \approx 300$ MeV, which is observed in the experiments on elliptic flow anisotropy [62, 63]. Of course, the question why the sideward anisotropy observed in the A+A collisions shows $K_o \approx 210$ MeV remains puzzling, but there is hope that in the coming years it will be clarified at the accelerator FAIR.

Then I presented an exact analytical solution [48, 49] of a simplified SMM found with my collaborators. The SMM [46] is a more profound statistical model and for many years it was a guide for both theoreticians and experimentalists in nuclear physics at intermediate energies. These results not only allowed me to explain the pitfalls of several numerical studies ("boiling point" [53, 54], numerical extraction of the SMM critical indices [83]), but also allowed me, for the first time, to find out the critical exponents of the SMM [56], to derive the scaling relations between them and show explicitly that SMM is in the other universality class ($\tau \leq 2$) than the famous FDM [44] ($\tau > 2$). The predicted range of the Fisher exponent $\tau = 1.799 - 1.846$ contradicts the FDM value $\tau \approx 2.16$, but is in a good agreement, $\tau_{EXP} \cong 1.8 - 1.9$, with the results of the ISiS collaboration [84] and the EOS collaboration [85]. Thus, for the first time, my results showed that the nuclear matter has the tricritical, rather than the critical, endpoint.

In addition, the calculation of the SMM critical exponents indicated that, despite the common beliefs, the fundamental scaling inequalities [76, 77] found in mid sixties, are not that well established as one might expect. Fisher's suggestion [75] to introduce a special index α_s instead of α "saves" the scaling inequalities, but it looks like a palliative. Hopefully, new experimental and theoretical studies of these inequalities may clarify this problem.

The SMM itself should be improved and developed further. One generalization of the SMM, the GSMM [112], which enables to include a more sophisticated EOS for the nuclear liquid phase,

is discussed above. It gives a possibility to avoid the problem with causality which exists in the present SMM at high baryonic densities. For this one can use, for instance, the mean-field EOS of nuclear matter [47] or similar models to describe the nuclear liquid phase. Another possibility to resolve the causality problem of such a typical nuclear EOS like the SMM, is to include the Lorentz contraction of the hard core repulsion of nuclear fragments. The latter is studied in the chapter 3. Another generalization of the SMM, the CSMM, is discussed in the next chapter concerning the possibility to rigorously study the PTs in finite systems.

CHAPTER 2

EXACTLY SOLVABLE STATISTICAL MODELS FOR FINITE NUCLEAR SYSTEMS

This chapter is devoted to the investigation of phase equilibrium in finite systems and accounting for finite size effects. Finite size effects are essential in the study of nuclei and other mesoscopic systems for opposite, but complementary reasons. In modern cluster physics, the problem of finite size arises when attempts are made to relate known properties of the infinite system to cluster properties brought to light by experiment [88]. For nuclear physics, the problem is the opposite: finite size effects dominate the physics at all excitations and one of the most important challenges is to generalize specific properties of a *drop* (nucleus) to a description of uncharged, symmetric infinite nuclear matter. This goal has been achieved already for cold nuclei by the liquid drop model. Finite size effects are also encountered in nuclear physics in efforts to generate a liquid-vapor phase diagram from heat capacity measurements [89] and fragment distributions [90].

The second of the most important challenges of nuclear physics is to formulate a rigorous theory of critical phenomena in finite systems. The point is that the experimental studies of PTs in nuclear systems require the development of theoretical approaches which would allow us to study the critical phenomena without going into the thermodynamic limit $V \rightarrow \infty$ (V is the volume of the system) because at finite nuclear densities such a limit does not exist due the long range Coulomb repulsion.

The general situation in the theory of critical phenomena for finite (small) systems is not very optimistic at the moment because theoretical progress in this field has been slow. It is well known that the mathematical theory of phase transitions was worked out by T. D. Lee and C. N. Yang [91, 92]. Unfortunately, there is no direct generic relation between the physical observables and zeros of the grand canonical partition in a complex fugacity plane. Therefore, we know very well

what are the gaseous phase and liquid at infinite volumes: mixture of multiparticle clusters of all sizes and, say, an ocean, respectively. This is known both for pure phases and for their mixture, but, despite some limited success [93], this general approach is not useful for the specific problems of critical phenomena in finite systems.

A tremendous complexity of critical phenomena in finite systems prevented their systematic and rigorous theoretical study. For instance, even the best formulation of the statistical mechanics and thermodynamics of finite systems by Hill [94] is not rigorous while discussing PTs. As a result, the absence of a well established definition of the liquid and mixed phase for finite volumes delays the progress of several related fields, including the theoretical and experimental searches for the reliable signals of several PTs which are expected to exist in strongly interacting matter.

Since the analysis of finite volume systems is very difficult, the problem was attacked by numerical codes. During more than two decades there were many successes achieved in this way [46, 95, 45, 96], but the problem is that the numerical simulations of this level do not provide us with any proof. On the other hand the developed analytical support was no match for the demands. As a result the absence of a firm theoretical ground led to formulation of such highly speculative “signals” of the nuclear liquid-vapor PT as negative heat capacity [97, 98], bimodality [99], which later on were disproved, in Refs [100] and [101], respectively.

Thus, there is a paradoxical situation in the nuclear multifragmentation community: there are many experimental data and facts, but there is no a single theoretical approach which is able to describe them. In fact, a similar state of the art is with the searches for QGP [102]: there is a lack of a firm and rigorous theoretical approach to describe the PTs in finite systems.

From these facts I concluded that to improve the present situation it is necessary to develop new theoretical methods which could break down the model EOS with PT in finite systems and use their exact solutions to understand the PT mechanism in finite system. Exactly solvable models with PTs always played a special role in statistical mechanics because they provide us with the information obtained directly from the first principles of statistical mechanics being unspoiled by mean-field or other simplifying approximations without which the analytical analysis is usually impossible. On the other hand an exact analytical solution gives the physical picture of PT,

which cannot be obtained by numerical evaluation. Therefore, one can expect that an extension of the exact analytical solutions to finite systems may provide us with the ultimate and reliable experimental signals of the nuclear liquid-vapor PT which are established on a firm theoretical ground of statistical mechanics. This, however, is a very difficult general task of the critical phenomena theory in finite systems.

Fortunately, we do not need to solve this very general task, but to find its solution for a specific problem of nuclear liquid-gas PT, which is less complicated and more realistic. In this case the straightforward way is to start from a few statistical models, like the FDM and/or SMM, which are successful in describing the main part of the experimental data. A systematic study of the various modifications of the FDM for finite volumes was performed by Moretto and collaborators [58] and it led to a discovery of thermal reducibility of the fragment charge spectra [45], to a determination of a quantitative liquid-vapor phase diagram containing the coexistence line up to critical temperature for small systems [103, 104], to the generalization of the FDM for finite systems and to a formulation of the complement concept [105, 106] which allows one to account for finite size effects of finite liquid drop on the properties of its vapor. This finding is very important for quantum chromodynamics because its universality class is expected to be the same as for 3-dimensional Ising model [107, 108, 109] studied in [106].

A comparable systematic analysis for the SMM was, however, not possible until recently, when its finite volume analytical solution was found in [110]. This exact solution was found with the help of new powerful method, which I named the Laplace-Fourier transform [110]. With this method I was able to analyze the Constrained SMM [110, 111, 112] and find out the rigorous definitions of the finite volume analogs of phases for the nuclear liquid-gas PT. However, the very same method I applied to the analytical solution of the GBM in finite volume [113], which will be discussed in the chapter 4 in connection with QGP searches, and to breaking down three statistical ensembles, including a novel one, for the HDM [114, 115]. The latter explains the origin of surface entropy and is very necessary to understand the linear temperature dependence of surface tension coefficient for a variety of cluster models (2- and 3-dimensional clusters of Ising model, nuclear clusters, the molecule clusters in real liquids and so on). From the above list of exact results it is clear that the

Laplace-Fourier transform method [110] can be used to form a common theoretical language for a few physical communities which study critical phenomena in finite systems, statistical mechanics of surfaces and physics of clusters.

Therefore, this chapter is devoted to such exact methods as the Complement [106] and Laplace-Fourier transform [110] methods and their applications to finite systems being in a phase equilibrium. The chapter is based on the following works: [106, 58, 110, 111, 112, 114, 115, 113].

2.1. The Complement Method for Finite Drop

Here I present a general approach to deal with finite size effects in phase transitions and illustrate it for liquid-vapor phase coexistence. A dilute, nearly ideal vapor phase is in equilibrium with a denser liquid phase; finiteness is realized when liquid phase is a finite drop. A finite drop's vapor pressure is typically calculated by including the surface energy in the molar vaporization enthalpy [116]. This concept of the complement is introduced to extend and quantify finite size effects down to drops as small as atomic nuclei. It generalizes Fisher's model [118, 120], deriving an expression for cluster concentrations of a vapor in equilibrium with a finite drop and recovers from it the Gibbs-Thomson formulae [121]. I demonstrate this approach with the lattice gas (Ising) model.

The complement method consists of evaluating the free energy change occurring when a cluster moves from one phase to another. For a finite liquid drop in equilibrium with its vapor, this is done by virtually transferring a cluster from the liquid drop to the vapor and evaluating the energy and entropy changes associated with *both* the vapor cluster *and* the residual liquid drop (complement). This method can be generalized to incorporate energy terms common in the nuclear case: symmetry, Coulomb (with caution [120]) and angular momentum energies.

In the framework of physical cluster theories of non-ideal vapors (which assume the monomer-monomer interaction is exhausted by the formation of clusters), clusters behave ideally and are independent of each other. The complement method is based upon this independence. Physical cluster theories state that the concentrations of vapor clusters of A constituents $n_A(T)$ depend on the free energy of cluster formation $\Delta G_A(T) = \Delta E_A(T) - T\Delta S_A(T)$. The epigon of physical

cluster theories is Fisher's model [118] which writes, at coexistence, $\Delta E = c_0 A^\sigma$ and $\Delta S_A(T) = \frac{c_0}{T_c} A^\sigma - \tau \ln A$. Thus

$$n_A(T) = \exp \left[-\frac{\Delta G_A(T)}{T} \right] = q_0 A^{-\tau} \exp \left(-\frac{c_0 A^\sigma \varepsilon}{T} \right) \quad (2.1)$$

where q_0 is a normalization, τ is Fisher's topological exponent, c_0 is the surface energy coefficient, σ is the surface to volume exponent, and $\varepsilon = (T_c - T)/T_c$. The leading term in $\Delta S_A(T)$, proportional to A^σ , permits the vanishing of the cluster free energy at a $T = T_c$ independent of size. Equation (2.1) (and the extension below) is valid only at phase coexistence for $T \leq T_c$. The direct physical interpretation of the parameters in $\Delta G_A(T)$ and their application to the nuclear case is the reason for this choice here, despite its limitations [122].

Eq. (2.1), valid for infinite liquid-vapor equilibrium, is generalized to the case of a vapor in equilibrium with a finite liquid drop. For each vapor cluster one can perform the gedanken experiment of extracting it from the liquid, determining entropy and energy changes of the drop and cluster, and then putting it back into the liquid (the equilibrium condition), as if, according to physical cluster theories, no other clusters existed. Fisher's expressions for $\Delta E_A(T)$ and $\Delta S_A(T)$ can be written for a drop of size A_d in equilibrium with its vapor as $\Delta E_A(T) = c_0 [A^\sigma + (A_d - A)^\sigma - A_d^\sigma]$ and $\Delta S_A(T) = \frac{c_0}{T_c} [A^\sigma + (A_d - A)^\sigma - A_d^\sigma] - \tau \ln [A(A_d - A)/A_d]$ giving

$$n_A(T) = q_0 \left[\frac{A(A_d - A)}{A_d} \right]^{-\tau} \exp \left\{ -\frac{c_0 \varepsilon}{T} [A^\sigma + (A_d - A)^\sigma - A_d^\sigma] \right\}. \quad (2.2)$$

The free energy cost of complement $(A_d - A)$ formation is determined just as the free energy cost of cluster (A) formation is determined. The resulting expression Eq. (2.2) reduces to Eq. (2.1) when A_d tends to infinity and contains exactly the same parameters. One can rewrite Eq. (2.2) as

$$n_A(T) = n_A^\infty(T) \exp \left(\frac{A \Delta \mu_{fs}}{T} \right) \quad (2.3)$$

with $n_A^\infty(T)$ given by Eq. (2.1). The finite size of the drop acts as an *effective* chemical potential, $\Delta \mu_{fs} = -\{c_0 \varepsilon [(A_d - A)^\sigma - A_d^\sigma] - T \tau \ln [(A_d - A)/A_d]\} / A$, increasing the vapor pressure [121].

In order to quantitatively demonstrate this method, I apply it to the canonical lattice gas (Ising) model [91, 92] with a fixed number of up spins, i.e. a fixed mean occupation density ρ_{fixed} lattice gas (equivalently, a fixed magnetization M_{fixed} Ising model) [105]. Up spins represent particles of

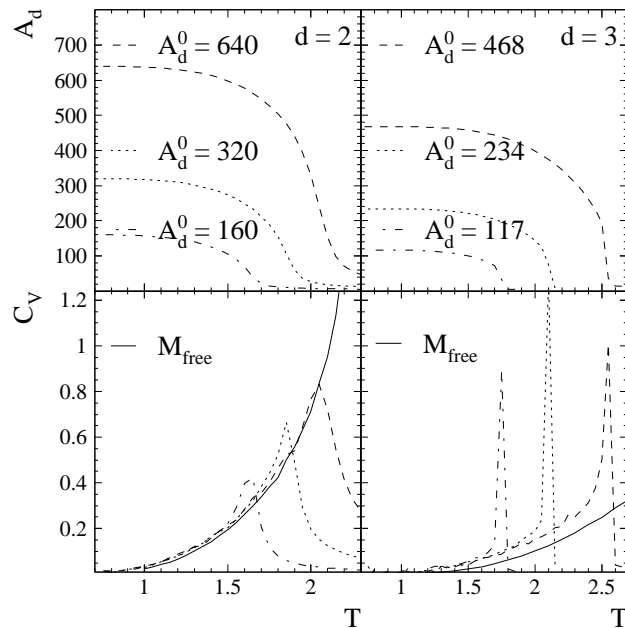


Figure 2.1. On the left (right), top to bottom: the $d = 2$ (3) liquid drop size A_d , specific heat C_V . See text for details.

the fluid forming monomers, dimers, drops etc. Down spins are empty space; the lattice is the container enclosing the fluid. The large lattices with periodic boundary conditions are chosen to minimize finite lattice effects, irrelevant to our study. For $d = 2$ (3) we used a square (simple cubic) lattice of side $L = 80$ (25) which leads to a shift in T_c of $\lesssim 0.5\%$ [123, 124] ($\lesssim 0.5\%$ [125, 126]). The M_{fixed} calculations were performed according to ref. [127]. For every (T, ρ_{fixed}) over 10^5 thermalized realizations were generated to produce the cluster concentrations. The calculations of M_{free} are performed for the same lattices as a benchmark in order to differentiate effects of a finite lattice from those of a finite drop.

For the M_{fixed} calculations at $T = 0$, the up spins aggregate into a single liquid drop in a vacuum: the ground state. At higher temperatures, the vacuum is filled with a vapor made of up spin clusters. Clusters in the vapor were identified via the Coniglio-Klein algorithm [128] to insure that their behavior is physical (i.e. cluster concentrations return Ising critical exponents and not percolation exponents). The largest cluster represents the liquid drop and is identified geometrically (all like spin nearest neighbors bonded) in order to capture the skin thickness associated with liquid drops [105]. Our choices of ground state liquid drops A_d^0 (shown in Fig.2.1) insure that the ground

state is approximately square (cubical) for $d = 2$ (3). Due to periodic boundary conditions the ground state shape changes with M_{fixed} [129].

Figure 2.1 shows that as T increases, the drop's size A_d decreases from A_d^0 ; the evaporating drop fills the container with vapor. At a temperature T_X , corresponding to the end of two phase coexistence, A_d falls quickly. The value of T_X varies with A_d^0 . For $T \lesssim T_X$ the specific heat C_V (measuring spin-spin interaction energy fluctuations only) agrees approximately with the M_{free} results (solid lines in Fig. 2.1) for all A_d^0 until fluctuations in A_d at $\sim T_X$ produce a C_V greater than that of the M_{free} results. As T increases further, C_V decreases.

To evaluate the efficacy of the complement, I examine the scaled cluster concentrations for our calculations: $n_A(T)/q_0 A^{-\tau}$ vs. $c_0 A^\sigma \varepsilon/T$. For M_{free} calculations it has been shown that this scaling collapses concentrations of clusters over a wide range in A and T [122]. Finite size liquid drop effects will be manifested in the cluster concentrations of the M_{fixed} calculations which should scale better according to Eq. (2.2) than to Eq. (2.1).

Table 2.1. Fit results for M_{free} calculations

-	Onsager	this analysis	theoretical values	this analysis
-	$d = 2$	$d = 2$	$d = 3$	$d = 3$
-	$L \rightarrow \infty$	$L = 80$	$L \rightarrow \infty$	$L = 25$
χ_ν^2	-	4.7	-	1972.2
T_c	2.26915	2.283 ± 0.004	4.51152 ± 0.00004	4.533 ± 0.002
c_0	≥ 8	8.6 ± 0.2	≥ 12	12.63 ± 0.04
σ	8/15	0.56 ± 0.01	0.63946 ± 0.0008	0.725 ± 0.003
τ	31/15	2.071 ± 0.002	2.209 ± 0.006	2.255 ± 0.001

Only clusters of $A \geq 9$ are included in the M_{free} fits for the $d = 2$ calculations. This is because only large clusters obey Fisher's ansatz for the cluster surface energy: $E_A = c_0 A^\sigma$. Small clusters are dominated by geometrical shell effects [58]. For the $d = 3$ M_{fixed} calculations, large clusters are very rare, so clusters of $A \geq 2$ are included in our analysis. Thus, the magnitudes of the χ_ν^2 values from the $d = 3$ calculations are due to the clusters analyzed not following closely Fisher's ansatz.

Table 2.2. χ_ν^2 results for M_{fixed} calculations.

A_d^0 ($d = 2$)	640	320	160
χ_ν^2 w/o complement	10.3	10.6	18.2
χ_ν^2 w complement	1.7	1.9	4.8
A_d^0 ($d = 3$)	468	234	117
χ_ν^2 w/o complement	14 825.9	7 938.6	3 516.0
χ_ν^2 w complement	1 553.4	838.6	258.1

In the thermodynamic limit, the highest temperature admitted by Eq. (2.1) or (2.2) is the temperature at which the system leaves coexistence. For the M_{free} calculations this occurs at $T = T_c$, while for the M_{fixed} calculations this occurs at $T \approx T_X$. However, due to the small size of our drops, fluctuations grow large before T_X and it is better to consider only $T \lesssim 0.85T_X$ ($0.75T_X$) for $d = 2$ (3).

To make a comparison between the scaling achieved with the M_{free} clusters and with the M_{fixed} clusters, the fit of the M_{free} clusters with Eq. (2.1) with the free parameters T_c , c_0 , σ and τ ; $q_0 = \zeta(\tau - 1)/2$ was performed. Results are given in Table 2.1 and shown in top panels of Figs. 2.2 and 2.3. The values of the T_c and τ returned by this procedure are within 1% of their established values. The value of c_0 shows that all clusters are not perfect squares (cubes) in $d = 2$ (3) for which $c_0 = 8$ (12) [122, 130]. The values of σ are within 5% (15%) of their established values for $d = 2$ (3). This level of inaccuracy arises from shell effects [58].

Next it is necessary to calculate χ_ν^2 for the M_{fixed} clusters using Eq. (2.1) and Eq. (2.2) with parameters fixed to the Table 2.1 values for the infinite system. This procedure frees one as much as possible from the drawbacks of Fisher's model so one can concentrate on the effect of the complement. Results are given in Table 2.2 and shown in the middle panels (without complement: concentrations scaled as $n_A(T)/q_0A^{-\tau}$) and the bottom panels (with complement: concentrations scaled as $n_A(T)/q_0A^{-\tau} \exp [A\Delta\mu_{\text{fs}}/T]$) of Figs. 2.2 and 2.3. The M_{fixed} χ_ν^2 values for the calculation with the complement are an order of magnitude smaller than the results without the complement

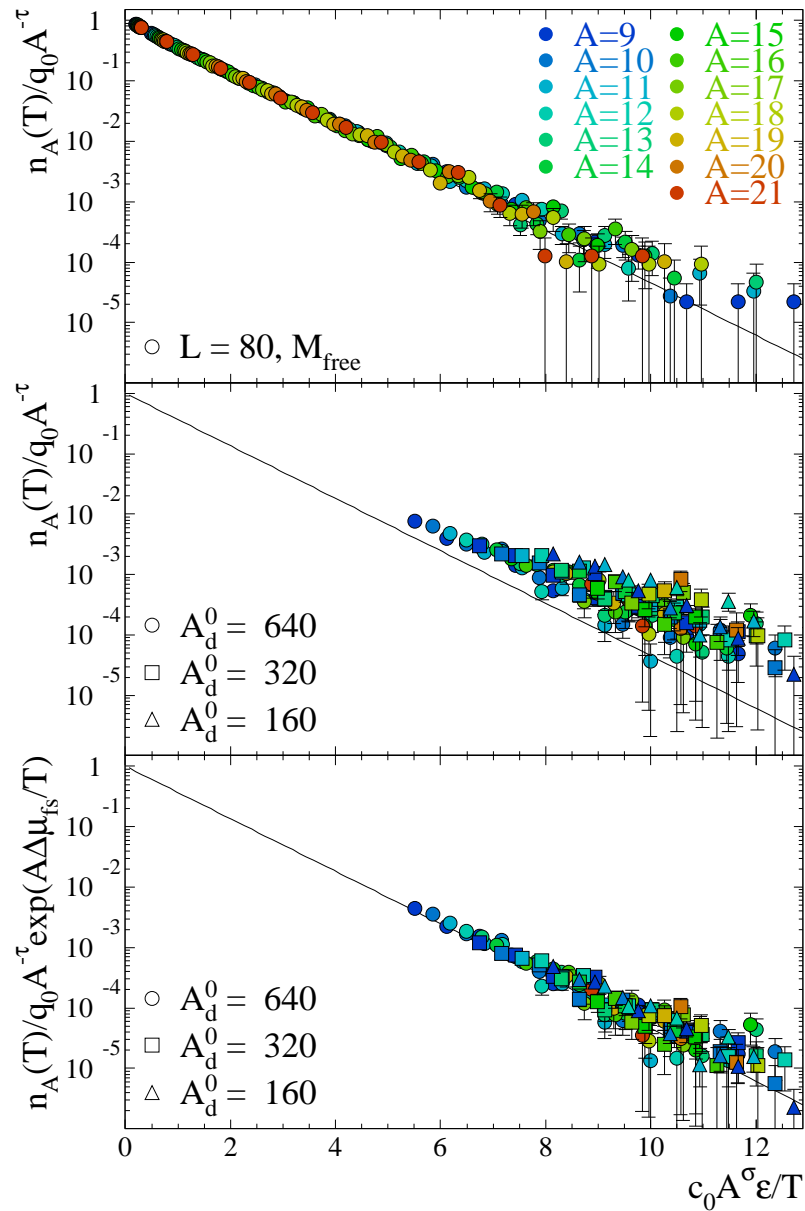


Figure 2.2. The cluster concentrations of the $d = 2$, $L = 80$ periodic boundary condition square lattice for: M_{free} calculations (top); M_{fixed} calculations with no complement (middle); M_{fixed} calculations with the complement (bottom).

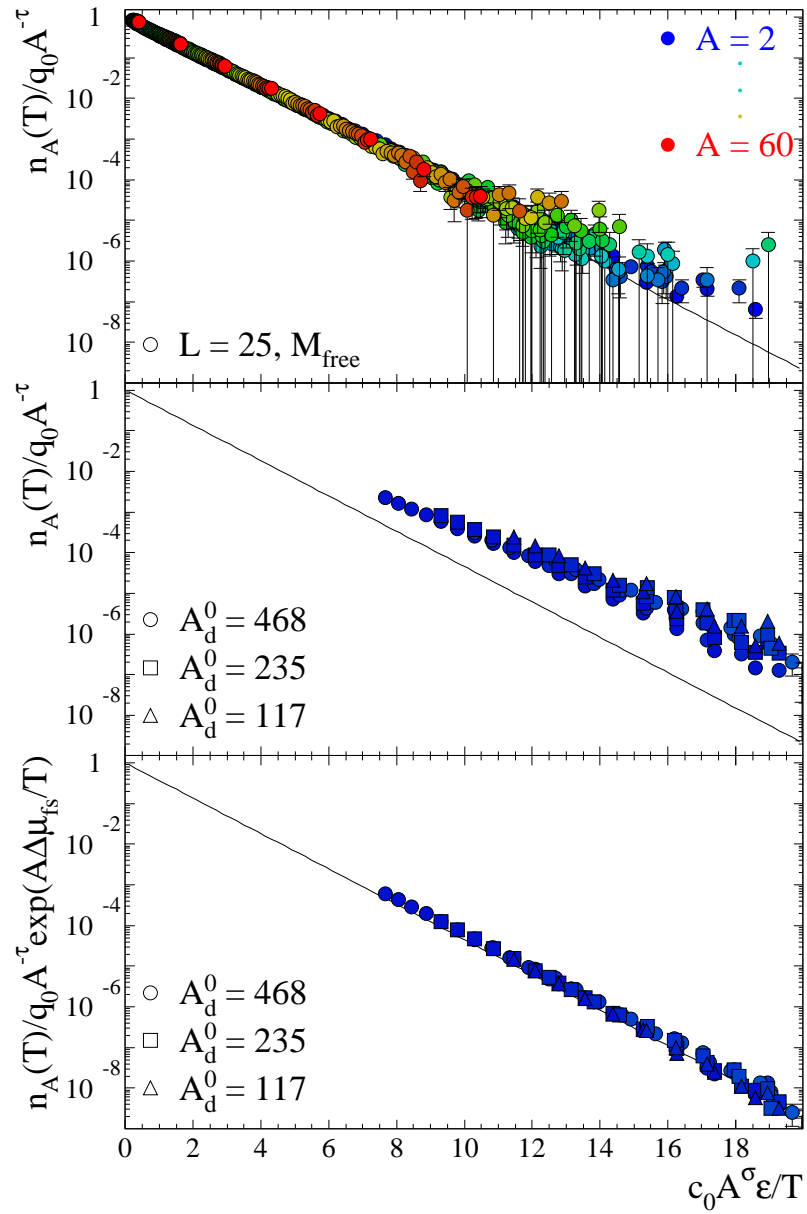


Figure 2.3. Same as Fig. 2.2 but for the $d = 3$, $L = 25$ periodic boundary condition simple cubic lattice.

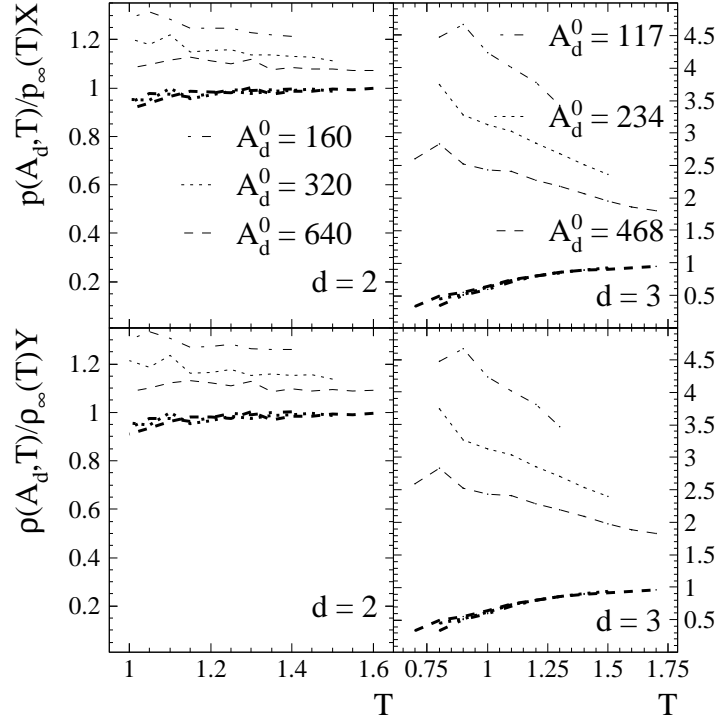


Figure 2.4. Left (right) the normalized pressure and density of a vapor in coexistence with a drop A_d for $d = 2$ (3). Thin [thick] lines show no complement results, $X = Y = 1$ [complement results, X and Y from Eqs. (2.5) and (2.6)].

and the data collapse is better.

The middle and bottom panels of Figs. 2.2 and 2.3 show the major point of this method: generalizing Fisher's model with the complement accounts for the finiteness of the liquid. The middle panels of Figs. 2.2 and 2.3 show that the M_{fixed} calculations do not scale as their M_{free} counterparts. The bottom panels of Figs. 2.2 and 2.3 show that when the complement effect is taken into account, the M_{fixed} calculations scale as their M_{free} counterparts.

Now in the integrated quantities, pressure $p(A_d, T) = T \sum_A n_A(T)$ and density $\rho(A_d, T) = \sum_A n_A(T)A$. For $A_d \gg A$, the expansion of $\Delta\mu_{\text{fs}}$ gives

$$\Delta\mu_{\text{fs}} = 1 + A \left(\frac{\tau}{A_d} + \frac{\sigma c_0 \varepsilon}{T A_d^{1-\sigma}} \right) + \dots \quad (2.4)$$

This leads to

$$p(A_d, T) \approx p_\infty(T) \exp \left[\left(\frac{\tau}{A_d} + \frac{\sigma c_0 \varepsilon}{T A_d^{1-\sigma}} \right) \frac{\sum_A n_A^\infty(T) A}{\sum_A n_A^\infty(T)} \right] \equiv p_\infty(T) X \quad (2.5)$$

and

$$\rho(A_d, T) \approx \rho_\infty(T) \exp \left[\left(\frac{\tau}{A_d} + \frac{\sigma c_0 \varepsilon}{T A_d^{1-\sigma}} \right) \frac{\sum_A n_A^\infty(T) A^2}{\sum_A n_A^\infty(T) A} \right] \equiv \rho_\infty(T) Y. \quad (2.6)$$

For a vapor of monomers as $A_d \gg \tau$ equations (2.5) and (2.6) yield the Gibbs-Thomson formulae [121].

Figure 2.4 shows the behavior of $p(A_d, T)$ and $\rho(A_d, T)$ for the M_{fixed} calculations compared to the bulk results. To free ourselves from finite lattice size effects $p_\infty(T)$, $\rho_\infty(T)$ and $n_A^\infty(T)$ are determined from the M_{free} calculations. As expected $p(A_d, T) > p_\infty(T)$ and $\rho(A_d, T) > \rho_\infty(T)$ (thin lines in Fig. 2.4); i.e. the ratio in question is > 1 . Accounting for the complement via equations (2.5) and (2.6) (using values in Table 2.1) collapses results from all the calculations to a single line recovering the bulk behavior (thick lines in Fig. 2.4); i.e. the ratio in question is ~ 1 . Deviations at low T are due to the increasing effects of monomers which have $c_0 = 8$ (12) in $d = 2$ (3).

Thus, a general approach in terms of the complement has been developed which allows one to account for finite liquid drop size effects and to extrapolate from finite to infinite systems. It was demonstrated the applicability of the suggested method using lattice gas model (Ising) calculations. This method can be generalized to include other energy factors present in the nuclear case (e.g. symmetry, Coulomb and angular momentum energies) which is another important step towards determining the liquid-vapor phase boundary of infinite, symmetric nuclear matter from experimental nuclear data. Also this general approach can be applied to a variety of cluster models, like the SMM, GSMM, CSMM and GBM, to deal with finite systems.

2.2. Constrained SMM in Finite Volumes

Despite the great success, the application of the exact solution [48, 50, 56] to the description of experimental data is limited because this solution corresponds to an infinite system and due to that it cannot account for a more complicated interaction between nuclear fragments. Therefore, it was necessary to extend the exact solution [48, 50, 56] to finite volumes. It is clear that for the finite volume extension it is necessary to account for the finite size and geometrical shape of

the largest fragments, when they are comparable with the system volume. For this one has to abandon the arbitrary size of largest fragment and consider the constrained SMM (CSMM) in which the largest fragment size is explicitly related to the volume V of the system. The latter is assumed to be a cubical one. Thus, the CSMM assumes a more strict constraint $\sum_k^{K(V)} k n_k = A$, where the size of the largest fragment $K(V) = \alpha V/b$ cannot exceed the total volume of the system (the parameter $\alpha \leq 1$ is introduced for convenience). The case of the fixed size of the largest fragment, i.e. $K(V) = Const$, analyzed numerically in Ref. [131] is also included in our treatment. A similar restriction should be also applied to the upper limit of the product in all partitions $Z_A^{id}(V, T)$, $Z_A(V, T)$ and $\mathcal{Z}(V, T, \mu)$ introduced above (how to deal with the real values of $K(V)$, see later). Then the model with this constraint, the CSMM, cannot be solved by the Laplace transform method, because the volume integrals cannot be evaluated due to a complicated functional V -dependence. However, the CSMM can be solved analytically with the help of the following identity [110]

$$G(V) = \int_{-\infty}^{+\infty} d\xi \int_{-\infty}^{+\infty} \frac{d\eta}{2\pi} e^{i\eta(V-\xi)} G(\xi), \quad (2.7)$$

which is based on the Fourier representation of the Dirac δ -function. The representation (2.7) allows us to decouple the additional volume dependence and reduce it to the exponential one, which can be dealt by the usual Laplace transformation in the following sequence of steps

$$\begin{aligned} \hat{\mathcal{Z}}(\lambda, T, \mu) &\equiv \int_0^\infty dV e^{-\lambda V} \mathcal{Z}(V, T, \mu) = \int_0^\infty dV' \int_{-\infty}^{+\infty} d\xi \int_{-\infty}^{+\infty} \frac{d\eta}{2\pi} e^{i\eta(V'-\xi)-\lambda V'} \\ &\times \sum_{\{n_k\}} \left[\prod_{k=1}^{K(\xi)} \frac{1}{n_k!} \left\{ V' \phi_k(T) e^{\frac{(\mu - (\lambda - i\eta) b T) k}{T}} \right\}^{n_k} \right] \Theta(V') \\ &= \int_0^\infty dV' \int_{-\infty}^{+\infty} d\xi \int_{-\infty}^{+\infty} \frac{d\eta}{2\pi} e^{i\eta(V'-\xi) - \lambda V' + V' \mathcal{F}(\xi, \lambda - i\eta)}. \end{aligned} \quad (2.8)$$

After changing the integration variable $V \rightarrow V' = V - b \sum_k^{K(\xi)} k n_k$, the constraint of Θ -function has disappeared. Then all n_k were summed independently leading to the exponential function. Now the integration over V' in Eq. (2.8) can be straightforwardly done resulting in

$$\hat{\mathcal{Z}}(\lambda, T, \mu) = \int_{-\infty}^{+\infty} d\xi \int_{-\infty}^{+\infty} \frac{d\eta}{2\pi} \frac{e^{-i\eta\xi}}{\lambda - i\eta - \mathcal{F}(\xi, \lambda - i\eta)}, \quad (2.9)$$

where the function $\mathcal{F}(\xi, \tilde{\lambda})$ is defined as follows

$$\mathcal{F}(\xi, \tilde{\lambda}) = \sum_{k=1}^{K(\xi)} \phi_k(T) e^{\frac{(\mu - \tilde{\lambda} b T)k}{T}} = \left(\frac{mT}{2\pi}\right)^{\frac{3}{2}} \left[z_1 e^{\frac{\mu - \tilde{\lambda} b T}{T}} + \sum_{k=2}^{K(\xi)} k^{-\tau} e^{\frac{(\mu + W - \tilde{\lambda} b T)k - \sigma k^{2/3}}{T}} \right]. \quad (2.10)$$

As usual, in order to find the GCE partition by the inverse Laplace transformation, it is necessary to study the structure of singularities of the isobaric partition (2.10).

2.2.1. Isobaric Partition Singularities at Finite Volumes. The isobaric partition (2.10) of the CSMM is, of course, more complicated than its SMM analog [48, 50] because for finite volumes the structure of singularities in the CSMM is much richer than in the SMM, and they match in the limit $V \rightarrow \infty$ only. To see this let us first make the inverse Laplace transform:

$$\begin{aligned} \mathcal{Z}(V, T, \mu) &= \int_{\chi - i\infty}^{\chi + i\infty} \frac{d\lambda}{2\pi i} \hat{\mathcal{Z}}(\lambda, T, \mu) e^{\lambda V} = \int_{-\infty}^{+\infty} d\xi \int_{-\infty}^{+\infty} \frac{d\eta}{2\pi} \int_{\chi - i\infty}^{\chi + i\infty} \frac{d\lambda}{2\pi i} \frac{e^{\lambda V - i\eta \xi}}{\lambda - i\eta - \mathcal{F}(\xi, \lambda - i\eta)} = \\ &= \int_{-\infty}^{+\infty} d\xi \int_{-\infty}^{+\infty} \frac{d\eta}{2\pi} e^{i\eta(V - \xi)} \sum_{\{\lambda_n\}} e^{\lambda_n V} \left[1 - \frac{\partial \mathcal{F}(\xi, \lambda_n)}{\partial \lambda_n} \right]^{-1}, \end{aligned} \quad (2.11)$$

where the contour λ -integral is reduced to the sum over the residues of all singular points $\lambda = \lambda_n + i\eta$ with $n = 1, 2, \dots$, since this contour in the complex λ -plane obeys the inequality $\chi > \max(\text{Re}\{\lambda_n\})$. Now both remaining integrations in (2.11) can be done, and the GCE partition becomes

$$\mathcal{Z}(V, T, \mu) = \sum_{\{\lambda_n\}} e^{\lambda_n V} \left[1 - \frac{\partial \mathcal{F}(V, \lambda_n)}{\partial \lambda_n} \right]^{-1}, \quad (2.12)$$

i.e. the double integral in (2.11) simply reduces to the substitution $\xi \rightarrow V$ in the sum over singularities. This is a remarkable result which was formulated in Ref. [110] as the following *theorem*: *if the Laplace-Fourier image of the excluded volume GCE partition exists, then for any additional V -dependence of $\mathcal{F}(V, \lambda_n)$ or $\phi_k(T)$ the GCE partition can be identically represented by Eq. (2.12)*. Now it clear that the above theorem can be applied to the finite volume formulations of a more general model, the GSMM [112]. However, in the following I will use the CSMM to keep presentation simple.

The simple poles in (2.11) are defined by the equation

$$\lambda_n = \mathcal{F}(V, \lambda_n). \quad (2.13)$$

In contrast to the usual SMM [48, 50] the singularities λ_n are (i) are volume dependent functions, if $K(V)$ is not constant, and (ii) they can have a non-zero imaginary part, but in this case there exist pairs of complex conjugate roots of (2.13) because the GCE partition is real.

Introducing the real R_n and imaginary I_n parts of $\lambda_n = R_n + iI_n$, one can rewrite Eq. (2.13) as a system of coupled transcendental equations

$$R_n = \sum_{k=1}^{K(V)} \tilde{\phi}_k(T) e^{\frac{\text{Re}(\nu_n)k}{T}} \cos(I_n bk), \quad (2.14)$$

$$I_n = - \sum_{k=1}^{K(V)} \tilde{\phi}_k(T) e^{\frac{\text{Re}(\nu_n)k}{T}} \sin(I_n bk), \quad (2.15)$$

where I have introduced the set of the effective chemical potentials $\nu_n \equiv \nu(\lambda_n)$ with $\nu(\lambda) = \mu + W(T) - \lambda bT$, and the reduced distribution functions $\tilde{\phi}_1(T) = \left(\frac{mT}{2\pi}\right)^{\frac{3}{2}} z_1 \exp(-W(T)/T)$ and $\tilde{\phi}_{k>1}(T) = \left(\frac{mT}{2\pi}\right)^{\frac{3}{2}} k^{-\tau} \exp(-\sigma(T) k^{2/3}/T)$ for convenience.

Consider the real root ($R_0 > 0, I_0 = 0$), first. For $I_n = I_0 = 0$ the real root R_0 exists for any T and μ . Comparing R_0 with the expression for vapor pressure of the analytical SMM solution [48, 50] shows that TR_0 is a constrained grand canonical pressure of the gas. As usual, for finite volumes the total mechanical pressure [94, 110] differs from TR_0 . Equation (2.15) shows that for $I_{n>0} \neq 0$ the inequality $\cos(I_n bk) \leq 1$ never become the equality for all k -values simultaneously. Then from Eq. (2.14) one obtains ($n > 0$)

$$R_n < \sum_{k=1}^{K(V)} \tilde{\phi}_k(T) e^{\frac{\text{Re}(\nu_n)k}{T}} \Rightarrow R_n < R_0, \quad (2.16)$$

where the second inequality (2.16) immediately follows from the first one. In other words, the gas singularity is always the rightmost one. This fact plays a decisive role in the thermodynamic limit $V \rightarrow \infty$.

The interpretation of the complex roots $\lambda_{n>0}$ is less straightforward. According to Eq. (2.12), the GCE partition is a superposition of the states of different free energies $-\lambda_n VT$. (Strictly speaking, $-\lambda_n VT$ has a meaning of the change of free energy, but I will use the traditional term for it.) For $n > 0$ the free energies are complex. Therefore, $-\lambda_{n>0}T$ is the density of free energy. The real part of the free energy density, $-R_n T$, defines the significance of the state's contribution to the partition: due to (2.16) the largest contribution always comes from the gaseous state and has

the smallest real part of free energy density. As usual, the states which do not have the smallest value of the (real part of) free energy, i. e. $-R_{n>0}T$, are thermodynamically metastable. For infinite volume they should not contribute unless they are infinitesimally close to $-R_0T$, but for finite volumes their contribution to the GCE partition may be important.

As one sees from (2.14) and (2.15), the states of different free energies have different values of the effective chemical potential ν_n , which is not the case for infinite volume [48, 50], where there exists a single value for the effective chemical potential. Thus, for finite V the states which contribute to the GCE partition (2.12) are not in a true chemical equilibrium.

The meaning of the imaginary part of the free energy density becomes clear from (2.14) and (2.15) [112]: as one can see from (2.14) the imaginary part $I_{n>0}$ effectively changes the number of degrees of freedom of each k -nucleon fragment ($k \leq K(V)$) contribution to the free energy density $-R_{n>0}T$. It is clear, that the change of the effective number of degrees of freedom can occur virtually only and, if $\lambda_{n>0}$ state is accompanied by some kind of equilibration process. Both of these statements become clear, if one recalls that the statistical operator in statistical mechanics and the quantum mechanical evolution operator are related by the Wick rotation [132]. In other words, the inverse temperature can be considered as an imaginary time. Therefore, depending on the sign, the quantity $I_n bT \equiv \tau_n^{-1}$ that appears in the trigonometric functions of the equations (2.14) and (2.15) in front of the imaginary time $1/T$ can be regarded as the inverse decay/formation time τ_n of the metastable state which corresponds to the pole $\lambda_{n>0}$ (for more details see next sections).

This interpretation of τ_n naturally explains the thermodynamic metastability of all states except the gaseous one: the metastable states can exist in the system only virtually because of their finite decay/formation time, whereas the gaseous state is stable because it has an infinite decay/formation time.

2.2.2. No Phase Transition Case. It is instructive to treat the effective chemical potential $\nu(\lambda)$ as an independent variable instead of μ . In contrast to the infinite V , where the upper limit $\nu \leq 0$ defines the liquid phase singularity of the isobaric partition and gives the pressure of a liquid phase $p_l(T, \mu) = TR_0|_{V \rightarrow \infty} = (\mu + W(T))/b$ [48, 50], for finite volumes and finite $K(V)$ the effective chemical potential can be complex (with either sign for its real part) and its value

defines the number and position of the imaginary roots $\{\lambda_{n>0}\}$ in the complex plane. Positive and negative values of the effective chemical potential for finite systems were considered [133] within the Fisher droplet model, but, to our knowledge, its complex values have never been discussed. From the definition of the effective chemical potential $\nu(\lambda)$ it is evident that its complex values for finite systems exist only because of the excluded volume interaction, which is not taken into account in the Fisher droplet model [44]. However, a recent study of clusters of the $d = 2$ Ising model within the framework of FDM (see the corresponding section in Ref. [58]) shows that the excluded volume correction improves essentially the description of the thermodynamic functions. Therefore, the next step is to consider the complex values of the effective chemical potential and free energy for the excluded volume correction of the Ising clusters on finite lattices.

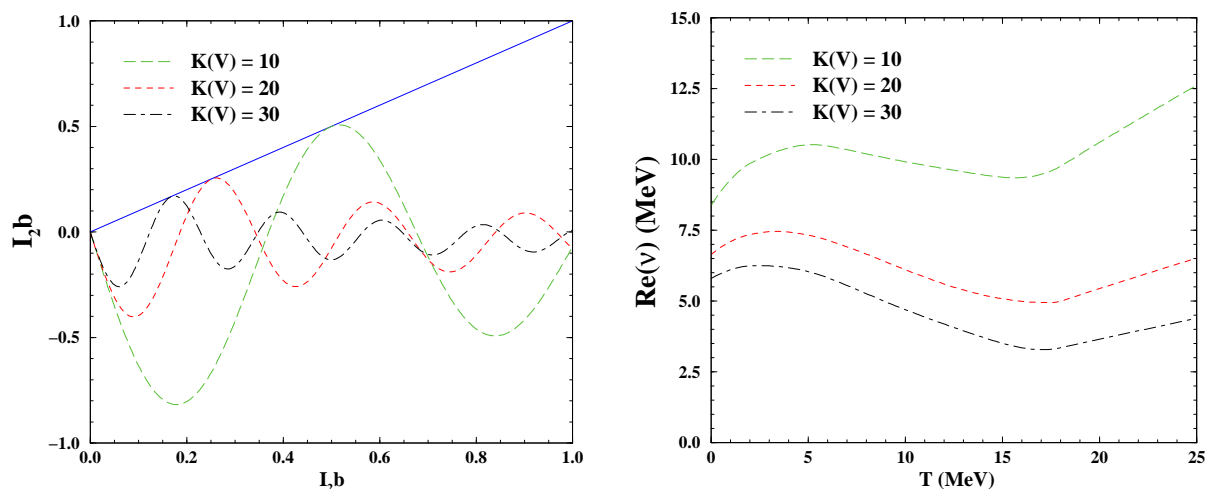


Figure 2.5. **Left panel:** A graphical solution of Eq. (2.15) for $T = 10$ MeV and $\tau = 1.825$. The l.h.s. (straight line) and r.h.s. of Eq. (2.15) (all dashed curves) are shown as the function of dimensionless parameter $I_1 b$ for the three values of the largest fragment size $K(V)$. The intersection point at $(0; 0)$ corresponds to a real root of Eq. (2.13). Each tangent point with the straight line generates two complex roots of (2.13).

Right panel: Each curve separates the $T - Re(\nu_n)$ region of one real root of Eq. (2.13) (below the curve), three complex roots (at the curve) and five and more roots (above the curve) for three values of $K(V)$ and the same parameters as in the left panel.

As it is seen from the left panel of Fig. 2.5, the r.h.s. of Eq. (2.15) is the amplitude and

frequency modulated sine-like function of dimensionless parameter $I_n b$. Therefore, depending on T and $Re(\nu)$ values, there may exist no complex roots $\{\lambda_{n>0}\}$, a finite number of them, or an infinite number of them. The left panel of Fig. 2.5 shows a special case which corresponds to exactly three roots of Eq. (2.13) for each value of $K(V)$: the real root ($I_0 = 0$) and two complex conjugate roots ($\pm I_1$). Since the r.h.s. of (2.15) is monotonously increasing function of $Re(\nu)$, when the former is positive, it is possible to map the $T - Re(\nu)$ plane into regions of a fixed number of roots of Eq. (2.13). Each curve in the right panel of Fig. 2.5 divides the $T - Re(\nu)$ plane into three parts: for $Re(\nu)$ -values below the curve there is only one real root (gaseous phase), for points on the curve there exist three roots, and above the curve there are four or more roots of Eq. (2.13).

For constant values of $K(V) \equiv K$ the number of terms in the r.h.s. of (2.15) does not depend on the volume and, consequently, in thermodynamic limit $V \rightarrow \infty$ only the rightmost simple pole in the complex λ -plane survives out of a finite number of simple poles. According to the inequality (2.16), the real root λ_0 is the rightmost singularity of isobaric partition (2.9). However, there is a possibility that the real parts of other roots $\lambda_{n>0}$ become infinitesimally close to R_0 , when there is an infinite number of terms which contribute to the GCE partition (2.12).

Let us show now that even for an infinite number of simple poles in (2.12) only the real root λ_0 survives in the limit $V \rightarrow \infty$. For this purpose consider the limit $Re(\nu_n) \gg T$. In this limit the distance between the imaginary parts of the nearest roots remains finite even for infinite volume. Indeed, for $Re(\nu_n) \gg T$ the leading contribution to the r.h.s. of (2.15) corresponds to the harmonic with $k = K$, and, consequently, an exponentially large amplitude of this term can be only compensated by a vanishing value of $\sin(I_n bK)$, i.e. $I_n bK = \pi n + \delta_n$ with $|\delta_n| \ll \pi$ (hereafter I will analyze only the branch $I_n > 0$), and, therefore, the corresponding decay/formation time $\tau_n \approx K[\pi n T]^{-1}$ is volume independent.

Keeping the leading term on the r.h.s. of (2.15) and solving for δ_n , one finds

$$I_n \approx (-1)^{n+1} \tilde{\phi}_K(T) e^{\frac{Re(\nu_n)K}{T}} \delta_n, \quad \text{with} \quad \delta_n \approx \frac{(-1)^{n+1} \pi n}{Kb \tilde{\phi}_K(T)} e^{-\frac{Re(\nu_n)K}{T}}, \quad (2.17)$$

$$R_n \approx (-1)^n \tilde{\phi}_K(T) e^{\frac{Re(\nu_n)K}{T}}, \quad (2.18)$$

where in the last step I used Eq. (2.14) and condition $|\delta_n| \ll \pi$. Since for $V \rightarrow \infty$ all negative

values of R_n cannot contribute to the GCE partition (2.12), it is sufficient to analyze even values of n which, according to (2.18), generate $R_n > 0$.

Since the inequality (2.16) can not be broken, a single possibility, when $\lambda_{n>0}$ pole can contribute to the partition (2.12), corresponds to the case $R_n \rightarrow R_0 - 0^+$ for some finite n . Assuming this, one finds $Re(\nu(\lambda_n)) \rightarrow Re(\nu(\lambda_0))$ for the same value of μ . Substituting these results into equation (2.14), one gets

$$R_n \approx \sum_{k=1}^K \tilde{\phi}_k(T) e^{\frac{Re(\nu(\lambda_0))k}{T}} \cos\left[\frac{\pi nk}{K}\right] \ll R_0. \quad (2.19)$$

The inequality (2.19) follows from the equation for R_0 and the fact that, even for equal leading terms in the sums above (with $k = K$ and even n), the difference between R_0 and R_n is large due to the next to leading term $k = K - 1$, which is proportional to $e^{\frac{Re(\nu(\lambda_0))(K-1)}{T}} \gg 1$. Thus, one arrives at a contradiction with our assumption $R_0 - R_n \rightarrow 0^+$, and, consequently, it cannot be true. Therefore, for large volumes the real root λ_0 always gives the main contribution to the GCE partition (2.12), and this is the only root that survives in the limit $V \rightarrow \infty$. Thus, I showed that the model with the fixed size of the largest fragment has no phase transition because there is a single singularity of the isobaric partition (2.9), which exists in thermodynamic limit.

2.2.3. Finite Volume Analogs of Phases. If $K(V)$ monotonically grows with the volume, the situation is different. In this case for positive value of $Re(\nu) \gg T$ the leading exponent in the r.h.s. of (2.15) also corresponds to a largest fragment, i.e. to $k = K(V)$. Therefore, we can apply the same arguments which were used above for the case $K(V) = K = const$ and derive similarly equations (2.17)–(2.18) for I_n and R_n . From $I_n \approx \frac{\pi n}{bK(V)}$ it follows that, when V increases, the number of simple poles in (2.11) also increases and the imaginary part of the closest to the real λ -axis poles becomes very small, i.e. $I_n \rightarrow 0$ for $n \ll K(V)$, and, consequently, the associated decay/formation time $\tau_n \approx K(V)[\pi n T]^{-1}$ grows with the volume of the system. Due to $I_n \rightarrow 0$, the inequality (2.19) cannot be established for the poles with $n \ll K(V)$. Therefore, in contrast to the previous case, for large $K(V)$ the simple poles with $n \ll K(V)$ will be infinitesimally close to the real axis of the complex λ -plane.

From Eq. (2.18) it follows that

$$R_n \approx \frac{p_l(T, \mu)}{T} - \frac{1}{K(V)b} \ln \left| \frac{R_n}{\tilde{\phi}_K(T)} \right| \rightarrow \frac{p_l(T, \mu)}{T} \quad (2.20)$$

for $|\mu| \gg T$ and $K(V) \rightarrow \infty$. Thus, it is proved that for infinite volume the infinite number of simple poles moves toward the real λ -axis to the vicinity of liquid phase singularity $\lambda_l = p_l(T, \mu)/T$ of the isobaric partition [48, 50] and generates an essential singularity of function $\mathcal{F}(V, p_l/T)$ in (2.10) *irrespective to the sign of the chemical potential μ* . In addition, as I showed above, the states with $Re(\nu) \gg T$ become stable because they acquire infinitely large decay/formation time τ_n in the limit $V \rightarrow \infty$. Therefore, these states should be identified as a liquid phase for finite volumes as well.

Now it is clear that each curve in the right panel of Fig. 2.5 is the finite volume analog of the phase boundary $T - \mu$ for a given value of $K(V)$: below the phase boundary there exists a gaseous phase, but at and above each curve there are states which can be identified with a finite volume analog of the mixed phase, and, finally, at $Re(\nu) \gg T$ there exists a liquid phase. When there is no phase transition, i.e. $K(V) = K = const$, the structure of simple poles is similar, but, first, the line which separates the gaseous states from the metastable states does not change with the volume, and, second, as shown above, the metastable states will never become stable. Therefore, a systematic study of the volume dependence of free energy (or pressure for very large V) along with the formation and decay times may be of a crucial importance for experimental studies of the nuclear liquid gas phase transition.

The above results demonstrate that, in contrast to Hill's expectations [94], the finite volume analog of the mixed phase does not consist just of two pure phases. The mixed phase for finite volumes consists of a stable gaseous phase and the set of metastable states which differ by the free energy. Moreover, the difference between the free energies of these states is not surface-like, as Hill assumed in his treatment [94], but volume-like. Furthermore, according to Eqs. (2.14) and (2.15), each of these states consists of the same fragments, but with different weights. As seen above for the case $Re(\nu) \gg T$, some fragments that belong to the states, in which the largest fragment is dominant, may, in principle, have negative weights (effective number of degrees of freedom) in the expression for $R_{n>0}$ (2.14). This can be understood easily because higher concentrations of

large fragments can be achieved at the expense of the smaller fragments and is reflected in the corresponding change of the real part of the free energy $-R_{n>0}VT$. Therefore, the actual structure of the mixed phase at finite volumes is more complicated than was expected in earlier works.

The Hills' ideas were developed further in Ref. [93], where the authors claimed to establish the one to one correspondence between the bimodal structure of the partition of measurable quantity B known on average and the properties of the Lee-Yang zeros of this partition in the complex g -plane. The starting point of Ref. [93] is to postulate the partition Z_g and the probability $P_g(B)$ of the following form

$$Z_g \equiv \int dB W(B) e^{-B \cdot g} \quad \Rightarrow \quad P_g(B) \equiv \frac{W(B) e^{-B \cdot g}}{Z_g}, \quad (2.21)$$

where $W(B)$ is the partition sum of the ensemble of fixed values of the observable $\{B\}$, and g is the corresponding Lagrange multiplier. Then the authors of Ref. [93] assume the existence of two maxima of the probability $P_g(B)$ (\equiv bimodality) and discuss their relation to the Lee-Yang zeros of Z_g in the complex g -plane.

The CSMM gives us a unique opportunity to verify the Chomaz and Gulminelli idea on the bimodality behavior of $P_g(B)$ using the first principle results. Let us use the equation (2.8) identifying the intensive variable g with λ and extensive one B with the available volume $V' \rightarrow \tilde{V}$. The evaluation of the r.h.s. of (2.8) is very difficult in general, but for a special case, when the eigen volume b is small this can be done analytically. Thus, approximating $\mathcal{F}(\xi, \lambda - i\eta) \approx \mathcal{F}(\xi, \lambda) - i\eta \partial \mathcal{F}(\xi, \lambda) / \partial \lambda$, one obtains the CSMM analog of the probability (2.21)

$$\begin{aligned} P_\lambda(\tilde{V}) \hat{\mathcal{Z}}(\lambda, T, \mu) &\equiv \int_{-\infty}^{+\infty} d\xi \int_{-\infty}^{+\infty} \frac{d\eta}{2\pi} e^{i\eta(\tilde{V}-\xi) - \lambda\tilde{V} + \tilde{V}\mathcal{F}(\xi, \lambda - i\eta)} \\ &\approx \int_{-\infty}^{+\infty} d\xi e^{\tilde{V}[\mathcal{F}(\xi, \lambda) - \lambda]} \delta\left[\tilde{V} - \xi - \frac{\partial \mathcal{F}(\xi, \lambda)}{\partial \lambda}\right], \end{aligned} \quad (2.22)$$

where I made the η integration after applying the approximation for $\mathcal{F}(\xi, \lambda - i\eta)$. Further evaluation of (2.22) requires to know all possible solutions of the average volume of the system $\xi_\alpha^*(\tilde{V}) = \tilde{V} - \partial \mathcal{F}(\xi_\alpha^*, \lambda) / \partial \lambda$ ($\alpha = \{1, 2, \dots\}$). Since the number of these solutions is either one or two [113], the probability (2.22) can be written as

$$P_\lambda(\tilde{V}) \hat{\mathcal{Z}}(\lambda, T, \mu) \approx \sum_\alpha \frac{1}{\left|1 + \frac{\partial^2 \mathcal{F}(\xi_\alpha^*, \lambda)}{\partial \lambda \partial \xi_\alpha^*}\right|} e^{\tilde{V}[\mathcal{F}(\xi_\alpha^*, \lambda) - \lambda]} \quad . \quad (2.23)$$

In contrast to the expectations of Ref. [93], the probability (2.23) cannot be measured experimentally, irrespective to the sign of the derivative $\frac{\partial \ln P_\Delta(\tilde{V})}{\partial \tilde{V}}$. Indeed, above it was rigorously proven that for any real ξ the IP $\hat{\mathcal{Z}}(\lambda, T, \mu)$ is defined on the real λ -axis only for $\mathcal{F}(\xi, \lambda) - \lambda < 0$, i.e. on the right hand side of the gaseous singularity λ_0 : $\lambda > \lambda_0$. However, as one can see from the equation (2.11), the “experimental” λ_n values belong to the other region of the complex λ -plane: $Re(\lambda_{n>0}) < \lambda_0$.

Thus, it turns out that the suggestion of Ref. [93] to analyze the probability (2.21) does not make any sense because, as I explicitly showed for the CSMM, it cannot be measured. It seems that the starting point of the Ref. [93] approach, i.e. the assumption that the left equation (2.21) gives the most general form of the partition of finite system, is problematic. Indeed, comparing (2.20) with the analytical result (2.23), one can see that for finite systems, in contrast to the major assumption of Ref. [93], the probability W of the CSMM depends not only on the extensive variable \tilde{V} , but also on the intensive variable λ , which makes unmeasurable the whole construct of Ref. [93]. Consequently, the conclusions of Ref. [93] on the relation between the bimodality and the phase transition existence are not general because they have a limited range of validity. In addition, the suggested construct [93] cannot be verified experimentally.

2.3. Gas of Bags in Finite Volumes

Now I will apply the formalism of the preceding sections to the analysis of the Gas of Bags Model (GBM) [134, 135] in finite volumes. In the low and high temperature domains the GBM reduces to two well known and successful models: the hadron gas model [136, 137] and the bag model of QGP [138]. Both of these models are surprisingly successful in describing the bulk properties of hadron production in high energy nuclear collisions, and, therefore, one may hope that their generalization, the GBM, may reflect basic features of the nature in the phase transition region.

The van der Waals gas consisting of n hadronic species, which are called bags in what follows, has the following GCE partition [134]

$$Z(V, T) = \sum_{\{N_k\}} \left[\prod_{k=1}^n \frac{[(V - v_1 N_1 - \dots - v_n N_n) \phi_k(T)]^{N_k}}{N_k!} \right] \theta(V - v_1 N_1 - \dots - v_n N_n) , \quad (2.24)$$

where $\phi_k(T) \equiv g_k \phi(T, m_k) \equiv \frac{g_k}{2\pi^2} \int_0^\infty p^2 dp \exp[-(p^2 + m_k^2)^{1/2}/T] = g_k \frac{m_k^2 T}{2\pi^2} K_2\left(\frac{m_k}{T}\right)$ is the particle density of bags of mass m_k and eigen volume v_k and degeneracy g_k . This expression differs slightly from the GCE partition of the simplified SMM (1.17), where $\mu = 0$ and the eigen volume of k -nucleon fragment kb is changed to the eigen volume of the bag v_k . Therefore, as for a simplified SMM the Laplace transformation (1.18) with respect to volume of Eq. (2.24) gives

$$\hat{Z}(s, T) = \left[s - \sum_{j=1}^n \exp(-v_j s) g_j \phi(T, m_j) \right]^{-1}. \quad (2.25)$$

In preceding sections I showed that as long as the number of types of bags, n , is finite, the only possible singularities of $\hat{Z}(s, T)$ (2.25) are simple poles. However, in the case of an infinite number of types of bags an essential singularity of $\hat{Z}(s, T)$ may appear. This property is used the GBM: the sum over different bag states in (2.24) can be replaced by the integral, $\sum_{j=1}^\infty g_j \dots = \int_0^\infty dm dv \dots \rho(m, v)$, if the bag mass-volume spectrum, $\rho(m, v)$, which defines the number of bag states in the mass-volume region $[m, v; m + dm, v + dv]$, is given. Then, the Laplace transform of $Z(V, T)$ reads [134]

$$\hat{Z}_{GB}(s, T) \equiv \int_0^\infty dV e^{-sV} Z(V, T) = \frac{1}{[s - F(T, s)]}, \quad (2.26)$$

where $F(s, T)$ is defined as

$$F(s, T) = \int_0^\infty dm dv \rho(m, v) e^{-vs} \phi(T, m). \quad (2.27)$$

Like in the simplified SMM, the pressure of infinite system is again given by the rightmost singularity: $p(T) = T s^*(T) = T \cdot \max\{s_H(T), s_Q(T)\}$. Similarly to the simplified SMM considered above, the rightmost singularity $s^*(T)$ of $\hat{Z}(s, T)$ (2.26) can be either the simple pole singularity $s_H(T) = F(s_H(T), T)$ of the isobaric partition (2.26) or the $s_Q(T)$ singularity of the function $F(s, T)$ (2.27) it-self. Note, that all singularities of the IP are defined by the equation [134, 48]:

$$s^*(T) = F(s^*, T). \quad (2.28)$$

The major mathematical difference between the simplified SMM and the GBM is that the latter employs the two parameters mass-volume spectrum. Thus, the mass-volume spectrum of the GBM

consists of the discrete mass-volume spectrum of light hadrons and the continuum contribution of heavy resonances [139]

$$\begin{aligned} \rho(m, v) &= \sum_{j=1}^{J_m} g_j \delta(m - m_j) \delta(v - v_j) \\ &+ \Theta(v - V_0) \Theta(m - M_0 - Bv) C v^\gamma (m - Bv)^\delta \exp \left[\frac{4}{3} \sigma_Q^{\frac{1}{4}} v^{\frac{1}{4}} (m - Bv)^{\frac{3}{4}} \right], \end{aligned} \quad (2.29)$$

respectively. Here $m_j < M_0$, $v_j < V_0$, $M_0 \approx 2$ GeV, $V_0 \approx 1$ fm³, C, γ, δ and B (the so-called bag constant, $B \approx 400$ MeV/fm³) are the model parameters and

$$\sigma_Q = \frac{\pi^2}{30} \left(g_g + \frac{7}{8} g_{q\bar{q}} \right) = \frac{\pi^2}{30} \left(2 \cdot 8 + \frac{7}{8} \cdot 2 \cdot 2 \cdot 3 \cdot 3 \right) = \frac{\pi^2}{30} \frac{95}{2} \quad (2.30)$$

is the Stefan-Boltzmann constant counting gluons (spin, color) and (anti-)quarks (spin, color and u, d, s -flavor) degrees of freedom.

Recently the grand canonical ensemble has been heavily criticized [140, 141], when it is used for the exponential mass spectrum. This critique, however, cannot be applied to the mass-volume spectrum (2.29) because it grows less fast than the Hagedorn mass spectrum discussed in [140, 141] and because in the GBM there is an additional suppression of large and heavy bags due to the van der Waals repulsion. Therefore, the spectrum (2.29) can be safely used in the grand canonical ensemble.

It can be shown [135] that the spectrum (2.29) generates the $s_Q(T) = \frac{\sigma_Q}{3} T^3 - \frac{B}{T}$ singularity, which reproduces the bag model pressure $p(T) = T s_Q(T)$ [138] for high temperature phase, and $s_H(T)$ singularity, which gives the pressure of the hadron gas model [136, 137] for low temperature phase. The transition between them can be of the first order or second order, depending on the model parameters.

However, for finite systems the volume of bags and their masses should be finite. The simplest finite volume modification of the GBM is to introduce the volume dependent size of the largest bag $n = n(V)$ in the partition (2.24). As we discussed earlier such a modification cannot be handled by the traditional Laplace transform technique used in [139, 135], but this modification can be easily accounted for by the Laplace-Fourier method [110]. Repeating all the steps of the CSMM analysis, one will obtain the equations (2.10)-(2.13), in which the function $\mathcal{F}(\xi, \tilde{\lambda})$ should be replaced by its

GBM analog $f(\lambda, V_B) \equiv F_H(\lambda) + F_Q(\lambda, V_B)$ defined via

$$F_H(\lambda) \equiv \sum_{j=1}^{J_m} g_j \phi(T, m_j) e^{-v_j s}, \quad \text{and} \quad F_Q(\lambda, V_B) \equiv V_0 \int_1^{V_B/V_0} dk a(T, V_0 k) e^{V_0(s_Q(T) - \lambda)k}. \quad (2.31)$$

In evaluating (2.31) I used the mass-volume spectrum (2.29) with the maximal volume of the bag V_B and changed integration to a dimensionless variable $k = v/V_0$. Here the function $a(T, v) = u(T)v^{2+\gamma+\delta}$ is defined by $u(T) = C\pi^{-1}\sigma_Q^{\delta+1/2} T^{4+4\delta}(\sigma_Q T^4 + B)^{3/4}$.

The above representation (2.31) generates equations for the real and imaginary parts of $\lambda_n \equiv R_n + iI_n$, which are very similar to the corresponding expressions of the CSMM (2.14) and (2.15). Comparing (2.31) with (2.13), one sees that their main difference is that the sum over k in (2.13) is replaced by the integral over k in (2.31). Therefore, the equations (2.14) and (2.15) remain valid for R_n and I_n of the GBM, respectively, if one replaces the k sum by the integral for $K(V) = V_B/V_0$, $b = V_0$, $\nu(\lambda) = V_0(s_Q(T) - \lambda)$ and $\tilde{\phi}_{k>1}(T) = V_0 a(T, V_0 k)$. Thus, the results and conclusions of our analysis of the R_n and I_n properties of the CSMM should be valid for the GBM as well. In particular, for large values of $K(V) = V_B/V_0$ and $R_n < s_Q(T)$ one can immediately find out $I_n \approx \pi n/V_B$ and the GBM formation/decay time $\tau_n = V_B[\pi n T V_0]^{-1}$. These equations show that the metastable $\lambda_{n>0}$ states can become stable in thermodynamic limit, if and only if $V_B \sim V$.

The finite volume modification of the GBM equation of state should be used for the quantities which have $V\lambda_0 \sim 1$. This may be important for the early stage of the relativistic nuclear collisions when the volume of the system is small, or for the systems that have small pressures. The latter can be the case for the pressure of strange or charm hadrons.

2.4. Hills and Dales Model and Source of Surface Entropy

During last forty years the FDM [44] has been successfully used to analyze the condensation of a gaseous phase (droplets or clusters of all sizes) into a liquid. The systems analyzed with the FDM are many and varied, but up to now the source of the surface entropy is not absolutely clear. In his original work Fisher postulated that the surface free-energy F_A of a cluster of A -constituents consists of surface ($A^{2/3}$) and logarithmic ($\ln A$) parts, i.e. $F_A = \sigma(T) A^{2/3} + \tau T \ln A$. Its surface part $\sigma(T) A^{2/3} \equiv \sigma_0[1 - T/T_c] A^{2/3}$ consists of the surface energy, i.e. $\sigma_0 A^{2/3}$, and

surface entropy $-\sigma_o/T_c A^{2/3}$. From the study of the combinatorics of lattice gas clusters in two dimensions, Fisher postulated the specific temperature dependence of the surface tension $\sigma(T)|_{\text{FDM}}$ which gives naturally an estimate for the critical temperature T_c . Surprisingly Fisher's estimate works for the 3-d Ising model [122], nucleation of real fluids [143, 144], percolation clusters [145] and nuclear multifragmentation [45].

2.4.1. Grand Canonical Surface Partition. To understand why the surface entropy has such a form I formulated a statistical model of surface deformations of the cluster of A -constituents, the Hills and Dales Model (HDM) [114]. For simplicity I consider cylindrical deformations of positive height $h_k > 0$ (hills) and negative height $-h_k$ (dales), with k -constituents at the base. It is assumed that for the deformation of the base of k -constituents the top (bottom) of the hill (dale) has the same shape as the surface of the original cluster of A -constituents. I also assume that: (i) the statistical weight of deformations $\exp(-\sigma_o|\Delta S_k|/s_1/T)$ is given by the Boltzmann factor due to the change of the surface $|\Delta S_k|$ in units of the surface per constituent s_1 ; (ii) all hills of heights $h_k \leq H_k$ (H_k is the maximal height of a hill with a base of k -constituents) have the same probability dh_k/H_k besides the statistical one; (iii) assumptions (i) and (ii) are valid for the dales. Then the HDM grand canonical surface partition (GCSP)

$$Z_{gc}(S_A) = \sum_{\{n_k^\pm=0\}} \left[\prod_{k=1}^{K_{max}} \frac{[z_k^+ \mathcal{G}_{gc}]^{n_k^+}}{n_k^+!} \frac{[z_k^- \mathcal{G}_{gc}]^{n_k^-}}{n_k^-!} \right] \Theta(s_1 \mathcal{G}_{gc}) \quad (2.32)$$

corresponds to the conserved (on average) volume of the cluster because the probabilities of hill z_k^+ and dale z_k^- of the same k -constituent base are identical [114]

$$z_k^\pm \equiv \int_0^{\pm H_k} \frac{dh_k}{\pm H_k} e^{-\frac{\sigma_o P_k |h_k|}{T s_1}} = \frac{T s_1}{\sigma_o P_k H_k} \left[1 - e^{-\frac{\sigma_o P_k H_k}{T s_1}} \right]. \quad (2.33)$$

Here P_k is the perimeter of the cylinder base.

The geometrical partition (degeneracy factor) of the HDM or the number of ways to place the center of a given deformation on the surface of the A -constituent cluster which is occupied by the set of $\{n_l^\pm = 0, 1, 2, \dots\}$ deformations of the l -constituent base I assume to be given in the van der Waals approximation [114]:

$$\mathcal{G}_{gc} = \left[S_A - \sum_{k=1}^{K_{max}} k (n_k^+ + n_k^-) s_1 \right] s_1^{-1}, \quad (2.34)$$

where $s_1 k$ is the area occupied by the deformation of k -constituent base ($k = 1, 2, \dots$), S_A is the full surface of the cluster, and $K_{max}(S_A)$ is the A -dependent size of the maximal allowed base on the cluster.

The $\Theta(s_1 \mathcal{G}_{gc})$ -function in (2.32) ensures that only configurations with positive value of the free surface of cluster are taken into account, but makes the analytical evaluation of the GCSP (2.32) very difficult. However, it is possible *to solve this GCSP exactly* for any surface dependence of $K_{max}(S_A)$ using the identity (2.7) of the Laplace-Fourier transform technique [110] discussed earlier:

$$Z_{gc}(S_A) = \sum_{\{\lambda_n\}} e^{\lambda_n S_A} \left[1 - \frac{\partial \mathcal{F}_{gc}(S_A, \lambda_n)}{\partial \lambda_n} \right]^{-1}. \quad (2.35)$$

The poles λ_n of the isochoric partition are defined by

$$\lambda_n = \mathcal{F}_{gc}(S_A, \lambda_n) \equiv \sum_{k=1}^{K_{max}(S_A)} \left[\frac{z_k^+}{s_1} + \frac{z_k^-}{s_1} \right] e^{-k s_1 \lambda_n}, \quad (2.36)$$

which can be cast as a system of two coupled transcendental equations

$$R_n = \sum_{k=1}^{K_{max}(S_A)} \left[z_k^+ + z_k^- \right] e^{-k R_n} \cos(I_n k), \quad (2.37)$$

$$I_n = - \sum_{k=1}^{K_{max}(S_A)} \left[z_k^+ + z_k^- \right] e^{-k R_n} \sin(I_n k), \quad (2.38)$$

for dimensionless variables $R_n = s_1 R e(\tilde{\lambda}_n)$ and $I_n = s_1 I m(\tilde{\lambda}_n)$.

To this point Eqs. (2.37) and (2.38) are general and can be used for particular models which specify the height of hills and depth of dales. But there exists an absolute supremum for the real root ($R_0; I_0 = 0$) of these equations. It is sufficient to consider the limit $K_{max}(S_A) \rightarrow \infty$, because for $I_n = I_0 = 0$ the right hand side (r.h.s.) of (2.14) is a monotonously increasing function of $K_{max}(S_A)$. Since $z_k^+ = z_k^-$ are the monotonously decreasing functions of H_k , the maximal value of the r.h.s. of (2.14) corresponds to the limit of infinitesimally small amplitudes of deformations, $H_k \rightarrow 0$. Then for $I_n = I_0 = 0$ Eq. (2.38) becomes an identity and Eq. (2.37) becomes

$$R_0 \rightarrow 2 \sum_{k=1}^{\infty} e^{-\frac{\sigma_0 P_k H_k}{2T s_1}} e^{-k R_0} = 2 \left[e^{R_0} - 1 \right]^{-1}, \quad (2.39)$$

and we have $R_0 = s_1 \tilde{\lambda}_0 \approx 1.06009$. Since for $I_n \neq 0$ defined by (2.38) the inequality $\cos(I_n k) \leq 1$ cannot become the equality for all values of k simultaneously, then it follows that the real root of

(2.37) obeys the inequality $R_0 > R_{n>0}$. The last result means that in the limit of infinite cluster, $S_A \rightarrow \infty$, the GCSP is represented by the farthest right singularity among all simple poles $\{\tilde{\lambda}_n\}$

$$Z(S_A) \Big|_{S_A \rightarrow \infty} \approx \frac{e^{\frac{R_0 S_A}{s_1}}}{1 + \frac{R_0(R_0+2)}{2}} \approx 0.3814 e^{\frac{R_0 S_A}{s_1}} \quad (2.40)$$

There are two remarkable facts regarding (2.40): first, this result is model independent because in the limit of vanishing amplitude of deformations all model specific parameters vanish; second, in evaluating (2.40) we did not specify the shape of the cluster under consideration, but only implicitly required that the cluster surface together with deformations is a regular surface without self-intersections. Therefore, for vanishing amplitude of deformations the latter means that Eq. (2.40) should be valid for any self-non-intersecting surfaces.

For spherical clusters the r.h.s. of (2.40) becomes familiar, $0.3814 e^{1.06009 A^{2/3}}$, which, combined with the Boltzmann factor of the surface energy $e^{-\sigma_o A^{2/3}/T}$, generates the following temperature dependent surface tension of the large cluster

$$\sigma(T) = \sigma_o \left[1 - 1.06009 \frac{T}{\sigma_o} \right] \quad (2.41)$$

which means that the actual critical temperature of the three dimensional Fisher model should be $T_c = \sigma_o/1.06009$, i.e. 6.009 % smaller in σ_o units than Fisher originally supposed. This equation for the critical temperature remains valid for the temperature dependent σ_o as well. Our result, given in Eq. (2.41), agrees with Fisher estimate of $\sigma(T)$. Agreement between our result and $\sigma(T)|_{SMM}$ occurs, if $\sigma_o = \sigma(T)|_{SMM} + 1.06009 T$.

Also equation (2.40) allows one, for the first time, to find the exact value of the degeneracy prefactor, 0.3814, which was unknown in the FDM and its extensions.

Now it is appropriate to ask which of two surface tension parameterizations, the FDM or SMM, is correct? On the one hand, the FDM linear T -dependence works well and can be derived in the limit of vanishing amplitudes of deformations within HDM, but on the other hand, the SMM prescription is based on the hyperscaling relation [146, 118] for the surface tension of macroscopic fluids $\sigma(T)|_{SMM} \rightarrow \Gamma_o \left[\frac{T_c - T}{T_c} \right]^{(d-1)\nu}$, which is nonlinear in T . Here ν is the critical exponent that also describes the divergence of the correlation length near the critical point and is related to other

exponents through the hyperscaling relation [146, 118]

$$d\nu = \gamma + 2\beta. \quad (2.42)$$

A possible solution of this problem is that the hyperscaling relation describes a single macroscopic drop, whereas the FDM and HDM are dealing with the ensemble of clusters or drops of a given volume (in fact, of a given mass) and they account for the mean surface or the surface of mean cluster [118]. The latter is measured in dimensionless units (in HDM it is written explicitly as the ratio of two surfaces S_A/s_1), whereas the hyperscaling is formulated for the surface S_A of the A -constituent drop. Therefore, in the relation between the surface tension coefficient used in hyperscaling and the surface of a mean Fisher cluster the temperature dependent density of liquids is involved via s_1 . The analysis performed for the real fluids [58] shows that the temperature dependent density of liquids, indeed, ‘compensates’ the extra power in temperature and makes the surface tension coefficient linear in T .

Before proceeding further let me consider the left equality in Eq. (2.16) which is valid for small deformation heights. It can be shown that for $S_A \gg s_1$ the deformation energy

$$\frac{\sigma_o P_k H_k}{2s_1} \rightarrow -\frac{3}{2} T k \frac{\tau}{\zeta} \frac{s_1}{S_A} \ln\left(\frac{s_1}{S_A}\right) \quad (2.43)$$

of a k -constituent base, indeed, generates the Fisher power law $A^{-\tau}$ for the GCSP (2.32) of an A -constituent cluster. Now one can see that besides the coefficient $3T\tau/(2\zeta)$ [where $\zeta^{-1} = 1 + \frac{2}{R_0(2+R_0)} \approx (0.61861)^{-1}$], the term $-k\frac{s_1}{S_A} \ln\left(\frac{s_1}{S_A}\right)$ on the right hand side of (2.43) is the entropy which gives an *a priori* uncertainty to measure the position of k constituents each of area s_1 on the surface of the cluster. A comparison of (2.43) with any $kR_n > 0$ in the left equality (2.16) shows that in the limit $S_A \gg s_1$ the ansatz (2.43) corresponds to a negligible correction compared to the exponentials $e^{\frac{R_n S_A}{s_1}}$. Therefore, the Fisher power law is too delicate for the present formulation of the surface partition model.

2.4.2. Special Ensembles for Surface Partition. Similarly one can introduce the surface partitions for the other ensembles [115]. The canonically constrained surface partition (CCSP) is built up to obey the volume conservation more strictly than it is done in the GCSP.

This is ensemble of pairs of deformations: the number of the hills n_k^+ of the k -constituent base is always identical to the number of corresponding dales, i.e. $n_k^- \equiv n_k^+ \equiv n_k$. Then the canonical geometrical partition can be cast as

$$\mathcal{G}_c = \left[S_A - 2 \sum_{k=1}^{K_{\max}} k n_k s_1 \right] (2s_1)^{-1}, \quad (2.44)$$

where the factor two in the denominator of the right hand side (r.h.s.) of (2.44) accounts for the fact that it is necessary to place simultaneously the centers of two k -constituent base deformations (hill and dale) out of $2n_k$ on the surface of cluster. Using the geometrical partition (2.44), one can obtain the partition function of canonical ensemble by formally replacing $\mathcal{G}_{gc} \rightarrow \mathcal{G}_c$ and inserting the Kronecker symbol $\delta_{n_k^+, n_k^-}$ for each k -multiplier in (2.32). I, however, consider each pair of hills and dales of the same base as a single degree of freedom. Therefore, the number of ways to place each pair out of n_k distinguishable pairs is still given by the canonical geometrical partition \mathcal{G}_c . Multiplying it with the probability of a pair of deformations $z_k^+ z_k^-$ and repeating this for n_k pairs, one obtains the CCSP, as follows

$$Z_{cc}(S_A) = \sum_{\{n_k=0\}}^{\infty} \left[\prod_{k=1}^{K_{\max}} \frac{[z_k^+ z_k^- \mathcal{G}_c]^{n_k}}{n_k!} \right] \Theta(2s_1 \mathcal{G}_c). \quad (2.45)$$

Applying the Laplace-Fourier transform technique to this partition, one can find that the CCSP has the same form as the GCSP (2.35), but the function \mathcal{F}_{gc} in (2.36) must be replaced with \mathcal{F}_{cc} :

$$\lambda_n = \mathcal{F}_{cc}(S_A, \lambda_n) = \sum_{k=1}^{K_{\max}(S_A)} \frac{z_k^+ z_k^-}{2 s_1} e^{-2 k s_1 \lambda_n}. \quad (2.46)$$

For the limit of the vanishing amplitudes of deformations it is possible to introduce one more ensemble for the surface deformations [115] which hereafter will be called as the *semi-grand canonical surface partition* (SGCSP). This ensemble occupies an intermediate position between the constrained canonical and grand canonical formulations. It corresponds to the case, when the hills and dales of the same base are considered to be indistinguishable. For that I would like to explore the fact that according to (2.33) the statistical probabilities of hills and dales of the same base are equal. Then for the infinitesimally small amplitudes of deformations the volume conservation constraint is fulfilled trivially. Below this ensemble will be used for the deformations of vanishing amplitude only, but it may be used also for finite amplitudes of deformations, if the volume is not

conserved. Then the SGCSF and its geometrical factor read as

$$Z_{\text{sg}}(S_A) = \sum_{\{n_k=0\}}^{\infty} \left[\prod_{k=1}^{K_{\text{max}}} \frac{[z_k^+ \mathcal{G}_{\text{sg}}]^{n_k}}{n_k!} \right] \Theta(s_1 \mathcal{G}_{\text{sg}}), \quad \mathcal{G}_{\text{sg}} = \left[S_A - \sum_{k=1}^{K_{\text{max}}} k n_k s_1 \right] s_1^{-1}. \quad (2.47)$$

Again, like in the case of the CCSP, only the equation for the simple poles of the isochoric partition should be modified

$$\lambda_n = \mathcal{F}_{\text{sg}}(S_A, \lambda_n) = \sum_{k=1}^{K_{\text{max}}(S_A)} \frac{z_k^+}{s_1} e^{-k s_1 \lambda_n}. \quad (2.48)$$

Eqs. (2.46) and (2.48) can be written for real and imaginary parts as follows

$$R_n^\alpha = \sum_{k=1}^{K_{\text{max}}(S_A)} \phi_k^\alpha e^{-k R_n^\alpha} \cos(I_n^\alpha k), \quad (2.49)$$

$$I_n^\alpha = - \sum_{k=1}^{K_{\text{max}}(S_A)} \phi_k^\alpha e^{-k R_n^\alpha} \sin(I_n^\alpha k), \quad (2.50)$$

for dimensionless variables defined as $R_n^\alpha = s_1 \text{Re}(\tilde{\lambda}_n)$ and $I_n^\alpha = s_1 \text{Im}(\tilde{\lambda}_n)$ for the GCSP and SGCSF, and as $R_n^{\text{cc}} = 2s_1 \text{Re}(\tilde{\lambda}_n)$ and $I_n^{\text{cc}} = 2s_1 \text{Im}(\tilde{\lambda}_n)$ for the CCSP. Here the function ϕ_k^α is given by the expression

$$\phi_k^\alpha = \begin{cases} z_k^+ + z_k^-, & \text{for } \alpha = gc, \\ z_k^+ z_k^-, & \text{for } \alpha = cc, \\ z_k^+, & \text{for } \alpha = sg. \end{cases} \quad (2.51)$$

Since the equation for the simple poles of all three surface partitions are reduced to the same system (2.49), (2.50), it is clear all the qualitative properties of the solutions discussed for the GCSP remain valid for the CCSP and SGCSF as well [115]. There is only a quantitative difference for the rightmost singularities R_0^α . Therefore, in the limit of the vanishing amplitudes of deformations for an infinite base of the largest deformation $K_{\text{max}}(S_A \rightarrow \infty) \rightarrow \infty$ each of these surface partitions will reach an *upper limit* defined by the corresponding value of the surface entropy coefficient ω_{U}^α , defined by the corresponding R_0^α :

$$\max\{Z_\alpha(S_A)\} \rightarrow g_\alpha e^{\omega_{\text{U}}^\alpha \frac{S_A}{s_1}} \quad \text{with} \quad \omega_{\text{U}}^\alpha = \begin{cases} \omega_{\text{U}}^{\text{gc}} = \max\{R_0^{\text{gc}}\} \approx 1.060090, & \alpha = gc, \\ \omega_{\text{U}}^{\text{cc}} = \max\{R_0^{\text{cc}}/2\} \approx 0.403233, & \alpha = cc, \\ \omega_{\text{U}}^{\text{sg}} = \max\{R_0^{\text{sg}}\} \approx 0.806466, & \alpha = sg, \end{cases} \quad (2.52)$$

where the degeneracy factor g_α is defined as follows: $g_{\text{gc}} \approx 0.38139$ and $g_{\text{cc}} = g_{\text{sg}} \approx 0.407025$. The rightmost singularities of these partitions are defined by the equation

$$R_0^\alpha = B^\alpha \sum_{k=1}^{\infty} e^{-k R_0^\alpha} = B^\alpha [e^{R_0^\alpha} - 1]^{-1}, \quad (2.53)$$

where $B^{\text{gc}} = 2$ and $B^{\text{cc}} = B^{\text{sg}} = 1$.

For large, but finite clusters it is necessary to take into account not only the farthest right singularity $\tilde{\lambda}_0$ in the corresponding surface partition, but all other roots of Eqs. (2.49) and (2.50) which have positive real part $R_{n>0}^\alpha > 0$. In this case for each $R_{n>0}^\alpha$ there are two roots $\pm I_n^\alpha$ of (2.50) because each surface partition function is real by definition. The roots of Eqs. (2.49) and (2.50) with largest real part are insensitive to the large values of $K_{\text{max}}(S_A)$, therefore, it is sufficient to keep $K_{\text{max}}(S_A) \rightarrow \infty$. Then for limit of vanishing amplitude of deformations Eqs. (2.49) and (2.50) can be, respectively, rewritten as

$$\frac{B^\alpha R_n^\alpha}{(R_n^\alpha)^2 + (I_n^\alpha)^2} = e^{R_n^\alpha} \cos(I_n^\alpha) - 1, \quad (2.54)$$

$$\frac{B^\alpha I_n^\alpha}{(R_n^\alpha)^2 + (I_n^\alpha)^2} = -e^{R_n^\alpha} \sin(I_n^\alpha). \quad (2.55)$$

After some algebra the system of (2.54) and (2.55) can be reduced to a single equation for R_n^α

$$\cos \left(\left[\frac{B^\alpha (B^\alpha + 2R_n^\alpha)}{e^{2R_n^\alpha} - 1} - (R_n^\alpha)^2 \right]^{1/2} \right) = \cosh R_n^\alpha - \frac{B^\alpha}{B^\alpha + 2 R_n^\alpha} \sinh R_n^\alpha, \quad (2.56)$$

and the quadrature $I_n^\alpha = \sqrt{\frac{B^\alpha (B^\alpha + 2R_n^\alpha)}{e^{2R_n^\alpha} - 1} - (R_n^\alpha)^2}$. The analysis shows that besides the opposite signs there are two branches of solutions, $I_n^{\alpha+}$ and $I_n^{\alpha-}$, for the same $n \geq 1$ value. Expanding both sides of (2.56) for $R_n^\alpha \ll 1$ and keeping the leading terms, for $n \geq 1$ one obtains

$$|I_n^{\alpha\pm}| \approx 2\pi n \pm \frac{B^\alpha}{2\pi n}, \quad (2.57)$$

$$R_n^\alpha \approx \frac{(B^\alpha)^2}{8\pi^2 n^2}. \quad (2.58)$$

The exact solutions $(R_n^\alpha; I_n^{\alpha\pm})$ for $n \geq 1$ which have the largest real part are shown in the left panel of Fig. 2.6 together with the curve parametrized by functions $I_x^{\alpha+}$ and R_x^α taken from Eqs. (2.57) and (2.58), respectively. From Eq. (2.58) and the left panel of Fig. 2.6 it is clear that for the GCSP the largest real part $R_1^{\text{gc}} \approx 0.0582$ is about 18 times smaller than R_0^{gc} , whereas for the

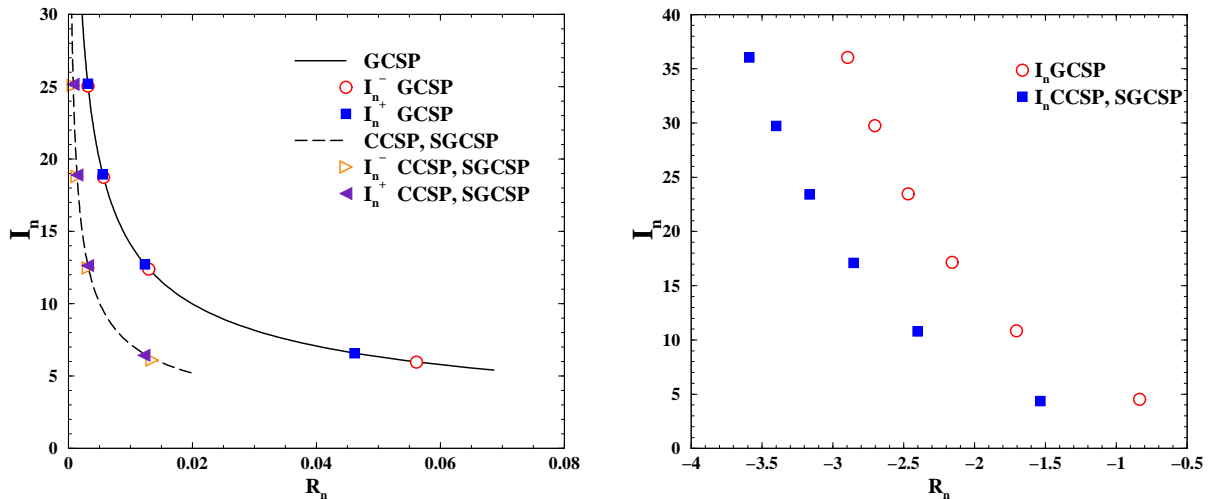


Figure 2.6. **Left panel:** The first quadrant of the complex plane $(R_n^\alpha + iI_n^\alpha) \equiv s_1 \lambda_n^\alpha L^\alpha$ shows the location of simple poles of the isochoric partitions for $n = 1, 2, 3, 4$. The symbols represent the two branches I_n^- and I_n^+ of the roots for the upper estimate of three surface partitions. The curves are defined by the approximation suggested in [115].

Right panel: The second quadrant of the complex plane $s_1 \tilde{\lambda}_n^\alpha \equiv R_n^\alpha + iI_n^\alpha$ shows the complex roots of the system of Eqs. (2.60) and (2.61) with the largest real parts. The circles and squares represent the roots for the lower estimate of the GCSP and CCSP(SGCSP), respectively.

CCSP and SGCSP the real part $R_1^{cc} = R_1^{sg}$ of the first most right complex root of Eqs. (2.49) and (2.50) is about 63.6 times smaller than $R_0^{cc} = R_0^{sg}$. Therefore, for a cluster of a few constituents the correction to the leading term in (2.52) is exponentially small for all considered partitions. Using the approximations (2.57) and (2.58), for $n > 2$ one can estimate the upper limit of the $(R_n^\alpha; I_n^{\alpha\pm})$ root contribution into left hand side Eq. (2.52)

$$\left| e^{\tilde{\lambda}_n S_A} \left[1 - \frac{\partial \mathcal{F}_\alpha(S_A, \tilde{\lambda}_n)}{\partial \tilde{\lambda}_n} \right]^{-1} \right| \leq e^{\frac{(B^\alpha)^2 S_A}{8\pi^2 n^2 s_1}} / (2\pi^2 n^2). \quad (2.59)$$

This result shows that for all three considered partition the total contribution of all complex poles into the corresponding surface partition is negligibly small compared to the leading term (2.52) even for a cluster of a few constituents.

2.4.3. The Lower Bounds for the Surface Entropy Coefficients. To

complete our analysis of the limit of vanishing deformations we would like to find the lower estimate

for the GCSP, CCSP and SGCSF for large clusters. This estimate corresponds to the absence of all other deformations except for those of smallest base. In other words, one has to substitute $K_{\max}(S_A) = 1$ in all corresponding expressions. Then equations (2.49) and (2.50), respectively become

$$R_n^\alpha = \phi_1^\alpha e^{-R_n^\alpha} \cos(I_n^\alpha), \quad (2.60)$$

$$I_n^\alpha = -\phi_1^\alpha e^{-R_n^\alpha} \sin(I_n^\alpha). \quad (2.61)$$

Similar to the previous consideration, the leading term of the lower estimate for the surface partitions is given by the real root ($R_0^\alpha; I_0^\alpha = 0$) of the system (2.60) and (2.61)

$$R_0^\alpha = \begin{cases} \omega_L^{gc} = \min\{\omega^{gc}\} \approx 0.852606, & \alpha = gc, \\ 2\omega_L^{cc} = 2 \min\{\omega^{cc}\} \approx 0.567143, & \alpha = cc, \\ \omega_L^{sg} = \min\{\omega^{sg}\} \approx 0.567143, & \alpha = sg. \end{cases} \quad (2.62)$$

Again, as in case of upper estimates one can show that the real root ($R_0^\alpha; I_0^\alpha = 0$) approximates well the lower estimate for the partition function for a system of a few constituents. In fact, each of three surface partitions has only a single root with positive real part which coincides with ($R_0^\alpha; I_0^\alpha = 0$). In the right panel of Fig. 2.6 a few complex roots of Eqs. (2.60) and (2.61) with the largest real parts are shown. Since all these roots have negative real part, they generate an exponentially small contribution to the lower estimate of surface partition for a system of a few constituents.

Table 2.3. The maximal and minimal values of the ω -coefficient for three HDM partitions.

Partition	$\max\{\omega^\alpha\}$	$\min\{\omega^\alpha\}$
GCSP	1.060090	0.852606
SGCSF	0.806466	0.567143
CCSP	0.403233	0.283572

The ω -coefficients for upper and lower estimates of all three surface partitions are summarized in the Table 2.3. A comparison with the corresponding coefficient for liquids should be made with

care because various contributions to the surface tension, i.e., eigen surface tension of the liquid drop, the geometrical degeneracy factor (surface partition), and the part induced by interaction between clusters, are not exactly known. Therefore, even the linear temperature dependence of the surface tension $\sigma(T) = \sigma_o(T_c - T)/T_c$ due to Fisher [44] applied to a nuclear liquid ($\sigma_o \approx 18$ MeV; $T_c \approx 18$ MeV [46]) may be used to estimate the ω -coefficient, if both the eigen surface tension and the interaction induced one are non-increasing functions of temperature. Under these assumptions one can get the following inequality for nuclear liquid

$$\omega_{nucl} \leq 1 < \omega_U^{gc} = 1.060090, \quad (2.63)$$

i.e. the upper estimate for the GCSP, indeed, provides the upper limit for surface partition of nuclear matter.

A similar analysis for real liquids is difficult because of complicated temperature dependence of the surface tension. Therefore, we would like to compare the ω -coefficients from Table 2.3 with the ω -coefficients for the large spin clusters of various 2- and 3-dimensional Ising models, which are listed in the Tables 2.4 and 2.5, respectively [118]. Such a comparison can be made because the surface entropy of large spin clusters on the Ising lattices are similar to the considered surface partitions [118].

The ω -coefficient for the d -dimensional Ising model is defined as the energy $2J$ required to flip a given spin interacting with its q -neighbors to opposite direction per $(d - 1)$ -dimensional surface divided by the value of critical temperature

$$\omega_{Lat} = \frac{q J}{T_c d}. \quad (2.64)$$

Here q is the coordination number for the lattice, and J denotes the coupling constant of the model. A comparison of the Tables 2.3 - 2.5 shows that all lattice ω_{Lat} -coefficients, indeed, lie between the upper estimates for the constrained canonical and grand canonical surface partitions

$$0.403233 = \omega_U^{cc} < \omega_{Lat} < \omega_U^{gc} = 1.060090, \quad (2.65)$$

i.e. ω_U^{cc} and ω_U^{gc} are the infimum and supremum for 2- and 3-dimensional Ising models, respectively.

Table 2.4. The values of the ω_{Lat} -coefficient for various 2-dimensional Ising models. For more details see the text.

Lattice type	$\omega_{Lat} = \frac{\sigma}{T_c}$
Honeycomb	0.987718
Kagome	0.933132
Square	0.881374
Triangular	0.823960
Diamond	0.739640

Table 2.5. The values of the ω_{Lat} -coefficient for various 3-dimensional Ising models.

Lattice type	$\omega_{Lat} = \frac{\sigma}{T_c}$
Simple cubic	0.44342
Body-centered cubic	0.41989
Face-centered cubic	0.40840

The HDM partitions do not have an explicit dependence on the dimension of the surface, but a comparison of the HDM and Ising model ω -coefficients shows that the HDM ensembles seem to possess some sort of internal dimension: the GCSP is close to honeycomb, kagome or square lattices, whereas the SGCSF is similar to triangular and diamond lattices, and the $\max\{\omega\}$ of the CCSP is closer to the 3-dimensional Ising models. In some cases the agreement with the lattice data is remarkable - ω_L^{gc} coincides with the arithmetical average of the ω -coefficients for square and triangular lattices up to a fifth digit, but in most cases the values agree within a few per cent. The latter is not surprising because the HDM estimates the surface entropy of a single cluster, whereas on the lattice the spin clusters do interact with each other and this, of course, changes the surface tension and, consequently, affects the value of critical temperature. It is remarkable that so oversimplified estimates of the surface partitions for a single large cluster reasonably approximate the ω -coefficients for 2- and 3-dimensional Ising models.

It would be interesting to check whether the lower estimate of the CCSP $\omega_L^{cc} \approx 0.283572$ is an infimum for the Ising lattices of higher dimensions $d > 3$. If this is the case, then we can give an upper limit for the critical temperature of those lattices using Eq. (2.64)

$$\frac{T_c}{J} \leq \frac{q}{\omega_L^{cc} d} \approx 3.5264 \frac{q}{d}. \quad (2.66)$$

On the other hand, the lower estimate for the critical temperature of Ising lattices, $\frac{T_c}{J} \geq \frac{q}{\omega_U^{cc} d}$, is provided by the supremum of the ω -coefficients of surface partitions.

2.5. Conclusions

An invention of a new powerful mathematical method [110], the Laplace-Fourier transform, is, perhaps, a major theoretical breakthrough in the statistical mechanics of finite systems of the last decade because it allowed us to solve exactly not only the simplified SMM for finite volumes [110], but also a variety of statistical surface partitions for finite clusters [114, 115] and to find out their surface entropy and to shed light on a source of the Fisher exponent τ . It was shown [110] that for finite volumes the analysis of the GCE partition of the simplified SMM is reduced to the analysis of the simple poles of the corresponding isobaric partition, obtained as a Laplace-Fourier transform of the GCE partition. Such a representation of the GCE partition allows one not only to show from the first principles that for finite systems there exist the complex values of the effective chemical potential, but to define the finite volume analogs of phases straightforwardly. Moreover, this method allows one to include into consideration all complicated features of the interaction (including the Coulomb one) which have been neglected in the simplified SMM because it was originally formulated for infinite nuclear matter. This can be done, for instance, by dividing the full system into the set of subsystems in which the gradient of a Coulomb field inside of each subsystem can be neglected, and considering each subsystem in a framework of the CSMM or finite volume formulation of the GSMM with electrostatic potential generated by the external subsystems.

Consequently, the Laplace-Fourier transform method opens a principally new possibility to study the nuclear liquid-gas phase transition directly from the partition of finite system without

taking its thermodynamic limit. Now this method is also applied [113] to the finite volume formulation of the GBM [134] which is used to describe the PT between the hadronic matter and QGP. Thus, the Laplace-Fourier transform method not only gives an analytical solution for a variety of statistical models with PTs in finite volumes, but provides us with a common framework for several critical phenomena in strongly interacting matter. Therefore, it turns out that further applications and developments of this method are very promising and important not only for the field of nuclear multifragmentation, but for several fields studying PTs in finite systems because this method may provide them with the firm theoretical foundations and a common theoretical language.

At the moment it is unclear how to experimentally verify the existence of the complex values of the effective chemical potential and measure the decay/formation time $\tau_n \approx K(V)[\pi n T]^{-1}$ predicted by the CSMM. From the expression for τ_n one concludes that the decay/formation time decreases with the decrease of the size of largest fragment in the system $K(V)$ and with in growth of temperature. Therefore, by varying these parameters, one can make the decay/formation time much smaller than the equilibration time $\tau_{eq} \gg \tau_n$ for all modes with $n \geq 1$. In this case only the stable state with λ_0 will be described by the hydrodynamics, whereas all the metastable states will not be describe by the hydrodynamics. Thus, searching for a failure of hydrodynamic description in the A+A collisions may indicate the metastable collective modes in finite systems. In principle, this can occur for both the nuclear multifragmetation and for the QGP-hadron gas PT. Perhaps, the systematic study of the A+A reactions with the nucleus of many sizes and in a wide range of energies which will be performed at the FAIR accelerator can locate the metastable collective modes qualitatively predicted by the CSMM.

Further on, with the help of the Laplace-Fourier transform method it was also possible to formulate and solve analytically three surface partitions within the HDM. It is remarkable that such a simple model of surface partition discussed above gives the upper and lower bounds of the ω -coefficients for all 2- and 3-dimensional Ising models. Also the HDM allowed me to resolve the puzzle of the success of Fisher parameterization of the linear temperature dependence of surface tension coefficient and exactly derive an analytical result which is just 6 % larger than Fisher assumed.

Also the canonically constrained surface partition, perhaps, is able to explain another long standing puzzle: why the curvature part of surface tension of clusters is not seen. In principle, this could happen for large clusters at (tri)critical point, where all other parts of free energy vanish, but this is not seen in the FDM, SMM and many systems described by the FDM. Moreover, a careful analysis of 2- and 3-dimensional Ising clusters performed by a Complement method [106] allows one not only to extract the critical temperature, surface tension coefficient and even the value of Fisher index τ of the infinite system, but also such delicate effects as the Gibbs-Thomson correction [121] to the free energy of a liquid drop. The Gibbs-Thomson corrections are much weaker than the curvature term, but the latter is not seen.

Therefore, let us imagine, that for each large cluster of regular shape the hills and dales of the same base have the same probability and appear in pairs, like in the CCSP, and that their shape is not a cylinder, but some smooth shape, say a gaussian like. Then, while summing up the free energy associated with a curvature of each surface deformation, one finds that the total curvature free energy of large cluster is exactly zero because the contribution of any hill is exactly compensated by the curvature free energy of a similar dale, which has an opposite sign, whereas the eigen curvature of the undeformed surface of large cluster vanishes due to large radius of a cluster.

While further intriguing facts can be found in the original work [115], here I mention only that the surface tension plays a very important role in many cluster models like the FDM, SMM and CSMM, but its influence on the properties of the phase diagram of QGP was realized very recently. This results I will present in the chapter 4. Another interesting problem of surface partition is to consider the fractal deformations within the HDM in order to elucidate the source of Fisher power law. It is believed that the fractals may give us a possible solution of the Fisher's power law problem.

CHAPTER 3

VIRIAL EXPANSION FOR THE LORENTZ

CONTRACTED RIGID SPHERES AND RELATIVISTIC

VDW EOS FOR HADRONIC BINARY MIXTURES.

Now I would like to turn from the nuclear matter EOS to that one of hadrons. In the chapter 1 the realistic mean-field EOS of nuclear matter [173] was discussed in details. The various extensions of the Walecka model [10] are very popular [11, 64], but their application is very limited both at very high and low energy densities. In the first case they are limited by the deconfinement transition to QGP, which will be discussed in the chapter 4, whereas in the second case there is a problem of their conversion to the gas of free hadrons. Also this problem is related to the experimental setup of A+A collisions, in which the observed hadrons are free particles with their vacuum values of masses, charges and dispersion relation. Therefore, the effective EOS can be applied to description of finite stage of the collision, if and only if they can be transformed into free streaming particles. This is impossible to do for the Walecka model [10] and any its extensions because even a relatively weak interaction between the nucleons at normal nuclear density is provided by the significant densities of the mean values of scalar and vector fields. Since at the level of EOS there is no well defined procedure to convert these mean fields into physical particles, it is unclear what to do with them, at the end of the collision process. Therefore, it was necessary to develop an alternative statistical description of the hadronic matter EOS.

Such statistical models of hadron gas [136, 137] are rather successful in description of many experimentally observed hadronic ratios at all available energies above 1 GeV per nucleon. On the one hand they are similar to the cluster models discussed in the chapters 1 and 2, where all hadrons

and hadronic resonances with masses below 1.8-2 GeV are accounted for as stable particles. On the other hand these statistical models take into account for the discrete part of the Hagedorn model [148, 149] with the hard core repulsion.

One might be very surprised by the fact that the mixture of hadrons and their resonances with the hard core repulsion is able to reproduce a vast amount of experimental data with only 3 or 4 fitting parameters. The explanation was found long ago [150], when the direct numerical analysis showed that from the statistical point of view the mixture of stable hadrons, interacting with each other in all known repulsive and attractive channels, accounted up to the quantum second virial coefficient do behave like the mixture of ideal gases of hadrons and their resonances with the shifted chemical potential due to hard core repulsion.

This description [136, 137], however, generated the problem of causality [150]. In statistical mechanics of relativistic particles such problem is known for awhile. In fact, since more than a century after the discovery of special relativity the statistical mechanics of extended relativistic objects does not exists! The problem is that the special relativity does not allow the existence of rigid bodies. If such particles would exists, then at their dense packing the density perturbation would propagate superluminously, i.e. with the speed higher that the speed of light, but the latter is forbidden by relativity. Thus, the causality problem appears at high densities in any hadronic or nuclear matter EOS, if hard core repulsion is used. Although in the most of applications for the nuclear matter EOS such a problem can be ignored because the studied systems are nonrelativistic, this problem cannot be ignored for dense and hot hadronic matter.

There were two unsuccessful tries to resolve the causality problem for the EOS with the relativistic hard core repulsion [151, 152], but in both of these works the second virial coefficient was mixed up with the eigen volume. Moreover, whereas in Ref. [152] the Lorentz transformation was used to contract the eigen volume of hadron, in Ref. [151] the very same arguments were used to extend the eigen volume of particles. There was a discussion of possible temperature dependence of the parameters of the Van der Waals EOS [153], but the weak point of that discussion is the absence of a connection between the parameters of EOS and the interparticle potentials that could generate them. Therefore, it was necessary to return to the foundations of statistical mechanics

and derive the cluster and virial expansions for the momentum dependent interparticle potentials [154]. Then it was necessary to formulate the Van der Waals EOS for relativistic particles [154]. The first EOS of this type has the temperature dependent second virial coefficient and can be safely used to describe the experimental data for the lightest hadrons (pions and kaons) at temperatures below 200 MeV and small baryonic densities [155].

However, such an improved EOS [154] cannot be used for higher temperatures and baryonic densities because at this region it breaks the causality. Therefore, it was necessary to develop an alternative relativistic Van der Waals extrapolation [156] to high pressures which can be used to describe the hadrons and their resonances and even the effective particles like in the Walecka model [10] far above the cross-over where, as the lattice quantum chromodynamics calculations show [157], they coexist with quarks and gluons up to large temperatures like $3T_c$. Very recently it was understood that in the deconfined phase there may exist bound states [181] and resonances [182].

The relativistic effects on the hard core repulsion may be important for a variety of the effective models of hadrons and hadronic matter such as the modified Walecka model [163], various extensions of the Nambu–Jona-Lasinio model [177], the quark-meson coupling model [178], the chiral SU(3) model [179] etc In fact, the relativistic hard core repulsion should be important for any effective model in which the strongly interacting particles have reduced masses compared to their vacuum values because with lighter masses the large portion of particles becomes relativistic. Nevertheless, the relativistic hard core repulsion was, so far, not incorporated into these models due to the absence of the required formalism.

In addition, the studies of the Lorentz contracted rigid spheres required the investigation of the the Van der Waals approximation for the different hard core radii because the Lorentz contraction affects stronger the lighter particles. If the excluded volumes of particles are different (binary mixture), then the Van der Waals extrapolation is not unique at high densities and one has to carefully study its properties. In [155, 158] such an analysis was performed for the Lorentz-Berthelot binary mixture [159, 160] and for the extrapolation suggested recently [161]. It was shown [155, 158] that for the temperatures below 200 MeV and small baryonic densities both

extrapolations give the identical results for the experimentally observed particle ratios. Later on I showed that the alternative relativistic Van der Waals extrapolation [156] resolves the non-uniqueness of Van der Waals extrapolation for the systems with the multicomponent hard core repulsion, if one requires the causal behavior at high pressures.

This chapter is based on the works [154, 155, 156].

3.1. The Van der Waals EOS for the Lorentz Contracted Hard Spheres

The Van der Waals (VdW) excluded volume model has been used to describe hadron yields in relativistic nucleus–nucleus collisions (see e.g. [9, 136, 137, 165, 166, 66, 167, 168, 169, 170, 171] and references therein). This model treats the hadrons as hard-core spheres and, therefore, takes into account the hadron repulsion at short distances. In a relativistic situation one should, however, include the Lorentz contraction of the hard core-hadrons. This problem was discussed in the literature (see e.g. Ref. [151, 152]). In this section the cluster and virial expansions are generalized to velocity dependent inter-particle potentials. This extension is used to construct the VdW model for Lorentz contracted rigid spheres which may be used to simulate hadrons.

The canonical partition function for the gas of N classical (Boltzmann) particles takes the form

$$Z_N(V, T) = \frac{1}{N!} \int \prod_{i=1}^N \left[\frac{g \, d\mathbf{r}_i d\mathbf{k}_i}{(2\pi)^3} \exp\left(-\frac{\omega_i}{T}\right) \right] \exp\left(-\frac{U}{T}\right), \quad (3.1)$$

where V and T are the system volume and temperature, g is the number of internal degrees of freedom (degeneracy factor) of the particles, $\omega_i = (m^2 + \mathbf{k}_i^2)^{1/2}$ is the dispersion relation of free particles with mass m . The particle interactions described by the function U in Eq. (3.1) are given by the sum over pair potentials:

$$U = \sum_{1 \leq i < j \leq N} u_{ij}. \quad (3.2)$$

In contrast to the usual statistical mechanic treatment of the pair potentials, the u_{ij} are assumed to be both coordinate and momentum dependent $u_{ij} \equiv u(\mathbf{r}_i, \mathbf{k}_i; \mathbf{r}_j, \mathbf{k}_j)$. This generalization is necessary, if Lorentz contraction effects of hard spheres are to be taken into account. Introducing

the Mayer functions

$$f_{ij} = \left[\exp\left(-\frac{u_{ij}}{T}\right) - 1 \right], \quad (3.3)$$

Eq. (3.1) can be presented as

$$Z_N(V, T) = \frac{1}{N!} \int d\mathbf{x}_1 \dots d\mathbf{x}_N \exp\left(-\frac{\omega_1 + \dots + \omega_N}{T}\right) \prod_{1 \leq i < j \leq N} (1 + f_{ij}), \quad (3.4)$$

with the short notation $d\mathbf{x}_i \equiv g d\mathbf{r}_i d\mathbf{k}_i / (2\pi)^3$. Similarly to the standard procedure one can introduce the cluster integrals [162]

$$b_1 = \frac{1}{V} \int d\mathbf{x}_1 \exp\left(-\frac{\omega_1}{T}\right) = \frac{g T^3}{2\pi^2} K_2\left(\frac{m}{T}\right) \equiv \phi(T), \quad (3.5)$$

$$b_2 = \frac{1}{2!V} \int d\mathbf{x}_1 d\mathbf{x}_2 \exp\left(-\frac{\omega_1 + \omega_2}{T}\right) f_{12}, \quad (3.6)$$

$$b_3 = \frac{1}{3!V} \int d\mathbf{x}_1 d\mathbf{x}_2 d\mathbf{x}_3 \exp\left(-\frac{\omega_1 + \omega_2 + \omega_3}{T}\right) (f_{12}f_{13} + f_{12}f_{23} + f_{13}f_{23} + f_{12}f_{23}f_{13}), \quad (3.7)$$

...

and present the canonical partition function in the familiar form

$$Z_N(V, T) = \sum'_{\{m_l\}} \prod_{l=1}^N \frac{(V b_l)^{m_l}}{m_l!}, \quad (3.8)$$

where the summation in Eq. (3.8) is taken over all sets of non-negative integer numbers $\{m_l\}$ satisfying the condition

$$\sum_{l=1}^N l m_l = N. \quad (3.9)$$

Note, however, that the cluster integrals defined above are different from those used in standard statistical mechanics [162] as here nontrivial momentum integrations are included. Condition (3.9) makes the calculation of Z_N (3.8) rather complicated. This problem can be avoided in the grand canonical ensemble: the grand canonical partition function can be calculated explicitly ($z \equiv \exp(\mu/T)$):

$$\mathcal{Z}(V, T, \mu) \equiv \sum_{N=0}^{\infty} \exp\left(\frac{\mu N}{T}\right) Z_N(V, T) = \exp\left(V \sum_{l=1}^{\infty} b_l z^l\right). \quad (3.10)$$

In the thermodynamical limit the pressure p and particle number density n are calculated in the grand canonical ensemble in terms of the asymptotic values of the cluster integrals:

$$p = T \lim_{V \rightarrow \infty} \frac{\ln \mathcal{Z}}{V} = T \sum_{l=1}^{\infty} b_l z^l, \quad (3.11)$$

$$n = \lim_{V \rightarrow \infty} \frac{1}{V} \frac{\partial \ln \mathcal{Z}}{\partial z} = \sum_{l=1}^{\infty} l b_l z^l. \quad (3.12)$$

The virial expansion represents the pressure in terms of a series of particle number density and takes the form

$$p = T \sum_{l=1}^{\infty} a_l n^l. \quad (3.13)$$

Substituting p (3.11) and n (3.12) into Eq. (3.13) and equating the coefficients of each power of z , one finds the virial coefficients a_l in terms of the cluster integrals

$$a_1 = 1, \quad a_2 = -\frac{b_2}{b_1^2}, \quad a_3 = \frac{4b_2^2}{b_1^4} - \frac{2b_3}{b_1^3}, \quad \dots \quad (3.14)$$

Let me recall, first, the derivation of the standard VdW excluded volume model. Then it is extended by adding the Lorentz contraction of the moving particles. Keeping the first two terms of the virial expansion (3.13) the following result is obtained:

$$p(T, n) = Tn (1 + a_2 n). \quad (3.15)$$

It is valid for small particle densities (i.e. $n \ll 1/a_2$). The usual (momentum independent) hard core potential for spherical particles with radius r_o is $u_{ij} = u(|\mathbf{r}_i - \mathbf{r}_j|)$. Here the function $u(r)$ equals to 0 for $r > 2r_o$ and ∞ for $r < 2r_o$. The second cluster integral (3.6) can easily be calculated in this case:

$$b_2 = -\phi^2(T) \frac{16\pi}{3} r_o^3. \quad (3.16)$$

Therefore $a_2 = 4v_o$, where $v_o = 4\pi r_o^3/3$ is the particle hard core volume. The VdW excluded volume model is obtained as the extrapolation of Eq. (3.15) to large particle densities in the form

$$p(T, n) = \frac{Tn}{1 - a_2 n}. \quad (3.17)$$

For practical use the pressure is given as a function of T and μ independent variables, i.e. in the grand canonical ensemble. This is done by substituting $n = (\partial p / \partial \mu)_T$ into Eq. (3.17), which

then turns into a partial differential equation for the function $p(T, \mu)$. For the VdW model (3.17) the solution of this partial differential equation can be presented in the form of a transcendental equation

$$p(T, \mu) = T\phi(T)e^{\mu/T} \exp\left(-\frac{a_2 p}{T}\right) \equiv p_{id}(T, \mu - a_2 p). \quad (3.18)$$

Eq. (3.18) was first obtained in Ref. [163] using the Laplas transform technique. With $p(T, \mu)$ (the solution of Eq. (3.18)) the particle number density, entropy density and energy density are calculated as ($\nu = \mu - a_2 p(T, \mu)$, $a_2 = 4v_o$):

$$n(T, \mu) \equiv \left(\frac{\partial p(T, \mu)}{\partial \mu}\right)_T = \frac{n_{id}(T, \nu)}{1 + a_2 n_{id}(T, \nu)}, \quad (3.19)$$

$$s(T, \mu) \equiv \left(\frac{\partial p(T, \mu)}{\partial T}\right)_\mu = \frac{s_{id}(T, \nu)}{1 + a_2 n_{id}(T, \nu)}, \quad (3.20)$$

$$\epsilon(T, \mu) \equiv Ts - p + \mu n = \frac{\epsilon_{id}(T, \nu)}{1 + a_2 n_{id}(T, \nu)}. \quad (3.21)$$

Here the superscripts *id* in the thermodynamical functions (3.18–3.21) indicate those of the ideal gas.

The excluded volume effect accounts for the blocked volume of two spheres when they touch each other. If hard-sphere particles move with relativistic velocities it is necessary to include their Lorentz contraction in the rest frame of the fluid. The model suggested in Ref. [152] is not satisfactory: the parameter $a_2 = 4v_o$ of the VdW excluded volume model is confused there with the proper volume of an individual particle – the contraction effect is introduced for the proper volume of each particle. In order to get the correct result it is necessary to account for the excluded volume of two Lorentz contracted spheres.

Let \mathbf{r}_i and \mathbf{r}_j be the coordinates of the i -th and j -th particle, respectively, and \mathbf{k}_i and \mathbf{k}_j be their momenta, $\hat{\mathbf{r}}_{ij}$ denotes the unit vector $\hat{\mathbf{r}}_{ij} = \mathbf{r}_{ij}/|\mathbf{r}_{ij}|$ ($\mathbf{r}_{ij} = |\mathbf{r}_i - \mathbf{r}_j|$). Then for a given set of vectors ($\hat{\mathbf{r}}_{ij}, \mathbf{k}_i, \mathbf{k}_j$) for the Lorentz contracted rigid spheres of radius r_o there exists the minimum distance between their centers $r_{ij}(\hat{\mathbf{r}}_{ij}; \mathbf{k}_i, \mathbf{k}_j) = \min|\mathbf{r}_{ij}|$. The dependence of the potentials u_{ij} on the coordinates $\mathbf{r}_i, \mathbf{r}_j$ and momenta $\mathbf{k}_i, \mathbf{k}_j$ can be given in terms of the minimal distance as follows

$$u(\mathbf{r}_i, \mathbf{k}_i; \mathbf{r}_j, \mathbf{k}_j) = \begin{cases} 0, & |\mathbf{r}_i - \mathbf{r}_j| > r_{ij}(\hat{\mathbf{r}}_{ij}; \mathbf{k}_i, \mathbf{k}_j), \\ \infty, & |\mathbf{r}_i - \mathbf{r}_j| \leq r_{ij}(\hat{\mathbf{r}}_{ij}; \mathbf{k}_i, \mathbf{k}_j). \end{cases} \quad (3.22)$$

The general approach to the cluster- and virial expansions described above is valid for this momentum dependent potential, and it leads to Eqs. (3.17,3.18) with

$$a_2(T) = \frac{1}{2\phi^2(T)} \int \frac{d\mathbf{k}_1 d\mathbf{k}_2}{(2\pi)^6} \exp\left(-\frac{\omega_1 + \omega_2}{T}\right) \int d\mathbf{r}_{12} \Theta(r_{12}(\hat{\mathbf{r}}_{12}; \mathbf{k}_1, \mathbf{k}_2) - |\mathbf{r}_{12}|) . \quad (3.23)$$

The new feature is the temperature dependence of the excluded volume a_2 (3.23) which is due to the Lorentz contraction of the rigid spheres. The pressure and particle number density are still given by Eqs. (3.18,3.19), but with temperature dependent $a_2(T)$ (3.23). However, Eqs. (3.20, 3.21) are now modified, e.g.

$$\epsilon(T, \mu) = \frac{\epsilon_{id}(T, \nu) - p^2 da_2(T)/dT}{1 + a_2 n_{id}(T, \nu)} . \quad (3.24)$$

In contrast to Eq. (3.21) the energy density (3.24) contains the extra term which appears also in the entropy density. The excluded volume $a_2(T)$ (3.23) is always smaller than $4v_o$. It has been proven rigorously that $a_2(T)$ is a monotonously decreasing function of T and, therefore, the additional term in Eq. (3.24) is always positive. Let us introduce the notation

$$a_2(T) = 4v_o f(T) . \quad (3.25)$$

The function $f(T)$ depends on the T/m ratio. It can be calculated numerically and its behavior is shown in Fig. 3.1. The simple analytical formula

$$f(T) = c + (1 - c) \frac{\rho_s(T)}{\phi(T)} \quad (3.26)$$

with

$$c = \left(1 + \frac{74}{9\pi}\right)^{-1} , \quad \rho_s = \frac{g}{(2\pi)^3} \int d\mathbf{k} \frac{m}{\omega} \exp\left(-\frac{\omega}{T}\right) ,$$

is found to be valid with an accuracy of a few percents for all temperatures. The asymptotic behavior of $f(T)$ is the following: $1 - O(T/m)$ at $T \ll m$ and $c + O(m/T)$ at $T \gg m$.

If one assumes that all types of hadrons have at rest the same hard core radius then the Lorentz contraction effect leads to different VdW excluded volumes for moving particles with different masses: for light particles (e.g. pions) the excluded volume (at given T) is smaller than that for heavy ones. Fig. 3.1 shows that at $T \cong 150$ MeV the value of a_2 in the nucleon gas ($m \cong 939$ MeV) decreases by 10% in comparison to its nonrelativistic value $4v_o$, whereas for pions ($m \cong 140$ MeV)

a_2 shrinks at the same T by almost a factor 2. This is simply because light particles are more relativistic than heavy ones at given temperature typical for high energy nuclear collisions, in which $T = 120 \div 170$ MeV.

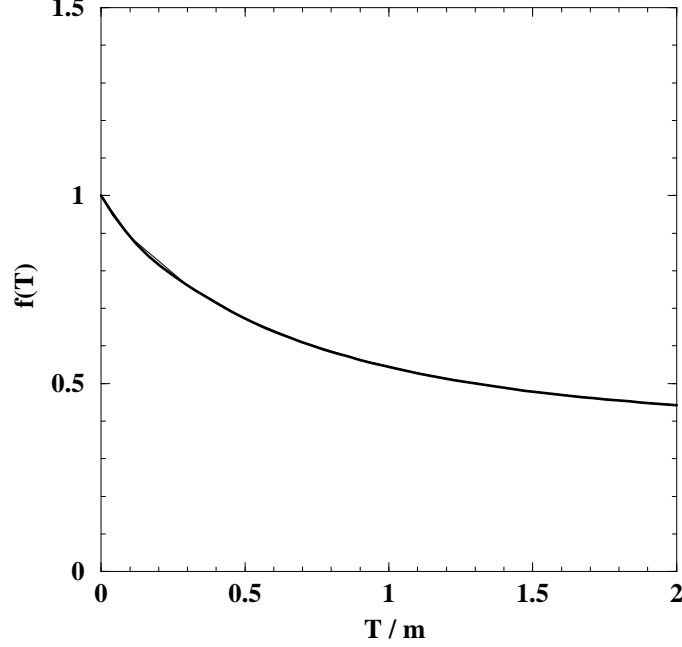


Figure 3.1. $f(T)$ as the function of the temperature-to-mass ratio. For heavy particles (e.g., nucleons $m \gg T$) the volume reduction is just a few per cents, whereas for pions ($m \approx T$) it is about 50%.

As an example, Fig. 3.2 shows the EOS of the pion gas ($\mu = 0, g = 3$) with $r_o = 0.5$ fm. The particle number density, shown in the left panel of Fig. 3.2, is calculated according to Eq. (3.19) for three different models: the ideal pion gas ($a_2 = 0$), the VdW model with constant excluded volume ($a_2 = 4v_o$) and the VdW model with Lorentz contraction ($a_2(T)$ is given by Eq. (3.23)). It can be seen from the left panel of Fig. 3.2 that at low T the pion density is small and excluded volume corrections are unimportant. Therefore, all three models are similar. The situation changes with increasing T : the suppression due to the excluded volume effects are large and different for $a_2 = 4v_o$ and $a_2(T)$ (3.23). The ratios of particle number densities and energy densities of the pion gas for two versions of the VdW model ($a_2 = 4v_o$ and $a_2(T)$ (3.23)) are shown in the right

panel of Fig. 3.2 as functions of the temperature. From this panel one can observe the deviations between these two models. These deviations increase with temperature. They are larger for the energy density due to the additional positive term in Eq. (3.24).

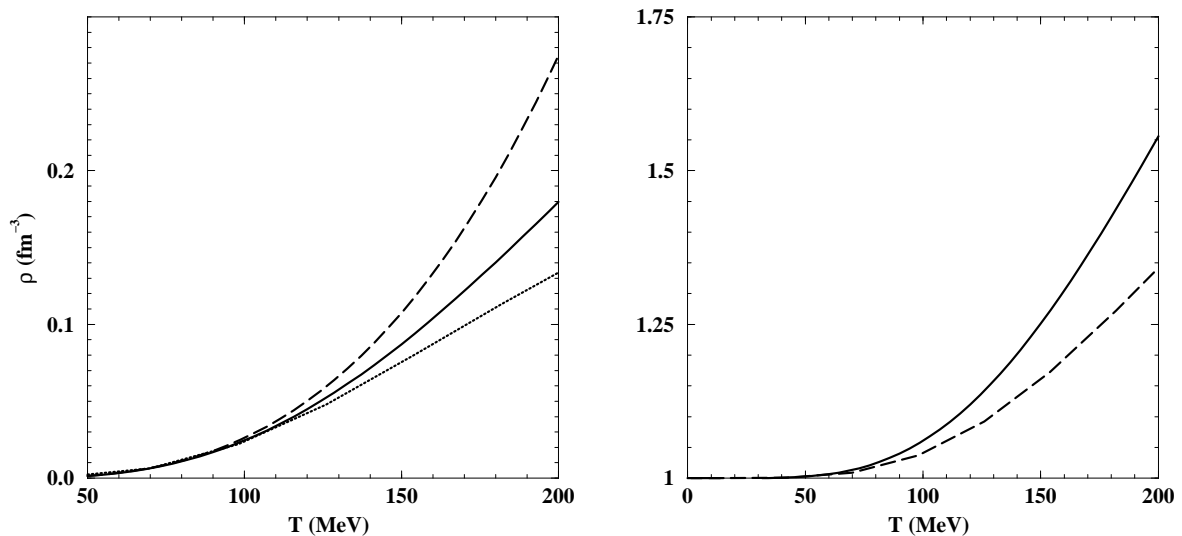


Figure 3.2. **Left panel:** The particle number density for three models of the pion gas ($\mu = 0, g = 3$): the solid line corresponds to the VdW model of the Lorentz contracted spheres ($r_o = 0.5$ fm), the dashed one corresponds to the ideal gas of point-like particles, and the dotted one corresponds to the VdW model without Lorentz contraction for the spheres of a constant radius 0.5 fm.

Right panel: The dashed line shows the ratio of the particle number densities of the pion gas ($g = 3, \mu = 0, r_o = 0.5$ fm): the VdW model with Lorentz contraction divided by the VdW model without Lorentz contraction. The solid line shows a similar ratio for the energy densities.

Thus, the traditional cluster and virial expansions can be consistently generalized to momentum dependent pair potentials. Hard-core potentials with Lorentz contraction effects lead to a VdW model with a temperature dependent excluded volume $a_2(T)$ (3.23). For light particles the effect of Lorentz contraction is, evidently, stronger than for heavy ones. Note that smaller values of the pion hard core radius r_π were introduced in Refs. [164, 165] within the standard VdW excluded volume model to fit hadron yield data better. The smaller value of the pion excluded volume

appears as a consequence of stronger Lorentz contraction for light particles.

3.2. Hadronic Binary Mixtures in Canonical Ensemble

As I showed in preceding section the Lorentz contraction affects lighter particles stronger. Therefore, to study the experimental particle yields it is necessary to consider the VdW description for the particles with different hard core radii. Since the VdW approximation is an extension of the low density expansion to high densities, the procedure is not unique as long as there is no constraints on the high density behavior.

The qualitative picture for the gas with the multicomponent hard core repulsion is as follows: as particle species with smaller hard core radii are closer to the ideal case, their particle densities are suppressed less. Consequently, their yield ratios to particle species with larger hard core radii are enhanced. This fact has been used in recent efforts [165] to explain the experimentally observed pion abundance for AGS and SPS data [172] by introducing a smaller hard core radius for pions R_π than for all other hadrons R_o . However, the resulting values are quite large, $R_o = 0.8$ fm and $R_\pi = 0.62$ fm. At the same time in Ref. [137] a reasonable fit of SPS data has been obtained, but for a distinctly smaller pair of hard core radii.

The excluded volume models used in [165, 137], however, are not correct in the case of different hard core radii. As will be shown below, these models correspond to a system where the components are separated from each other by a mobile wall and hence cannot mix.

A more realistic approach requires a two-component partition function including a term for the repulsion between particles of different hard core radii. In the case of two components, however, the VdW approximation is not uniquely defined. The simplest possibility yields the Lorentz-Berthelot mixture, which was originally postulated by Van der Waals for binary mixtures, see Refs. [159, 160]. Another VdW approximation was recently proposed in Ref. [161]. These two formulations contain a suppression of particle densities similar to the one-component VdW gas, which is *reduced to different extend* for each formulation. In this section I will study and apply both of these formulations.

There is yet another cause for a reduced excluded volume suppression. Particles are considered

to be rigid spheres in the usual VdW model. As was shown above, at high energies as achieved in nuclear collisions, however, relativistic effects cannot be neglected [154]. Within the logic of the VdW model it is absolutely necessary to take into account the Lorentz contraction of the spheres. Below I will use an approach developed in Ref. [156] providing approximative formulae for relativistic excluded volumes: naturally, they decrease with rising temperature, and the effect is stronger for lighter particles. At high temperatures, consequently, it is not possible to use a *one-component* VdW description (i. e. a *common* excluded volume for *all* particle species) for a system of species with various masses. Since different masses cause different reductions of the excluded volumes at a given temperature, a *multi-component* VdW description is required.

To illustrate the influence of different excluded volumes in what follows I will restrict myself to the simplest 'multi-component' case, the two-component case. The crucial extension from the one- to the two-component case is to include the repulsion between particles of two *different* hard core radii. As it will be illustrated, a generalization to the multi-component case is straightforward and will yield no essential differences [158].

In this section a derivation of the one-component canonical partition function with (constant) excluded volumes is presented. The generalization to the two-component case is made and two possible VdW approximations are analysed: the Lorentz-Berthelot mixture [160] and the recently proposed approximation of Ref. [161].

First it is necessary to derive the canonical partition function (CPF) for the one-component VdW gas by estimating the excluded volumes of particle clusters. Then this procedure will be generalised to the two-component case.

Here I use the Boltzmann statistics to avoid the complications due to quantum statistics. The deviations from quantum statistics are negligible as long as the density over temperature ratio is small. This is the case for the hadron gas at temperatures and densities typical for heavy ion collisions, see e. g. Ref. [165].

Note that here the term VdW is used for the van der Waals excluded volume model, not for the general van der Waals model which includes attraction.

3.2.1. The Van der Waals Excluded Volume Model.

Let me consider N identical particles with temperature T kept in a sufficiently large volume V , so that finite volume effects can be neglected. The partition function of this system reads

$$Z(T, V, N) = \frac{\phi^N}{N!} \int_{V^N} d^3x_1 \cdots d^3x_N \exp \left[-\frac{U_N}{T} \right]. \quad (3.27)$$

Here, $\phi \equiv \phi(T; m, g)$ denotes the momentum integral of the one particle partition

$$\phi(T; m, g) = \frac{g}{2\pi^2} \int_0^\infty dk k^2 \exp \left[-\frac{E(k)}{T} \right], \quad (3.28)$$

where $E(k) \equiv \sqrt{k^2 + m^2}$ is the relativistic energy and $g = (2S + 1)(2I + 1)$ counts the spin and isospin degeneracy. For a hard core potential U_N of N spherical particles with radii R the potential term in Eq. (3.27) reads

$$\exp \left[-\frac{U_N}{T} \right] = \prod_{i < j \leq N} \theta(|\vec{x}_{ij}| - 2R), \quad (3.29)$$

where \vec{x}_{ij} denotes the relative position vector connecting the centers of the i -th and j -th particle.

Hence one can write

$$\begin{aligned} \int_{V^N} d^3x_1 \cdots d^3x_N \exp \left[-\frac{U_N}{T} \right] &= \int_{V^N} d^3x_1 \cdots d^3x_N \prod_{1 \leq i < j \leq N} \theta(|\vec{x}_{ij}| - 2R) \\ &= \int_V d^3x_1 \int_V d^3x_2 \theta(|\vec{x}_{12}| - 2R) \cdots \int_V d^3x_N \prod_{1 \leq i \leq N-1} \theta(|\vec{x}_{i,N}| - 2R) \\ &\equiv \int_V d^3x_1 \int_{\{\vec{x}_1\}} d^3x_2 \cdots \int_{\{\vec{x}_1 \dots \vec{x}_{N-1}\}} d^3x_N. \end{aligned} \quad (3.30)$$

Here, $\int_{\{\vec{x}_1 \dots \vec{x}_j\}} d^3x_{j+1}$ denotes the available volume for \vec{x}_{j+1} , which is the center of the particle with number $j + 1$, if the j other particles are configurated as $\{\vec{x}_1 \dots \vec{x}_j\}$. I will show now that this volume is estimated by $\int_{\{\vec{x}_1 \dots \vec{x}_j\}} d^3x_{j+1} \geq (V - 2bj)$, where $2b \equiv \frac{4\pi}{3}(2R)^3$ is the excluded volume of an isolated particle seen by a second one. Then, $2bj$ estimates the total volume which is excluded by all particle clusters occuring in the configuration $\{\vec{x}_1 \dots \vec{x}_j\}$.

It is sufficient to prove that the excluded volume of a cluster of k particles is less than the excluded volume of k isolated particles. A group of k particles forms a k -cluster, if for any of these particles there is a neighboring particle of this group at a distance less than $4R$. The *exact* excluded volume of a k -cluster, $v_{(k)}$, obviously depends on the configuration of the k particles. If one considers two isolated particles, i. e. two 1-clusters, and reduces their distance below $4R$, their

excluded volumes will overlap. They form now a 2-cluster with the excluded volume $v_{(2)} = 4b - 1v_{\text{ov}}$, where v_{ov} denotes the overlap volume.

Evidently, one can construct any k -cluster by attaching additional particles and calculate its excluded volume by subtracting each occurring overlap volume from $2bk$. It follows that $v_{(k)} < 2bk$ is valid for any k -cluster, and this inequality leads to the above estimate. Obviously, its accuracy improves with the diluteness of the gas.

Using these considerations one can approximate the r. h. s. of Eq. (3.30): starting with $j+1 = N$ one gradually replaces all integrals $\int_{\{\vec{x}_1 \dots \vec{x}_j\}} d^3x_{j+1}$ by $(V - 2bj)$. One has to proceed from the right to the left, because only the respective rightmost of these integrals can be estimated in the described way. Hence one finds

$$Z(T, V, N) \geq \frac{\phi^N}{N!} \prod_{j=0}^{N-1} (V - 2bj) . \quad (3.31)$$

In this treatment the VdW approximation consists of two assumptions concerning Eq. (3.31). Firstly, the product can be approximated by

$$\prod_{j=0}^{N-1} \left(1 - \frac{2b}{V} j\right) \cong \exp \left[-\sum_{j=0}^{N-1} \frac{2b}{V} j\right] \exp \left[-\frac{b}{V} (N-1)N\right] \cong \left(1 - \frac{b}{V} N\right)^N , \quad (3.32)$$

where $\exp[-x] \cong (1-x)$ is used for dilute systems, i. e. for low densities $2bN/V \ll 1$. The second assumption is to take the equality instead of the inequality in Eq. (3.31). Then the CPF takes the VdW form,

$$Z_{\text{VdW}}(T, V, N) = \frac{\phi^N}{N!} (V - bN)^N . \quad (3.33)$$

As usual, the VdW CPF is obtained as an approximation for dilute systems, but when used for high densities it should be considered as an *extrapolation*.

Finally, one obtains the well-known VdW pressure formula from the thermodynamical identity $p(T, V, N) \equiv T \partial \ln[Z(T, V, N)] / \partial V$,

$$p_{\text{VdW}}(T, V, N) = \frac{TN}{V - bN} , \quad (3.34)$$

using the logarithm of the Stirling formula.

Now let me briefly investigate a system of volume V containing two components with *different* hard core radii R_1 and R_2 which are separated by a wall and occupy the volume fractions xV and

$(1-x)V$, respectively. According to Eq. (3.34) their pressures read

$$p_{\text{vdW}}(T, xV, N_1) = \frac{T N_1}{xV - N_1 b_{11}}, \quad (3.35)$$

$$p_{\text{vdW}}(T, (1-x)V, N_2) = \frac{T N_2}{(1-x)V - N_2 b_{22}}, \quad (3.36)$$

where the particle numbers N_1, N_2 and the excluded volumes $b_{11} = \frac{16\pi}{3} R_1^3$, $b_{22} = \frac{16\pi}{3} R_2^3$ correspond to the components 1 and 2, respectively.

If the separating wall is mobile, the pressures (3.35) and (3.36) must be equal. In this case the fraction x can be eliminated and one obtains the common pressure of the whole system

$$p_{\text{vdW}}(T, xV, N_1) = p_{\text{vdW}}(T, (1-x)V, N_2) = p^{\text{sp}}(T, V, N_1, N_2) \equiv \frac{T(N_1 + N_2)}{V - N_1 b_{11} - N_2 b_{22}}. \quad (3.37)$$

Since the components are separated in this model system it will be referred to as the *separated* model [158].

The pressure formula (3.37) corresponds to the Boltzmann approximation of the commonly used two-component VdW models of Refs. [165, 137]. It is evident that p^{sp} (3.37) does not describe the general two-component situation without a separating wall. Therefore, it is necessary to find a more realistic model, i. e. an approximation from a *two-component* partition function. This will be done in the following.

3.2.2. Generalization to the Two-component Case. Recall the simple estimate (3.30–3.33), which gives a physically transparent derivation of the one-component CPF in the VdW approximation. Let us use it now for a *two-component* gas of spherical particles with radii R_1 and R_2 , respectively. It is important to mention that each component may consist of several particle species as long as these species have one common hard core radius, i. e. the number of necessary VdW components is determined by the number of different excluded volume terms b_{qq} . In the case of two radii the potential term (3.29) becomes

$$\exp\left[-\frac{U_{N_1+N_2}}{T}\right] = \prod_{i < j \leq N_1} \theta(|\vec{x}_{ij}| - 2R_1) \times \prod_{k < \ell \leq N_2} \theta(|\vec{x}_{k\ell}| - 2R_2) \times \prod_{\substack{m \leq N_1 \\ n \leq N_2}} \theta(|\vec{x}_{mn}| - (R_1 + R_2)). \quad (3.38)$$

The integration is carried out in the way described above: e. g. firstly over the coordinates of the particles of the second component, then over those of the first component. For the estimation of

the excluded volume of a k -cluster now *two different* particle sizes have to be considered. One obtains

$$\begin{aligned} Z(T, V, N_1, N_2) &\geq \frac{\phi_1^{N_1}}{N_1!} \frac{\phi_2^{N_2}}{N_2!} \left\{ \prod_{i=0}^{N_1-1} (V - 2b_{11} i) \right\} \left\{ \prod_{j=0}^{N_2-1} (V - 2b_{12} N_1 - 2b_{22} j) \right\} \\ &\cong \frac{\phi_1^{N_1}}{N_1!} \frac{\phi_2^{N_2}}{N_2!} V^{N_1+N_2} \exp \left[-\frac{N_1^2 b_{11} + 2N_1 N_2 b_{12} + N_2^2 b_{22}}{V} \right], \end{aligned} \quad (3.39)$$

where it is $\phi_q \equiv \phi(T; m_q, g_q)$, and $2b_{pq} \equiv \frac{4\pi}{3} (R_p + R_q)^3$ denotes the excluded volume of a particle of the component p seen by a particle of the component q ($p, q = 1, 2$ hereafter). Approximating the above exponent by $\exp[-x] \cong (1-x)$ yields the *simplest* possibility of a VdW approximation for the *two-component* CPF,

$$Z_{\text{VdW}}^{\text{nl}}(T, V, N_1, N_2) \equiv \frac{\phi_1^{N_1}}{N_1!} \frac{\phi_2^{N_2}}{N_2!} \left(V - \frac{N_1^2 b_{11} + 2N_1 N_2 b_{12} + N_2^2 b_{22}}{N_1 + N_2} \right)^{N_1+N_2} \quad (3.40)$$

$$= \frac{\phi_1^{N_1}}{N_1!} \frac{\phi_2^{N_2}}{N_2!} \left(V - N_1 b_{11} - N_2 b_{22} + \frac{N_1 N_2}{N_1 + N_2} D \right)^{N_1+N_2}, \quad (3.41)$$

where the non-negative coefficient D is given by

$$D \equiv b_{11} + b_{22} - 2b_{12}. \quad (3.42)$$

This approximation will be called the *non-linear* approximation as the volume correction in (3.41) contains non-linear terms in N_1, N_2 . The corresponding pressure follows from the thermodynamical identity,

$$p^{\text{nl}}(T, V, N_1, N_2) = p_1^{\text{nl}} + p_2^{\text{nl}} \equiv \frac{T(N_1 + N_2)}{V - N_1 b_{11} - N_2 b_{22} + \frac{N_1 N_2}{N_1 + N_2} D}. \quad (3.43)$$

This canonical formula corresponds to the Lorentz-Berthelot mixture (without attraction terms) known from the theory of fluids [160]. It was postulated by van der Waals [159] and studied as well by Lorentz and Berthelot [160].

The crucial step from the one- to the two-component gas is to include b_{pq} terms ($p \neq q$) additionally to the $b_{qq} \equiv b|_{R=R_q}$ terms. For the multi-component gas no further essential extension is necessary. Consequently, the generalization of the above procedure to the multi-component case, i. e. an arbitrary number of different hard core radii, is straightforward [158].

In Ref. [161] a *more involved* approximation has been suggested for the two-component VdW gas. This follows from splitting the exponent in the CPF (3.39) by introducing *two generalised*

excluded volume terms \tilde{b}_{12} and \tilde{b}_{21} (instead of a *single* and symmetric term $2b_{12}$) for the mixed case,

$$Z(T, V, N_1, N_2) \cong \frac{\phi_1^{N_1}}{N_1!} \frac{\phi_2^{N_2}}{N_2!} V^{N_1+N_2} \exp \left[-\frac{N_1^2 b_{11} + N_1 N_2 (\tilde{b}_{12} + \tilde{b}_{21}) + N_2^2 b_{22}}{V} \right], \quad (3.44)$$

which leads to an alternative two-component VdW CPF,

$$Z_{\text{VdW}}^{\text{lin}}(T, V, N_1, N_2) \equiv \frac{\phi_1^{N_1}}{N_1!} (V - N_1 b_{11} - N_2 \tilde{b}_{21})^{N_1} \frac{\phi_2^{N_2}}{N_2!} (V - N_2 b_{22} - N_1 \tilde{b}_{12})^{N_2}. \quad (3.45)$$

Since the particle numbers N_1, N_2 appear solely linearly in the volume corrections, these formulae will be referred to as the *linear* approximation. In this approximation one obtains [161] for the pressure

$$p^{\text{lin}}(T, V, N_1, N_2) = p_1^{\text{lin}} + p_2^{\text{lin}} \equiv \frac{T N_1}{V - N_1 b_{11} - N_2 \tilde{b}_{21}} + \frac{T N_2}{V - N_2 b_{22} - N_1 \tilde{b}_{12}}. \quad (3.46)$$

The choice of the generalised excluded volume terms \tilde{b}_{pq} is not unique in the sense that all choices which satisfy the basic constraint $\tilde{b}_{12} + \tilde{b}_{21} = 2b_{12}$ are consistent with the second order virial expansion [161]. Therefore, additional conditions are necessary to fix these generalised excluded volumes. In Ref. [161] they were chosen as

$$\tilde{b}_{12} \equiv b_{11} \frac{2b_{12}}{b_{11} + b_{22}}, \quad \tilde{b}_{21} \equiv b_{22} \frac{2b_{12}}{b_{11} + b_{22}}. \quad (3.47)$$

For this choice, the linear approximation reproduces a traditional VdW gas behavior, i.e. *one-component-like*, in the two limits $R_2 = R_1$ and $R_2 = 0$ as readily checked. The factor $2b_{12}/(b_{11} + b_{22}) = 1 - D/(b_{11} + b_{22})$ is always smaller than unity for $R_1 \neq R_2$, consequently, the \tilde{b}_{pq} terms are smaller than the corresponding terms b_{pp} . Note that there are many possible choices for \tilde{b}_{12} and \tilde{b}_{21} , e.g. additionally dependent on the particle numbers N_1 and N_2 , whereas the non-linear approximation (3.40) contains no such additional parameters.

The formulae of the linear approximation are generally valid for *any* choice of \tilde{b}_{12} and \tilde{b}_{21} satisfying the constraint $\tilde{b}_{12} + \tilde{b}_{21} = 2b_{12}$. In the following, however, I will restrict this study to the special choice given in the Eqs. (3.47). The canonical (and grand canonical) formulae for the multi-component case are given in Ref. [161].

3.2.3. Comparison of Two-component VdW Approximations. As the

VdW approximation is a low density approximation it is evident that the linear and non-linear formulae are equivalent for such densities. Deviations, however, occur at high densities, where any VdW approximation generally becomes inadequate.

The differences between both approximations result from the fact that the linear pressure (3.46) has two poles, $v_1^{\text{lin}} = V$ and $v_2^{\text{lin}} = V$, whereas the non-linear pressure (3.43) has solely one pole, $v^{\text{nl}} = V$. For constant volume V these poles define limiting densities, e. g. $\hat{n}_1 = \max(N_1/V)$ as functions of $n_2 = N_2/V$,

$$v_q^{\text{lin}}(N_1, N_2) = V \quad \rightsquigarrow \quad \hat{n}_1(n_2) \equiv \hat{n}_{1,q}^{\text{lin}}(n_2) \quad (3.48)$$

$$\text{or } v^{\text{nl}}(N_1, N_2) = V \quad \rightsquigarrow \quad \hat{n}_1(n_2) \equiv \hat{n}_1^{\text{nl}}(n_2), \quad (3.49)$$

which represent the domains of the two pressure formulae in the n_2 - n_1 -plane. The explicit fomulae are discussed in App. 6.4. .

In Fig. 3.3(a) an example of these limiting densities is shown for $R_2/R_1 = 0.4$. It is clearly seen that the non-linear domain (below the solid line) is larger than the linear domain (below both dashed lines), which is generally the case for $R_2 \neq R_1$. Especially for $R_2 \ll R_1$ the non-linear domain is distinctly larger for high densities of the large component, $n_1 b_{11} > n_2 b_{22}$, whereas both domains are similar for high densities of the small component, $n_2 b_{22} > n_1 b_{11}$.

The linear approximation is constructed in traditional VdW spirit; the densities n_q^{lin} achieved in this approximation are below the maximum density of the corresponding *one-component* VdW gas $\max(n_q^{\text{oc}}) = 1/b_{qq}$, which is defined by the pole of $p_q^{\text{oc}} \equiv p_{\text{VdW}}(T, V, N_q; b_{qq})$ from Eq. (3.34).

In the non-linear approximation, however, the possible densities of the larger particles n_1^{nl} can exceed $1/b_{11}$ due to the occurrence of negative partial derivatives of the pressure, $\partial p^{\text{nl}}/\partial N_2 < 0$. In this context it is necessary to state that this behavior does not lead to a thermodynamical instability of the non-linear approximation as proven in App. 6.4. . The linear approximation shows no such behavior, it is always $\partial p^{\text{lin}}/\partial N_1 > 0$ and $\partial p^{\text{lin}}/\partial N_2 > 0$.

The condition $\partial p^{\text{nl}}/\partial N_2 = 0$ defines the boundary $\hat{n}_1^{\text{nl, bd}}(n_2)$ of the region of negative partial derivatives of the non-linear pressure. In Fig. 3.3(a) this boundary is shown by the dotted line for $R_2/R_1 = 0.4$; the values of $\partial p^{\text{nl}}/\partial N_2$ are negative above this line.

Densities larger than $n_1^{\text{nl}} = 1/b_{11}$ can only occur, if R_2 is smaller than a critical radius,

$$R_2 < R_{2,\text{crit}}(R_1) = (\sqrt[3]{4} - 1) R_1 \approx R_1/1.7. \quad (3.50)$$

Then, the boundary $\hat{n}_1^{\text{nl,bd}}(n_2)$ starts inside the non-linear domain, see App. 6.4. for details.

The reason for this behavior is the ratio of the amounts of small and large particles. There are much more small than large particles in the system for densities n_1, n_2 along the boundary $\hat{n}_1^{\text{nl,bd}}(n_2)$ at high densities n_1 : here, the fewer large particles are surrounded by many small particles. Therefore, the excluded volume interaction of the large particles in the non-linear pressure (3.43) is governed not by the simple term b_{11} but by the mixed term b_{12} , which is distinctly smaller than b_{11} for $R_2 \ll R_1$. The maximum density achieved in the non-linear approximation $\max(\hat{n}_1^{\text{nl}}) = 4/b_{11}$ is obtained for $R_2 \rightarrow 0$ and $N_2 \gg N_1$, i.e. these formulae go far *beyond* the traditional VdW results in the corresponding situation.

An example of pressure profiles for p_1^{lin} , p_2^{lin} and p^{nl} for $n_1 b_{11} = 0.9$ is shown in Fig. 3.3 (b), where it is $R_2/R_1 = 0.4$ as in Fig. 3.3 (a). The non-linear pressure (solid line) firstly decreases as the densities n_1, n_2 correspond to the region of negative partial derivatives, see Fig. 3.3 (a). The partial pressures of the linear approximation are shown by dashed lines. The non-linear domain is seen to be larger since it is one of the linear partial pressures which diverges first for increasing n_2 .

I conclude that the linear and non-linear approximation show a drastically different behavior for high values of the large component's density n_1 . In the linear approximation (3.46) the possible density values are below $1/b_{11}$ and $1/b_{22}$, respectively, and the derivatives $\partial p^{\text{lin}}/\partial N_q$ are always positive. Whereas in the non-linear approximation (3.43) higher densities $n_1 > 1/b_{11}$ are possible due to the occurrence of negative derivatives $\partial p^{\text{nl}}/\partial N_2 < 0$. This may be considered as pathological – or used as an advantage to describe special situations, e.g. densities $1/b_{11} < n_1 < \hat{n}_1^{\text{nl}}$ for $R_2 \ll R_1$ (see App. 6.4.).

However, the use of any VdW approximation is in principle problematic for densities near $1/b_{qq}$. For low densities the non-linear and linear approximation are practically equivalent, and the non-linear approximation is preferable since the formulae are essentially simpler.

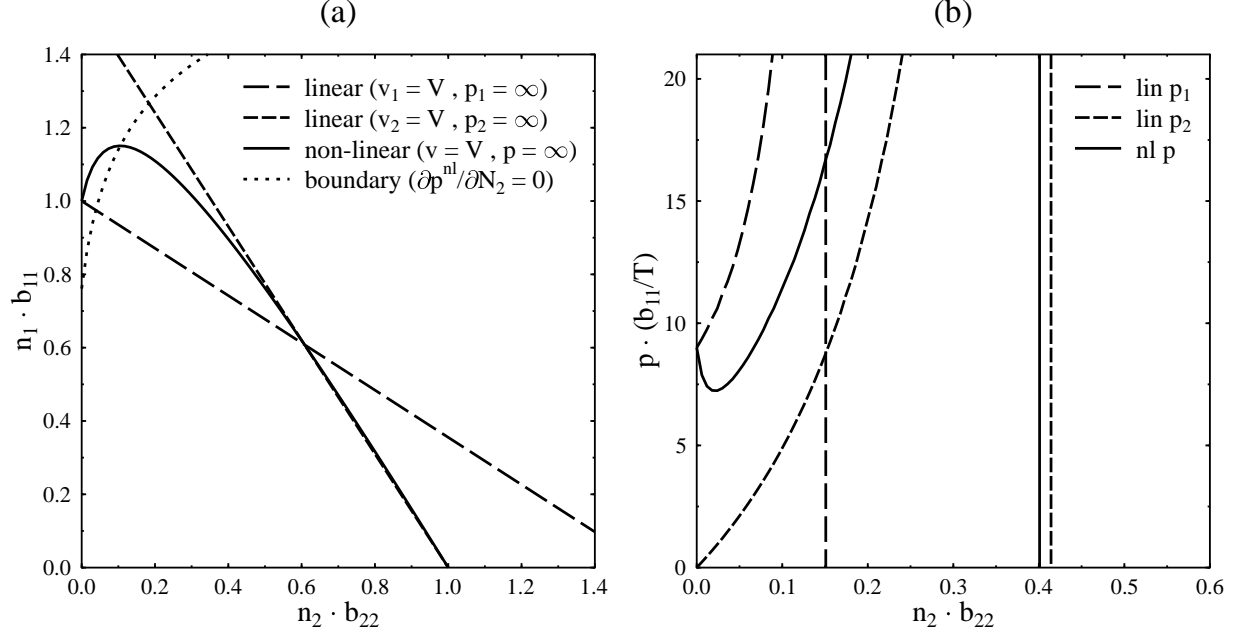


Figure 3.3. (a) Domains of the linear and non-linear approximation for $R_2/R_1 = 0.4$: limiting densities \hat{n}_1 (isobars for $p_q(n_1, n_2) = \infty$) and the lower boundary $\hat{n}_1^{\text{nl, bd}}$ to the region of negative partial derivatives of the non-linear pressure. The dashed lines correspond to the two poles of the linear pressure, and the solid line corresponds to the pole of the non-linear pressure. For given n_2 the possible densities n_1^{lin} are below both dashed lines, whereas the possible densities n_1^{nl} are below the solid line. Negative derivatives $\partial p^{\text{nl}}/\partial N_2 < 0$ occur only above the dotted line.

(b) Pressure profiles in dimensionless units for $R_2/R_1 = 0.4$ as in (a) at fixed $n_1 b_{11} = 0.9$. The dashed lines show the partial pressures of the linear approximation p_1^{lin} and p_2^{lin} , while the solid line shows the total pressure of the non-linear approximation p^{nl} with initial decrease due to negative $\partial p^{\text{nl}}/\partial N_2$.

3.3. Grand Canonical Treatment of Binary Mixtures

Let me now turn to the GCE. The grand canonical partition function is built using the CPF,

$$\mathcal{Z}(T, V, \mu_1, \mu_2) = \sum_{N_1=0}^{\infty} \sum_{N_2=0}^{\infty} \exp\left[\frac{\mu_1 N_1 + \mu_2 N_2}{T}\right] Z(T, V, N_1, N_2), \quad (3.51)$$

whereas the chemical potentials μ_1 and μ_2 correspond to the components 1 and 2, respectively. For the VdW CPF (3.41) or (3.45) there are limiting particle numbers $\hat{N}_1(N_2)$ or $\hat{N}_2(N_1)$, where each

CPF becomes zero. For this reason the above sum contains only a finite number of terms. Then it can be shown that in the thermodynamical limit (i. e. in the limit $V \rightarrow \infty$ for $N_q/V = \text{const.}$) the grand canonical pressure $p(T, \mu_1, \mu_2) \equiv T \ln[\mathcal{Z}(T, V, \mu_1, \mu_2)]/V$ depends only on the *maximum term* of the double sum (3.51), where $N_1 = \mathcal{N}_1$ and $N_2 = \mathcal{N}_2$. One obtains

$$p(T, \mu_1, \mu_2) = \lim_{V \rightarrow \infty} \frac{T}{V} \ln \left[\exp \left[\frac{\mu_1 \mathcal{N}_1 + \mu_2 \mathcal{N}_2}{T} \right] Z(T, V, \mathcal{N}_1, \mathcal{N}_2) \right], \quad (3.52)$$

wheras \mathcal{N}_1 and \mathcal{N}_2 are the *average* particle numbers.

3.3.1. The Two VdW Approximations. For the non-linear VdW approximation (3.41) the last expression takes the form

$$p^{\text{nl}}(T, \mu_1, \mu_2) = \lim_{V \rightarrow \infty} \frac{T}{V} \ln \left[\frac{A_1^{\mathcal{N}_1}}{\mathcal{N}_1!} \frac{A_2^{\mathcal{N}_2}}{\mathcal{N}_2!} \left(V - \mathcal{N}_1 b_{11} - \mathcal{N}_2 b_{22} + \frac{\mathcal{N}_1 \mathcal{N}_2}{\mathcal{N}_1 + \mathcal{N}_2} D \right)^{\mathcal{N}_1 + \mathcal{N}_2} \right], \quad (3.53)$$

where $A_q = A(T, \mu_q; m_q, g_q) \equiv \exp[\mu_q/T] \phi_q$. The evaluation of both maximum conditions for the grand canonical pressure

$$0 \stackrel{!}{=} \frac{\partial}{\partial \mathcal{N}_q} \left\{ \ln \left[\frac{A_1^{\mathcal{N}_1}}{\mathcal{N}_1!} \frac{A_2^{\mathcal{N}_2}}{\mathcal{N}_2!} \left(V - \mathcal{N}_1 b_{11} - \mathcal{N}_2 b_{22} + \frac{\mathcal{N}_1 \mathcal{N}_2}{\mathcal{N}_1 + \mathcal{N}_2} D \right)^{\mathcal{N}_1 + \mathcal{N}_2} \right] \right\},$$

yields a system of two coupled transcendental equations,

$$\xi_1^{\text{nl}}(T, \mu_1, \mu_2) = A_1 \exp \left[-(\xi_1^{\text{nl}} + \xi_2^{\text{nl}}) b_{11} + \frac{\xi_2^{\text{nl}2}}{\xi_1^{\text{nl}} + \xi_2^{\text{nl}}} D \right], \quad (3.54)$$

$$\xi_2^{\text{nl}}(T, \mu_1, \mu_2) = A_2 \exp \left[-(\xi_1^{\text{nl}} + \xi_2^{\text{nl}}) b_{22} + \frac{\xi_1^{\text{nl}2}}{\xi_1^{\text{nl}} + \xi_2^{\text{nl}}} D \right], \quad (3.55)$$

where ξ_1^{nl} and ξ_2^{nl} are defined as

$$\xi_1^{\text{nl}} \equiv \frac{\mathcal{N}_1}{V - \mathcal{N}_1 b_{11} - \mathcal{N}_2 b_{22} + \frac{\mathcal{N}_1 \mathcal{N}_2}{\mathcal{N}_1 + \mathcal{N}_2} D}, \quad (3.56)$$

$$\xi_2^{\text{nl}} \equiv \frac{\mathcal{N}_2}{V - \mathcal{N}_1 b_{11} - \mathcal{N}_2 b_{22} + \frac{\mathcal{N}_1 \mathcal{N}_2}{\mathcal{N}_1 + \mathcal{N}_2} D}. \quad (3.57)$$

In the thermodynamical limit the average particle numbers \mathcal{N}_1 and \mathcal{N}_2 are proportional to V as $\mathcal{N}_q = n_q^{\text{nl}} V$. Then the volume V disappears in the definitions of ξ_1^{nl} and ξ_2^{nl} given by Eqs. (3.56, 3.57), and they can be solved for either the density n_1^{nl} or n_2^{nl} ,

$$n_1^{\text{nl}}(T, \mu_1, \mu_2) = \frac{\xi_1^{\text{nl}}}{1 + \xi_1^{\text{nl}} b_{11} + \xi_2^{\text{nl}} b_{22} - \frac{\xi_1^{\text{nl}} \xi_2^{\text{nl}}}{\xi_1^{\text{nl}} + \xi_2^{\text{nl}}} D}, \quad (3.58)$$

$$n_2^{\text{nl}}(T, \mu_1, \mu_2) = \frac{\xi_2^{\text{nl}}}{1 + \xi_1^{\text{nl}} b_{11} + \xi_2^{\text{nl}} b_{22} - \frac{\xi_1^{\text{nl}} \xi_2^{\text{nl}}}{\xi_1^{\text{nl}} + \xi_2^{\text{nl}}} D}. \quad (3.59)$$

The $\xi_q^{\text{nl}} = \xi_q^{\text{nl}}(T, \mu_1, \mu_2)$ are the solutions of the coupled Eqs. (3.54) and (3.55), respectively.

Hence, the pressure (3.53) can be rewritten in terms of ξ_1^{nl} (3.54) and ξ_2^{nl} (3.55),

$$p^{\text{nl}}(T, \mu_1, \mu_2) = T \left(\xi_1^{\text{nl}} + \xi_2^{\text{nl}} \right) , \quad (3.60)$$

supposed that Eqs. (3.58, 3.59) are taken into account. If the definitions (3.56) and (3.57) are used for ξ_1^{nl} and ξ_2^{nl} , the pressure formula (3.60) coincides with the canonical expression (3.43) for $N_1 = \mathcal{N}_1$ and $N_2 = \mathcal{N}_2$.

Since the formulation is thermodynamically self-consistent the identity $n_q \equiv \partial p(T, \mu_1, \mu_2) / \partial \mu_q$ leads to Eqs. (3.58, 3.59) as well.

The grand canonical formulae of the linear approximation [161] are obtained exactly as presented for the non-linear case in Eqs. (3.53–3.60). In the linear case the system becomes

$$\xi_1^{\text{lin}}(T, \mu_1, \mu_2) = A_1 \exp \left[-\xi_1^{\text{lin}} b_{11} - \xi_2^{\text{lin}} \tilde{b}_{12} \right] , \quad (3.61)$$

$$\xi_2^{\text{lin}}(T, \mu_1, \mu_2) = A_2 \exp \left[-\xi_2^{\text{lin}} b_{22} - \xi_1^{\text{lin}} \tilde{b}_{21} \right] , \quad (3.62)$$

$$\text{where } \xi_1^{\text{lin}} \equiv \frac{\mathcal{N}_1}{V - \mathcal{N}_1 b_{11} - \mathcal{N}_2 \tilde{b}_{21}} , \quad (3.63)$$

$$\xi_2^{\text{lin}} \equiv \frac{\mathcal{N}_2}{V - \mathcal{N}_2 b_{22} - \mathcal{N}_1 \tilde{b}_{12}} . \quad (3.64)$$

The particle densities are found by solving Eqs. (3.63, 3.64) for either n_1^{lin} or n_2^{lin} ,

$$n_1^{\text{lin}}(T, \mu_1, \mu_2) = \frac{\xi_1^{\text{lin}}(1 + \xi_2^{\text{lin}}[b_{22} - \tilde{b}_{21}])}{1 + \xi_1^{\text{lin}}b_{11} + \xi_2^{\text{lin}}b_{22} + \xi_1^{\text{lin}}\xi_2^{\text{lin}}[b_{11}b_{22} - \tilde{b}_{12}\tilde{b}_{21}]} , \quad (3.65)$$

$$n_2^{\text{lin}}(T, \mu_1, \mu_2) = \frac{\xi_2^{\text{lin}}(1 + \xi_1^{\text{lin}}[b_{11} - \tilde{b}_{12}])}{1 + \xi_1^{\text{lin}}b_{11} + \xi_2^{\text{lin}}b_{22} + \xi_1^{\text{lin}}\xi_2^{\text{lin}}[b_{11}b_{22} - \tilde{b}_{12}\tilde{b}_{21}]} . \quad (3.66)$$

For the linear case the pressure (3.52) can be rewritten in terms of ξ_1^{lin} (3.61) and ξ_2^{lin} (3.62),

$$p^{\text{lin}}(T, \mu_1, \mu_2) = T \left(\xi_1^{\text{lin}} + \xi_2^{\text{lin}} \right) , \quad (3.67)$$

if Eqs. (3.65, 3.66) are taken into account, like in the non-linear case.

Let me briefly return to the usual VdW case, the one-component case. The corresponding transcendental equation is obtained from either Eqs. (3.54, 3.55) or (3.61, 3.62) by setting $R_1 = R_2 \equiv R$ and $A_1 = A_2 \equiv A$,

$$\xi^{\text{oc}}(T, \mu) = A \exp[-\xi^{\text{oc}} b] , \quad (3.68)$$

whereas $b \equiv b_{11} = b_{22}$. The *transcendental factor* $\exp[-\xi^{\text{oc}} b]$ has the form of a suppression term, and the solution $\xi^{\text{oc}} \equiv p^{\text{oc}}/T$ of this transcendental equation evidently decreases with increasing b for constant T and μ . Then in turn, the corresponding particle density $n^{\text{oc}} = \xi^{\text{oc}}/(1 + \xi^{\text{oc}} b)$ is suppressed in comparison with the ideal gas due to the lower ξ^{oc} and the additional denominator. Thus, a transcendental factor corresponds to a suppression of particle density.

Now it can be seen from Eqs. (3.54, 3.55) and (3.61, 3.62) that the transcendental factors of both *two-component* approximations contain as well this usual *one-component-* or *VdW-like* suppressive part $\exp[-(p/T) b_{qq}]$. But since it is $D \geq 0$ and $\tilde{b}_{pq} < b_{pp}$, respectively, there is furthermore an attractive part in each corresponding transcendental factor.

In the non-linear approximation the attractive part can even dominate the suppressive part for the smaller component, e. g. in Eq. (3.55) for $R_2 < R_1$. Then the larger component can reach densities n_1^{nl} higher than $1/b_{11}$, analogous to the CE.

High densities in the canonical treatment correspond to large values of the chemical potentials in the grand canonical treatment. In the limit

$$\mu_1/T \rightarrow \infty \quad (T, \mu_2 = \text{const.}) \quad \text{or} \quad \xi_1^{\text{nl}} \rightarrow \infty \quad (3.69)$$

the solution of Eq. (3.55), ξ_2^{nl} , can be enhanced for increasing ξ_1^{nl} instead of being suppressed, if R_2 is sufficiently small. This may be called the *non-linear enhancement*. The behavior of the non-linear approximation in the limit (3.69) depends only on the ratio of the two radii R_1/R_2 and is characterised by the coefficient

$$a_2 \equiv \sqrt{D/b_{22}} - 1. \quad (3.70)$$

A negative a_2 relates to a suppressive transcendental factor in Eq. (3.55). For equal radii $R_2 = R_1$ it is $a_2 = -1$, and the suppression is evidently not reduced but *VdW-like*. For $-1 < a_2 < 0$ this suppression is reduced, the most strongly for $a_2 \approx 0$.

In the case $a_2 = 0$ the suppression for ξ_2^{nl} (3.55) disappears in the limit (3.69), one has $\xi_2^{\text{nl}} \rightarrow A_2 = \text{const.}$ This case provides the critical radius $R_{2, \text{crit}}$ (3.50).

For $a_2 > 0$ or $R_2 < R_{2, \text{crit}}$ the non-linear enhancement of ξ_2^{nl} occurs for increasing ξ_1^{nl} ; it is the stronger the larger a_2 is. Then n_1^{nl} (3.58) can exceed $\max(n_1^{\text{oc}}) = 1/b_{11}$, whereas n_2^{nl} (3.59) does not vanish. The density $\max(\hat{n}_1^{\text{nl}}) = 4/b_{11}$ is achieved for $a_2 \rightarrow \infty$ or $R_2 \rightarrow 0$.

The suppression in the transcendental factor of ξ_1^{nl} (3.54) is generally reduced for $R_2 < R_1$, the more strongly the smaller R_2 is, but there is no enhancement possible in the limit (3.69).

3.3.2. Relativistic Excluded Volumes. In this section I will investigate the influence of relativistic effects on the excluded volumes of fast moving particles by accounting for their ellipsoidal shape due to Lorentz contraction. In Ref. [156] a quite simple, ultra-relativistic approach has been made to estimate these effects: instead of ellipsoids two cylinders with the corresponding radii have been used to calculate approximately the excluded volume term b_{pq} for the two-component mixture. The resulting relativistic excluded volumes depend on the temperature and contain the radii and the *masses* as parameters. The simple, non-mixed term reads [154]

$$b_{qq}(T) = \alpha_{qq} \left(\frac{37\pi}{9} \frac{\sigma_q}{\phi_q} + \frac{\pi^2}{2} \right) R_q^3, \quad (3.71)$$

where $\sigma_q \equiv \sigma(T; m_q, g_q)$ denotes the *ideal gas* scalar density,

$$\sigma(T; m, g) = \frac{g}{2\pi^2} \int_0^\infty dk k^2 \frac{m}{E(k)} \exp \left[-\frac{E(k)}{T} \right]. \quad (3.72)$$

The expression for the mixed case can be derived similarly from [156],

$$b_{12}(T) = \alpha_{12} \left\{ \left(\frac{\sigma_1}{\phi_1} f_1 + \frac{\pi^2 R_2}{4 R_1} \right) R_1^3 + \left(\frac{\sigma_2}{\phi_2} f_2 + \frac{\pi^2 R_1}{4 R_2} \right) R_2^3 \right\}, \quad (3.73)$$

whereas the abbreviations f_1 and f_2 are dimensionless functions of both radii,

$$f_1 = \frac{\pi}{3} \left(2 + \frac{3R_2}{R_1} + \frac{7R_2^2}{6R_1^2} \right), \quad f_2 = \frac{\pi}{3} \left(2 + \frac{3R_1}{R_2} + \frac{7R_1^2}{6R_2^2} \right).$$

The normalization factors

$$\alpha_{11} = \alpha_{22} = \frac{16}{\frac{37}{3} + \frac{3\pi}{2}}, \quad (3.74)$$

$$\alpha_{12} = \frac{\frac{2\pi}{3} (R_1 + R_2)^3}{\left(f_1 + \frac{\pi^2 R_2}{4 R_1} \right) R_1^3 + \left(f_2 + \frac{\pi^2 R_1}{4 R_2} \right) R_2^3} \quad (3.75)$$

are introduced to normalise the ultra-relativistic approximations (3.71, 3.73) for $T = 0$ to the corresponding non-relativistic results. For the hadron gas, however, these Boltzmann statistical formulae will only be used at high temperatures, where effects of quantum statistics are negligible.

Note that it is *not appropriate* to consider temperature dependent hard core radii $R_p(T)$ or $R_q(T)$ since the $b_{pq}(T)$ terms give the Lorentz-contracted excluded *volumes* and are involved functions of T, m_p, m_q, R_p and R_q . However, for a given value of $b_{pq}(T)$ the necessary hard core radii R_p and R_q will obviously depend on the temperature.

It is evident that the formulae (3.71, 3.73) suffice already for the multi-component case, because even a multi-component VdW formulation contains only b_{pq} terms.

For both approximations the expressions for the pressure (3.60) or (3.67) and corresponding particle densities (3.58, 3.59) or (3.65, 3.66) remain unchanged. However, due to the temperature dependence of the relativistic excluded volumes the entropy density is modified

$$s(T, \mu_1, \mu_2) \equiv \frac{\partial}{\partial T} p(T, \mu_1, \mu_2) \equiv s_{\text{rel}} + s_{\text{rel}}(\partial_T b_{11}, \partial_T b_{22}, \partial_T b_{12}) . \quad (3.76)$$

The additional term s_{rel} depends on temperature derivatives of the relativistic excluded volumes, $\partial_T b_{pq} \equiv \partial b_{pq} / \partial T$, which represent their thermal compressibility.

Furthermore, the term s_{rel} generates additional terms for the energy density, according to $e \equiv Ts - p + \mu_1 n_1 + \mu_2 n_2$. In the non-linear approximation one obtains

$$e^{\text{nl}}(T, \mu_1, \mu_2) = n_1^{\text{nl}} \frac{\epsilon_1}{\phi_1} + n_2^{\text{nl}} \frac{\epsilon_2}{\phi_2} - (n_1^{\text{nl}} + n_2^{\text{nl}}) T^2 \left(\xi_1^{\text{nl}} \partial_T b_{11} + \xi_2^{\text{nl}} \partial_T b_{22} - \frac{\xi_1^{\text{nl}} \xi_2^{\text{nl}}}{\xi_1^{\text{nl}} + \xi_2^{\text{nl}}} \partial_T D \right) , \quad (3.77)$$

and the linear approximation yields

$$\begin{aligned} e^{\text{lin}}(T, \mu_1, \mu_2) = & n_1^{\text{lin}} \frac{\epsilon_1}{\phi_1} + n_2^{\text{lin}} \frac{\epsilon_2}{\phi_2} - n_1^{\text{lin}} T^2 \left(\xi_1^{\text{lin}} \partial_T b_{11} + \xi_2^{\text{lin}} \partial_T \tilde{b}_{12} \right) \\ & - n_2^{\text{lin}} T^2 \left(\xi_2^{\text{lin}} \partial_T b_{22} + \xi_1^{\text{lin}} \partial_T \tilde{b}_{21} \right) , \end{aligned} \quad (3.78)$$

whereas $\epsilon_q \equiv \epsilon(T; m_q, g_q)$ denotes the *ideal gas* energy density

$$\epsilon(T; m, g) = \frac{g}{2\pi^2} \int_0^\infty dk k^2 E(k) \exp \left[-\frac{E(k)}{T} \right] . \quad (3.79)$$

The additional terms in the entropy density (3.76) and in the energy density (3.77) or (3.78) which contain temperature derivatives do evidently not occur in the case of the usual non-relativistic, i. e. constant excluded volumes.

Let me now study the hadronic equation of state generated by each of the two-component VdW approximations and their modifications due to relativistic excluded volumes. When used to

describe *hadrons*, the hard core radii R_q should be considered as *parameters* rather than particle radii. The first component is identified as nucleons ($m_1 \equiv m_n = 939 \text{ MeV}$, $\mu_1 \equiv \mu_n = \mu_B$ and $g_1 \equiv g_n = 4$ for symmetric nuclear matter) and the second as pions ($m_2 \equiv \bar{m}_\pi = 138 \text{ MeV}$, $\mu_2 \equiv \mu_\pi = 0$ and $g_2 \equiv g_\pi = 3$). Quantum statistical effects other than the degeneracy factors g_q are neglected. To reproduce experimental data, however, it would be necessary to consider all hadrons and hadronic resonances as well as the contributions from hadronic decays into daughter hadrons.

For some examples the temperature dependence of the relativistic excluded volumes is shown in Fig. 3.4 (a), given in units of the corresponding non-relativistic terms, $b_{pq} = b_{pq}(0)$. The solid line and the short dashes show the basic excluded volumes $b_{11}(T)$ and $b_{22}(T)$, respectively. In these relative units the decreases of $b_{11}(T)$ and $b_{22}(T)$ depend only on the corresponding masses. It is apparent that the pion excluded volume $b_{22}(T)$ is affected much stronger than the excluded volume of the nucleons, $b_{11}(T)$. The dotted line shows the mixed volume term $b_{12}(T)$, and the long dashes show the compound volume term $D(T) \equiv b_{11}(T) + b_{22}(T) - 2b_{12}(T)$. These two terms depend obviously on both masses and both radii.

The curves for the generalised excluded volume terms of the linear approximation $\tilde{b}_{12}(T)$ and $\tilde{b}_{21}(T)$ behave similarly to $b_{12}(T)$.

Introduction of the relativistic excluded volumes $b_{pq}(T)$, however, has two effects. First, the maximum densities become larger since it is generally $1/b_{qq}(T) > 1/b_{qq}$ as seen in Fig. 3.4 (a). Furthermore, the balance between the lighter and the heavier species is changed because the lighter species is affected more than the heavier at the same temperature: For the above parameters it is $b_{22}(T)/b_{22} \leq b_{11}(T)/b_{11}$.

In the non-linear approximation this balance is characterised by the coefficient a_2 defined by Eq. (3.70). In Fig. 3.4 (b) the temperature dependence of $a_2(T) \equiv (\sqrt{D(T)/b_{22}(T)} - 1)$ is shown for three different values of R_2 . The *relativistic* coefficient $a_2(T)$ increases with T , i. e. the non-linear enhancement becomes stronger for higher temperatures. For some values of R_2 , e. g. $R_2 = 0.4 \text{ fm}$, a primary suppression $a_2(0) \equiv a_2 < 0$, turns into an enhancement $a_2(T) > 0$, when the temperature is sufficiently high. For temperature dependent excluded volumes $R_{2,\text{crit}}$ loses its meaning; here,

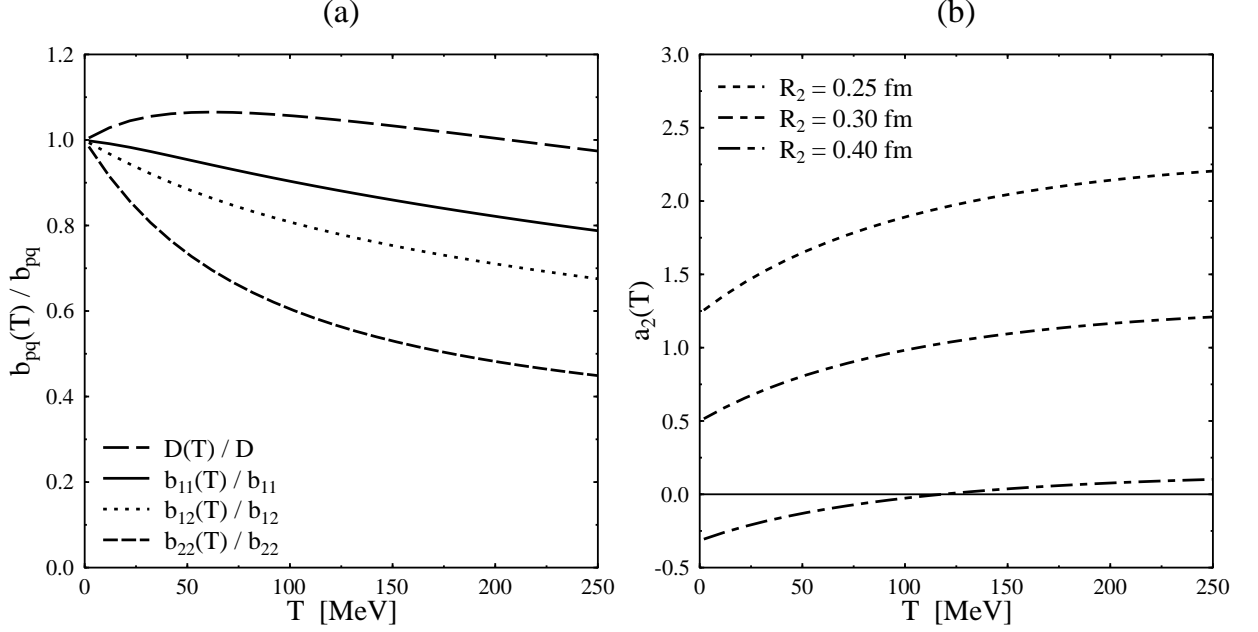


Figure 3.4. Temperature dependence of the relativistic excluded volume terms for $m_1 = m_n, m_2 = \bar{m}_\pi, R_1 = 0.6$ fm.

(a) Relative values for $R_2 = 0.3$ fm: $b_{11}(T)/b_{11}$, $b_{12}(T)/b_{12}$, $b_{22}(T)/b_{22}$ and $D(T)/D$ (solid line, dotted line, short and long dashes, respectively). The relativistic excluded volume of light species ($b_{22}(T)/b_{22}$) is affected more strongly by temperature.

(b) The characteristic coefficient of the non-linear approximation $a_2(T) = (\sqrt{D(T)/b_{22}(T)} - 1)$ for various $R_2 = 0.25, 0.3$ and 0.4 fm. The non-linear enhancement ($a_2(T) > 0$) becomes stronger due to the decrease of the relativistic excluded volumes with increasing temperature.

only $a_2(T) > 0$ is the valid condition for the occurrence of the non-linear enhancement or densities $n_1^{\text{nl}} > 1/b_{11}(T)$.

The linear coefficient, $\tilde{a}_2(T) = -2b_{12}(T)/(b_{11}(T) + b_{22}(T))$, is not strongly affected by temperature for the above choice of hadronic parameters: It increases slightly with T but remains negative. Hence, changes in the balance between the lighter and the heavier species play a minor role for the linear approximation.

Particle densities for nucleons and pions in units of $n_0 = 0.16 \text{ fm}^{-3}$ vs. $\mu_1/m_1 \equiv \mu_n/m_n$ are shown in Figs. 3.5(a) and (b) for $T = 185$ MeV. The linear and non-linear results are shown for

constant excluded volumes with short dashes and solid lines, respectively, and further for relativistic excluded volumes with dotted lines and long dashes, respectively. At this high temperature the relativistic results are significantly higher than the non-relativistic result. A difference between the linear and the non-linear approximation due to the non-linear enhancement becomes noticeable only for high $\mu_n/m_n > 0.8$. Thus, for $R_n = R_1 = 0.6$ fm from above, the linear and non-linear approximation are practically equivalent for nucleon densities below $n_n \approx 0.8 n_0$, i. e. for densities below about $n_1 \approx 1/(2b_{11})$. On the other hand, due to the strong decrease of $b_{22}(T)$ with increasing temperature, the influence of the relativistic excluded volumes is essential for temperatures of the order of $T \approx m_\pi$.

The presence of the additional terms containing temperature derivatives in the energy density (3.77) or (3.78) makes it impossible to convert a VdW gas with relativistic excluded volumes into a gas of free streaming particles. Therefore, it is problematic to use these formulae for the post-freeze-out stage. For the latter the quantities of the free streaming particles without any interaction should be used, see discussion in [173, 174, 175] and references therein. However, these equations of state may be used to describe the stage between chemical and thermal freeze-out, i. e. a pre-freeze-out stage in terms of Refs. [173, 174, 175]. This is exemplified in the next section.

3.3.3. Hard-core Radii from Particle Yield Ratios. As a simple application of the equations of state presented above, let me re-evaluate the thermal model fit parameters for particle yield ratios of Ref. [165], namely the hard core radii of pions R_π and other hadrons R_o . A two-component VdW excluded volume model has been used there to explain the pion abundance in A+A-collisions by a smaller hard core radius for the pions than for the other hadrons. The ratios has been fitted to BNL AGS (Au+Au at 11 A GeV) and CERN SPS (Pb+Pb at 160 A GeV) data [172] within a thermal model, including all resonances up to 2 GeV and using quantum statistics.

The applied model, however, corresponds to the incorrect separated model as pointed out in previous section. For convenience I give these formulae in Boltzmann approximation. Within the

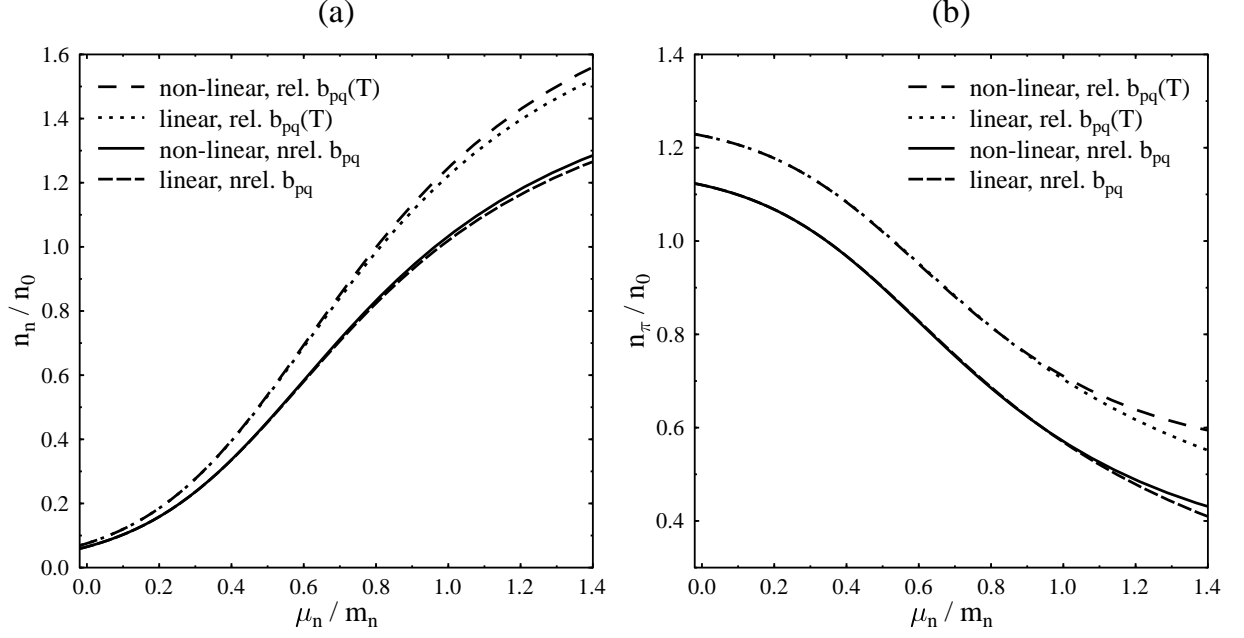


Figure 3.5. Comparison of the model predictions for the nucleon (a) and pion (b) density n_n and n_π , respectively, vs. μ_n/m_n ($R_1 = 0.6$ fm, $R_2 = 0.3$ fm and $T = 185$ MeV, densities in units of $n_0 = 0.16$ fm $^{-3}$). In both figures the two upper lines correspond to relativistic excluded volumes $b_{pq}(T)$ and the two lower lines to non-relativistic excluded volumes b_{pq} . The results of the linear and non-linear approximation coincide – only for extremely large μ_n/m_n the non-linear results lie slightly higher than the corresponding linear results. The deviations due to relativistic excluded volumes are significant.

previously defined notation the two coupled transcendental equations read

$$\xi_1^{\text{SP}}(T, \mu_1, \mu_2) = A_1 \exp[-(\xi_1^{\text{SP}} + \xi_2^{\text{SP}}) b_{11}] , \quad (3.80)$$

$$\xi_2^{\text{SP}}(T, \mu_1, \mu_2) = A_2 \exp[-(\xi_1^{\text{SP}} + \xi_2^{\text{SP}}) b_{22}] , \quad (3.81)$$

wheras $p^{\text{SP}}(T, \mu_1, \mu_2) = T (\xi_1^{\text{SP}} + \xi_2^{\text{SP}})$. In this context A_1 represents a sum over the contributions of all hadron species but pions, while A_2 corresponds to the pions only.

The expressions for the particle densities are obtained from $n_q^{\text{SP}} \equiv \partial p^{\text{SP}} / \partial \mu_q$,

$$n_1^{\text{SP}}(T, \mu_1, \mu_2) = \frac{\xi_1^{\text{SP}}}{1 + \xi_1^{\text{SP}} b_{11} + \xi_2^{\text{SP}} b_{22}} , \quad (3.82)$$

$$n_2^{\text{SP}}(T, \mu_1, \mu_2) = \frac{\xi_2^{\text{SP}}}{1 + \xi_1^{\text{SP}} b_{11} + \xi_2^{\text{SP}} b_{22}} . \quad (3.83)$$

Solving these equations for ξ_1^{SP} and ξ_2^{SP} one recovers the canonical pressure formula of the separated model (3.37) as announced earlier.

Due to the separation of both components in this model there is no excluded volume term b_{12} for the interaction between different components at all. This is an essential difference to both the linear and the non-linear approximation. Note that the separated model is *not* a two-component VdW *approximation* because it cannot be obtained by approximating the CPF (3.39).

The transcendental factors of the formulae (3.80, 3.81) exhibit a constant VdW-like suppression $\exp[-(p/T)b_{qq}]$. There is a reduction of this suppression in the linear and in the non-linear approximation, as shown above. The VdW-like suppression is reduced, if b_{12} appears in the corresponding formulae since b_{12} is smaller than b_{11} for $R_2 < R_1$. It is evident that the deviation of the linear and non-linear approximation from the separated model is the larger the more R_1 and R_2 differ from each other.

In the first step of the fit procedure of Ref. [165] only the hadron ratios excluding pions have been taken to find the freeze-out parameters. For AGS $T \approx 140$ MeV, $\mu_B \approx 590$ MeV and for SPS $T \approx 185$ MeV, $\mu_B \approx 270$ MeV have been obtained. In the second step, a parameter introduced as the *pion effective chemical potential* μ_π^* has been fitted to the pion-to-hadron ratios. Using Boltzmann statistics it can be shown that the pion enhancement is thoroughly regulated by the value of μ_π^* [165]; one has obtained $\mu_\pi^* \approx 100$ MeV for AGS and $\mu_\pi^* \approx 180$ MeV for SPS data, respectively.

The pion effective chemical potential depends explicitly on the excluded volumes but also on the pressure. The pressure itself is a transcendental function depending solely on the excluded volumes since T and μ_B are already fixed by step one. In Ref. [165] the formula $\mu_\pi^* \equiv (v_o - v_\pi)p(v_o, v_\pi)$ has been obtained for the separated model, where $v_\pi \equiv b_{22}$ and $v_o \equiv b_{11}$ are the excluded volumes corresponding to the hard core radii of pions $R_\pi \equiv R_2$ and other hadrons $R_o \equiv R_1$, respectively. Thus, the μ_π^* values for AGS and SPS data define two curves in the R_π - R_o -plane. The main conclusion of Ref. [165] is that the intersection point of these two curves ($R_\pi = 0.62$ fm, $R_o = 0.8$ fm) gives the correct pair of hard core radii for pions and for the other hadrons, i. e. AGS and SPS data are fitted simultaneously within the applied model.

In Ref. [137] these values of R_o and R_π have been criticised for being unreasonably large. There, a complete fit of solely SPS data has been performed within a separated model. The best fit has been obtained for equal hard core radii, $R_\pi = R_o = 0.3$ fm, motivated by nucleon scattering data. Good agreement has been found as well for a *baryon* hard core radius, $R_{\text{Bar}} = 0.3$ fm, and a common hard core radius for *all mesons*, $R_{\text{Mes}} = 0.25$ fm, chosen in accord with the above ratio of radii, $R_o/R_\pi = 0.8/0.62$. Larger hard core radii, especially those of Ref. [165], are quoted as giving distinctly worse agreement.

Assuming the validity of Boltzmann statistics, I have re-calculated the $R_o(R_\pi)$ -curves for the above μ_π^* values; firstly in the separated model (3.80–3.83), i. e. as presented in [165]. The resulting curves, shown as thin lines in Fig. 3.6 (a), naturally match the results of the underlying fit of Ref. [165], which are indicated by markers.

Then I have considered the linear and the non-linear approximation. Due to the occurrence of b_{12} terms in these two cases, both functional forms of μ_π^* are essentially different from the separated case. Consequently, the shapes of the $R_o(R_\pi)$ -curves are different as well. Thus, one finds distinct deviations from the separated model, especially for $R_\pi \rightarrow 0$, and the values for the intersection point are slightly lower; see thin lines in Fig. 3.6 (b) for the linear extrapolation. The non-linear approximation gives identical results for this purpose because the hadron densities are too small for a noticeable non-linear enhancement.

The crucial point is now to turn on the relativistic temperature dependence of the excluded volumes. To keep the analysis simple I treat only pions this way since they give the strongest effect.

Although the other hadrons are assumed to have equal hard core radii, their relativistic excluded volumes would be different for $T > 0$, according to their different masses. To check the influence of relativistic excluded volumes for *all* particles, I have used *one average* mass of 1 GeV for *all other* hadrons. The corresponding change in the R_o -values are below 5%.

The results of the fit for relativistic excluded volumes for pions are shown in Figs. 3.6 (a) and (b) as thick lines. Though this approach is more realistic, there is *no* intersection point for *any* of the three models even for very large radii $R_o, R_\pi \gg 0.5$ fm. For the approximated case of a

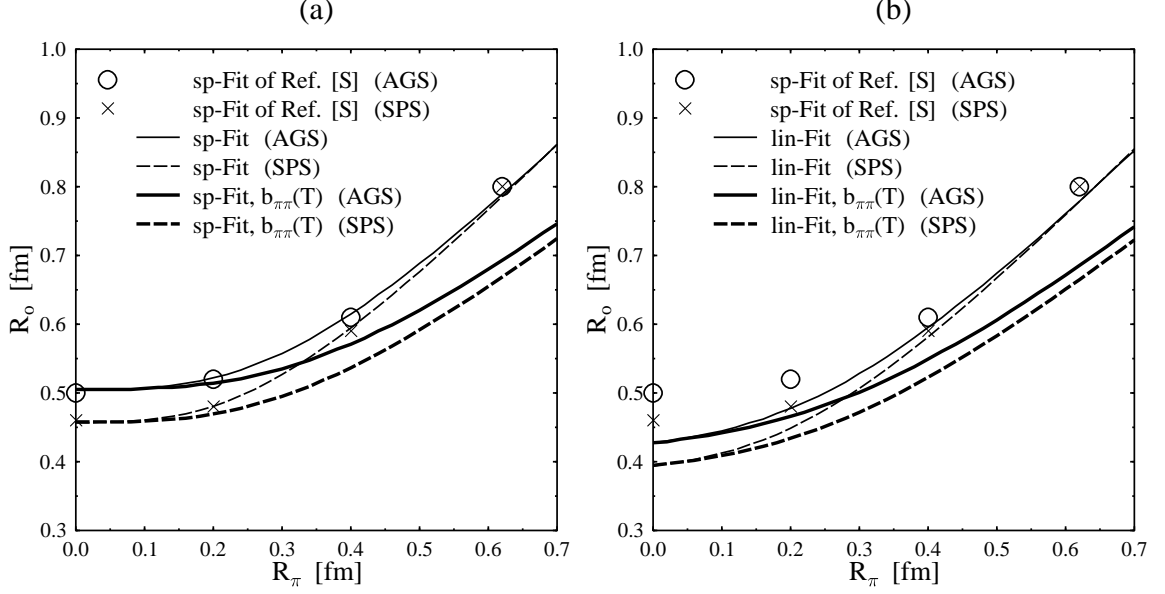


Figure 3.6. Fits of particle yield ratios for AGS and SPS data [172] with the separated model and the linear approximation. The thin lines show the fits for the separated model (a) and the linear approximation (b); the non-linear approximation gives identical results for the latter case.

The thick lines in (a) and (b) show the corresponding curves for relativistic excluded volumes $v_\pi = b_{22}(T)$: there is no intersection for either of the three models. In both figures the results of the fit from Ref. [165] for AGS and SPS data are indicated by circles and crosses, respectively, and are referred as Ref. [S].

single averaged hadron mass there is no intersection either. Because of the different freeze-out temperatures for AGS and SPS the $v_\pi(T) \equiv b_{22}(T)$ values are changed differently in both cases, and so are the scales for the corresponding R_π .

Due to the errors in experimental data one ought to obtain a corridor instead of a curve for each set of data. Consequently, the particle yield ratios can be reproduced well by e. g. $R_0 \approx 0.4$ fm, $R_\pi \approx 0.2$ fm or larger values for any of the models with relativistic excluded volumes. Therefore, I conclude that the fit procedure proposed in Ref. [165] is *not* suitable to find a *unique* pair of hard core radii for pions and other hadrons, as long as a best fit is searched for just two sets of data of particle yield ratios. The use of a relativistic excluded volume for pions along with a correct approximation reduce the value of the necessary nucleon hard core radius essentially towards more

realistic values.

3.3.4. Intermediate Conclusions. In this section several EOS for the two-component VdW excluded volume model are derived and investigated in details. Two essentially different formulations have been discussed, the linear and the non-linear approximation.

The non-linear approximation is the simplest possibility. Here, the large component can reach higher densities n_1 than the usual limiting VdW density $1/b_{11}$, if the other component has a sufficiently small hard core radius, $R_2 < R_{2,\text{crit}}$. In the linear approximation the densities cannot exceed the usual limiting VdW densities $1/b_{11}$ and $1/b_{22}$, but generalised excluded volume terms have to be introduced.

For both approximations the suppression factors of the grand canonical formulae contain a VdW-like term, proportional to $\exp[-(p/T)b_{qq}]$, which however is reduced non-trivially. In the linear case there is a slight reduction, whereas in the non-linear case this reduction can turn the suppression even into an enhancement for the smaller component, which leads to exceeding of $1/b_{11}$ for the density of the larger component n_1 .

The commonly used formulae of the separated model are shown to be not suitable for the two-component case, because they correspond to a system where both components are separated from each other and cannot mix. In this model the grand canonical suppression factor is just VdW-like and has no reduction of the suppression.

Furthermore relativistic, i. e. Lorentz-contracted, excluded volumes have been introduced. Naturally, the relativistic excluded volume per particle decreases with rising temperature. This effect is the stronger the lighter the particle species is. The suppression of particle densities in VdW models is lower for a component of smaller excluded volume in comparison with a component of larger excluded volume. Therefore, the temperature dependence of the relativistic excluded volumes causes a reduction of the particle densities suppression.

The full equations of state have been presented, for both the linear and non-linear approximation, with constant and with relativistic excluded volumes. For the entropy density and energy density there are additional terms containing temperature derivatives of the relativistic excluded volume terms due to their 'thermal compressibility'. In comparison with the non-relativistic case,

the expressions for the pressure and the particle densities remain unchanged, but the possible range of values is obviously wider, since it is generally $1/b_{11}(T) \geq 1/b_{11}$ and $1/b_{22}(T) \geq 1/b_{22}$.

As an application of the derived formulations a fit of particle yield ratios for SPS and AGS has been re-evaluated. In Ref. [165] this fit had been done in a separated model by adjusting the hard core radii for the pions R_π and for the other hadrons R_o . The results of the new fit are essentially different from the separated model but coincide for both the linear and non-linear approximation. The picture changes drastically, however, if relativistic excluded volumes are adopted for pions. The basic idea of the fit – one pair of hard core radii suffices to fit AGS and SPS data simultaneously – does not lead to a result anymore. This is the case for the separated model and for both approximations, linear and non-linear. Experimental uncertainties lead to a *region* of possible values in the R_o - R_π -plane; one could describe the data for $R_o \geq 0.4$ fm and $R_\pi \geq 0.2$ fm.

I conclude that there are two causes of an *enhancement* of particle densities, e. g. the thermal pion abundance, in VdW descriptions: First, the density suppression is generally lower for the smaller component in two-component models. Second, there is a further reduction of the density suppression due to the relativistic excluded volumes. The latter are essentially smaller for light hadron species than for heavy species, especially for temperatures $T \gg 50$ MeV.

When applied to the hadron gas, the linear and non-linear results almost coincide for nucleon densities up to $n_0 \approx 0.16$ fm⁻³ (for $R_o \leq 0.6$ fm) since the non-linear enhancement does not appear there, but the deviation from the incorrect separated model is distinct. However, the formulae of the non-linear approximation are essentially simpler than these of the linear approximation.

The influence of relativistic effects on the excluded volumes becomes indispensable for temperatures typical for heavy ion collisions. However, the EOS presented above become acausal above the cross-over where the usual hadrons can coexist with quarks and gluons [157]. Therefore, in order to extend the hadron gas description above the cross-over it is necessary to return back to the VdW extrapolation suggested in [154] and find the reason why the relativistic excluded volumes do not vanish at high pressures.

3.4. Relativization of the VdW EOS

As was shown in the preceding section the relativistic VdW equation obtained in the traditional way leads to the reduction of the second virial coefficient (analog of the excluded volume) compared to nonrelativistic case. However, in the high pressure limit the second virial coefficient remains finite. This fact immediately leads to the problem with causality in relativistic mechanics - the speed of sound exceeds the speed of light [150].

At the moment there are few guesses on how to formulate the statistical mechanics of this state, but it is possible that the relevant quasiparticle degrees of freedom may include the dressed constituent quarks or/and their hadron-like bound states. In this case one can think about the possibility to describe such states in terms of relativistic particles with the hard core repulsion on short distances. In fact, according to Shuryak [184] the recent study of the strongly coupled colored classical plasma does include the short range repulsion of the inverse distance square type. Also it is quite possible that the huge values of the partonic cross-sections which are necessary to reproduce the values of elliptic flow observed at RHIC energies [185] do evidence that during the course of heavy ion collision the partons are acquiring some finite transversal size.

In addition, the VdW EOS which obeys the causality condition in the limit of high density and simultaneously reproduces the correct low density behavior has a significant theoretical value for the relativity because, due to some unclear reasons, such an EOS was not formulated during the century that passed after the special relativity birth. This section is devoted to the investigation of the necessary assumptions to formulate such an equation of state.

Similarly to the nonrelativistic VdW case [150] this leads to the problem with causality at very high pressures. Of course, in this formulation the superluminal speed of sound should appear at very high temperatures which are unreachable in hadronic phase. Thus the simple “relativization” of the virial expansion is much more realistic than the nonrelativistic description used in Refs. [136, 137], but it does not solve the problem completely.

The reason why the simplest generalization (3.18) fails is rather trivial. Eq. (3.18) does not take into account the fact that at high densities the particles disturb the motion of their neighbors. The latter leads to the more compact configurations than predicted by Eqs. (3.18 - 3.21), i.e., the

motion of neighboring particles becomes correlated due to a simple geometrical reason. In other words, since the N -particle distribution is a monotonically decreasing function of the excluded volume, the most probable state should correspond to the configurations of smallest excluded volume of all neighboring particles. This subject is, of course, far beyond the present paper. Although I will touch this subject slightly while discussing the limit $\mu/T \gg 1$ below, my primary task here will be to give a relativistic generalization of the VdW EOS, which at low pressures behaves in accordance with the relativistic virial expansion presented above, and at the same time is free of the causality paradox at high pressures.

In the treatment below I will completely neglect the angular rotations of the Lorentz contracted spheres because their correct analysis can be done only within the frame work of quantum scattering theory which is not used here. However, it is clear that the rotational effects can be safely neglected at low densities because there are not so many collisions in the system. At the same time the rotations of the Lorentz contracted spheres at very high pressures, which are of my main interest, can be neglected too, because at so high densities the particles should be so close to each other, that they must prevent the rotations of neighboring particles. Thus, for these two limits one can safely ignore the rotational effects and proceed further on like for the usual VdW EOS.

Eq. (3.18) is only one of many possible VdW extrapolations to high density. As in nonrelativistic case one can write many expressions which will give the first two terms of the full virial expansion exactly, and the difference will appear in the third virial coefficient. In relativistic case there is an additional ambiguity: it is possible to perform the momentum integration, first, and make the VdW extrapolation next, or vice versa. The result will, evidently, depend on the order of operation.

As an example let me give a brief “derivation” of Eq. (3.18), and its counterpart in the grand canonical ensemble. The two first terms of the standard cluster expansion read as [162, 154]

$$p = T \rho_t(T) e^{\frac{\mu}{T}} \left(1 - a_2 \rho_t(T) e^{\frac{\mu}{T}} \right) . \quad (3.84)$$

Now I approximate the last term on the right hand side as $\rho_t(T) e^{\frac{\mu}{T}} \approx \frac{p}{T}$. Then I extrapolate it to high pressures by moving this term into the exponential function as

$$p \approx T \rho_t(T) e^{\frac{\mu}{T}} \left(1 - a_2 \frac{p}{T} \right) \approx T \rho_t(T) \exp \left(\frac{\mu - a_2 p}{T} \right) . \quad (3.85)$$

The resulting expression coincides with Eq. (3.18), but the above manipulations make it simple and transparent. Now I will repeat all the above steps while keeping both momentum integrations fixed

$$\begin{aligned}
p &\approx \frac{T g^2 e^{\frac{\mu}{T}}}{\rho_t(T)} \int \frac{d\mathbf{k}_1}{(2\pi)^3} \frac{d\mathbf{k}_2}{(2\pi)^3} e^{-\frac{E(k_1)+E(k_2)}{T}} \left(1 - \frac{v(\mathbf{k}_1, \mathbf{k}_2) p}{T} \right) \\
&\approx \frac{T g^2}{\rho_t(T)} \int \frac{d\mathbf{k}_1}{(2\pi)^3} \frac{d\mathbf{k}_2}{(2\pi)^3} e^{\frac{\mu - v(\mathbf{k}_1, \mathbf{k}_2) p - E(k_1) - E(k_2)}{T}}.
\end{aligned} \tag{3.86}$$

The last expression contains the relativistic excluded volume (3.21) explicitly and, as can be shown, is free of the causality paradox. This is so because at high pressures the main contribution to the momentum integrals corresponds to the smallest values of the excluded volume (3.21). It is clear that such values are reached when the both spheres are ultrarelativistic and their velocities are collinear.

With the help of the following notations

$$\langle \mathcal{O} \rangle \equiv \frac{g}{\rho_t(T)} \int \frac{d\mathbf{k}}{(2\pi)^3} \mathcal{O} e^{-\frac{E(k)}{T}}, \tag{3.87}$$

$$\langle \langle \mathcal{O} \rangle \rangle \equiv \frac{g^2}{\rho_t^2(T)} \int \frac{d\mathbf{k}_1}{(2\pi)^3} \frac{d\mathbf{k}_2}{(2\pi)^3} \mathcal{O} e^{-\frac{v(\mathbf{k}_1, \mathbf{k}_2) p + E(k_1) + E(k_2)}{T}} \tag{3.88}$$

for the averages one can define all other thermodynamic functions as

$$n(T, \mu) = \frac{\partial p(T, \mu)}{\partial \mu} = \frac{p}{T \left(1 + e^{\frac{\mu}{T}} \rho_t(T) \langle \langle v(\mathbf{k}_1, \mathbf{k}_2) \rangle \rangle \right)}, \tag{3.89}$$

$$s(T, \mu) = \frac{\partial p(T, \mu)}{\partial T} = \frac{p}{T} + \frac{1}{T} \frac{\left(2 e^{\frac{\mu}{T}} \rho_t(T) \langle \langle E \rangle \rangle - [\mu + \langle E \rangle] p T^{-1} \right)}{1 + e^{\frac{\mu}{T}} \rho_t(T) \langle \langle v(\mathbf{k}_1, \mathbf{k}_2) \rangle \rangle}, \tag{3.90}$$

$$\varepsilon(T, \mu) = T s(T, \mu) + \mu n(T, \mu) - p(T, \mu) = \frac{2 e^{\frac{\mu}{T}} \rho_t(T) \langle \langle E \rangle \rangle - [\mu + \langle E \rangle] p T^{-1}}{1 + e^{\frac{\mu}{T}} \rho_t(T) \langle \langle v(\mathbf{k}_1, \mathbf{k}_2) \rangle \rangle}. \tag{3.91}$$

Here $n(T, \mu)$ is the particle density, while $s(T, \mu)$ and $\varepsilon(T, \mu)$ denote the entropy and energy density, respectively.

In the low pressure limit $4 p v_0 T^{-1} \ll 1$ the corresponding exponent in (3.88) can be expanded and the mean value of the relativistic excluded volume can be related to the second virial coefficient $a_2(T)$ as follows

$$\langle \langle v(\mathbf{k}_1, \mathbf{k}_2) \rangle \rangle \approx a_2(T) - \frac{p}{T} \langle \langle v^2(\mathbf{k}_1, \mathbf{k}_2) \rangle \rangle, \tag{3.92}$$

which shows that at low pressures the average value of the relativistic excluded volume should match the second virial coefficient $a_2(T)$, but should be smaller than $a_2(T)$ at higher pressures and this behavior is clearly seen in Fig. 3.7.

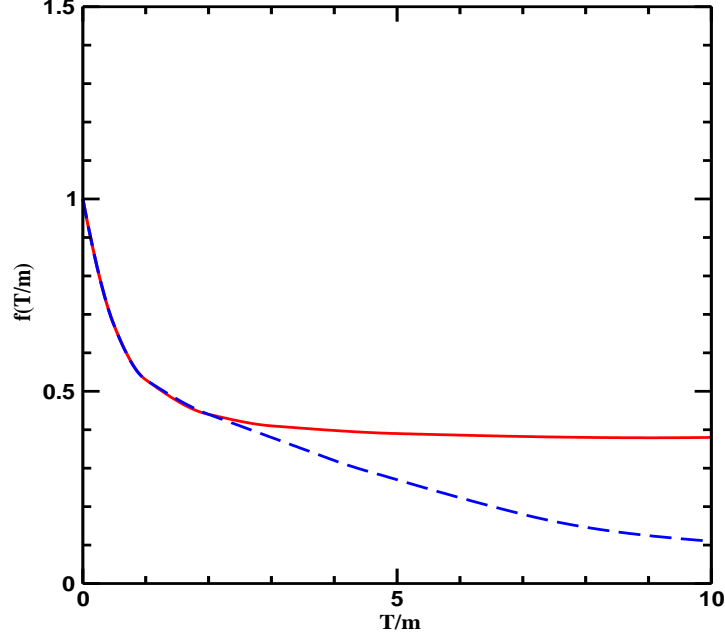


Figure 3.7. Comparison of the exact value of the second virial coefficient $a_2(T)/a_2(0)$ (solid curve) with the averaged value of the relativistic excluded volume $\alpha \langle \langle v^{Urel}(\mathbf{k}_1, \mathbf{k}_2) \rangle \rangle / (2a_2(0))$ (dashed curve) given by Eq. (3.93) for $\mu = 0$. The normalization coefficient $\alpha \approx 1/1.065$ (6.39) is introduced to reproduce the low density results.

A comparison of the particle densities (3.19) and (3.89) shows that despite the different formulae for pressure the particle densities of these models have a very similar expression, but in (3.89) the second virial coefficient is replaced by the averaged value of the relativistic excluded volume $\langle \langle v(\mathbf{k}_1, \mathbf{k}_2) \rangle \rangle$. Such a complicated dependence of the particle density (3.89) on T and μ requires a nontrivial analysis for the limit of high pressures.

To analyze the high pressure limit $p \rightarrow \infty$ analytically I need an analytic expression for the excluded volume. For this purpose I will use the ultrarelativistic expression derived in the Appendix 6.4.:

$$v(\mathbf{k}_1, \mathbf{k}_2) \approx \frac{v^{Urel}(\mathbf{k}_1, \mathbf{k}_2)}{2} \equiv \frac{v_o}{2} \left(\frac{m}{E(\mathbf{k}_1)} + \frac{m}{E(\mathbf{k}_2)} \right) \left(1 + \cos^2 \left(\frac{\Theta_v}{2} \right) \right)^2 + \frac{3v_o}{2} \sin(\Theta_v) . \quad (3.93)$$

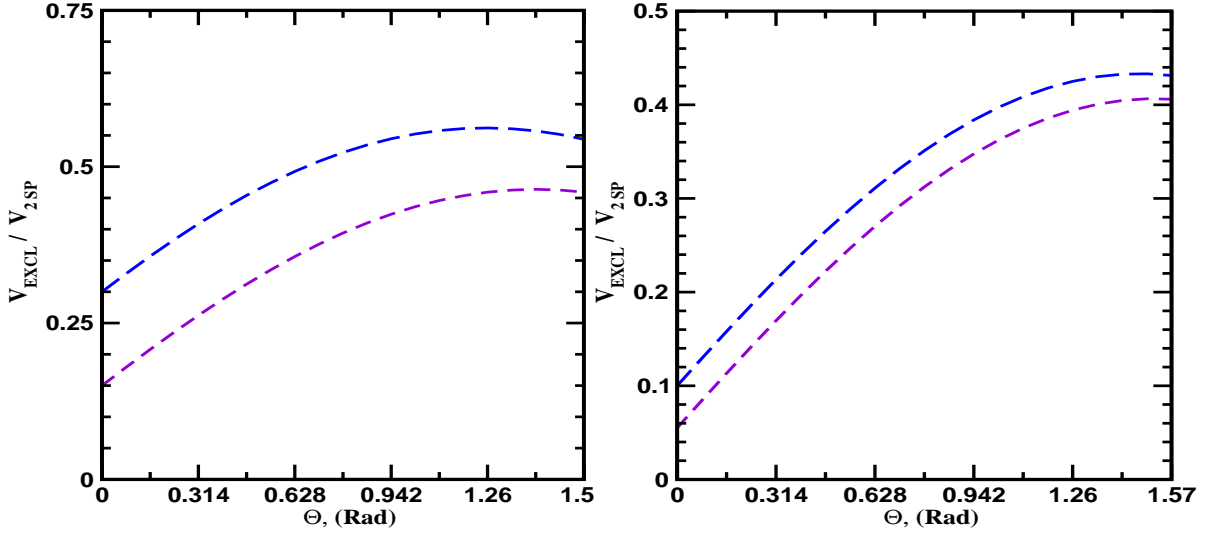


Figure 3.8. Comparison of the relativistic excluded volumes for highly contracted spheres. In the left panel the long dashed curve corresponds to $\frac{E(k_1)}{m} = 2$ and $\frac{E(k_2)}{m} = 10$ whereas the short dashed curve is found for $\frac{E(k_1)}{m} = 5$ and $\frac{E(k_2)}{m} = 10$. The corresponding values in the right panel are $\frac{E(k_1)}{m} = 10$, $\frac{E(k_2)}{m} = 10$ (long dashed curve) and $\frac{E(k_1)}{m} = 10$, $\frac{E(k_2)}{m} = 100$ (short dashed curve). It shows that the excluded volume for Θ_v close to $\frac{\pi}{2}$ is finite always, while for the collinear velocities the excluded volume approaches zero, if both spheres are ultrarelativistic.

As usual the total excluded volume $v^{Urel}(\mathbf{k}_1, \mathbf{k}_2)$ is taken per particle. Eq. (3.93) is valid for $0 \leq \Theta_v \leq \frac{\pi}{2}$, to use it for $\frac{\pi}{2} \leq \Theta_v \leq \pi$ one has to make a replacement $\Theta_v \rightarrow \pi - \Theta_v$ in (3.93). Here the coordinate system is chosen in such a way that the angle Θ_v between the 3-vectors of particles' momenta \mathbf{k}_1 and \mathbf{k}_2 coincides with the usual spherical angle Θ of spherical coordinates (see the Appendix 6.4.). To be specific, the OZ-axes of the momentum space coordinates of the second particle is chosen to coincide with the 3-vector of the momentum \mathbf{k}_1 of the first particle.

The Lorentz frame is chosen to be the rest frame of the whole system because otherwise the expression for pressure becomes cumbersome. Here v_0 stands for the eigen volume of particles which, for simplicity, are assumed to have the same hard core radius and the same mass.

Despite the fact that this equation was obtained for ultrarelativistic limit, it is to a within few per cent accurate in the whole range of parameters (see Fig. 3.7 and Appendix 6.4. for the details), and, in addition, it is sufficiently simple to allow one the analytical manipulations.

3.4.1. Proof of Causality in the High Pressure Limit. As it is seen from the expression for the relativistic excluded volume (3.93) for very high pressures only the smallest values of the relativistic excluded volume will give a non-vanishing contribution to the angular integrals of thermodynamic functions. This means that only Θ_v -values around 0 and around π will contribute into the thermodynamic functions (see Fig. 3.8). Using the variable $x = \sin^2(\Theta_v/2)$, one can rewrite the \mathbf{k}_2 angular integration as follows

$$I_{\Theta}(k_1) = \int \frac{d\mathbf{k}_2}{(2\pi)^3} e^{-\frac{v(\mathbf{k}_1, \mathbf{k}_2)p}{T}} = 4 \int \frac{d k_2 k_2^2}{(2\pi)^2} \int_0^{0.5} dx e^{-\left(AC\left(1-\frac{x}{2}\right)^2 + B\sqrt{x(1-x)}\right)}, \quad (3.94)$$

$$\text{with } A = 2v_0 \frac{p}{T}; \quad B = \frac{3}{2}A; \quad C = \left(\frac{m}{E(k_1)} + \frac{m}{E(k_2)} \right), \quad (3.95)$$

where I have accounted for the fact that the integration over the polar angle gives a factor 2π and that one should double the integral value in order to integrate over a half of the Θ_v range.

Since $C \leq 2$ in (3.95) is a decreasing function of the momenta, then in the limit $A \gg 1$ one can account only for the \sqrt{x} dependence in the exponential in (3.94) because it is the leading one. Then integrating by parts one obtains

$$I_{\Theta}(k_1) \approx 4 \int \frac{d k_2 k_2^2}{(2\pi)^2} e^{-AC} \int_0^{0.5} dx e^{-B\sqrt{x}} \approx 8 \int \frac{d k_2 k_2^2}{(2\pi)^2} e^{-AC} \frac{1}{B^2}. \quad (3.96)$$

Applying the result above to the pressure (3.86), in the limit under consideration one finds that the momentum integrals are decoupled and one gets the following equation for pressure

$$p(T, \mu) \approx \frac{16 T^3 e^{\frac{\mu}{T}}}{9 v_0^2 p^2 \rho_t(T)} \left[g \int \frac{d k k^2}{(2\pi)^2} e^{-\frac{E(k)}{T} - \frac{2v_0 m}{TE(k)} p} \right]^2. \quad (3.97)$$

Our next step is to perform the gaussian integration in Eq. (3.97). Analyzing the function

$$F \equiv 2 \ln k - \frac{E(k)}{T} - A \frac{m}{E(k)} \quad (3.98)$$

for $A \gg 1$, one can safely use the ultrarelativistic approximation for particle momenta $k \approx E(k) \rightarrow \infty$. Then it is easy to see that the function F in (3.98) has an extremum at

$$\frac{\partial F}{\partial E} = \frac{2}{E} - \frac{1}{T} + A \frac{m}{E^2} = 0 \quad \Rightarrow \quad E = E^* \approx \frac{A m}{\sqrt{1 + \frac{A m}{T}} - 1} \equiv T \left(\sqrt{1 + \frac{A m}{T}} + 1 \right), \quad (3.99)$$

which turns out to be a maximum, since the second derivative of F (3.98) is negative

$$\left. \frac{\partial^2 F}{\partial E^2} \right|_{E=E^*} \approx -\frac{2}{(E^*)^2} - 2A \frac{m}{(E^*)^3} < 0. \quad (3.100)$$

There are two independent ways to increase pressure: one can increase the value of chemical potential while keeping temperature fixed and vice versa. I will consider the high chemical potential limit $\mu/T \gg 1$ for finite T first, since this case is rather unusual. In this limit the above expressions can be simplified further on

$$E^* \approx \sqrt{2 m v_o p}, \quad \Rightarrow \quad \left. \frac{\partial^2 F}{\partial E^2} \right|_{E=E^*} \approx -\frac{2}{T \sqrt{2 m v_o p}}. \quad (3.101)$$

Here in the last step I explicitly substituted the expression for A . Performing the gaussian integration for momenta in (3.97), one arrives at

$$\int \frac{d k k^2}{(2\pi)^2} e^{-\frac{E(k)}{T} - \frac{2 v_o m}{T E(k)} p} \approx \frac{(E^*)^2}{(2\pi)^2} \sqrt{\pi T E^*} e^{-\frac{2 E^*}{T}}, \quad (3.102)$$

which leads to the following equation for the most probable energy of particle E^*

$$E^* \approx D T^4 e^{\frac{\mu - 4 E^*}{T}}, \quad D \equiv \frac{8 g^2 m^3 v_o}{9 \pi^3 \rho_t(T)}. \quad (3.103)$$

As one can see, Eq. (3.103) defines pressure of the system. Close inspection shows that the high pressure limit can be achieved, if the exponential in (3.103) diverges much slower than μ/T . The latter defines the EOS in the leading order as

$$E^* \approx \frac{\mu}{4}, \quad \Rightarrow \quad p \approx \frac{\mu^2}{32 m v_o}. \quad (3.104)$$

The left hand side equation above demonstrates that in the $\mu/T \gg 1$ limit the natural energy scale is given by chemical potential. This is a new and important feature of the relativistic VdW EOS compared to the previous findings.

The right hand side Eq. (3.104) allows one to find all other thermodynamic functions in this limit from thermodynamic identities:

$$s \approx 0, \quad n \approx \frac{2 p}{\mu}, \quad \varepsilon \equiv T s + \mu n - p \approx p. \quad (3.105)$$

Thus, it was shown that for $\mu/T \gg 1$ and finite T the speed of sound c_s in the leading order does not exceed the speed of light since

$$c_s^2 = \left. \frac{\partial p}{\partial \varepsilon} \right|_{s/n} = \frac{d p}{d \varepsilon} = 1. \quad (3.106)$$

From Eq. (3.103) it can be shown that the last result holds in all orders.

It is interesting that the left hand side Eq. (3.101) has a simple kinetic interpretation. Indeed, recalling that the pressure is the change of momentum during the collision time one can write (3.99) as follows (with $E^* = k^*$)

$$p = \frac{(k^*)^2}{2 m v_o} = \frac{2 k^*}{\pi R_o^2} \cdot \frac{3 v^* \gamma^*}{8 R_o} \cdot \frac{1}{2}. \quad (3.107)$$

In the last result the change of momentum during the collision with the wall is $2k^*$, which takes the time $\frac{8R_o}{3v^*\gamma^*}$. The latter is twice of the Lorentz contracted height ($4/3R_o$) of the cylinder of the base πR_o^2 which is passed with the speed v^* . Here the particle velocity v^* and the corresponding gamma-factor γ^* are defined as $v^*\gamma^* = k^*/m$. The rightmost factor $1/2$ in (3.107) accounts for the fact that only a half of particles moving perpendicular to the wall has the momentum $-k^*$. Thus, Eq. (3.107) shows that in the limit under consideration the pressure is generated by the particle momenta which are perpendicular to the wall. This, of course, does not mean that all particles in the system have the momenta which are perpendicular to a single wall. No, this means that in those places near the wall where the particles' momenta are not perpendicular (but are parallel) to it, the change of momentum $2k^*$ is transferred to the wall by the particles located in the inner regions of the system whose momenta are perpendicular to the wall. Also it is easy to deduce that such a situation is possible, if the system is divided into the rectangular cells or boxes inside which the particles are moving along the height of the box and their momenta are collinear, but they are perpendicular to the particles' momenta in all surrounding cells. Of course, inside of such a box each Lorentz contracted sphere would generate an excluded volume which is equal to a volume of a cylinder of height $\frac{2R_o}{\gamma^*}$ and base πR_o^2 . This cylinder differs from the one involved in Eq. (3.107), but one notes that exactly the hight $\frac{4R_o}{3\gamma^*}$ is used in the derivation of the ultrarelativistic limit for the relativistic excluded volume (6.38) (see the Appendix 6.4. for details). Thus, it is remarkable that the low density EOS extrapolated to very high values of the chemical potential, at which it is not supposed to be valid, gives a reasonable estimate for the pressure at high densities.

Another interesting conclusion that follows from this limit is that for the relativistic VdW systems existing in the nonrectangular volumes the relativistic analog of the dense packing maybe unstable.

The analysis of the limit $T/\mu \gg 1$ and finite μ also starts from Eqs. (3.97)–(3.99). The function F from (3.98) again has the maximum at $E^* \equiv E(k^*) = k^*$ defined by the right hand side Eq. (3.99). Now the second derivative of function F becomes

$$\left. \frac{\partial^2 F}{\partial E^2} \right|_{E=E^*} \approx -\frac{2}{(E^*)^2} - 2A \frac{m}{(E^*)^3} = -\frac{2\sqrt{1 + \frac{Am}{T}}}{(E^*)^2}. \quad (3.108)$$

This result allows one to perform the gaussian integration for momenta in (3.97) for this limit as

$$\int \frac{d k k^2}{(2\pi)^2} e^{-\frac{E(k)}{T} - \frac{3v_0 m}{TE(k)} p} \approx \frac{(E^*)^3 e^{-2\left(1 + \frac{Am}{T}\right)^{\frac{1}{2}}}}{(2\pi)^2 \left(1 + \frac{Am}{T}\right)^{\frac{1}{4}}} I_\xi \left(1 + \frac{Am}{T}\right), \quad (3.109)$$

where the auxiliary integral I_ξ is defined as follows

$$I_\xi(x) \equiv \int_{-\sqrt{x}}^{+\infty} d\xi e^{-\xi^2}. \quad (3.110)$$

The above results can be used to find the thermal density $\rho_t(T)$ in the limit $T \rightarrow \infty$ by the substitution $A = 0$. Using (3.109), one can rewrite the equation for pressure (3.97) as the equation for the unknown variable $z \equiv Am/T$

$$z^3 \approx e^{\frac{\mu}{T}} \phi(z), \quad \phi(z) \equiv \frac{3 g v_0 m^3 I_\xi^2(1+z) \left(1 + (1+z)^{\frac{1}{2}}\right)^3}{(2\pi e^{\sqrt{1+z}})^2 I_\xi(1)(1+z)^{\frac{1}{2}}}. \quad (3.111)$$

Before continuing this analysis further on it is necessary to make the two comments concerning Eq. (3.111). First, rewriting the right hand side Eq. (3.111) in terms of pressure, one can see that the value of chemical potential is formally reduced exactly in three times. In other words, it looks like that in the limit of high temperature and finite μ the pressure of the relativistic VdW gas is created by the particles with the charge being equal to the one third of their original charge. Second, due to the nonmonotonic dependence of $\phi(z)$ in the right hand side Eq. (3.111) it is possible that the left hand side Eq. (3.111) can have several solutions for some values of parameters. Leaving aside the discussion of this possibility, I will further consider only such a solution of (3.111) which corresponds to the largest value of the pressure (3.97).

Since the function $\phi(z)$ does not have any explicit dependency on T or μ , one can establish a very convenient relation

$$\frac{\partial z}{\partial T} = -\frac{\mu}{T} \frac{\partial z}{\partial \mu} \quad (3.112)$$

between the partial derivatives of z given by the left hand side Eq. (3.111). Using it, one can calculate all the thermodynamic functions from the pressure $p = \alpha T^2 z$ (with $\alpha \equiv (3 m v_o)^{-1}$) as:

$$n \approx \alpha T^2 \frac{\partial z}{\partial \mu}, \quad (3.113)$$

$$s \approx \alpha \left[2T z + T^2 \frac{\partial z}{\partial T} \right] = \frac{2p - \mu n}{T}, \quad (3.114)$$

$$\varepsilon \equiv Ts + \mu n - p \approx p. \quad (3.115)$$

The last result leads to the causality condition (3.106) for the limit $T/\mu \gg 1$ and finite μ as well. In fact, the above result can be extended to any $\mu > -\infty$ and any value of T satisfying the inequality

$$E^* \approx T \left(\sqrt{1+z} + 1 \right) \gg m, \quad (3.116)$$

which is sufficient to derive Eq. (3.111). To show this it is sufficient to see that for $z = 0$ one has the inequality $z^3 < e^{\frac{\mu}{T}} \phi(z)$, which changes to the opposite inequality $z^3 > e^{\frac{\mu}{T}} \phi(z)$ for $z = \infty$. Consequently, for any value of μ and T satisfying (3.116) the left hand side Eq. (3.111) has at least one solution $z^* > 0$ for which one can establish Eqs. (3.112)–(3.115) and prove the validity of the causality condition (3.106).

The model (3.86) along with the analysis of high pressure limit can be straightforwardly generalized to include several particle species. For the pressure $p(T, \{\mu_i\})$ of the mixture of N -species with masses m_i ($i = \{1, 2, \dots, N\}$), degeneracy g_i , hard core radius R_i and chemical potentials μ_i is defined as a solution of the following equation

$$p(T, \{\mu_i\}) = \int \frac{d^3 \mathbf{k}_1}{(2\pi)^3} \frac{d^3 \mathbf{k}_2}{(2\pi)^3} \sum_{i,j=1}^N \frac{T g_i g_j}{\rho_{tot}(T, \{\mu_l\})} e^{\frac{\mu_i + \mu_j - v_{ij}(\mathbf{k}_1, \mathbf{k}_2) p - E_i(k_1) - E_j(k_2)}{T}}, \quad (3.117)$$

where the relativistic excluded volume per particle of species i (with the momentum \mathbf{k}_1) and j (with the momentum \mathbf{k}_2) is denoted as $v_{ij}(\mathbf{k}_1, \mathbf{k}_2)$, $E_i(k_1) \equiv \sqrt{k_1^2 + m_i^2}$ and $E_j(k_2) \equiv \sqrt{k_2^2 + m_j^2}$ are the corresponding energies, and the total thermal density is given by the expression

$$\rho_{tot}(T, \{\mu_i\}) = \int \frac{d^3 \mathbf{k}}{(2\pi)^3} \sum_{i=1}^N g_i e^{\frac{\mu_i - E_i(k)}{T}}. \quad (3.118)$$

The excluded volume $v_{ij}(\mathbf{k}_1, \mathbf{k}_2)$ can be accurately approximated by $\alpha v_{12}^{Urel}(R_i, R_j)/2$ defined by Eqs. (6.38) and (6.39).

The multicomponent generalization (3.117) is obtained in the same sequence of steps like the one component expression (3.86). The only difference is in the definition of the total thermal density (3.118) which now includes the chemical potentials. Note also that the expression (3.117) by construction recovers the virial expansion up to the second order at low particle densities, but it cannot be reduced to any of two extrapolations which are suggested in [159] and [161] for the multicomponent mixtures and carefully analyzed in Ref. [155]. Thus, the expression (3.117) removes the non-uniqueness of the VDW extrapolations to high densities, if one requires a causal behavior in this limit.

3.4.2. A Few Remarks on Possible Observables. In the preceding section I considered a relativistic analog of the VdW EOS which reproduces the virial expansion for the gas of the Lorentz contracted rigid spheres at low particle densities and, as was shown above, is causal at high densities. As one can see from the expression for particle density (3.89) the one-particle momentum distribution function has a more complicated energy dependence than the usual Boltzmann distribution function, which would be interesting to check up experimentally. This, of course, is a very difficult task since the particle spectra measured in high energy nuclear collisions involve a strong collective flow which can easily hide or smear the additional energy dependence. However, it is possible that such a complicated energy dependence of the momentum spectra and excluded volumes of lightest hadrons, i.e. pions and kaons, can be verified for highly accurate measurements, if the collective flow is correctly taken into account. The latter is a tremendously difficult task because it is related to the freeze-out problem in relativistic hydrodynamics [173] or hydro-cascade approach [263].

Perhaps, it would be more realistically to incorporate the developed approach into the effective models of nuclear/hadronic matter [163, 177, 178, 179], and check the obtained EOS on the huge amount of data collected by the nuclear physics of intermediate energies. Since the suggested relativization of the VdW EOS makes it softer at high densities and, hence, one can hope to improve the description of the nuclear/hadronic matter properties (compressibility constant, elliptic flow, effective nucleon masses etc) at low temperatures and high baryonic densities [63].

Also it is possible that the momentum spectra of this type can help to extend the hydrodynamic

description into the region of large transversal momenta of hadrons ($p_T > 1.5 - 2$ GeV) which are usually thought to be too large to follow the hydrodynamic regime [186].

Another possibility to verify the suggested model is to study the angular correlations of the hard core particles emitted from the neighboring regions and the enhancement of the particle yield of those hadrons which appear due to the coalescence of the constituents with the strong short range repulsion. As was proven in the preceding sections (see also Fig. 3.8) the present model predicts that the probability to find the neighboring particles with the collinear velocities is higher than to find the neighboring particles with the non-collinear velocities. Due to this reason the coalescence of particles with the collinear velocities should be enhanced. This effect gets strong, if pressure is high and if particles are relativistic in the local rest frame. Therefore, it would be interesting to study the coalescence of any relativistic constituents with hard core repulsion (quarks or hadrons) at high pressures in a spirit of the recombination model of Ref. [187] and extend its results for light hadrons to lower values of transversal momenta. Perhaps, the inclusion of such an effect into consideration may essentially improve not only our understanding of the quark coalescence process, but also the formation of deuterons and other nuclear fragments in relativistic nuclear collisions. This subject is, however, outside the scope of the present work.

As a typical VdW EOS the present model should be valid for the low particle densities, but the above analysis of the limit $\mu/T \gg 1$ for fixed T led to a surprisingly clear kinetic expression for the system's pressure (3.107). Therefore, it is possible that this low density result may provide us with the correct hint to study the relativistic analog of the dense packing problem. Thus, it would be interesting to verify, whether the above approach remains valid for relativistic quantum treatment because there are several unsolved problems for the systems of relativistic bosons and/or fermions which, on the one hand, are related to the problems discussed here and which, on the other hand, maybe potentially important for relativistic nuclear collisions and for nuclear astrophysics.

3.5. Conclusions

In this chapter I presented the generalization of the virial and cluster expansions for the momentum dependent interparticle potentials. This is necessary generalization of the corresponding

nonrelativistic expansions. Such a generalization allowed me to formulate a new class of the hadronic matter EOS for the Lorentz contracted rigid spheres. The first representative from this class, Eq. (3.18), is obtained as the usual VdW extrapolation to high densities. It accounts for the Lorentz contraction of the relativistic hard core repulsion at low densities, but breaks causality at high densities. Since the Lorentz contraction stronger affects the lighter particles, the hadronic EOS of this type require the statistical treatment with the multicomponent hard core repulsion between the different particle species.

A detailed analysis of canonical and grand canonical descriptions of the hadronic mixtures with the multicomponent hard core repulsion shows that the two VdW extrapolations, considered in this chapter, give practically the identical results for the particle ratios observed at AGS and highest SPS energies. Also such an analysis showed that the major conclusion of Ref. [165] on the values of hadronic hard core radii is wrong, whereas the relativistic treatment of pion hard core repulsion presented here, is consistent with the results reported in Ref. [137].

Further on I considered another VdW extrapolation for the Lorentz contracted rigid spheres, Eq. (3.86), and showed that in the limit of high pressure it obeys a causality. The suggested EOS, of course, is not a rigorous result based on the exact summation of the relativistic virial expansion, but, similarly to its nonrelativistic counterpart, it gives a qualitatively correct estimate for high pressures. A new element of this EOS is that its average excluded volume coincides with the relativistic second virial coefficient at small pressures only, whereas at high pressures the average excluded volume is smaller than the relativistic second virial coefficient. As I showed above this fact leads to an interesting kinetic interpretation of the systems pressure (3.107) at $\mu/T \gg 1$ and finite T , which corresponds to the relativistic analog of dense packing. Thus, the suggested model EOS for the Lorentz contracted rigid spheres predicts the existence of relativistic polycrystalline structure in hadronic matter at $\mu/T \gg 1$ and finite T , if the deconfinement PT to QGP occurs at sufficiently high pressure. Perhaps, this can be the case for the effective nucleons in the Walecka-like models (see chapter 1) with the relativistic hard core repulsion which can be applied to various astrophysical objects.

Since the suggested EOS obeys a causality in high pressure limit, it can be used for the liquid

phase of nuclear matter within the GSMM concept introduced in the chapter 2. Also this EOS is a good candidate to describe the EOS of lightest hadrons (pions, kaons e.t.c.), which, according to lattice quantum chromodynamics (see a discussion in the next chapter), can coexist with heavy QGP bags at high temperatures above the cross-over transition.

At high pressures the suggested EOS for the Lorentz contracted rigid spheres favors the collinear velocities for neighboring particles because they occupy less volume and, hence, the surrounding media is "disturbed" less, whereas the configurations with the perpendicular velocities of neighboring particles are highly suppressed. Perhaps, such an angular asymmetry can improve our understanding of statistical aspects of a coalescence process of any relativistic constituents (nucleons or quarks) in a dense media.

Finally, the relativistic analog of the VdW EOS (3.86) resolves the problem of non-uniqueness of the VdW extrapolation to the systems with the multiple hard core repulsion between the constituents, if one requires the causal behavior of the EOS at high pressures.

CHAPTER 4

EXACTLY SOLVABLE PHENOMENOLOGICAL EOS OF THE DECONFINEMENT PT

A natural step to generalize the hadron gas model analyzed in the previous chapter could be its extension to infinitely heavy hadronic states. Thus, one could include into statistical description all known hadronic states and the hypothetical hadronic states which may be arbitrarily heavy. Then, using the properties of the cluster models like the FDM and SMM, one could analyze the obtained model for the PT existence. But historically this happened differently: the infinitely heavy hadronic states were introduced into statistical mechanics by Rolf Hagedorn [148, 149], first, and then it was realized that the limiting temperature, the Hagedorn temperature, generated by the statistical bootstrap model (SBM) [188] for the systems of all hadrons consisting of other hadrons, evidences for a new physics beyond the Hagedorn temperature. Based on the Hagedorn results, Cabibbo and Parisi concluded that the limiting temperature is the phase transition temperature [189] to the state of partonic degrees of freedom, to quarks and gluons. This was the beginning of relativistic nuclear physics.

Thus, from the very beginning the SBM [148, 149, 188] gave the first evidence that an exponentially growing hadronic mass spectrum $g_H(m) = \exp[m/T_H] (m_o/m)^a$ for $m \rightarrow \infty$ (the constants m_o and a will be defined later) could lead to new thermodynamics above the Hagedorn temperature T_H . Originally, the divergence of thermodynamic functions at temperatures T above T_H was interpreted as the existence of a limiting temperature for hadrons. In other words, it is impossible to build the hadronic thermostat above T_H . A few years later an exponential form of the asymptotic mass spectrum was found in the MIT bag model [138] and the associated limiting temperature was correctly interpreted as the phase transition temperature to the partonic degrees of freedom [189]. These results initiated extensive studies of hadronic thermodynamics within the

framework of the GBM [195, 196]. The SBM with a non-zero proper volume [192] of hadronic bags was solved analytically [134] by the Laplace transform to the isobaric ensemble (see chapters 1 and 2) and the existence of phase transition from hadronic to partonic matter, nowadays known as QGP, was shown. Since then the more sophisticated formulations of the SBM [193, 225] were suggested.

The major achievement of the SBM is that it naturally explains why the temperature of secondary hadrons created in collisions of elementary particles at high energies cannot exceed T_H . However, this result is based on *two related assumptions*. First, the grand canonical formulation for the SBM is appropriate, and second, the resonances of infinite mass should contribute to thermodynamic functions.

However, the story with the SBM is not over yet because very recently, using the microcanonical formulation, my collaborators and I showed [140, 190] that in the absence of any restrictions on the mass, resonances with the Hagedorn mass spectrum behave as perfect thermostats and perfect chemical reservoirs, i.e. they impart the Hagedorn temperature T_H to particles which are in thermal contact and force them to be in chemical equilibrium. These findings led to the following significant conclusions [140]: (i) canonical and/or grand canonical formulations of the statistical mechanics of any system coupled to a Hagedorn thermostat are not equivalent to the microcanonical one; (ii) in the presence of the Hagedorn thermostat *it is improper to include any temperature other than T_H* into the canonical and/or grand canonical description; (iii) the Hagedorn thermostat generates a volume independent concentration of the particles in chemical equilibrium with it [140].

The first of these results was obtained by R. D. Carlitz [191], who analyzed the nonequivalence conditions for the canonical and microcanonical formulations of the SBM. However, Carlitz's somewhat complicated and detailed mathematical analysis of the problem prevented the observation of the consequences (ii) and (iii) regarding the themostatic properties of Hagedorn systems. Therefore, the entire framework of the SBM and GBM, which is also based on the two major assumptions discussed above, should be revisited. In other words, it is necessary to return to the foundations of the statistical mechanics of hadrons and study the role of the Hagedorn mass spectrum for finite masses of hadronic resonances above the cut-off value m_o , below which the hadron mass spectrum

is discrete. Such an analysis for an arbitrary value of a in $g_H(m)$ was done in [141].

The results on thermostatic properties of heavy hadronic resonances maybe important for the elementary particle collisions, in which the short range repulsion, perhaps, can be ignored, but to use it to model A+A collisions one must get rid of the artificial singularities in the GCE. For this purpose it is necessary to use some additional physical input. In the chapter 2 I considered the GBM solution in finite volume. This model generalizes the SBM and accounts for the hard core repulsion between hadronic bags. In the GCE such a treatment (at least in the simplest case) generates an exponential decreasing mass spectrum which removes an artificial singularities of the SBM. This exactly solvable model [134], however, is just a toy model which cannot be used to describe simultaneously the 1st deconfinement PT and a cross-over. A recent try [135] to revitalize the GBM does not look reasonable because the main assumption of Ref. [135] about the existence of the line along which the order of PT gradually increases contradicts the whole concept of critical phenomena which is based on a assumption that any PT occurs due to the break down of certain symmetry in the system under consideration. However, as I will show below the GBM lacks the surface free energy of large hadronic bags. If the latter is included into statistical treatment, then such a model [240, 241], the quark-gluon bags with surface tension (QGBST) model, is able to simultaneously describe the 1st deconfinement PT and cross-over.

Another possibility to remove the artificial singularities of the SBM in the GCE is to use the properties of the Mott transition and introduce the special mass dependent width of heavy resonances [200, 225, 226]. Such a model allows one to describe the data on thermodynamic functions obtained by the lattice quantum chromodynamics simulations. Also it explains the reason why very heavy hadronic resonances are not observed experimentally.

The chapter is based on the following works [113, 140, 141, 142, 200, 225, 226, 240, 241, 242].

4.1. Microcanonical Analysis of the Hagedorn Model

The microcanonical analysis of the Hagedorn model is important for understanding the differences and similarities between A+A and elementary particle collisions at high energies. There are two temperatures measured in A+A collisions that are very close to the transition temperature T_{Tr} ,

from hadron gas to QGP calculated from the lattice quantum chromodynamics [194] at vanishing baryonic density. The first is the chemical freeze-out temperature at vanishing baryonic density $T_{Chem} \approx 175 \pm 10$ MeV of the most abundant hadrons (pions, kaons, nucleons *etc*) extracted from particle multiplicities at highest SPS [136, 137] and all RHIC [198, 199] energies. Within the error bars $T_{Tr} \approx T_{Chem}$ is also very close to the kinetic freeze-out temperature T_{Kin} (i.e. hadronization temperature) found from the transverse mass spectra of heavy, weakly interacting hadrons such as Ω hyperons, J/ψ and ψ' mesons at the highest SPS energy [205, 206, 207], and Ω -hyperons [208, 209, 210, 211, 212] and ϕ meson [208, 209, 212, 213] at $\sqrt{s} = 130$ A·GeV and $\sqrt{s} = 200$ A·GeV energies of RHIC. The existence of the deconfinement transition naturally explains the same value for all these temperatures.

Can the same logic be applied to the collisions of elementary particles, where the formation of a deconfined quark gluon matter is rather problematic? The fact that the hadronization temperature [201] and inverse slopes of the transverse mass spectra of various hadrons [197] found in elementary particle collisions at high energies are similar to those ones for A+A collisions is tantalizing.

Hagedorn noted that the hadronic mass spectrum (level density) has the asymptotic ($m \rightarrow \infty$) form

$$\rho_{\mathcal{H}}(m) \approx \exp(m/T_{\mathcal{H}}), \quad (4.1)$$

where m is the mass of the hadron in question and $T_{\mathcal{H}}$ is the parameter (temperature) controlling the exponential rise of the mass spectrum [148, 149]. The question of the mass range over which (4.1) is valid is still under discussion [225].

The M.I.T. bag model [138] of partonic matter produces the same behavior via a constant pressure B of the containing “bag” [195, 196]. In the absence of conserved charges the bag pressure B forces a constant temperature T_B and energy density ϵ from which it follows that the bag entropy is

$$S = \epsilon V/T_B = m/T_B \quad (4.2)$$

where V and m are the volume and mass of the bag respectively. This leads to a bag mass spectrum $\exp(S)$ identical to Eq. (4.1) [195, 196]. This property implies the lack of any surface energy associated with the bag.

A variety of experiments with high energy ($\sqrt{s} \geq 30 - 50$ GeV) elementary particle collisions on very different systems indicate a constant temperature characterizing both chemical and thermal equilibrium at vanishing baryonic densities [204, 197, 201]. It is interesting to explore the connection of these empirical temperatures with the Hagedorn temperature $T_{\mathcal{H}}$ on one hand and the bag temperature T_B on the other.

I will show that the temperature of any such \mathcal{H} system is not affected by the extrinsic injection of energy into the system but it is encoded and strictly enforced by the fixed temperature of the mass spectrum.

The insertion of an exponential spectrum such as Eq. (4.1) in the partition function

$$\mathcal{Z}(T) = \int_{E_{min}}^{\infty} \rho_{\mathcal{H}}(E) e^{-\frac{E}{T}} dE \quad (4.3)$$

led to the incorrect conclusion that the entire range of temperatures $0 \leq T < T_{\mathcal{H}}$ would be accessible and that $T_{\mathcal{H}}$ is the limiting temperature of the system.

In order to see the origin of this erroneous conclusion, let me consider the following illuminating exercise. Consider a system A composed of ice and water at standard pressure. For such a system the temperature (kelvin) is $T_A = 273$ K. Because of coexistence, one can feed or extract heat to/from the system without changing T_A . The system A is a thermostat.

If a quantity Q of heat is added to the sytem, the change in entropy is

$$\Delta S = Q/T_A. \quad (4.4)$$

The level density of A is then

$$\rho(Q) = S_0 e^{Q/T_A} \approx K e^{E/T_A}. \quad (4.5)$$

The level density, or spectrum, is exponential in E and depends only on the intrinsic "parameter" T_A . Let us calculate the partition function of A :

$$Z(T) = \int e^{E/T_A} e^{-E/T} dE = \int e^{-\left(\frac{1}{T} - \frac{1}{T_A}\right)E} dE = \frac{T_A T}{T_A - T} \quad (4.6)$$

This seems to indicate that A can assume *any* temperature $0 \leq T < T_A$. But, by hypothesis, the only temperature possible for A is T_A . What is the trouble?

Let me consider two systems A, B with level densities ρ_A and ρ_B . Let the systems be thermally coupled to each other with total energy E . Now I can calculate the distribution in energies between the two systems,

$$\rho_T(x) = \rho_A(E - x)\rho_B(x) \quad (4.7)$$

Let A be a "thermostat", i.e. $\rho_A = e^{\epsilon/T_A}$. Then

$$\rho_T(x) = \exp\left(\frac{E - x}{T_A}\right)\rho_B(x) = e^{E/T_A}e^{-x/T_A}\rho_B(x). \quad (4.8)$$

Let me integrate over x for macroscopic systems and macroscopic value of E

$$\int \rho_T(x)dx = e^{E/T_A} \int e^{-x/T_A}\rho_B(x)dx = e^{E/T_A}Z_B(T_A). \quad (4.9)$$

This is the origin of the partition function $Z_B(T_A)$ and the meaning of "implicit" thermostat. By changing "thermostat" one can change T_A and the temperature of B .

Thus, every time we construct a partition function, we imply the gedanken experiment of connecting the system to a thermostat, and that this experiment is actually possible for the system we are studying. Does this always work?

To see this, let us look for the most probable value of the distribution $\rho_T(x)$, which defines the equilibrium partition, by taking the log and differentiating:

$$\ln \rho_T(x) = \ln \rho_A(E - x) + \ln \rho_B(x) \quad (4.10)$$

$$\partial \ln \rho_T(x)/\partial x = - \partial \ln \rho_A/\partial x + \partial \ln \rho_B/\partial x = 0 \quad (4.11)$$

or

$$1/T_A = 1/T_B. \quad (4.12)$$

For this to be possible, it is necessary that ρ_A and ρ_B admit the *same* logarithmic derivative somewhere in the allowed range of energy x .

Usually, and always for concave functions, $S(x) = \ln \rho(x)$ and $T = (\partial S/\partial x)^{-1}$ is such that $0 \leq T \leq \infty$. Thus, for such systems it is possible to match derivatives for whatever value of E . Thermal equilibrium is achievable over a broad range of temperatures.

However, if $S_A(E) = \ln \rho_A(E)$ is linear in E , then $T_A = (\partial S / \partial E)^{-1}$ is a constant, independent of E . In this case, it is up to B to look for the value of x at which its logarithmic derivative matches $1/T_A$. The system A is a “thermostat” at $T = T_A$ and B can only try to assume the value $T = T_B = T_A$, if it can do so.

Now suppose that also $S_B(E) = \ln \rho_B(E)$ is linear in E with an inverse slope T_B . This means that only if $T_A = T_B$ is equilibrium possible, and the partition function of B , Z_B is meaningfully defined only for $T = T_B$ and not for $0 \leq T \leq T_B$. One cannot force a temperature $T \neq T_B$ on a thermostat. It can only have its own intrinsic temperature T_B .

Placing systems A and B into contact will lead to a continuous heat flow from one system to the other. Thermal equilibrium is not achievable.

Summarizing: it is permissible to calculate a system’s partition function only, if its $S(E)$ admits as inverse derivatives values such as one wants to impose through the Laplace transform. Failing that, the resulting partition function does not satisfy any thermodynamic criterion.

Carlitz noticed [191] that Eq. (4.1) leads to a nonequivalence between the (grand)canonical and microcanonical descriptions. However, the striking consequences of this fact reported in above were not noticed and appreciated.

I show here that the exponential form of the mass spectrum in Eq. (4.1) forces the unique temperature $T_{\mathcal{H}}$ on both the chemical and thermal equilibria associated with it. Below the consequences of this hitherto unappreciated fact are discussed.

To begin, I show that a system \mathcal{H} possessing a Hagedorn-like spectrum, characterized by an entropy of the form (4.2), not only has a unique microcanonical temperature $T_{\mathcal{H}}$

$$T_{\mathcal{H}} = (dS/dE)^{-1} = T_B, \quad (4.13)$$

but also imparts this same temperature to any other system to which \mathcal{H} is coupled. In the language of thermodynamics: \mathcal{H} is a perfect thermostat with the constant temperature $T_{\mathcal{H}}$.

Incidentally, it is worth noting that a perfect thermostat is indifferent to the transfer of any portion of its energy to any parcel within itself, no matter how small. In other words, it is at the limit of phase stability and the internal fluctuations of its energy density are maximal. Therefore it does not matter whether this thermostat is one large bag or it is fragmented in an arbitrary number

of smaller bags or, equivalently, it is a system of hadrons with a spectrum given by Eq. (4.1). This has no consequences on the properties of \mathcal{H} as one can see below.

4.1.1. Harmonic Oscillator Coupled to \mathcal{H} . In order to demonstrate the thermostatic behavior of a Hagedorn system, let me begin by coupling \mathcal{H} to a one dimensional harmonic oscillator and use a microcanonical treatment. The unnormalized probability $P(\varepsilon)$ for finding an excitation energy ε in the harmonic oscillator out of the system's total energy E is

$$P(\varepsilon) \sim \rho_{\mathcal{H}}(E - \varepsilon)\rho_{\text{osc}}(\varepsilon) = \exp\left(\frac{E - \varepsilon}{T_{\mathcal{H}}}\right) = \rho_{\mathcal{H}}(E) \exp\left(-\frac{\varepsilon}{T_{\mathcal{H}}}\right). \quad (4.14)$$

Recall that for a one dimensional harmonic oscillator ρ_{osc} is a constant. The energy spectrum of the oscillator is canonical up to the upper limit $\varepsilon_{\text{max}} = E$ with an inverse slope (temperature) of $T_{\mathcal{H}}$ independent of E . The mean value of the energy of the oscillator is

$$\bar{\varepsilon} = T_{\mathcal{H}} \left[1 - \frac{E/T_{\mathcal{H}}}{\exp(E/T_{\mathcal{H}}) - 1} \right]. \quad (4.15)$$

Thus in the limit that $E \rightarrow \infty$: $\bar{\varepsilon} \rightarrow T_{\mathcal{H}}$, i.e. no temperature other than $T_{\mathcal{H}}$ is admitted. In the standard language of statistical mechanics this example means that a one dimensional harmonic oscillator can be used as an ideal thermometer.

4.1.2. An Ideal Vapor Coupled to \mathcal{H} . For a physically more relevant example, let me consider a vapor of $N \gg 1$ non-interacting particles of mass m coupled to \mathcal{H} . The microcanonical level density of the vapor with kinetic energy ε is

$$\rho_{\text{vapor}}(\varepsilon) = \frac{V^N}{N! \left(\frac{3}{2}N\right)!} \left(\frac{m\varepsilon}{2\pi}\right)^{\frac{3}{2}N}, \quad (4.16)$$

where V is the volume. The microcanonical partition of the total system is

$$\rho_{\text{total}}(E, \varepsilon) = \rho_{\mathcal{H}}(E - \varepsilon)\rho_{\text{vapor}}(\varepsilon) = \frac{V^N}{N! \left(\frac{3}{2}N\right)!} \left(\frac{m\varepsilon}{2\pi}\right)^{\frac{3}{2}N} e^{\frac{E - mN - \varepsilon}{T_{\mathcal{H}}}}. \quad (4.17)$$

The distribution of the vapor is exactly canonical up to $\varepsilon_{\text{max}} = E$, if the particles are independently present, or $\varepsilon_{\text{max}} = E - mN$, if the particles are generated by \mathcal{H} . In either case, the temperature of the vapor is always $T_{\mathcal{H}}$.

At fixed N the maximum of $\rho_{\text{total}}(E, \varepsilon)$ with respect to ε gives the most probable kinetic energy per particle as

$$\frac{\partial \ln \rho_{\text{total}}(E, \varepsilon)}{\partial \varepsilon} = \frac{3N}{2\varepsilon} - \frac{1}{T_{\mathcal{H}}} = 0 \Rightarrow \frac{\varepsilon}{N} = \frac{3}{2}T_{\mathcal{H}}, \quad (4.18)$$

provided that $E \geq mN + \frac{3}{2}NT_{\mathcal{H}}$. For $mN < E < mN + \frac{3}{2}NT_{\mathcal{H}}$, the most probable kinetic energy per particle value is $\frac{\varepsilon}{N} = \frac{E}{N} - m < \frac{3}{2}T_{\mathcal{H}}$; for $E \leq mN$, $\frac{\varepsilon}{N} = 0$. $T_{\mathcal{H}}$ is the sole temperature characterizing the distribution up to the microcanonical cut off, which may be above or below the maximum of the distribution, since the form of $\rho_{\text{total}}(E, \varepsilon)$ is E -independent.

The maximum of $\rho_{\text{total}}(E, \varepsilon)$ with respect to N at fixed V is given by

$$\frac{\partial \ln \rho_{\text{total}}(E, \varepsilon)}{\partial N} = -\frac{m}{T_{\mathcal{H}}} + \ln \left[\frac{V}{N} \left(\frac{mT_{\mathcal{H}}}{2\pi} \right)^{\frac{3}{2}} \right] = 0, \quad (4.19)$$

where Eq. (4.18) was used for ε . Thus the most probable particle density of the vapor is *independent* of V :

$$\frac{N}{V} = \left(\frac{mT_{\mathcal{H}}}{2\pi} \right)^{\frac{3}{2}} e^{-\frac{m}{T_{\mathcal{H}}}} \equiv n_{\mathcal{H}}. \quad (4.20)$$

Equation (4.20) demonstrates that not only is \mathcal{H} a perfect thermostat but also a perfect particle reservoir. Particles of different mass m will be in chemical equilibrium with each other. At equilibrium, particles emitted from \mathcal{H} form a saturated vapor at coexistence with \mathcal{H} at temperature $T_{\mathcal{H}}$. This describes a first order phase transition (hadronic to partonic). Coexistence occurs at a single temperature fixed by the bag pressure. Different arguments lead to a similar conclusion concerning the existence of a phase transition [191].

These key results explain the common value of: the hadronization temperatures obtained within the statistical hadronization model at vanishing baryonic densities [201]; the inverse slopes of the transverse mass spectra of hadrons observed in high energy elementary particle collisions with the transverse momenta $p_T \leq 1$ GeV [204, 197]; and the transition temperature from lattice QCD calculations for low baryonic density [194]. For further discussion see [141].

Let me consider the case in which the vapor particle mass m is free. The system's level density $\rho_{\text{total}}(E, \varepsilon)$ is still given by Eq. (4.17). Using Eqs. (4.18) and (4.20), one finds the most probable value of the system's level density as $\rho_{\text{total}}^*(E, \varepsilon) \approx \exp[S^*]$, where the entropy is $S^* = E/T_{\mathcal{H}} + N$.

Differentiating $\rho_{\text{total}}^*(E, \varepsilon)$ with respect to m and applying Eq. (4.20) gives

$$\frac{\partial \ln \rho_{\text{total}}^*(E, \varepsilon)}{\partial m} = N \left[\frac{3}{2m} - \frac{1}{T_{\mathcal{H}}} \right] = 0 \Rightarrow m = \frac{3}{2} T_{\mathcal{H}}, \quad (4.21)$$

i.e. the last equality provides the maximum of level density for $N \neq 0$. Since all the intrinsic statistical weights in $\rho_{\text{total}}^*(E, \varepsilon)$ are factored into a single \mathcal{H} , the system breaks into fragments with $m = \frac{3}{2} T_{\mathcal{H}}$ except for one whose mass is determined by mass/energy conservation.

Substituting the most probable value of ε and m into the most probable value of N gives the vapor concentration

$$\frac{N}{V} = \left(\frac{3}{4\pi e} \right)^{\frac{3}{2}} T_{\mathcal{H}}^3. \quad (4.22)$$

The vapor density of nonrelativistic particles acquires the typical ultrarelativistic limit form.

If the mass given by Eq. (4.21) does not exist, then the level density's most probable value $\rho_{\text{total}}^*(E, \varepsilon)$ corresponds to the mass m^* nearest to $\frac{3}{2} T_{\mathcal{H}}$ and $N(m^*)$ given by Eq. (4.20). The value of m^* that maximizes the level density $\rho_{\text{total}}^*(E, \varepsilon)$ is the pion mass.

4.1.3. \mathcal{H} as a Radiant Bag. Do the emitted particles need to remain in the proximity of \mathcal{H} to insure equilibrium? Let me assume that \mathcal{H} is a bag thick enough to absorb any given particle of the vapor striking it. Then, detailed balance requires that on average \mathcal{H} radiates back the same particle. Under these conditions particles can be considered to be effectively emitted from the surface of \mathcal{H} . *Thus the relevant fluxes do not depend in any way upon the inner structure of \mathcal{H} , nor on the presence of the outer vapor.*

The results in equations (4.18) and (4.20) show that the saturated vapor concentration depends only on m and $T_{\mathcal{H}}$ as long as \mathcal{H} is present. A decrease in V does not increase the vapor concentration, but induces a condensation of the corresponding amount of energy out of the vapor into \mathcal{H} . An increase in V keeps the vapor concentration constant via evaporation of the corresponding amount of energy out of \mathcal{H} into the vapor. This is reminiscent of liquid-vapor equilibrium at fixed temperature, except that here coexistence occurs at a single temperature $T_{\mathcal{H}}$, rather than over a range of temperatures as in ordinary fluids.

The bag wall is Janus faced: one side faces the partonic world, and, aside from conserved

charges, radiates a partonic black body radiation responsible for balancing the bag pressure; the other side faces the hadronic world and radiates a hadronic black body radiation, mostly pions. Both sides of the bag wall are at temperature $T_{\mathcal{H}}$. It is tempting to attribute most, if not all, of the hadronic and partonic properties to the wall itself, possibly even the capability to enforce conservation laws globally (quantum number conductivity). Despite the fact that this wall is an insurmountable horizon, hadronic measurements such as bag size and total radiance can yield some properties of the partonic world, e.g. the number of degrees of freedom [204].

One can estimate an upper limit for the emission time using the outward energy flux of particles radiated from the bag. At equilibrium the in-going and out-going fluxes must be the same, thus the outward flux of particles in the nonrelativistic approximation using Eq. (4.20) is

$$\varphi_{n_{\mathcal{H}}} \simeq \frac{n_{\mathcal{H}}}{4} \left(\frac{m}{m + 2T_{\mathcal{H}}} \right) \sqrt{8 \frac{T_{\mathcal{H}}}{\pi m}}. \quad (4.23)$$

Using the techniques of [173, 258], one finds the energy flux $\varphi_{E_{\mathcal{H}}}$ and momentum flux p_{rad} as

$$\varphi_{E_{\mathcal{H}}} \simeq (m + 2T_{\mathcal{H}}) \varphi_{n_{\mathcal{H}}}, \quad p_{\text{rad}} = n_{\mathcal{H}} T_{\mathcal{H}} / 2. \quad (4.24)$$

The pressure p_{rad} exerted on the bag by its radiation can be compared to the intrinsic bag pressure B : for pions $p_{\text{rad}} \sim 0.02B$. The time τ for the bag to dissolve into its radiation is

$$\tau \simeq \frac{3\pi \exp\left(\frac{m}{T_{\mathcal{H}}}\right) E_0}{g_m (m^2 T_{\mathcal{H}}^2) R_0^2}, \quad (4.25)$$

g_m is the particle degeneracy and R_0 and E_0 are the radius and total energy of the initial bag.

The fluxes written in Eqs. (4.23) and (4.24) (particle or energy per unit surface area) are integrated over an assumed spherical bag to give the result in Eq. (4.25). However, because of the lack of surface tension, the bag's maximum entropy corresponds to either an elongated (cylinder) or a flattened shape (disc). Thus, Eq. (4.25) should be interpreted as an upper limit.

The decoupling between the vapor concentration and m and $T_{\mathcal{H}}$ occurs when \mathcal{H} has completely evaporated (i.e. $E - Nm - \frac{3}{2}NT_{\mathcal{H}} = 0$) at a volume of

$$V_d \simeq \frac{1}{n_{\mathcal{H}}} \frac{E}{m + \frac{3}{2}T_{\mathcal{H}}}. \quad (4.26)$$

The disappearance of \mathcal{H} allows the vapor concentration to decrease as $N/V = n_{\mathcal{H}} V_d / V$.

For $V > V_d$ due to energy and particle number conservation the temperature is fixed at $T_{\mathcal{H}}$. This assumes the Hagedorn spectrum extends to $m = 0$. However, there may be a lower cut off

at m_0 which modifies the results as follows. For energies $E - mN - \varepsilon \gg m_0$ and $V < V_d$ the above results hold. For $V \gg V_d$, the situation is different: \mathcal{H} evaporates until its mass is m_0 . If the entire mass of \mathcal{H} is transformed into vapor particles as the volume increases further, then the excess particles increases the concentration and decreases the temperature. As the volume increases further, the concentration varies as

$$\frac{N}{V} = \frac{n_{\mathcal{H}}V_d + \frac{m_0}{m}}{V}, \quad (4.27)$$

while the temperature remains constant at

$$T = \frac{n_{\mathcal{H}}V_d}{n_{\mathcal{H}}V_d + \frac{m_0}{m}}T_{\mathcal{H}}. \quad (4.28)$$

The threshold m_0 is absolute regardless of bag multiplicity. Many bags in equilibrium have a global Hagedorn threshold m_0 so particle-particle collisions are identical to heavy ion reactions.

4.1.4. Fragmentation of \mathcal{H} . What is the stability of \mathcal{H} against fragmentation? Is the situation of a vapor of \mathcal{H} -like particles different than that of a single \mathcal{H} -like particle? If the translational degrees of freedom are neglected, \mathcal{H} is indifferent to fragmentation into an arbitrary number of particles of arbitrary mass (within the constraints of mass/energy conservation). This follows from the exponential mass spectrum of Eq. (4.1) and the consequent lack of surface energy.

If \mathcal{H} fragments totally into a number N of equal sized fragments but one all with translational degrees of freedom and with an exponential mass spectrum (4.1), then

$$\rho_T = \frac{e^{\frac{E-Nm-\varepsilon}{T_{\mathcal{H}}}} e^{\frac{Nm}{T_{\mathcal{H}}}} V^N}{N! \left(\frac{3}{2}N\right)!} \left[\frac{m\varepsilon}{2\pi}\right]^{\frac{3}{2}N} = \frac{e^{\frac{E}{T_{\mathcal{H}}}} V^N}{N!} \left[\frac{mT_{\mathcal{H}}}{2\pi}\right]^{\frac{3}{2}N}. \quad (4.29)$$

In the last step I substituted the kinetic energy's most probable value (4.18) and used the Stirling formula for $\left(\frac{3}{2}N\right)!$. Equation (4.29) shows that all Hagedorn factors collapse to a single one with the m -independent argument E . Maximization of (4.29) with respect to m leads to

$$\partial \ln \rho_T / \partial m = 3N/2m = 0, \quad (4.30)$$

which is consistent with $N = 0$ and $m = E$: a single \mathcal{H} particle with all available mass.

This again illustrates the indifference of \mathcal{H} toward fragmentation. Of course Eq. (4.18) gives directly the mass distribution of the Hagedorn fragments under the two conditions discussed above.

These results justify the assumption of the canonical formulation of the statistical hadronization model that smaller clusters appear from a single large cluster [202].

It can be shown similarly that for N identical \mathcal{H} resonances of mass $m \gg T_{\mathcal{H}}$ the most probable value of kinetic energy of the system is $\varepsilon \approx \frac{3}{2}NT_{\mathcal{H}}$. Furthermore, the most probable value of N can be found by the equation (4.20), in which one has to insert the exponential degeneracy of \mathcal{H} and approximate the \mathcal{H} mass as $m \approx \frac{E}{N}$.

As was shown above \mathcal{H} system is a perfect thermostat at fixed temperature $T_{\mathcal{H}}$ and a perfect particle reservoir. Particles in equilibrium with or emitted by \mathcal{H} are in thermal and chemical equilibrium with themselves and with \mathcal{H} . They constitute a saturated vapor. This defines a first order PT in a finite system and a phase coexistence completely controlled by the bag pressure. The hadronic side of \mathcal{H} radiates particles in preexisting thermal and chemical equilibrium just as a black body radiates photons in thermal and chemical equilibrium. An \mathcal{H} system is nearly indifferent to fragmentation into smaller \mathcal{H} systems. This invariance with respect to fragmentation makes this model relevant to elementary particle and heavy ion collisions. A lower cut off in the mass spectrum does not alter the above results.

4.2. Hagedorn Thermostat Model

In this section I would like to show that the results of A+A and elementary particle collisions can be understood and explained on the same footing by the Hagedorn thermostat concept. For this purpose let me study the properties of microcanonical equilibrium of Boltzmann particles which are in contact with Hagedorn thermostats and elucidate the effect of the mass cut-off m_0 of the Hagedorn spectrum on the temperature of a system at given energy. The microcanonical formulation of the Hagedorn thermostat model (HTM) is given in section 4.2.1. Section 4.2.2. is devoted to the analysis of the most probable state of a single heavy Hagedorn thermostat of mass $m \geq m_0$ and N_B Boltzmann particles. Section 4.2.3. contains my conclusions and possible experimental consequences.

4.2.1. A Single Hagedorn Thermostat Case. Let me consider the microcanonical ensemble of N_B Boltzmann point-like particles of mass m_B and degeneracy g_B , and N_H hadronic point-like resonances of mass m_H with a mass spectrum

$$g_H(m_H) = \exp[m_H/T_H](m_o/m_H)^a \text{ for } m_H \geq m_o, \quad (4.31)$$

which obeys the inequalities $m_o \gg T_H$ and $m_o > m_B$. A recent analysis [214] suggests that the Hagedorn mass spectrum can be established for $m_o < 2$ GeV.

In the SBM [188] and the MIT bag model [195] it was found that for $m_H \rightarrow \infty$ the parameter $a \leq 3$. For finite resonance masses the value of a is unknown, so it will be considered as a fixed parameter.

The microcanonical partition of the system, with volume V , total energy U and zero total momentum, can be written as follows

$$\Omega(U, N_H, N_B) = \frac{V^{N_H}}{N_H!} \left[\prod_{k=1}^{N_H} g_H(m_H) \int \frac{d^3 Q_k}{(2\pi)^3} \right] \frac{V^{N_B}}{N_B!} \left[\prod_{l=1}^{N_B} g_B \int \frac{d^3 p_l}{(2\pi)^3} \right] \delta \left(U - \sum_{i=1}^{N_H} \epsilon_i^H - \sum_{j=1}^{N_B} \epsilon_j^B \right), \quad (4.32)$$

where the quantity $\epsilon_i^H = \epsilon(m_H, Q_i)$ ($\epsilon_j^B = \epsilon(m_B, p_j)$) with the notation $\epsilon(M, P) \equiv \sqrt{M^2 + P^2}$ denotes the energy of the Hagedorn (Boltzmann) particle with the 3-momentum \vec{Q}_i (\vec{p}_j). In order to simplify the presentation of my idea, Eq. (4.32) accounts for energy conservation only and neglects momentum conservation.

The microcanonical partition (4.32) can be evaluated by the Laplace transform in total energy U [55]. Then the momentum integrals in (4.32) are factorized and can be performed analytically. The inverse Laplace transform in the conjugate variable λ can be done analytically for the nonrelativistic and ultrarelativistic approximations of the one-particle momentum distribution function ($K_2(z)$ is the modified Bessel function)

$$\int_0^\infty \frac{d^3 p}{(2\pi)^3} e^{-\lambda \epsilon(M,p)} = \frac{M^2 K_2(M \lambda)}{2 \pi^2 \lambda} \approx \begin{cases} \left[\frac{2M}{\lambda} \right]^{\frac{3}{2}} I_{\frac{1}{2}} e^{-M\lambda}, & M \text{Re}(\lambda) \gg 1, \\ \frac{2}{\lambda^3} I_2 e^{-M\lambda}, & M \text{Re}(\lambda) \ll 1, \end{cases} \quad (4.33)$$

where the auxiliary integral can be expressed in terms of the gamma function as follows

$$I_b \equiv \int_0^\infty \frac{d\xi}{(2\pi)^2} \xi^b e^{-\xi} = \frac{\Gamma(b+1)}{(2\pi)^2}. \quad (4.34)$$

Since the formal steps of further evaluation are similar for both cases, I discuss in detail the nonrelativistic limit only, and later present the results for the other case. The nonrelativistic approximation ($MRe(\lambda) \gg 1$) for Eq. (4.32) is as follows

$$\Omega_{nr} = \frac{[Vg_H(m_H) [2m_H]^{\frac{3}{2}} I_{\frac{1}{2}}]^{N_H}}{N_H!} \frac{[Vg_B [2m_B]^{\frac{3}{2}} I_{\frac{1}{2}}]^{N_B}}{N_B!} \frac{E_{kin}^{\frac{3}{2}(N_H+N_B)-1}}{(\frac{3}{2}(N_H+N_B)-1)!}, \quad (4.35)$$

where $E_{kin} = U - m_H N_H - m_B N_B$ is the kinetic energy of the system.

As shown below, the most realistic case corresponds to the nonrelativistic treatment of the Hagedorn resonances because the resulting temperature is much smaller than their masses. Therefore, it is sufficient to consider the ultrarelativistic limit for the Boltzmann particles only. In this case ($MRe(\lambda) \ll 1$) the equation (4.32) can be approximated as

$$\Omega_{ur} = \frac{[Vg_H(m_H) [2m_H]^{\frac{3}{2}} I_{\frac{1}{2}}]^{N_H}}{N_H!} \frac{[Vg_B 2I_2]^{N_B}}{N_B!} \frac{E_{kin}^{\frac{3}{2}(N_H+2N_B)-1}}{(\frac{3}{2}(N_H+2N_B)-1)!}, \quad (4.36)$$

where the kinetic energy does not include the rest energy of the Boltzmann particles, i.e. $E_{kin} = U - m_H N_H$.

Within the adopted assumptions the above results are general and can be used for any number of particles, provided $N_H + N_B \geq 2$. It is instructive to consider first the simplest case $N_H = 1$. This oversimplified model, in which a Hagedorn thermostat is always present, allows one to study the problem rigorously. For $N_H = 1$ and $N_B \gg 1$ I treat the mass of Hagedorn thermostat m_H as a free parameter and determine the value which maximizes the entropy of the system. The solution $m_H^* > 0$ of

$$\frac{\delta \ln \Omega_{nr}(N_H = 1)}{\delta m_H} = \frac{1}{T_H} + \left(\frac{3}{2} - a\right) \frac{1}{m_H^*} - \frac{3(N_B + 1)}{2 E_{kin}} = 0 \quad (4.37)$$

provides the maximum of the system's entropy, if for $m_H = m_H^*$ the second derivative is negative

$$\frac{\delta^2 \ln \Omega_{nr}(N_H = 1)}{\delta m_H^2} = - \left(\frac{3}{2} - a\right) \frac{1}{m_H^{*2}} - \frac{3(N_B + 1)}{2 E_{kin}^2} < 0. \quad (4.38)$$

If the inequality (4.38) is satisfied, then the extremum condition (4.37) defines the temperature of the system of $(N_B + 1)$ nonrelativistic particles

$$T^*(m_H^*) \equiv \frac{2 E_{kin}}{3(N_B + 1)} = \frac{T_H}{1 + \left(\frac{3}{2} - a\right) \frac{T_H}{m_H^*}}. \quad (4.39)$$

Thus, as $m_H^* \rightarrow \infty$ it follows that $T^*(m_H^*) \rightarrow T_H$, while for finite $m_H^* \gg T_H$ and $a > \frac{3}{2}$ ($a < \frac{3}{2}$) the temperature of the system is slightly larger (smaller) than the Hagedorn temperature, i.e. $T^* > T_H$ ($T^* < T_H$). Formally, the temperature of the system in equation (4.39) may differ essentially from T_H for a light thermostat, i.e. for $m_H^* \leq T_H$. However, it is assumed that the Hagedorn mass spectrum exists above the cut-off mass $m_o \gg T_H$, thus $m^* \gg T_H$.

4.2.2. The Role of the Mass Cut-off. Now I would like to study the effect of the mass cut-off of the Hagedorn spectrum on the inequality (4.38) in more detail. For $a \leq \frac{3}{2}$ the condition (4.38) is satisfied. For $a > \frac{3}{2}$ the inequality (4.38) is equivalent to

$$\frac{m_H^{*2}}{\left(a - \frac{3}{2}\right) T^*(m_H^*)} > \frac{3}{2} (N_B + 1) T^*(m_H^*), \quad (4.40)$$

which means that a Hagedorn thermostat should be massive compared to the kinetic energy of the system.

A more careful analysis shows that for a negative value of the determinant D_{nr} ($\tilde{N} \equiv N_B - \frac{2}{3}a$)

$$D_{nr} \equiv \left(U - m_B N_B - \frac{3}{2} T_H \tilde{N}\right)^2 - 4 \left(a - \frac{3}{2}\right) T_H (U - m_B N_B) < 0, \quad (4.41)$$

equation (4.37) has two complex solutions, while for $D_{nr} = 0$ there exists a single real solution of (4.37). Solving (4.41) for $(U - m_B N_B)$, shows that for $\tilde{N} > \frac{2}{3}a - 1$, i.e. for $N_B > \frac{4}{3}a - 1$ the inequality (4.41) does not hold and $D_{nr} > 0$. Therefore, in what follows I will assume that $N_B > \frac{4}{3}a - 1$ and only analyze the case $D_{nr} > 0$. For this case equation (4.37) has two real solutions

$$m_H^\pm = \frac{1}{2} \left[U - m_B N_B - \frac{3}{2} T_H \tilde{N} \pm \sqrt{D_{nr}} \right]. \quad (4.42)$$

For $a \leq \frac{3}{2}$ only m_H^+ solution is positive and corresponds to a maximum of the microcanonical partition Ω_{nr} .

For $a > \frac{3}{2}$ both solutions of (4.37) are positive, but only m_H^+ is a maximum. From the two limiting cases:

$$\frac{\delta \ln \Omega_{nr}(N_H = 1)}{\delta m_H} \approx \left(\frac{3}{2} - a\right) \frac{1}{m_H} \quad \text{for } m_H \approx 0, \quad (4.43)$$

$$\frac{\delta \ln \Omega_{nr}(N_H = 1)}{\delta m_H} \approx \frac{3(N_B + 1)}{2 E_{kin}} \quad \text{for } E_{kin} \approx 0, \quad (4.44)$$

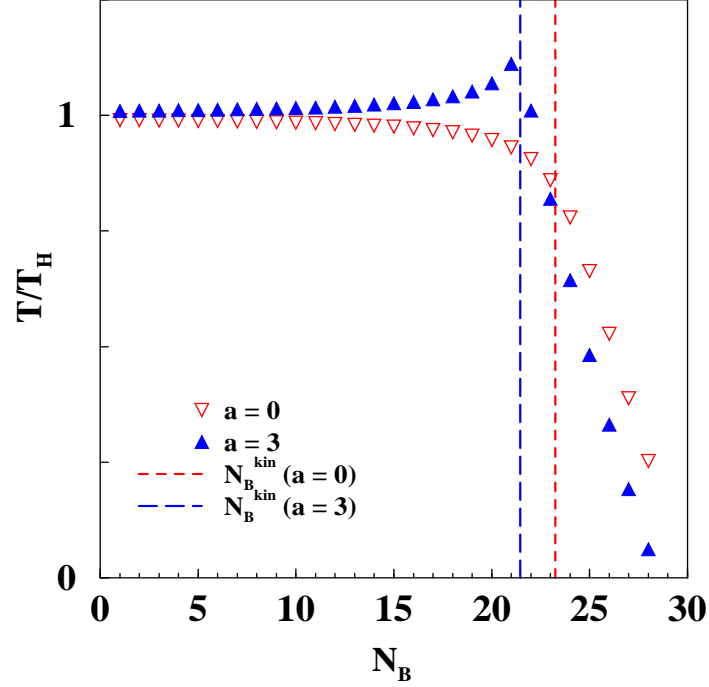


Figure 4.1. A typical behavior of the system's temperature as the function of the number of Boltzmann particles N_B for $a = 3$ and $a = 0$ for the same value of the total energy $U = 30 m_B$. Due to the thermostatic properties of a Hagedorn resonance the system's temperature is nearly constant up to the kinematically allowed value N_B^{kin} given by (4.46).

and the fact that m_H^\pm obey the inequalities

$$0 < m_H^- \leq m_H^+ < U - m_B N_B, \quad (4.45)$$

it is clear that $m_H^* = m_H^-$ is a local minimum of the microcanonical partition Ω_{nr} , while $m_H^* = m_H^+$ is a local maximum of the partition Ω_{nr} .

Using Eq. (4.42) for m_H^+ , it is clear that for any value of a the constraint $m_H^+ \geq m_o$ is equivalent to the inequality

$$N_B \leq N_B^{kin} \equiv \frac{U - [\frac{m_o}{T_H} - a] T^*(m_o)}{m_B + \frac{3}{2} T^*(m_o)}. \quad (4.46)$$

Thus, at fixed energy U for all $N_B \leq N_B^{kin}$ at $m_H^* = m_H^+$ there is a local maximum of the microcanonical partition Ω_{nr} with the temperature $T = T^*(m_H^+)$. For $N_B > N_B^{kin}$ the maximum of the partition Ω_{nr} cannot be reached due to the cut-off constraint and, consequently, the most

probable state corresponds to $m_H = m_o$ with $T \leq T^*(m_o)$ from Eq. (4.39). In other words, for $N_B > N_B^{kin}$ the amount of energy U is insufficient for the mass of the Hagedorn thermostat to be above the cut-off m_o and simultaneously maintain the temperature of the Boltzmann particles according to Eq. (4.39). By assumption there is a single Hagedorn thermostat in the system, therefore, as N_B grows the temperature of the system decreases from $T^*(m_o)$ value. Thus, the equality (4.46) defines the kinematical limit for reaching the maximum of the microcanonical partition.

To prove that the maximum of the microcanonical partition at $m_H = m_H^\dagger$ is global it is sufficient to show that the constraint $m_H^\dagger \geq m_o$ is not consistent with the condition $m_H^- > m_o$. For $a \leq \frac{3}{2}$ the maximum is global because for $0 < m_H < m_H^\dagger$ ($m_H > m_H^\dagger$) the partition $\Omega_{nr}(N_H = 1, m_H)$ monotonically increases (decreases) with m_H . For $a > \frac{3}{2}$ it is clear that the maximum at $m_H = m_H^\dagger$ is local, if the state with mass $m_H = m_o$ is more probable, i.e. $\Omega_{nr}(N_H = 1, m_o) > \Omega_{nr}(N_H = 1, m_H^\dagger)$. Due to (4.45) this can occur, if $m_H^- > m_o$. Substituting Eq. (4.42) into the last inequality, shows that this inequality reduces to the condition $N_B > N_B^{kin}$. This contradicts the constraint $m_H^\dagger \geq m_o$ in the form of Eq. (4.46). Thus, the maximum of the microcanonical partition is global.

To complete this consideration of the nonrelativistic case let me express the partition (4.35) in terms of the temperature (4.39). Applying the Stirling approximation to the factorial $(\frac{3}{2}(N_B + 1) - 1)!$ for $N_B^{kin} > N_B \gg 1$ and reversing the integral representations (4.33) and (4.34) for $\lambda = 1/T^*(m_H^\dagger)$, one finds

$$\Omega_{nr}(N_H = 1) = \frac{V g_H(m_H^\dagger)}{T^*(m_H^\dagger)} \int \frac{d^3Q}{(2\pi)^3} e^{-\frac{\sqrt{m_H^{\dagger 2} + Q^2}}{T^*(m_H^\dagger)}} \frac{e^{\frac{U}{T^*(m_H^\dagger)}}}{N_B!} \left[V g_B \int \frac{d^3p}{(2\pi)^3} e^{-\frac{\sqrt{m_B^2 + p^2}}{T^*(m_H^\dagger)}} \right]^{N_B}. \quad (4.47)$$

This is just the grand canonical partition of $(N_B + 1)$ Boltzmann particles with temperature $T^*(m_H^\dagger)$. If $N_B > N_B^{kin} \gg 1$, then $T^*(m_H^\dagger)$ in (4.47) should be replaced by $T_o(N_B) \equiv \frac{2(U - m_B N_B - m_o)}{3(N_B + 1)}$.

Fig. 4.1 shows that for $a > \frac{3}{2}$ the system's temperature $T = T^*(m_H^\dagger)$ as a function of N_B remains almost constant for $N_B < N_B^{kin}$, reaches a maximum at N_B^{kin} and rapidly decreases like $T = T_o(N_B)$ for $N_B > N_B^{kin}$. For $a < \frac{3}{2}$ the temperature has a plateau $T = T^*(m_H^\dagger)$ for $N_B < N_B^{kin}$, and rapidly decreases for $N_B > N_B^{kin}$ according to $T_o(N_B)$.

The same results are valid for the ultrarelativistic treatment of Boltzmann particles. Comparing

the nonrelativistic and ultrarelativistic expressions for the microcanonical partition, i.e. equations (4.35) and (4.36), respectively, one finds that the derivation of the ultrarelativistic limit requires only the substitution $N_B \rightarrow 2N_B$ and $m_B/T_H \rightarrow 0$ in equations (4.37 – 4.47). Note that this substitution does not alter the expression for the temperature of the system, i.e. the right hand side of (4.39).

Finally, it can be shown that for a heavy Hagedorn thermostat ($m_H^\dagger \gg m_o$) these results remain valid for a single Hagedorn thermostat split into N_H pieces of the same mass.

Substituting $m_H \rightarrow m_H N_H$ in the nonrelativistic expressions (4.35) and minimizing it with respect to m_H , one finds that the temperature of the system in the form of equation (4.39) is $T^*(m_H^* N_H)$, where the mass of N_H Hagedorn thermostats m_H^* is related to the solution m_H^\dagger of equation (4.42) as $m_H^* = m_H^\dagger / N_H$. Since the original single thermostat of mass m_H^\dagger was assumed to be heavy, it follows $T^*(m_H^* N_H) = T^*(m_H^\dagger) \rightarrow T_H$. A more careful study (see also [140]) using an exact expression for the microcanonical partition of N_H Hagedorn thermostats of the same mass m_H gives the same result, if $m_H \gg m_o$. A generalization of these statements to the case of N_H heavy Hagedorn thermostats of different masses also leads to the same result. Thus, splitting a single heavy Hagedorn thermostat into an arbitrary number of heavy resonances (heavier than m_o) does not change the temperature of the system.

4.2.3. Concluding Remarks on the HTM. In the present section I generalized the SBM results [188] to systems of finite energy by showing explicitly that even a single resonance with the Hagedorn mass spectrum degeneracy, i.e. *a Hagedorn thermostat*, keeps an almost constant temperature close to T_H for any number of Boltzmann particles $3 < N_B \leq N_B^{kin}$. For the high energy limit $U \gg m_o$ this means that a single Hagedorn resonance defines the temperature of the system to be only slightly different from T_H until the energy of the Hagedorn thermostat is almost negligible compared to U . In contrast to the grand canonical formulation of the original SBM [188], in the presence of a Hagedorn thermostat the temperature T_H can be reached at any energy density.

The thermostatic nature of a Hagedorn system obviously explains the ubiquity of both the inverse slopes of measured transverse mass spectra [197] and hadronization temperature found in

numerical simulations of hadrons created in elementary particle collisions at high energies [202, 201, 203]. By a direct evaluation of the microcanonical partition I showed that in the presence of a single Hagedorn thermostat the energy spectra of particles become exponential with no additional assumptions, e.g. *phase space dominance* [215] or *string tension fluctuations* [216, 217]. Also the limiting temperature found in the URQMD calculations made in a finite box [218] can be explained by the effect of the Hagedorn thermostat. One expects that, if the string parametrization of the URQMD in a box [218] was done microcanonically instead of grand canonically, then the same behavior would be found.

The Hagedorn thermostat model generalizes the statistical hadronization model which successfully describes the particle multiplicities in nucleus-nucleus and elementary collisions [202, 201, 203]. The statistical hadronization model accounts for the decay of heavy resonances (clusters in terms of Refs. [202, 201, 203]) only and does not consider the additional particles, e.g. light hadrons, free quarks and gluons, or other heavy resonances. As I showed, the splitting of a single heavy Hagedorn resonance into several does not change the temperature of the system. This finding justifies the main assumption of the canonical formulation of the statistical hadronization model [202] that smaller clusters may be reduced to a single large cluster. Also the present model explains the results of a new statistical model of resonance decay [219] that the only temperature available to the system is the Hagedorn temperature T_H .

Thus, recalling the MIT Bag model interpretation of the Hagedorn mass spectrum [195, 196], I conclude that quark gluon matter confined in heavy resonances (hadronic bags) controls the temperature of surrounding particles close to T_H , and, therefore, this temperature can be considered as a coexistence temperature for confined color matter and hadrons. Moreover, as I showed, the emergence of a coexistence temperature does not require the actual deconfinement of the color degrees of freedom, which, in terms of the GBM [134], is equivalent to the formation of the infinitely large and infinitely heavy hadronic bag.

A similar conclusion on the phase transition existence was given in Ref. [191]. However, Carlitz's argument for phase transition is based on the condensation properties of heavy resonances, assuming that the Hagedorn mass spectrum is truncated from the above. On contrary, the approach

that I formulate here refers exclusively to the thermostatic properties of the Hagedorn systems.

Within the framework of the Hagedorn thermostat model it was found that, even for a single Hagedorn thermostat and $a > \frac{3}{2}$, the system's temperature $T = T^*(m_H^+)$ as a function of N_B remains almost constant for $N_B < N_B^{kin}$, reaches a maximum at N_B^{kin} and rapidly decreases for $N_B > N_B^{kin}$ (see Fig. 4.1). For $a < \frac{3}{2}$ the temperature has a plateau $T = T^*(m_H^+)$ for $N_B < N_B^{kin}$, and rapidly decreases for $N_B > N_B^{kin}$. If such a characteristic behavior of the hadronization temperature or the hadronic inverse slopes can be measured as a function of event multiplicity, it may be possible to experimentally determine the value of a . For quantitative predictions it is necessary to include more hadronic species into the model, but this will not change qualitatively these result.

If one applies the HTM to elementary particle collisions at high energies, and thus at vanishing baryonic densities, then, as shown above, the temperature of created particles will be defined by the most probable mass of the Hagedorn thermostat. If the most probable resonance mass grows with the energy of collision, then the hadronization temperature should decrease (increase) to T_H for $a > \frac{3}{2}$ ($a < \frac{3}{2}$). Such a decrease is observed in reactions of elementary particles at high energies, see Table 1 in Ref. [203].

In order to apply these results in a more realistic fashion to the quark gluon plasma formation in relativistic nucleus-nucleus collisions (where the excluded volume effects are known to be important [192, 134, 136, 137, 220, 155] for all hadrons) the eigen volumes of all particles should be incorporated into the model. For pions this should be done in relativistic fashion [154, 156], as was discussed in the chapter 3. Also, as will be shown in the next section, the effect of finite width of Hagedorn resonances may be important [225] and should be studied.

4.3. Mott-Hagedorn Model for QGP

The lattice quantum chromodynamics simulations not only provide the strongest theoretical support of the QGP existence, but they also give detailed information on the properties of strongly interacting matter over a wide range of temperatures. A recent analysis [222] of the lattice energy density showed that a hadron gas model with lattice value of hadron masses can perfectly explain

the steep rise in the number of degrees of freedom at $T \approx T_c$. On the other hand, lattice quantum chromodynamics has also revealed that hadronic correlations persist for $T > T_c$ [223, 224]. The question arises whether it is more appropriate to describe the hot quantum chromodynamics matter in terms of hadronic correlations rather than in terms of quarks and gluons. Therefore, in the present section, I would like to discuss a generalization [200, 225, 226] of the Hagedorn model, i.e. the SBM, which allows for the extension of a hadronic description above T_c .

The SBM [148] is based on the hypothesis that hadrons are made of hadrons, with constituent and compound hadrons being treated on the same footing. This implies an exponentially growing form of the hadronic mass spectrum (4.31) for $m \rightarrow \infty$. The the Hagedorn temperature T_H was interpreted as a limiting temperature reached at infinite energy density. As was discussed at the beginning of this chapter, the extensive investigation of the SBM has led to a formulation of both the important physical ideas and the mathematical methods for modern statistical mechanics of strongly interacting matter [193].

However, up to now the formulation of the SBM had some severe problems. The first one is the absence of a width for the heavy resonances. From the Particle Data Group [227] it is known that heavy resonances with masses $m \geq 3.5$ GeV may have widths comparable to their masses. Taking the widths into account will effectively reduce the statistical weight of the resonance. The second problem arises while discussing the results of the hadron gas model [136, 137, 198]. The hadron gas model accounts for all strong decays of resonances according their partial width given in [227], and, hence, it describes remarkably well the light hadron multiplicities measured in nucleus-nucleus collisions at CERN SPS [136, 137] and BNL RHIC [198] energies. This model is nothing else than the SBM of light hadrons which accounts for the proper volume of hadrons with masses below 2.5 GeV, but neglects the contribution of the exponentially growing mass spectrum.

Thus, one immediately faces a severe problem: “Why do the heavy resonances with masses above 2.5 GeV predicted by the SBM not contribute in the particle spectra measured in heavy-ion collisions at SPS and RHIC energies?” Note that the absence of heavy resonance contributions in the particle ratios cannot be due to the statistical suppression of the Hagedorn mass spectrum because the latter should not be strong in the quark-hadron phase transition region, where those

ratios are believed to be formed [136, 137, 198].

In the present section I discuss the possibility that the introduction of a finite width of the resonances can solve the above problems of the SBM. In the subsection 4.3.1. I formulate a simple statistical model that incorporates besides of the Hagedorn mass spectrum also medium dependent resonance widths due to the hadronic Mott effect, and analyze its mathematical structure. In the subsection 4.3.2. I discuss a model fit to recent lattice data of quantum chromodynamics thermodynamics [222] and some possible consequences for heavy-ion physics, whereas the subsection 4.3.3. is devoted to the discussion of the J/ψ anomalous suppression within the model developed here.

4.3.1. Resonance Width Model: Mott Transition. According to quantum chromodynamics, hadrons are not elementary, point-like objects but rather color singlet bound states of quarks and gluons with a finite spatial extension of their wave function. While at low densities a hadron gas description can be sufficient, at high densities and temperatures, when hadronic wave functions overlap, nonvanishing quark exchange matrix elements between hadrons occur in order to fulfill the Pauli principle. This leads to a Mott-Anderson type delocalization transition with frequent rearrangement processes of color strings (string-flip [228, 229]) so that hadronic resonances become off-shell with a finite, medium-dependent width. Such a Mott transition has been thoroughly discussed for light hadron systems in [230] and has been named *soft deconfinement*. The Mott transition for heavy mesons may serve as the physical mechanism behind the anomalous J/ψ suppression phenomenon [231].

For this purpose the width Γ of a resonance in the statistical model with the Hagedorn mass spectrum is introduced through the spectral function

$$A(s, m) = N_s \frac{\Gamma m}{(s - m^2)^2 + \Gamma^2 m^2}, \quad (4.48)$$

a Breit-Wigner distribution of virtual masses with a maximum at $\sqrt{s} = m$ and the normalization factor

$$N_s = \left[\int_{m_B^2}^{\infty} ds \frac{\Gamma m}{(s - m^2)^2 + \Gamma^2 m^2} \right]^{-1} = \frac{1}{\frac{\pi}{2} + \arctan\left(\frac{m^2 - m_B^2}{\Gamma m}\right)}. \quad (4.49)$$

The energy density of this model with zero resonance proper volume for given temperature T and baryonic chemical potential μ can be cast in the form

$$\varepsilon(T, \mu) = \sum_{i=\pi, g, \dots} g_i \varepsilon_M(T, \mu_i; m_i) + \sum_{A=M, B} \int_{m_A}^{\infty} dm \int_{m_B^2}^{\infty} ds g_H(m) A(s, m) \varepsilon_A(T, \mu_A; \sqrt{s}), \quad (4.50)$$

where the energy density per degree of freedom with a mass m is

$$\varepsilon_A(T, \mu_A; m) = \int \frac{d^3k}{(2\pi)^3} \frac{\sqrt{k^2 + m^2}}{\exp\left(\frac{\sqrt{k^2 + m^2} - \mu_A}{T}\right) + \delta_A}, \quad (4.51)$$

with the degeneracy g_A and the baryonic chemical potential μ_A of hadron A . For mesons, $\delta_M = -1$, $\mu_M = 0$ and for baryons $\delta_B = 1$ and $\mu_B = \mu$, respectively. According to Eq. (4.50) the energy density of hadrons consists of the contribution of light hadrons for $m_i < m_A$ and the contribution of the Hagedorn mass spectrum $g_H(m)$ for $m \geq m_A$.

A new element of Eq. (4.50) in comparison to the SBM is the presence of the \sqrt{s} -dependent spectral function. The analysis shows that, depending on the behavior of the resonance width Γ in the limit $m \rightarrow \infty$, there are the following possibilities:

- For vanishing resonance width, $\Gamma = 0$, Eq. (4.50) evidently reproduces the usual SBM.
- For final values of the resonance width, $\Gamma = \text{const}$, Eq. (4.50) diverges for all temperatures T because, in contrast to the SBM, the statistical factor in Eq. (4.50) behaves as $\{\exp[(m_B - \mu_A)/T] + \delta_A\}^{-1}$ so that it cannot suppress the exponential divergence of the Hagedorn mass spectrum $g_H(m)$.
- For a resonance width growing with mass like the Hagedorn spectrum $\Gamma \sim C_\Gamma \exp\left[\frac{m}{T_H}\right]$ or faster, Eq. (4.50) converges again.

Indeed, in the latter case the Breit-Wigner spectral function behaves as

$$N_s \frac{\Gamma m}{(s - m^2)^2 + \Gamma^2 m^2} \Big|_{m \rightarrow \infty} \rightarrow \frac{2}{\pi \Gamma} \sim \exp\left(-\frac{m}{T_H}\right) \quad (4.52)$$

and cancels the exponential divergence of the Hagedorn mass spectrum. Hence, the energy density remains finite. Note that both the analytical properties of model (4.50) and the right hand side of Eq. (4.52) remain the same, if a Gaussian shape of the spectral function is chosen instead of the Breit-Wigner one.

It can be shown that the behavior of the width at finite resonance masses is not essential for the convergence of the energy density (4.50). In other words, for a convergent energy density (4.50) above T_H it is sufficient to have a very small probability density (4.52) (or smaller) for a resonance of mass m to be found in the state with the virtual mass \sqrt{s} . Since there is no principal difference between the high and low mass resonances, one can use the same functional dependence of the width Γ for all masses. Thus, for the following model ansatz

$$\Gamma(T) = \begin{cases} 0, & \text{for } T \leq T_H, \\ C_\Gamma \left(\frac{m}{T_H}\right)^{N_m} \left(\frac{T}{T_H}\right)^{N_T} \exp\left(\frac{m}{T_H}\right), & \text{for } T > T_H, \end{cases} \quad (4.53)$$

the energy density (4.50) is finite for all temperatures and the divergence of the SBM is removed. At $T = T_H$, depending on choice of parameters, it may have either a discontinuity or its partial T derivative may be discontinuous. As discussed above, for $T \leq T_H$ such a model corresponds to the usual SBM, but for high temperatures $T > T_H$ it remains finite for a wide choice of powers N_m .

The idea behind the exponentially mass dependent width of resonances (4.52) is as follows: to have a possibility for resonances of different masses to transform into each other one has at least to allow the transformations of resonances of a given mass m into the resonances being located within some finite interval of masses Δ_m about m and assume a finite (non-vanishing) partial width Γ_p for each mass state within this interval; since in the immediate vicinity of a given mass m the number of all resonance states is given by the Hagedorn spectrum, i.e. is roughly about $\exp\left(\frac{m}{T_H}\right)$, then the total width of the resonances of mass is approximately $\Gamma_p \exp\left(\frac{m}{T_H}\right) \Delta_m$.

As was shown in the preceding sections the CGE should be applied to the SBM with some care. Thus, although the ansatz (4.53) removes the artificial singularity above T_H , it, strictly speaking, cannot be used below T_H . Therefore, a more suitable ansatz for the width reads as:

$$\Gamma(T) = \begin{cases} C'_\Gamma \left(\frac{m}{T_H}\right)^{N_m} \left(\frac{T}{T_H}\right)^{N_T} \exp\left(\frac{m}{T_H}\right), & \text{for } T \leq T_H, \\ C_\Gamma \left(\frac{m}{T_H}\right)^{N_m} \left(\frac{T}{T_H}\right)^{N_T} \exp\left(\frac{m}{T_H}\right), & \text{for } T > T_H, \end{cases} \quad (4.54)$$

with $C'_\Gamma \gg C_\Gamma$. The latter inequality ensures that the continuous spectrum generated by the ansatz (4.54) does not contribute into energy density (4.50) for $T \leq T_H$. Also the ansatz (4.54)

numerically matches the original parameterization of Ref. [222] for $T < T_H$, where the hadron gas model can be described by the lightest hadron species (lighter than 1 GeV), but with their lattice values of masses. Moreover, a numerical analysis of (4.53) and (4.54) parameterizations shows that, although the ansatz (4.54) is physically correct, their results for the energy densities are the indistinguishable. Therefore, in what follows I will use the data obtained with (4.53) because they require less efforts.

Note that for heavy resonances having the widths (4.53) or (4.54) the resulting mass distribution will be a power law which is seen both in hadron-hadron reactions [232] and nucleus-nucleus reactions [233] at high energies.

Also one should remember that the representation of energy density (4.50) by the spectral function is chosen for the sake of simplicity. In fact, such a representation can be assumed for pressure or entropy density. The latter is preferable, if one needs to build thermodynamically consistent description of all available lattice data, but this is not the main point of the present discussion. Therefore, in what follows I will always choose the most convenient thermodynamic function just for simplicity.

4.3.2. Applications to Lattice Quantum Chromodynamics and Heavy-Ion Collisions. As one can see from Fig. 4.2 the hadron gas model [222] correctly reproduces the lattice quantum chromodynamics results below the critical temperature T_c and just in a vicinity above T_c , but not for large temperatures. On the other hand Fig. 4.3 shows a comparison of the same lattice quantum chromodynamics data [222] with the Mott-Hagedorn gas (4.53) where the parameters of the spectral function are $N_T = 2.325$, $N_m = 2.5$ and $T_H = 165$ MeV and $m_A = m_B = 1$ GeV. The successful description of the lattice energy density [222] indicates that above T_c the strongly interacting matter may be well described in terms of strongly correlated hadronic degrees of freedom. This result is based on the concept of soft deconfinement and provides an alternative to the conventional explanation of the deconfinement transition as the emergence of quasifree quarks and gluons.

Another interesting feature of the model (4.53) is that it allows to explain naturally the absence of heavy resonance contributions to the particle yields measured at highest SPS and all RHIC

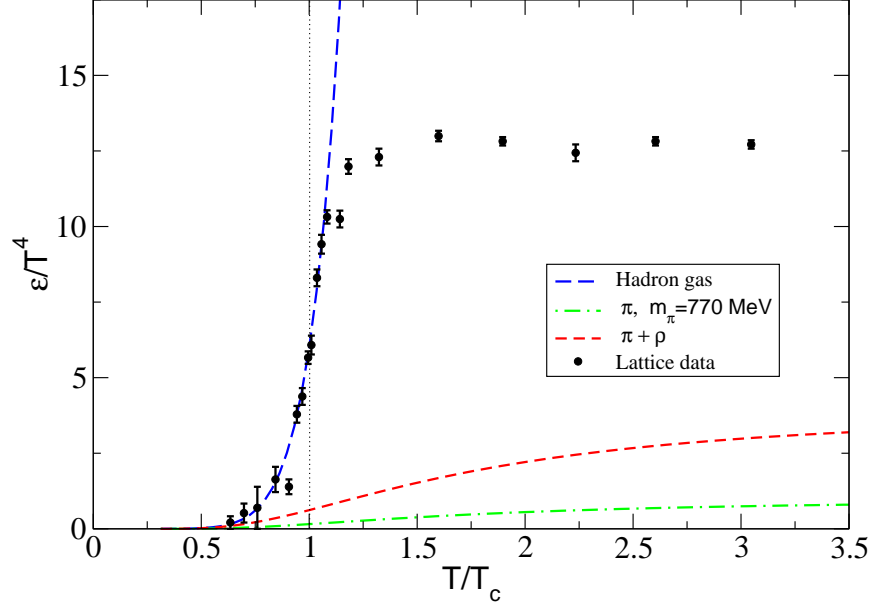


Figure 4.2. Fit of the lattice quantum chromodynamics data [222] with the hadron gas model of Ref. [222].

energies, where QGP conditions are expected [136, 137, 198]. In order to find out whether a given resonance has a chance to survive till the freeze-out it is necessary to compare its lifetime with the typical timescale in the system. There are two typical timescales usually discussed in nucleus-nucleus collisions, the equilibration time τ_{eq} and the formation time τ_f . The equilibration time tells when the matter created in collision process reaches a thermal equilibrium which allows to use the hydrodynamic and thermodynamic descriptions. For Au + Au collisions at RHIC energies it was estimated to be about $\tau_{eq} \approx 0.5$ fm [234]. On the other hand in transport calculations the formation time is used: the time for constituent quarks to form a hadron. The formation time depends on the momentum and energy of the created hadron, but is of the same order $\tau_f \approx 1 - 2$ fm [235] as the equilibration time.

Since within this model the QGP is equivalent to a resonance gas with medium dependent widths, all hadronic resonances with life time $\Gamma^{-1}(m)$ shorter than $\max\{\tau_f, \tau_{eq}\}$ will have no chance to be formed in the system. Therefore, the upper limit of the the integrals over the resonance mass

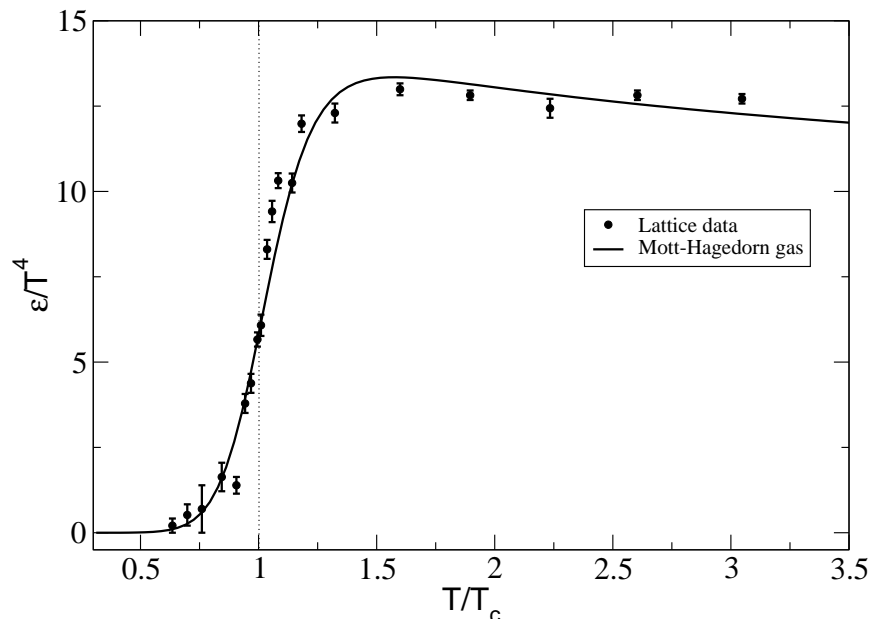


Figure 4.3. Fit of the lattice quantum chromodynamics data [222] with the Mott-Hagedorn resonance gas model (4.53). For details see text.

m and over the virtual mass \sqrt{s} in Eq. (4.50) should be reduced to a resonance mass defined by

$$\Gamma(m)^{-1} = \max\{\tau_f, \tau_{eq}\}. \quad (4.55)$$

This reduction may essentially weaken the energy density gap at the transition temperature or even make it vanish. Thus, the explicit time dependence should be introduced into the resonance width model (4.50) while applying it to nuclear collisions, and this finite time (size) effect, as I discussed, may change essentially the thermodynamics of the hadron resonances formed in the nucleus-nucleus collisions.

4.3.3. Anomalous J/ψ Suppression. The phenomenon of anomalous J/ψ suppression as observed by the NA50 collaboration at CERN-SPS with ultrarelativistic Pb-Pb collisions at 158 GeV/A did not yet find a satisfactory explanation. It has been demonstrated that the extrapolation from results with pA collisions and light ion beams (O, S) fails to describe the E_T dependence of the J/ψ survival probability (production cross section) above $E_T \sim 40$ GeV. Successful fits to the data are obtained with models assuming a critical phenomenon where the

conditions for the onset of the new phase are fulfilled at the above E_T value. Among these models are in particular:

- percolation (Satz) [237, 238]
- J/ψ Mott transition (Blaizot/Ollitrault) [239]
- D-meson Mott transition (Blaschke/Bureau) [231]

Here I would like to generalize the kinetic theory approach to J/ψ suppression as it was formulated in Ref. [231] and study charmonium dissociation in a Mott-Hagedorn resonance gas. Besides the impact by off-shell π and ρ mesons which has been studied in [231], the resonance gas (4.50)-(4.53) consists of more massive resonances so that no reaction threshold occurs for the breakup into open-charm hadrons (D-mesons, Σ_c , Λ_c , excited states).

The key quantities for the solution of a kinetic equation of the charmonium distribution function are the rate coefficients which can be estimated within the binary collision approximation. This approximation shall be applicable since the first collision is expected to destroy the charmonium and thus determines the lifetime as long as the charm density is too low for the reverse process of charmonium gain (fusion of $D\bar{D}$, $\Lambda_c \bar{D}$, ...).

One can estimate the charmonium lifetime to be

$$\tau_\psi^{-1}(T) = \sigma_{\psi R \rightarrow X} v n_R(T) \quad (4.56)$$

under the assumption that the charmonium breakup cross section is rather universal and may be estimated by the value for ψ absorption measured in pA collision experiments of charm hadroproduction. In pA and S-U collisions an absorption cross section σ_{abs} of 4.4 ± 0.5 mb has been extracted from the data by using a Glauber model analysis [236]. The velocity of a typical hadron resonance is of the order of 0.5 and the number density of resonances at a given temperature is given by

$$n_R(T) = \sum_{i=\pi, g, \dots} g_i n_M(T, \mu; m_i) + \sum_{A=M, B} \int_{m_A}^{\infty} dm \int_{m_B^2}^{\infty} ds g_H(m) A(s, m) n_A(T, \mu_A; \sqrt{s}), \quad (4.57)$$

where the number density per degree of freedom is as follows

$$n_A(T, \mu_A; m) = \int \frac{d^3k}{(2\pi)^3} \frac{1}{e^{(\sqrt{k^2+m^2}-\mu_A)/T} + \delta_A}, \quad (4.58)$$

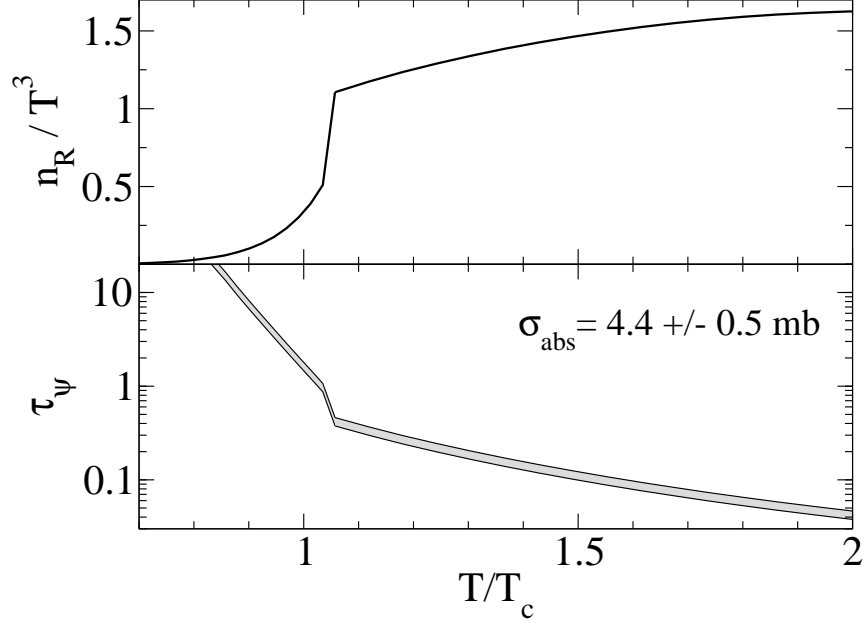


Figure 4.4. Density of resonances (upper panel) and mean J/ψ lifetime (lower panel) in a Mott-Hagedorn resonance gas.

see Fig. 4.4 (upper panel). The result for the charmonium lifetime is given in Fig. 4.4 and exhibits a sharp drop at the critical temperature for the Mott transition in the resonance gas. This behavior is then reflected in a threshold-like behavior of the charmonium survival probability

$$S(T_0) = \exp \left(- \int_{\tau_0}^{\infty} d\tau \tau_\psi^{-1}(T(\tau)) \right) , \quad (4.59)$$

estimated within the one-dimensional hydrodynamic expansion (Bjorken scenario) with the following dependence $T^3(\tau)\tau = T^3(\tau_0)\tau_0$ of the temperature of the system on the proper time τ .

The result is shown in Fig. 4.5. As soon as the initial temperature $T_0 = T(\tau_0)$ is above the critical one, the survival probability drops according to the increase in the effective density of degrees of freedom measured by $n_R(T)$, see Fig. 4.4. Therefore, the present model suggests that the step-like drop in the J/ψ production cross section in Pb-Pb collisions at SPS energies can be explained by the dramatic increase in the number of hadronic resonances at the Hagedorn temperature in the resonance gas.

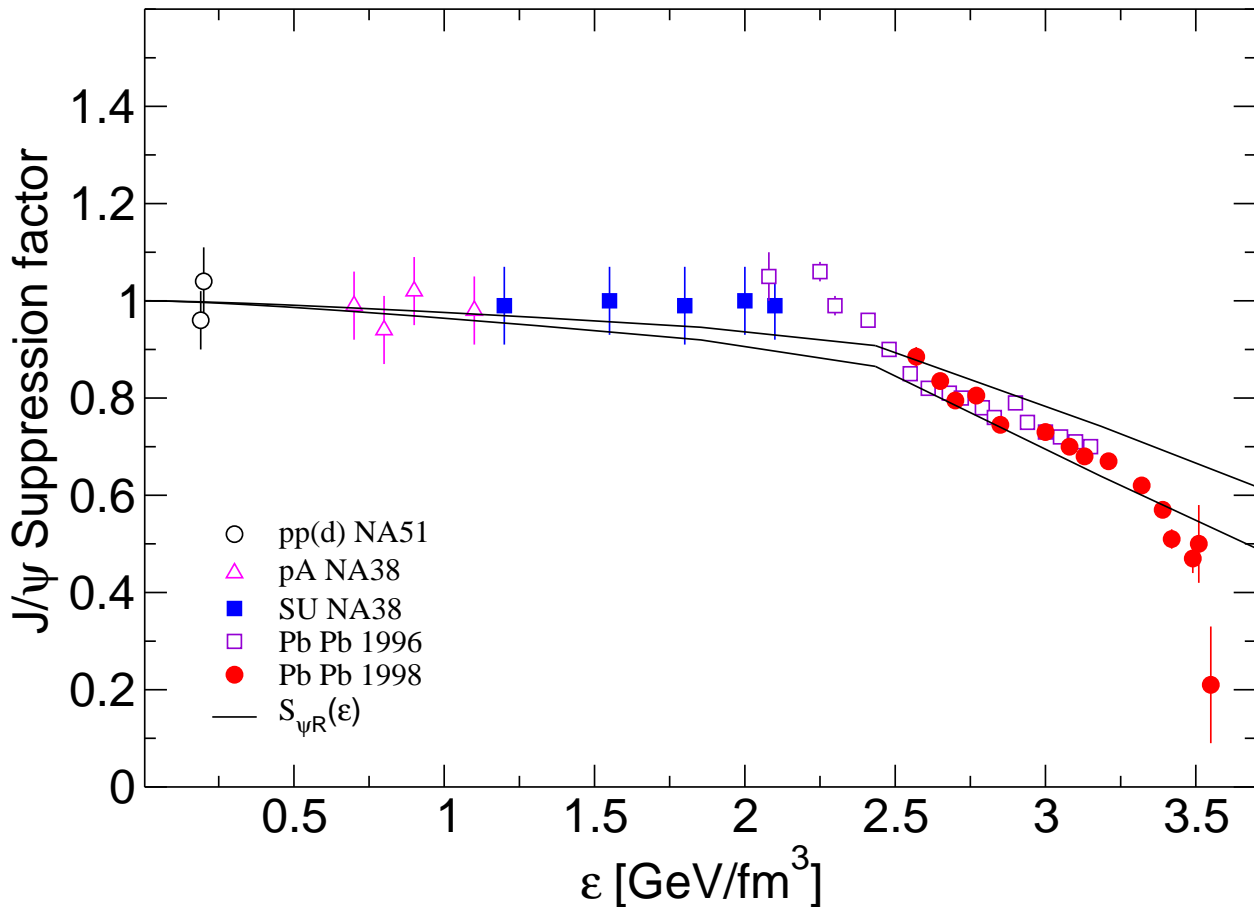


Figure 4.5. J/ψ survival probability in a Mott-Hagedorn resonance gas as a function of the energy density. Data are from the NA50 collaboration [236].

Thus, the statistical bootstrap model allows one to interpret the QGP as the hadron resonance gas dominated by the state of infinite mass (and infinite volume). As was shown, it is necessary to include the resonance width into the SBM in order to avoid the contradiction with experimental data on hadron spectroscopy. One can see that the simple model (4.50)-(4.53) may not only eliminate the divergence of the thermodynamic functions above T_H , but it is also able to successfully describe the lattice quantum chromodynamics data [222] for energy density. Such a model also explains the absence of heavy resonance contributions in the fit of the experimentally measured particle ratios at SPS and RHIC energies.

However, such a modification of the SBM requires an essential change in our view on QGP: it is conceivable that hadrons of very large masses which should be associated with a QGP cannot be formed in nucleus-nucleus collisions because of their very short lifetime.

As also was shown the dramatic increase in the number of hadronic resonances at the Hagedorn temperature of this model can explain the step-like drop in the J/ψ production cross section in Pb-Pb collisions at SPS energies.

It is also necessary to mention that the presented model should be applied to experimental data with care: it can be successfully applied to describe either the quantities associated with the chemical freeze-out, i.e. particle ratios or spectra of Ω hyperons, ϕ , J/ψ and ψ' mesons that are freezing out at hadronization [205, 206, 207, 208, 261, 262]. But as discussed in Refs. [173, 263, 264] the model presented here should not be used for the post freeze-out momentum spectra of other hadrons produced in the nucleus-nucleus collisions. Perhaps only such weakly interacting hadrons like Ω , ϕ , J/ψ and ψ' will allow us to test the model presented here.

4.4. Quark Gluon Bags with Surface Tension

This section is devoted to the reformulation of the GBM [134, 192, 195], which was analyzed in the chapter 2 for finite volumes. Its present generalization, the QGBST model [240, 241, 242], is more realistic than the GBM and maybe useful for the experimental location of the (tri)critical endpoint of quantum chromodynamics which is hoped to be done at BNL RHIC, CERN SPS, GSI FAIR and, perhaps, at JINR NICA.

The GBM [134, 192, 195] itself contains two well-known models of deconfined and confined phases: the bag model of QGP [138, 243] and the hadron gas model [136, 137]. Since, on the one hand, the MIT Bag Model [138] is able to simultaneously describe the hadron mass spectrum, i.e. the hadron masses and their proper volumes, and the properties of the deconfined phase [243] and, on the other hand, the hadron gas model is rather successful in describing the experimental particle yields [136, 137, 198, 199], there were hopes [135] that an exact analytical solution of the GBM found in [134] could be helpful in understanding the properties of strongly interacting matter. However, this solution does not allow one to introduce the critical end point of the strongly

interacting matter phase diagram. Also, a complicated construction of the line, along which the phase transition order gradually increases, suggested in [135], does look too artificial. Therefore, the present GBM formulation lacks an important physical input and is interesting only as a toy example which can be solved analytically.

On the other hand, the models, which can correctly reproduce the expectation [107, 108, 109] that the end point of the 1st order phase transition (PT) line to QGP should be the 2nd order critical point, are indeed necessary for heavy ion phenomenology. In addition, such phenomenological models can provide us with the information about the phase structure and equation of state of strongly interacting matter which is located between the critical endpoint and the region of the color superconductivity because such an information is unavailable otherwise. Therefore, the present section is devoted to the extension of the GMB. I think that the GMB can be drastically improved by the inclusion of such a vitally important element as the surface tension of the quark-gluon bags.

The dynamical surface tension of the quark-gluon bags was estimated long ago [244, 245], but it was never used in statistical description of the equation of state. Moreover, the estimate of the bag surface tension made in [245] is negligible for u and d quarks of and, hence, can be safely neglected in the present treatment. The situation with the surface tension of the quark-gluon bags is somewhat unclear: the early estimates within the MIT Bag Model [246, 247] indicate that small hadronic bubbles can exist in the hot QGP, whereas the analysis based on the effective potential of the 1st order PT in early Universe [248] does not support the results of Refs. [246, 247]. Thus, it turns out that the surface energy may play an important role for the properties of hadronic bubbles [246, 247, 248] and QGP bags [142], but the surface tension of large bags was not included into a consistent statistical description of QGP. Therefore, the present paper is devoted to the investigation and analysis of the critical properties of the model of quark-gluon bags with surface tension (QGBST model hereafter).

In statistical mechanics there are several exactly solvable cluster models with the 1st order PT which describe the critical point properties very well. These models are built on the assumptions that the difference of the bulk part (or the volume dependent part) of free energy of two phases disappears at phase equilibrium and that, in addition, the difference of the surface part (or the

surface tension) of free energy vanishes at the critical point. The most famous of them is the Fisher droplet model (FDM) [44, 190] which has been successfully used to analyze the condensation of a gaseous phase (droplets of all sizes) into a liquid (see chapter 2). The FDM has been applied to many different systems, including nuclear multifragmentation [45], nucleation of real fluids [143], the compressibility factor of real fluids [144], clusters of the Ising model [122] and percolation clusters [145].

As was discussed in the chapter 2, the analytical results [48, 56] for a simplified SMM version [53, 54] give a very strong evidence that the SMM, and, thus, the nuclear matter, has a tricritical endpoint rather than a critical endpoint.

Such a success of the SMM initiated the studies of the surface partitions of large clusters within the Hills and Dales Model [114, 115] and led to a discovery of the origin of the temperature independent surface entropy similar to the FDM. As a consequence, the surface tension coefficient of large clusters consisting of the discrete constituents should linearly depend on the temperature of the system [114] and must vanish at the critical endpoint. However, the present formulation of the Hills and Dales Model [114, 115], which successfully estimates the upper and lower bounds of the surface deformations of the discrete physical clusters, does not look suitable for quark-gluon bags. Therefore, in this section I will assume a certain dependence of the surface tension coefficient on temperature and baryonic chemical potential, and concentrate on the impact of surface tension of the quark-gluon bags on the properties of the deconfinement phase diagram and the quantum chromodynamics critical endpoint. A discussion of the origin of the surface tension is a subject of a future research.

Here I will show that the existence of a cross-over at low values of the baryonic chemical potential along with the 1st order deconfinement PT at high baryonic chemical potentials leads to the existence of an additional PT of the 2nd or higher order along the curve where the surface tension coefficient vanishes. Thus, it turns out that the QGBST model predicts the existence of the tricritical rather than critical endpoint.

In the subsection 4.4.1. I formulate the basic ingredients of the QGBST model and analyze all possible singularities of its isobaric partition for vanishing baryonic densities. This analysis is

generalized to non-zero baryonic densities in the subsection 4.4.2.. The subsection 4.4.3. is devoted to the analysis of the surface tension induced PT which exists above the deconfinement PT. The conclusions and research perspectives are summarized in the subsection 4.5.

4.4.1. The Role of Surface Tension. Again, like in the chapter 2, I consider the isobaric partition (the notations are the same as in chapter II):

$$\hat{Z}(s, T) \equiv \int_0^\infty dV \exp(-sV) Z(V, T) = \frac{1}{[s - F(s, T)]} \quad (4.60)$$

where the function $F(s, T)$ is defined as follows

$$F(s, T) \equiv F_H(s, T) + F_Q(s, T) = \sum_{j=1}^n g_j e^{-v_j s} \phi(T, m_j) + u(T) \int_{V_0}^\infty dv \frac{\exp[-v(s - s_Q(T))]}{v^\tau}. \quad (4.61)$$

At the moment the particular choice of function $F_Q(s, T)$ in (4.61) is not important. The key point of my treatment is that it should have the form of Eq. (4.61) which has a singularity at $s = s_Q$ because for $s < s_Q$ the integral over the bag volume v diverges at its upper limit. Note that the exponential in (4.61) is nothing else, but a difference of the bulk free energy of a bag of volume v , i.e. $-Tsv$, which is under external pressure Ts , and the bulk free energy of the same bag filled with QGP, i.e. $-Ts_Qv$. At phase equilibrium this difference of the bulk free energies vanishes. Despite all positive features, Eq. (4.61) lacks the surface part of free energy of bags, which will be called a surface energy hereafter. In addition to the difference of the bulk free energies the realistic statistical models which demonstrated their validity, the FDM [44] and SMM [46], have the contribution of the surface energy which plays an important role in defining the phase diagram structure [48, 113]. Therefore, I modify Eq. (4.61) by introducing the surface energy of the bags in a general fashion [56]:

$$F_Q(s, T) = u(T) \int_{V_0}^\infty dv \frac{\exp[(s_Q(T) - s)v - \sigma(T)v^\kappa]}{v^\tau}, \quad (4.62)$$

where the ratio of the temperature dependent surface tension coefficient to T (the reduced surface tension coefficient hereafter) which has the form $\sigma(T) = \frac{\sigma_o}{T} \cdot \left[\frac{T_{cep} - T}{T_{cep}} \right]^{2k+1}$ ($k = 0, 1, 2, \dots$). Here $\sigma_o > 0$ can be a smooth function of the temperature, but for simplicity I fix it to be a constant. For $k = 0$ the two terms in the surface (free) energy of a v -volume bag have a simple interpretation

[44]: thus, the surface energy of such a bag is $\sigma_0 v^\varkappa$, whereas the free energy, which comes from the surface entropy $\sigma_o T_{cep}^{-1} v^\varkappa$, is $-T \sigma_o T_{cep}^{-1} v^\varkappa$. Note that the surface entropy of a v -volume bag counts its degeneracy factor or the number of ways to make such a bag with all possible surfaces. This interpretation can be extended to $k > 0$ on the basis of the Hills and Dales Model [114, 115].

In choosing such a simple surface energy parameterization I follow the original Fisher idea [44] which allows one to account for the surface energy by considering some mean bag of volume v and surface v^\varkappa . The consideration of the general mass-volume-surface bag spectrum I leave for the future investigation. The power $\varkappa < 1$ which describes the bag's effective surface is a constant which, in principle, can differ from the typical FDM and SMM value $\frac{2}{3}$. This is so because near the deconfinement PT region QGP has low density and, hence, like in the low density nuclear matter [250], the non-spherical bags (spaghetti-like or lasagna-like [250]) can be favorable (see also [246, 247] for the bubbles of complicated shapes). A similar idea of "polymerization" of gluonic quasiparticles was introduced recently [251].

The second essential difference with the FDM and SMM surface tension parameterization is that I do not require the vanishing of $\sigma(T)$ above the CEP. As will be shown later, this is the most important assumption which, in contrast to the GBM, allows one to naturally describe the cross-over from hadron gas to QGP. Note that negative value of the reduced surface tension coefficient $\sigma(T)$ above the CEP does not mean anything wrong. As was discussed above, the surface tension coefficient consists of energy and entropy parts which have opposite signs [44, 114, 115]. Therefore, $\sigma(T) < 0$ does not mean that the surface energy changes the sign, but it rather means that the surface entropy, i.e. the logarithm of the degeneracy of bags of a fixed volume, simply exceeds their surface energy. In other words, the number of non-spherical bags of a fixed volume becomes so large that the Boltzmann exponent, which accounts for the energy "costs" of these bags, cannot suppress them anymore.

Finally, the third essential difference with the FDM and SMM is that I assume that the surface tension in the QGBST model vanishes at some line in $\mu_B - T$ plane, i.e. $T_{cep} = T_{cep}(\mu_B)$. However, below I will consider $T_{cep} = Const$ for simplicity and will discuss the necessary modifications of the model with $T_{cep} = T_{cep}(\mu_B)$.

The surface energy should, in principle, be introduced into a discrete part of the mass-volume spectrum F_H , but a successful fitting of the particle yield ratios [136, 137] with the experimentally determined hadronic spectrum F_H does not indicate such a necessity.

In principle, besides the bulk and surface parts of free energy, the spectrum (4.62) could include the curvature part as well, which may be important for small hadronic bubbles [246, 247] or for cosmological PT [248]. It is necessary to stress, however, that the critical properties of the present model are defined by the infinite bag, therefore the inclusion in (4.62) of a curvature term of any sign could affect the thermodynamic quantities of this model at $s = s_Q(T)$ and $\sigma(T) = 0$, which is possible at (tri)critical endpoint only (see below). If, the curvature term was really important for the cluster models like the present one, then it should have been seen also at (tri)critical points of the FDM, SMM and many systems described by the FDM [45, 143, 144, 122, 145], but this is not the case. Indeed, recently the Complement method [106] was applied to the analysis of the largest, but still mesoscopic drop of a radius R_{dr} representing the liquid in equilibrium with its vapor. The method allows one to find out the concentrations of the vapor clusters in finite system in a whole range of temperatures and determine the free energy difference of two phases with high precision. The latter enables me not only to extract the critical temperature, surface tension coefficient and even the value of Fisher index τ of the infinite system, but also such a delicate effects as the Gibbs-Thomson correction [252] to the free energy of a liquid drop. Note that the Gibbs-Thomson correction behaves as R_{dr}^{-1} , but the Complement method [106] allows one to find it, whereas the curvature part of free energy, which is proportional to R_{dr} , is not seen both for a drop and for smaller clusters. Such a result is directly related to the QGP bags because quantum chromodynamics is expected to be in the same universality class [107] as the 3-dimensional Ising model whose clusters were analyzed in [106]. Therefore, admitting that for finite QGP bags the curvature effects may be essential, I leave them out because the critical behavior of the present model is defined by the properties of the infinite bag.

According to the general theorem [134] the analysis of PT existence of the GCP is now reduced to the analysis of the rightmost singularity of the isobaric partition (4.60). Depending on the sign of the reduced surface tension coefficient, there are three possibilities. Since at this point the

present model essentially differs from the FDM and GBM, it is necessary to study all possibilities in details.

(I) The first possibility corresponds to $\sigma(T) > 0$. Its treatment is very similar to the GBM choice (4.61) with $\tau > 2$ [134]. In this case at low temperatures the QGP pressure $Ts_Q(T)$ is negative and, therefore, the rightmost singularity is a simple pole of the isobaric partition $s^* = s_H(T) = F(s_H(T), T) > s_Q(T)$, which is mainly defined by a discrete part of the mass-volume spectrum $F_H(s, T)$. The last inequality provides the convergence of the volume integral in (4.62) (see Fig. 4.6). On the other hand at very high T the QGP pressure dominates and, hence, the rightmost singularity is the essential singularity of the isobaric partition $s^* = s_Q(T)$. The phase transition occurs, when the singularities coincide:

$$s_H(T_c) \equiv \frac{p_H(T_c)}{T_c} = s_Q(T_c) \equiv \frac{p_Q(T_c)}{T_c}, \quad (4.63)$$

which is nothing else, but the Gibbs criterion. The graphical solution of Eq. (2.28) for all these possibilities is shown in Fig. 4.6. Like in the GBM [134, 135], the necessary condition for the PT existence is the finiteness of $F_Q(s_Q(T), T)$ at $s = s_Q(T)$. It can be shown that the sufficient conditions are the following inequalities: $F_Q(s_Q(T), T) > s_Q(T)$ for low temperatures and $F(s_Q(T), T) < s_Q(T)$ for $T \rightarrow \infty$. These conditions provide that at low T the rightmost singularity of the isobaric partition is a simple pole, whereas for high T the essential singularity $s_Q(T)$ becomes its rightmost one (see Fig. 4.6 and a detailed analysis of case $\mu_B \neq 0$).

The PT order can be found from the T -derivatives of $s_H(T)$. Thus, differentiating (2.28) one finds

$$s'_H = \frac{G + u \mathcal{K}_{\tau-1}(\Delta, -\sigma) \cdot s'_Q}{1 + u \mathcal{K}_{\tau-1}(\Delta, -\sigma)}, \quad (4.64)$$

where the functions G and $\mathcal{K}_{\tau-a}(\Delta, -\sigma)$ are defined as

$$G \equiv F'_H + \frac{u'}{u} F_Q + \frac{(T_{cep} - 2kT)\sigma(T)}{(T_{cep} - T)T} u \mathcal{K}_{\tau-\kappa}(\Delta, -\sigma), \quad (4.65)$$

$$\mathcal{K}_{\tau-a}(\Delta, -\sigma) \equiv \int_{V_0}^{\infty} dv \frac{\exp[-\Delta v - \sigma(T)v^\tau]}{v^{\tau-a}}, \quad (4.66)$$

where $\Delta \equiv s_H - s_Q$.

Now it is easy to see that the transition is of the 1st order, i.e. $s'_Q(T_c) > s'_H(T_c)$, provided $\sigma(T) > 0$ for any τ . The 2nd or higher order phase transition takes place provided $s'_Q(T_c) = s'_H(T_c)$

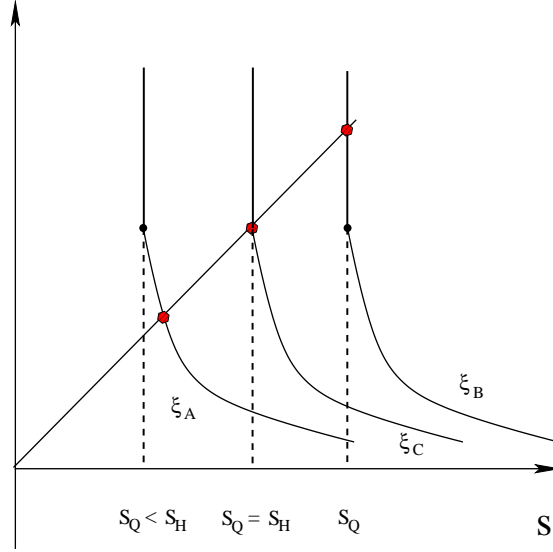


Figure 4.6. Graphical solution of Eq. (2.28) which corresponds to a PT. The solution of Eq. (2.28) is shown by a filled hexagon. The function $F(s, \xi)$ is shown by a solid curve for a few values of the parameter ξ . The function $F(s, \xi)$ diverges for $s < s_Q(\xi)$ (shown by dashed lines), but is finite at $s = s_Q(\xi)$ (shown by black circle). At low values of the parameter $\xi = \xi_A$, which can be either T or μ_B , the simple pole s_H is the rightmost singularity and it corresponds to hadronic phase. For $\xi = \xi_B \gg \xi_A$ the rightmost singularity is an essential singularity $s = s_Q(\xi_B)$, which describes QGP. At intermediate value $\xi = \xi_C$ both singularities coincide $s_H(\xi_C) = s_Q(\xi_C)$ and this condition is a Gibbs criterion.

at $T = T_c$. The latter condition is satisfied when $\mathcal{K}_{\tau-1}$ diverges to infinity at $T \rightarrow (T_c - 0)$, i.e. for T approaching T_c from below. Like for the GBM choice (4.61), such a situation can exist for $\sigma(T_c) = 0$ and $\frac{3}{2} < \tau \leq 2$. Studying the higher T -derivatives of $s_H(T)$ at T_c , one can show that for $\sigma(T) \equiv 0$ and for $(n+1)/n \leq \tau < n/(n-1)$ ($n = 3, 4, 5, \dots$) there is a n^{th} order phase transition

$$\begin{aligned} s_H(T_c) &= s_Q(T_c), \quad s'_H(T_c) = s'_Q(T_c), \quad \dots \\ s_H^{(n-1)}(T_c) &= s_Q^{(n-1)}(T_c), \quad s_H^{(n)}(T_c) \neq s_Q^{(n)}(T_c), \end{aligned} \quad (4.67)$$

with $s_H^{(n)}(T_c) = \infty$ for $(n+1)/n < \tau < n/(n-1)$ and with a finite value of $s_H^{(n)}(T_c)$ for $\tau = (n+1)/n$.

(II) The second possibility, $\sigma(T) \equiv 0$, described in the preceding paragraph, does not give anything new compared to the GBM [134, 135]. If the PT exists, then the graphical picture of singularities is

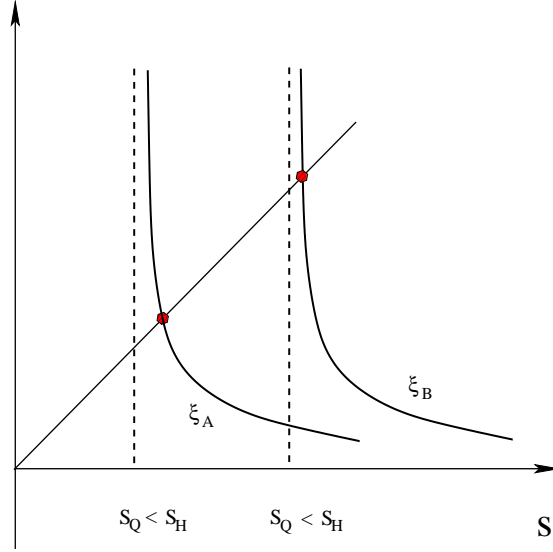


Figure 4.7. Graphical solution of Eq. (2.28) which corresponds to a cross-over. The notations are the same as in Fig. 4.6. Now the function $F(s, \xi)$ diverges at $s = s_Q(\xi)$ (shown by dashed lines). In this case the simple pole s_H is the rightmost singularity for any value of ξ .

basically similar to Fig. 1. The only difference is that, depending on the PT order, the derivatives of $F(s, T)$ function with respect to s should diverge at $s = s_Q(T_c)$.

(III) A principally new possibility exists for $T > T_{cep}$, where $\sigma(T) < 0$. In this case there exists a cross-over, if for $T \leq T_{cep}$ the rightmost singularity is $s_H(T)$, which corresponds to the leftmost curve in Fig. 4.6. Under the latter, its existence can be shown as follows. Let me solve the equation for singularities (2.28) graphically (see Fig. 4.7). For $\sigma(T) < 0$ the function $F_Q(s, T)$ diverges at $s = s_Q(T)$. On the other hand, the partial derivatives $\frac{\partial F_H(s, T)}{\partial s} < 0$ and $\frac{\partial F_Q(s, T)}{\partial s} < 0$ are always negative. Therefore, the function $F(s, T) \equiv F_H(s, T) + F_Q(s, T)$ is a monotonically decreasing function of s , which vanishes at $s \rightarrow \infty$. Since the left hand side of Eq. (2.28) is a monotonically increasing function of s , then there can exist a single intersection s^* of s and $F(s, T)$ functions. Moreover, for finite $s_Q(T)$ values this intersection can occur on the right hand side of the point $s = s_Q(T)$, i.e. $s^* > s_Q(T)$ (see Fig. 4.7). Thus, in this case the essential singularity $s = s_Q(T)$ can become the rightmost one for infinite temperature only. In other words, the pressure of the pure QGP can be reached at infinite T , whereas for finite T the hadronic mass spectrum gives a non-zero contribution into all thermodynamic functions. Note that such a behavior is typical for

the lattice quantum chromodynamics data at zero baryonic chemical potential [157].

It is clear that in terms of the present model a cross-over existence means a fast transition of energy or entropy density in a narrow T region from a dominance of the discrete mass-volume spectrum of light hadrons to a dominance of the continuous spectrum of heavy QGP bags. This is exactly the case for $\sigma(T) < 0$ because in the right vicinity of the point $s = s_Q(T)$ the function $F(s, T)$ decreases very fast and then it gradually decreases as function of s -variable. Since, $F_Q(s, T)$ changes fast from $F(s, T) \sim F_Q(s, T) \sim s_Q(T)$ to $F(s, T) \sim F_H(s, T) \sim s_H(T)$, their s -derivatives should change fast as well. Now, recalling that the change from $F(s, T) \sim F_Q(s, T)$ behavior to $F(s, T) \sim F_H(s, T)$ in s -variable corresponds to the cooling of the system (see Fig. 4.7), I conclude that there exists a narrow region of temperatures, where the T derivative of system pressure, i.e. the entropy density, drops down from $\frac{\partial p}{\partial T} \sim s_Q(T) + T \frac{ds_Q(T)}{dT}$ to $\frac{\partial p}{\partial T} \sim s_H(T) + T \frac{ds_H(T)}{dT}$ very fast compared to other regions of T , if system cools. If, however, in the vicinity of $T = T_{cep} - 0$ the rightmost singularity is $s_Q(T)$, then for $T > T_{cep}$ the situation is different and the cross-over does not exist. A detailed analysis of this situation is given in the subsection 4.4.3.

Note also that all these nice properties would vanish, if the reduced surface tension coefficient is zero or positive above T_{cep} . This is one of the crucial points of the present model which puts forward certain doubts about the vanishing of the reduced surface tension coefficient in the FDM [44] and SMM [46]. These doubts are also supported by the first principle results obtained by the Hills and Dales Model [114, 115], because the surface entropy simply counts the degeneracy of a cluster of a fixed volume and it does not physically affect the surface energy of this cluster.

4.4.2. Generalization to Non-Zero Baryonic Densities. The possibilities (I)-(III) discussed in the preceding section remain unchanged for non-zero baryonic numbers. The latter should be included into consideration to make this model more realistic. To keep the presentation simple, I do not account for strangeness. The inclusion of the baryonic charge of the quark-gluon bags does not change the two types of singularities of the isobaric partition (4.60) and the corresponding equation for them (2.28), but it leads to the following modifications of the F_H

and F_Q functions:

$$F_H(s, T, \mu_B) = \sum_{j=1}^n g_j e^{\frac{b_j \mu_B}{T} - v_j s} \phi(T, m_j), \quad (4.68)$$

$$F_Q(s, T, \mu_B) = u(T, \mu_B) \int_{V_0}^{\infty} dv \frac{\exp[(s_Q(T, \mu_B) - s)v - \sigma(T)v^\tau]}{v^\tau}. \quad (4.69)$$

Here the baryonic chemical potential is denoted as μ_B , the baryonic charge of the j -th hadron in the discrete part of the spectrum is b_j . The continuous part of the spectrum, F_Q can be obtained from some spectrum $\rho(m, v, b)$ in the spirit of Ref. [139, 249], but this will lead the discussion away from the main subject.

The QGP pressure $p_Q = Ts_Q(T, \mu_B)$ can be also chosen in several ways. Here I use the bag model pressure

$$p_Q = \frac{\pi^2}{90} T^4 \left[\frac{95}{2} + \frac{10}{\pi^2} \left(\frac{\mu_B}{T} \right)^2 + \frac{5}{9\pi^4} \left(\frac{\mu_B}{T} \right)^4 \right] - B, \quad (4.70)$$

but the more complicated model pressures, even with the PT of other kind like the transition between the color superconducting QGP and the usual QGP, can be, in principle, used.

The sufficient conditions for a PT existence are

$$F((s_Q(T, \mu_B = 0) + 0), T, \mu_B = 0) > s_Q(T, \mu_B = 0), \quad (4.71)$$

$$F((s_Q(T, \mu_B) + 0), T, \mu_B) < s_Q(T, \mu_B), \forall \mu_B > \mu_A. \quad (4.72)$$

The condition (4.71) provides that the simple pole singularity $s^* = s_H(T, \mu_B = 0)$ is the rightmost one at vanishing $\mu_B = 0$ and given T , whereas the condition (4.72) ensures that $s^* = s_Q(T, \mu_B)$ is the rightmost singularity of the isobaric partition for all values of the baryonic chemical potential above some positive constant μ_A . This can be seen in Fig. 4.6 for μ_B being a variable. Since $F(s, T, \mu_B)$, where it exists, is a continuous function of its parameters, one concludes that, if the conditions (4.71) and (4.72), are fulfilled, then at some chemical potential $\mu_B^c(T)$ the both singularities should be equal. Thus, one arrives at the Gibbs criterion (4.63), but for two variables

$$s_H(T, \mu_B^c(T)) = s_Q(T, \mu_B^c(T)). \quad (4.73)$$

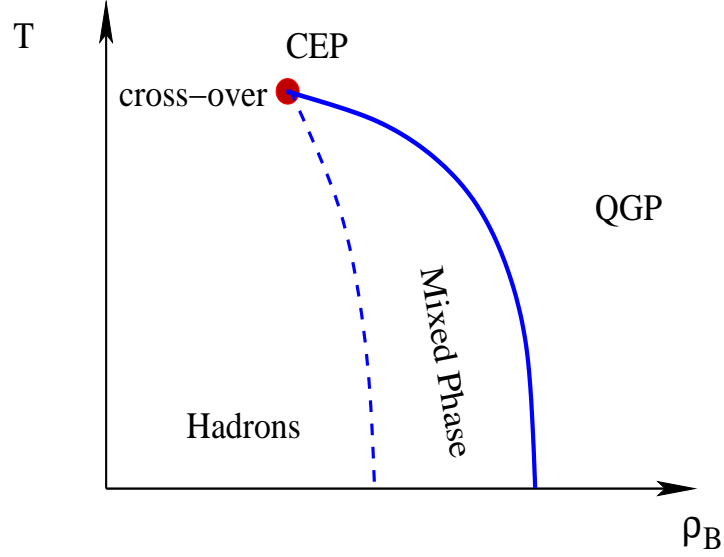


Figure 4.8. A schematic picture of the deconfinement phase transition diagram in the plane of baryonic density ρ_B and T for the 2^{nd} order PT at the critical endpoint (CEP), i.e. for $\frac{3}{2} < \tau \leq 2$. For the 3^{rd} (or higher) order PT the boundary of the mixed and hadronic phases (dashed curve) should have the same slope as the boundary of the mixed phase and QGP (solid curve) at the CEP.

It is easy to see that the inequalities (4.71) and (4.72) are the sufficient conditions of a PT existence for more complicated functional dependencies of $F_H(s, T, \mu_B)$ and $F_Q(s, T, \mu_B)$ than the ones used here.

For the choice (4.68), (4.69) and (4.70) of $F_H(s, T, \mu_B)$ and $F_Q(s, T, \mu_B)$ functions the PT exists at $T < T_{cep}$, because the sufficient conditions (4.71) and (4.72) can be easily fulfilled by a proper choice of the bag constant B and the function $u(T, \mu_B) > 0$ for the interval $T \leq T_{up}$ with the constant $T_{up} > T_{cep}$. Clearly, this is the 1^{st} order PT, since the surface tension is finite and it provides the convergence of the integrals (4.65) and (4.66) in the expression (4.64), where the usual T -derivatives should be now understood as the partial ones for $\mu_B = const$.

Assuming that the conditions (4.71) and (4.72) are fulfilled by the correct choice of the model parameters B and $u(T, \mu_B) > 0$, one can see now that at $T = T_{cep}$ there exists a PT as well, but its order is defined by the value of τ . As was discussed in the preceding section for $\frac{3}{2} < \tau \leq 2$ there exists the 2^{nd} order PT. For $1 < \tau \leq \frac{3}{2}$ there exist the PT of higher order, defined by the

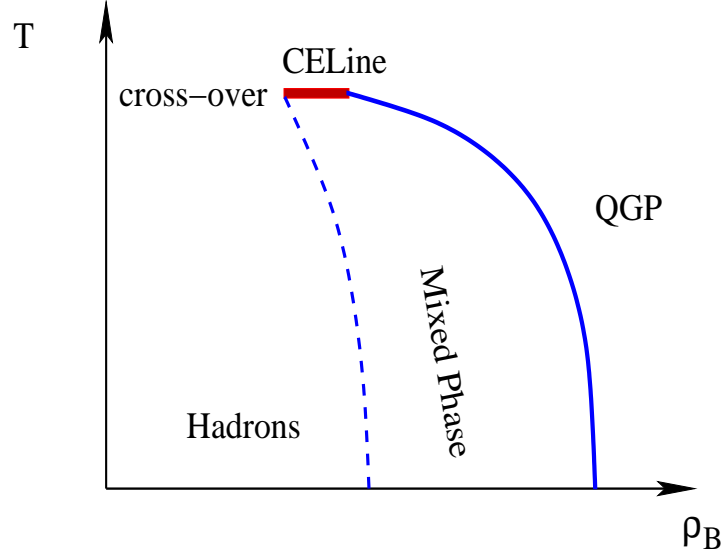


Figure 4.9. A schematic picture of the deconfinement phase transition diagram in the plane of baryonic density ρ_B and T for $\tau > 2$. The critical endpoint in the $\mu_B - T$ plane generates the critical end line (CELine) in the $\rho_B - T$ plane shown by the thick horizontal line. This occurs because of the discontinuity of the partial derivatives of s_H and s_Q functions with respect to μ_B and T .

conditions formulated in Eq. (4.67). This is a new possibility, which, to my best knowledge, does not contradict to any general physical principle (see Fig. 4.8).

The case $\tau > 2$ can be ruled out because there must exist the first order PT for $T \geq T_{cep}$, whereas for $T < T_{cep}$ there exists the cross-over. Thus, the critical endpoint in $T - \mu_B$ plane will correspond to the critical interval in the temperature-baryonic density plane. Since such a structure of the phase diagram in the variables temperature-density has, to my knowledge, never been observed, I conclude that the case $\tau > 2$ is unrealistic (see Fig. 4.9). Note that a similar phase diagram exists in the FDM with the only difference that the boundary of the mixed and liquid phases (the latter in the QGBST model corresponds to QGP) is moved to infinite particle density.

4.4.3. Surface Tension Induced Phase Transition. Using the results for the case (III) of the preceding subsection, I conclude that above T_{cep} there is a cross-over, i.e. the QGP and hadrons coexist together up to the infinite values of T and/or μ_B . Now, however, it is

necessary to answer the question: How can the two different sets of singularities that exist on two sides of the line $T = T_{cep}$ provide the continuity of the solution of Eq. (2.28)?

It is easy to answer this question for $\mu_B < \mu_B^c(T_{cep})$ because in this case all partial T derivatives of $s_H(T, \mu_B)$, which is the rightmost singularity, exist and are finite at any point of the line $T = T_{cep}$. This can be seen from the fact that for the considered region of parameters $s_H(T, \mu_B)$ is the rightmost singularity and, consequently, $s_H(T, \mu_B) > s_Q(T, \mu_B)$. The latter inequality provides the existence and finiteness of the volume integral in $F_Q(s, T, \mu_B)$. In combination with the power T dependence of the reduced surface tension coefficient $\sigma(T)$ the same inequality provides the existence and finiteness of all its partial T derivatives of $F_Q(s, T, \mu_B)$ regardless to the sign of $\sigma(T)$. Thus, using the Taylor expansion in powers of $(T - T_{cep})$ at any point of the interval $T = T_{cep}$ and $\mu_B < \mu_B^c(T_{cep})$, one can calculate $s_H(T, \mu_B)$ for the values of $T > T_{cep}$ which are inside the convergency radius of the Taylor expansion.

The other situation is for $\mu_B \geq \mu_B^c(T_{cep})$ and $T > T_{cep}$, namely in this case above the deconfinement PT there must exist a weaker PT induced by the disappearance of the reduced surface tension coefficient. To demonstrate this I have solved Eq. (2.28) in the limit, when T approaches the curve $T = T_{cep}$ from above, i.e. for $T \rightarrow T_{cep} + 0$, and study the behavior of T derivatives of the solution of Eq. (2.28) s^* for fixed values of μ_B . For this purpose I have to evaluate the integrals $\mathcal{K}_\tau(\Delta, \gamma^2)$ introduced in Eq. (4.66). Here the notations $\Delta \equiv s^* - s_Q(T, \mu_B)$ and $\gamma^2 \equiv -\sigma(T) > 0$ are introduced for convenience.

To avoid the unpleasant behavior for $\tau \leq 2$ it is convenient to transform (4.66) further on by integrating by parts:

$$\mathcal{K}_\tau(\Delta, \gamma^2) \equiv g_\tau(V_0) - \frac{\Delta}{(\tau - 1)} \mathcal{K}_{\tau-1}(\Delta, \gamma^2) + \frac{\varkappa \gamma^2}{(\tau - 1)} \mathcal{K}_{\tau-\varkappa}(\Delta, \gamma^2), \quad (4.74)$$

where the regular function $g_\tau(V_0)$ is defined as

$$g_\tau(V_0) \equiv \frac{1}{(\tau - 1) V_0^{\tau-1}} \exp \left[-\Delta V_0 + \gamma^2 V_0^\varkappa \right]. \quad (4.75)$$

For $\tau - a > 1$ one can change the variable of integration $v \rightarrow z/\Delta$ and rewrite $\mathcal{K}_{\tau-a}(\Delta, \gamma^2)$ as

$$\mathcal{K}_{\tau-a}(\Delta, \gamma^2) = \Delta^{\tau-a-1} \int_{V_0 \Delta}^{\infty} dz \frac{\exp \left[-z + \frac{\gamma^2}{\Delta^\varkappa} z^\varkappa \right]}{z^{\tau-a}} \equiv \Delta^{\tau-a-1} \mathcal{K}_{\tau-a} \left(1, \gamma^2 \Delta^{-\varkappa} \right). \quad (4.76)$$

This result shows that in the limit $\gamma \rightarrow 0$, when the rightmost singularity must approach $s_Q(T, \mu_B)$ from above, i.e. $\Delta \rightarrow 0^+$, the function (4.76) behaves as $\mathcal{K}_{\tau-a}(\Delta, \gamma^2) \sim \Delta^{\tau-a-1} + O(\Delta^{\tau-a})$. This is so because for $\gamma \rightarrow 0$ the ratio $\gamma^2 \Delta^{-\varkappa}$ cannot go to infinity, otherwise the function $\mathcal{K}_{\tau-1}(1, \gamma^2 \Delta^{-\varkappa})$, which enters into the right hand side of (4.74), would diverge exponentially and this makes impossible an existence of the solution of Eq. (2.28) for $T = T_{cep}$. The analysis shows that for $\gamma \rightarrow 0$ there exist two possibilities: either $\nu \equiv \gamma^2 \Delta^{-\varkappa} \rightarrow Const$ or $\nu \equiv \gamma^2 \Delta^{-\varkappa} \rightarrow 0$. The most straightforward way to analyze these possibilities for $\gamma \rightarrow 0$ is to assume the following behavior

$$\Delta = A \gamma^\alpha + O(\gamma^{\alpha+1}), \quad (4.77)$$

$$\frac{\partial \Delta}{\partial T} = \frac{\partial \gamma}{\partial T} [A \alpha \gamma^{\alpha-1} + O(\gamma^\alpha)] \sim \frac{(2k+1)A \alpha \gamma^\alpha}{2(T - T_{cep})}, \quad (4.78)$$

and find out the α value by equating (4.78) with the T derivative (4.64).

Indeed, using (4.64), (4.65) and (4.66), one can write

$$\begin{aligned} \frac{\partial \Delta}{\partial T} &= \frac{G_2 + u \mathcal{K}_{\tau-\varkappa}(\Delta, \gamma^2) 2 \gamma \gamma'}{1 + u \mathcal{K}_{\tau-1}(\Delta, \gamma^2)} \approx \frac{\Delta^{2-\tau} G_2}{u \mathcal{K}_{\tau-1}(1, \nu)} + \\ &\frac{2 \gamma \gamma' \Delta^{1-\varkappa} [\nu \varkappa \mathcal{K}_{\tau-2\varkappa}(1, \nu) - \mathcal{K}_{\tau-1-\varkappa}(1, \nu)]}{(\tau - 1 - \varkappa) \mathcal{K}_{\tau-1}(1, \nu)}, \end{aligned} \quad (4.79)$$

where the prime denotes the partial T derivative. Note that the function $G_2 \equiv F' + u' \mathcal{K}_\tau(\Delta, \gamma^2) - s'_Q$ can vanish for a few values of μ_B only. In the last step of deriving (4.79) I used the identities (4.74) and (4.76) and dropped the non-singular terms. As was discussed above, in the limit $\gamma \rightarrow 0$ the function ν either remains a constant or vanishes, then the term $\nu \varkappa \mathcal{K}_{\tau-2\varkappa}(1, \nu)$ in (4.79) is either of the same order as the constant $\mathcal{K}_{\tau-1-\varkappa}(1, \nu)$ or vanishes. Thus, to reveal the behavior of (4.79) for $\gamma \rightarrow 0$ it is sufficient to find a leading term out of $\Delta^{2-\tau}$ and $\gamma \gamma' \Delta^{1-\varkappa}$ and compare it with the assumption (4.77).

The analysis shows that for $\Delta^{2-\tau} \leq \gamma \gamma' \Delta^{1-\varkappa}$ the last term in the right hand side of (4.79) is the leading one. Consequently, equating the powers of γ of the leading terms in (4.78) and (4.79), one finds

$$\gamma^{\alpha-2} \sim \Delta^{1-\varkappa} \Rightarrow \alpha \varkappa = 2 \quad \text{for } \tau \leq 1 + \frac{\varkappa}{2k+1}, \quad (4.80)$$

where the last inequality follows from the fact that the term $\gamma \gamma' \Delta^{1-\varkappa}$ in (4.79) is the dominant one.

Similarly, for $\Delta^{2-\tau} \geq \gamma\gamma'\Delta^{1-\varkappa}$ one obtains $\gamma^{\alpha-1}\gamma' \sim \Delta^{2-\tau}$ and, consequently,

$$\alpha = \frac{2}{(\tau-1)(2k+1)} \quad \text{for } \tau \geq 1 + \frac{\varkappa}{2k+1}. \quad (4.81)$$

Summarizing the above results for $\gamma \rightarrow 0$ as

$$\frac{\partial\Delta}{\partial T} \sim \frac{T_{cep}\gamma^\alpha}{T-T_{cep}} = \begin{cases} \left[\frac{T-T_{cep}}{T_{cep}} \right]^{\frac{2k+1}{\varkappa}-1}, & \tau \leq 1 + \frac{\varkappa}{2k+1}, \\ \left[\frac{T-T_{cep}}{T_{cep}} \right]^{\frac{2-\tau}{\tau-1}}, & \tau \geq 1 + \frac{\varkappa}{2k+1}, \end{cases} \quad (4.82)$$

one can also write the expression for the second derivative of Δ as

$$\frac{\partial^2\Delta}{\partial T^2} \sim \begin{cases} \left[\frac{T-T_{cep}}{T_{cep}} \right]^{\frac{2k+1}{\varkappa}-2}, & \tau \leq 1 + \frac{\varkappa}{2k+1}, \\ \left[\frac{T-T_{cep}}{T_{cep}} \right]^{\frac{3-2\tau}{\tau-1}}, & \tau \geq 1 + \frac{\varkappa}{2k+1}. \end{cases} \quad (4.83)$$

The last result shows that, depending on \varkappa and k values, the second derivatives of s^* and $s_Q(T, \mu_B)$ can differ from each other for $\frac{3}{2} < \tau < 2$ or can be equal for $1 < \tau \leq \frac{3}{2}$. In other words, one finds that at the line $T = T_{cep}$ there exists the 2^{nd} order PT for $\frac{3}{2} < \tau < 2$ and the higher order PT for $1 < \tau \leq \frac{3}{2}$, which separates the pure QGP phase from the region of a cross-over, i.e. the mixed states of hadronic and QGP bags. Since it exists at the line of a zero surface tension, this PT will be called the *surface induced PT*. For instance, from (4.83) it follows that for $k = 0$ and $\varkappa > \frac{1}{2}$ there is the 2^{nd} order PT, whereas for $k = 0$ and $\varkappa = \frac{1}{2}$ or for $k > 0$ and $\varkappa < 1$ there is the 3^d order PT, and so on.

Since the analysis performed in the present section did not include any μ_B derivatives of Δ , it remains valid for the μ_B dependence of the reduced surface tension coefficient, i.e. for $T_{cep}(\mu_B)$. Only it is necessary to make a few comments on a possible location of the *surface tension null line* $T_{cep}(\mu_B)$. In principle, such a null line can be located anywhere, if its location does not contradict to the sufficient conditions (4.71) and (4.72) of the 1^{st} deconfinement PT existence. Thus, the surface tension null line must cross the deconfinement line in the $\mu_B - T$ plane at a single point which is the tricritical endpoint $(\mu_B^{cep}; T_{cep}(\mu_B^{cep}))$, whereas for $\mu_B > \mu_B^{cep}$ the null line should have higher temperature for the same μ_B than the deconfinement one, i.e. $T_{cep}(\mu_B) > T_c(\mu_B)$ (see Fig 4.10). Clearly, there exist two distinct cases for the surface tension null line: either it is endless, or it

ends at zero temperature. But recalling that at low temperatures and high values of the baryonic chemical potential there may exist the Color-Flavor-Locked phase [253], it is possible that the null line may also cross the boundary of the Color-Flavor-Locked phase and, perhaps, it may create another special point at this intersection. From the present lattice quantum chromodynamics data the case C in Fig. 4.10 is the least possible.

One may wonder why this surface induced PT was not observed so far. The main reason is that the lattice quantum chromodynamics calculations at non-zero μ_B are very difficult, and because of this the identification of the precise location of the critical endpoint is highly nontrivial task [108, 109, 107]. Therefore, the identification of the 2^{nd} or higher order PT which might be located in the vicinity of the deconfinement PT could be a real challenge. In addition, for all $\mu_B > \mu_B^{cep}$ the surface induced PT may lie so close to the deconfinement PT line that it would be extremely difficult to observe it at the present lattices.

To understand the meaning of the surface induced PT it is instructive to quantify the difference between phases by looking into the mean size of the bag:

$$\langle v \rangle \equiv - \left. \frac{\partial \ln F(s, T, \mu_B)}{\partial s} \right|_{s=s^*-0}. \quad (4.84)$$

As was shown in hadronic phase $\Delta > 0$ and, hence, it consists of the bags of finite mean volumes, whereas, by construction, the QGP phase is a single infinite bag. For the cross-over states $\Delta > 0$ and, therefore, they are the bags of finite mean volumes, which gradually increase, if the rightmost singularity approaches $s_Q(T, \mu_B)$, i.e. at very large values T and/or μ_B . Such a classification is useful to distinguish quantum chromodynamics phases of present model: it shows that hadronic and cross-over states are separated from the QGP phase by the 1^{st} order deconfinement PT and by the 2^{nd} or higher order PT, respectively.

4.5. Conclusions and Perspectives

In this chapter I discussed three related models - the SBM (or rather its microcanonical version, the HTM), the Mott-Hagedorn resonance gas model and the QGBST model. The latter two originate from the Hagedorn model. All these models are exactly solved. Whereas the Mott-Hagedorn

gas model was just constructed in a way that the expressions for thermodynamic functions are analytical, the QGBST required an involved analysis of its PTs. The most unusual surprise was given by the microcanonical analysis of the Hagedorn model. Surprisingly, after so many years of studies it was possible to rigorously prove [140, 141, 190] by the finite volume treatment that this model has, indeed, has a PT. Thus, the old guesses based on a formal analogy [191] and on a deep understanding of physics [189] turned out to be right. Of course, at first glance this result seems simply curious, but at the second glance one realizes that the underlying physics of this model is highly non-trivial and this is the reason of why it took so many years to clarify the thermostatic properties of heavy Hagedorn resonances, although the nonequivalence of microcanonical and (grand)canonical ensembles for the exponential mass spectrum of resonances is known for a while [191].

Also it is possible that further development of statistical mechanics of multihadron production in elementary particle collisions on the basis of statistical hadronization model [171, 201, 202, 203] or comparable models [221] can lead to further refinement of the HTM after which the model can be used for quantitative analysis of the data.

One generalization of the SBM, the Mott-Hagedorn gas model, which employs the properties of the Mott transition to generate the large width of heavy resonances [200, 225, 226] was presented above. This model removes the singularity of the SBM in the GCE by a similar mass dependence of a width of heavy resonances. Such a mathematical trick might look somewhat artificial, but this model naturally explains the reason why the heavy resonances which are expected to be produced in A+A and elementary particle collisions are not observed experimentally. Also, using a few parameters, this model reproduces the energy density found by the lattice quantum chromodynamic simulations [222] and is able to describe the anomalous suppression of J/ψ mesons which is observed experimentally at SPS energies [236]. Therefore, I conclude that the medium dependent resonance width should be incorporated in a more elaborate statistical description of the cross-over states and the role of the Mott effect should elucidated by both the lattice quantum chromodynamic simulations and experimental studies.

Then I discussed an analytically solvable statistical model, the QGBST model [240, 241, 242],

which simultaneously describes the 1st and 2nd order PTs with a cross-over. The suggested approach is general and can be used for more complicated parameterizations of the hadronic mass-volume spectrum, if in the vicinity of the deconfinement PT region the discrete and continuous parts of this spectrum can be expressed in the form of Eqs. (4.68) and (4.69), respectively. Also the actual parameterization of the QGP pressure $p = Ts_Q(T, \mu_B)$ was not used so far, which means that these result can be extended to more complicated functions, that can contain other phase transformations (chiral PT, or the PT to color superconducting phase) provided that the sufficient conditions (4.71) and (4.72) for the deconfinement PT existence are satisfied.

In this model the desired properties of the deconfinement phase diagram are achieved by accounting for the temperature dependent surface tension of the quark-gluon bags. As I showed, it is crucial for the cross-over existence that at $T = T_{cep}$ the reduced surface tension coefficient vanishes and remains negative for temperatures above T_{cep} . Then the deconfinement $\mu_B - T$ phase diagram has the 1st PT at $\mu_B > \mu_B^c(T_{cep})$ for $\frac{3}{2} < \tau \leq 2$, which degenerates into the 2nd order PT (or higher order PT for $\frac{3}{2} \geq \tau > 1$) at $\mu_B = \mu_B^c(T_{cep})$, and a cross-over for $0 \leq \mu_B < \mu_B^c(T_{cep})$. These two ingredients drastically change the critical properties of the GBM [134] and resolve the long standing problem of a unified description of the 1st and 2nd order PTs and a cross-over, which, despite all claims, was not resolved in Ref. [135]. In addition, I found that at the null line of the surface tension there must exist the surface induced PT of the 2nd or higher order, which separates the pure QGP from the mixed states of hadrons and QGP bags, that coexist above the cross-over region (see Fig. 4.10). Thus, the QGBST model predicts that for $\tau \leq 2$ the quantum chromodynamics critical endpoint is the tricritical endpoint. It would be interesting to verify this prediction with the help of the lattice quantum chromodynamics analysis. For this it will be necessary to study the behavior of the bulk and surface contributions to the free energy of the QGP bags and/or the string connecting the static quark-antiquark pair.

In contrast to popular mean-field models the PT mechanism in the QGBST model is clear: it happens due to the competition of the rightmost singularities of the isobaric partition function. Since the GCP function of the QGBST model does not depend on any (baryonic or entropy or energy) density, but depends exclusively on T, μ_B and V , its phase diagram does not contain any

back bending and/or spinodal instabilities [96] which are typical for the mean-field (= classical) models. The found exact analytical solution does not require a complicated and artificial procedure of conjugating the two parts of the equation of state in the vicinity of the critical endpoint like it is done by hands in Refs. [254, 255] because all this is automatically included in the statistical description.

Also in the QGBST model the pressure of the deconfined phase is generated by the infinite bag, whereas the discrete part of the mass-volume spectrum plays an auxiliary role even above the cross-over region. Therefore, there is no reason to believe that any quantitative changes of the properties of low lying hadronic states generated by the surrounding media (like the mass shift of the ω and ρ mesons [256]) would be the robust signals of the deconfinement PT. On the other hand, the QGP bags created in the experiments have finite mass and volume and, hence, the strong discontinuities which are typical for the 1st order PT should be smeared out which would make them hardly distinguishable from the cross-over. Thus, to seriously discuss the signals of the 1st order deconfinement PT and/or the tricritical endpoint, one needs to solve the finite volume version of the QGBST model like it was done for the CSMM [110] and the GBM [113] in the chapter 2. This, however, is not sufficient because, in order to make any reliable prediction for experiments, the finite volume EOS must be used in hydrodynamic equations which, unfortunately, are not suited for such a purpose. As was discussed at the end of the chapter 2 the short lived metastable modes with decay/formation time τ_n being shorter than the expansion time cannot be described by hydrodynamics. Also at the moment it is unclear how to build up the corresponding kinetic description. Thus, the studies of the strongly interacting matter EOS in finite systems face us with a necessity to return to the foundations of heavy ion phenomenology and to modify them according to the requirements of the experiments.

The QGBST model indicates how difficult it will be to locate the tricritical point of QGP. In principal it can be found, if the mass spectrum of heavy resonances becomes a power like. This occurs only, if the system is in a mixed phase and if the surface tension coefficient of heavy bags vanishes. Unfortunately, there are two complications: the first one is that for finite systems the 1st order PT behaves like a cross-over, and, the second complication is that the heavy QGP bags

cannot be detected directly, but through the resonance decays only. Therefore, it is possible that, although the mass distribution of heavy QGP bags is reconstructed, due to the little difference between the 1st order PT and a cross-over in finite systems the power law will exist, perhaps, not only at the tricritical endpoint, but at some line of thermodynamic parameters.

Although the QGBST model has a great advantage compared to other models because, in principle, it can be formulated on the basis of the experimental data on the degeneracies, masses and eigen volumes of hadronic resonances in the spirit of Ref. [139], it requires further improvements to make it suitable for the quantitative estimates. Thus, above the surface tension null line the hadrons can coexist with QGP at high temperatures. Consequently, the nonrelativistic consideration of hard core repulsion in the present model should be modified to its relativistic treatment for light hadrons like it was discussed in the chapter 3. Also, the realistic EOS requires the inclusion of the temperature and mass dependent width of heavy resonances into a continuous part of the mass-volume spectrum which may essentially modify our understanding of the cross-over mechanism in a spirit of the Mott-Hagedorn resonance gas model considered in this chapter.

Finally, a precise temperature dependence of the surface tension coefficient along with the role of the curvature part of free energy of the bags should be investigated and their relation to the interquark string tension should be studied in detail. For this purpose I would like to modify the Hills and Dales Model (see chapter 2) in order to include the surface deformations with the base of arbitrary size whereas its present formulation is suited for discrete clusters and, hence, for discrete bases of surface deformations.

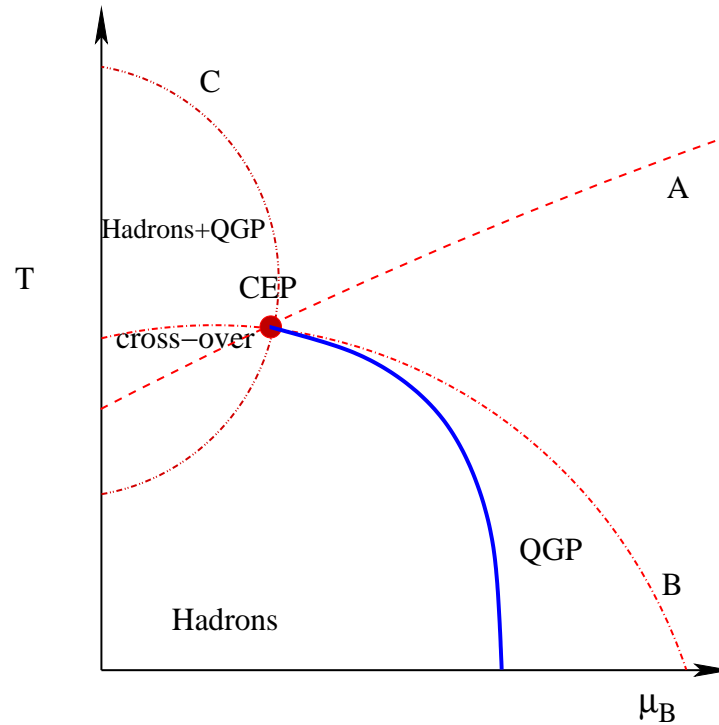


Figure 4.10. A schematic picture of the deconfinement phase transition diagram (full curve) in the plane of baryonic chemical potential μ_B and T for the 2^{nd} order PT at the tricritical endpoint (CEP). The model predicts an existence of the surface induced PT of the 2^{nd} or higher order (depending on the model parameters). This PT starts at the CEP and goes to higher values of T and/or μ_B . Here it is shown by the dashed curve CEP-A, if the phase diagram is endless, or by the dashed-dot curve CEP-B, if the phase diagram ends at $T = 0$, or by the dashed-double-dot curve CEP-C, if the phase diagram ends at $\mu_B = 0$. Below (above) each of A or B curves the reduced surface tension coefficient is positive (negative). For the curve C the surface tension coefficient is positive outside of it.

CHAPTER 5

FREEZE-OUT PROBLEM OF RELATIVISTIC HYDRODYNAMICS AND HYDROKINETICS

From its birth relativistic hydrodynamics [268] became the most powerful theoretical tool to study the dynamics of PTs in A+A collisions at high energies. During last 20 years it was successfully used to model the deconfinement PT between QGP and hadronic matter [9, 269, 270, 102]. So far, only within the hydro approach it was possible to predict the three major signals of the deconfinement transition seen at SPS energies, i.e. the Kink [266], the Strangeness Horn [267] and the Step [265]. Nevertheless, the hydro modeling of relativistic heavy ion collisions is difficult and even not straightforward.

Relativistic hydrodynamics is a set of the partial differential equations which describe the local energy-momentum and charge conservation [271]

$$\partial_\mu T_f^{\mu\nu}(x, t) = 0, \quad T_f^{\mu\nu}(x, t) = (\epsilon_f + p_f) u_f^\mu u_f^\nu - p_f g^{\mu\nu}, \quad (5.1)$$

$$\partial_\mu N_f^\mu(x, t) = 0, \quad N_f^\nu(x, t) = n_f u_f^\nu. \quad (5.2)$$

Here the components of the energy-momentum tensor $T_f^{\mu\nu}$ of the perfect fluid and its (baryonic) charge 4-current N_f^μ are given in terms of energy density ϵ_f , pressure p_f , charge density n_f and 4-velocity of the fluid u_f^ν . This is a simple indication that hydrodynamic description directly probes the equation of state of the matter under investigation.

As usual to complete the system (5.1) and (5.2) it is necessary to provide

- (A) *the initial conditions* on some hypersurface and
- (B) *equation of state* (EOS).

The tremendous complexity of (A) and (B) transformed each of them into a specialized direction of research of relativistic heavy ion community. However, there are several specific features

of relativistic hydrodynamics which have to be mentioned. In contrast to nonrelativistic hydrodynamics which is an exact science, the relativistic one applied to collisions of hadrons or/and heavy nuclei faces a few problems from the very beginning. Since collisions occur in vacuum there are no specific boundary conditions. Moreover, since the system created during the collision process is small and short lived there were always questions whether hydro description is good and accurate and whether the system thermalizes sufficiently fast in order that hydro description can be used [272].

It is clear that the last two questions cannot be answered within the framework of hydrodynamics. One has to study these problems in a wider frame, and there was some progress achieved on this way [102]. However, to be applicable and realistic, relativistic hydrodynamics requires the knowledge of

(C) *boundary conditions* which must be consistent with conservation laws (5.1) and (5.2).

The latter is known as the *freeze-out problem* (FO), and it has two basic aspects [268]:

(C1) hydrodynamic equations should be terminated at some freeze-out hypersurface (FO HS) $\Sigma_{fr}(x, t)$;

(C2) at the FO HS $\Sigma_{fr}(x, t)$ all interacting particles should be converted into the free-streaming particles which go to detector.

The complications come from the fact that the FO HS cannot be found a priori without solving hydrodynamic equations (5.1) and (5.2). This is a consequence of relativistic causality on the time-like (t.l.) parts of the FO HS defined by positive 4-interval $ds^2 = dt^2 - dx^2 > 0$ in Landau-Lifshitz convention [271]. Therefore, the *freeze-out criterion* is usually formulated as an additional equation (constraint) $F(x^*, t) = 0$ with the solution $\{x^*\} \Leftrightarrow x^{1*} = x^1(x^2, x^3, t)$, which has to be inserted into conservation laws and solved simultaneously with them. In what follows I will mostly use the 1+1 dimensional formulation for simplicity and convenience, but the main results will be formulated in 3+1 dimensional space-time.

There were many unsuccessful tries [273, 274, 275, 276, 277, 278] to solve this problem by imposing the form of the FO HS a priori, but all of them led to severe difficulties - either to negative number of particles or break up of conservation laws. The major difficulty is that the

hydro equations should be terminated in such a way, that their solution remains unmodified by this very fact. This is known as the recoil problem. Clearly this problem cannot be postponed to later times, as it is usually done in hydro simulations [269, 270, 278, 279, 186], because at the boundary with vacuum the particles start to evaporate from the very beginning of hydro expansion, and this fact should be accounted by equations as well. Thus, one has to account for the emission of particles from the FO HS and modify the hydro equations accordingly.

However this is only a part of the trouble. Another one comes from the problem of calculating the particle spectra on a t.l. hypersurface. For a space-like (s.l.) FO HS (i.e. with negative 4-interval $s^2 < 0$) the correct answer for the spectra of particles is given by the formula of Cooper and Frye [275]. However, one cannot use this formula for t.l. hypersurfaces, since it leads to negative numbers of particles. This is due to the fact that it was obtained only for the s.l. case, where the decay of one element of gas does not affect the decay of adjacent elements.

The freeze-out problem was completely solved in [173] and developed further in Refs. [258, 257, 259, 260]. Although Sinykov's effort [276, 277] did not resolve this problem, was a very descent try to solve it by purely hydrodynamic approach and, hence, it was very useful to me. The solution of the FO problem was found after a realization of a fact that at the t.l. parts of FO HS there is a *fundamental difference between the particles of fluid and the particles emitted from its surface*: the EOS of the fluid can be anything, but it implies a zero value for the mean free path, whereas the emitted particles cannot interact at all because they have an infinite mean free path. Therefore, it was necessary to extend the conservation laws (5.1) and (5.2) from a fluid alone to a system consisting of a fluid and the particles of gas emitted (gas of free particle) from the FO HS. As I will prove below on the t.l. parts of the FO HS these solution inevitably includes a new type of shock wave, which I called the FO shock [173]. As I showed, such a FO shock not only resolves the recoil problem, but also it provides an absence of the causal paradoxes at the t.l. parts of FO HS.

After the solution of the freeze-out problem was found in Ref. [173], there were two basic directions to develop it further on the basis of the transport simulations. Thus, there were two hydro groups which wanted to improve the solution [173]. The Bergen group wanted to justify and improve my approach using kinetic "equations" [280, 281, 282, 283, 284]. All these tries seems

to be unsuccessful because none of those “equations” was ever derived. The Bergen group used an intuition to postulate their equations and the hand waving arguments to justify them. These tries, of course, cannot be even closely compared with the rigorous analysis which was worked out in Ref. [173, 258, 257, 259, 260]. The San Paolo group [285, 286] tried to establish the continuous emission of particles in space and time. But again the suggested equations [285, 286] are used without any physical justification. Moreover, until the work of Sinyukov and collaborators [287], those equations for the escape probability had elementary mathematical mistakes.

Furthermore, from the very beginning it was also clear that the relaxation type equations considered as an improvement of the formalism developed in my works [173, 258, 257, 259, 260] cannot be applied to the actual hydro simulations because they do not conserve energy, momentum and baryonic charge. In this sense, the approach of the Bergen group was a step back because even a naive use of the Cooper-Frye formula respects all conservation laws.

The San Paolo group went ahead with the idea of the volume emission (see the full list of references in [286]). However, I think this group failed to understand three major points:

(I) if the mean free path of the fluid particles is small compared to the characteristic size of the system (usually it is transversal size), then the volume emission of the particles is reduced to the surface emission and the previous analysis becomes a perfect approximation;

(II) if, on contrary, the mean free path of the fluid particles is compared to the size of the system, then there is no reason to believe in thermal equilibrium at all and one has to abandon the whole hydro treatment pursuing by the San Paolo group;

(III) a real improvement of the hydrodynamic solution [173, 258, 257, 259, 260] of the freeze-out problem requires a far more fundamental approach which should be based on a new formalism.

A more solid attempt to study the validity of the solution [173] was presented in Ref. [288]. However, the conclusions on the applicability of the *freeze-out shock* model were too general. In contrast, the results of comparable simulations [289] indicate that the freeze-out shock approximation is valid within 15 % at the t.l. parts of the FO HS because about 85 % of all particles are born within a narrow region of the width about 0.5 - 1.2 fm, whereas the main problem with the narrow freeze-out hypersurface exists at the s.l. parts of the FO HS. The latter is a typical region

where the usual hydrodynamics and the Cooper-Frye formula [275] were traditionally believed to be valid. These conclusions of Ref. [289] were the first evidence that the hadronic rescattering and decay of heavy hadronic resonances should be treated with the transport approach.

Again there appeared two major directions of research: a simplified theoretical approach for hadronic rescattering was suggested in [287], whereas Bass and Dumitru suggested a principally new numerical approach to this problem [261] - the “*hydro-cascade*” model (or BD model) which was further developed in [262] (TLS model). This approach is a combination of hydro simulations with kinetics (hydrokinetic) and it assumes that the nucleus-nucleus collisions proceed in three stages: hydrodynamic expansion (“hydro”) of the QGP, phase transition from the QGP to the hadron gas and the stage of hadronic rescattering and resonance decays (“cascade”). The switch from hydro to cascade modeling takes place at the boundary between the mixed and hadronic phases. The spectrum of hadrons leaving this hypersurface of the transition between QGP and hadron gas is taken as an input for the cascade.

This approach incorporates the best features of both the hydrodynamic and cascade descriptions. It allows for, on one hand, the calculation of the phase transition between the quark gluon plasma and hadron gas using hydrodynamics and, on the other hand, the freeze-out of hadron spectra using the cascade description. This approach allows one to overcome the usual difficulty of transport models in modeling phase transition phenomenon. For this reason, this approach has been rather successful in explaining a variety of collective phenomena that has been observed at the CERN SPS and Brookhaven RHIC energies. However, both the BD and TLS models face some fundamental difficulties which cannot be ignored (see a detailed discussion in [263, 264]). Thus, within the BD approach the initial distribution for the cascade is found using the Cooper-Frye formula [275], which takes into account particles with all possible velocities, whereas in the TLS model the initial cascade distribution is given by the cut-off formula [173, 257], which accounts for only those particles that can leave the phase boundary. As shown in Ref. [263] the Cooper-Frye formula leads to causal and mathematical problems in the present version of the BD model because the phase boundary between QGP and hadron gas inevitably has t.l. parts. On the other hand, the TLS model does not conserve energy, momentum and number of charges and this,

as proved in [263, 264], is due to the fact that the equations of motion used in [262] are incomplete and, hence, should be modified.

These difficulties are likely in part responsible for the fact that the existing hydro-cascade models, like the more simplified ones, fail to explain the *HBT puzzle* [102], i.e. the fact that the experimental HBT radii at RHIC are very similar to those found at SPS, even though the center of mass energy is larger by an order of magnitude. Therefore, it turns out that the hydro-cascade approach successfully *parameterizes* the one-particle momentum spectra and their moments, but does not *describe* the space-time picture of the nuclear collision as probed by two-particle interferometry.

After I realized that the main difficulty of the hydro-cascade approach looks similar to the traditional problem of freeze-out in relativistic hydrodynamics [173, 258, 257, 259, 260], I started to work out the correct set of hydro-cascade equations. It turned out that in both cases the domains (subsystems) have t.l. boundaries through which the exchange of particles occurs and this fact should be taken into account. In relativistic hydrodynamics this problem was solved by the constraints which appear on the FO HS hypersurface and provide the global energy-momentum and charge conservation [173, 258, 257, 259, 260] between the perfect fluid domain and the domain of the gas of free particles. Similarly, it was necessary to generalize the usual Boltzmann equation in order to account for the exchange of particles through the t.l. boundary between the domains. As derived in [263] the generalized Boltzmann equations necessarily contain the δ -like source terms. By integrating the Boltzmann equation of the fluid domain over particle momenta, I derived the desired set of hydro-cascade equations [263] and analyzed them in [264]. The approach developed in [263, 264], is a new tool to model the PT dynamics in finite systems. Already the present formulation allows one, in principal, to consider the phase evolution of many domains of one phase being surrounded by the other phase. For instance, it can be used to model a hadronization of any number of the QGP droplets or bags which cannot be described the usual hydro equations.

In this chapter I present the FO model which is based on the conservation laws of energy and momentum between the perfect fluid and the gas of free particles and give a derivation of the hydrokinetic equations from the first principles and explain their analysis in details.

This chapter is based on the following works [173, 258, 257, 259, 260, 263, 264].

5.1. Freeze-out Problem in Relativistic Hydrodynamics

Before reformulating the hydrodynamic equations I will consider the problem of negative numbers of particles which was a nightmare of hydro simulations since the Cooper-Frye formula's invention [275]. This is necessary in order to understand the source of problem which puzzled the researches for almost four decades.

5.1.1. Decay of Perfect Fluid into the Gas of Free Particles. In order to obtain the particle spectra for the gas, I will use the method suggested by Gorenstein and Sinyukov [290]. Suppose there is a boundary between fluid and gas. Let me consider the decay of a small element Δx of the gas of free particles in its rest frame. The gas is supposed to be located in the left hemisphere and to have the freeze-out temperature $T = T^*$. (I suppose that the derivative to the freeze-out hypersurface v_σ in the $t - x^1$ plane is positive). Note that this frame is the rest frame of the gas *before* decay. Hereafter I will call it the reference frame of the gas (RFG). Suppose the particles in the gas have an equilibrium distribution function $\phi\left(\frac{p_0}{T^*}\right)$.

First I consider the contribution from particles with negative momenta that leave the element Δx (see Fig. 5.1)

$$\frac{dN_1}{d^2p_\perp \Delta S_\perp} = \phi\left(\frac{p_0}{T^*}\right) \Delta x dp \Theta(-p) , \quad (5.3)$$

where p_\perp is the transverse momentum of the particle, and ΔS_\perp the transverse size of the element. The second contribution is given by particles with negative momenta from the element $-\frac{p}{p_0} \Delta t$

$$\frac{dN_2}{d^2p_\perp \Delta S_\perp} = -\phi\left(\frac{p_0}{T^*}\right) \frac{p}{p_0} \Delta t dp \Theta(-p) . \quad (5.4)$$

Finally, the third contribution comes from particles with positive momenta from the element $\Delta x - \frac{p}{p_0} \Delta t$. However, those particles will cross the freeze-out hypersurface only if their velocity is smaller than the derivative to the hypersurface v_σ in the $t - x$ plane. Thus, the third term reads as follows (see Fig. 5.2):

$$\frac{dN_3}{d^2p_\perp \Delta S_\perp} = \phi\left(\frac{p_0}{T^*}\right) \left[\Delta x - \frac{p}{p_0} \Delta t \right] dp \Theta(p) \Theta\left(v_\sigma - \frac{p}{p_0}\right) . \quad (5.5)$$

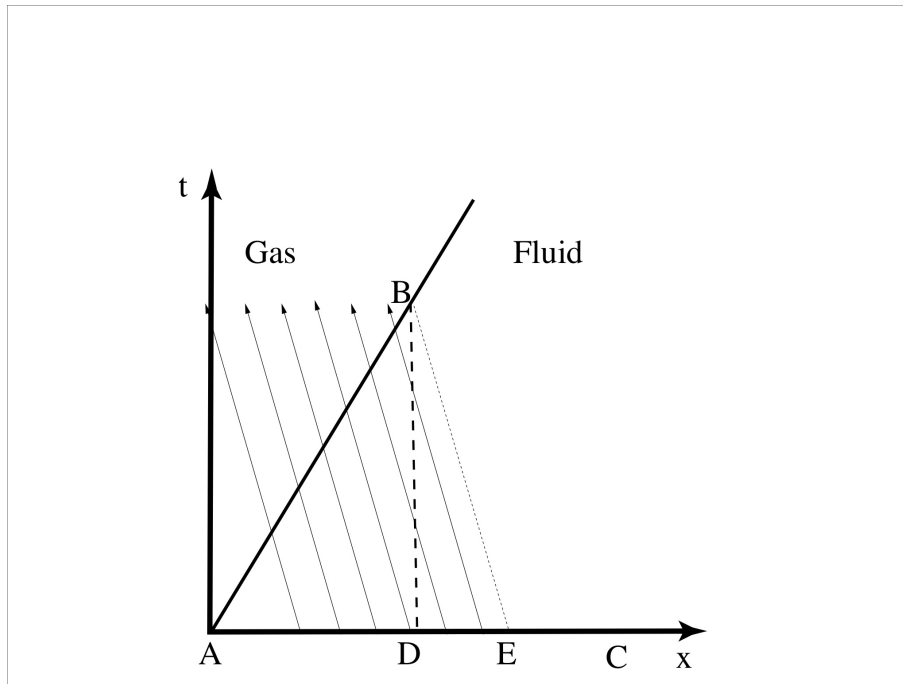


Figure 5.1. Decay of the element $\Delta x = AD$. Particles with negative momenta are leaving elements AD and $DE = -p/p_0 \Delta t$. The trajectories of free streaming particles are indicated by the lines with small arrows.

After some simple algebra one obtains the formula for the spectrum of the gas of free particles

$$\frac{dN_{tot}}{d^2p_{\perp} dp \Delta S_{\perp}} = \phi \left(\frac{p_0}{T^*} \right) \left[\Delta x - \frac{p}{p_0} \Delta t \right] \Theta \left(v_{\sigma} - \frac{p}{p_0} \right). \quad (5.6)$$

As will be shown below, the modification of the spectrum due to the Θ -function will lead to an energy-momentum tensor that differs from the equilibrium case.

Our last step is to write the formula for the spectrum in a fully relativistic form. For that one has to change the energy of the particles appearing in the distribution function in the RFG to the product of the four-vectors of momentum and hydrodynamic velocity, $p_{\mu} u^{\mu}$, and change the integration over the hypersurface of freeze-out to the product of the four-vectors of momentum and normal vector to the freeze-out hypersurface, $p_{\mu} d\sigma^{\mu}$. Finally, one has

$$p_0 \frac{dN_{tot}}{d^3p} = \phi \left(\frac{p_{\mu} u^{\mu}}{T^*} \right) p_{\nu} d\sigma^{\nu} \Theta (p_{\rho} d\sigma^{\rho}), \quad (5.7)$$

where the vector $d\sigma_{\mu} = (v_{\sigma}, -1) dt \Delta S_{\perp}$ is the normal vector to the freeze-out hypersurface in the left hemisphere. It is, however, easy to check that the above formula is valid for the right hemisphere as well.

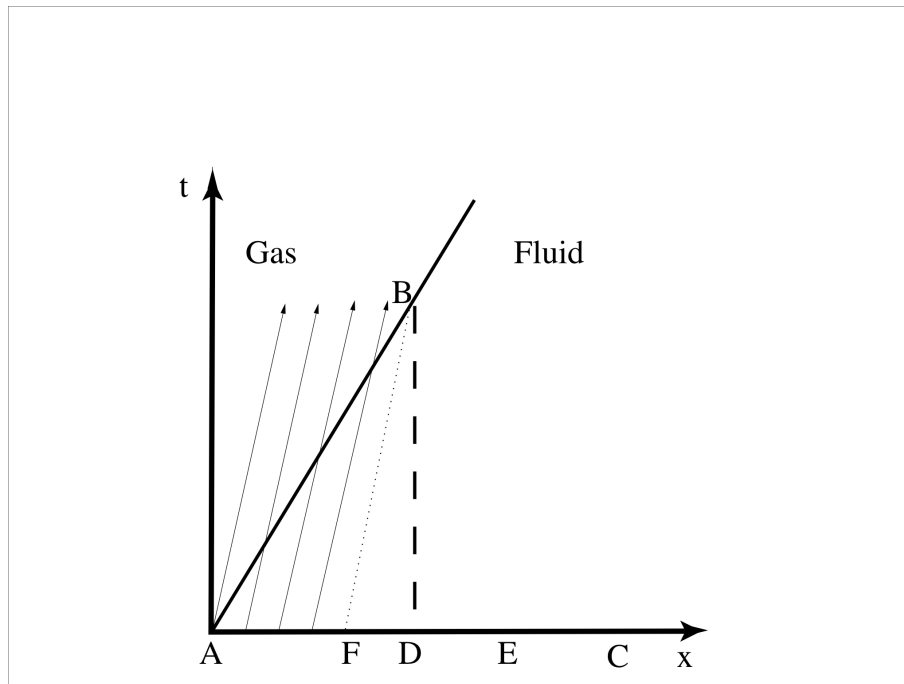


Figure 5.2. Decay of the element $\Delta x = AD$. Particles with positive momenta are leaving elements $AF = \Delta x - p/p_0 \Delta t$. Note that particles emitted from the element FD are returning to fluid's interior. The trajectories of free streaming particles are indicated by the lines with small arrows.

Integrating (5.7) over the whole FO HS, one gets

$$p_0 \frac{dN_{tot}}{d^3p} = \int_{\Sigma_{fr}} \phi \left(\frac{p_\mu u^\mu}{T^*} \right) p_\nu d\sigma^\nu \Theta(p_\rho d\sigma^\rho) , \quad (5.8)$$

The meaning of this nice result is that this is the formula of Cooper and Frye [275], but without negative particle numbers! Thus, Eq. (5.7) accounts for outgoing particles only (see Figs. 5.3 and 5.4 for more details), whereas other particles are returning to fluid and, hence, should not be taken into account! For this reason I named the distribution function (5.7) as *the cut-off distribution function*.

It is easy to see that for a s.l. hypersurface, where $v_\sigma > 1$, the above expression gives the result obtained by Cooper and Frye [275].

The energy-momentum tensor of free particles in the RFG reads as:

$$T_g^{\mu\nu}(v_\sigma) = \int \frac{d^3p}{p_0} p^\mu p^\nu \Theta \left(v_\sigma - \frac{p}{p_0} \right) \phi \left(\frac{p_0}{T} \right) . \quad (5.9)$$

It is easy to calculate this tensor for the case of noninteracting massless particles; it has the form:

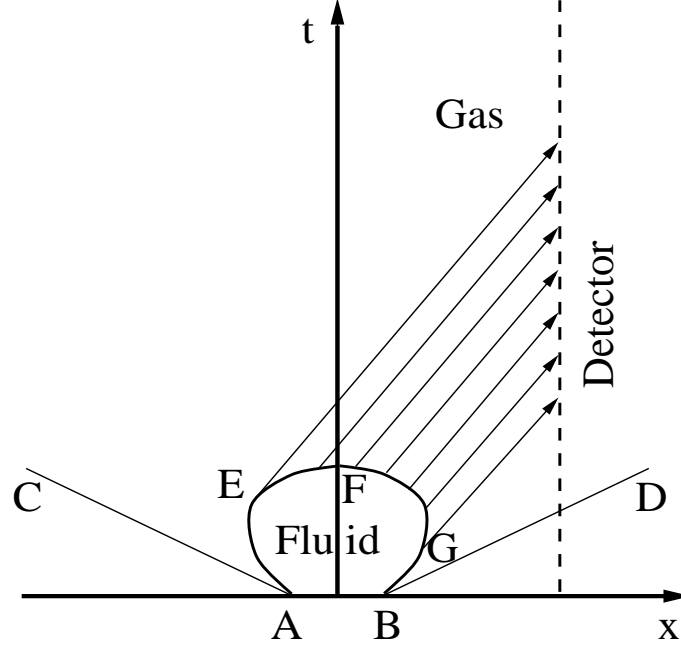


Figure 5.3. Decay of the fluid into the gas of free particles on the convex freeze-out hypersurface $AEFGB$. Trajectories of the particles are indicated by the lines with arrows. Dashed line represents the detector's world line. Lines AC and BD denote the light cones. For the given particle velocity $v = \frac{v^x}{p^0}$ the integration limits in coordinate space, points E and G , are found from the condition $p_\rho d\sigma^\rho = 0$. The geometrical meaning of points E and G is evident from the construction: they are the tangent points of the particle velocity to the freeze-out hypersurface in $t-x$ plane. In contrast to the cut-off formula for invariant spectra which ensures such limits automatically, the Cooper-Frye one takes into account the particles emitted from all points of the FO HS $AEFGB$.

$$T_g^{00}(v_\sigma) = \epsilon(T^*) \frac{1 + v_\sigma}{2}, \quad (5.10)$$

$$T_g^{01}(v_\sigma) = \epsilon(T^*) \frac{v_\sigma^2 - 1}{4}, \quad (5.11)$$

$$T_g^{11}(v_\sigma) = \epsilon(T^*) \frac{v_\sigma^3 + 1}{6}, \quad (5.12)$$

where ϵ is the usual energy density. The above result is valid for the left hemisphere. The corresponding formulae for the right hemisphere can be obtained in the same way. The general

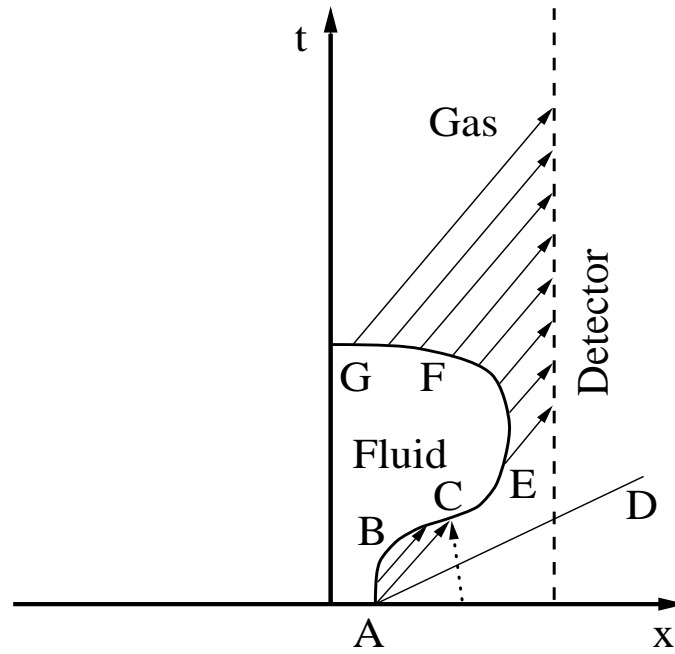


Figure 5.4. Decay of the fluid into the gas of free particles on the concave freeze-out hypersurface $ABCEFG$. Notations correspond to the previous figure. In this case, however, one has to take into account the particles feeding back into the fluid on the part ABC of the freeze-out hypersurface. These particles were emitted earlier and do not appear from the rescattering. The latter is forbidden by the assumption that the particle spectra are "frozen" once they belong to the gas of free particles. Hence, the particle trajectories, like the one shown by the dotted line, are not allowed in the freeze-out picture because those particles appear from nothing.

formulae for $T_g^{\mu\nu}(v_\sigma)$ can be found in [258]. Now one can see that for the case $v_\sigma = 1$ the above expressions give the usual formula for the ideal gas. For $v_\sigma = -1$ no particle can cross such a HS and, hence, all components of the gas tensor vanish.

In Sinyukov's works [276, 277] another model for freeze-out was suggested. The author of [276, 277] considered the decay from a box and did not account for the additional contributions from the intrinsic volume of the gas, namely from the element $-\frac{p}{p_0}\Delta t$ (see Fig. 5.1). Due to that, the energy-momentum tensor obtained in these papers is not symmetric which means that the orbital momentum of the considered system is not locally conserved!

On the other hand, in [276, 277] considered an *ad hoc* model of deflagration from a very

hot pionic matter into the gas of free particles. However, such an oversimplified picture does not correspond to the real situation in A+A collisions, since the solution of the hydrodynamic equations [269, 270, 278, 279] does not exhibit the pure shock-like transition in the expansion of hot and dense pionic matter. Moreover, in contrast to the assumption of Refs. [276, 277]. the hydro solutions must necessarily have the s.l. parts of the FO HS.

Now I would like to clarify an important question: "What is the difference between a perfect fluid and the gas of free particles at the FO?" It seems that the main difference is that they have different values of the mean free path. Due to that, there are collisions in the fluid which lead to thermodynamical equilibrium. In contrast, there are about no collisions in the gas of free particles (and I will neglect them completely), because the mean free path is very large. Of course, fluid and gas have somewhat different values of temperature, but due to the fact that the mean free-path strongly depends on the temperature, this difference should not be too large. It was found [291] that for pions the mean free-path depends on the fifth power of the inverse temperature: $\lambda \approx \frac{const}{T^5}$. Thus, the difference between the temperatures of the fluid and the gas should be small, but due to the strong dependence of the collision cross-section on the temperature, their mean free-paths should be very different. Such a conclusion was also demonstrated by [289] with the transport simulations which show that at the t.l. parts of the FO HS about 85 % of all particles are born (or scattered last time) within a narrow region of the width about 0.5 - 1.2 fm. Also these simulations showed that the main problem with the validity of the narrow freeze-out hypersurface existence comes from the s.l. parts of the FO HS due to decay of hadronic resonances. Thus, keeping these facts in mind, I will assume that the FO HS has a zero width. As one sees these is reasonable assumption for the t.l. parts of the FO HS, whereas the decay of resonances can be accounted after the FO, since this is necessary to work out *a purely hydrodynamic solution of the freeze-out problem*. As will be seen this concept is based on the conservation laws at the discontinuity between the perfect fluid and the gas of free particles.

However, before completing this subsection it is necessary to generalize the obtained results (5.7) and (5.8) in order to account for feed back of the particles emitted earlier from the concave parts of the FO HS (see Fig. 5.4 for details). This can be done by accounting for the incoming

particles with $\phi_{g.fback}(\mathbf{p}) \Theta(-p_\rho d\sigma^\rho)$. In order to distinguish the corresponding distributions of the gas of free particles, hereafter they are labeled by additional subscript:

$$\phi_g \left(\frac{p_\rho u_g^\rho}{T_g}, d\sigma_\mu \right) \Big|_{x^{1*}} = \left(\phi_{g.emit}(\mathbf{p}) \Theta(p^\mu d\sigma_\mu) + \phi_{g.fback}(\mathbf{p}) \Theta(-p^\mu d\sigma_\mu) \right) \Big|_{x^{1*}}, \quad (5.13)$$

where I have dropped the space-time dependence in the distribution functions above for the sake of convenience. An important assumption of this approach is that the post FO distribution function at the moment of emission, i.e. $\phi_{g.emit}(\mathbf{p})$, is an equilibrium one. This assumption implies that the outgoing free particles are emitted from the region in which the collision rate is sufficient high to keep thermodynamic equilibrium. This might look strange, but it seems to be very reasonable because the hydrodynamic approach is valid in the same range as equilibrium thermodynamics [268, 271].

5.1.2. Conservation Laws at the Freeze-out Hypersurface. The FO problem was solved in [173] and developed further in Refs. [258, 257, 259, 260]. It was found after a realization of a fact that at the t.l. parts of FO HS there is a fundamental difference between the particles of fluid and the particles emitted from its surface: the EOS of the fluid can be anything, but it implies a zero value for the mean free path, whereas the emitted particles cannot interact at all because they have an infinite mean free path. Mixing these two different objects the researches were confused for decades. However, once they are distinguished it clear that it is necessary to extend the conservation laws (5.1) and (5.2) from a fluid alone to a system consisting of a fluid and the particles of gas emitted (gas of free particle) from the FO HS. The resulting energy-momentum tensor and baryonic current (for a single particle species) of the system can be, respectively, cast as

$$T_{tot}^{\mu\nu}(x, t) = \Theta_f^* T_f^{\mu\nu}(x, t) + \Theta_g^* T_g^{\mu\nu}(x, t), \quad (5.14)$$

$$N_{tot}^\mu(x, t) = \Theta_f^* N_f^\mu(x, t) + \Theta_g^* N_g^\mu(x, t), \quad (5.15)$$

where at the FO HS the energy-momentum tensor of the gas $T_g^{\mu\nu}$ and its baryonic current N_g^μ are given in terms of *the cut-off* distribution function of particles that have the 4-momentum p^μ , i.e.

(5.13),

$$T_g^{\mu\nu}(x^*, t) = \int \frac{d^3p}{p_0} p^\mu p^\nu \phi_g(x^*, t, p, d\sigma_\mu) , \quad (5.16)$$

$$N_g^\mu(x^*, t) = \int \frac{d^3p}{p_0} p^\mu \phi_{c.g}(x^*, t, p, d\sigma_\mu) . \quad (5.17)$$

Here $\phi_g(x^*, t, p)$ and $\phi_{c.g}(x^*, t, p)$ denote the equilibrium distribution function of number of particles and charges, respectively. $d\sigma_\mu$ are the components of the external normal 4-vector to the FO HS $\Sigma_{fr}(x^*, t)$ [173, 257, 259, 260].

The important feature of equations (5.13)-(5.14) is the presence of several Θ -functions. The $\Theta_g^* = \Theta(F(x, t))$ function of the gas and $\Theta_f^* = 1 - \Theta_g^*$ function of the fluid can be explicitly expressed in terms of the freeze-out criterion and can automatically ensure that the energy-momentum tensor of the gas (liquid) is not vanishing only in the domain where the gas (liquid) exists.

The equations of motion of the full system are just the conservation laws:

$$\partial_\mu T_{tot}^{\mu\nu}(x, t) = 0 , \quad \partial_\mu N_{tot}^\mu(x, t) = 0 \quad (5.18)$$

Let me study *the boundary conditions* first. I will do it for the energy-momentum tensor only, since for the charge it can be done similarly. Integrating equations (5.18) over the 4-volume around the vicinity of the FO HS, namely $x^1 \in [x^{1*} - \delta^2; x^{1*} + \delta^2]$ and the corresponding finite limits for the other coordinates, and applying the Gauss theorem as it was done in previous subsection, one obtains the energy-momentum conservation for the corresponding part of the FO HS Σ_{fr}

$$\int_{\Sigma_{fr}-\delta^2} d\sigma_\mu T_{tot}^{\mu\nu} = \int_{\Sigma_{fr}+\delta^2} d\sigma_\mu T_{tot}^{\mu\nu} , \quad (5.19)$$

where in both sides of the equality $d\sigma_\mu$ is the external normal with respect to the fluid.

Then in the limit $\delta \rightarrow 0$ one easily gets the energy-momentum (the charge) conservation at the FO HS from Eqs. (5.16)

$$d\sigma_\mu T_f^{\mu\nu} \Big|_{x^{1*}} = d\sigma_\mu T_g^{\mu\nu} \Big|_{x^{1*}} , \quad (5.20)$$

$$d\sigma_\mu N_{c.f}^\mu \Big|_{x^{1*}} = d\sigma_\mu N_{c.g}^\mu \Big|_{x^{1*}} , \quad (5.21)$$

or, writing it explicitly,

$$d\sigma_\mu \int \frac{d^3\mathbf{p}}{p^0} p^\mu p^\nu \phi_f \left(\frac{p_\rho u_f^\rho}{T} \right) \Big|_{x^{1*}} = d\sigma_\mu \int \frac{d^3\mathbf{p}}{p_0} p^\mu p^\nu \left(\phi_{g.emit}(\mathbf{p}) \Theta(p^\mu d\sigma_\mu) + \phi_{g.fback}(\mathbf{p}) \Theta(-p^\mu d\sigma_\mu) \right) \Big|_{x^{1*}}, \quad (5.22)$$

$$d\sigma_\mu \int \frac{d^3\mathbf{p}}{p^0} p^\mu \phi_{c.f} \left(\frac{p_\rho u_f^\rho}{T} \right) \Big|_{x^{1*}} = d\sigma_\mu \int \frac{d^3\mathbf{p}}{p_0} p^\mu \left(\phi_{c.g.emit}(\mathbf{p}) \Theta(p^\mu d\sigma_\mu) + \phi_{c.g.fback}(\mathbf{p}) \Theta(-p^\mu d\sigma_\mu) \right) \Big|_{x^{1*}}, \quad (5.23)$$

with the evident notations for fluid distribution functions.

From the expressions (5.22) and (5.23) it is clear that there are two distinct cases, namely **(i)** when the distribution function of the gas of free particles coincides with that one of the fluid (or the EOS is the same for both) and **(ii)** when they are entirely different. In the latter case there is no criterion which equation of state is preferable. This should be defined by the physics of the considered task. I believe that the full solution of the problem can be given within the kinetic approach only. However, since we adopted the hydrodynamical approach which implies also the thermodynamical equilibrium, in what follows it is assumed that at least the emission part is described by the equilibrium distribution function.

Statement 1: If the fluid and the gas have same EOS, then on the s.l. parts of the FO HS their distribution functions are identical, on the convex parts of the t.l. FO HS there exists a *freeze-out shock* transition, and on the concave ones there is a *parametric freeze-out shock* transition (see below).

Let me demonstrate this. Indeed, a simple analysis shows that for the case **(i)** there are the following possibilities:

(i.a) if $\Theta(p^\mu d\sigma_\mu) = 1$ for $\forall \mathbf{p}$, i.e., on *the s.l.* parts of the FO HS or on the light cone, there is no feedback and then there is only a trivial solution given by the Cooper-Frye formula $\phi_f \left(\frac{p_\rho u_f^\rho}{T} \right) \Big|_{x^{1*}} = \phi_{g.emit}(\mathbf{p}) \Big|_{x^{1*}}$ with the fluid temperature being equal to the FO one. Note that the discontinuity through such a hypersurface (or the t.l. shocks, as the authors of Ref. [294] call it) is impossible in this case as it was shown in [295].

(i.b) for *the convex t.l.* parts of the FO HS the feedback term vanishes as was discussed

before (see Fig. 5.3) and hence there is a *freeze-out shock* between the fluid and the gas of free particles (actually, the same fluid, but with the FO temperature and cut-off distribution function; for details see later). It is reasonable to call it this way because the pressure and the energy density of the gas of free particles are not the usual ones, but have extra dependence on the parameters of the FO HS. The hydrodynamic parameters of the fluid should be found from the conservation laws on the discontinuity

$$d\sigma_\mu \int \frac{d^3\mathbf{P}}{p_0} p^\mu p^\nu \phi_f \left(\frac{p_\rho u_f^\rho}{T} \right) \Big|_{x^{1*}} = d\sigma_\mu \int \frac{d^3\mathbf{P}}{p_0} p^\mu p^\nu \phi_f \left(\frac{p_\rho u_f^\rho}{T^*} \right) \Theta(p^\mu d\sigma_\mu) \Big|_{x^{1*}}, \quad (5.24)$$

$$d\sigma_\mu \int \frac{d^3\mathbf{P}}{p_0} p^\mu \phi_{c.f} \left(\frac{p_\rho u_f^\rho}{T} \right) \Big|_{x^{1*}} = d\sigma_\mu \int \frac{d^3\mathbf{P}}{p_0} p^\mu \phi_{c.f} \left(\frac{p_\rho u_f^\rho}{T^*} \right) \Theta(p^\mu d\sigma_\mu) \Big|_{x^{1*}}. \quad (5.25)$$

(i.c) for *the concave t.l.* parts of the FO HS the feedback term does not vanish (see also Fig. 5.4) and hence it is a new type of shock between the fluid and the gas of free particles which can be called a *parametric freeze-out shock* with the contribution of the feedback particles being a parameter in the general meaning. In this case the equations on the discontinuity, i.e. Eqs. (5.22) and the similar one for the conserved charge, should be studied. However, it requires the knowledge of the expressions for the feedback particles emitted from arbitrary hypersurface which is outside the scope of this dissertation. In addition, the assumption of the instant thermalization of the feedback particles has to be investigated, but this is far beyond the hydrodynamical approach.

Statement 2: If the fluid and the gas have entirely different EOS, then on the s.l. parts of the FO HS the t.l. shocks [294] can exist, whereas on the convex parts of the t.l. FO HS there is a *freeze-out shock* transition, and on the concave ones there is a *parametric freeze-out shock*.

The proof is similar to the previous consideration. If the fluid and the gas EOS are different, [case (ii)], one has the following cases:

(ii.a) if $\Theta(p^\mu d\sigma_\mu) = 1$ for $\forall \mathbf{p}$, i.e., on *the s.l.* parts of the FO HS or on the light cone, again the feedback contribution is zero, but there is no trivial solution in contrast to the case (i.a), and the t.l. shocks [294] are possible as it was discussed in Ref. [295]. They are defined by the following

conservation laws

$$d\sigma_\mu \int \frac{d^3\mathbf{p}}{p_0} p^\mu p^\nu \phi_f \left(\frac{p_\rho u_f^\rho}{T} \right) \Big|_{x^{1*}} = d\sigma_\mu \int \frac{d^3\mathbf{p}}{p_0} p^\mu p^\nu \phi_{g.emit} \left(\frac{p_\rho u'^\rho}{T^*} \right) \Big|_{x^{1*}}, \quad (5.26)$$

$$d\sigma_\mu \int \frac{d^3\mathbf{p}}{p_0} p^\mu \phi_{c.f} \left(\frac{p_\rho u_f^\rho}{T} \right) \Big|_{x^{1*}} = d\sigma_\mu \int \frac{d^3\mathbf{p}}{p_0} p^\mu \phi_{c.g.emit} \left(\frac{p_\rho u'^\rho}{T^*} \right) \Big|_{x^{1*}}, \quad (5.27)$$

where the equilibrium distribution functions for the gas $\phi_{g.emit} \left(\frac{p_\rho u'^\rho}{T^*} \right)$ and $\phi_{c.g.emit} \left(\frac{p_\rho u'^\rho}{T^*} \right)$ are used.

More recent results on this subject can be found in Refs. [297, 293]. However, this kind of solutions can probably exist only under very special conditions, namely for the supercooled quark-gluon plasma, since it is difficult to imagine any reason for the fluid near the FO state (when all interactions between particles are very weak) to convert suddenly without any cause into the gas of free particles with entirely different EOS.

(ii.b) for *the convex t.l.* parts of the FO HS the feedback term again vanishes and therefore there is a shock transition between the fluid and the gas of free particles but now fluid and gas being completely different states! Therefore, the gas should be described by the cut-off distribution function. In this case the hydrodynamic parameters of the fluid are defined by the conservation laws on the discontinuity

$$d\sigma_\mu \int \frac{d^3\mathbf{p}}{p_0} p^\mu p^\nu \phi_f \left(\frac{p_\rho u_f^\rho}{T} \right) \Big|_{x^{1*}} = d\sigma_\mu \int \frac{d^3\mathbf{p}}{p_0} p^\mu p^\nu \phi_{g.emit} \left(\frac{p_\rho u'^\rho}{T^*} \right) \Theta(p^\mu d\sigma_\mu) \Big|_{x^{1*}}, \quad (5.28)$$

$$d\sigma_\mu \int \frac{d^3\mathbf{p}}{p_0} p^\mu \phi_{c.f} \left(\frac{p_\rho u_f^\rho}{T} \right) \Big|_{x^{1*}} = d\sigma_\mu \int \frac{d^3\mathbf{p}}{p_0} p^\mu \phi_{c.g.emit} \left(\frac{p_\rho u'^\rho}{T^*} \right) \Theta(p^\mu d\sigma_\mu) \Big|_{x^{1*}}. \quad (5.29)$$

(ii.c) for *the concave t.l.* parts of the FO HS the feedback term does not vanish and therefore the *parametric freeze-out shock* introduced above should exist. This kind of the shock solution should satisfy the conservation laws in the most general form of Eqs. (5.22) and (5.23). However, the detailed consideration of such a solution would lead us too far off the main topic of the present discussion, although a similar discontinuity will be discussed in the section on hydrokinetics.

Thus, the full analysis of all possible boundary conditions is performed. The conservation laws discussed above have to be solved together with the equations of motion of the fluid in order to find out the FO HS. Next subsection is devoted to the derivation of the equations of motion of the fluid alone and their consistency with the boundary conditions.

There are several papers [276, 292, 293] on a shock-like treatment of the freeze-out problem. However, in my opinion these approaches are *ad hoc*, since the existence of such a shock is postulated and not obtained as a result of equations of motion. For instance, the conservation laws on the boundary between the fluid and the gas of free particles discussed in [280] (see Eqs. (6), (7) therein) were just postulated and are not related to any hydrodynamical evolution of the fluid at all. Moreover, those equations, in the integral form as presented in Ref. [280], cannot be used to solve them together with the hydrodynamical equations of the fluid.

To summarize, I have presented above the full and complete analysis of the possible boundary conditions, following the original idea of the paper [173]. The derived formalism allows one not only to find out the new class of the shock transitions, i.e. *the parametric freeze-out shock*, but also to formulate the hydrodynamical approach in the way consistent with the emission of the particles from an arbitrary FO HS.

5.1.3. Consistency Theorem. Let me study the consistency of the equations of motion for the whole system with the boundary conditions derived in the previous subsection. At the moment the explicit form of the energy-momentum tensor and 4-current for the gas of free particles is not important, but one should remember that these quantities have to satisfy the conservation laws in the differential form, since the gas particles move freely along the straight lines:

$$\partial_\mu T_g^{\mu\nu} = 0, \quad (5.30)$$

$$\partial_\mu N_{c.g}^\mu = 0 \quad (5.31)$$

in the domain where the gas of free particles exists. Exploiting this fact, one can rewrite the original conservation laws (5.18) as the equations of motion of the fluid alone

$$\begin{aligned} \partial_\mu \left\{ \Theta_f^* T_f^{\mu\nu} \right\} &= - \sum_a \delta(F(x_a^*, t)) n_\mu(f_a) \times \\ &\int \frac{d^3\mathbf{p}}{p_0} p^\mu p^\nu \left(\phi_{g.emit}(\mathbf{p}) \Theta(p^\mu n_\mu(f_a)) + \phi_{g.fback}(\mathbf{p}) \Theta(-p^\mu n_\mu(f_a)) \right) \Big|_{x_a^{1*}}, \quad (5.32) \end{aligned}$$

$$\begin{aligned} \partial_\mu \left\{ \Theta_f^* N_f^\mu \right\} &= - \sum_a \delta(F(x_a^*, t)) n_\mu(f_a) \times \\ &\int \frac{d^3\mathbf{p}}{p_0} p^\mu \left(\phi_{c.g.emit}(\mathbf{p}) \Theta(p^\mu n_\mu(f_a)) + \phi_{c.g.fback}(\mathbf{p}) \Theta(-p^\mu n_\mu(f_a)) \right) \Big|_{x_a^{1*}}, \quad (5.33) \end{aligned}$$

where $n_\mu(f_a)$ is the external normal 4-vector with respect to the fluid which is defined as

$$n_\mu(f_a) \equiv \partial_\mu F(x_a^*, t) \quad (5.34)$$

for all solutions of the FO criterion equation that labeled by the subscript a.

Eqs. (5.32) and (5.33) look like the hydrodynamical equations of motion with the source terms, the first of them describes *the loss* of the energy-momentum flux through the FO HS due to emission of the "frozen" particles and the second one is responsible for *the gain* by the reentering particles at the concave parts of the t.l. FO HS. It is evident because the Θ -function in the first term takes into account only positive values of the product $p^\mu n_\mu(f_a) > 0$, while the second one is nonvanishing only for its negative values, i.e., $p^\mu n_\mu(f_a) < 0$.

However, it is easy to show that, in fact, there are no source terms because they disappear due to the boundary conditions studied in the previous subsection! Indeed, taking derivatives of the remaining Θ -functions in the left hand side of Eqs. (5.32) and (5.33), one obtains the source-like terms with the fluid energy-momentum tensor and with the conserved 4-current, respectively, which exactly cancel the source terms in the r.h.s of (5.32) and (5.33). Then the equations of motion of the fluid acquire a familiar form:

$$\Theta_f^* \partial_\mu T_f^{\mu\nu}(x, t) = 0, \quad \Theta_f^* \partial_\mu N_f^\mu(x, t) = 0, \quad (5.35)$$

These equations complete the proof of the following *Theorem 1*: If the gas of free particles with the emission part defined by cut-off distribution and with known feedback part is described by the equations of motion (5.30) and (5.31), then the equations of motion of the whole system consisting of the perfect fluid and the gas of free particles split up into the system of the fluid's equations of motion (5.35) and of the boundary conditions in the general form of Eqs. (5.22) and (5.23) on the FO HS.

There is a fundamental difference between the equations of motion (5.1) of traditional hydrodynamics and the corresponding equations (5.35) of hydrodynamics with particle emission although they look very similar: if the FO HS is found, then, in contrast to usual hydrodynamics, the equations (5.35) automatically vanish in the domain where the fluid is absent. Evidently, a solution of the traditional hydrodynamic equations under the given additional conditions is also a solution of

Eqs. (5.35). Moreover, the solution of the latter has to be understood this way. Thus, the effect of the particle emission is implicitly taken into account by the equations of motion of the fluid alone, and is expressed explicitly in the boundary conditions between the fluid and the gas.

Theorem 1 leads also to the fact that inclusion of the source terms which are proportional to the δ -function on the FO HS into the equations of motion of the fluid will always require their vanishing, unless the derivatives of the fluid's energy-momentum tensor or the gas one contain similar singularities. This is a very important consequence of the *Theorem 1* which is easy to understand recalling the fact that singularities like δ -function and its derivatives (if they appear) are of different order and should be considered independently. Therefore, if these singularities enter the same equality, then singularities of the same order will generate independent equations.

Now we are ready to consider the consistency problem of the energy-momentum and the current conservation of the fluid given by Eqs. (5.13) with the emission of the "frozen" particles of the gas described by the cut-off distribution function.

Theorem 2: Energy, momentum and charge of the initial fluid together with the corresponding contribution of the reentering particles from the concave parts of the FO HS are equal to the corresponding quantities of the emitted from this hypersurface free particles with the cut-off momentum distribution function, i.e., those quantities are conserved.

Proof. First I integrate the derived equations (5.35) of the fluid evolution over the 4-volume and use the Gauss theorem to write the 4-volume integral over the integral of the corresponding closed HS. Then by splitting the closed HS into the initial and FO parts one obtains an integral form of the energy-momentum conservation for the fluid alone

$$P_{f.in}^\nu \equiv - \int_{\Sigma_{in}} d\sigma_\mu T_f^{\mu\nu}(x, t) = \int_{\Sigma_{fr}} d\sigma_\mu T_f^{\mu\nu}(x^*, t). \quad (5.36)$$

Due to the boundary conditions (5.22) on the FO HS one can rewrite the r.h.s of Eq. (5.36) in terms of the gas distribution function and obtain the following equality

$$\begin{aligned} & - \int_{\Sigma_{in}} d\sigma_\mu T_f^{\mu\nu}(x, t) - \int_{\Sigma_{fr}} d\sigma_\mu \int \frac{d^3\mathbf{p}}{p_0} p^\mu p^\nu \phi_{g.back}(\mathbf{p}) \Theta(-p^\mu d\sigma_\mu) \Big|_{x^{1*}} = \\ & \int_{\Sigma_{fr}} d\sigma_\mu \int \frac{d^3\mathbf{p}}{p_0} p^\mu p^\nu \phi_{g.emit}(\mathbf{p}) \Theta(p^\mu d\sigma_\mu) \Big|_{x^{1*}}, \end{aligned} \quad (5.37)$$

which actually states the energy-momentum conservation in the integral form and also shows that the sum of the energy-momentum of the fluid and the particles reentering the fluid during its evolution are exactly transformed into the energy-momentum of the emitted particles with the correct distribution function!

A proof for the conserved current can be obtained in a similar way.

Recently there appeared an attempt to resolve the FO problem by introducing the sources into the hydrodynamic equations [296]. As it is seen from the text of Ref. [296] the source terms modify the solution of the hydrodynamic equations essentially and such a modification should have been long ago found in the experiments on nonrelativistic hydrodynamics. In addition the problem of negative numbers of particles is not resolved in [296] and in this approach there exist a typical causal paradox that the post FO state in the inner part of a fluid is reached before it is reached in its outer part. Consequently, the gas of free particles “waits”, when the outer parts of the fluid “tells” it to freely go to the detector. Therefore, I conclude that the attempt of Ref. [296] is unsuccessful.

5.2. Equations for the Freeze-out Hypersurface

The conservation laws (5.22) and (5.23) are the partial differential equation for the FO HS. Here I will discuss the general scheme of how to solve these equations together with the hydro equations. In what follows I will neglect the contribution of the feedback particles in order to simplify presentation, and, hence, the freeze-out and the parametric freeze-out shocks will not be distinguished.

From academic and numeric points of view it is worth to closely inspect these equations. As a good example to apply the derived scheme, I consider an important problem of relativistic hydrodynamics – the freeze-out of a simple wave.

5.2.1. Freeze-out Calculus: General Scheme. Let me obtain now the full system of all necessary equations. First, I suppose that the FO HS exists and then I will derive its equations. For this it is convenient to evaluate the boundary conditions in the rest frame of

the fluid (hereafter RFF) before the FO shock, where the energy-momentum tensor of the fluid is diagonal. I choose the local coordinate system with one of the axis, let it be the X -axis, being parallel to the normal 3-vector. The latter then is reduced to

$$n_\mu(f_a) = \left(-\partial_0 x_a^{1*}; 1; 0; 0 \right) \begin{cases} -1, & a \in \text{left hemisphere}, \\ +1, & a \in \text{right hemisphere}. \end{cases} \quad (5.38)$$

Next, I mention that the velocity of the gas of free particles cannot have nonzero projection on any tangential direction to the normal 3-vector in this frame. It can be shown directly by manipulation with formulae, but it is evident from the simple reason that an oblique shock (see corresponding chapter in Ref. [271]) should have continuous tangent velocities on the both sides of shock. Then it follows for the RFF that the gas velocity can be parallel or antiparallel to the normal 3-vector only.

This statement is valid for the RFG as well, and the expression for the normal 4-vector in this frame is evidently similar to Eq. (5.38). In order to distinguish them, hereafter I will write the corresponding subscript.

Boundary conditions (5.22) and (5.23) have a simplest representation in the RFG since the moments of the cut-off distribution function do not look too much complicated in this frame:

$$T_f^{X0}(v_{f\mathbf{G}}) - T_f^{00}(v_{f\mathbf{G}})v_{s\mathbf{G}} = T_g^{X0}(v_{s\mathbf{G}}) - T_g^{00}(v_{s\mathbf{G}})v_{s\mathbf{G}}, \quad (5.39)$$

$$T_f^{XX}(v_{f\mathbf{G}}) - T_f^{X0}(v_{f\mathbf{G}})v_{s\mathbf{G}} = T_g^{XX}(v_{s\mathbf{G}}) - T_g^{X0}(v_{s\mathbf{G}})v_{s\mathbf{G}}, \quad (5.40)$$

$$N_{c.f}^X(v_{f\mathbf{G}}) - N_{c.f}^0(v_{f\mathbf{G}})v_{s\mathbf{G}} = N_{c.g}^X(v_{s\mathbf{G}}) - N_{c.g}^0(v_{s\mathbf{G}})v_{s\mathbf{G}}, \quad (5.41)$$

where the energy-momentum tensor and 4-current of the fluid have standard form of Eqs. (5.1) and (5.2), respectively, with the 3-velocity $v_{f\mathbf{G}}$. In the above formula the velocity $v_{s\mathbf{G}} = \partial_0 x^{1*}$ is the time derivative of the FO hypersurface in the RFG, or velocity of the shock in this frame. Note, however, that in contrast to the usual shocks the above equations look like the conservation laws in the arbitrary Lorentz frame (not the rest frame of the gas!) where the nondiagonal components of the energy-momentum tensor are nonzero.

Introducing the following notations for the "effective" energy density, pressure and charge

density of the gas of free particles

$$\tilde{\varepsilon}_g(v_{s\mathbf{G}}) = T_g^{00}(v_{s\mathbf{G}}) - T_g^{X0}(v_{s\mathbf{G}})v_{s\mathbf{G}}^{-1}, \quad (5.42)$$

$$\tilde{p}_g(v_{s\mathbf{G}}) = T_g^{XX}(v_{s\mathbf{G}}) - T_g^{X0}(v_{s\mathbf{G}})v_{s\mathbf{G}}, \quad (5.43)$$

$$\tilde{n}_{c.g}(v_{s\mathbf{G}}) = N_{c.g}^0(v_{s\mathbf{G}}) - N_{c.g}^X(v_{s\mathbf{G}})v_{s\mathbf{G}}^{-1}, \quad (5.44)$$

one can transform the right-hand side of Eqs. (5.39) – (5.41) to the familiar expressions of the relativistic shocks [271] written in the rest frame of the matter behind the discontinuity. In contrast to the usual shock, however, Eqs. (5.39) – (5.41) do not form the closed system together with the EOS, but they are dynamical equations for the FO HS. Then velocities of fluid and shock in the RFG can be expressed by the standard relations

$$v_{f\mathbf{G}}^2 = \frac{(\varepsilon_f - \tilde{\varepsilon}_g(v_{s\mathbf{G}}))(p_f - \tilde{p}_g(v_{s\mathbf{G}}))}{(\varepsilon_f + \tilde{p}_g(v_{s\mathbf{G}}))(p_f + \tilde{\varepsilon}_g(v_{s\mathbf{G}}))}, \quad (5.45)$$

$$v_{s\mathbf{G}}^2 = \frac{(p_f - \tilde{p}_g(v_{s\mathbf{G}}))(\varepsilon_f + \tilde{p}_g(v_{s\mathbf{G}}))}{(\varepsilon_f - \tilde{\varepsilon}_g(v_{s\mathbf{G}}))(p_f + \tilde{\varepsilon}_g(v_{s\mathbf{G}}))}. \quad (5.46)$$

Now it is clearly seen that last relation is a transcendental equation for the $v_{s\mathbf{G}}$ – velocity of the FO HS in the RFG. It cannot be solved analytically for an arbitrary EOS. In addition it is necessary to transform it to the fluid rest frame in order to complete it with the solution of the hydrodynamical equations for the fluid

$$v_{s\mathbf{F}} = \frac{v_{s\mathbf{G}} - v_{f\mathbf{G}}}{1 - v_{s\mathbf{G}} v_{f\mathbf{G}}}. \quad (5.47)$$

Fortunately, there exist a simple expression for the square of this velocity, namely

$$v_{s\mathbf{F}}^2 = \frac{(p_f - \tilde{p}_g(v_{s\mathbf{G}}))(p_f + \tilde{\varepsilon}_g(v_{s\mathbf{G}}))}{(\varepsilon_f - \tilde{\varepsilon}_g(v_{s\mathbf{G}}))(\varepsilon_f + \tilde{p}_g(v_{s\mathbf{G}}))}, \quad (5.48)$$

which can be easily understood if one recalls that in the theory of relativistic shocks the above relation has a meaning of the shock velocity in the rest frame of the initial fluid.

Equation for the charge density becomes

$$n_{c.f}^2 = \tilde{n}_{c.g}^2(v_{s\mathbf{G}}) \frac{(p_f + \varepsilon_f)}{(p_f + \tilde{\varepsilon}_g(v_{s\mathbf{G}}))} \cdot \frac{(\tilde{p}_g(v_{s\mathbf{G}}) + \varepsilon_f)}{(\tilde{p}_g(v_{s\mathbf{G}}) + \tilde{\varepsilon}_g(v_{s\mathbf{G}}))}. \quad (5.49)$$

Evidently, it can be cast in the form of usual Taub adiabat [298]. Together with equations for the shock velocity in RFG and RFF, Eqs. (5.46) and (5.48) respectively, it forms a complete system of boundary conditions.

Let me discuss the boundary conditions and how to solve these equations together with the hydrodynamic equations for the fluid. In what follows I will assume that the solution of hydrodynamical equations (5.13) for the fluid is known in the center of mass frame (hereafter CM) for the whole available space-time volume, and hydrodynamical quantities, for instance, T_f, μ_f and $u_{fCM}^\nu = (1; \mathbf{v}_{fCM}) / \sqrt{1 - \mathbf{v}_{fCM}^2}$, are given in each space-time point X_{fCM}^ν with $\nu \in \{0; 1; 2; 3\}$. Having this solution, one can map it into the RFF by the Lorentz transformation

$$X_{\mathbf{F}}^i = \frac{1}{\sqrt{1 - \mathbf{v}_{fCM}^2}} \left(X_{CM}^i - X_{CM}^0 v_{fCM}^i \right), \quad (5.50)$$

$$X_{\mathbf{F}}^0 = \frac{1}{\sqrt{1 - \mathbf{v}_{fCM}^2}} \left(X_{CM}^0 - X_{CM}^i v_{fCM}^i \right), \quad (5.51)$$

with $i \in \{1; 2; 3\}$. Then all hydrodynamical quantities are defined in the RFF.

After this transformation into the RFF, the obtained coordinate system does not necessarily coincide with the original system which was used for the derivation of the shock-like expressions (5.46), (5.48) and (5.49) at the boundary between fluid and gas. Let assume that in the RFF the 3-vector of the shock velocity $v_{s\mathbf{F}}$ is described by the standard set of spherical coordinates with the angles ϕ and θ . Exploiting this fact, one can derive a differential equation for the FO HS in the RFF [258, 259]. Projecting the 3 vector of FO shock velocity onto the spacial coordinates (5.50) in the RFF, rewriting them in terms of the standard spherical coordinates and getting rid of spherical angles, one obtains the following partial differential equation for $X^{*1} (X^2; X^3; X^0)$ [258]:

$$\left. \frac{\partial X^{*1}}{\partial X^0} \right|_{s\mathbf{F}}^2 \left[1 + \left. \frac{\partial X^{*1}}{\partial X^3} \right|_{s\mathbf{F}}^2 \left(1 + \left. \frac{\partial X^{*1}}{\partial X^2} \right|_{s\mathbf{F}}^{-2} \right) \right] = v_{s\mathbf{F}}^2 \left. \frac{\partial X^{*1}}{\partial X^3} \right|_{s\mathbf{F}}^2, \quad (5.52)$$

which has to be solved in the RFF along with the boundary conditions (5.46), (5.48) and (5.49) and with the solution of the hydrodynamic equations for the fluid.

To show how to find the solution of this system, let me rewrite it in a more convenient form with the help of both EOS:

$$F_{nf}(T_f, \mu_f, \mu_g, v_{s\mathbf{G}}) \equiv \frac{n_{c,f}^2}{\tilde{n}_{c,g}^2(v_{s\mathbf{G}})} - \frac{(p_f + \varepsilon_f)}{(p_f + \tilde{\varepsilon}_g(v_{s\mathbf{G}}))} \cdot \frac{(\tilde{p}_g(v_{s\mathbf{G}}) + \varepsilon_f)}{(\tilde{p}_g(v_{s\mathbf{G}}) + \tilde{\varepsilon}_g(v_{s\mathbf{G}}))} = 0, \quad (5.53)$$

$$F_{v_{s\mathbf{F}}}(T_f, \mu_f, \mu_g, v_{s\mathbf{G}}, v_{s\mathbf{F}}) \equiv v_{s\mathbf{F}}^2 - \frac{(p_f - \tilde{p}_g(v_{s\mathbf{G}}))(p_f + \tilde{\varepsilon}_g(v_{s\mathbf{G}}))}{(\varepsilon_f - \tilde{\varepsilon}_g(v_{s\mathbf{G}}))(\varepsilon_f + \tilde{p}_g(v_{s\mathbf{G}}))} = 0, \quad (5.54)$$

$$F_{v_{s\mathbf{G}}}(T_f, \mu_f, \mu_g, v_{s\mathbf{G}}) \equiv v_{s\mathbf{G}}^2 - \frac{(p_f - \tilde{p}_g(v_{s\mathbf{G}}))(\varepsilon_f + \tilde{p}_g(v_{s\mathbf{G}}))}{(\varepsilon_f - \tilde{\varepsilon}_g(v_{s\mathbf{G}}))(p_f + \tilde{\varepsilon}_g(v_{s\mathbf{G}}))} = 0, \quad (5.55)$$

where only the most important arguments are shown.

The preceding analysis can be summarized in the following *Theorem 3*: If the solution of the transcendental Eqs. (5.53) – (5.55) exists, then the FO HS at the t.l. boundary between the fluid and the gas of free particles is given by the differential equation (5.52).

To prove this theorem let me, first, resolve the transcendental equation (5.55) for the solution of hydrodynamic equations given in the RFF. Suppose it exists and is denoted as

$$v_{s\mathbf{G}} = v_{s\mathbf{G}}(T_f(X^{*1}), \mu_f(X^{*1}), \mu_g) . \quad (5.56)$$

Substituting it into the equation of charge conservation (5.53), one finds the relation between the chemical potential of the gas of free particles μ_g , the chemical potential of fluid μ_f , and fluid's temperature T_f . Assume it can be expressed as follows

$$\mu_g = \mu_g(T_f(X^{*1}), \mu_f(X^{*1})) . \quad (5.57)$$

Inserting this solution into Eq. (5.56) and then substituting the both obtained equations into the expression (5.54), one defines the shock velocity $v_{s\mathbf{F}}(T_f(X^{*1}), \mu_f(X^{*1}))$ in terms of the hydrodynamical solution mapped into the RFF. The last result completes the differential equation (5.52) for the t.l. parts of the FO HS in the RFF. The s.l. ones should be obtained in accordance with the traditional Cooper-Frye prescription. On the light cones both parts should match and this is a requirement to choose the correct root of the transcendental equations for the t.l. FO HS.

In the case of zero charge the above consideration simplifies because both chemical potentials and equation of charge conservation should be left out.

Thus, the principal way how to find the t.l. FO HS is described. Now let me consider the FO problem in 1 + 1 dimensions.

5.2.2. Freeze-out in 1 + 1 Dimensional Hydrodynamics. According to *Theorems 1* and *3* one has to conjugate the *freeze-out shock* with the hydrodynamical solution for the fluid. In 1+1 dimensions the original system of equations (5.52) – (5.55) for the FO HS is greatly simplified. Setting formally $dX^{*2}, dX^{*3} \rightarrow 0$ in Eq. (5.52), one finds then in the RFF

$$\left. \frac{dX^*}{dX^0} \right|_{s\mathbf{F}} = v_{s\mathbf{F}}(T_f(X^*)), \quad (5.58)$$

or, rewriting it in the CM frame, one gets

$$\left. \frac{dX^*}{dX^0} \right|_{s_{CM}} = \frac{v_{f_{CM}} + v_{s_{\mathbf{F}}}}{1 + v_{f_{CM}} v_{s_{\mathbf{F}}}} \quad (5.59)$$

by the relativistic addition of the fluid velocity in the CM frame.

Dividing Eq. (5.55) by Eq. (5.54), one obtains the following important expression after getting rid of the squares

$$v_{s_{\mathbf{G}}}^{\pm} = \pm v_{s_{\mathbf{F}}} \frac{\varepsilon_f + \tilde{p}_g(v_{s_{\mathbf{G}}})}{p_f + \tilde{\varepsilon}_g(v_{s_{\mathbf{G}}})}. \quad (5.60)$$

Substituting Eq. (5.60) into Eq. (5.55), one obtains the second equation for velocities

$$v_{s_{\mathbf{F}}} v_{s_{\mathbf{G}}}^{\pm} = \pm \frac{p_f - \tilde{p}_g(v_{s_{\mathbf{G}}})}{\varepsilon_f - \tilde{\varepsilon}_g(v_{s_{\mathbf{G}}})}, \quad (5.61)$$

where I denote the possible sign values by the corresponding superscript.

For the sake of simplicity I will consider the fluid and gas without charge. Then Eq. (5.53) becomes an identity. In what follows I impose that the EOS of the fluid is $p_f = c_s^2 \sigma_f T_f^{\frac{1+c_s^2}{c_s^2}} = c_s^2 \varepsilon_f$, and gas of free particles has the EOS of the ideal gas of massless particles $p_g = \frac{\sigma_g}{3} T_g^4 = \varepsilon_g/3$.

Such an example is meaningful because intuitively it is clear that once the interaction is not important for the gas and its particles are nearly free, then the most natural choice for its EOS is the ideal gas one. In order to simplify presentation I consider the massless gas. However, this simple choice will demonstrate the conceptually most important physical features of the FO model.

The same might be valid for the fluid as well, but I would like to study a more general case of the fluid EOS. Then, the case when both EOS are the same is included by the proper choice of the speed of sound $c_s = \sqrt{\frac{dp}{d\varepsilon}}$ of the fluid.

The effective energy density and the pressure of the gas of free particles can be cast as:

$$\tilde{\varepsilon}_g = -\varepsilon_g(T^*) \frac{(1 - v_{s_{\mathbf{G}}})^2}{4v_{s_{\mathbf{G}}}}, \quad (5.62)$$

$$\tilde{p}_g = \varepsilon_g(T^*) \frac{(1 - v_{s_{\mathbf{G}}})^2 (2 + v_{s_{\mathbf{G}}})}{12}, \quad (5.63)$$

where I give the results for the right hemisphere. In what follows, for definiteness, I will consider only a single boundary between the fluid and the gas of free particles, assuming that at the beginning of the FO process the fluid occupies the left hemisphere, whereas the gas starts to fill the right hemisphere.

In this subsection I will use the simplest FO criterion $T_g(x, t) = T^* = \text{const}$. Of course, one could consider different freeze-out criteria. For instance, one could fix the FO criterion by the constant value of energy density in the Landau-Lifshitz frame (see Appendix B of Ref. [258]), or by the constant value of effective energy density (5.62). My choice is aimed to simplify the presentation, while keeping its essence.

Introducing the new variable

$$R \equiv \frac{[\sigma_f(T_f)]^{\frac{1+c_s^2}{c_s^2}}}{\sigma_g(T^*)^4} > 0, \quad (5.64)$$

one can rewrite

$$v_{s\mathbf{G}}^\pm = \mp 2v_{s\mathbf{F}} \frac{1+c_s^2}{v_{s\mathbf{F}}^2+c_s^2} - 3. \quad (5.65)$$

For the left hemisphere one has to change only the overall sign in the left-hand side of the above equation.

Then I will analyze the solution $v_{s\mathbf{G}}^+$ only, because other case can be obtained by the substitution $v_{s\mathbf{F}} \rightarrow -v_{s\mathbf{F}}$. From the inequality $|v_{s\mathbf{G}}^+| < 1$ the available range of the velocity $v_{s\mathbf{F}}$ follows

$$-1 < v_{s\mathbf{F}} < -c_s^2. \quad (5.66)$$

The maximal value of $v_{s\mathbf{G}}^+$ corresponds to $v_{s\mathbf{F}} = -c_s$ (see the left panel of Fig. 5.5).

Inequalities (5.66) show the limiting values of the shock velocity in the RFF which are derived by the conservation laws and relativistic causality condition. However, the entropy growth condition will give the narrower interval for the allowed values of the velocity $v_{s\mathbf{F}}$ (see below).

After some algebra from Eq. (5.66) one can get the following expression for the unknown R [258, 257, 259]:

$$R^+ = \frac{(2c_s^2 + 2v_{s\mathbf{F}}^2 + v_{s\mathbf{F}}(1+c_s^2))^2 (v_{s\mathbf{F}} - 1)}{3 (v_{s\mathbf{F}} + c_s^2) (v_{s\mathbf{F}}^2 + c_s^2)^2}. \quad (5.67)$$

Finally, the result for the unknown fluid temperature on the boundary with the gas reads as

$$T_f = \left[\frac{\sigma_g(T^*)^4 (2c_s^2 + 2v_{s\mathbf{F}}^2 + v_{s\mathbf{F}}(1+c_s^2))^2 (v_{s\mathbf{F}} - 1)}{3 \sigma_f (v_{s\mathbf{F}} + c_s^2) (v_{s\mathbf{F}}^2 + c_s^2)^2} \right]^{\frac{c_s^2}{1+c_s^2}}. \quad (5.68)$$

The formal solution of the freeze-out problem in 1+1 dimensions follows from the last equation: solving it for $v_{s\mathbf{F}}(T_f(X^*))$ and integrating Eq. (5.59) with the known hydrodynamical solution for the fluid, one finds the desired answer.

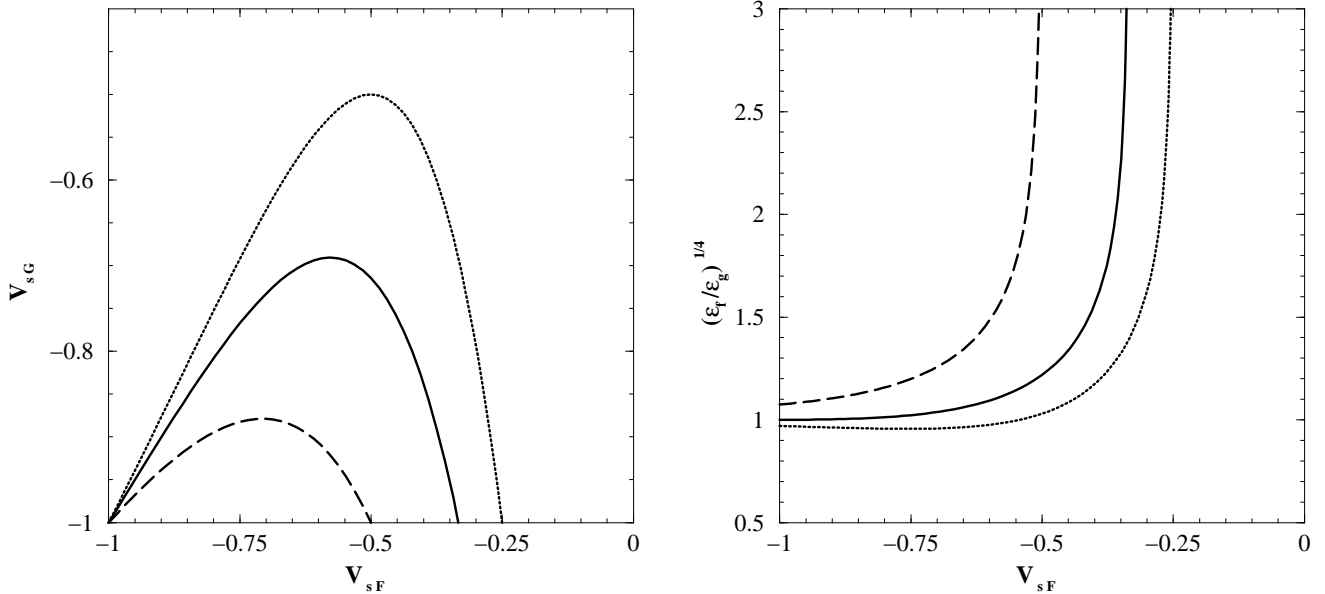


Figure 5.5. **Left panel.** Dependence of the FO shock velocity v_{sG} in the RFG upon the the shock velocity v_{sF} in the RFF for the three different EOS of fluid. The values of the fluid’s speed of sound are: $c_s = \frac{1}{\sqrt{3}}$ (solid line), $c_s = \frac{1}{\sqrt{2}}$ (dashed line) and $c_s = \frac{1}{\sqrt{4}}$ (dotted line).

Right panel. Ratio of the energy densities on the both sides of the FO shock as the function of the shock velocity v_{sF} in the RFF for the same EOS of fluid as in the left panel.

From Eq. (5.68) it is seen that FO criteria $T_g = T^* = const$ and $T_f = T^* = const$ are not equivalent in general. The only exception is when the FO HS is a straight line in (X^0, X) plane. This occurs in the FO process of the simple wave (see later). The criterion $T_f = T^*$ looks technically simpler because the time derivative of the FO HS $v_{sF}(T_F(X^*))$ is defined by the hydrodynamical solution for the fluid. Then one has to find the gas temperature. However, it might be that under a ”bad choice” of the FO criterion, the gas temperature may drop too low (in the limit $v_{sF}(T_F(X^*)) \rightarrow -c_s^2$ it follows $T_g \rightarrow 0$) for the applicability of both thermodynamics and hydrodynamics.

This fact is a reflection of the relativistic causality which tells us that the pre FO fluid cannot “know” that in the next moment is has to freeze-out into the gas of noninteracting particles. The

information about the necessity to freeze-out the particle distributions is “stored” in the local density and cross-sections of the post FO state (gas), but there is no physical agent to “inform” the pre FO fluid about this because the agent should move backwards in time.

Dependence of the fluid temperature on $v_{s\mathbf{F}}$ for $c_s^2 = \frac{1}{3}$ is presented in Fig. 5.5. From the right panel of Fig. 5.5 it is seen that the fluid temperature is always larger than the gas one. This fact is born in a more general statement, namely the energy density of the fluid $\varepsilon_f(T_f)$ always exceeds the gas one $\varepsilon_g(T^*)$ one for $c_s^2 \geq \frac{1}{3}$ [258, 259].

5.2.3. Entropy Production in the Freeze-out Shock. Next I would like to study the problem of the thermodynamical stability, or in other words the entropy production in the FO shock. This question is of a special interest for me because it clearly demonstrates that the FO shock is a new kind of the discontinuity in which entropy increases in the rarefaction transition for thermodynamically normal media [299].

The fluid entropy flux through the FO HS in an arbitrary Lorentz frame is given by

$$s_f^\mu = s_f u_f^\mu, \quad (5.69)$$

$$\mathcal{S}_f = \int_{\Sigma_{fr}} d\sigma_\mu s_f^\mu. \quad (5.70)$$

With the help of the previous section the entropy flux in RFG can be written in the general form

$$s_f^\mu n_\mu = s_f \left(\frac{(p_f - \tilde{p}_g(v_{s\mathbf{G}})) (\tilde{\varepsilon}_g(v_{s\mathbf{G}}) + \tilde{p}_g(v_{s\mathbf{G}}))}{(\varepsilon_f - \tilde{\varepsilon}_g(v_{s\mathbf{G}})) (p_f + \varepsilon_f)} \right)^{\frac{1}{2}}, \quad (5.71)$$

where the normal vector n_μ acquires the form $n_\mu = (-v_{s\mathbf{G}}; 1)$ in $1 + 1$ dimensions.

The corresponding expression for the gas of free particles has to be found from the cut-off distribution function. In the RFG it is evident that the entropy of outgoing particles is accounted by the change of the momentum integration volume $d^3p \rightarrow \Theta(p_\rho d\sigma^\rho) d^3p$ in the standard expressions for both classical and quantum statistics. For the Boltzmann distribution function ϕ [304], for example, it yields

$$s_g^\mu = \int \frac{d^3\mathbf{P}}{p^0} p^\mu \phi [1 - \ln \phi] \Theta(p_\rho d\sigma^\rho), \quad (5.72)$$

$$\mathcal{S}_g = \int_{\Sigma_{fr}} d\sigma_\mu s_g^\mu. \quad (5.73)$$

From the expressions for the entropy flux of the massless gas

$$s_g^\nu(v_{s\mathbf{G}}, T) = s_g(T^*) \left(\frac{1 - v_{s\mathbf{G}}}{2}; \frac{1 - v_{s\mathbf{G}}^2}{4} \right), \quad (5.74)$$

$$\mathcal{S}_g = \int_{\Sigma_{fr}} dX^0 n_\mu s_g^\mu, \quad (5.75)$$

where $s_g(T^*)$ is the entropy density of the gas at the freeze-out temperature, one can find the ratio of the entropy flux on the both sides of the FO shock:

$$P_s = \left(\frac{s_g^\mu n_\mu}{s_f^\mu n_\mu} \right)^4, \quad (5.76)$$

which becomes

$$P_s^+ \Big|_{c_s^2 = \frac{1}{3}} = \frac{\sigma_g (3 v_{s\mathbf{F}}^2 + 1)^2 (3 v_{s\mathbf{F}} + 1)}{16 \sigma_f v_{s\mathbf{F}}^4 (v_{s\mathbf{F}} - 1)} \quad (5.77)$$

for the solution $v_{s\mathbf{F}}^+$ with $c_s^2 = \frac{1}{3}$.

The left panel of Fig. 5.6 shows the limiting values of $v_{s\mathbf{F}}$ obtained by the thermodynamical stability criterion

$$P_s^+ \Big|_{c_s^2 = \frac{1}{3}} \geq 1 \Rightarrow -1 < v_{s\mathbf{F}} \leq -0.479 \text{ for } \sigma_g = \sigma_f. \quad (5.78)$$

The maximal value of the entropy production in the FO shock for the same EOS of the fluid is

$$\max \left(P_s^+ \Big|_{c_s^2 = \frac{1}{3}} \right)^{\frac{1}{4}} \approx 1.01088 \left(\frac{\sigma_g}{\sigma_f} \right)^{\frac{1}{4}}, \quad (5.79)$$

i.e., is about one percent for the same number of the internal degrees of freedom of fluid and gas.

Another problem of stability is the mechanical stability (see, for example, Refs. [300, 301, 302, 303] and references therein) of the *FO shock*. It is of crucial importance for the FO process because it is related to the recoil problem of the FO process on the fluid expansion. Usually one might argue that the FO of the small fluid element would affect the hydrodynamical solution in the whole future cone of this element.

However, it is known [300, 301, 302, 303] that in rest frame of the thermodynamically normal matter the perturbations of small amplitudes propagate with the speed of sound and the rarefaction shocks propagate with the subsonic velocity. Since the FO process corresponds to a decompression (the gas is more dilute than the fluid), it follows that in a normal media near the FO state the information about the emission of particles from the FO HS can be transmitted interior fluid by

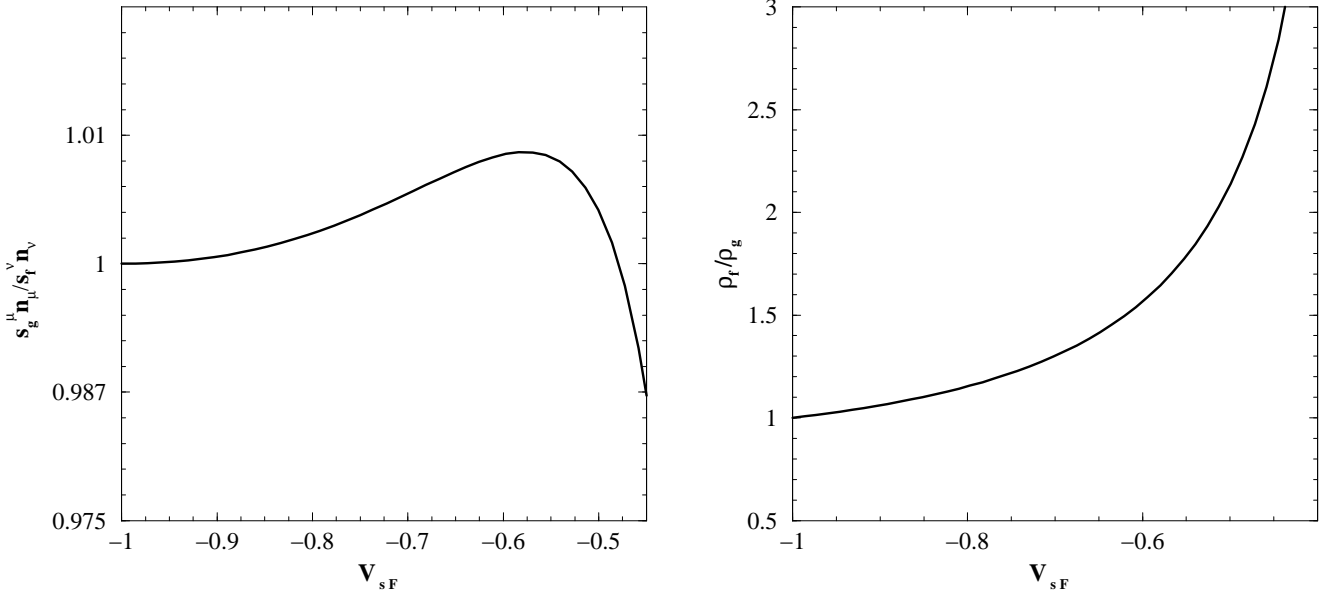


Figure 5.6. Ratio of the entropies (left panel) and particle densities (right panel) on the both sides of the FO shock as a function of the shock velocity v_{sF} in the RFF for the fluid velocity of sound $c_s = \frac{1}{\sqrt{3}}$. In the left panel the states to the right of the maximum are mechanically unstable (see text).

a simple wave or a rarefaction shock, whereas the compression shock is ruled out. Therefore, one concludes that a FO shock with the shock velocity in the following range

$$-1 < v_{sF}^+ \leq -c_s \tag{5.80}$$

is also mechanically stable with respect to the small perturbations of the fluid state [257] (c.f. the left panel of Fig. 5.6). Thus, we proved the *Statement 3*: For the EOS under consideration the perturbations of the fluid state at the t.l. FO HS are slower than the supersonic FO shock and, hence, they do not affect the hydrodynamical evolution of the fluid inside the FO HS.

Now one can see that, in contrast to the usual approach, the recoil problem is resolved for the supersonic velocities of the FO shock in the RFF. This is one of the main goals of the suggested FO scheme. However, an investigation of the mechanical stability of the FO shock in full requires a special consideration.

It is now important to verify the validity of the adopted approximations comparing of the mean free path λ in the fluid and in the gas of free particles. Since λ contains a cross-section, I would like to study the ratio of the particle density on both sides of the FO shock. Such an estimation gives the lower limit of applicability because of the inequality

$$R_\rho \Big|_{c_s^2=\frac{1}{3}} = \frac{\rho_f}{\rho_g} \leq \frac{\lambda_g}{\lambda_f}. \tag{5.81}$$

Substituting the densities found in the corresponding rest frames (for the gas of free particles there used the results obtained in the Eckart frame [304]), one gets

$$R_\rho^+ \Big|_{c_s^2=\frac{1}{3}} = \left(\frac{\sigma_f (v_{s\mathbf{F}} - 1)^3 (3v_{s\mathbf{F}}^2 + 1)^2}{16 \sigma_g (3 v_{s\mathbf{F}} + 1)^3 v_{s\mathbf{F}}^2} \right)^{\frac{1}{4}} \tag{5.82}$$

for $c_s^2 = \frac{1}{3}$. It is easy to prove that for the same EOS with the same number of degrees of freedom the particle density in the fluid is larger than in the gas of free particles, i.e., the following inequalities hold (see also the right panel of Fig. 5.6)

$$\frac{\lambda_g}{\lambda_f} \geq R_\rho^+ \Big|_{c_s^2=\frac{1}{3}} \geq 1. \tag{5.83}$$

It would be a problem of internal consistency otherwise, because the fluid with the larger mean free path should freeze-out before the gas of free particles and, hence, the whole consideration would become questionable.

Now it is clear that a very large mean free path in the gas of free particles might lead to the reduction of the collision rate and, hence, the usage of the cut-off equilibrium distribution function would not be justified. However, such a region of the velocity $v_{s\mathbf{F}} \rightarrow -c_s^2$ is not allowed by the thermodynamical stability condition (c. f. Eq. (5.78)). Thus, it is shown that the considered freeze-out scheme in 1 + 1 dimensions does not have internal contradictions.

5.2.4. Freeze-out of the Simple Wave. Let me consider the FO of the semi-infinite homogeneous normal matter without charge, occupying the left hemisphere in 1+1 dimensions. Then the hydrodynamical solution for the fluid is known – it is a simple wave [271]. This simple isentropic flow describes the propagation of the perturbations with small amplitudes in the thermodynamically normal media [299]. The characteristics of the simple wave and, therefore, its

isotherms are just straight lines in the space-time variables originating at the initial position of the boundary with the vacuum. It is important to remind also that characteristics are the t.l. HS and, therefore, are of a special interest. A short and clear description of the simple wave can be found in the Appendix A of Ref. [301].

Adopting the EOS of the previous subsections one can apply their results straightforwardly to describe the FO of the simple wave. Making the consideration in the RFF, I conclude that the shock velocity in this frame, namely $v_{s\mathbf{F}}$, has to be equal to the velocity of the simple wave there, i.e., to the velocity of sound c_s . Since both waves move to the left-hand side in RFF, one can write

$$v_{s\mathbf{F}} = -c_s . \quad (5.84)$$

Consequently, the FO of the simple wave corresponds to a particular choice of the FO shock velocity which one has to substitute in all necessary formulae of the preceding subsection.

Thus, substitution of Eq. (5.84) into Eq. (5.65) yields

$$v_{s\mathbf{G}}^{\pm} = \pm \frac{1 + c_s^2}{c_s} - 3 . \quad (5.85)$$

The latter equation leads to the restrictions on the fluid EOS. Indeed, requiring the validity of the inequality $|v_{s\mathbf{G}}^+| < 1$, one gets the lower limit of the velocity of sound in the fluid, i.e.,

$$c_s^- \equiv 2 - \sqrt{3} < c_s < 1 < c_s^+ \equiv 2 + \sqrt{3} . \quad (5.86)$$

The lower boundary of the velocity of sound corresponds to the extremely soft EOS with $c_s^- \approx 0.26795$ or with the power of the temperature in the expression for the pressure being $\frac{1+c_s^2}{c_s^2} \approx 15$.

The ratio of the energy densities becomes

$$R^+ \Big|_{S.W.} = \frac{(1 - 4c_s + c_s^2)^2 (1 + c_s)}{12 c_s^3 (1 - c_s)} , \quad (5.87)$$

and the temperature of the fluid in the simple wave reduces to the expression

$$T_f \Big|_{S.W.} = \left[\frac{\sigma_g (T^*)^4 (1 - 4c_s + c_s^2)^2 (1 + c_s)}{12 \sigma_f c_s^3 (1 - c_s)} \right]^{\frac{c_s^2}{1+c_s^2}} . \quad (5.88)$$

In order to illustrate the scale of quantities let me study the case $c_s = \frac{1}{\sqrt{3}} \approx 0.57735$. Then the shock velocity in the RFG is $v_{s\mathbf{G}}^+ = \frac{4}{\sqrt{3}} - 3 \approx -0.6906$, and the ratio R^+ is $R^+ \Big|_{S.W.} = \frac{8}{3\sqrt{3}} \approx 1.5396$.

The freeze-out temperature of the fluid in the simple wave is

$$T_f \Big|_{S.W.} = \left[\frac{8 \sigma_g}{3 \sigma_f \sqrt{3}} \right]^{\frac{1}{4}} T^* \approx 1.1139 \left[\frac{\sigma_g}{\sigma_f} \right]^{\frac{1}{4}} T^* . \quad (5.89)$$

If the fluid and the gas of free particles possess the same number of the degrees of freedom, then the fluid temperature exceeds the freeze-out one only by 11 percent. Thus, no dramatical difference for the temperatures should be expected when both EOS are same.

The entropy growth in the simple wave corresponds to the maximal possible value

$$\left(P_s^+ \right)^{\frac{1}{4}} \Big|_{S.W.} = \max \left(P_s^+ \Big|_{c_s^2 = \frac{1}{3}} \right)^{\frac{1}{4}} \approx 1.01088 \left(\frac{\sigma_g}{\sigma_f} \right)^{\frac{1}{4}} . \quad (5.90)$$

The ratio of the mean free path on the both sides of FO shock satisfies the inequality

$$\frac{\lambda_g}{\lambda_f} \Big|_{S.W.} \geq R_\rho^+ \Big|_{S.W.} \approx 1.655 \left(\frac{\sigma_f}{\sigma_g} \right)^{\frac{1}{4}} . \quad (5.91)$$

Thus, the FO scheme of the simple wave is thermodynamically stable and leads to the increase of the mean free path in the gas of free particles compared to the fluid.

The described FO scheme of the simple wave should be used in relativistic nuclear collisions with more realistic EOS. However, for illustrative purpose I will analyze the FO of the expanding pion rich matter with Landau initial conditions. Already this example will demonstrate us the reduction of the emission volume in comparison with the standard Cooper-Frye FO picture. This is so because the same FO temperature of the emitted particles in the picture with FO shock and without it corresponds to the different energy densities of the pre FO fluid in the simple wave. In the FO shock the pre FO fluid temperature is higher than the FO temperature, whereas in the traditional approach they are equal. It follows now that for the same initial condition the fluid velocity prior the FO is smaller for the larger energy density, i.e., in the picture with the FO shock.

Due to this fact one should expect some reduction of the emission volume for the same expansion time for the suggested FO of the simple wave in comparison with the traditional Cooper-Frye estimations. This is a clear indication of the "influence effect" of the particle emission on the evolution of the fluid in the simple wave.

Let me now find the spectra of massless particles (bosons to be specific) emitted by the simple wave within the cut-off FO scheme and compare it with corresponding result obtained by the

traditional Cooper-Frye one. Adopting the standard cylindric geometry (X-axis is longitudinal) in momentum space, one gets the following expression for the invariant spectra in the CM frame (after the angular integration)

$$\frac{dN^{cut-off}}{p_t dp_t dy_{CM} dS_{\perp} dt} = \frac{E_t \cosh(y_{CM}) (\tanh(y_{CM}) - v_{\sigma}) \Theta(\tanh(y_{CM}) - v_{\sigma})}{(2\pi)^2 \left(e^{\frac{E_t \cosh(y_{CM} - \eta_G) - \mu_c}{T^*}} - 1 \right)}, \quad (5.92)$$

where $E_t = \sqrt{p_t^2 + m^2}$ is the transverse energy of the particle, p_t is its transverse momentum, y_{CM} is the CM particle rapidity, η_G is the rapidity of the RFG in the CM frame, and v_{σ} is a velocity of the *FO shock* in the CM frame. For simplicity I consider only one internal degree of freedom.

For the massless particles without charge ($\mu_c = 0$) it is convenient to introduce the dimensionless variable $\tilde{p}_t = \frac{p_t}{T^*}$. Then Eq. (5.92) becomes

$$T^{*-3} \frac{dN^{cut-off}}{\tilde{p}_t d\tilde{p}_t dy_{CM} dS_{\perp} dt} = \frac{\tilde{p}_t \cosh(y_{CM}) (\tanh(y_{CM}) - v_{\sigma}) \Theta(\tanh(y_{CM}) - v_{\sigma})}{(2\pi)^2 (e^{\tilde{p}_t \cosh(y_{CM} - \eta_G)} - 1)}. \quad (5.93)$$

Let me assume that initial fluid has the temperature T_{in} . Then the velocity v_f and the temperature T_f of the fluid in the simple wave are related through the expression

$$v_f(T_f) = \tanh\left(c_s^{-1} \ln\left(\frac{T_{in}}{T_f}\right)\right). \quad (5.94)$$

The *FO shock* velocity in the CM frame is given by the formula

$$v_{\sigma} = \frac{v_f(T_f) - c_s}{1 - c_s v_f(T_f)}, \quad (5.95)$$

where the fluid temperature is taken on the FO boundary with the gas and it is defined by Eq. (5.68).

For $v_{s\mathbf{F}} = -c_s$ one finds the RFG velocity in the CM frame [258, 259]:

$$\tanh(\eta_G) = \frac{v_f(T_f) - v_{f\mathbf{G}}^+(-c_s)}{1 - v_{f\mathbf{G}}^+(-c_s)v_f(T_f)}. \quad (5.96)$$

Fig. 5.7 shows v_f and v_{σ} velocities for the fluid EOS $c_s^2 = \frac{1}{3}$ as a function of the initial temperature T_{in} . For such an EOS the FO temperature of the fluid is given by Eq. (5.89). Assuming that fluid and gas have the same number of degrees of freedom, one obtains

$$v_f \Big|_{c_s^2 = \frac{1}{3}}^{cut-off} \approx \tanh\left(\sqrt{3} \ln\left(\frac{T_{in}}{1.1139T^*}\right)\right), \quad (5.97)$$

$$v_{f\mathbf{G}}^+ \Big|_{c_s^2 = \frac{1}{3}}^{cut-off} \approx -0.18835. \quad (5.98)$$

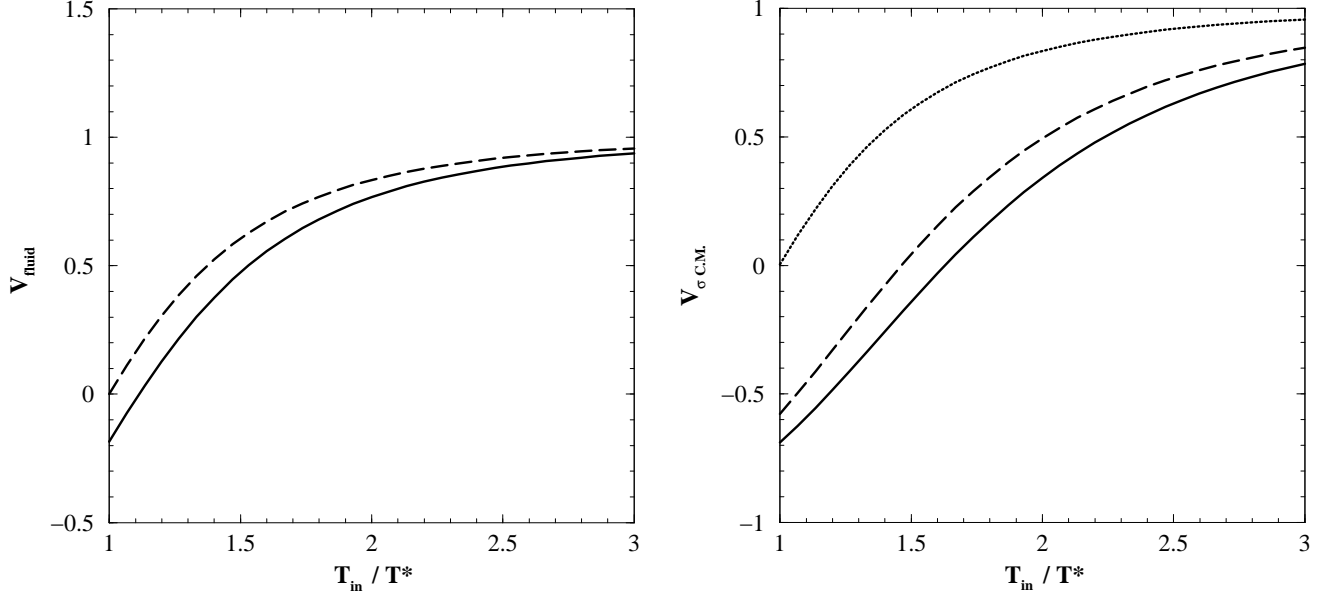


Figure 5.7. **Left panel.** Fluid velocity v_f in the simple wave at the FO HS as a function of the initial temperature of the fluid T_{in} . The dashed line corresponds to the Cooper-Frye FO scheme, and the solid one corresponds to the cut-off FO scheme.

Right panel. Velocity of the FO boundary v_σ in the CM frame as a function of the initial temperature of the fluid T_{in} . The dashed line corresponds to the Cooper-Frye FO scheme, and the solid one corresponds to the cut-off FO scheme. The dotted line represents the velocity of the RFG in the CM frame.

The traditional FO scheme based on the Cooper-Frye formula has several important differences. First of all, spectrum does not contain the cut-off Θ -function

$$T^{*-3} \frac{dN^{\text{Cooper-Frye}}}{\tilde{p}_t d\tilde{p}_t dy_{CM} dS_\perp dt} = \frac{\tilde{p}_t \cosh(y_{CM}) (\tanh(y_{CM}) - v_\sigma)}{(2\pi)^2 (e^{\tilde{p}_t \cosh(y_{CM} - \eta_G)} - 1)}. \tag{5.99}$$

Second, the FO fluid temperature coincides with the gas one, i.e., $T_f = T^*$. Thus, the FO in the traditional scheme happens at smaller energy density and at larger velocity of the fluid in comparison with the one explained above. And, third, there is no difference between the rest frame of fluid and the frame of its decay. Therefore, the fluid velocity and the relative velocity of

the emitted particles read as

$$v_f \Big|_{c_s^2=\frac{1}{3}}^{Cooper-Frye} = \tanh \left(\sqrt{3} \ln \left(\frac{T_{in}}{T^*} \right) \right) , \quad (5.100)$$

$$v_{fG}^+ \Big|_{c_s^2=\frac{1}{3}}^{Cooper-Frye} = 0 . \quad (5.101)$$

Now it is easy to see that for the same initial temperature of the fluid the hydrodynamic motion of the fluid in the Cooper-Frye FO scheme is more developed (see Fig. 5.7 for details), i.e.,

$$v_\sigma \Big|_{c_s^2=\frac{1}{3}}^{Cooper-Frye} (T_{in}) > v_\sigma \Big|_{c_s^2=\frac{1}{3}}^{cut-off} (T_{in}) , \quad (5.102)$$

whereas the CM rapidities are nearly equal

$$\eta_G \Big|_{c_s^2=\frac{1}{3}}^{Cooper-Frye} (T_{in}) \leq \eta_G \Big|_{c_s^2=\frac{1}{3}}^{cut-off} (T_{in}) . \quad (5.103)$$

The first inequality above leads to the important consequences: for the cut-off FO scheme (i) the energy emission per unit time from the FO HS is larger, and (ii) the C.M. rapidity interval with the positive values of the particle spectra is more broad. Inequality (5.103) has a negligible effect on the difference of the cut-off and the Cooper-Frye results. Therefore, one immediately gets the following inequality

$$\frac{dN^{cut-off}}{\tilde{p}_t d\tilde{p}_t dy_{CM} dS_\perp dt} \geq \frac{dN^{Cooper-Frye}}{\tilde{p}_t d\tilde{p}_t dy_{CM} dS_\perp dt} , \quad (5.104)$$

which, evidently, holds for the spectra integrated over rapidity or transversal momentum.

Due to these reasons the integrated spectra in both schemes are very different. Figs. 5.8–5.11 show some typical examples of the spectra integrated over the rapidity and the transverse momenta for both schemes. Evidently, the spectra integrated in the small rapidity window about $y_{CM} \approx 0$ are extremely different - for the high initial temperatures the Cooper-Frye formula gives negative particle numbers everywhere (see Figs. 5.8 and 5.9). This feature is hidden, if integration is carried for positive values of the rapidity (see Fig. 5.10). Nevertheless, the quantitative difference remains. The spectra integrated over the transverse momenta have, basically, similar features. However, these simple examples of the spectra show that some previous results based on the Cooper-Frye formula may be considerably revised while the correct FO scheme is used.

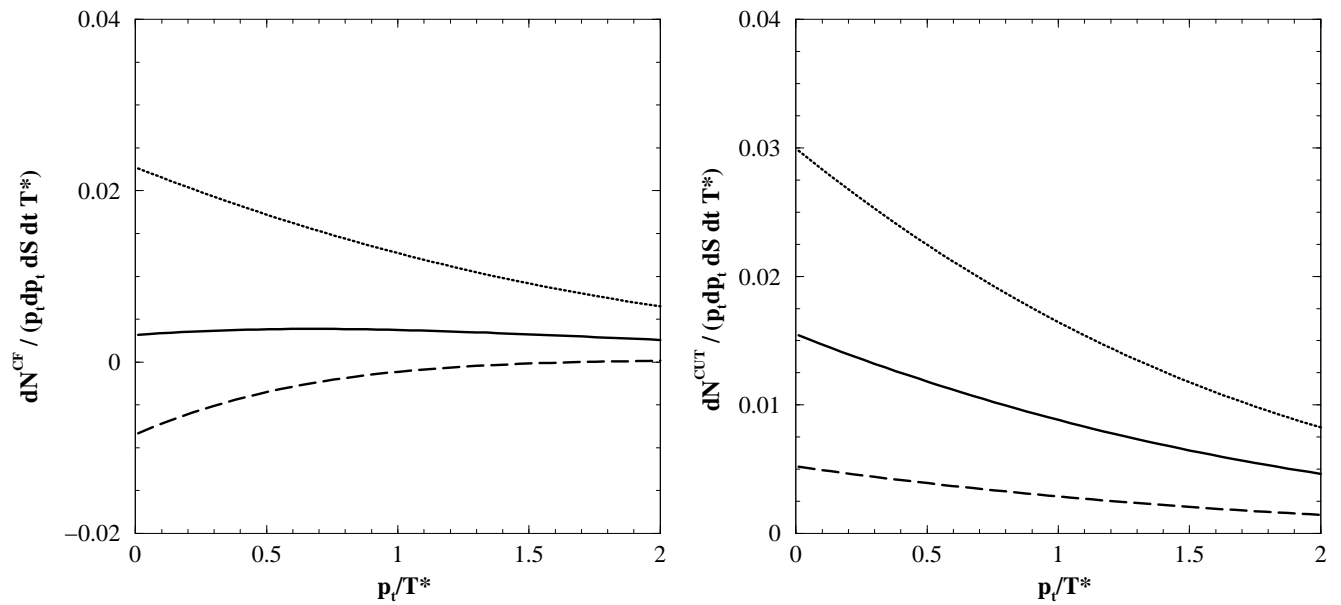


Figure 5.8. **Left panel.** Momentum distribution function of the Cooper-Frye FO scheme integrated over the CM rapidity $y_{CM} \in [-1; 1]$. The spectra are found for three values of the initial temperature of the fluid: $T_{in} = 1.1T^*$ (dotted line), $T_{in} = 1.5T^*$ (solid line), and $T_{in} = 1.9T^*$ (dashed line).

Right panel. Same as in the left panel, but for the cut-off s FO scheme.

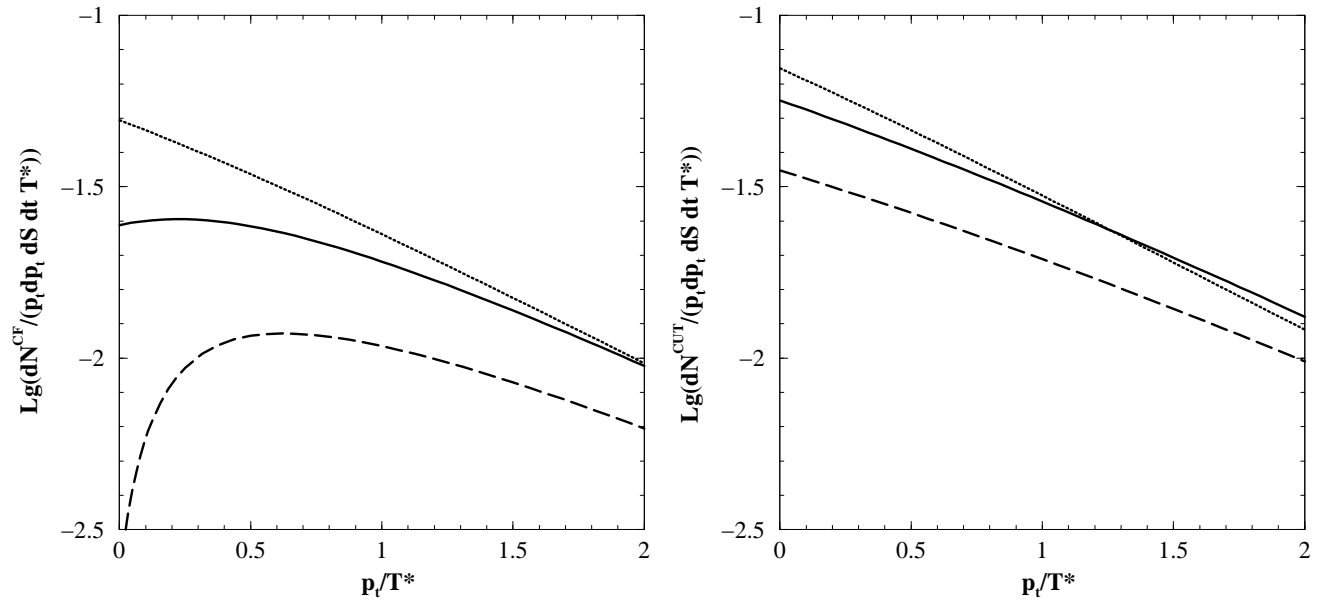


Figure 5.9. Comparison of the Cooper-Frye (left panel) and cut-off (right panel) FO schemes. The notations are the same as in Fig. 5.8, but the spectra were integrated over the CM rapidity $y_{CM} \in [-2; 2]$.

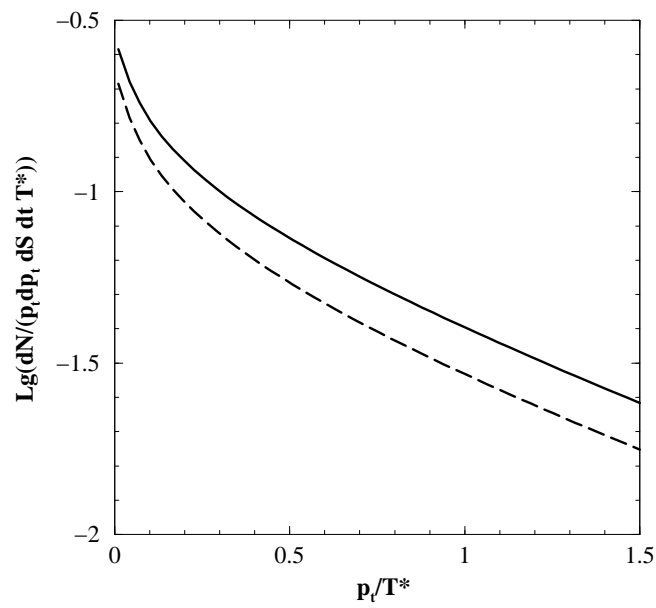


Figure 5.10. Comparison of the momentum distribution of the Cooper-Frye (dashed line) and the cut-off (solid line) FO schemes integrated over the CM rapidity $y_{CM} \in [-1; 6]$. Initial temperature of the fluid is $T_{in} = 1.5T^*$.

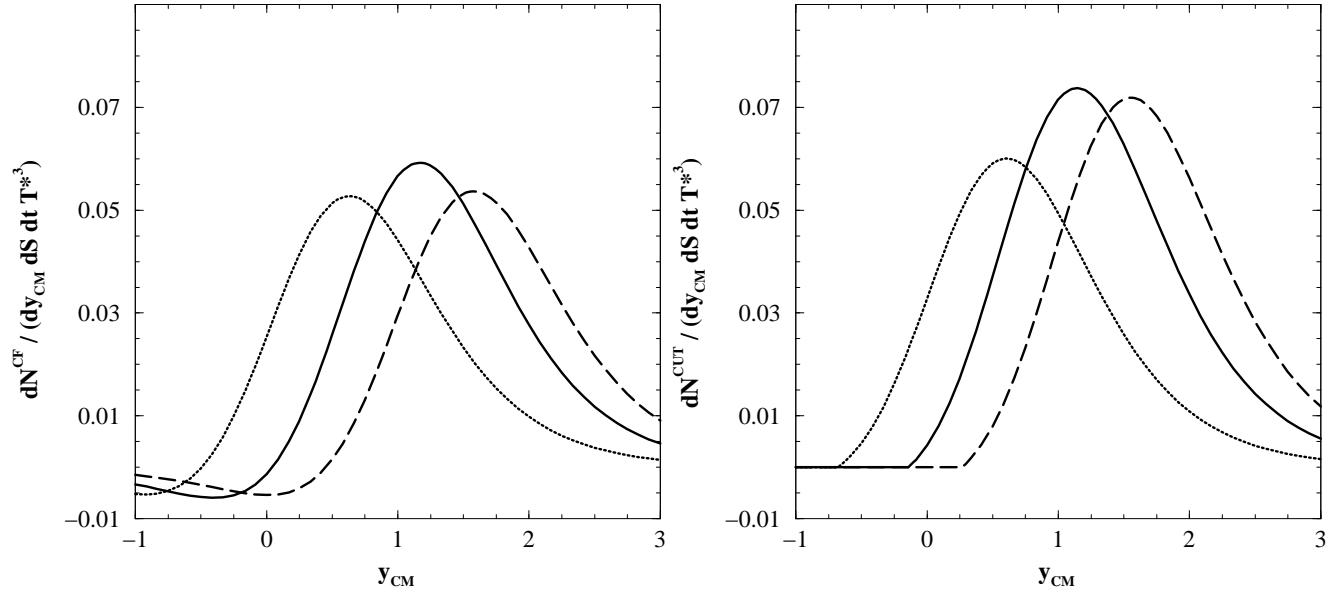


Figure 5.11. Comparison of the Cooper-Frye (left panel) and cut-off (right panel) FO schemes. The momentum distribution of both FO schemes was integrated over the CM transverse momentum $p_t \in [0.01; 6]T^*$. Initial temperatures of the fluid are: $T_{in} = 1.1T^*$ (dotted line), $T_{in} = 1.5T^*$ (solid line), and $T_{in} = 1.9T^*$ (dashed line). The left panel clearly demonstrates the presence of negative particle numbers in the Cooper-Frye FO scheme, which is not the case for the cut-off FO scheme. Also one can see, that the height of distribution function at maximum are different for these FO schemes.

As discussed above to describe the FO in finite systems requires one needs to know the hydrodynamic evolution of the system. Nevertheless, as it was argued earlier the fluid volume for the cut-off FO scheme is reduced on the magnitude of about

$$\int \left(S_{\perp}^{CF}(t_{em}) v_{\sigma}^{CF} - S_{\perp}^{CO}(t_{em}) v_{\sigma}^{CO} \right) dt_{em}$$

in comparison with the Cooper-Frye one ($S_{\perp}(t_{em})$ is the area of the FO 3-surface at the emission time t_{em}). The maximal difference of the velocities is about $v_{\sigma}^{CF} - v_{\sigma}^{CO} \approx 0.18$ and it corresponds to the initial temperature $T_{in} \approx 1.5T^*$. Taking a typical emission time of 10 fm one can roughly estimate the reduction of emission transverse radius of fireball on about 2 fm compared to the Cooper-Frye FO scheme. Such a reduction of the emitting source size is in a better agreement with the results of the HBT analysis of the relativistic nuclear collisions.

In the considered example I gave a complete solution of the FO problem for the simple wave. Due to the fact that characteristics and isotherms of the fluid in the simple wave are just straight lines in any Lorentz frame, one can show that the ratio of the partial derivatives of the temperatures on both sides of the shock is the same, i.e., $\frac{\partial_x T_f}{\partial_t T_f} = \frac{\partial_x T^*}{\partial_t T^*}$ in any frame. This is the simplest example against the statement of Ref. [280] that such a condition is unphysical. As was shown in this section, it is unnecessarily strong for the derivation of the equation for the FO HS as it was supposed in the paper [173], but it appears in particular applications like the freeze-out of the simple wave.

The momentum and rapidity spectra of the two compared schemes are different, but the negative numbers of particles in the Cooper-Frye FO scheme are usually hidden by the positive contributions which are coming from the s.l. parts of the FO HS. Therefore, one should look into some integrated characteristics of the hydrodynamic systems, like emission volume, which cannot be correctly described by the Cooper-Frye FO scheme.

5.3. Relativistic Kinetic Equations for Finite Domains

In the preceding sections I have considered the FO problem in relativistic hydrodynamics. Now I would like to analyze a new approach to resolve this problem which was invented by Bass and

Dumitru (BD model) [261] and further developed by Teaney, Lauret and Shuryak (TLS model) [262]. These hydrocascade models assume that the nucleus-nucleus collisions proceed in three stages: hydrodynamic expansion (hydro) of the quark gluon plasma (QGP), phase transition from the QGP to the hadron gas and the stage of hadronic rescattering and resonance decays (cascade). The switch from hydro to cascade modeling takes place at the boundary between the mixed and hadronic phases. The spectrum of hadrons leaving this HS of the QGP-hadron gas transition is taken as input for the cascade.

This approach incorporates the best features of both the hydrodynamical and cascade descriptions. It allows for, on one hand, the calculation of the phase transition between the quark gluon plasma and hadron gas using hydrodynamics and, on the other hand, the FO of hadron spectra using the cascade description. This approach allows one to overcome the usual difficulty of transport models in modeling phase transition phenomenon. For this reason, this approach has been rather successful in explaining a variety of collective phenomena that has been observed at the CERN SPS and Brookhaven RHIC energies. However, both the BD and TLS models face some fundamental difficulties which cannot be ignored (see a detailed discussion in [263]). Thus, within the BD approach the initial distribution for the cascade is found using the Cooper-Frye formula [275], which takes into account particles with all possible velocities, whereas in the TLS model the initial cascade distribution is given by the *cut-off* formula [173, 258], which accounts for only those particles that can leave the phase boundary. As shown in Ref. [263] the Cooper-Frye formula leads to causal and mathematical problems in the present version of the BD model because the QGP-hadron gas phase boundary inevitably has time-like parts. On the other hand, the TLS model does not conserve energy, momentum and number of charges and this, as will be demonstrated later, is due to the fact that the equations of motion used in [262] are incomplete and, hence, should be modified.

These difficulties are likely in part responsible for the fact that the existing hydrocascade models, like the more simplified ones, fail to explain the *HBT puzzle* [102], i.e. the fact that the experimental HBT radii at RHIC are very similar to those found at SPS, even though the center of mass energy is larger by an order of magnitude. Therefore, it turns out that the hydrocas-

cade approach successfully *parameterizes* the one-particle momentum spectra and their moments, but does not *describe* the space-time picture of the nuclear collision as probed by two-particle interferometry.

The main difficulty of the hydrocascade approach looks similar to the traditional problem of FO in relativistic hydrodynamics [173, 258]. In both cases the domains (subsystems) have time-like boundaries through which the exchange of particles occurs and this fact should be taken into account. In relativistic hydrodynamics this problem was solved by the constraints which appear on the FO HS and provide the global energy-momentum and charge conservation [173, 258, 259]. A generalization of the usual Boltzmann equation which accounts for the exchange of particles on the time-like boundary between domains in the relativistic kinetic theory was given recently in Ref. [263]. It was shown that the kinetic equations describing the exchange of particles on the time-like boundary between subsystems should necessarily contain the δ -like source terms. From these kinetic equations the correct system of hydrocascade equations to model the relativistic nuclear collision process was derived without specifying the properties of the separating HS. However, both an explicit switch off criterion from the hydro equation to the cascade one and the boundary conditions between them were not considered in [263]. The present section is devoted to the analysis of the boundary conditions for the system of hydrocascade equations. This is necessary to formulate the numerical algorithm for solving the hydrocascade equations.

This section is organized as follows. A brief derivation of the set of kinetic equations is given and source terms are obtained first. Then the analog of the collision integrals is discussed and a fully covariant formulation of the system of coupled kinetic equations is found. The relation between the system obtained and the relativistic Boltzmann equation is also considered. The correct equations of motion for the hydrocascade approach and their boundary conditions are analyzed next. It is also shown that the existence of strong discontinuities across the space-like boundary, the time-like shocks, is in contradiction with the basic assumptions of a transport approach. The solutions of boundary conditions between the hydro and cascade domains for a single degree of freedom and for many degrees of freedom are discussed in details.

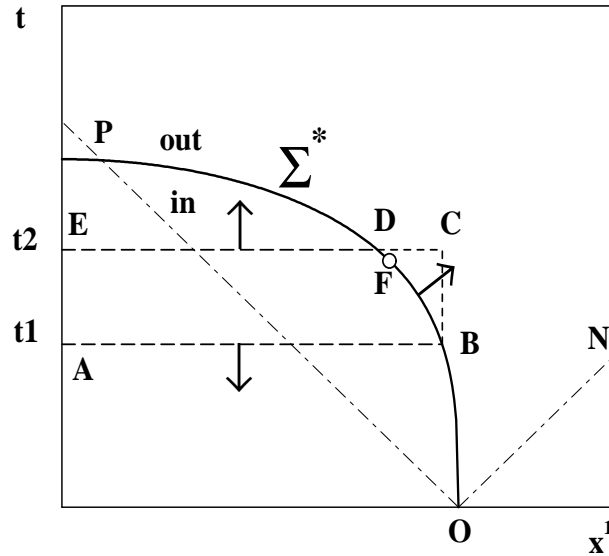


Figure 5.12. Schematic two dimensional picture of the boundary HS Σ^* (solid curve). Arrows show the external normal vectors. The light cone NOP is shown by the dash-dotted line. The point F divides Σ^* into the time-like (OF) and space-like (FP) parts.

5.3.1. Drift Term for Semi-Infinite Domain. Let me consider two semi-infinite domains, “in” and “out”, separated by the HS Σ^* which, for the purpose of presenting the idea, I assume to be given in (3+1) dimensions by a single valued function $t = t^*(\vec{x}) = x_0^*(\vec{x})$. The latter is assumed to be a unique solution of the equation $\mathcal{F}^*(t, \vec{x}) = 0$ (a *switch off criterion*) which has a positive time derivative $\partial_0 \mathcal{F}^*(t^*, \vec{x}) > 0$ on the HS Σ^* . Hereafter all quantities defined at Σ^* will be marked with an asterisk. The distribution function $\phi_{in}(x, p)$ for $t \leq t^*(\vec{x})$ is assumed to belong to the “in” domain, whereas $\phi_{out}(x, p)$ denotes the distribution function of the “out” domain for $t \geq t^*(\vec{x})$ (see Fig. 5.12). In this treatment it is assumed that the initial conditions for $\phi_{in}(x, p)$ are given, whereas on Σ^* the function $\phi_{out}(x, p)$ is allowed to differ from $\phi_{in}(x, p)$ and this will modify the kinetic equations for both functions. For simplicity I consider a classical gas of point-like Boltzmann particles.

Similar to Ref. [304] I derive the kinetic equations for $\phi_{in}(x, p)$ and $\phi_{out}(x, p)$ from the requirement of particle number conservation. Therefore, the particles leaving one domain and crossing the HS Σ^* should be subtracted from the corresponding distribution function and added to the other. Now consider the closed HS of the “in” domain, Δx^3 (shown as the contour $ABDE$ in

Fig. 5.12), which consists of two semi-planes σ_{t1} and σ_{t2} of constant time $t1$ and $t2$, respectively, that are connected from $t1$ to $t2 > t1$ by the arc BD of the boundary $\Sigma^*(t1, t2)$ in Fig. 5.12. The original number of particles on the HS σ_{t1} is given by the standard expression [304]

$$N_1 = - \int_{\sigma_{t1}} d\Sigma_\mu \frac{d^3p}{p^0} p^\mu \phi_{in}(x, p), \quad (5.105)$$

where $d\Sigma_\mu$ is the external normal vector to σ_{t1} and, hence, the product $p^\mu d\Sigma_\mu \leq 0$ is non-positive. It is clear that these particles can cross either HS σ_{t2} or $\Sigma^*(t1, t2)$. The corresponding numbers of particles are as follows

$$N_2 = \int_{\sigma_{t2}} d\Sigma_\mu \frac{d^3p}{p^0} p^\mu \phi_{in}(x, p), \quad (5.106)$$

$$N_{loss}^* = \int_{\Sigma^*(t1, t2)} d\Sigma_\mu \frac{d^3p}{p^0} p^\mu \phi_{in}(x, p) \Theta(p^\nu d\Sigma_\nu). \quad (5.107)$$

The Θ -function in the *loss* term (5.107) is very important because it accounts for the particles leaving the “in” domain (see also discussion in [173, 259]). For the space-like parts of the HS $\Sigma^*(t1, t2)$ which are defined by negative sign $ds^2 < 0$ of the squared line element, $ds^2 = dt^*(\vec{x})^2 - d\vec{x}^2$, the product $p^\nu d\Sigma_\nu > 0$ is always positive and, therefore, particles with all possible momenta can leave the “in” domain through the $\Sigma^*(t1, t2)$. For the time-like parts of $\Sigma^*(t1, t2)$ (with sign $ds^2 > 0$) the product $p^\nu d\Sigma_\nu$ can have either sign, and the Θ -function *cuts off* those particles which return to the “in” domain.

Similar one has to consider the particles coming to the “in” domain from outside. This is possible through the time-like parts of the HS $\Sigma^*(t1, t2)$, if the particle momentum satisfies the inequality $-p^\nu d\Sigma_\nu > 0$. In terms of the external normal $d\Sigma_\mu$ with respect to the “in” domain (this normal vector is shown as an arrow on the arc BD in Fig. 5.12 and will be used hereafter for all integrals over the HS $\Sigma^*(t1, t2)$) the number of gained particles

$$N_{gain}^* = - \int_{\Sigma^*(t1, t2)} d\Sigma_\mu \frac{d^3p}{p^0} p^\mu \phi_{out}(x, p) \Theta(-p^\nu d\Sigma_\nu) \quad (5.108)$$

is, evidently, non-negative. Since the total number of particles is conserved, i.e. $N_2 = N_1 - N_{loss}^* + N_{gain}^*$, one can use the Gauss theorem to rewrite the obtained integral over the closed HS Δx^3 as

an integral over the 4-volume Δx^4 (area inside the contour $ABDE$ in Fig. 5.12) surrounded by Δx^3

$$\int_{\Delta x^4} d^4x \frac{d^3p}{p^0} p^\mu \partial_\mu \phi_{in}(x, p) = \int_{\Sigma^*(t1, t2)} d\Sigma_\mu \frac{d^3p}{p^0} p^\mu [\phi_{in}(x, p) - \phi_{out}(x, p)] \Theta(-p^\nu d\Sigma_\nu). \quad (5.109)$$

Note that in contrast to the usual case [304], i.e. in the absence of a boundary Σ^* , the right-hand side (rhs) of Eq. (5.109) does not vanish identically.

The rhs of Eq. (5.109) can be transformed further to a 4-volume integral in the following sequence of steps. First one has to express the integration element $d\Sigma_\mu$ via the normal vector n_μ^* as follows ($dx^j > 0$, for $j = 1, 2, 3$)

$$d\Sigma_\mu = n_\mu^* dx^1 dx^2 dx^3; \quad n_\mu^* \equiv \delta_{\mu 0} - \frac{\partial t^*(\vec{x})}{\partial x^\mu} (1 - \delta_{\mu 0}), \quad (5.110)$$

where $\delta_{\mu\nu}$ denotes the Kronecker symbol. Then, using the identity $\int_{t1}^{t2} dt \delta(t - t3) = 1$ for the Dirac δ -function with $t1 \leq t3 \leq t2$, one can rewrite the rhs integral in (5.109) as

$$\int_{\Sigma^*(t1, t2)} d\Sigma_\mu \cdots \equiv \int_{V_\Sigma^4} d^4x \delta(t - t^*(\vec{x})) n_\mu^* \cdots, \quad (5.111)$$

where short hand notations are introduced for the corresponding 4-dimensional volume $V_\Sigma^4 = (t2 - t1) \int_{\Sigma^*(t1, t2)} dx^1 dx^2 dx^3$ which is shown as the rectangle $GBCD$ in Fig. 5.12 ($|GB| = |CD|$). Evidently, the Dirac δ -function allows one to extend integration in (5.111) to the unified 4-volume $V_U^4 = \Delta x^4 \cup V_\Sigma^4$ of Δx^4 and V_Σ^4 (the volume V_U^4 is shown as the area $ABCE$ in Fig. 5.12). Finally, with the help of notations

$$\Theta_{out} \equiv \Theta(t - t^*(\vec{x})); \quad \Theta_{in} \equiv 1 - \Theta_{out} \quad (5.112)$$

it is possible to extend the left hand side (lhs) integral in Eq. (5.109) from Δx^4 to V_U^4 . Collecting all the above results, from Eq. (5.109) one obtains

$$\int_{V_U^4} d^4x \frac{d^3p}{p^0} \Theta_{in} p^\mu \partial_\mu \phi_{in} = \int_{V_U^4} d^4x \frac{d^3p}{p^0} p^\mu n_\mu^* [\phi_{in} - \phi_{out}] \Theta(-p^\nu n_\nu^*) \delta(t - t^*(\vec{x})). \quad (5.113)$$

Since the volumes Δx^4 and V_U^4 are arbitrary, one obtains the kinetic equation for the distribution function of the “in” domain

$$\Theta_{in} p^\mu \partial_\mu \phi_{in}(x, p) = C_{in}(x, p) + p^\mu n_\mu^* [\phi_{in}(x, p) - \phi_{out}(x, p)] \Theta(-p^\nu n_\nu^*) \delta(t - t^*(\vec{x})). \quad (5.114)$$

Note that the general solution of Eq. (5.113) contains an arbitrary function $C_{in}(x, p)$ (the first term in the rhs of (5.114)) which identically vanishes while being integrated over the invariant momentum measure d^3p/p_0 . Such a property is typical for a collision integral [304], and I will discuss its derivation in the next subsection. To shorten the notation, the domain of each distribution function will be denoted as a subscripted Latin capital letter A or B ($A, B \in \{in, out\}$) to avoid confusion with Greek 4-indices.

Similar one can obtain the equation for the distribution function of the “out” domain

$$\Theta_{out} p^\mu \partial_\mu \phi_{out}(x, p) = C_{out}(x, p) + p^\mu n_\mu^* [\phi_{in}(x, p) - \phi_{out}(x, p)] \Theta(p^\nu n_\nu^*) \delta(t - t^*(\vec{x})), \quad (5.115)$$

where the normal vector n_ν^* is given by (5.110). Note the asymmetry between the rhs of Eqs. (5.114) and (5.115): for the space-like parts of HS Σ^* the source term with $\Theta(-p^\nu n_\nu^*)$ vanishes identically because $p^\nu n_\nu^* > 0$. This reflects the causal properties of the equations above: propagation of particles faster than light is forbidden, and hence no particle can (re)enter the “in” domain.

5.3.2. Collision Term for Semi-Infinite Domain. Since in the general case $\phi_{in}(x, p) \neq \phi_{out}(x, p)$ on Σ^* , the δ -like terms in the rhs of Eqs. (5.114) and (5.115) cannot vanish simultaneously on this HS. Therefore, the functions $\Theta_{in}^* \equiv \Theta_{in}|_{\Sigma^*} \neq 0$ and $\Theta_{out}^* \equiv \Theta_{out}|_{\Sigma^*} \neq 0$ do not vanish simultaneously on Σ^* as well. The $\Theta(x)$ is not uniquely defined at $x = 0$, and, therefore, there is some freedom to choose a convenient value at $x = 0$. Since there is no preference between “in” and “out” domains it is assumed that

$$\Theta_{in}^* = \Theta_{out}^* = \Theta(0) = \frac{1}{2}, \quad (5.116)$$

but the final results are independent of this choice. This result can be understood by considering the limit $a \rightarrow 0$ of the following definition: $\Theta(x) \equiv \frac{1}{2} \lim_{a \rightarrow 0} [\tanh(x/|a|) + 1]$.

Now the collision terms for Eqs. (5.114) and (5.115) can be readily obtained. Adopting the usual assumptions for the distribution functions [305, 304, 306], one can repeat the standard derivation of the collision terms [304, 306] and get the desired expressions. I will not recapitulate this standard part, but only discuss how to modify the derivation for this purpose. First of all, one has to start the derivation in the Δx^4 volume of the “in” domain and then extend it to the unified

4-volume $V_U^4 = \Delta x^4 \cup V_\Sigma^4$ similarly to the preceding section. Then the first part of the collision term for Eq. (5.114) reads ($A, B \in \{in, out\}$)

$$C_{in}^I(x, p) = \Theta_{in}^2 \left(I^G[\phi_{in}, \phi_{in}] - I^L[\phi_{in}, \phi_{in}] \right), \quad (5.117)$$

$$I^G[\phi_A, \phi_B] \equiv \frac{1}{2} \int D^9 P \phi_A(p') \phi_B(p'_1) W_{p p_1 | p' p'_1}, \quad (5.118)$$

$$I^L[\phi_A, \phi_B] \equiv \frac{1}{2} \int D^9 P \phi_A(p) \phi_B(p_1) W_{p p_1 | p' p'_1}, \quad (5.119)$$

where the invariant measure of integration is denoted by $D^9 P \equiv \frac{d^3 p_1}{p_1^0} \frac{d^3 p'}{p'^0} \frac{d^3 p'_1}{p'_1^0}$ and $W_{p p_1 | p' p'_1}$ is the transition rate in the elementary reaction with energy-momentum conservation given in the form $p^\mu + p_1^\mu = p'^\mu + p'_1^\mu$. The rhs of (5.117) contains the standard gain and loss terms which are defined by Eqs. (5.118) and (5.119), respectively, weighted by the “probability” of collision between particles from the “in” domain given by the square of the Θ_{in} -function. The value $\Theta_{in}^2 \equiv 1$ is found inside of the “in” domain, whereas $\Theta_{in}^2 = \Theta_{in}^{*2} = 1/4$ at the boundary Σ^* because according to (5.116), for each value of the distribution function ϕ_{in} in the rhs of (5.117), only half of the boundary Σ^* belongs to the “in” domain. This can be better understood by considering, first, the above mentioned tangent representation for the Θ -function, and then taking the limit $a \rightarrow 0$ next.

It is easy to understand that on Σ^* the second part of the collision term (according to Eq. (5.116)) is defined by the collisions between particles of “in” and “out” domains

$$C_{in}^{II}(x, p) = \Theta_{in} \Theta_{out} \left(I^G[\phi_{in}, \phi_{out}] - I^L[\phi_{in}, \phi_{out}] \right). \quad (5.120)$$

Again, the product $\Theta_{in} \Theta_{out} = 0$ everywhere, except at the HS Σ^* , where it corresponds to the “probability” of collision at Σ^* for the particles coming from both domains. This can be easily seen from the hyperbolic tangent representation of the Θ -function.

Combining (5.114), (5.117) and (5.120), one gets the kinetic equation for the “in” domain

$$\begin{aligned} \Theta_{in} p^\mu \partial_\mu \phi_{in}(x, p) &= C_{in}^I(x, p) + C_{in}^{II}(x, p) + p^\mu n_\mu^* \times \\ &[\phi_{in}(x, p) - \phi_{out}(x, p)] \Theta(-p^\nu n_\nu^*) \delta(t - t^*(\vec{x})). \end{aligned} \quad (5.121)$$

The kinetic equation for the “out” domain can be derived similarly and then it can be represented in the form

$$\begin{aligned} \Theta_{out} p^\mu \partial_\mu \phi_{out}(x, p) &= C_{out}^I(x, p) + C_{out}^{II}(x, p) + p^\mu n_\mu^* \times \\ &[\phi_{in}(x, p) - \phi_{out}(x, p)] \Theta(p^\nu n_\nu^*) \delta(t - t^*(\vec{x})), \end{aligned} \quad (5.122)$$

where the evident notations for the collision terms $C_{out}^I \equiv \Theta_{out}^2 \left(I^G[\phi_{out}, \phi_{out}] - I^L[\phi_{out}, \phi_{out}] \right)$ and $C_{out}^{II} \equiv \Theta_{in} \Theta_{out} \left(I^G[\phi_{out}, \phi_{in}] - I^L[\phi_{out}, \phi_{in}] \right)$ are used.

The equations (5.121) and (5.122) can be represented also in a covariant form with the help of the function $\mathcal{F}^*(t, \vec{x})$. Indeed, applying the definition of the derivative of the implicit function to $\partial_\mu t^*(\vec{x})$, one can rewrite the external normal vector (5.110) as $n_\mu^* \equiv \partial_\mu \mathcal{F}^*(t, \vec{x}) / \partial_0 \mathcal{F}^*(t, \vec{x})$. Now using the inequality $\partial_0 \mathcal{F}^*(t^*, \vec{x}) > 0$ and the following identities $\delta(\mathcal{F}^*(t, \vec{x})) = \delta(t - t^*(\vec{x})) / \partial_0 \mathcal{F}^*(t^*, \vec{x})$, $\Theta_A \equiv \Theta(S_A \mathcal{F}^*(t, \vec{x}))$ one can write Eqs. (5.121) and (5.122) in a fully covariant form

$$\begin{aligned} \Theta_A p^\mu \partial_\mu \phi_A(x, p) &= C_A^I(x, p) + C_A^{II}(x, p) + p^\mu \partial_\mu \mathcal{F}^* \times \\ &[\phi_{in}(x, p) - \phi_{out}(x, p)] \Theta(S_A p^\nu \partial_\nu \mathcal{F}^*) \delta(\mathcal{F}^*(t, \vec{x})), \end{aligned} \quad (5.123)$$

where the notations $A \in in, S_{in} = -1$ ($A \in out, S_{out} = 1$) are introduced for “in” (“out”) domain.

For the continuous distribution functions on Σ^* , i.e. $\phi_{out}|_{\Sigma^*} = \phi_{in}|_{\Sigma^*}$, the δ -like source terms on the rhs of Eqs. (5.121) and (5.122) vanish and one recovers the Boltzmann equations. Moreover, with the help of the evident relations

$$-\partial_\mu \Theta_{in} = \partial_\mu \Theta_{out} = \delta(\mathcal{F}^*(t, \vec{x})) \partial_\mu \mathcal{F}^*(t, \vec{x}), \quad (5.124)$$

$$C_{in}^I + C_{in}^{II} + C_{out}^I + C_{out}^{II} = I^G[\Phi, \Phi] - I^L[\Phi, \Phi], \quad (5.125)$$

where $\Phi(x, p) \equiv \Theta_{in} \phi_{in}(x, p) + \Theta_{out} \phi_{out}(x, p)$, one can get the following result summing up Eqs. (5.121) and (5.122)

$$p^\mu \partial_\mu \Phi(x, p) = I^G[\Phi, \Phi] - I^L[\Phi, \Phi]. \quad (5.126)$$

In other words, the usual Boltzmann equation follows from the system (5.123) automatically *without any assumption* about the behavior of ϕ_{in} and ϕ_{out} on the boundary HS Σ^* . Also Eq. (5.126) is valid not only under condition (5.116), but for *any choice* $0 < \Theta_A^* < 1$ obeying Eq. (5.112).

In fact the system (5.123) generalizes the relativistic kinetic equation to the case of the strong temporal and spatial inhomogeneity, i.e., for $\phi_{in}(x, p) \neq \phi_{out}(x, p)$ on Σ^* . Of course, one has to be extremely careful while discussing the strong temporal inhomogeneity (or discontinuity on the space-like parts of Σ^*) such as the so called *time-like shocks* [294, 307] because, as shown below, their existence contradicts the usual assumptions [305, 304, 306] adopted for distribution functions.

From the system (5.123) it is possible to derive the macroscopic equations of motion for the energy-momentum tensor by multiplying the corresponding equation with p^ν and integrating it over the invariant measure. Thus, Eq. (5.123) generates the following expression ($T_A^{\mu\nu} \equiv \int \frac{d^3p}{p^0} p^\mu p^\nu \phi_A(x, p)$)

$$\Theta_A \partial_\mu T_A^{\mu\nu} = \int \frac{d^3p}{p^0} p^\nu C_A^{II}(x, p) + \int \frac{d^3p}{p^0} p^\nu p^\mu \partial_\mu \mathcal{F}^* \times [\phi_{in}(x, p) - \phi_{out}(x, p)] \Theta(S_A p^\rho \partial_\rho \mathcal{F}^*) \delta(\mathcal{F}^*(t, \vec{x})). \quad (5.127)$$

Similar to the usual Boltzmann equation the momentum integral of the collision term C_{in}^I vanishes due to its symmetries [304], but it can be shown that the integral of the second collision term C_{in}^{II} does not vanish because it involves two different distribution functions.

The corresponding system of equations for the conserved current $N_A^\mu \equiv \int \frac{d^3p}{p^0} p^\mu \phi_A(x, p)$ can be obtained by direct integration of the system (5.123) with the invariant measure

$$\Theta_A \partial_\mu N_A^\mu = \int \frac{d^3p}{p^0} p^\mu \partial_\mu \mathcal{F}^* [\phi_{in}(t, \vec{x}) - \phi_{out}(t, \vec{x})] \times \Theta(S_A p^\rho \partial_\rho \mathcal{F}^*) \delta(\mathcal{F}^*(t, \vec{x})). \quad (5.128)$$

The above equation does not contain the contribution from antiparticles (just for simplicity), but the latter can be easily recovered. Note that in contrast to (5.127) the momentum integral of both collision terms vanish in Eq. (5.128) due to symmetries.

5.4. Derivation of Conservation Laws for Hydrokinetics

It is clear that Eqs. (5.123), (5.127) and (5.128) remain valid both for finite domains and for a multiple valued function $t = t^*(\vec{x})$ as well. To derive the whole system of these equations in the latter case, one has to divide the function $t^*(\vec{x})$ into the single valued parts, but this discussion is beyond the scope of this analysis. Using Eqs. (5.123), (5.127) and (5.128) one can analyze the boundary conditions on the HS Σ^* . The simplest way to get the boundary conditions is to integrate Eqs. (5.127) and (5.128). Indeed, integrating (5.127) over the 4-volume V_Σ^4 (shown as the area ABCD in Fig. 5.13) containing part $\tilde{\Sigma}$ of the HS Σ^* , one obtains the energy-momentum conservation. Before applying the Gauss theorem to the lhs of (5.127), I note that the corresponding

Θ_A -function reduces the 4-volume V_{Σ}^4 to its part which belongs to the A -domain. The latter is shown as area $ALMD$ ($BCML$) for $A \in in$ ($A \in out$) in Fig. 5.12. Then in the limit of a vanishing maximal distance $\Delta \rightarrow 0$ between the HSs AD and BC in Fig. 5.12, the volume integral of the lhs of Eq. (5.127) can be rewritten as the two integrals $\int d\sigma_{\mu} T_A^{\mu\nu}$: the first integral is performed over the HS $\tilde{\Sigma}$ shown as an arc LM in Fig. 5.12, and the second integral reduces to the same HS but taken in the opposite direction, i.e. the ML arc in Fig. 5.12. Thus, the volume integral of the lhs of Eq. (5.127) vanishes in this limit for tensors $T_A^{\mu\nu}$ being continuous functions of coordinates, and one obtains

$$0 = \int_{V_{\Sigma}^4} d^4x \Theta_A \partial_{\mu} (T_A^{\mu\nu}(x, p)) \equiv \int_{V_{\Sigma}^4} d^4x \frac{d^3p}{p^0} p^{\nu} C_A^{II}(x, p) + \int_{V_{\Sigma}^4} d^4x \frac{d^3p}{p^0} \delta(\mathcal{F}^*(t, \vec{x})) p^{\nu} p^{\mu} \partial_{\mu} \mathcal{F}^* [\phi_{in}(x, p) - \phi_{out}(x, p)] \Theta(S_A p^{\rho} \partial_{\rho} \mathcal{F}^*). \quad (5.129)$$

Similarly to the previous treatment, in the limit $\Delta \rightarrow 0$ the second integral on the rhs of (5.129) can be reexpressed as an integral over the closed HS. Since the latter is arbitrary, then Eq. (5.129) can be satisfied, if and only if the energy-momentum conservation occurs for every point of the HS Σ^*

$$T_{in\pm}^{\mu\nu} \partial_{\mu} \mathcal{F}^*(t^*, \vec{x}) = T_{out\pm}^{\mu\nu} \partial_{\mu} \mathcal{F}^*(t^*, \vec{x}), \text{ with } T_{A\pm}^{\mu\nu} \equiv \int \frac{d^3p}{p^0} p^{\mu} p^{\nu} \phi_A(x, p) \Theta(\pm p^{\rho} \partial_{\rho} \mathcal{F}^*). \quad (5.130)$$

In deriving (5.130) from (5.129) I used the fact that the 4-volume integral of the second collision term C_A^{II} vanishes for finite values of distribution functions because of the Kronecker symbols. The results for the conserved current follows similarly from Eq. (5.128) after integrating it over the 4-volume V_{Σ}^4 and taking the limit $\Delta \rightarrow 0$

$$N_{in\pm}^{\mu} \partial_{\mu} \mathcal{F}^*(t^*, \vec{x}) = N_{out\pm}^{\mu} \partial_{\mu} \mathcal{F}^*(t^*, \vec{x}), \text{ with } N_{A\pm}^{\mu} \equiv \int \frac{d^3p}{p^0} p^{\mu} \phi_A(x, p) \Theta(\pm p^{\rho} \partial_{\rho} \mathcal{F}^*). \quad (5.131)$$

The fundamental difference between the conservation laws (5.130), (5.131) and the ones of the usual hydrodynamics is that the systems (5.130) and (5.131) conserve the quantities of the outgoing from ($S_A = 1$) and incoming to ($S_A = -1$) “in” domain particles *separately*, whereas in the usual hydrodynamics only the sum of these contributions is conserved.

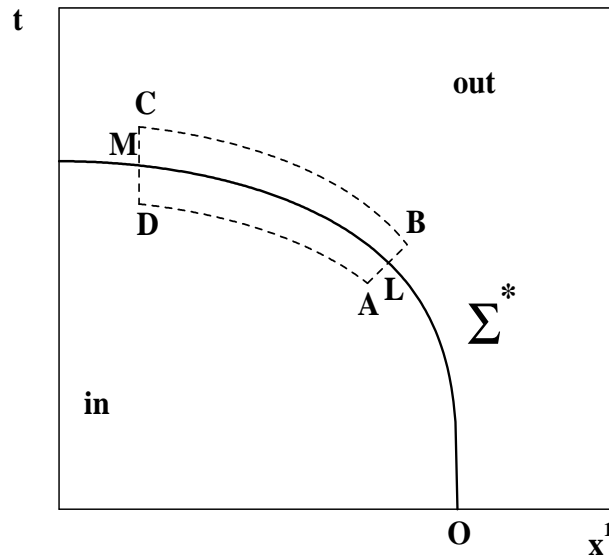


Figure 5.13. Schematic two dimensional picture of the integration contour to derive the boundary conditions (5.129) - (5.131) between the “in” and “out” domains. In the limit of a vanishing maximal distance $\Delta \rightarrow 0$ between the HSs AD and BC , both of these HSs are reduced to the part $\tilde{\Sigma}$ (an arc LM) of the boundary Σ^* between domains.

The trivial solution of Eqs. (5.130) and (5.131) corresponds to a continuous transition between “in” and “out” domains

$$\phi_{out}(x, p) \Big|_{\Sigma^*} = \phi_{in}(x, p) \Big|_{\Sigma^*} . \quad (5.132)$$

This choice corresponds to the BD model [261]. The BD model gives a correct result for an oversimplified kinetics considered here. However, in the case of the first order phase transition (or a strong cross-over) which was a prime target of the hydrocascade models [261, 262] the situation is different. In the latter case the speed of sound either vanishes (or becomes very small) [308, 309] and, hence, the rarefaction shock waves become possible [310, 311, 301]. The reason why the rarefaction shocks may exist lies in the anomalous thermodynamic properties [301] of the media near the phase transition region. In other words, on the boundary between the mixed and hadronic phases the rarefaction shocks are mechanically stable [301], whereas the compression shocks are mechanically unstable. This is also valid for the vicinity of the generalized mixed phase of a strong cross-over.

One important consequence of the shock mechanical stability criterion (see also the preceding subsections of this chapter) is that the stable shocks necessarily are supersonic in the media where they propagate. The latter means that the continuous rarefaction flow in the region of phase transition is mechanically unstable as well, since a rarefaction shock, if it appears, propagates inside the fluid faster than the sound wave and, hence, it should change the fluid's state. Due to this reason the unstable hydrodynamic solutions simply do not appear [271, 302].

Applying these arguments to the BD model, one concludes: for the first order phase transition or strong cross-over the sound wave in the (generalized) mixed phase may be unstable and the strong discontinuities of the thermodynamic quantities are possible [310, 311, 301]. The latter corresponds to the non-trivial solution of the conservation laws (5.130) and (5.131), which allows a discontinuity of the distribution function on two sides of the HS Σ^* . Since there is twice the number of conservation laws compared to the usual hydrodynamics, it is impossible, as shown below, to build up the nontrivial solution of Eqs. (5.130) and (5.131), if the distribution functions on both sides of the HS Σ^* , i.e. ϕ_{in} and ϕ_{out} , are taken to be the equilibrium ones.

Consider first the space-like parts of the HS Σ^* . Then Eqs. (5.130) and (5.131) for $S_A = -1$ vanish identically because of the inequality $p^\mu \partial_\mu \mathcal{F}^*(t^*, \vec{x}) > 0$, whereas for $S_A = 1$ Eqs. (5.130) and (5.131) recover the usual hydrodynamical conservation laws at the discontinuity. However, it can be shown that the existence of strong discontinuities across the space-like HSs, the *time-like shocks* [294, 307], is rather problematic because it leads to a contradiction of the basic assumptions adopted for the distribution function, even though the conservation laws (5.130) and (5.131) are formally fulfilled.

Indeed, according to the Bogolyubov's classification [305], a one-particle treatment can be established for a typical time Δt which, on one hand, should be much larger than the collision time τ_{Coll} , and, on the other hand, it should be much smaller than the relaxation time τ_{Relax}

$$\tau_{Coll} \ll \Delta t \ll \tau_{Relax} . \quad (5.133)$$

Similar to the usual Boltzmann equation (see also discussions in [305, 306]), in deriving the collision terms of Eq. (5.123) one implicitly adopted the requirement that the distribution function does not change substantially for times Δt less than the relaxation time τ_{Relax} . However, at the discon-

tinuities on the space-like parts of Σ^* , suggested in [294, 307], the distribution function changes suddenly, i.e. $\Delta t = 0$, and the left inequality (5.133) cannot be fulfilled at the *time-like shock*. Therefore, according to the Bogolyubov's classification [305], such a process, which is shorter than the typical collision time, belongs to a prekinetic or chaotic stage and, hence, cannot be studied at the level of a one-particle distribution function. It would instead require the analysis of a hierarchy of N -particle distribution functions, where N is the number of particles in the system. Thus, the existence of time-like shocks contradicts the adopted assumptions for a one-particle distribution. Their existence should be demonstrated first within the higher order distributions. This statement applies to several papers published by the Bergen group during the last few years where *time-like shocks* were attenuated in time using a phenomenological quasi-kinetic approach [284]. For the same reason, the use of equilibrium values for temperature and chemical potential in an attenuated time-shock is rather problematic for time scales shorter than τ_{Coll} . Note, however, that the discontinuities at the time-like parts of Σ^* (usual shocks) have no such restrictions and, hence, in what follows I will analyze only these discontinuities.

5.4.1. Boundary Conditions at Σ^* for a Single Degree of Freedom.

Now it is necessary to find out whether it is possible to obtain the nontrivial solution of systems (5.130) and (5.131) using the parts of equilibrium distributions on the time-like segments of the HS Σ^* . To simplify the presentation, first I consider the same kind of particles in both domains. It is convenient to transform the coordinate system $(t^*(\vec{x}); \vec{x})$ into the special local frame $(t_L^*(\vec{x}_L); \vec{x}_L)$ which is the rest-frame of discontinuity between the distributions ϕ_{in} and ϕ_{out} . This coordinate system will be indicated by the subscript L . The special local frame is defined as follows: the x -axis should coincide with the local external normal vector to the HS Σ^* , y - and z -axes belong to the tangent hyperplane of Σ^* . In this case the external normal vector to the time-like parts of Σ^* is $n_\mu^* = (0; \partial_1 \mathcal{F}_L^*; 0; 0)$, and one can readily check that the value of the derivative $\partial_1 \mathcal{F}_L^*$ plays an important role in the conservation laws (5.130) and (5.131) only through the *cut-off* Θ function. Then, as in the theory of usual relativistic shocks [271, 301, 302], it can be shown that equations for the y - and z -components of system (5.130) degenerate into the identities because of the symmetries of the energy-momentum tensor. Therefore, the number of independent equations

at the discontinuity is 7: a switch off criterion and six independent equations out of systems (5.130) and (5.131) (t - and x -equations (5.130) and one equation (5.131) for two choices of $S_A = \{-1; +1\}$).

On the other hand the number of unknowns is 6 only: temperature T_{in}^* and baryonic chemical potential μ_{in}^* of the “in” domain, temperature T_{out}^* and baryonic chemical potential μ_{out}^* of the “out” domain, the collective velocity v_{in}^* of the “in” domain particles, and the collective velocity v_{out}^* of the particles of “out” domain, which should be collinear to the normal vector n_μ^* in the rest-frame of the discontinuity. A formal counting of equations and unknown shows that it is impossible to satisfy the conservation laws (5.130) and (5.131) if the distribution functions on both sides are the equilibrium ones.

The last result means that instead of a traditional discontinuity one has to search for a principally new boundary condition on the HS Σ^* . The analysis shows that there are two such possibilities with the equilibrium distribution function in the “in” domain and a special superposition of two *cut-off* equilibrium distributions for the “out” domain. The first possibility is to choose ϕ_{out} as follows:

$$\phi_{out}\Big|_{\Sigma^*} = \phi_{in}(T_{in}^*, \mu_{in}^*, v_{in}^*) \Theta(p^1 \partial_1 \mathcal{F}_L^*) + \phi_{out}(T_{out}^*, \mu_{out}^*, v_{out}^*) \Theta(-p^1 \partial_1 \mathcal{F}_L^*), \quad (5.134)$$

i.e. the distribution of outgoing particles from the “in” domain (the first term in the rhs of Eq. (5.134)) is continuous on the HS Σ^* , whereas the distribution of the particles entering the “in” domain (the second term in the rhs of Eq. (5.134)) has a discontinuity on Σ^* which conserves the energy, momentum and baryonic charge because of the following boundary conditions ($\nu = \{0; 1\}$)

$$T_{in-}^{1\nu}(T_{in}^*, \mu_{in}^*, v_{in}^*) = T_{out-}^{1\nu}(T_{out}^*, \mu_{out}^*, v_{out}^*), \quad (5.135)$$

$$N_{in-}^1(T_{in}^*, \mu_{in}^*, v_{in}^*) = N_{out-}^1(T_{out}^*, \mu_{out}^*, v_{out}^*). \quad (5.136)$$

The above choice of boundary conditions at Σ^* reduces systems (5.130) and (5.131) for $S_A = 1$ to the identities, and, hence, from the systems (5.130) and (5.131) there remain only three independent equations (5.135), (5.136) for $S_A = -1$. Along with a switch off criterion, these four equations can now be solved for six independent variables with the two variables chosen to be free for a moment. Thus, both the outgoing and incoming parts of the distribution function (5.134) can be chosen as the equilibrium ones, but with different temperatures, chemical potentials and non-zero relative

velocity $v_{rel}^* \equiv (v_{out}^* - v_{in}^*) / (1 - v_{out}^* v_{in}^*)$ with respect to the distribution function ϕ_{in} .

Note a principal difference between this discontinuity and all the ones known in relativistic hydrodynamics: the “out” domain state consists, in general, of two different subsystems (fluxes) that have individual hydrodynamic parameters. It is clear that it is impossible to reduce three of those hydrodynamical parameters of one flux to those three of another flux because there are only two free variables out of six. Thus, together with the “in” domain flux there are in total three fluxes involved in this discontinuity. Therefore, it is appropriate to name it a *three flux discontinuity* in order to distinguish it from the ordinary shocks that are defined by maximum of two fluxes.

The outgoing component of the distribution (5.134) coincides with the choice of the boundary conditions suggested in the TLS model [262], whereas the equations (5.135) and (5.136) are missing in this model. For this reason, the TLS model fails to conserve energy, momentum and charge. Note also that the lower values of the temperature $T_{out}^* \leq T_{in}^*$ and baryonic chemical potential $\mu_{out}^* \leq \mu_{in}^*$, which are typical for the rarefaction process considered in [262], should be compensated by an extra flow from the incoming particles to the “in” domain, i.e. v_{rel}^* should be opposite to the external normal vector n_μ^* in the rest-frame of the *three flux discontinuity*. Therefore, such a discontinuity is analogous to the compression shock wave in relativistic hydrodynamics, and cannot appear in the rarefaction process for any of the hadronic species considered in Ref. [262].

Similarly, one can find another non-trivial solution of the systems (5.130) and (5.131) which corresponds to opposite choice to Eq. (5.134)

$$\phi_{out} \Big|_{\Sigma^*} = \phi_{in} (T_{in}^*, \mu_{in}^*, v_{in}^*) \Theta(-p^1 \partial_1 \mathcal{F}_L^*) + \phi_{out}(T_{out}^*, \mu_{out}^*, v_{out}^*) \Theta(p^1 \partial_1 \mathcal{F}_L^*), \quad (5.137)$$

i.e., the incoming to the “in” domain component of the distribution above (the first term in the rhs of Eq. (5.137)) is continuous on HS Σ^* , but the component leaving the “in” domain has a discontinuity on Σ^* which obeys the following conservation laws ($\nu = \{0; 1\}$):

$$T_{in+}^{1\nu} (T_{in}^*, \mu_{in}^*, v_{in}^*) = T_{out+}^{1\nu} (T_{out}^*, \mu_{out}^*, v_{out}^*), \quad (5.138)$$

$$N_{in+}^1 (T_{in}^*, \mu_{in}^*, v_{in}^*) = N_{out+}^1 (T_{out}^*, \mu_{out}^*, v_{out}^*). \quad (5.139)$$

It is clear that both the outgoing and incoming components of the distribution (5.137) can be chosen as the equilibrium distribution functions. A simple analysis of the system (5.138), (5.139)

shows that for $T_{out}^* \leq T_{in}^*$ and $\mu_{out}^* \leq \mu_{in}^*$ the relative velocity v_{rel} in the local frame should be collinear to the external normal vector n_μ^* . Such a discontinuity is analogous to the rarefaction shock wave in the relativistic hydrodynamics. Thus, in contrast to the TLS choice, Eq. (5.137) should be used as the initial conditions for the “out” domain while studying the rarefaction process of matter with anomalous thermodynamic properties.

Now it is appropriate to discuss how the non-trivial solutions (5.134) and (5.137) will modify the system of the hydrocascade equations (5.123), (5.127) and (5.128). In what follows I assign the hydrodynamic equations to the “in” domain and the cascade ones to the “out” domain (the opposite case can also be considered). Inserting (5.134), (5.135) and (5.136) into the “in” Eqs. (5.127), (5.128), and into the “out” Eq. (5.123), one obtains the following system:

$$\Theta_{in} \partial_\mu T_{in}^{\mu\nu} = \int \frac{d^3p}{p^0} p^\nu C_{in}^{II}(x, p), \quad (5.140)$$

$$\Theta_{in} \partial_\mu N_{in}^\mu = 0, \quad (5.141)$$

$$\Theta_{out} p^\mu \partial_\mu \phi_{out}(x, p) = C_{out}^I(x, p) + C_{out}^{II}(x, p), \quad (5.142)$$

i.e., due to the boundary conditions (5.134) – (5.136) the δ -like terms have disappeared from the original system of equations. It is clear also that the source term in the rhs of Eq. (5.140) does not play any role because it is finite on the HS Σ^* and vanishes everywhere outside Σ^* .

In order to obtain the system of hydrocascade equations (5.140) – (5.142) for the non-trivial solution defined by Eqs. (5.137) – (5.139), the hydrodynamic description has to be extended to the outer ε -vicinity ($\varepsilon \rightarrow 0$) of the HS Σ^*

$$\Theta_{out} \partial_\mu T_{out}^{\mu\nu} = \int \frac{d^3p}{p^0} p^\nu C_{out}^{II}(x, p), \quad (5.143)$$

$$\Theta_{out} \partial_\mu N_{out}^\mu = 0, \quad (5.144)$$

which in practice means that for Eqs. (5.137) – (5.139) one has to solve the cascade equation (5.142) a bit inside of the “out” domain infinitesimally close to Σ^* in order to remove the δ -like term in (5.142) and move this term to the discontinuity on the HS Σ^* .

The remarkable feature of the system of hydrocascade equations (5.140) – (5.144) is that each equation automatically vanishes outside the domain where it is specified. Also, by the construction, it is free of the principal difficulties of the BD and TLS models discussed above. The question how

to conjugate the *three flux discontinuity* with the solution of the hydro equations (5.140), (5.141), (5.143) and (5.144) will be discussed in the next section.

5.4.2. Boundary Conditions at Σ^* for Many Degrees of Freedom. In order to apply the above results to the description of the QGP-hadron gas phase transition occurring in relativistic nuclear collisions it is necessary to take into account the fact that the real situation differs from the previous consideration in two respects. The first one is that in the realistic case inside the “in” domain there should exist the QGP, whereas it should not appear in the “out” domain. Of course, the discussion of the QGP kinetic theory is a much more complicated problem and lies beyond the scope of this analysis. For my purpose it is sufficient to generalize the equations of motion (5.140) - (5.144) inside domains and the conservation laws (5.130) and (5.131) between these domains to the realistic case. Such a generalization can be made because in the case of the QGP-hadron gas phase transition there will also be an exchange of particles between the “in” and “out” domains which must be accounted for by the δ -like source terms in the transport equations. The only important difference from the formalism developed in the preceding sections is that QGP must hadronize while entering the “out” domain, whereas the hadrons should melt while entering the “in” domain. Note, however, that in relativistic hydrodynamics one has to assume that all reactions, i.e. the QGP hadronization and melting of hadrons in this case, occur instantaneously. Under this assumption one can justify the validity of the equations of motion (5.140) - (5.144) and the conservation laws between the QGP and the hadron gas at the boundary Σ^* .

The second important fact to be taken into account is that some hadrons have the large scattering cross-sections with other particles and some hadrons have the small cross-sections, because of this, different hadrons participate in the collective flow differently. A recent effort [205, 206] to classify the inverse slopes of the hadrons at SPS lab. energy 158 GeV·A led to the conclusion that the most abundant hadrons, e.g. pions, kaons, (anti)nucleons, Λ hyperons e.t.c., participate in the hadron rescattering and resonance decay till the very late time of expansion, whereas Ω hyperons, J/ψ and ψ' mesons practically do not interact with the hadronic media and, hence, the FO of their transverse momentum spectra (*kinetic FO*) may occur just at hadronization temperature

T_H . Therefore, the inverse slopes of the Ω , J/ψ and ψ' particles are a combination of the thermal motion and the transversal expansion of the media from which these particles are formed.

These results for the Ω baryons and ϕ mesons were obtained within the BD and TLS models, whereas for the J/ψ and ψ' mesons it was suggested for the first time in Refs. [205, 206]. Later these results were further refined in Ref. [207] by the simultaneous fit with only one free parameter (the maximal value of transversal velocity) of the measured Ω [312, 313], J/ψ and ψ' [314] transverse momentum spectra in Pb+Pb collisions at 158 GeV·A that are frozen-out at hadronization temperature T_H . The experimental situation with the ϕ mesons at SPS is, unfortunately, not clarified yet because the results of the NA49 [315] and NA50 [316] Collaborations disagree. The analysis of the transverse momentum spectra of Ω hyperons [208, 209, 212] and ϕ mesons [208] reported by the STAR Collaboration for energies $\sqrt{s} = 130$ A·GeV in Refs. [211] and [213], respectively, and for $\sqrt{s} = 200$ A·GeV in Ref. [212] shows that this picture remains valid for RHIC energies as well.

It is easy to find that for particles like ϕ , Ω , J/ψ and ψ' , which weakly interact with other hadrons, the distribution function ϕ_{out} should coincide with ϕ_{in}

$$\phi_{out} \Big|_{\Sigma^*} = \phi_{in} (T_{in}^*, \mu_{in}^*, v_{in}^*) \Theta(p^1 \partial_1 \mathcal{F}_L^*), \quad (5.145)$$

where, in contrast to (5.134), there is no incoming component of the distribution because the non-interacting particles cannot rescatter and change their velocity. Note also that a small modification of the incoming part of J/ψ momentum distribution due to decay of heavier charmonia in the “out” domain can be safely neglected. Remarkably, the cascade initial condition (5.145) exactly coincides with the one used in the TLS model. Therefore, the main TLS conclusions [262] on the ϕ mesons and Ω hyperons remain unchanged, whereas for hadrons with large scattering cross-sections the TLS conclusions may change significantly.

Omitting the contributions of weakly interacting hadrons from the components of the energy-momentum tensor and baryonic 4-current, one can generalize the boundary conditions (5.130) and (5.131) on the HS Σ^* between the domains and formulate the energy-momentum and charge conservation laws in terms of the parts of the *cut-off* distribution functions. For definiteness I will consider the first order phase transition between QGP and hadronic matter through out the rest of

this section. The case of the second order phase transition can be analyzed similarly. In terms of the local coordinates $(t_L^*(\vec{x}_L); \vec{x}_L)$, introduced previously, the conservation laws (5.130) and (5.131) can be generalized as follows ($\nu = \{0; 1\}$)

$$\alpha_q \sum_{Q=q, \bar{q}, \dots} T_{Q\pm}^{1\nu} (T_{in}^*, Z_Q \cdot \mu_{in}^*, v_{in}^*) + (1 - \alpha_q) \sum_{H=\pi, K, \dots} T_{H\pm}^{1\nu} (T_{in}^*, Z_H \cdot \mu_{in}^*, v_{in}^*) = \sum_{H=\pi, K, \dots} T_{H\pm}^{1\nu} (T_{out}^\pm, Z_H \cdot \mu_{out}^\pm, v_{out}^\pm), \quad (5.146)$$

$$\alpha_q \sum_{Q=q, \bar{q}, \dots} N_{Q\pm}^1 (T_{in}^*, Z_Q \cdot \mu_{in}^*, v_{in}^*) + (1 - \alpha_q) \sum_{H=\pi, K, \dots} N_{H\pm}^1 (T_{in}^*, Z_H \cdot \mu_{in}^*, v_{in}^*) = \sum_{H=\pi, K, \dots} N_{H\pm}^1 (T_{out}^\pm, Z_H \cdot \mu_{out}^\pm, v_{out}^\pm) \quad (5.147)$$

where α_q is the volume fraction of the QGP in a mixed phase, and the Q -sums of the energy-momentum tensor and baryonic 4-current components, denoted as

$$T_{Q\pm}^{\mu\nu} \equiv \int \frac{d^3p}{p^0} p^\mu p^\nu \phi_Q(x, p) \Theta(\pm p^\rho \partial_\rho \mathcal{F}^*), \quad (5.148)$$

$$N_{Q\pm}^\mu \equiv \int \frac{d^3p}{p^0} p^\mu Z_Q \phi_Q(x, p) \Theta(\pm p^\rho \partial_\rho \mathcal{F}^*), \quad (5.149)$$

run over all corresponding degrees of freedom of QGP. The H -sums also run over all hadronic degrees of freedom. In Eqs. (5.146) and (5.147) Z_Q and Z_H denote the baryonic charge of the corresponding particle species.

Now from Eqs. (5.148) and (5.149) it is clearly seen that the correct hydrocascade approach requires more detailed information about the microscopic properties of QGP than is usually provided by traditional equations of state. To proceed further I assume that those components are known. The general approach to calculate the angular and momentum integrals in Eqs. (5.148) and (5.149) was developed in Ref. [258] and was applied to the massive Boltzmann gas description in [317, 258].

The important difference between conservation laws (5.146), (5.147) and (5.130), (5.131) is that in the “out” domain the temperature T_{out}^- , chemical potential μ_{out}^- and relative velocity v_{out}^- of the incoming to Σ^* hadrons should differ from the corresponding quantities T_{out}^+ , μ_{out}^+ and v_{out}^+ of the outgoing from Σ^* particles, and both sets should differ from the quantities T_{in}^* , μ_{in}^* and v_{in}^* of the “in” domain. In order to prove this statement, it is necessary to compare the number of equations and number of unknowns for the two distinct cases. Namely, (i) if the initial state is in the mixed

QGP-hadron gas phase, and (ii) if the initial state belongs to the QGP.

In case (i) there are 10 equations and 10 unknowns:

- The equations are as follows: 6 conservation laws from Eqs. (5.146) and (5.147); value of the initial energy; value of the initial baryonic density; the relation between initial temperature T_{in}^* and the baryonic chemical potential μ_{in}^* taken at the phase boundary; and the switch off criterion.
- The unknowns are as follows: three temperatures T_{in}^* , T_{out}^- , T_{out}^+ ; three chemical potentials μ_{in}^* , μ_{out}^- , μ_{out}^+ ; three velocities v_{in}^* , v_{out}^- , v_{out}^+ defined in the rest frame of a discontinuity; and the QGP fraction volume α_q .

Thus, in this case, one can find a desired solution of the system of ten transcendental equations, which is the most general form of the three flux discontinuity introduced by Eqs. (5.134) - (5.136).

To complete the solution of hydro equations (5.140), (5.141), (5.143) and (5.144) one must find the value of velocity v_{in}^* from the system of ten transcendental equations discussed above. This velocity then defines an ordinary differential equation $dx_L^1/dt_L^* = -v_{in}^*$ for the HS Σ^* in the rest frame of matter of the “in” domain, which must be solved simultaneously with the hydro equations.

If initial state belongs to the interior of the QGP phase, case (ii), then the usual hydro solution will be valid till the system reaches the boundary with the mixed phase, from which the non-trivial discontinuity described by Eqs. (5.146) and (5.147) will begin. The differences from the previously considered case are now clear: in contrast to case (i), the volume fraction of QGP is fixed to unit $\alpha_q = 1$; the energy and baryonic charge densities are no longer independent, but are completely defined by the temperature and baryonic chemical potential, which are connected by the entropy conservation for the continuous hydro solution in QGP.

Therefore, in case (ii) there are 9 equations and 9 unknowns, which are as follows:

- The equations are: 6 conservation laws from Eqs. (5.146) and (5.147); temperature dependence of the baryonic chemical potential $\mu_{in}^* = \mu_{in}^*(T_{in}^*)$ due to the entropy conservation; the relation connecting temperature T_{in}^* and baryonic chemical potential μ_{in}^* , since they belong to the phase boundary; and the switch off criterion.
- The unknowns, except for the fixed volume fraction $\alpha_q = 1$, are the same as in case (i).

Again the number of unknowns matches the number of equations, and the procedure to solve the

system of hydro equations (5.140), (5.141), (5.143) and (5.144) simultaneously with the boundary conditions (5.146) and (5.147) is the same as in case (i).

Now it is appropriate to discuss the switch off criterion $\mathcal{F}^*(t, \vec{x}) = 0$ in more details. By the construction of the hydrocascade approach, the cascade treatment should be applied when hydrodynamics starts to lose its applicability: according to the original assumption the hydro equations (5.140), (5.141), (5.143) and (5.144) work well inside of the 4-volume surrounded by the HS Σ^* and in the outer ε -vicinity ($\varepsilon \rightarrow 0$) of Σ^* [see also a discussion after Eq. (5.142)], whereas just outside of this domain the thermal equilibrium dismantles and one cannot use the *cut-off* equilibrium distributions interior of the “out” domain. Consequently, a switch off criterion should be formulated solely for some quantity defined in the outer ε -vicinity of HS Σ^* , and it has to define the bounds of applicability of thermal equilibration and/or hydrodynamic description. Note that in the BD and TLS models this did not matter because both groups kept the cascade initial conditions as close as possible to the output of hydro. However, in the case of the *three flux discontinuity* on the time-like parts of HS Σ^* the proper use of the switch off criterion plays a decisive role in the construction of the mathematically correct hydrocascade solution (see also a discussion of the FO criterion in Refs. [173, 258]). It is clear that, in contrast to the BD and TLS formulations, the switch off criterion may generate a sizable effect while applied to interior of hadronic phase. This is so, because even a small difference (just a few MeV) between the temperature T_{in}^* , which belongs to the phase transition region, and temperatures T_{out}^- and T_{out}^+ of the “out” domain may lead to a tremendous flow of outgoing hadrons because of the enormous latent heat of the QGP.

5.5. Concluding Remarks

In this chapter the solution of the FO problem in relativistic hydrodynamics is given within a zero width approximation for the FO HS. I analyzed the difference between the Cooper-Frye procedure and its *cut-off* generalization for the t.l. FO HS. I showed that a reformulation of the traditional

hydrodynamic is necessary in order to include the particle emission from the t.l. parts of the FO HS. The modified self-consistent hydrodynamics with the specific boundary conditions is formulated and different types of shock-like FO are studied. It is shown that the momentum spectra of the particles emitted from the t.l. parts of the FO HS are described by the cut-off distribution function and particle emission looks as a discontinuity in the hydrodynamical motion (FO shock). This is the new kind of hydrodynamic discontinuities.

The correct boundary conditions enable me to derive the equations of motion of the fluid alone, which do not contain any source term. I have also proved the energy-momentum and charge conservation in the integral form for the hydrodynamics with specific boundary conditions, if the *cut-off* distribution function is used.

I analyzed the equations for the t.l. parts of the FO HS and showed how to solve them together with the equations of motion of the fluid. A complete analysis of the FO problem for the t.l. parts of the FO HS in 1+1 dimensions is presented. The entropy growth and mechanical stability conditions as well as the “recoil problem” for the shock-like FO are studied. As an application of the general scheme, the FO of the simple wave is considered, and analytical solution of this problem for the massless gas of free particles is given. The spectra of the emitted particles are calculated and compared to those obtained by the Cooper-Frye FO procedure.

Then I considered a more complicated, but mathematically similar problem: the correct boundary conditions for hydrokinetic approach. To reach this goal I have derived a system of relativistic kinetic equations which describe the particle exchange between two domains separated by the HS of arbitrary properties. I showed that the usual Boltzmann equation for the following sum of two distributions $\Phi(x, p) \equiv \Theta_{in} \phi_{in}(x, p) + \Theta_{out} \phi_{out}(x, p)$ automatically follows from the derived system, but not vice versa. Integrating the kinetic equations I derived the system of the hydrocascade equations for a single degree of freedom. Remarkably, the conservation laws on the boundary between two domains conserve the incoming and outgoing components of the energy, momentum and baryonic charge separately leading to twice the number of conservation laws on the separating HS compared to the usual relativistic hydrodynamics. Then I showed that for a single degree of freedom these boundary conditions between domains can be satisfied only by a special superposi-

tion of two *cut-off* equilibrium distributions for the “out” domain. Since the obtained discontinuity has three irreducible fluxes, it is named a *three flux discontinuity*, in contrast to usual shocks defined by two fluxes. It was also shown that the TLS-like choice of the boundary conditions, in contrast to expectation of [262], corresponds to an analog of the compression shock in traditional hydrodynamics, and, therefore, cannot be used to model the rarefaction process.

Then I showed that existence of the *time-like shocks* [294, 307], formally rederived by this formalism, contradicts the usual assumptions adopted for the one-particle distributions and, hence, the solution of this problem requires the analysis of higher order distribution functions. Therefore, in the rest of this chapter I concentrated on a detailed analysis of the discontinuities at the time-like HSs, i.e. the space-like shocks in terms of Refs. [294, 307]. These results were then generalized to a more realistic case: when the mixed QGP and hadron gas phase exists in the “in” domain and hadrons exist in the “out” domain. Such a generalization also required the exclusion of the hadrons with the small scattering cross-section (like Ω , J/ψ and ψ' particles) from the boundary conditions between domains. As was showed in the preceding subsection, the presence of the first order phase transition makes the resulting system of transcendental equations more complicated than in the case of a single degree of freedom.

It turns out that a minimal number of variables in this discontinuity is either 9 or 10, depending on the location of the initial state on the phase diagram. Therefore, on the hadronic side the *three flux discontinuity* should have two different flows with their own temperatures, chemical potentials and collective velocities. This solution has a number of unique features in comparison with usual shocks:

- This discontinuity may generate a very strong, explosive like, flow of outgoing particles from the “in” domain, first, because a huge latent heat of QGP is involved, and, second, due to an extra momentum associated with the *cut-off* distribution. Indeed, considering the outgoing component of the distribution $\phi_{out} \Theta(p^1 \partial_1 \mathcal{F}_L^*)$ for massless pions in the frame where this function maximally resembles the non-cut Boltzmann distribution, i.e. in the rest-frame of the latter, one finds a nonvanishing collective velocity $v_\pi = \frac{(1+v_\sigma)}{2}$. Here $v_\sigma \equiv \frac{dR_\perp}{dt}$ ($|v_\sigma| \leq 1$ for time-like parts of Σ^*) denotes the transversal radius velocity in this frame.

- The strong explosive flow of outgoing particles is localized at the time-like parts of the HS Σ^* , whereas at the space-like parts of Σ^* there will be a continuous flow. It is even possible that for some choice of parameters the space-like boundary may be absent.
- The particle density of outgoing pions will strongly depend on the speed of the transversal radius expansion. Thus, for massless pions the particle density found according to the Eckart definition [304] is $\rho_\pi = \frac{\rho_\pi(T_{out}^+)}{4} \sqrt{(1 - v_\sigma)^3 (3 + v_\sigma)}$, i.e. it is smaller for all $v_\sigma > -1$ than the thermal particle density $\rho_\pi(T_{out}^+)$. Therefore, the two particle correlations off the low particle density regions should be reduced. Since the situation $v_\sigma \gg -1$ is typical for the beginning of the transversal expansion [262], the main contribution to the transversal pion correlations will come from the later times of expansion. Thus, it is possible that the space-time region which defines the side and out pion correlation radii will be essentially more localized both in space and time than in traditional hydrodynamic solutions.
- Because there are two fluxes in the “out” domain, they will interact with each other. The resulting distribution should be, of course, found by the cascade simulations, but it is clear that the fastest of them will decelerate and the cold one will reheat. Besides the possibility to accelerate or decelerate the outgoing transversal flow more rapidly than in the BD and TLS models, the *three flux discontinuity* may naturally generate some *turbulence* patterns in the “out” domain.

Taking into account all these features alone with the fact that neither the BD nor TLS boundary conditions have such a strong discontinuity, I conclude that the *three flux discontinuity* opens a principally new possibility not only to resolve the HBT puzzle [102], but also to study some new phenomena, like a turbulence pattern, associated with a new kind of shock, a *three flux discontinuity*, in relativistic hydrocascade approach.

Despite the reasonably good description of the one-particle spectra of the most abundant hadrons, even such sophisticated model as the TLS one badly overestimates both of the transverse radii measured by pion interferometry like other hydrodynamic models. This is a strong indication that the hydro part of all existing hydrocascade and hydrodynamic models requires an

essential revision. How this revision will affect the present BD and TLS results is unclear at the moment, but the solution of the HBT puzzle [102] should serve as a good test for the correct picture of the space-time evolution during the post-hadronization stage. The additional tests for the correct hydrocascade equations should be the reproduction of three recently established signals of the deconfinement phase transition, i.e. the pion Kink [267, 266] seen at lab. energy of ~ 30 GeV·A, the K^+/π^+ peak at the same lab. energy [267] (the Strangeness Horn) and the plateau [265] in the inverse slope of the K^\pm transverse momentum spectra at the whole range of the SPS energies (the Step in caloric curves) measured by the NA49 Collaboration [318, 319]. It is also necessary to check other predictions of the Statistical Model of the Early Stage [267], namely the anomalies in the entropy to energy fluctuations [320] (the “Shark Fin”) and in strangeness to energy fluctuations [321] (the “Tooth”), because both the “Shark Fin” and “Tooth” may be sensitive to the turbulence behavior due to energy dissipation.

Note, however, that the completion of this task requires an additional research of the hydro-cascade approach. First, it is necessary to develop further the microscopic models of the QGP equation of state in order to find out the required by Eqs. (5.146) - (5.149) components of the *cut-off* energy-momentum tensor and baryonic 4-current. This can be done, for example, within the phenomenological extensions [134, 322, 200] of the Hagedorn model. Second, a similar problem for hadrons should be solved as well, otherwise, as I discussed above, the *switch off* criterion from the hydro to cascade cannot be formulated correctly within the hydrocascade approach. And, finally, for practical modeling it is necessary to formulate a mathematical algorithm to solve simultaneously the system of hydrocascade equations (5.140) - (5.144) with the boundary conditions (5.146) and (5.147) between the hydro and cascade domains. These problems, however, are out of the scope of the present dissertation.

CHAPTER 6

EXPERIMENTAL SIGNALS OF THE DECONFINEMENT TRANSITION

The concepts of chemical (hadron multiplicities) and kinetic (hadron momentum spectra) FOs were introduced to interpret data on hadron production in relativistic A+A collisions. The equilibrium hadron gas model describes remarkably well the light hadron multiplicities measured in A+A collisions at the SPS [136, 137, 220] and RHIC [198, 199] energies, where the creation of the QGP is expected. Recently it was found [323] also that charmonium yield systematics in nuclear collisions at the SPS [236] follow the pattern predicted by the hadron gas model. The hadronization temperature parameter extracted from the fits to the hadron multiplicities is similar for both energies: $T_H = 170 \pm 10$ MeV. It is close to an estimate of the temperature T_C for the QGP to hadron gas transition at zero baryonic density.

Experimental results on inclusive hadron spectra and correlations evidence for a hydrodynamic expansion of the matter created in heavy ion collisions. Strong transverse flow effects in Pb+Pb collisions at the SPS (average collective transverse velocity is approximately $0.5 \div 0.6$) are firmly established from the combined analysis [337, 325, 338] of the pion transverse mass spectra and correlations. The kinetic ('thermal') FO of pions and nucleons seems to occur at a rather late stage of an A+A reaction. The thermal FO temperature parameter of pions measured by the NA49 Collaboration [336] for central Pb+Pb collisions at the SPS is $T_f \cong 120$ MeV.

Further exploration of idea of the statistical J/ψ production [323] led me and my collaborators to the formulation of the hypothesis that the kinetic FO of J/ψ and ψ' mesons takes place directly at hadronization [205, 206]. This means that chemical and thermal FOs occur simultaneously for those mesons and they, therefore, carry information on the flow velocity of strongly interacting matter just after the transition to the hadron gas phase. A possible influence of the

effect of rescattering in the hadronic phase on the transverse momentum (p_T) spectra was recently studied within a hydrocascade approach [261, 262]. As I discussed in the preceding chapter, the hydrocascade approach splits the A+A collisions into three stages: hydrodynamic QGP expansion (“hydro”), transition from QGP to hadron gas (“switching”) and the stage of hadronic rescattering and resonance decays (“cascade”). The switching from hydro to cascade takes place at $T = T_C$, where the spectrum of hadrons leaving the surface of the QGP to hadron gas transition is taken as an input for the subsequent cascade calculations. The results [261, 262] suggest that the p_T spectrum of Ω s is only weakly affected during the cascade stage. The corresponding calculation for charmonia are not yet performed within this model, but a similar result may be expected due to their very high masses and low interaction cross sections.

In my next work [207] devoted to the analysis of the SPS data it was demonstrated that the measured transverse mass ($m_T = \sqrt{p_T^2 + m^2}$) spectra of Ω^\pm hyperons [312] and J/ψ and ψ' mesons [314] produced in Pb+Pb at 158 A·GeV collisions can be reproduced within a hydrodynamical approach using the same FO parameters: hadronization temperature $T \cong 170$ MeV and the mean transverse flow velocity $\bar{v}_T \cong 0.2$. Within such an approach the value of the \bar{v}_T parameter extracted in this way should be interpreted as the mean flow velocity of the hadronizing QGP.

The next step was, of course, to verify such a hypothesis using the available RHIC data. Employing the estimates of the hydrocascade model [262] for the transverse velocity it was possible to predict [208] the inverse slopes of the early hadronizing particles which, within the error bars, agreed with the results for the Ω^\pm hyperons reported by the STAR Collaboration at the conference “Quark Matter 2002” [210] for the center of mass energy $\sqrt{s_{NN}} = 130$ GeV. Since up to now the charmonia data are not available at RHIC energies, to test the hypothesis of early hadronization it was possible to use the measured transverse spectra of multistrange hadrons - ϕ -meson and Ω -hyperons. Their fitting at fixed value of hadronization temperature $T = 170 \pm 5$ MeV, i.e. with a single parameter, allowed me to determine the mean transverse collective velocity and predict the inverse slopes for the charmonia and charmed meson transverse spectra [209]. Moreover, it was possible to find out the mean emission volume at the QGP hadronization (see below) which agrees well with the hydrocascade calculations estimate [262].

The analysis of the multistrange hadrons data once more indicated me a very special role playing by the strange quark. The first solid evidence for such a role was demonstrated by the Strangeness Horn [267], i.e. by the peak of the ratio of positive kaons to positive pions yields as the function of colliding energy. On the other hand, the existing hydrocascade simulations [262] demonstrated that in the deconfinement region the inverse slopes of kaon transverse momentum spectra are not affected by hadronic reactions after the QGP hadronization. The reason for such a behavior was not clear and it initiated my interest in analyzing the experimental data.

A qualitative analysis showed me that the kaons emitted from the deconfinement region are affected by the rescattering and by the resonance decays. However, it turned out that both of these effects do modify the kaon distribution at soft momenta, but in opposite directions and, hence, they almost compensate each other. This is the qualitative explanation of the of the hydrocascade results on the kaon inverse slopes [262]. Then the existing data indicated a nonmonotonic behavior of the kaon inverse slopes as the function of the colliding energy [265]. The analysis of these data led me and my collaborators to the formulation of a new signal of the deconfinement, known as the Step [265].

This chapter is based on the following works [205, 206, 207, 208, 209, 265].

6.1. Statistical Production of Particles.

J/ψ suppression in nuclear collisions was suggested by T. Matsui and H. Satz to be a signal of the deconfinement PT. Nowadays there are several models which mainly differ from the original idea of the J/ψ suppression in the mechanism of charmonia dissociation either in quark gluon or in nuclear media. Such an approach I discussed in the subsection on the Mott-Hagedorn resonance gas of the present dissertation. Recently a principally different picture of the statistical charm production was suggested [323]. The next breakthrough in this field, the statistical coalescence model, suggests [324] that charmonium is generated by the coalescence of earlier produced c and \bar{c} quarks. However, important questions, what happens after hadronization and what are the transversal mass spectra of J/ψ and ψ' mesons, were not considered in [324]. Therefore, I will mainly concentrate on the problem of the J/ψ and ψ' FO and will analyze their apparent

temperature. Then I will answer the question, “What can we learn from experimental data about hadronization of QGP?”

The idealized concept of chemical and thermal FOs enables one to interpret data on hadron production in relativistic A+A collisions. The first experimental results on yields and transverse mass spectra suggested the following scenario: for the most abundant hadron species (π, N, K, Λ) the chemical FO which seems to coincide with the hadronization of the QGP, is followed by the thermal or kinetic FO occurring at a rather late stage of the A+A reaction. Thus, for the central Pb+Pb collisions at 158 A·GeV the temperature of the chemical FO was extracted from the fit of the multiplicity data to be $T_H = 175 \pm 10$ MeV [136, 137]. The thermal FO parameters, i.e., temperature T_F and averaged transversal velocity $\langle v_T \rangle$, for pions were determined from the results of two pion correlations [325] to be quite different

$$T_F = 120 \pm 12 \text{ MeV}, \quad \langle v_T \rangle = 0.5 \pm 0.12 . \quad (6.1)$$

On the other hand from hadronic cascade simulations it is known that thermal FO of multi-strange hadrons (ϕ, Ξ, Ω) happens, probably, earlier than the kinetic FO of pions. Now the main question is, “When does the J/ψ FO occur? Late or early?”

The convolution of the transverse flow velocity of the matter element with the thermal motion of hadrons in the rest frame of this element leads to a nearly exponential shape of final m_T spectrum $\frac{1}{m_T} \cdot \frac{dN}{d m_T} \approx C \cdot e^{-m_T/T^*}$ with the apparent temperature (AT) T^* which is defined from the p_T^2 distribution at fixed longitudinal rapidity y_p of the particle as

$$T^* = - \left[2m_T \frac{d}{dp_T^2} \ln \left(\frac{dN}{dy_p dp_T^2} \right) \right]^{-1} . \quad (6.2)$$

In the limit $m_T \gg T$ and $p_T \rightarrow 0$ the AT depends on the particle mass and $\langle v_T \rangle$ as follows

$$T^* = T_F + \alpha \cdot m \cdot \langle v_T \rangle^2 . \quad (6.3)$$

For the spherical fireball Eq. (6.3) was first found in Ref. [326]. For the cylindrical geometry, surprisingly, there are two answers which differ by the value of the coefficient α : there is a *naive result* $\alpha = \frac{1}{2}$ [327] and the *more elaborate one* $\alpha = \frac{2}{\pi}$ [328]. Therefore, before going further it is necessary to discuss the origin of the difference between the results of Refs. [327] and [328].

6.1.1. Particle Spectra and Apparent Temperature.

The general expression for the momentum distribution of the outgoing particle having the 4-vector of momentum $p^\mu = (m_T \cosh y_p, p_T \cos(\phi_p), p_T \sin(\phi_p), m_T \sinh y_p)$ which is emitted from the arbitrary FO HS Σ by the fluid element having the hydrodynamical 4-velocity parameterized as $u^\mu = \gamma_T(\cosh y_L, v_T \cos(\phi_u), v_T \sin(\phi_u), \sinh y_L)$ is given by the *cut-off distribution function* [173, 258] (see also the preceding chapter)

$$E \frac{d^3 N}{dp^3} = \int_{\Sigma} p^\mu d\Sigma_\mu \varphi \left(\frac{p^\nu u_\nu}{T} \right) \Theta(p^\rho d\Sigma_\rho), \quad (6.4)$$

where the standard notations are assumed for 4-vectors (y_p , y_T and y_L are particle longitudinal, fluid transversal and fluid longitudinal rapidities, respectively, and ϕ denotes the corresponding polar angles), $\gamma_T = 1/\sqrt{1-v_T^2}$ is the relativistic γ -factor, $d\Sigma_\mu$ denotes the 4-vector of external normal to the FO HS Σ and φ is the one-particle phase space distribution function. The Θ -function in (6.4) is of crucial importance because it makes sure that only outgoing particles are counted from both the t.l. and s.l. FO HS.

For further analysis I will neglect the contributions coming from the t.l. parts of the FO HS and then comment on general case. Now the product $p^\rho d\Sigma_\rho > 0$ is positive for any momentum and the *cut-off distribution* (6.4) automatically reproduces the famous Cooper-Frye result [275]. For the Boltzmann distribution $\varphi = \frac{g}{(2\pi)^3} e^{-\frac{p^\nu u_\nu}{T}}$ of particles emitted from the FO HS $R^* = R^*(t, z)$ one obtains from (6.4)

$$\frac{d^2 N}{dy_p dp_T^2} = \frac{g}{(2\pi)^2} \int_{\Sigma} dz dt R^* e^{-\frac{m_T \gamma_T \cosh(y_p - y_L)}{T}} m_T \cosh y_p I_\phi \left(\frac{p_T v_T \gamma_T}{T} \right), \quad (6.5)$$

$$I_\phi \left(\frac{p_T v_T \gamma_T}{T} \right) = \int_0^{2\pi} d\phi_p \left(\frac{\partial R^*}{\partial t} - \tanh y_p \frac{\partial R^*}{\partial z} - \frac{p_T \cos(\phi_p)}{m_T \cosh y_p} \right) e^{\frac{p_T v_T \gamma_T \cos(\phi_p)}{T}}. \quad (6.6)$$

Now it is clearly seen that the main contribution to the integral (6.6) corresponds to the small angles ϕ_p between a 3-momentum of particle and a 3-vector of the hydrodynamic velocity, whereas contributions coming from the large angles ϕ_p are suppressed exponentially.

Neglecting the term with $\frac{p_T}{m_T}$ in Eq. (6.6) for $p_T \ll m_T$ and expanding the Bessel function $I_0(x) \approx 1 + (0.5x)^2$ for $p_T v_T \gamma_T \ll T$, one finds from (6.2) the following result for the AT

$$\frac{1}{T^*} \approx \left\langle \left\langle \frac{\gamma_T \cosh(y_p - y_L) - \frac{m_T v_T^2 \gamma_T^2}{2T}}{T} \right\rangle \right\rangle \approx \left\langle \frac{\gamma_T - \frac{m_T v_T^2 \gamma_T^2}{2T}}{T} \right\rangle \quad (6.7)$$

where the double averaging means a double integration over time and longitudinal coordinate with the weight function defined by Eq. (6.5). For the longitudinal expansion depending on the rapidity y_L only (e.g. Bjorken expansion) the integration over z -coordinate can be done because for heavy particles the Boltzmann exponential behaves like a Kronecker δ -function, i.e., $e^{-m_T \gamma_T \cosh(y_p - y_L)/T} \cong \delta(y_p - y_L)$. This leads to a single averaging over the evolution time (last equality in Eq. (6.7)) with a slightly modified weight function. The next approximation in (6.7) implies the nonrelativistic transversal expansion and $m_T \rightarrow m$

$$T^* \approx T + \frac{m \langle v_T^2 \rangle}{2} \approx T + \frac{m \langle v_T \rangle^2}{2}, \quad \text{for } m v_T^2 \gamma_T \ll T, \quad (6.8)$$

where the last equality is fulfilled within 10-15 % for the linear dependence of the velocity on the transversal radius. Note, however, that a popular expression (6.8) was obtained under the condition which is hardly fulfilled in practice for heavy particles and, hence, Eq. (6.8) cannot be established from Eq. (6.7). Moreover, for particles of $m_T \geq 1$ GeV, freezing out under conditions (6.1), Eq. (6.7) leads to negative contributions to the AT and even to negative values of the AT! The latter follows from the fact that contributions coming from the small transversal radii (and, hence, small v_T) in (6.5) are suppressed.

Thus, an accurate examination of the derivation of Ref. [327] shows that **negative AT** can be seen, if the FO HS is a s.l. one. In the preceding chapter I discussed some explicit examples that **negative AT** exist, if the Cooper-Frye formula is applied to the t.l. HS, whereas the cut-off formula (6.4) generates positive AT in that case. Discussion of the AT for the arbitrary HS is out of the scope of this chapter. I mention only that negative AT which are not seen experimentally may be an artifact of the Cooper-Frye formula.

In contrast to the rightmost equality in (6.8), a more sophisticated derivation of Ref. [328] accounts for the finiteness of the system and is partly free of the problems discussed above. In [328] the Cooper-Frye formula is modified by an additional factor $\exp\{-a(\cosh y_T - 1)\}$ (with $a = 1/(\langle R^* \rangle v_T'(0))^2$) which in case of nonrelativistic transversal expansion reduces to $\exp\{-\frac{R^{*2}}{2\langle R^* \rangle^2}\}$. Here $\langle R^* \rangle$ is the mean transverse radius and $v_T'(0)$ is the transverse velocity derivative at the center of the fireball. The large radii contributions in (6.7) are suppressed due to such a factor and, hence, they do not lead to negative AT values. Further evaluation ends in (6.3) with $\alpha = \frac{2}{\pi}$ which appears

from the additional factor and reflects the cylindrical symmetry. Therefore, the latter is used in the next subsection, whereas a more elaborate estimate I will consider afterwards.

6.1.2. Freeze-out of J/ψ Meson. Recently it was found that the data on J/ψ and ψ' yields in central Pb+Pb collisions at 158 A·GeV are consistent with the results of the statistical model for the typical value of $T_H \cong 175$ MeV extracted from light hadron systematics (see Refs. in [323, 208]). The hypothesis of statistical J/ψ production at hadronization can be further tested using data on m_T spectra. New NA50 data [314] on transverse mass spectra of J/ψ mesons in central Pb+Pb collisions at 158 A·GeV confirm this expectation: the spectrum is nearly exponential with $T^*(J/\psi) = 245 \pm 5$ MeV. The measured $T^*(J/\psi)$ value is significantly smaller than expected one from Eq. (6.3) for the pion FO parameters (6.1) ($T^* \cong 610$ MeV).

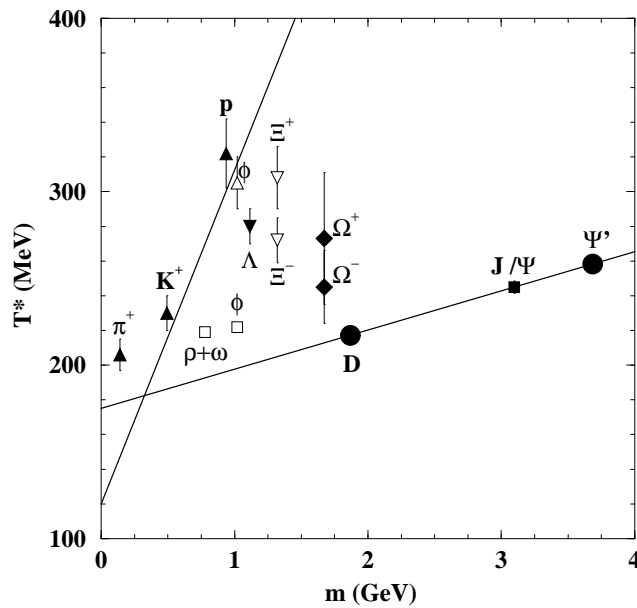


Figure 6.1. The inverse slope parameter as a function of the particle mass for central Pb+Pb collisions at 158 A·GeV. The results are compiled from: [330] (filled \triangle), [316] (open \square), [315] (open \triangle), [331] (filled ∇), [332] (open ∇), [333] (filled \diamond), [314] (filled \square). The filled circles are predictions of the model for ψ' and D mesons. The upper solid line is given by Eq. (6.3) with $\alpha = \frac{2}{\pi}$ for the FO parameters (6.1). The lower solid line is given by Eq. (6.9) with $T_H = 175$ MeV and $\langle v_T^H \rangle = 0.19$ which correspond to the QGP hadronization.

The ‘low’ value of T^* for J/ψ suggests its rather early thermal FO. The low interaction cross

section of the J/ψ meson with the most abundant hadrons [329] and its large mass lead to a very low probability of the J/ψ rescattering on hadrons. All this suggests that the thermal FO of J/ψ coincides with the hadronization of QGP, i.e., that the J/ψ meson does not participate in the hadronic rescattering after hadronization. It is, however, natural to expect that there is a significant collective transverse flow of hadronizing QGP developed at the early stage of partonic rescattering. Consequently the AT of the J/ψ meson as well as all other hadrons for which chemical and thermal FOs coincide with hadronization can be expressed as:

$$T_H^*(m) = T_H + \frac{2}{\pi} \cdot m \cdot \langle v_T^H \rangle^2, \quad (6.9)$$

where $\langle v_T^H \rangle$ is the mean transverse flow velocity of the QGP at the hadronization. Assuming $T_H = 175$ MeV and using the measured value of $T^*(J/\psi) = 245$ MeV one finds from Eq.(6.9): $\langle v_T^H \rangle \cong 0.19$. As expected the obtained transverse flow velocity of QGP at hadronization is significantly smaller than the transverse flow velocity of pions (≈ 0.5). The linear m -dependence of T_H^* (6.9) is shown in Fig. 6.1 by the lower solid line. Within the approach discussed here, Eq. (6.9) can be used to obtain a next estimate of the lower limit of the measured AT for all hadrons. In fact, the values of the parameter T^* for all light hadrons are higher than $T_H^*(m)$. The recent results [314] on the m_T spectra of the ψ' meson indicate that $T^*(\psi') \approx T_H^*(\psi') = 258 \pm 5$ MeV, which suggests that the ψ' meson (like J/ψ) does not participate in the hadronic rescattering either.

One may expect that the thermal FO may coincide with hadronization also for D and Υ mesons. Under this assumption one can calculate the value of the apparent temperature for those mesons : $T^*(D) \cong T_H^*(D) \cong 217$ MeV and $T^*(\Upsilon) \cong T_H^*(\Upsilon) \cong 392$ MeV, respectively.

For the production of open and hidden charm particles in A+A collisions at RHIC energies one can expect stronger transverse collective flow effects than at the SPS. This will lead to a linear mass dependence (6.9) of the AT with approximately the same value of $T_H \cong 175$ MeV, but with a larger value of $\langle v_T^H \rangle$. A recent analysis [334] of the RHIC data leads to the above value $T_H \cong 175$ MeV of the chemical FO temperature.

Since the RHIC data for J/ψ mesons are not measured yet, one can use the hydrodynamic calculations of Ref. [335] which predict the value of $\langle v_T^H \rangle \cong 0.30$ at the QGP hadronization for

the low collision energy at RHIC. This will lead to an increase of the AT of charmed hadrons at RHIC in comparison to those values at SPS, e.g., $T^*(J/\psi) \cong T_H^*(J/\psi) \cong 350$ MeV and $T^*(D) \cong T_H^*(D) \cong 280$ MeV. If bottomonium experiences the same FO conditions at RHIC like J/ψ meson, then its apparent temperature will be about $T^*(\Upsilon) \cong T_H^*(\Upsilon) \cong 720$ MeV.

To end this subsection, I conclude that the recent results on transverse mass spectra of J/ψ and ψ' mesons in central Pb+Pb collisions at 158 A·GeV are considered. It is shown that these data support the hypothesis of the statistical production of charmonia at hadronization and suggest a simultaneous hadronization and the thermal FO for J/ψ and ψ' mesons. Based on this approach the collective transverse velocity of hadronizing quark gluon plasma is estimated to be $\langle v_T^H \rangle \approx 0.2$. Predictions for transverse mass spectra of hidden and open charm along with hidden bottom mesons at SPS and RHIC are discussed. Now I would like to perform a finer analysis of the data.

6.1.3. Ω , J/ψ and ψ' Early Hadronization at SPS Energies. The equilibrium hadron gas model describes remarkably well the hadron multiplicities measured in A+A collisions at top SPS [136, 137, 220] and RHIC [198, 199] energies, where the creation of QGP is expected. The extracted hadronization temperature parameter is similar for both energies $T_H = 170 \pm 10$ MeV. This is close to an estimate of the temperature T_C for the QGP to hadron gas transition obtained in Lattice QCD simulations at zero baryonic density (see e.g. [194]). One may therefore argue that the QGP created in high energy heavy ion collisions hadronizes into an (approximately) locally equilibrated hadron gas and the chemical composition of this hadron gas is weakly affected by rescattering during the expansion of the hadronic system [340].

As was discussed in the preceding subsection, I and my collaborators for the first time formulated the hypothesis that the kinetic FO of J/ψ and ψ' mesons takes place directly at hadronization and that those mesons therefore carry information on the flow velocity of strongly interacting matter just after the transition to the hadron gas. Based on the measured J/ψ and ψ' spectra in Pb+Pb collisions at 158 A·GeV [314] and using the hypothesis of the statistical production of charmonia at hadronization [323, 324, 342], it was possible to extract a mean transverse collective flow velocity of hadronizing matter: $\langle v_T^H \rangle \cong 0.2$. Here I would like to verify these results more carefully and include the Ω^\pm hyperons into consideration.

The effect of the rescattering in the hadronic phase was recently studied within a hydrocascade approach [261, 262]. The results of Refs. [261, 262] suggest that the transverse momentum (p_T) spectrum of Ω may be weakly affected during the cascade stage even for central Pb+Pb collisions at the top SPS energy. This is because of the small hadronic cross section and large mass of the Ω hyperon [339]. The corresponding calculations for charmonia are not yet performed within this model.

Thus, we are faced with an intriguing problem: if the above considerations for charmonia [205] and Ω [261, 262] are correct, their p_T spectra should be simultaneously reproduced using the same hydrodynamic parameters: the hadronization temperature T_H and the mean transverse velocity \bar{v}_T (the latter notation will be used hereafter to distinguish it from the notation of the previous discussion). In the present subsection I demonstrate that such a description is, indeed, possible. The transverse mass spectra around midrapidity in Pb+Pb collisions at the SPS (158 A·GeV) were recently measured for Ω by WA97 Collaboration [312, 313] and for J/ψ and ψ' by NA50 Collaboration [314]. These spectra will be the subject of the analysis below.

Assuming kinetic FO of matter at constant temperature T , the transverse mass spectrum of i -th hadron species (with mass m_i) in cylindrically symmetric and longitudinally boost invariant fluid expansion within the blast wave model can be approximated as [341]:

$$\frac{dN_i}{m_T dm_T} \propto m_T \int_0^R r dr K_1 \left(\frac{m_T \cosh y_T}{T} \right) I_0 \left(\frac{p_T \sinh y_T}{T} \right), \quad (6.10)$$

where $y_T = \tanh^{-1} v_T$ is the transverse fluid rapidity, R is the transverse system size, K_1 and I_0 are the modified Bessel functions. The spectrum (6.10) is obtained under assumption that the freeze-out occurs at constant longitudinal proper time $\tau = \sqrt{t^2 - z^2}$, where t is the time and z is the longitudinal coordinate. Thus, the FO time t is independent of the transverse coordinate r [341]. The analysis of the numerical calculations of Ref. [262] shows that the latter is approximately fulfilled. The quality of the approximation made gets better for considered here heavy particles and small transverse flow velocities because a possible deviation from Eq. (6.10) is proportional to $p_T^2 v_T / (2m_T T)$ and hence it decreases with increasing particle mass at constant p_T .

In order to calculate (6.10) the function $y_T(r)$ has to be given. A linear flow profile, $y_T(r) = y_T^{max} \cdot r/R$, is often assumed in phenomenological fits [341]. The numerical calculations of Ref. [262]

justify this assumption. For heavy hadrons analysed in here the condition $m_i \gg T$ is always satisfied and, therefore, the asymptotic form for large arguments of $K_1(x) \sim x^{-1/2} \exp(-x)$ can be used in Eq. (6.10). At SPS energies typical values of v_T are small ($v_T^2 \ll 1$) and consequently $\cosh y_T \cong 1 + \frac{1}{2}v_T^2$ and $\sinh y_T \cong v_T$.

The experimental m_T -spectra are usually parametrised by a function:

$$\frac{dN_i}{m_T dm_T} \propto \sqrt{m_T} \exp\left(-\frac{m_T}{T_i^*}\right), \quad (6.11)$$

where the inverse slope T_i^* is extracted from the fit to the data. Formally this corresponds to neglecting the transverse flow ($v_T \equiv 0$ in Eq. (6.10)), but introducing instead an “effective” temperature. However, when Eq. (6.11) is considered as an approximation of Eq. (6.10), the inverse slopes T_i^* should depend on both m_i and p_T . The limiting cases of T_i^* behavior at low and high p_T can be easily studied using the small and large argument asymptotic of the modified Bessel function I_0 in Eq. (6.10):

$$T_i^*(p_T \rightarrow 0) = \frac{T}{1 - \frac{1}{2}\bar{v}_T^2 (m_i/T - 1)} \approx T + \frac{1}{2} m_i \bar{v}_T^2, \quad (6.12)$$

$$T_i^*(p_T \rightarrow \infty) \equiv T^* = \frac{T}{1 - v_T^{max} + \frac{1}{2} (v_T^{max})^2}, \quad (6.13)$$

where the average velocity \bar{v}_T in Eq. (6.12) is defined as $\bar{v}_T^2 = \int_0^R r dr v_T^2(r) / \int_0^R r dr$. The maximum velocity v_T^{max} in Eq. (6.13) is related to \bar{v}_T as $\bar{v}_T^2 = (v_T^{max})^2/2$ provided a linear flow profile is assumed, $v_T(r) = v_T^{max} \cdot r/R$. Note that T^* in Eq. (6.13) is equivalent to the well known “blue shifted” temperature, $T[(1 + v_T^{max})/(1 - v_T^{max})]^{1/2}$ (see e.g. [262, 341]), calculated for $(v_T^{max})^2 \ll 1$. The shape of the “high- p_T ” tail ($p_T \gg m_i$) of the m_T distribution (6.10) is “universal”, i.e. T^* given by Eq. (6.13) is independent of particle mass m_i . On the other hand, the inverse slopes T_i^* (6.12) at “low- p_T ” are strongly dependent on m_i . Two remarks are appropriate here. First, for heavy particles like Ω and J/ψ the term $\frac{1}{2}m_i\bar{v}_T^2/T$ in Eq. (6.12) is not small compared to unity and thus the second (approximate) equality in this equation is violated. Second, a condition of the validity of Eq. (6.12), $p_T\bar{v}_T \ll T$, is too restrictive for heavy hadrons, e.g. for $T \cong 170$ MeV and $\bar{v}_T \cong 0.2$ discussed below it leads to $m_T - m_i \ll 0.3 \text{ GeV}^2/m_i$. This means that Eq. (6.12) is valid for the values of $m_T - m_i$ which are much smaller than 0.2 GeV for Ω and than 0.1 GeV for J/ψ .

Consequently: (a) none of the asymptotic regimes (6.12) or (6.13) can be clearly seen in the experimental m_T spectra, i.e. neither “low- p_T ” ($m_T - m_i \ll 0.3 \text{ GeV}^2/m_i$) nor “high- p_T ” ($m_T - m_i \gg m_i$) approximations are useful ones (at least for studying the available m_T spectra of Ω and charmonia); (b) fitting the experimental m_T spectrum of i -th hadron species by Eq. (6.11) one finds, in fact, the “average inverse slopes” which depend not only on particle mass m_i , but also on the $m_T - m_i$ interval covered in a given experiment (see also Ref. [262], where T_i^* have been discussed separately for $m_T - m_i < 0.6 \text{ GeV}$ and for $0.6 \text{ GeV} < m_T - m_i < 1.6 \text{ GeV}$).

For small values of v_T relevant to our discussion a good approximation of Eq. (6.10) at $m_T - m_i < m_i$ can be obtained by substituting the v_T distribution in Eq. (6.10) by its average value \bar{v}_T and by using large argument K_1 asymptotic:

$$\frac{dN_i}{m_T dm_T} \propto \sqrt{m_T} \exp\left(-\frac{m_T(1 + \frac{1}{2}\bar{v}_T^2)}{T}\right) I_0\left(\frac{p_T \bar{v}_T}{T}\right). \quad (6.14)$$

It was checked numerically that the values of the parameter \bar{v}_T extracted from the fits (see below) to Eqs. (6.10) and (6.14) assuming a linear velocity profile differ by about 5%.

Let me turn now to the test of the hypothesis of the kinetic FO of J/ψ , ψ' and Ω occurring directly at hadronization i.e. at $T = T_H = 170 \text{ MeV}$. The m_T -spectra of these hadrons are measured around midrapidity [314, 312] for Pb+Pb collisions at 158 A·GeV. The fit to these data performed using Eq. (6.14) with $T = T_H = 170 \text{ MeV}$ yields $\bar{v}_T = 0.194 \pm 0.017$ and $\chi^2/dof = 1.3$. The value of \bar{v}_T varies by ∓ 0.016 when T_H is changed within its uncertainty $\pm 10 \text{ MeV}$. Note that T and \bar{v}_T parameters are anti-correlated. A surprisingly good agreement (see Fig. 6.2) of this model with the data on m_T -spectra serves as a strong support of the hypothesis of statistical nature of J/ψ and ψ' production [323] and their kinetic FO occurring directly at hadronization [205].

The dependence of the J/ψ and ψ' transverse mass spectrum on the centrality (quantified by the neutral transverse energy E_T) of Pb+Pb collisions at 158 A·GeV was also measured by NA50 Collaboration [314]. An increase of $\langle p_T \rangle$ and $\langle p_T^2 \rangle$ from peripheral collisions to the most central collisions can be explained, within the present approach, by an increase of the model parameter \bar{v}_T with E_T . Note that the increase of mean flow velocity and consequently an increase of $\langle p_T \rangle$ and $\langle p_T^2 \rangle$ with a centrality of the collision as well as an increase of $\langle p_T \rangle$ and $\langle p_T^2 \rangle$ with particle mass m_i are characteristic features of hydrodynamics. In contrast to J/ψ and ψ' mesons the m_T -spectra

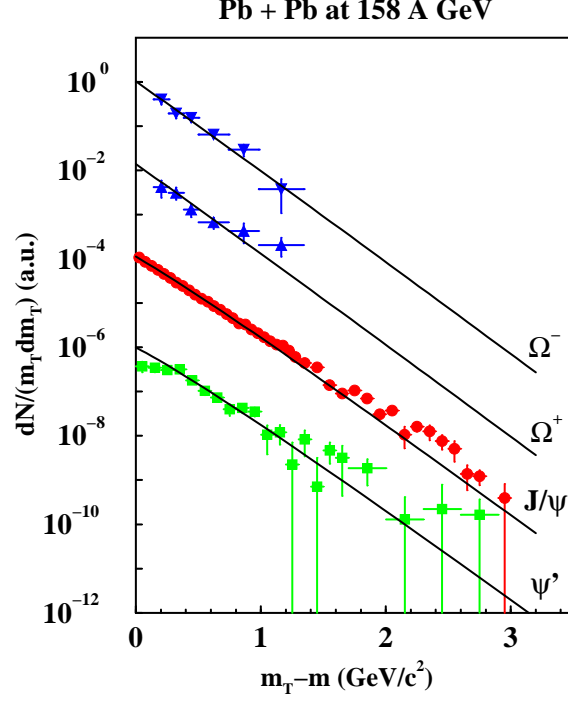


Figure 6.2. The transverse mass spectra of Ω^- (triangles down) and Ω^+ (triangles up) [312] as well as J/ψ (circles) and ψ' (squares) [314] produced in Pb+Pb collisions at 158 A·GeV. The solid lines indicate a prediction of the model (6.14) assuming kinetic FO of heavy hadrons directly after hadronization of expanding quark gluon plasma. The FO parameters are: $T = 170$ MeV and $\bar{v}_T = 0.194$.

of the Drell–Yan pairs (dileptons with invariant mass $M > 4.2$ GeV) do not show this type of hydrodynamical behavior. The values of $\langle p_T \rangle$ and $\langle p_T^2 \rangle$ [314] for the Drell–Yan pairs are smaller than those for J/ψ and ψ' and do not change significantly with E_T .

The kinetic FO parameters of pions were extracted from the analysis of single- and two-pion spectra measured for central Pb+Pb collisions at 158 A·GeV by the NA49 Collaboration [337, 325, 338]. The results are: $T_f \cong 120$ MeV and $\bar{v}_T \cong 0.55$, i.e. they are very different than those obtained here from the analysis of heavy hadron spectra. In fact, it was checked that the parameters obtained for pions lead to the m_T spectra of heavy hadrons which strongly disagree with the data. A decrease of temperature and an increase of transverse flow velocity with time is a

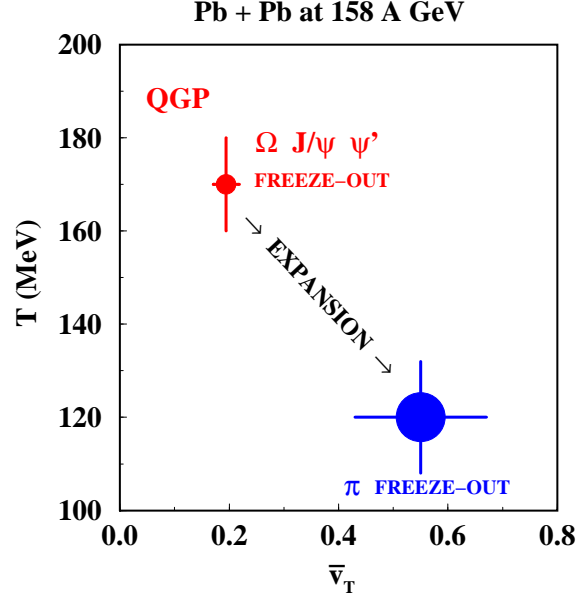


Figure 6.3. The expansion history of strongly interacting matter created in Pb+Pb collisions at 158 A·GeV. The points indicate the temperature T and the mean transverse flow velocity \bar{v}_T of matter at the time of Ω , J/ψ and ψ' FO (upper point) and at the time of pion kinetic FO (lower point).

general property of expanding systems. The different kinetic FO times of heavy hadrons and pions allowed us to establish the expansion history of the hadron gas phase created in Pb+Pb collisions at 158 A·GeV for the first time. The FO points of heavy hadrons and pions extracted from the data are plotted in Fig. 6.3 defining the path of the expanding hadron system in the $T - \bar{v}_T$ plane.

Thus, the m_T -spectra of Ω , J/ψ and ψ' produced in Pb+Pb collisions at 158 A·GeV are analysed within the hydrodynamical model of the QGP expansion and hadronization. The spectra are in agreement with the hypothesis of kinetic FO of these heavy hadrons occurring directly after the transition from the quark gluon plasma to the hadron gas. A mean collective transverse flow of hadronizing matter of $\bar{v}_T \cong 0.2$ is extracted from the fit to the spectra using temperature $T_H \cong 170$ MeV fixed by the analysis of hadron multiplicities [136, 137, 220]. This result together with a previously obtained parameters of pion FO ($T_f \cong 120$ MeV and $\bar{v}_T \cong 0.55$) allowed for the first time to establish the history of the expanding hadron matter [207] created in nuclear

collisions.

In the RHIC energy range the temperature parameter is approximately the same $T = T_H \cong 170$ MeV [198, 199], whereas the transverse hydrodynamic flow at $T = T_H$ is expected to be stronger. The model predictions for the m_T -spectra of Ω and charmonia at the RHIC energies will be presented in the next section.

6.2. Hadron Spectra and QGP Hadronization in Au+Au Collisions at RHIC

The recent measurements [336] of the energy dependence of pion and kaon production in central collisions of heavy nuclei indicate [267] that the transient state of deconfined matter is created at the early stage of these collisions for energies higher than about 30 A·GeV, i.e. at high SPS and RHIC energies. Analysis of the hadron multiplicities measured in these collisions within statistical models at the SPS [136, 137, 220] and RHIC [198, 199] energies shows that the chemical FO takes place near the boundary between the quark–gluon and hadron phases. The values of the temperature parameter extracted from the data are similar for both energies, $T_H = 170 \pm 10$ MeV, and, as discussed above, they are close to the value of the deconfinement transition temperature at zero baryonic density estimated in the lattice QCD (see e.g. Ref. [194]).

The analysis of the experimental data at the SPS [337, 338] and a numerical modeling of the hadron cascade stage in A+A collisions at SPS and RHIC energies [261, 262] indicate that the kinetic (i.e., particle spectra) FO of the most abundant hadrons takes place at temperatures significantly lower than T_H . Nevertheless, as was argued in the preceding subsection, one may expect that the kinetic FO of some heavy and weakly interacting hadrons (e.g. Ω hyperons and ϕ , J/ψ , ψ' mesons) occurs directly at the QGP hadronization stage or close to it. Thus, for these hadrons the chemical and kinetic FOs coincide and are determined by the features of the QGP hadronization. For Ω hyperons and ϕ mesons this expectation is based on the results of hydrocascade approach [261, 262]. For J/ψ and ψ' mesons such a result I obtained with my collaborators [205, 207, 206]. It is a straightforward consequence of the recently proposed statistical

mechanism of charmonia production at the QGP hadronization [323, 324, 342, 343]. As I showed above, within this approach the transverse mass spectra of the Ω , J/ψ and ψ' measured in Pb+Pb collisions at the SPS can be described successfully. The transverse mass spectra of Ω hyperons [210] and ϕ mesons [212, 213] produced in central Au+Au collisions at $\sqrt{s_{NN}} = 130$ GeV were recently measured by the STAR Collaboration. These data allow to test the present model in the new energy regime. They also give a unique opportunity to extract parameters of the QGP hadronization at RHIC energies and consequently predict spectra of J/ψ and ψ' mesons.

Within a hydrodynamical approach of the QGP hadronization the transverse mass spectrum of i -th hadron in the central rapidity region can be written as (see, e.g., Ref. [344]):

$$\left. \frac{dN_i}{m_T dm_T dy} \right|_{y=0} = \frac{d_i \lambda_i \gamma_i^{n_i}}{\pi} \tau_H R_H^2 \int_0^1 \xi d\xi K_1 \left(\frac{m_T \cosh y_T}{T_H} \right) I_0 \left(\frac{p_T \sinh y_T}{T_H} \right), \quad (6.15)$$

where y is the particle longitudinal rapidity and $y_T(\xi) = \tanh^{-1} v_T$ is the fluid transverse rapidity. R_H and τ_H are, respectively, the transverse system size and proper time at the hadronization (i.e., at the boundary between the mixed phase and hadron matter), $\xi = r/R_H$ is a relative transverse coordinate. The particle degeneracy and fugacity are denoted as d_i and λ_i , respectively. Parameter γ_i in Eq. (6.15) (γ_S [345] for $i = \phi, \Omega$ and γ_C [324, 342] for $i = J/\psi, \psi'$) describes a possible deviation of strange and charm hadrons from complete chemical equilibrium ($n_i = 2$ for $\phi, J/\psi, \psi'$ and $n_i = 3$ for Ω).

The spectrum (6.15) is obtained under the assumption that the hydrodynamic expansion is longitudinally boost invariant and that the FO occurs at constant longitudinal proper time $\tau = \sqrt{t^2 - z^2}$ (see Eq. (6.10) for the notations), i.e. the FO time t is independent of the transverse coordinate r . The formula (6.15) is a more careful expression of Eq. (6.10), which I use here to extract $\tau_H R_H^2$ value from the absolute normalization of spectra.

In order to complete Eq. (6.15) the functional form of the transverse rapidity distribution of hadronizing matter $y_T(\xi)$ has to be given. A linear flow profile, $y_T(\xi) = y_T^{max} \cdot \xi$, used in this model is justified by the numerical calculations of Ref. [262] and by an excellent fit [207] of the SPS transverse momentum spectra for Ω^\pm , J/ψ , and ψ' particles.

Thus, in the present model, the QGP hadronization is described by the following parameters: temperature T_H , "volume" $\tau_H R_H^2$, maximum flow rapidity y_T^{max} , fugacities λ_i , and saturation factors

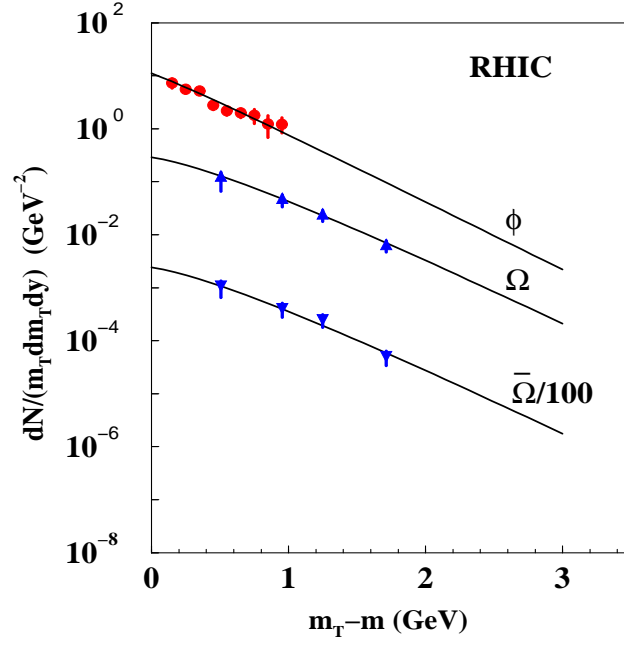


Figure 6.4. The hadron transverse mass spectra in Au+Au collisions at $\sqrt{s_{NN}} = 130$ GeV are shown. The points indicate experimental data for the Ω [210] and ϕ [213] measured by STAR. The model results are shown by full lines.

γ_i . Note that the $\phi, J/\psi, \psi'$ have no conserved charges and $\lambda_i = 1$ for these particles. I use the fixed values of the parameters $T_H = 170$ MeV, $\gamma_S = 1.0$, $\lambda_{\Omega^-} = 1/\lambda_{\Omega^+} = 1.09$ (note that $\lambda_{\Omega^-} \equiv \exp[(\mu_B - 3\mu_S)/T]$, where μ_B and μ_S are, respectively, baryon and strange chemical potentials). These (average) values of the *chemical freeze-out* parameters have been found in the hadron gas analysis [198, 199] of the full set of the midrapidity particle number ratios measured in central Au+Au collisions at $\sqrt{s_{NN}} = 130$ GeV. The fit to the m_T -spectra of Ω^\pm hyperons [210, 211] and ϕ mesons [212, 213] measured in central (14% for Ω^\pm and 11% for ϕ) Au+Au collisions at $\sqrt{s_{NN}} = 130$ GeV is shown in Fig. 6.4. The fit results are: $y_T^{max} = 0.74 \pm 0.09$, $\tau_H R_H^2 = 275 \pm 70$ fm³ and $\chi^2/ndf \cong 0.46$. In the calculation of errors of the two free parameters of the model the uncertainties of T_H (± 5 MeV), γ_S (± 0.05) and λ_{Ω^-} (± 0.06) were taken into account.

A simple exponential approximation of the spectra is usually utilized to parameterize the experimental data:

$$\left. \frac{dN}{m_T dm_T dy} \right|_{y=0} = C \exp\left(-\frac{m_T}{T^*}\right). \quad (6.16)$$

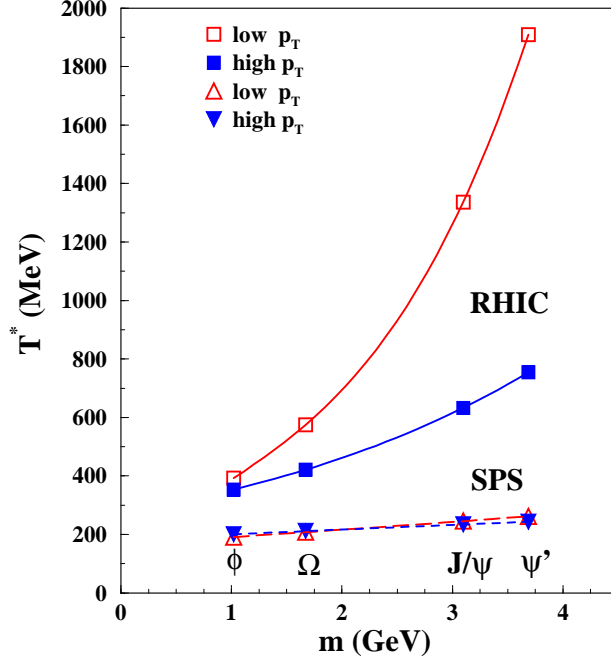


Figure 6.5. The values of the inverse slope parameters T^* for two different m_T domains – “low- p_T ” ($m_T - m < 0.6$ GeV) and “high- p_T ” (0.6 GeV $< m_T - m < 1.6$ GeV) – in Au+Au collisions at $\sqrt{s_{NN}} = 130$ GeV are presented. They are found using Eq. (6.15) with $T_H = 170$ MeV and $y_T^{max} = 0.74$. For comparison, the values of T^* extracted from fitting the data in Pb+Pb collisions at the SPS (Eq. (6.15) with $T_H = 170$ MeV, $y_T^{max} = 0.28$, see Ref. [207]) are also shown.

Note that in Refs. [205, 207, 206] an additional factor $m_T^{1/2}$ was present in the r.h.s. of Eq. (6.16). It led to smaller values of T^* when fitting the same spectrum. The m_T -spectrum (6.15) may, however, deviate significantly from a purely exponential one and its shape depends on the magnitude of the transverse flow and the mass of the particle. The normalization factors C and the inverse slope parameters T^* in different intervals of $m_T - m$ can be found from the ϕ , Ω , J/ψ and ψ' spectra given by Eq. (6.15) using the maximum likelihood method. The average values of T^* for the m_T domains of “low- p_T ” ($m_T - m < 0.6$ GeV) and “high- p_T ” (0.6 GeV $< m_T - m < 1.6$ GeV), discussed in Refs. [262, 206], are shown in Fig. 6.5. The values of T^* determined in the preceding section by fitting the Ω^\pm , J/ψ and ψ' data in Pb+Pb collisions at 158 A·GeV ($T_H = 170$ MeV, $y_T^{max} = 0.28$) are also shown for comparison. The observed increase of T^* with increase of the hadron mass is much stronger at RHIC than at SPS energies. It is caused by larger transverse

flow velocity of hadronizing QGP at RHIC ($\bar{v}_T \cong 0.44$) than at SPS ($\bar{v}_T \cong 0.19$). The increase of T^* is much more pronounced in “low- p_T ” region than in “high- p_T ” one. In this model the m_T -spectra of charmonia are extraordinarily affected by the stronger transverse flow at RHIC due to enormous masses of these hadrons. Thus, the data on J/ψ and ψ' production in Au+Au collisions, soon to be obtained at RHIC, should allow to test the hypothesis of their formation at the QGP hadronization.

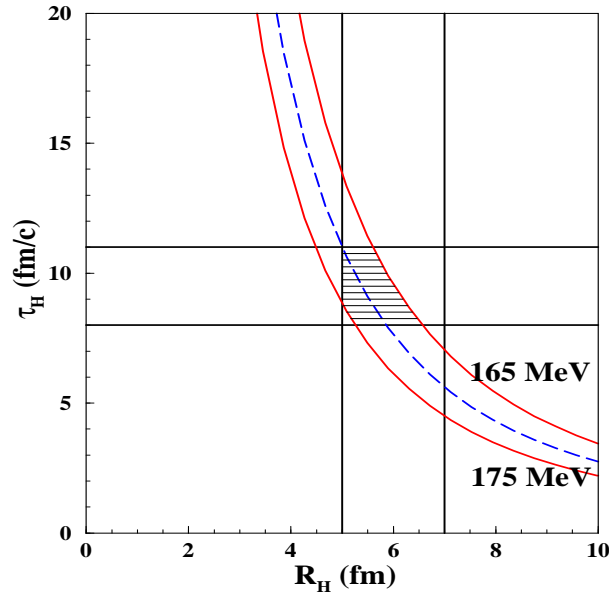


Figure 6.6. The lines $\tau_H = A(T_H) \cdot R_H^{-2}$ of constant “volume parameter” $A(T_H)$ are shown: $T_H = 170$ MeV corresponds to the dashed line, $T_H = 165$ MeV and $T_H = 175$ MeV correspond to the lower and upper solid lines, respectively. The dashed area is the intersection of the R_H - τ_H region between the $T_H = 165$ MeV and $T_H = 175$ MeV lines with the region of $R_H = 5 \div 7$ fm and $\tau_H = 8 \div 11$ fm estimated from Ref. [262].

One should note here that at present there exists an uncertainty in the estimates of the γ_C factor, therefore, the predictions concerning charmonia multiplicities in Au+Au collisions at RHIC within statistical approaches significantly vary and their discussion goes beyond the scope of the present discussion.

The “volume parameter” $\tau_H R_H^2 \equiv A(T_H)$ extracted from the fit to the Ω and ϕ spectra defines the line $\tau_H = A(T_H) \cdot R_H^{-2}$ in the R_H - τ_H plane. The allowed region in the R_H - τ_H plane can be estimated by varying the temperature parameter within its limits, $T_H = 165$ MeV and $T_H =$

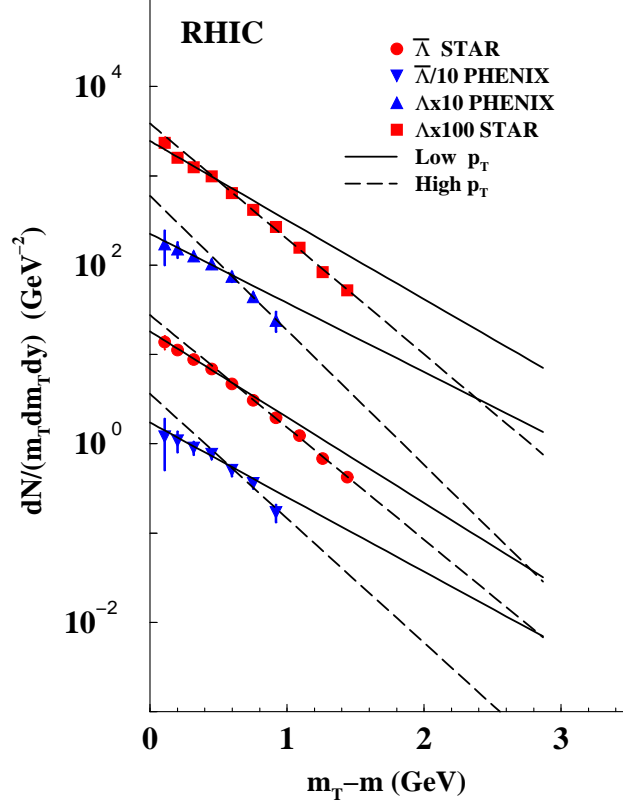


Figure 6.7. The points indicate the experimental m_T -spectra of the Λ and $\bar{\Lambda}$ in central Au+Au collisions at $\sqrt{s_{NN}} = 130$ GeV measured by the STAR [349] and PHENIX [351] Collaborations. The “straight lines” are the exponential approximations of the spectra with Eq. (6.16) in the low- p_T (solid lines) and high- p_T (dashed lines) regions.

175 MeV. The resulting lines are shown in Fig. 6.6. The transverse radius $R_H = 5 \div 7$ fm and the proper time $\tau_H = 8 \div 11$ fm at the QGP hadronization can be estimated from the hydrodynamical calculations of [262] for central Au+Au collisions at $\sqrt{s_{NN}} = 130$ GeV (see Fig. 3 in Ref. [262]). These model boundaries and their intersection with the R_H - τ_H region found in my analysis are shown in Fig. 6.6.

Within the present approach the m_T -spectra of ϕ , Ω , J/ψ , ψ' are assumed to be frozen at the space-time hyper-surface where the hadron phase starts. This assumption is justified by the small hadronic cross sections and large masses of these particles (in addition, the m_T -spectra of these hadrons are almost not affected by the resonance feeding). However, the m_T -spectra of many other hadrons are expected to be significantly modified by hadronic rescattering. Contrary to

this expectation it was recently postulated [346, 347] that the simultaneous chemical and kinetic freeze-out in Au+Au collisions at RHIC occurs for all hadrons (a single freeze-out model). Do experimental data allow us to distinguish between these two approaches?

Table 6.1. The values of inverse slope parameters T^* for (anti)protons and (anti)lambdas in Au+Au collisions at $\sqrt{s_{NN}} = 130$ GeV are presented. The experimental values are taken as the average ones over the STAR and PHENIX results (a difference in the results for particle and its anti-particle is small).

	$T_{low-p_T}^*$ (MeV)	$T_{high-p_T}^*$ (MeV)	Refs.
DATA p, \bar{p}	455 ± 105	290 ± 40	[348, 350]
Hydro+RQMD	480	300	[262]
Single freeze-out	315	310	[346, 347]
DATA $\Lambda, \bar{\Lambda}$	505 ± 60	320 ± 30	[349, 351]
Hydro+RQMD	440	310	[262]
Single freeze-out	360	330	[347]

The hydrocascade approach [262] predicts for central Au+Au collisions at $\sqrt{s_{NN}} = 130$ GeV that the hadron cascade stage modifies the m_T -spectra of nucleons and Λ hyperons substantially. In particular a large increase of the inverse slope parameter in the low- p_T region is expected for these hadrons as a result of hadronic rescattering and resonance decay effects. Thus, the measurements of (anti)proton and (anti)lambda m_T -spectra should allow to distinguish between the single freeze-out model and models which assume different kinetic freeze-out conditions for different hadrons. I performed the T^* analysis of the present RHIC data from STAR [348, 349] and PHENIX [350, 351]. The resulting T^* values are summarized in Table 6.1. together with the predictions of the single FO model [346, 347] and hydrocascade model [262]. The m_T -spectra of the Λ and $\bar{\Lambda}$ are also shown in Fig. 6.7. There are significant systematic differences between T^* parameters obtained from the STAR and PHENIX data. In view of this fact, the values quoted in the Table 6.1. are calculated

as an arithmetic average of both results, whereas the (systematic) error was estimated to be a half of the difference between them.

Despite the large uncertainties, the data seem to favor the hydrocascade model over the single FO model. Additional data in the low- p_T region and their theoretical analysis would be helpful to clarify presence of the hadron cascade stage and its influence on $T_{low-p_T}^*$ of (anti)protons and (anti)lambdas.

The results on m_T -spectra of charmonia in central Au+Au collisions at the RHIC energies are expected to be available soon. They should allow to test a statistical approach to the charmonia production at the QGP hadronization in high energy nuclear collisions. In particular, within this approach, I predict a strong (a few times) increase of the inverse slope parameter T^* of the charmonia m_T -spectra at RHIC in comparison with that at SPS. The higher is the energy the larger inverse slope is expected due to increasing transverse flow of hadronizing QGP. Thus, at $\sqrt{s_{NN}} = 200$ GeV the increase of T^* should become even more pronounced than at $\sqrt{s_{NN}} = 130$ GeV. Due to strong sensitivity of the charmonia spectra to the hadronization temperature and transverse flow velocity, their analysis should significantly improve the discussed estimate of these parameters.

6.3. Transverse Caloric Curves of Kaons as the Signal of Deconfinement Transition in A+A Collisions

The statistical model of the early stage of A+A collisions suggests [267] that the onset of the deconfinement phase transition at the early stage of the collisions may be signaled by the anomalous energy dependence of several hadronic observables. In particular, following earlier suggestions [353], the behavior of strangeness and pion yields in the transition region was studied in detail. Recent measurements [336] of pion and kaon production in central Pb+Pb collisions at the CERN SPS, indeed, indicate that the transient state of deconfined matter is created in these collisions for energies larger than about 40 A·GeV. The present data show a maximum of the strangeness to pion ratio at this energy. An exact position and the detailed structure of this

maximum is clarified by the recent results from the 2002 Pb run at 30 A·GeV [352].

In the present section I discuss another well known observable, which may be sensitive to the onset of deconfinement, the transverse momentum, p_T , spectra of produced hadrons. It was suggested by Van Hove [354] more than 20 years ago to identify the deconfinement phase transition in high energy proton–antiproton interactions by an anomalous behavior (a plateau-like structure) of the average transverse momentum as a function of hadron multiplicity. Let me briefly recall Van Hove’s arguments. According to the general concepts of the hydrodynamical approach the hadron multiplicity reflects the entropy, whereas the transverse hadron AT reflects the combined effects of temperature and collective transverse expansion. The entropy is assumed to be created at the early stage of the collision and is approximately constant during the hydrodynamic expansion. The multiplicity is proportional to the entropy, $S = s \cdot V$, where s is the entropy density and V is the effective volume occupied by particles. During the hydrodynamic expansion, s decreases and V increases with $s \cdot V$, being approximately constant because, as I showed earlier, the FO shocks generate just about 1 % of entropy. The large multiplicity at high energies means a large entropy density at the beginning of the expansion (and consequently a larger volume at the end). A large value of s at the early stage of the collisions means normally high temperature T_0 at this stage. This, in turn, leads to an increase of transverse hadron AT, a flattening of the transverse momentum spectra. Therefore, with increasing collision energy one expects to observe an increase of both the hadron multiplicity and average transverse momentum per hadron. In the original Van Hove suggestion the correlation between average transverse momentum and hadron multiplicity was discussed for proton-antiproton collisions at fixed energy. Today it is possible to study A+A collisions at different energies.

However, the presence of the deconfinement phase transition would change this correlation. In the phase transition region the initial entropy density (and hence the final hadron multiplicity) increases with collision energy, but temperature $T_0 = T_C$ and pressure $p_0 = p_C$ remain constant. The equation of state presented in the form $p(\varepsilon)/\varepsilon$ versus energy density ε shows a minimum (the ‘softest point’ [355, 308]) at the boundary of the (*generalized* [308]) mixed phase and the QGP. Consequently, the shape of the p_T spectrum is approximately independent of the multiplicity or

collision energy. The transverse expansion effect may even decrease when crossing the transition region [354]. Thus one expects an anomaly in the energy dependence of transverse hadron AT: the average transverse momentum increases with collision energy when the early stage matter is either in pure confined or in pure deconfined phases, and it remains approximately constant when the matter is in the mixed phase.

A simplified picture with $T = T_C = \text{const}$ inside the mixed phase is changed, if the created early stage matter has a non-zero baryonic density. It was, however, demonstrated [309] that the main qualitative features ($T \cong \text{const}$, $p \cong \text{const}$, and a minimum of the function $p(\varepsilon)/\varepsilon$ vs ε) are present also in this case. In the statistical model of the early stage model [267], which correctly predicted the energy dependence of pion and strangeness yields, the modification of the equation of state due to the deconfinement phase transition is located between the lab. energy of 30 and about 200 A-GeV. Thus, the anomaly in energy dependence of transverse hadron AT may be expected in this energy range. Can one see this anomaly in the experimental data?

The experimental data on transverse mass spectra are usually parameterized by a simple exponential dependence:

$$\frac{dN}{m_T dm_T} = C \exp\left(-\frac{m_T}{T^*}\right), \quad (6.17)$$

where the inverse slope parameter T^* is sensitive to both the thermal and collective motion in the transverse direction. In the parameterization (6.17) the shape of the m_T spectrum is fully determined by a single parameter, the inverse slope T^* . In particular, the average transverse mass, $\langle m_T \rangle$, can be expressed as:

$$\langle m_T \rangle = T^* + m + \frac{(T^*)^2}{m + T^*}. \quad (6.18)$$

The energy dependence of the inverse slope parameter fitted to the K^+ and K^- spectra for central Pb+Pb (Au+Au) collisions is shown in Fig. 6.8. The results obtained at AGS [356], SPS [336] and RHIC [357] energies are compiled. The striking features of the data can be summarized and interpreted as follows.

- The T^* parameter increases strongly with collision energy up to the lowest (40 A-GeV) SPS energy point. This is an energy region where the creation of confined matter at the early stage of the collisions is expected. Increasing collision energy leads to an increase of the early stage

temperature and pressure. Consequently, the transverse AT of produced hadrons, measured by the m_T spectra, increases with increasing energy.

- The T^* parameter is approximately independent of the collision energy in the SPS energy range. In this energy region the transition between confined and deconfined matter is expected to be located. The resulting modification of the equation of state “suppresses” the hydrodynamical transverse expansion and leads to the observed plateau structure in the energy dependence of the T^* parameter.
- At higher energies (RHIC data) the T^* again increases with collision energy. The equation of state at the early stage becomes again stiff, the early stage temperature and pressure increase with collision energy. This results in increase of T^* with energy.

Surprisingly, such a plateau-like behavior is typical for the caloric curves of nuclear multifragmentation data [6] and reflects the system’s evolution within the mixed phase [48, 49, 50]. Since the kaon AT behavior is similar in shape and in physics to the usual caloric curves of nuclear multifragmentation, I suggest to call it the transverse caloric curve.

The anomalous energy dependence of the m_T spectra is a characteristic feature of the kaon data. Why is this the case? How do the m_T spectra of other hadrons look like? The answer is rather surprising: among the measured hadron species the kaons are the best and unique particles for observing the effect of the modification of the equation of state due to the onset of deconfinement. The arguments are as follows.

- The kaon m_T -spectra are only weakly affected by the hadron re-scattering and resonance decays during the post-hydrodynamic hadron cascade [261, 262]. In fact, both effects should have modified the low p_T range of kaon spectra, but into opposite directions. As a result, both effects almost compensate each other for kaons.
- A simple one parameter exponential fit (6.17) is quite accurate up to $m_T - m \cong 1$ GeV for K^+ and K^- mesons in A+A collisions at all energies. This means that the energy dependence of the average transverse mass $\langle m_T \rangle$ and average transverse momentum $\langle p_T \rangle$ for kaons is

qualitatively the same as that for the parameter T^* . This simplifies the analysis of the experimental data.

- The high quality data on m_T spectra of K^+ and K^- mesons in central Pb+Pb (Au+Au) collisions are available in the full range of relevant energies.

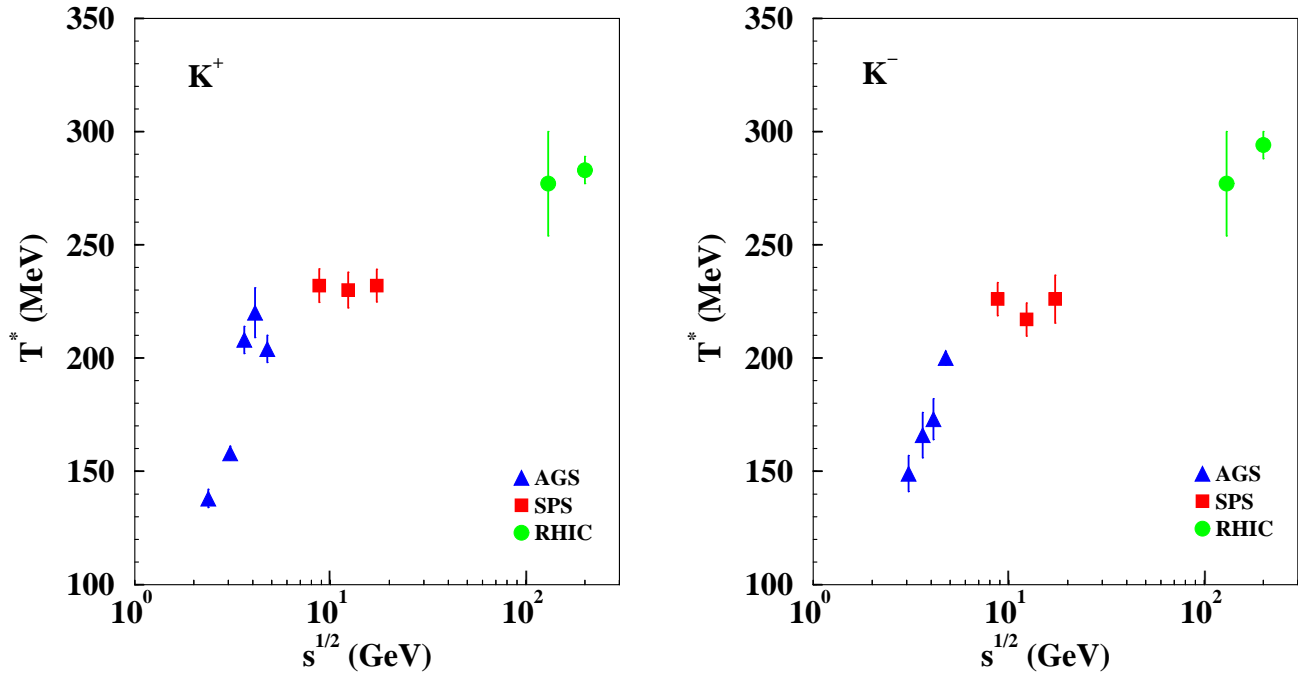


Figure 6.8. The energy dependence of the inverse slope parameter T^* for K^+ (left panel) and K^- (right panel) mesons produced at mid-rapidity in central Pb+Pb (Au+Au) collisions at AGS [356] (triangles), SPS [336] (squares) and RHIC [357] (circles) energies. Note that the abscissa has a logarithmic scale because in the linear one it would be a huge plateau.

The hydrocascade approach [261, 262] predicts a strong modification of the m_T -spectra of protons and lambdas during the hadron cascade stage in A+A collisions at both the SPS and RHIC. As the hadron gas expands, the pions excite Δ and Σ^* resonances and transform some part of their transverse energy in the nucleon and hyperon sectors. Therefore, the hadron re-scattering and resonance decays lead to significant increase (about 40% [262]) of the inverse slope parameters T^* for (anti)nucleons and (anti)lambdas at the expense of the pion transverse energy (also see discussion in Ref. [205]). These changes of the slopes T^* are not directly related to the equation

of state of the matter at the early stage. It is rather difficult to separate these hadron-cascade effects and in any case, this separation will be strongly model dependent. Note also that a simple exponential fit (6.17) neither works for π -mesons ($T_{low-p_T}^* > T_{high-p_T}^*$) [348, 349, 350] nor for protons and lambdas ($T_{low-p_T}^* < T_{high-p_T}^*$) [350, 351]. This means that the average transverse masses, $\langle m_T \rangle$, and their energy dependence are not connected to the behavior of the slope parameters in the simple way described by Eq. (6.18): one should separately consider both $T_{low-p_T}^*$ and $T_{high-p_T}^*$ slopes for these hadrons (see also Ref. [262] for details).

The transverse AT of Ω hyperons and ϕ mesons should, as in the case of kaons, be sensitive to the matter equation of state at the early stage of the collisions. These particles seem to decouple just after the hadronization is over and they do not participate in the hadron cascade stage [261, 262, 205, 208]. Unfortunately the spectra of Ω hyperons are measured only at top SPS [313] and RHIC energies [210]. More data exist for ϕ meson production [315, 316, 358]. However, the large uncertainties in the experimental results do not allow to draw a definite conclusion on the possible anomaly in the energy dependence of m_T spectra.

Thus, one observes an anomalous energy dependence of transverse mass spectra of K^+ and K^- mesons produced in central Pb+Pb (Au+Au) collisions. The inverse slopes of the m_T -spectra increase with energy in the AGS and RHIC energy domains, whereas they remain constant in the intermediate SPS energy range. As was argued above, this anomaly is caused by a modification of the equation of state in the transition region between confined and deconfined matter. Now this observation is considered as a new signal, in addition to the previously reported anomalies in energy dependence of the pion and strangeness production, of the onset of deconfinement located at the low SPS energies.

6.4. Concluding Remarks

Here I discussed the possible experimental signatures of the deconfinement transition. Note that none of the signals suggested in 80-th and 90-th was ever observed in a way as it was suggested. Therefore, the formulation of a reliable signal of the deconfinement transition is highly non-trivial task. So far, there are only three signals of the deconfinement which have been observed experi-

mentally. They are: the Kink in the ratio of pion yield to number of wounded nucleons [266], the Strangeness Horn [267] in K^+ to π^+ numbers ratio and the Step [265] in kaon AT presented in this chapter. All these irregularities are emerging at the very same lab. energy of about 30 GeV·A.

On the other hand the early hadronization of multistrange and charmed (open and hidden) hadrons is indirect, but, nevertheless, firm evidence for thermalization and collective flow of the QGP at the stage of its hadronization. A systematic study of A+A collisions with the nuclei of different sizes (including the small ones) based on the suggested hypothesis of early hadronization will, perhaps, find out the threshold for the QGP collective flow.

Conclusions

In the present dissertation I discussed two main PTs that are studied in the strongly interacting matter: the nuclear liquid-gas PT and the transition of liberating the color degrees of freedom from hadrons known as the deconfinement transition. Since the quantum chromodynamics, which is the fundamental theory of strong interaction, has not reached yet the stage when it can be directly applied to the description of the experimental data obtained in the relativistic heavy ion collisions, we are faced with the necessity to develop the phenomenological approaches to model the EOS of strongly interacting matter in a very wide range of densities - from the one third of normal nuclear density at which the break up of nuclear systems occurs in the reaction of nuclear multifragmentation up to hundreds of normal nuclear densities which are expected to be created at LHC. In fact, the results of the experiments cannot be interpreted without the underlying statistical descriptions.

However, the construction of the realistic EOS is not a straightforward procedure because it is necessary to take into account the specific features of strong interaction and combine them with some general requirements, like thermodynamic self-consistency, causality e.t.c. One important additional requirement, which I adopted in my research, is to reduce as much as possible the mean-field approximation for statistical models. So far, I suggested a single phenomenological mean-field EOS of nuclear matter from thermodynamically self-consistent class of Walecka-like models, but analytically I solved the SMM, the Mott-Hagedorn resonance gas and QGBST models in thermodynamic limit, and the CSMM, the GSMM, the GBM, the HTM and the HDM for finite systems. Note that only two of these statistical models, the SMM and the GBM, were formulated by other researchers, whereas all the rest was formulated in my works with collaborators.

This additional requirement to study and develop truly statistical, i.e. non mean-field, models led to several very valuable results. The first of these results is that the solution of a simplified SMM and calculation of the critical exponents of nuclear matter allowed me and my former student

P. T. Reuter to predict a narrow range for the Fisher index $\tau \approx 1.825 \pm 0.025$ which, in contrast to the Fisher value $\tau \approx 2.16$, is consistent with the experimental results $\tau \approx 1.8 - 1.9$ obtained by the ISiS and EOS Collaborations. Such a value of τ shows that the nuclear matter belongs to other universality class ($\tau < 2$) than the Fisher droplet model ($\tau > 2$) and that the nuclear liquid-gas PT has the tricritical endpoint rather than the critical one.

However, the analysis of the SMM critical indices showed me that the definition of the α index via the critical isochore is not a well established definition. For instance, the critical isochore in a simplified SMM belongs to the boundary of the mixed and liquid phases and, hence, it explicitly breaks down the implicit Fisher assumption which is necessary to prove the validity of the scaling inequalities for critical exponents. Since there exist substances with rather complicated phase diagrams, where the critical isochore (partially) lies out of the mixed phase, one has to search for an alternative definition. Fisher's suggestion to use a specially defined index α_s "saves" the scaling inequalities for known models, but it does not have such a simple and clear meaning like α and has to be justified further. Perhaps, new models and new experimental tests of the inequalities of critical indices will clarify this problem.

The second result of high value obtained in this dissertation on a firm ground of statistical mechanics is an exact analytical solution of several statistical models for finite systems. This was possible because of the invention of a new and powerful mathematical method, the Laplace-Fourier transform. This method allows one to identically rewrite the GCE partition via the sum over the simple poles of the isobaric partition. The analysis of the behavior of these singularities for the case with a PT and without it led me to the formulation of the finite volume analogs of phases and their phase diagram in the temperature – real part of the effective chemical potential plane. These definitions based on the first principles of statistical mechanics allowed me to clarify the pitfalls of the definition of phases suggested in works of T. Hill, Ph. Chomaz, F. Gulminelly and others for finite systems.

Also such a representation shows that in the CSMM, the GSMM and the GBM the low density phase, i.e the gas of nuclear fragments in the CSMM and the GSMM and hadron gas in the GBM, are the only stable states which have a real value of free energy, whereas all other states

are metastable and they have complex values of free energy and effective chemical potential. The different values of the real part of the effective chemical potential generated by interaction indicate that in finite system the states which belong to the same partition and have the same value of chemical potential are not in true chemical equilibrium with each other. As discussed in the dissertation, the imaginary part of free energy of these λ_n states gives us an estimate for the formation/decay time τ_n of the state λ_n ($n = 0, 1, 2, \dots$). At high densities the formation/decay time τ_n of the λ_n state of the system having volume V is $\tau_n(V) \approx \frac{V}{V_o \pi n T}$. Here V_o denotes an eigen volume of the nucleon (minimal volume of the QGP bag) for the CSMM or the GSMM (the GBM). The existence of the finite decay time puts some restriction on the application of hydrodynamic and even kinetic methods to describe such collective λ_n states in A+A collisions.

Indeed, to apply the hydrodynamic description to the λ_n state defined in the local rest frame RF* it is necessary that its decay time τ_n being larger than the typical hydro time $t_H = [\partial_\mu \cdot u^\mu]^{-1}$, i.e. $\tau_n \geq t_H$. In other words, the only λ_n modes which live longer than the hydro expansion rate (u^μ is the 4-vector of hydrodynamic velocity) can be described by relativistic hydrodynamics. Since the volume $V_h = \rho^3 \frac{\partial x_1^*}{\partial \rho} \frac{\partial x_2^*}{\partial \rho} \frac{\partial x_3^*}{\partial \rho}$ here should be understood as the homogeneity volume in the local RF* defined in terms of the spatial derivatives of the local particle (charge) density ρ , one can see that for large n and/or very high gradients $\frac{\partial \rho}{\partial x_i^*}$ the inequality $\tau_n(V_h) \geq t_H$ cannot be fulfilled. The hope that such λ_n states which cannot be described by hydro, but can be described by relativistic Boltzmann equation, is also questionable because there may exist so large n that its decay time $\tau_n = \rho^3 \frac{\partial x_1^*}{\partial \rho} \frac{\partial x_2^*}{\partial \rho} \frac{\partial x_3^*}{\partial \rho} \frac{1}{V_o \pi n T}$ will be shorter than the collision time $t_{Coll} \approx [\sigma \langle v \rangle \rho]^{-1}$ (σ is the typical cross-section of the elastic scattering and $\langle v \rangle$ is the mean thermal velocity of particles in the local RF*) which, according to Bogolyubov classification, does not allow to apply the one-particle kinetic treatment and keep thermodynamic equilibrium. Consequently, if the metastable $\lambda_{n>0}$ states with large n are created in the relativistic A+A collisions, then they can be, in principle, detected via the failure of the hydrodynamic description and/or via the absence of the local thermodynamic equilibrium. In addition, this discussion indicates us the necessity to develop some new microscopic methods to describe the metastable and short-lived collective states at phase equilibrium.

Despite these difficulties the invention of the Laplace-Fourier transform method allows one to

rigorously describe the PTs in the presence of the long-range interaction which leads to the absence of thermodynamic limit. As I discussed in the chapter 2, now such a problem can be reduced to the analysis of a PT in each finite subsystem with nearly constant external field generated by the surrounding subsystems. Of course, the necessary condition for this method is that the whole system under investigation can be divided into the set of subsystems with small gradients of the external long-range field. Such a condition can generate some restrictions on the application of this method, but from the theoretical point of view it is an important step towards the rigorous treatment of PTs in finite systems.

At the moment it is unclear whether with the help of the Laplace-Fourier transform method one can establish the experimental signals of the 2^{nd} order PT in nuclear matter, predicted by a simplified SMM. But, perhaps, the refined theoretical methods can help us in resolving this problem.

The Laplace-Fourier method allowed me to formulate and solve analytically the HDM and find out the upper and lower bounds for the surface partition of large physical clusters consisting from the constituents of finite size. With the help of these exact results it was possible to derive and improve the Fisher parameterization for the surface tension coefficient of large clusters. Also these results clearly showed me that the GBM lacks a very important ingredient – the surface free energy of the QGP bags. An inclusion of the temperature and chemical potential dependent surface tension coefficient into the GBM led to a formulation of a new and more realistic exactly solvable model, the QGBST model, which describes the 1^{st} and 2^{nd} order PTs with the cross-over and demonstrates that for $\tau \leq 2$ the quantum chromodynamics has the tricritical point. This is the third principal results of the present dissertation.

The QGBST model predicts an existence of an additional PT to the deconfinement one at the null line of the surface tension coefficient of the QGP bags (see chapter 4 for details). Perhaps, its unique property, the power-like mass distribution of the QGP bags, at the tricritical point can be verified experimentally. Such a research requires the normalization of the QGBST model onto existing thermodynamic functions obtained by the lattice quantum chromodynamic simulations and its extension to finite systems using the Laplace-Fourier transformation method.

An important feature of the statistical methods developed in the present dissertation is that they are similar for both of PTs discussed here. Thus, the suggested Laplace-Fourier transform method can be a good starting point to create a common theoretical language for the communities which are studying the nuclear liquid-gas PT and the deconfinement PT. Moreover, I believe that the results obtained in this dissertation on the PTs in finite systems along with the hydrokinetic equations derived here are two key elements to build up the microscopic kinetic theory of 1st PTs in finite systems. As I discussed on several occasions in the present work, such a truly microscopic kinetic theory is vitally necessary for several fields. I think that it can be build up in a few years and can be verified experimentally. A similarity and difference of the nuclear liquid-gas and deconfinement PTs can be used to successfully work out such a theory. Thus, the absence of a strong flow in the nuclear multifragmentation experiments is an attractive feature of these experiments which can be used for a detailed justification of the whole concept of the microscopic kinetic theory of 1st PTs in finite systems, which later on can be applied to the more complicated searches for the QGP and deconfinement PT.

The author is cordially thankful to the coauthors, friends and colleagues of the Department of High Energy Densities Physics at the Bogolyubov ITP of National Academy of Sciences of Ukraine whose discussions and remarks were important and fruitful to my research. The special thanks are to the friends of mine Blokhin A. L., Borisenko O. A. and Blaschke D. B., to my former teacher Gorenstein M. I. and to Zinovjev G. M. for their persistent support. The most cordial thanks go to my dear wife Tanya whose permanent care and efficient help in preparing this manuscript were indispensable to me.

Appendices

Appendix A

In the following I would like to study the differences between the linear and the non-linear approximation: the total excluded volumes $v_q = v_q(N_1, N_2)$ of the corresponding partial pressures. In the linear pressure formula (3.46) each component has its own total excluded volume given by

$$v_1^{\text{lin}} \equiv N_1 b_{11} + N_2 \tilde{b}_{21} , \quad v_2^{\text{lin}} \equiv N_1 \tilde{b}_{12} + N_2 b_{22} , \quad (6.19)$$

whereas in the non-linear pressure formula (3.43) there is a *common* total excluded volume for both components

$$v_1^{\text{nl}} = v_2^{\text{nl}} = v^{\text{nl}} \equiv N_1 b_{11} + N_2 b_{22} - \frac{N_1 N_2}{N_1 + N_2} D . \quad (6.20)$$

It can be readily checked that it is either $v_1^{\text{lin}} \leq v^{\text{nl}} \leq v_2^{\text{lin}}$ or $v_1^{\text{lin}} \geq v^{\text{nl}} \geq v_2^{\text{lin}}$, i. e. the pole of the non-linear pressure always lies between both poles of the linear pressure. Hence, there are values N_1, N_2 , where the non-linear pressure is still finite, but the linear pressure formula is yet invalid since one of the partial pressures has already become infinite. Consequently, the domain of the non-linear approximation is larger.

For given V the two domains can be expressed by the limiting densities (3.48) and (3.49), which are defined by the poles $v_q(N_1, N_2) = V$ of the corresponding pressure. In the linear approximation one obtains the expressions

$$\hat{n}_{1,1}^{\text{lin}}(n_2) = \frac{1 - \tilde{b}_{21} n_2}{b_{11}} , \quad \hat{n}_{1,2}^{\text{lin}}(n_2) = \frac{1 - b_{22} n_2}{\tilde{b}_{12}} . \quad (6.21)$$

For given n_2 , therefore, the domain of p^{lin} (3.46) is

$$0 \leq n_1^{\text{lin}} < \min \lambda \{ \hat{n}_{1,1}^{\text{lin}}(n_2), \hat{n}_{1,2}^{\text{lin}}(n_2) \rho \} . \quad (6.22)$$

In the non-linear approximation there is solely one limiting density

$$\hat{n}_1^{\text{nl}}(n_2) = \frac{1 - 2b_{12}n_2 + \sqrt{(1 - 2b_{12}n_2)^2 + 4b_{11}n_2(1 - b_{22}n_2)}}{2b_{11}} . \quad (6.23)$$

Consequently, for given n_2 the domain of p^{nl} (3.43) is

$$0 \leq n_1^{\text{nl}} < \hat{n}_1^{\text{nl}}(n_2) . \quad (6.24)$$

In the non-linear approximation there is furthermore a region where the pressure has negative partial derivatives with respect to the smaller particles' number, $\partial p^{\text{nl}}/\partial N_2 < 0$. The condition $\partial p^{\text{nl}}/\partial N_2 = 0$ defines the boundary of this region

$$\hat{n}_1^{\text{nl, bd}}(n_2) = \frac{1-2(b_{12}-b_{22})n_2 + \sqrt{(1-2(b_{12}-b_{22})n_2)^2 + 8(b_{11}-b_{12})n_2}}{4(b_{11}-b_{12})} . \quad (6.25)$$

For given n_2 a negative derivative $\partial p^{\text{nl}}/\partial N_2 < 0$ occurs only at a density $n_1 > \hat{n}_1^{\text{nl, bd}}$, while the derivative $\partial p^{\text{nl}}/\partial N_1$ is always positive for $R_2 \leq R_1$ as readily checked.

In Fig. 3.3(a) the functions $\hat{n}_1(n_2)$ are presented in *dimensionless* variables $\hat{n}_1 b_{11}$ and $n_2 b_{22}$. The properties of these dimensionless functions depend only on the ratio of the two radii R_2/R_1 . The smaller this ratio is, the higher is the maximum value of \hat{n}_1^{nl} , while the region of negative derivatives $\partial p^{\text{nl}}/\partial N_2$ becomes narrower. The straight line $\hat{n}_{1,1}^{\text{lin}}(n_2)$ starts always at $1/b_{11}$, but its slope decreases for smaller R_2/R_1 , whereas $\hat{n}_{1,2}^{\text{lin}}(n_2)$ ends at $1/b_{22}$ and its slope increases. The pressure of the *separated model* (3.37) would yield one straight line from $n_1 b_{11} = 1$ to $n_2 b_{22} = 1$ in Fig. 3.3(a), for any ratio of the radii R_1 and R_2 .

For very small ratios R_2/R_1 , i. e. for $R_2 \rightarrow 0$, one finds from Eq. (6.20) that $v^{\text{nl}} \rightarrow N_1 b_{11} [1 - \frac{3}{4} N_2 / (N_1 + N_2)]$. This yields the maximum density $\max(\hat{n}_1^{\text{nl}}) = 4/b_{11}$ for $N_2 \gg N_1$. Thus \hat{n}_1^{nl} exceeds the maximum density of the linear approximation or of the corresponding one-component *VdW* gas, $\max(\hat{n}_{1,1}^{\text{lin}}) = \max(n_1^{\text{oc}}) = 1/b_{11}$, by a factor of four in this case.

Note that the value $4/b_{11}$ appears in the linear approximation as well: For $v_2^{\text{lin}} \rightarrow V$ it is $\max(\hat{n}_{1,2}^{\text{lin}}) = 4/b_{11}$ at $n_2 = 0$, but this density cannot be achieved because $p_1^{\text{lin}}(n_1, n_2)$ is infinite for $n_1 \geq 1/b_{11}$.

Let us consider now the consequences of negative derivatives $\partial p^{\text{nl}}/\partial N_2 < 0$ in the non-linear approximation. If a negative $\partial p^{\text{nl}}/\partial N_2$ occurs for a density $n_1' = \text{const.}$ at $n_2 = 0$, the pressure $p^{\text{nl}}(n_1', n_2)$ has a minimum at a certain density $n_{2, \text{min}} > 0$, which is determined by the boundary $\hat{n}_1^{\text{nl, bd}}(n_2)$. For increasing n_1 along the boundary, consequently, the non-linear pressure is always lower than for increasing n_1 at fixed $n_2 = 0$. Hence along the boundary higher densities can be achieved, in particular $n_1 > 1/b_{11}$.

Therefore, exceeding of $n_1^{\text{nl}} = 1/b_{11}$ requires that the boundary starts inside the the non-linear domain at $n_2 = 0$. Thus the condition $\hat{n}_1^{\text{nl, bd}}(0) < 1/b_{11}$ provides the critical radius $R_{2, \text{crit}}$ (3.50),

$$b_{11} < 2b_{12} \quad \rightsquigarrow \quad R_{2, \text{crit}}(R_1) = (\sqrt[3]{4} - 1) R_1 . \quad (6.26)$$

On the other hand the boundary starts at $n_1 = 8/(14b_{11})$ for $R_2 \rightarrow 0$ at $n_2 = 0$, i. e. for any density $b_{11}n_1 \leq 8/14 \approx 1/2$ negative values of $\partial p^{\text{nl}}/\partial N_2$ do not occur for any radii.

Although it is pathological that for *high* densities n_1 the non-linear pressure firstly decreases, if particles of the second and smaller component are added to the system, there is a reasonable explanation for the lowered pressure along the boundary (6.25) for small radii $R_2 < R_{2, \text{crit}}$.

Consider, for instance, $n_1b_{11} = 0.9$ in Fig. 3.3 (a). Since it is $R_2/R_1 = 0.4$, the dimensionless density of the small particles at the boundary $\hat{n}_1^{\text{nl, bd}}(n_2)$ nearly vanishes, $n_2b_{22} \approx 0.05$, whereas the absolute amounts of the small and large particles are about equal. For the excluded volume interaction of the large particles in the pressure formula (3.43), therefore, the influence of the mixed term b_{12} becomes comparable to that of the distinctly larger non-mixed term b_{11} .

For $R_2/R_1 \ll 1$ one obtains $n_2 \gg n_1$ near the boundary at $n_1b_{11} = 0.9$, i. e. the large particles are completely surrounded by the smaller particles and interact mostly with these but hardly with other large particles anymore. In this situation, consequently, the excluded volume interaction of the large particles is governed by the essentially smaller b_{12} and not by $b_{11} \leq 8b_{12}$.

One might interpret this behaviour as an effective attraction between small and large particles, but it is rather a strong reduction of the large particles' excluded volume suppression.

As *VdW* approximations are low density approximations they coincide for these densities, but they evidently become inadequate near the limiting densities: both discussed formulations do evidently not match the real *gas of rigid spheres* there.

For high densities the linear approximation behaves natural, i. e. it is $\partial p^{\text{lin}}/\partial N_q > 0$ always. However, one has to introduce the additional terms \tilde{b}_{12} and \tilde{b}_{21} . For the choice (3.47) these terms provide a one-component-like behaviour in the limits $R_2 = R_1$ and $R_2 = 0$, but they have no concrete physical meaning.

In the non-linear approximation there occur pathologic pressure derivatives $\partial p^{\text{nl}}/\partial N_2 < 0$ for $R_2 \ll R_1$. However, the non-linear formulae may be used for special purposes, e. g. for $n_1 > 1/b_{11}$

at intermediate $n_2 b_{22}$, where the linear approximation is yet invalid.

The non-linear enhancement in the GCE or the occurrence of negative values for $\partial p^{\text{nl}}/\partial N_q$ in the CE suggest a further investigation concerning the thermodynamical stability of the non-linear approximation.

One can readily check that in the CE it is $\partial p^{\text{nl}}/\partial V < 0$ generally, so there is no *mechanical* instability. To investigate whether there is a *chemical* instability [176] it is necessary to study partial derivatives with respect to the particle numbers, $\partial/\partial N_q$, of the *chemical potentials*

$$\mu_p(T, V, N_1, N_2) \equiv -T \frac{\partial}{\partial N_p} \ln[Z(T, V, N_1, N_2)] . \quad (6.27)$$

Partial derivatives of the *pressure* with respect to the particle numbers $\partial p/\partial N_q$ have no relevance here.

For the examination of chemical stability it is appropriate to switch from the *free energy* of the CE, $F(T, V, N_1, N_2) \equiv -T \ln[Z(T, V, N_1, N_2)]$, to the *Gibbs free energy* or *free enthalpie*

$$G(T, p, N_1, N_2) \equiv F + pV = \mu_1 N_1 + \mu_2 N_2 , \quad (6.28)$$

where $\mu_q(T, p, N_1, N_2) \equiv \partial G/\partial N_q$. This requires that $p(T, V, N_1, N_2)$ can be solved for $V(T, p, N_1, N_2)$, which is the case for the non-linear approximation,

$$V^{\text{nl}}(T, p, N_1, N_2) = \frac{N_1 + N_2}{p/T} + N_1 b_{11} + N_2 b_{22} - \frac{N_1 N_2}{N_1 + N_2} D .$$

Further it is useful to introduce the molar free enthalpie $g \equiv G/(N_1 + N_2) = g(T, p, x_1)$ with the molar fractions $x_1 \equiv N_1/(N_1 + N_2)$ and $(1 - x_1) = x_2 \equiv N_2/(N_1 + N_2)$ of component 1 and 2, respectively. Then the chemical stability of a binary mixture [176] corresponds to the condition

$$\frac{\partial^2}{\partial x_1^2} g(T, p, x_1) = \frac{\partial \mu_1(T, p, x_1)}{\partial x_1} - \frac{\partial \mu_2(T, p, x_1)}{\partial x_1} > 0 . \quad (6.29)$$

For the non-linear approximation one obtains

$$\begin{aligned} g^{\text{nl}}(T, p, x_1) &= x_1 \lambda \{ T \ln \lambda \left[\frac{x_1}{\phi_1} \frac{p}{T} \rho \right] + p \lambda (b_{11} - (1 - x_1)^2 D \rho) \rho \} \\ &+ (1 - x_1) \lambda \{ T \ln \lambda \left[\frac{1 - x_1}{\phi_2} \frac{p}{T} \rho \right] + p \lambda (b_{22} - x_1^2 D \rho) \rho \} , \end{aligned} \quad (6.30)$$

and thus condition (6.29) is satisfied:

$$\frac{\partial^2}{\partial x_1^2} g^{\text{nl}}(T, p, x_1) = \frac{T}{x_1} + \frac{T}{1 - x_1} + p 2D > 0 . \quad (6.31)$$

Therefore, the system described by the non-linear approximation is thermodynamically stable – despite the pathologic behaviour in special cases. Due to the equivalence of the thermodynamical ensembles this is true for any representation of the model.

Appendix B

In order to study the high pressure limit it is necessary to find out the excluded volume of two ellipsoids which are obtained by the Lorentz contraction of the spheres. This is rather involved problem. Fortunately, the analysis below requires to know only the ultrarelativistic limit when the mean energy per particle is very high compared to the mass of particle. The problem can be simplified further since it is sufficient to find an analytical expression for the relativistic excluded volume the collinear particle velocities because the configurations with the noncollinear velocities have larger excluded volume and, hence, are suppressed. Therefore, one can safely consider the excluded volume produced by two contracted cylinders (disks) having the same eigen volumes as the ellipsoids. For this purpose the cylinder's height in the local rest frame is fixed to be $\frac{4}{3}$ of a sphere radius.

Let me introduce the different radii R_1 and R_2 for the cylinders, and consider a zero height for the second cylinder $h_2 = 0$ and non-zero height h_1 for the first one. Suppose that the center of the coordinate system coincides with the geometrical center of the first cylinder and the OZ -axis is perpendicular to the cylinder's base. Then the angle Θ_v between the particle velocities is also the angle between the bases two cylinders. To simplify the expression for pressure the Lorentz frame is chosen to be the rest frame of the whole system.

In order to estimate the excluded volume one should fix the particle velocities and translate the second cylinder around the first one keeping the angle Θ_v fixed. The desired excluded volume is obtained as the volume occupied by the center of the second cylinder under these transformations. Considering the projection on the XOY plane (see the panel a) of Fig. 6.9), one should transform the ellips of the radii $R_x = R_2 \cos(\Theta_v)$ and $R_y = R_2$ around the circle of radius R_1 . We approximate it by the circle of the averaged radius of the ellips $\langle R_{XOY} \rangle = R_1 + (R_x + R_y)/2 = R_1 + R_2(1 + \cos(\Theta_v))/2$. Then the first contribution to the excluded volume is the volume of the cylinder of

the radius $\langle R_{XOY} \rangle$ and the height $h_1 = CC_1$ of the cylinder $OABC$ in the panels .a) and b) of Fig. 6.9), i.e.,

$$v_I(h_1) = \pi \left(R_1 + \frac{R_2(1 + \cos(\Theta_v))}{2} \right)^2 h_1 . \quad (6.32)$$

Projecting the picture onto the XOZ plane as it is shown in the pabel b) of Fig. 6.9, one finds that the translations of a zero width disk over the upper and lower bases of the first cylinder (the distance between the center of the disk and the base CA is, evidently, $CD_1 = R_2 |\sin(\Theta_v)|$) generate the second conrtibution to the excluded volume

$$v_{II}(h_1) = \pi R_1^2 2 R_2 |\sin(\Theta_v)| . \quad (6.33)$$

The last contribution follows from the translation of the disk from the cylinder's base to the cylinder's side as it is shown for the YOZ plane in the panel c) of Fig.6.9. The area BB_1F is the part of the ellips segment which magnitude depends on the x-coordinate. However, one can approximate it as the quarter of the disk area projected onto the YOZ plane and can get a simple answer $\pi R_2^2 |\sin(\Theta_v)|/4$. Since there are four of such transformations and one has to consider them for all x-coordinates of the first cylinder (the length is $2 R_1$), then one finds the third contribution as follows

$$v_{III}(h_1) = \pi R_1^2 2 R_1 |\sin(\Theta_v)| . \quad (6.34)$$

Collecting all the contributions, one obtains the excluded volume for the two cylinders of zero and non-zero heights

$$v_{2c}(h_1) = \pi \left(R_1 + R_2 \cos^2 \left(\frac{\Theta_v}{2} \right) \right)^2 h_1 + 2 \pi R_1 R_2 (R_1 + R_2) |\sin(\Theta_v)| . \quad (6.35)$$

The above equation, evidently, gives an exact result for a zero angle and arbitrary height of the first cylinder. Comparing it with the exact answer for $\Theta_v = \frac{\pi}{2}$

$$v_{2c}^E \left(h_1, \Theta_v = \frac{\pi}{2} \right) = R_1 (\pi R_1 + 4 R_2) h_1 + 2 \pi R_1 R_2 (R_1 + R_2) , \quad (6.36)$$

one finds that the dominant terms (the second terms in (6.35) and (6.36)) again are exact, whereas the corresponding corrections which are proportional to h_1 are related to each other as $\frac{28.27}{28.56} \approx 0.9897$ (approximated to exact and for $R_2 = R_1$). Therefore, Eq. (6.35) also gives a good approximation for the intermediate angles and small heights.

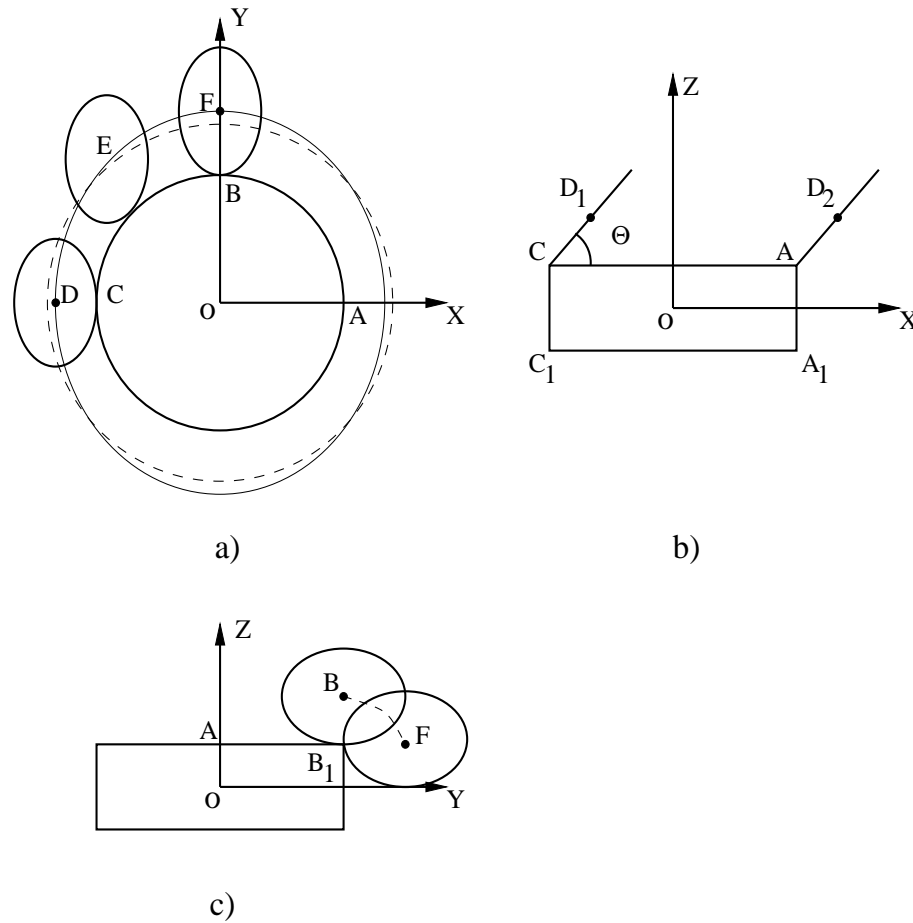


Figure 6.9. Relativistic excluded volume derivation for relativistic cylinder $OABC$ and ultrarelativistic cylinder (disk) DC with radii R_1 and R_2 , respectively. Θ is the angle between their velocities. Pictures a - c show the projections onto different planes. The transformation of the cylinder DC around the side of the cylinder $OABC$ is depicted in Fig. 3.a. The solid curve DEF corresponds to the exact result, whereas the dashed curve corresponds to the average radius approximation $\langle R_{XOY} \rangle = OA + (DC + BF)/2 = R_1 + R_2(1 + \cos(\Theta))/2$.

The transformation of the cylinder $DC = DC_1 = AD_2$ along the upper base of the cylinder $OABC = ACC_1A_1$ is shown in panel b. Its contribution to the excluded volume is a volume of the cylinder with the base $AC = 2R_1$ and the height $CD_1 \sin(\Theta) = R_2 \sin(\Theta)$. A similar contribution corresponds to the disk transformation along the lower base of the cylinder A_1C_1 .

The third contribution to the relativistic excluded volume arises from the transformation of the cylinder $DC = BB_1 = FB_1$ from the upper base of the cylinder $OABC = AB_1O$ to its side, and it is schematically shown in Fig. 3.c. The area $BB_1F \approx \pi/4R_2^2 \sin(\Theta)$ is approximated as the one quarter of the area of the ellipse BB_1 .

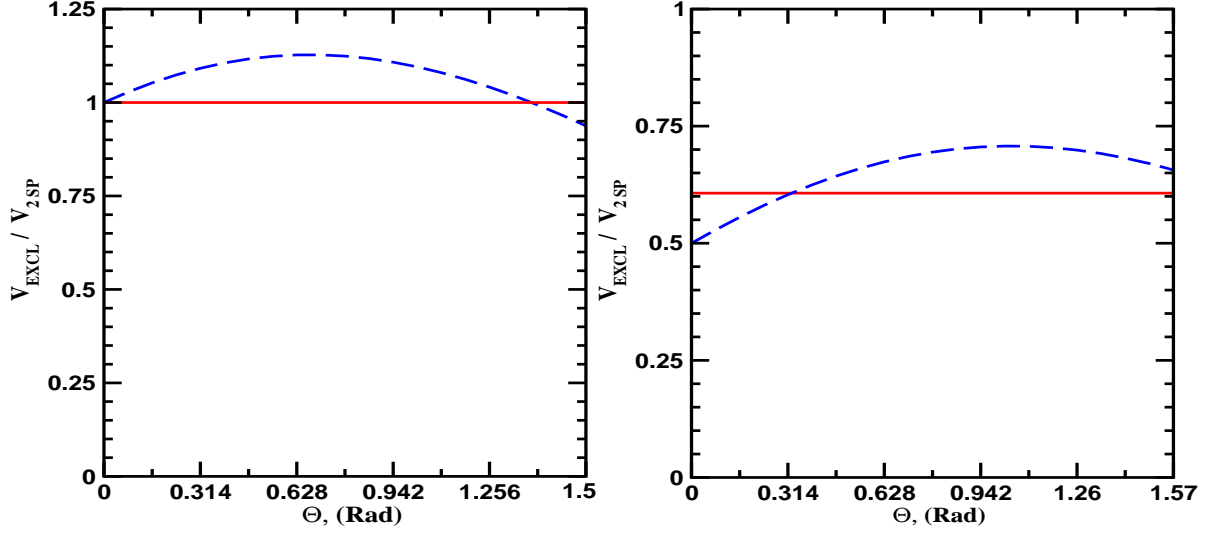


Figure 6.10. Comparison of the relativistic excluded volume obtained by the approximative ultra-relativistic formula with the exact results. The left panel shows the quality of the approximation $V_{EXCL} \equiv v^{Urel}(R, R)$ (6.38) to describe the excluded volume of two nonrelativistic spheres V_{2SP} of same radius R as a function of the spherical angle Θ , whereas the right panel depicts the approximation to the excluded volume of the nonrelativistic sphere and disk. In both panels the solid curve corresponds to the exact result and the long dashed one corresponds to the ultrarelativistic approximation by two cylinders. The averaged ultrarelativistic excluded volume in the left panel is $\frac{\langle V_{EXCL} \rangle_{\Theta}}{V_{2SP}} \approx 1.065$. The corresponding averaged value for the right panel is $\frac{\langle V_{EXCL} \rangle_{\Theta}}{V_{2SP}} \approx 0.655$, which should be compared with the exact value $\frac{\langle V_{EXCL} \rangle_{\Theta}}{V_{2SP}} \approx 0.607$.

In order to get an expression for the non-zero heights of the second cylinder I note that the answer should be symmetric under the permutation of indexes 1 and 2. The lowest order correction in powers of the height comes from the contribution $v_I(h_1)$. Adding the symmetric contribution $v_I(h_2)$ to $v_{2c}(h_1)$ (6.35), one obtains the full answer

$$\begin{aligned}
 v_{2c}(h_1, h_2) &= \pi \left(R_1 + R_2 \cos^2 \left(\frac{\Theta_v}{2} \right) \right)^2 h_1 + \pi \left(R_2 + R_1 \cos^2 \left(\frac{\Theta_v}{2} \right) \right)^2 h_2 \\
 &+ 2 \pi R_1 R_2 (R_1 + R_2) \sin(\Theta_v) .
 \end{aligned} \tag{6.37}$$

The above expression gives an exact result for a zero angle and arbitrary heights of cylinders. It also gives nearly exact answer for $\Theta_v = \frac{\pi}{2}$ in either limit h_1 or $h_2 \rightarrow 0$.

Choosing the heights to reproduce the proper volume of each of the Lorentz contracted spheres,

one gets an approximation for the excluded volume of contracted spheres in ultrarelativistic limit

$$v^{Urel}(R_1, R_2) = \frac{4}{3}\pi \frac{R_1}{\gamma_1} \left(R_1 + R_2 \cos^2 \left(\frac{\Theta_v}{2} \right) \right)^2 + \frac{4}{3}\pi \frac{R_2}{\gamma_2} \left(R_2 + R_1 \cos^2 \left(\frac{\Theta_v}{2} \right) \right)^2 + 2\pi R_1 R_2 (R_1 + R_2) \sin(\Theta_v) . \quad (6.38)$$

The corresponding γ_q -factors ($\gamma_q \equiv E(\mathbf{k}_q)/m_q$, $q = \{1, 2\}$) are defined in the local rest frame of the whole system for particles of mass m_q . The last result is valid for $0 \leq \Theta_v \leq \frac{\pi}{2}$, to use it for $\frac{\pi}{2} \leq \Theta_v \leq \pi$ one has to replace $\Theta_v \rightarrow \pi - \Theta_v$ in it.

It is necessary to mention that the above formula gives a surprisingly good approximation even in nonrelativistic limit for the excluded volume of two spheres. For $R_2 = R_1 \equiv R$ one finds that the maximal excluded volume corresponds to the angle $\Theta_v = \frac{\pi}{4}$ and its value is $\max\{v^{Urel}(R, R)\} \approx \frac{36}{3}\pi R^3$, whereas an exact result for nonrelativistic spheres is $v_{2s} = \frac{32}{3}\pi R^3$, i.e., the ultrarelativistic formula (6.38) describes a nonrelativistic situation with the maximal deviation of about 10% (see the left panel in Fig. 6.10).

Eq. (6.38) also describes the excluded volume $v_{sd} = \frac{10+3\pi}{3}R^3$ for a nonrelativistic sphere and ultrarelativistic ellipsoid with the maximal deviation from the exact result of about 15% (see the right panel in Fig. 6.10).

In order to improve its accuracy for the nonrelativistic case, I introduce a factor α to normalize the integral of the excluded volume (6.38) over the whole solid angle to the volume of two spheres

$$v^{Nrel}(R_1, R_2) = \alpha v^{Urel}(R_1, R_2); \quad \alpha = \frac{4\pi (R_1 + R_2)^3}{3 \int_0^\pi d\Theta_v \sin(\Theta_v) v^{Urel}(R_1, R_2) \Big|_{\gamma_1=\gamma_2=1}} . \quad (6.39)$$

For equal hard core radii and equal masses of particles the normalization factor reduces to the following value $\alpha \approx \frac{1}{1.0654}$, i.e., it compensates the most of the deviations discussed above. With such a correction the excluded volume (6.39) can be safely used for the nonrelativistic domain because in this case the VdW excluded volume effect is itself a correction to the ideal gas and, therefore, the remaining deviation (less than 1.7 % for the whole available range of parameters) from the exact result is of higher order.

It is useful to have the relativistic excluded volume expressed in terms of 3-momenta

$$\begin{aligned}
v^{Urel}(R_1, R_2) &= \frac{v_{01}}{\gamma_1} \left(1 + R_2 \frac{|\mathbf{k}_1||\mathbf{k}_2| + |\mathbf{k}_1 \cdot \mathbf{k}_2|}{2 R_1 |\mathbf{k}_1||\mathbf{k}_2|} \right)^2 + \frac{v_{02}}{\gamma_1} \left(1 + R_1 \frac{|\mathbf{k}_1||\mathbf{k}_2| + |\mathbf{k}_1 \cdot \mathbf{k}_2|}{2 R_2 |\mathbf{k}_1||\mathbf{k}_2|} \right)^2 \\
&+ 2 \pi R_1 R_2 (R_1 + R_2) \frac{|\mathbf{k}_1 \times \mathbf{k}_2|}{|\mathbf{k}_1||\mathbf{k}_2|}, \tag{6.40}
\end{aligned}$$

where v_{0q} denote the corresponding eigen volumes $v_{0q} = \frac{4}{3}\pi R_i^3$, $q = \{1, 2\}$.

For the practical calculations it is necessary to express the relativistic excluded volume in terms of the three 4-vectors - the two 4-momenta of particles, $k_{q\mu}$, and the collective 4-velocity $u^\mu = \frac{1}{\sqrt{1-\mathbf{v}^2}}(1, \mathbf{v})$. For this purpose one should reexpress the gamma-factors and at least one of trigonometric functions in (6.38) in a covariant form

$$\gamma_q = \frac{\sqrt{m^2 + \mathbf{k}_q^2}}{m} = \frac{k_q^\mu u_\mu}{m}, \quad \cos(\Theta_v) = \frac{k_1^\mu u_\mu k_2^\nu u_\nu - k_1^\mu k_{2\mu}}{\sqrt{((k_1^\mu u_\mu)^2 - m^2)((k_2^\mu u_\mu)^2 - m^2)}}. \tag{6.41}$$

Using Eq. (6.41), one can express any trigonometric function of Θ_v in a covariant form.

THE LIST OF USED SOURCES

- [1] Weisskopf V. Statistics and nuclear reactions // Phys. Rev. 1937. Vol. 52, N 4, P.295-303.
- [2] Pochadzalla J. et. al. Probing the nuclear liquid - gas phase transition // Phys. Rev. Lett. 1995. Vol. 75, N6. P. 1040-1043.
- [3] Hauger J.A. et. al. Two-stage multifragmentation of 1A GeV Kr, La, and Au. // Phys. Rev. C. 2000. Vol. 62, N 024616, P. 1-14.
- [4] Kwiatkowski K. et. al. Heating nuclear matter with GeV He-3 beams // Phys. Lett. B. 1998. Vol. 423, N 1-2, P. 21-26.
- [5] Morley K.B. et. al. 4 pi studies of the 1.8-GeV - 4.8-GeV He-3 + Ag (nat), Au-197 reactions: 1. Energy deposition // Phys. Rev. C. 1996. Vol. 54, N 2, P. 737-748.
- [6] Natowitz J.B. et. al. Caloric Curves and Critical Behavior in Nuclei // Phys. Rev. C. 2002. Vol. 65, N 034618, P. 1-9.
- [7] Bonche P., Levit S., Vautherin H. Properties of highly excited nuclei //Nucl. Phys. A. 1984. Vol. 427, N 2, P. 278-296.
- [8] Bondorf J.P. et. al. Statistical multifragmentation of nuclei: (I). Formulation of the model // Nucl. Phys. A. 1985. Vol. 443, N 2, P. 321-347.
- [9] Stöcker H., Greiner W. High-Energy Heavy Ion Collisions: Probing the Equation of State of Highly Excited Hadronic Matter// Phys. Rep. 1986. Vol. 137, N5-6, P.227-392.
- [10] Walecka J.D. A theory of highly condensed matter //Ann. Phys. 1974. Vol. 83, N 2, P.491-529.
- [11] Serot B.D., Walecka J.D. Properties of finite nuclei in a relativistic quantum field theory.//Phys. Lett. B. 1979. Vol. 87, N 3, P.172-176.

- [12] Jaqaman H. et al. Nuclear Condensation // Phys. Rev. C. 1983. Vol. 27, N 6, P.2782-2791.
- [13] Jaqaman H. et al. Liquid-gas phase transitions in finite nuclear matter // Phys. Rev. C. 1984. Vol. 29, N 6, P.2067-2074.
- [14] Goodman A.L. et al. Liquid-gas phase instabilities and droplet formation in nuclear reactions // Phys. Rev. C. 1984. Vol. 30, N 3, P.851-865.
- [15] Bonche P., Levit S., Vautherin D. Statistical properties and stability of hot nuclei // Nucl. Phys. A. 1985. Vol. 436, N 2, P.265-293.
- [16] Levit S., Bonche P. Coulomb instability in hot compound nuclei approaching liquid-gas transition // Nucl. Phys. A. 1985. Vol. 437, N 2, P.426-442.
- [17] Glendenning N.K., Csernai L.P., Kapusta J.I. Liquid-gas phase separation in nuclear collisions // Phys. Rev. C. 1986. Vol. 33, N 4, P.1299-1302.
- [18] Muller H., Serot B.D. Phase transitions in warm, asymmetric nuclear matter // Phys. Rev. C. 1995. Vol. 52, N 4, P.2072-2091.
- [19] Bauer W., Dean D.R., Mosel U., Post U. New approach to fragmentation reactions: The nuclear lattice model // Phys. Lett. B. 1985. Vol. 150, N 1-3, P.53-56.
- [20] Campi X. Signals of a phase transition in nuclear multifragmentation // Phys. Lett. B. 1988. Vol. 208, N 3-4, P.351-354.
- [21] Bauer W. Extraction of signals of a phase transition from nuclear multifragmentation // Phys. Rev. C. 1988. Vol. 38, N 3, P.1297-1303.
- [22] Phair L. et al. Multifragment emission in $^{36}\text{Ar}+^{197}\text{Au}$ and $^{129}\text{Xe}+^{197}\text{Au}$ collisions. Percolation model // Phys. Lett. B. 1992. Vol. 285, N 2, P.10-14.
- [23] Phair L., Bauer W., Gelbke C.K. Percolation with bubbles and toroids // Phys. Lett. B. 1993. Vol. 314, N 3-4, P.271-274.

- [24] Li T. et al. Mass dependence of critical behavior in nucleus-nucleus collisions // Phys. Rev. C. 1994. Vol. 49, N 3, P.1630-1634.
- [25] Elliott J.B. et al. Extraction of critical exponents from very small percolation lattices // Phys. Rev. C. 1994. Vol. 49, N 6, P.3185-3191.
- [26] Pan J., Das Gupta S. A schematic model for fragmentation and phase transition in nuclear collisions // Phys. Lett. B. 1995. Vol. 344, N 1-4 P.29-34.
- [27] Pan J., Das Gupta S. Unified description for the nuclear equation of state and fragmentation in heavy-ion collisions // Phys. Rev. C. 1995. Vol. 51, N3, P.1384-1392.
- [28] Bauer W., Botvina A. Pre-equilibrium particle emission, and critical exponent analysis// Phys. Rev. C. 1995. Vol. 52, N 5, P.R1760-R1763.
- [29] Das Gupta S., Pan J. Lattice gas model for fragmentation: From argon on scandium to gold on gold// Phys. Rev. C. 1996. Vol. 53, N 3, P.1319-1324.
- [30] Gulminelli F., Chomaz Ph. Critical Behavior in the Coexistence Region of Finite Systems // Phys. Rev. Lett. 1999. Vol. 82, N 7, P.1402-1405.
- [31] Carmona J.M. et al. Finite size effects and the order of a phase transition in fragmenting nuclear systems// Phys. Rev. C. 2000. Vol. 61, N 3, P.037304-1-037304-4.
- [32] Gulminelli F. et al. Scaling in the lattice gas model// Phys. Rev. C. 2002. Vol. 65, N5, P.051601-1-051601-4.
- [33] Latora V. et al. Dynamics of Instabilities and Intermittency // Phys. Rev. Lett. 1994. Vol. 73, N 13, P.1765-1768.
- [34] Pratt S. Balancing nuclear matter between liquid and gas // Phys. Lett. B. 1995. Vol. 349, N 3, P.261-266.
- [35] Belkacem M. et al. Critical evolution of a finite system // Phys. Rev. C. 1995. Vol. 52, N 1, P.271-285.

- [36] Finocchiaro P. et al. Second order phase transitions: From infinite to finite systems// Nucl. Phys. A. 1996. Vol. 600, N 2, P.236-250.
- [37] Dorso C.O., Strachan A. Onset of fragment formation in periodic expanding systems // Phys. Rev. B, 1996. Vol. 54, N 1, P.236-243.
- [38] Kondratyev V.N., Lutz H.O., Ayik S. Critical evolution of hot van der Waals droplets // J. Chem. Phys. 1997. Vol. 106, N 18, P.7766-7776.
- [39] Strachan A., Dorso C.O. Temperature and energy partition in fragmentation // Phys. Rev. C. 1999. Vol. 59, N 1, P.285-294.
- [40] Ma Y.G. Cluster emission and phase transition behaviours in nuclear disassembly//J. Phys. G. 2001. Vol. 27, N 12, P.2455-2470.
- [41] Gulminelli F. et al. Scaling in the lattice gas model // Phys. Rev. C. 2002. Vol. 65, N 5, P.051601-1-051601-4.
- [42] Balenzuela P. et al. Time Dependence of Critical Behavior in Multifragmentation//Phys. Rev. C. 2002. Vol. 66, N 2, P.024613-1-024613-6.
- [43] Moretto L.G., Elliott J.B., Phair L. Compound nuclear decay and the liquid to vapor phase transition: A Physical picture// Phys. Rev. C. 2005. Vol. 72, N 6, P.064605-1-064605-6.
- [44] Fisher M.E. Theory of condensation and critical point // Physics. 1967. Vol. 3, N 5, P.255-283.
- [45] Moretto L.G. et al. Reducibility and thermal scaling in multifragmentation// Phys. Rep. 1997. Vol. 287, N 3, P.249-336.
- [46] Bondorf J.P. et al. Statistical multifragmentation of nuclei// Phys. Rep. 1995. Vol. 257, N 3, P.133-221.
- [47] Gorenstein M.I., Rischke D.H., Stöcker H., Greiner W., Bugaev K.A. A self-consistent equation of state for nuclear matter//J. Phys. G. 1993. Vol. 19, N 4, P.L69-75.

- [48] Bugaev K.A., Gorenstein M.I., Mishustin I.N., Greiner W. Exactly Soluble Model for Nuclear Liquid-Gas Phase Transition// Phys. Rev. C. 2000. Vol. 62, N 4, P.044320-1–044320-7;
- [49] Bugaev K.A., Gorenstein M.I., Mishustin I. N., Greiner W. Exact Solution of the Statistical Multifragmentation Model and Liquid–Gas Phase Transition in Nuclear Matter / “Nucleus-Nucleus Collisions”, Proceedings of the conference “*Structure of the Nucleus at the Dawn of the Century*”, Bologna, Italy, May 29 - June 3, 2000. Edited by Bonsignori G. C., Bruno M., Ventura A., Vretenar D. and Zichichi A. World Scientific Pub. Co. Inc. 2001. P. 285-292.
- [50] Bugaev K.A., Gorenstein M.I., Mishustin I.N., Greiner W. Statistical Multifragmentation in Thermodynamic Limit// Phys. Lett. B. 2001. Vol. 498, N3-4, P.144-148.
- [51] Bugaev K.A., Gorenstein M.I., Mishustin I.N., Greiner W. Exactly Soluble Model for Nuclear Liquid-Gas Phase Transition. Book of abstracts of the conference “*Nucleus Nucleus Collisions 2000*”, Strasbourg, France, July 3-7, 2000, AI.
- [52] Bugaev K.A., Gorenstein M.I., Mishustin I.N., Greiner W. Statistical Multifragmentation in Thermodynamical Limit: Exact Solution for Phase Transitions / “Exploring Quark Matter”, Proceedings of the conference “*Quark Matter in Astro- and Particle Physics*”, Rostock, November 27–29, 2000. Edited by G. Burau R.G., Blaschke D.B. and Schmidt S.M. Rostock University, Germany, March 2001, 185–199.
- [53] Das Gupta S., Mekjian A.Z. Phase transition in a statistical model for nuclear multifragmentation //Phys. Rev. C. 1998. Vol. 57, N 3, P.1361-1365.
- [54] Das Gupta S., Majumder A., Pratt S., Mekjian A. A soluble statistical model for nuclear fragmentation// arXiv:nucl-th/9903007.
- [55] Pathria R.K. “Statistical Mechanics”, Pergamon Press, 1972, Oxford.
- [56] Reuter P.T., Bugaev K.A. Critical Exponents of the Statistical Multifragmentation Model// Phys. Lett. B. 2001. Vol. 517, N 1-2, P.233-238.

- [57] Bugaev K.A., Reuter P.T. Critical Indices of the Statistical Multifragmentation Model / Book of abstracts of the conference “*INPC2001*” Berkeley, California, USA, July 30 – August 3, 2001, p.279.
- [58] Elliott J.B., Bugaev K.A., Moretto L.G., Phair L. Yield Scalings of Clusters with Fewer than 100 Nucleons / arXiv:nucl-ex/0608022 (2006) 36 p.
- [59] Glendenning N.K. Equation of state from nuclear and astrophysical evidence // Phys. Rev. C. 1988. Vol. 37, N 6, P.2733-2743.
- [60] Blaizot J.P. Nuclear compressibilities // Phys. Rep. 1980. Vol. 64, N 4, P.171-248.
- [61] Treiner J., Krivine H., Bohigas O., Martorell J. Nuclear incompressibility: From finite nuclei to nuclear matter // Nucl. Phys. A. 1981. Vol. 371, N 2, P.253-287
- [62] Danielewicz P., Lacey R., Lynch W.G. Determination of the equation of state of dense matter// Science 2002. Vol. 298, N 5598, P.1592-1596.
- [63] Danielewicz P., Nuclear Equation of State: Picture from Medium Energy Heavy Ion Collisions, arXiv:nucl-exp/0512009 (2005) 7p.
- [64] Boguta J., Bodmer A.R. Relativistic Calculation of Nuclear Matter and the Nuclear Surface //Nucl. Phys. A. 1977. Vol. 292, N 3, P.413-428.
- [65] Friedman B., Pandharipande V.R. Hot and cold, nuclear and neutron matter//Nucl. Phys. A. 1981. Vol. 361, N 2, P.502-520.
- [66] Stöcker H., Greiner W., Scheid W. Dependence of particle production in high-energy heavy ion collisions on the nuclear equation of state //Z. Phys. A. 1978. Vol. 286, N 1, P.121-122.
- [67] Bugaev K.A., Gorenstein M.I. Thermodynamically self-consistent class of nuclear matter EOS and compression shocks in relativistic nuclear collisions//Z. Phys. C. 1989. Vol. 43, N 2, P.261-265.
- [68] Hugenholtz N.M., van Hove L. A theorem on the single particle energy in a Fermi gas with interaction // Physica 1958. Vol. 24, N 1-5, P.363-376.

- [69] Weisskopf V.F. The problem of an effective mass in nuclear matter // Nucl. Phys. 1957. Vol. 3, N 3, P.423-432.
- [70] Boguta J., Stöcker H. Systematics of nuclear matter properties in a non-linear relativistic field theory // Phys. Lett. B. 1983. Vol. 120, N 4-6, P.289-293.
- [71] Waldhauser B.M., Maruhn J.A., Stöcker H., Greiner W. Nuclear equation of state from the nonlinear relativistic mean field theory// Phys. Rev. C. 1988. Vol. 38, N 2, P.1003-1009.
- [72] Rischke D.H., Friman B.L., Stöcker H., Greiner W. Phase transition from hadron gas to quark gluon plasma : influence of the stiffness of the nuclear equation of state // J. Phys. G. 1988. Vol. 14, N 2, P. 191-204.
- [73] Zimanyi J., Lukacs B., Levai J., Bondorf J., Balazs N.L. An interpretable family of equations of state for dense hadronic matter// Nucl. Phys. A. 1988. Vol. 484, N 3-4, P.647-660.
- [74] Yang C.N., Yang C.P. Critical Point in Liquid-Gas Transitions //Phys. Rev. Lett. 1964. Vol. 13, N 9, P.303-305.
- [75] Fisher M.E., Felderhof B.U. Phase transitions in one-dimensional cluster-interaction fluids. IB. Critical behavior //Ann. of Phys. 1970. Vol. 58, N 1, P. 217-267.
- [76] Fisher M.E. Correlation functions and the critical region of simple fluids // J. Math. Phys. 1964. Vol. 5, N 7, P.944-962.
- [77] Griffiths R.B. Ferromagnets and simple fluids near critical point - some thermodynamic inequalities // J. Chem. Phys. 1965. Vol. 43, N 6, P.1958-1968.
- [78] Liberman D.A. Another relation between thermodynamic functions near the critical point of a simple fluid // J. Chem. Phys. 1966. Vol. 44, N 1, P.419-420.
- [79] Gilkes M.L. et al. Determination of critical exponents from the multifragmentation of gold nuclei // Phys. Rev. Lett. 1994. Vol. 73, N 12, P.1590-1593.
- [80] Bauer W., Friedman W.A. Nuclear multifragmentation critical exponents// Phys. Rev. Lett. 1995. Vol. 75, N , P. 767-767.

- [81] Huang K. *Statistical Mechanics*, J. Wiley, New York, 1987.
- [82] Guida R., Zinn-Justin J. Critical exponents of the N-vector model // J. Phys. A. 1998. Vol. 31, N 40, P.8103-8121.
- [83] Elliott J.B., Hirsch A.S. Standard thermodynamic quantities as determined via models of nuclear multifragmentation // Phys. Rev. C. 2000. Vol. 61, N 5, P.054605-1–054605-17.
- [84] Beaulieu L. et al. Thermal excitation of heavy nuclei with 5-15 - GeV/c anti-proton, proton and pion beams//Phys. Lett. B. 1999. Vol. 463, N 2-4, P.159-167.
- [85] Elliott J.B. et al. (The EOS Collaboration) Statistical signatures of critical behavior in small systems // Phys. Rev. C. 2000. Vol. 62, N 6, P.064603-1–064603-33.
- [86] Karnaukhov V.A. et al. Critical temperature for the nuclear liquid-gas phase transition //Phys. Rev. C. 2003. Vol. 67, N 1, P.011601R-1–011601R-4.
- [87] Buyukcizmeci N., Ogul R., Botvina A.S. Isospin and symmetry energy effects on nuclear fragment production in liquid-gas type phase transition region. //Eur. Phys. J. A. 2005. Vol.25, N 1, P.57-64.
- [88] Schmidt M. et al. Negative Heat Capacity for a Cluster of 147 Sodium Atoms// Phys. Rev. Lett. 2001. Vol. 86, N 7, P.1191-1194.
- [89] D'Agostino M. et al. Negative heat capacity in the critical region of nuclear fragmentation: an experimental evidence of the liquid-gas phase transition // Phys. Lett. B. 2000. Vol. 473, N 3, P.219-225.
- [90] Elliott J.B. et al. The Liquid to vapor phase transition in excited nuclei// Phys. Rev. Lett. 2002. Vol. 88, N 4, P.042701-1–042701-4.
- [91] Lee T.D., Yang C.N. Statistical theory of equations of state and phase transitions. 1. Theory of condensation//Phys. Rev. 1952. Vol. 87, N 3, P.404-409.
- [92] Lee T.D., Yang C.N. Statistical theory of equations of state and phase transitions. II. Lattice gas and ising model //Phys. Rev. 1952. Vol. 87, N 3, P.410-419.

- [93] Chomaz Ph., Gulminelli F. First-order phase transitions: equivalence between bimodalities and the Yang-Lee theorem // *Physica A*. 2003. Vol. 330, N 3-4, P.451-458.
- [94] Hill T.L. *Thermodynamics of Small Systems*// Dover Publications, New York., 1994.
- [95] Gross D.H.E. Microcanonical thermodynamics and statistical fragmentation of dissipative systems. The topological structure of the N-body phase space // *Phys. Rep.* 1997. Vol. 279, N 3-4, P.119-201.
- [96] Chomaz P., Colonna M., Randrup J. Nuclear spinodal fragmentation // *Phys. Rep.* 2004. Vol. 389, N 5-6, P.263-440.
- [97] Gulminelli F. et al. Critical Behavior in the Coexistence Region of Finite Systems // *Phys. Rev. Lett.* 1999. Vol. 82, N 7, P.1402-1405.
- [98] D'Agostino M. et al. Negative heat capacity in the critical region of nuclear fragmentation: An Experimental evidence of the liquid gas phase transition// *Phys. Lett. B*. 2000. Vol. 473, N3-4, P.219-225.
- [99] Chomaz Ph., Gulminelli F., Duflot V. Topology of event distributions as a generalized definition of phase transitions in finite systems // *Phys. Rev. E*. 2001. Vol. 64, N 4, P.046114-1–046114-4.
- [100] Moretto L.G. et al. Negative heat capacities and first order phase transitions in nuclei // *Phys. Rev. C*. 2002. Vol. 66, N 4, P.041601(R)-1–041601-5.
- [101] Moretto L.G., Elliott J.B., Phair L.W. “**Mesoscopy and Thermodynamics**”, talk given at the conference “*World Consensus Initiative III*”, Texas A & M University, College Station, Texas, USA, February 11-17, 2005. (see http://cyclotron.tamu.edu/wci3/newer/chapVI_4.pdf)
- [102] Gyulassy M. Theory of high-energy A+A at RHIC// *Lect. Notes Phys.* 2002. Vol. 583, P.37-79.

- [103] Elliott J.B. et al. Liquid to Vapor Phase Transition in Excited Nuclei //Phys. Rev. Lett. 2002. Vol. 88, N 4, P.042701-1–042701-4.
- [104] Elliott J.B. et al. Constructing the phase diagram of finite neutral nuclear matter // Phys. Rev. C. 2003. Vol. 67, N 2, P.024609-1–024609-14.
- [105] Elliott J.B., Moretto L.G., Phair L. Saturated vapor properties and scaling in the lattice gas model//Phys. Rev. C. 2005. Vol. 71, N 2, P.024607-1–024607-5.
- [106] Moretto L.G., Bugaev K.A., Elliott J.B., Ghetti R., Helgesson J., Phair L.//The Complement: a Solution to Liquid Drop Finite Size Effects in Phase Transitions, Phys. Rev. Lett. 2005. Vol. 94, N 20, P.202701-1–202701-4.
- [107] Stephanov M.A. The phase diagram of QCD and the critical point //Acta Phys. Polon. B. 2004. Vol. 35, N 12, P. 2939-2962.
- [108] Fodor Z., Katz S.D. Lattice determination of the critical point of QCD at finite T and μ // JHEP 2002. Vol. 0203, N 3, P.014.
- [109] Karsch F. et. al. Where is the chiral critical point in 3-flavor QCD?// Nucl. Phys. Proc. Suppl. 2004. Vol. 129, N 3, P.614-616.
- [110] Bugaev K.A. Exact Analytical Solution of the Constrained Statistical Multifragmentation Model// Acta. Phys. Pol. B. 2005. Vol. 36, N 10, P.3083-3094.
- [111] Bugaev K.A., Reuter P.T. Exactly Solvable Models: The Road Towards a Rigorous Treatment of Phase Transitions in Finite Nuclear Systems // Ukr. J. Phys. 2007. Vol. 52, N 5, P.489-510.
- [112] Bugaev K.A. Exact Analytical Solution of the Constrained Statistical Multifragmentation Model and Phase Transitions in Finite Systems// arXiv:nucl-th/0507028, 7 p.
- [113] Bugaev K.A. Exactly Solvable Models: The Road Towards a Rigorous Treatment of Phase Transitions in Finite Systems// Phys. Part. Nucl. 2007. Vol. 38, N 4, P.447-468.

- [114] Bugaev K.A., Phair L., Elliott J.B. Surface Partition of Large Fragments//Phys. Rev. E. 2005. Vol. 72, N 4, P.047106-1–047106-4.
- [115] Bugaev K.A., Elliott J.B. Exactly Soluble Models for Surface Partition//Ukr. J. Phys. 2007. Vol. 52, N 3, P.301-308.
- [116] Moretto L.G. et al. Negative heat capacities and first order phase transitions in nuclei// Phys. Rev. C. 2002. Vol. 66, N 4, P.041601(R)-1–041601(R)-5.
- [117] Stanley H. E. Scaling, universality, and renormalization: Three pillars of modern critical phenomena // Rev. Mod. Phys. 1999. Vol. 71, N 2, S358-S366 (1999).
- [118] Fisher M.E. The theory of equilibrium critical phenomena// Rep. Prog. Phys. 1967. Vol. 30, P.615-730.
- [119] Wilson K.G., Kogut J.B. The Renormalization group and the epsilon expansion // Phys. Rep. 1974. Vol. 12, N 2, P.75-200.
- [120] Moretto L.G. et al. Resistible effects of Coulomb interaction on nucleus-vapor phase coexistence//Phys. Rev. C. 2003. Vol 68, N 6, P.1602-1606.
- [121] Krishnamachari B. et al. Gibbs-Thomson formula for small island sizes: Corrections for high vapor densities // Phys. Rev. B. 1996. Vol. 54, N 12, P.8899-8907.
- [122] Mader C.M. et al. The Three-dimensional Ising model and its Fisher analysis: A paradigm of liquid vapor coexistence in nuclear multiclustering// Phys. Rev. C. 2003. Vol. 68, N 6, P.064601-1–064601-6.
- [123] Ferdinand A.E., Fisher M.E. Bounded and Inhomogeneous Ising Models. I. Specific-Heat Anomaly of a Finite Lattice // Phys. Rev. 1969. Vol. 185, N 2, P.832-846.
- [124] Landau D.P. Finite-size behavior of the Ising square lattice // Phys. Rev. B. 1976. Vol. 13, N 7, P.2997-3011.
- [125] Landau D.P. Finite-size behavior of the simple-cubic Ising lattice //Phys. Rev. B. 1976. Vol. 14, N 1, P.255-262.

- [126] Ferrenberg A.M., Landau D.P. Critical behavior of the three-dimensional Ising model: A high-resolution Monte Carlo study //Phys. Rev. B. 1991. Vol. 44, N 10, P.5081-5091.
- [127] Blöte H.W.J., Luijten E., J R Heringa J.R. Ising universality in three dimensions: a Monte Carlo study // J. Phys. A. 1995. Vol. 28, N 22, P.6289-6313.
- [128] Coniglio A., Klein W. Clusters and Ising critical droplets: a renormalisation group approach //J. Phys. A. 1980. Vol. 13, N 8, P.2775-2780.
- [129] Binder K. Finite size scaling analysis of Ising model block distribution functions//Z. Phys. B. 1981. Vol. 43, N 2, P.119-140.
- [130] Stauffer D. Scaling theory of percolation clusters // Phys. Rep. 1979. Vol 54, N 1, P.1-74.
- [131] Das C.B., Das Gupta S., Mekjian A.Z. Specific heat at constant volume in the thermodynamic model // Phys. Rev. C. 2003. Vol. 68, N 3, P.031601-1–031601-4.
- [132] Feynman R.P. *“Statistical Mechanics”*, Westview Press, Oxford, 1998.
- [133] Elliott J.B. et al. (ISiS Collaboration) Liquid to Vapor Phase Transition in Excited Nuclei , Phys. Rev. Lett. 2002. Vol. 88, N 4, P.042701-042704.
- [134] Gorenstein M.I., Petrov V.K., Zinovjev G.M. Phase transition in the hadron gas model// Phys. Lett. B. 1981. Vol. 106, N 4, P.327-330.
- [135] Gorenstein M.I., Gazdzicki M., Greiner W. Critical line of the deconfinement phase transitions // Phys. Rev. C. 2005. Vol. 72, N 2, P.024909-1–024909-9.
- [136] Yen G.D., Gorenstein M.I. Analysis of particle multiplicities in Pb+Pb collisions at 158A GeV/c within hadron gas models // Phys. Rev. C. 1999. Vol. 59, N 5, P.2788-2791.
- [137] Braun-Munzinger P., Heppe I., Stachel J. Chemical equilibration in Pb + Pb collisions at the SPS//Phys. Lett. B. 1999. Vol. 465, N 1-4, P.15-20.
- [138] Chodos A. et al. New extended model of hadrons //Phys. Rev. D. 1974. Vol. 9, N 12, P.3471-3495.

- [139] Gorenstein M.I., Zinovjev G.M., Petrov V.K., Shelest V.P. Exactly solvable model of phase transition between hadron and quark-gluon matter // Teor. Mat. Fiz. 1982.(Russ) Vol. 52, N 3, P.346-362.
- [140] Moretto L.G., Bugaev K.A., Elliott J.B., Phair L. The Hagedorn Thermostat// Europhys. Lett. 2006. Vol. 76, N 3, P.402-408
- [141] Bugaev K.A., Elliott J.B., Moretto L.G., Phair L. Hagedorn Thermostat: A Novel View of Hadronic Thermodynamics, LBNL preprint **57363**; arXiv: hep-ph/0504011.
- [142] Moretto L.G., Bugaev K.A., Elliott J.B., Phair L. The Quark-Gluon Plasma: a Perfect Thermostat and a Perfect Particle Reservoir, LBNL preprint **59103**; Preprint nucl-th/0511180 (2005) 15 p.
- [143] Dillmann A., Meier G.E.A. A refined droplet approach to the problem of homogeneous nucleation from the vapor phase // J. Chem. Phys. 1991. Vol. 94, N 5, P.3872-3884.
- [144] Kiang C.S. Use of Liquid-Droplet Model in Calculations of the Critical Exponent δ // Phys. Rev. Lett. 1970. Vol. 24, N 2, P.47-50.
- [145] Stauffer D., Aharony A. "Introduction to Percolation", Taylor and Francis, Philadelphia, 2001.
- [146] Kadanoff L.P. et al. Static phenomena near critical points: Theory and experiment //Rev. Mod. Phys. 1967. Vol. 39, N 2, P.395-431.
- [147] Cleymans J., Oeschler H., Redlich K., Wheaton S. Comparison of chemical freeze-out criteria in heavy-ion collisions // Phys. Rev. C. 2006. Vol. 73, N 3, P.034905-1–034905-10.
- [148] Hagedorn R. Statistical thermodynamics of strong interactions at high-energies//Suppl. Nuovo Cimento 1965. Vol. 3, N 2, P.147-186.
- [149] Hagedorn R., Ranft J. Statistical thermodynamics of strong interactions at high-energies. 2. Momentum spectra of particles produced in p p collisions. //Suppl. Nuovo Cimento 1968. Vol. 6, N 2, P.169-354.

- [150] Venugopalan R., Prakash M. Thermal properties of interacting hadrons//Nucl. Phys. A. 1992. Vol. 546, N 4, P.718-760.
- [151] Kapusta J.I., Olive K.A. Thermodynamics of hadrons: Delimiting the temperature//Nucl. Phys. A. 1983. Vol. 408, N 3, P.478-494.
- [152] Zhang Q.R. Relativistic finite baryon size effect and the mass limit for neutron stars//Z. Phys. A. 1995. Vol. 353, N 3, P.345-348.
- [153] Bugrii A. I., Trushevsky A.A. The Van der Waals equation for the system of ultrarelativistic particles, Preprint ITP-78-82E, 19p.
- [154] Bugaev K.A., Gorenstein M.I., Stöcker H., Greiner W. Van der Waals Excluded Volume Model for Lorentz Contracted Rigid Spheres// Phys. Lett. B. 2000. Vol. 485, N 1-3, P.121-125.
- [155] Zeeb G., Bugaev K.A., Reuter P.T., Stöcker H. Equation of State for the Two-component Van der Waals Gas with Relativistic Excluded Volumes// Ukr J. Phys. 2008. Vol. 53, N 3, P.279-295.
- [156] Bugaev K.A. The Van-der-Waals Gas EOS for the Lorentz Contracted Spheres// Nucl. Phys. A. 2008. Vol. 807, N 3-4, P.251-268.
- [157] Karsch F., Laermann E. in “Quark-Gluon Plasma 3”, edited by R. C. Hwa and X.-N. Wang (World Scientific, Singapore, 2004), p. 1.
- [158] Zeeb G.: Diploma thesis, Zweikomponentige *Van-der-Waals-Zustandsgleichungen* mit relativistischen Eigenvolumentermen für das hadronische Gas // Frankfurt am Main 2002.
- [159] Гельфер Я.М. История и методология термодинамики и статистической физики // Высшая Школа. 1981. Москва, 536с.
- [160] Münster A. Statistical Thermodynamics // Springer-Verlag. Heidelberg. 1974. Vol. II, 581p.
- [161] Gorenstein M.I., Kostyuk A.P., Krivenko Y.D. Van der Waals excluded volume model of multicomponent hadron gas// J. Phys. G. 1999. Vol. 25, N 9, P.L75-L83.

- [162] Майер Дж., Гепперт-Майер М. Статистическая Механика // Мир. Москва. 1980, 544с.
- [163] Rischke D.H., Gorenstein M.I., Stöcker H., Greiner W. Excluded volume effect for the nuclear matter equation of state// Z. Phys. C. 1991. Vol. 51, N 3, P.485-489.
- [164] Ritchie R.A., Gorenstein M.I., Miller H.G. The excluded volume hadron gas model and pion production at the SPS//Z. Phys. C. 1997. Vol. 75, N 3, P.535-538.
- [165] Yen G.D., Gorenstein M.I., Greiner W., Yang S.N. Excluded volume hadron gas model for particle number ratios in A + A collisions//Phys. Rev. C. 1997. Vol. 56, N 4, P.2210-2218.
- [166] Gorenstein M.I., Greiner W., Yang S.N. Phase transitions in the gas of bags//J. Phys. G. 1998. Vol. 24, N 4, P.725-744.
- [167] Greiner C., Stöcker H. Distillation and survival of strange quark matter droplets in ultrarelativistic heavy ion collisions//Phys. Rev. D. 1991. Vol. 44, N 11, P.3517-3529.
- [168] Koch P., Müller B., Rafelski J. Strangeness in relativistic heavy ion collisions// Phys. Rep. 1986. Vol. 142, N 4, P.167-262.
- [169] Cleymans J., Satz H. Thermal hadron production in high-energy heavy ion collisions, Z. Phys. C. 1993. Vol. 57, N 1,P.135-148.
- [170] Braun-Munzinger P., Stachel J., Wessels J.P., Xu N. Thermal equilibration and expansion in nucleus-nucleus collisions at the AGS// Phys. Lett. B. 1995. Vol. 344, N 1-4, P.43-48.
- [171] Becattini F., Heinz U.W. Thermal hadron production in pp and p anti-p collisions//Z. Phys. C. 1997. Vol. 76, N 2, P.269-286.
- [172] Proceedings of the Quark Matter '96, 12th International Conference on Ultrarelativistic Nucleus Nucleus Collisions, Heidelberg, Germany, May 20-24, 1996, edited by P. Braun-Munzinger, H.J. Specht, R. Stock, H. Stöcker //Nucl. Phys. A. 1996. Vol. 610, 1c.
- [173] Bugaev K.A. Shock-like Freeze-out in Relativistic Hydrodynamics// Nucl. Phys. A. 1996. Vol. 606, N 3-4, P.559-567.

- [174] Magas V.K. et al. Freeze-out in hydrodynamical models in relativistic heavy ion collisions//Nucl. Phys. A. 1999. Vol. 661, N 1-4, P.596-599.
- [175] Anderlik C. et al. Freeze out in hydrodynamical models// Phys. Rev. C. 1999. Vol. 59, N 6, P.3309-3316.
- [176] Reichl L.E. "A Modern Course in Statistical Physics", 2nd Edition, J. Wiley & Sons, New York 1998, 55, 153.
- [177] Nambu Y., Jona-Lasinio G. Dynamical Model of Elementary Particles Based on an Analogy with Superconductivity. I // Phys. Rev. 1961. Vol. 122, N 1, P.345-358.
- [178] Guichon P.A.M. A possible quark mechanism for the saturation of nuclear matter//Phys. Lett. B. 1988. Vol. 200, N 3, P.235-240.
- [179] Papazoglou P. et. al. Chiral Lagrangian for strange hadronic matter//Phys. Rev. C. 1998 Vol. 57, N 5, P.2576-2588.
- [180] Karsch F. et. al. Hadron correlators, spectral functions and thermal dilepton rates from lattice QCD // Nucl. Phys. A. 2003. Vol. 715, P.701-704.
- [181] Shuryak E.V., Zahed I. Towards a theory of binary bound states in the quark gluon plasma//Phys. Rev. D. 2004. Vol. 70, N 5, P.054507-1-054507-16.
- [182] Mannarelli M., Rapp R. Hadronic Modes and Quark Properties in the Quark-Gluon Plasma//Phys.Rev. C. 2005. Vol. 72, N 6, P.064905-1-064905-10.
- [183] Shuryak E.V., Zahed I. Rethinking the properties of the quark gluon plasma at T approximately T(c)//Phys. Rev. C. 2004. Vol. 70, N 2, P.021901(R)-1-021901(R)-4.
- [184] Shuryak E.V. Toward the theory of strongly coupled quark-gluon plasma // In Proceedings of the 18th International Conference on Ultra-Relativistic Nucleus-Nucleus Collisions Budapest "QUARK MATTER 2005", Hungary 04-09 August 2005. Edited by Tamas Csorgo, Gabor David, Peter Levai and Gabor Papp / Nucl. Phys. A. 2006. Vol. 774, P.387-396.

- [185] Molnar D., Gyulassy M. Saturation of elliptic flow and the transport opacity of the gluon plasma at RHIC//Nucl. Phys. A. 2002. Vol. 697, N 1-2, P.495-520.
- [186] Heinz U. Equation of state and collective dynamics//J. Phys. Conf. Ser. 2006. Vol. 50, P.230-237.
- [187] Fries R.J., Muller B., Nonaka C., Bass S.A. Hadron production in heavy ion collisions: Fragmentation and recombination from a dense parton phase//Phys. Rev. C. 2003. Vol. 68, N 4, P.044902-1-044902-23.
- [188] Hamer C.J., Frautschi S.C. Determination of asymptotic parameters in the statistical bootstrap model // Phys. Rev. D. 1971. Vol. 4, N 7, P.2125-2137.
- [189] Cabibbo N., Parisi G. Exponential Hadronic Spectrum and Quark Liberation//Phys. Lett. B. 1975. Vol. 59, N 1, P.67-69.
- [190] Moretto L.G., Bugaev K.A., Elliott J.B., Phair L. Can a Hagedorn System Have a Temperature Other Than T_C or Can a Thermostat Have a Temperature Other Than Its Own?//Preprint LBNL-59191. 2006. 4p.
- [191] Carlitz R.D. Hadronic matter at high density. //Phys. Rev. D. 1972. Vol. 5, N 12, P.3231-3242.
- [192] Hagedorn R., Rafelski J. Hot Hadronic Matter and Nuclear Collisions//Phys. Lett. B. 1980. Vol. 97, N 1, P.136-142.
- [193] Letessier J., Rafelski J., Tounsi A. Strangeness and particle freezeout in nuclear collisions at 14.6-GeV/A//Phys. Lett. B. 1994. Vol. 328, N 3-4, P.499-505.
- [194] Karsch F. Lattice QCD at finite temperature and density /Proceedings of the XVIIth International Symposium on Lattice Field Theory Pisa, Italy, 29 June - 3 July 1999 // Nucl. Phys. Proc. Suppl. 2000. Vol. 83-84, P.14-23.
- [195] Kapusta J.I. Asymptotic mass spectrum and thermodynamics of the Abelian bag model//Phys. Rev. D. 1981. Vol. 23, N 10, P.2444-2453.

- [196] Kapusta J.I. Asymptotic level density of constrained and interacting fields//Nucl. Phys. B. 1982. Vol. 196, N 1, P.1-10.
- [197] Kliemant M., Lungwitz B., Gazdzicki M. Energy dependence of transverse mass spectra of kaons produced in $p + p$ and $p + \bar{p}$ interactions: a compilation//Phys. Rev. C. 2004. Vol. 69, N 4, P.044903-1-044903-7.
- [198] Braun-Munzinger P. et al. Hadron production in Au–Au collisions at RHIC//Phys. Lett. B. 2001. Vol.518, N 1-2, P.41-46.
- [199] Becattini F. The Canonical effect in statistical models for relativistic heavy ion collisions//J. Phys. G. 2002. Vol. 28, N 7, P.2041-2046.
- [200] Blaschke D.B., Bugaev K.A. Hadronic Correlations above the Chiral / Deconfinement Transition//Fizika B. 2004. Vol. 13, N 2, 491-500.
- [201] Becattini F., Ferroni L. Statistical hadronization and microcanonical ensemble//Acta Phys. Polon. B. 2004. Vol. 35, N 1, P.207-211.
- [202] Becattini F., Passaleva G. Statistical hadronisation model and transverse momentum spectra of hadrons in high energy collisions//Eur. Phys. J. C. 2002. Vol. 23, N 3, P.551-583.
- [203] Becattini F., Ferroni L. Statistical hadronization and hadronic microcanonical ensemble//Eur. Phys. J. C. 2004. Vol.38, N 2, P.225-246.
- [204] Alexopoulos T. et al. Evidence for hadronic deconfinement in $\bar{p} - p$ collisions at 1.8 TeV //Phys. Lett. B. 2002. Vol. 528, N 1-2, P.43-48.
- [205] Bugaev K.A., Gazdzicki M., Gorenstein M.I. Transverse Momentum Spectra of J/ψ and ψ' Mesons from Quark Gluon Plasma Hadronization in Nuclear Collisions// Phys. Lett. B. 2001. Vol. 523, N 3-4, P.255-259.
- [206] Bugaev K.A. Transverse Momentum Spectra of J/ψ and ψ' Mesons from Quark Gluon Plasma Hadronization at CERN SPS//J. Phys. G. 2002. Vol. 28, N 7, P.1981-1986.

- [207] Gorenstein M.I., Bugaev K.A., Gazdzicki M. Ω , J/ψ and ψ' production in nuclear collisions from quark gluon plasma hadronization//Phys. Rev. Lett. 2002. Vol. 88, N 13, P.132301-1–132301-4.
- [208] Bugaev K.A., Gazdzicki M., Gorenstein M.I. Ω , J/ψ and ψ' Transverse Mass Spectra at RHIC//Phys. Lett. B. 2002. Vol. 544, N 1-2, P.127-131.
- [209] Bugaev K.A., Gazdzicki M., Gorenstein M.I. Hadron spectra and QGP hadronization in Au+Au collisions at RHIC//Phys. Rev. C. 2003. Vol. 68, N 1, P.017901-1–017901-4.
- [210] van Buren G. Soft physics in STAR / Proceedings of the 16th International Conference on Ultra-Relativistic Nucleus-Nucleus Collisions // Nucl. Phys. A. 2003. Vol. 715, P. 129-139.
- [211] Adams J. et al. Multistrange baryon production in Au-Au collisions at $\sqrt{S_{NN}} = 130$ GeV (STAR Collab.)//Phys. Rev. Lett. 2004. Vol. 92, N 18, P.182301-1–182401-4.
- [212] Suire C. et al. Ω^- and $\bar{\Omega}^+$ production in Au+Au collisions at $\sqrt{S_{NN}} = 130$ and 200 GeV (STAR Collab.)/ Proceedings of the 16th International Conference on Ultra-Relativistic Nucleus-Nucleus Collisions //Nucl. Phys. A. 2003. Vol. 715, P.470-473.
- [213] Adler C. et al. Midrapidity ϕ production in Au+Au collisions at $\sqrt{s_{NN}} = 130$ GeV(STAR Collab.)//Phys. Rev. C. 2002. Vol.65, N 4, P.041901(R)-1–041901(R)-5.
- [214] Broniowski W., Florkowski W., Glozman L.Y. Update of the Hagedorn mass spectrum//Phys. Rev. D. 2004. Vol.70, N 11, P.117503-1–117503-4.
- [215] Rischke D.H. Remarks on the extraction of freezeout parameters//Nucl. Phys. A. 2002. Vol. 698, N 1-4, P.153-163.
- [216] Bialas A. Fluctuations of string tension and transverse mass distribution//Phys. Lett. B. 1999. Vol. 466, N 2-4, P.301-304.
- [217] Florkowski W. Schwinger tunneling and thermal character of hadron spectra//Acta. Phys. Polon. B. 2004. Vol. 35, N 2, P.799-808.

- [218] Belkacem M. et al. Equation of state, spectra and composition of hot and dense infinite hadronic matter in a microscopic transport model//Phys. Rev. C. 1998. Vol.58, N 3, P.1727-1733.
- [219] Pal S., Danielewicz P. Hadron production from resonance decay in relativistic collisions //Phys. Lett. B. 2005. Vol. 627, N 1-4, P.55-63.
- [220] Becattini F., Cleymans J., Keranen A., Suhonen E., Redlich K. Features of particle multiplicities and strangeness production in central heavy ion collisions between 1.7A and 158A GeV/c //Phys. Rev. C. 2001. Vol. 64, N 2, P.024901-1-024001-9.
- [221] Greiner C. et. al. Chemical equilibration due to heavy Hagedorn states//J. Phys. G. 2005, Vol. 31, N 6, P.S725-S732.
- [222] Karsch F., Redlich K., Tawfik A. Hadron resonance mass spectrum and lattice QCD thermodynamics//Eur. Phys. J. C. 2003. Vol. 29, N 4, P.549-556.
- [223] Wetzorke I. et al. Meson spectral functions at finite temperature // Nucl. Phys. Proc. Suppl. 2002. Vol. 106-107, P.510-512.
- [224] Asakawa M., Hatsuda T., Nakahara Y. Hadronic spectral functions above the QCD phase transition/ Proceedings of the 16th International Conference on Ultra-Relativistic Nucleus-Nucleus Collisions// Nucl. Phys. A. 2003. Vol. 715, P.863-866.
- [225] Blaschke D.B., Bugaev K.A. J/psi suppression in the Mott-Hagedorn resonance gas//Prog. Part. Nucl. Phys. 2004. Vol. 53, N 1, P.197-205.
- [226] Blaschke D.B., Bugaev K.A. Thermodynamics of resonances with finite width//Phys. Part. Nucl. Lett. 2005. Vol. 2, P.305-308.
- [227] Particle Data Group// Phys. Lett. B. 2004. Vol. 591, N 1-4, P.1.
- [228] Blaschke D. et al. Mott mechanism and the hadronic to quark matter phase transition// Phys. Lett. B. 1985. Vol. 151, N 5-6, P.439-443.

- [229] Röpke G., Blaschke D., Schulz H. Pauli quenching effects in a simple string model of quark / Nuclear Matter // Phys. Rev. D. 1986. Vol. 34, N 11, P.3499-3513.
- [230] Hüfner J., Klevansky S.P., Rehberg P. Soft deconfinement critical phenomena at the Mott transition in a field theory for quarks and mesons // Nucl. Phys. A. 1996. Vol. 606, N 1-2, P.260-282.
- [231] Bureau G., Blaschke D., Kalinovsky Yu. Mott effect at the chiral phase transition and anomalous J/ψ suppression // Phys. Lett. B. 2001. Vol. 506, N 3-4, P.297-302.
- [232] Gazdzicki M., Gorenstein M.I. Power law in hadron production // Phys. Lett. B. 2001. Vol. 517, N 3-4, P.250-254.
- [233] Schaffner-Bielich J., Kharzeev D., McLerran L., Venugopalan R. Generalized scaling of the transverse mass spectrum at the Relativistic Heavy-Ion Collider // Nucl. Phys. A. 2002. Vol. 705, N 3-4, P.494-507.
- [234] Wang X.-N., Gyulassy M., Plümer M. The LPM effect in QCD and radiative energy loss in a quark gluon plasma // Phys. Rev. D. 1995. Vol. 51, N 7, P.3436-3446.
- [235] Bass S.A. et al. Microscopic models for ultrarelativistic heavy ion collisions, Prog. Part. Nucl. Phys. 1998. Vol. 41, P.225-370.
- [236] Abreu M.C. et al. (NA50 Collaboration) Evidence for deconfinement of quarks and gluons from the J/ψ suppression pattern measured in Pb + Pb collisions at the CERN SPS. // Phys. Lett. B. 2000. Vol. 477, N 1-3, P.28-36.
- [237] Nardi M., Satz H. String clustering and J/ψ suppression in nuclear collisions // Phys. Lett. B. 1998. Vol. 442, N 1-4, P.14-19.
- [238] Digal S., Fortunato S., Petreczky P., Satz H. Parton percolation and J/ψ suppression // Phys. Lett. B. 2002. Vol. 549, N 1-2, P.101-108.
- [239] Blaizot J.P., Ollitrault J.Y. J/ψ suppression in Pb–Pb collisions: A Hint of quark-gluon plasma production? // Phys. Rev. Lett. 1996. Vol. 77, N 9, P.1703-1706.

- [240] Bugaev K.A. Quark-Gluon Bags with Surface Tension // Phys. Rev. C. 2007. Vol. 76, N. 1, P. 014903-1–014903-10.
- [241] Bugaev K.A. The Role of Surface Tension for the EOS of Quark-Gluon Bags // talk given at the international school-seminar “New Physics and Quantum Chromodynamics at External Conditions”, Dniepropetrovsk, Ukraine, May 3-6, 2007; e-print arXiv:0707.2263 [nucl-th] (2007) 10p.
- [242] Bugaev K.A. Exactly Solvable Model for the QCD Tricritical Endpoint // Phys. Atom. Nucl. 2008. Vol. 71, N 9, P. 1615-1623.
- [243] Shuryak E.V. Quantum Chromodynamics and the Theory of Superdense Matter // Phys. Rep. 1980. Vol. 61, N 2, P.71-158.
- [244] Farhi E., Jaffe R.L. Strange Matter // Phys. Rev. D. 1984. Vol. 30, N 11, P.2379-2390.
- [245] Berger M.S., Jaffe R.L. Radioactivity in strange quark matter // Phys. Rev. C. 1987. Vol. 35, N 1, P.213-225; and Erratum-ibid. C 44, 566 (1991).
- [246] Mardor I., Svetitsky B. Bubble free energy at the quark-hadron phase transition // Phys. Rev. D. 1991. Vol. 44, N 3, P.878-886.
- [247] Neergaard G., Madsen J. Does the quark-gluon plasma contain stable hadronic bubbles? // Phys. Rev. D. 2000. Vol. 62, N 3, P.034005-1–034005-5.
- [248] Ignatius J. Bubble free energy in cosmological phase transitions // Phys. Lett. B. 1993. Vol. 309, N 3-4, P.252-257.
- [249] Zakout I., Greiner C., Schaffner-Bielich J. The Order, shape and critical point for the quark-gluon plasma phase transition // Nucl. Phys. A. 2007. Vol. 781, N 1-2, P.150-200.
- [250] Ravenhall D.G., Pethick C.J., Wilson J.R. Structure of matter below nuclear saturation density // Phys. Rev. Lett. 1983. Vol. 50, N 26, P.2066-2069.
- [251] Liao J., Shuryak E.V. What do lattice baryonic susceptibilities tell us about quarks, diquarks, and baryons at $T > T_c$? // Phys. Rev. D. 2006. Vol. 73, N 1, P.014509-1–014509-11.

- [252] Krishnamachari B. et al. Gibbs-Thomson formula for small island sizes: Corrections for high vapor densities //Phys. Rev. B. 1996. Vol. 54, N 12, P.8899-8907.
- [253] Alford M.G., Rajagopal K., Wilczek F. Color-flavor locking and chiral symmetry breaking in high density QCD //Nucl. Phys. B. 1999. Vol. 537, N 1-3, P.443-458.
- [254] Nonaka C., Asakawa M. Hydrodynamical evolution near the QCD critical end point //Phys. Rev. C. 2005. Vol. 71, N 4, P.044904-1–044904-12.
- [255] Antoniou N.G., Diakonou F.K., Kapoyannis A.S. The Critical endpoint of bootstrap and lattice QCD matter// Nucl. Phys. A. 2005. Vol. 759, N 3-4, P.417-438.
- [256] Shuryak E. Interactions between hadrons are strongly modified near the QCD (tri)critical point// arXiv:hep-ph/0504048, 2005, 9pp.
- [257] Bugaev K.A., Gorenstein M.I. Particle freeze-out in self-consistent relativistic hydrodynamics// University of Hannover Preprint ITP-UH-03/99 1999. 70p.
- [258] Bugaev K.A., Gorenstein M.I., Greiner W. Particle Freeze-out and discontinuities in relativistic hydrodynamics//J. Phys. G. 1999. Vol. 25, N 10, P.2147-2160.
- [259] Bugaev K.A., Gorenstein M.I., Greiner W. Discontinuities in Relativistic Hydrodynamics Across Space-like and Time-like Hypersurfaces. Proceedings of the conference “*Non-Euclidean Geometry in Modern Physics*”, Nyiregyha’za, Hungary, July 7-10, 1999, Heavy Ion Phys. 1999. Vol. 10, N 10, P.333-343.
- [260] Bugaev K.A. Particle Freeze-out within the Self-Consistent Hydrodynamics // Acta. Phys. Pol. B. 2009. Vol. 40, N 4, 1045-1051.
- [261] Bass S.A., Dumitru A. Dynamics of hot bulk QCD matter: From the quark gluon plasma to hadronic freezeout//Phys. Rev. C. 2000. Vol. 61, N 6, P.064909-1–064909-24.
- [262] Teaney D., Lauret J., Shuryak E.V. Flow at the SPS and RHIC as a quark-gluon plasma signature // Phys. Rev. Lett. 2001. Vol. 86, N 21, P.4783-4786.

- [263] Bugaev K.A. Relativistic kinetic equations for finite domains and freeze-out problem // Phys. Rev. Lett. 2003. Vol. 90, N 25, P. 252301-1–252301-4.
- [264] Bugaev K.A. Boundary conditions of the hydro-cascade model and relativistic kinetic equations for finite domains// Phys. Rev. C. 2004. Vol. 70, N 3, P.034903-1-034903-11.
- [265] Gorenstein M.I., Gazdzicki M., Bugaev K.A. Transverse activity of kaons and the deconfinement phase transition in nucleus nucleus collisions// Phys. Lett. B. 2003. Vol. 567, N 3-4, P.175-178.
- [266] Gazdzicki M. Entropy in nuclear collisions//Z.Phys. C. 1995. Vol. 66, N 4, P.659-662.
- [267] Gazdzicki M., Gorenstein M.I. On the early stage of nucleus nucleus collisions// Acta Phys. Polon. B. 1999. Vol. 30, N 9, P.2705-2742.
- [268] Landau L.D. On the multiparticle production in high-energy collisions// Izv. Akad. Nauk Ser. Fiz. 1953. Vol. 17, N 1, P.51-64.
- [269] Mishustin I.N., Russkikh V.N., Satarov L.M. Relativistic fluid-dynamical approach for nuclear collisions at energies from 1 to 100 GeV per nucleon. Moscow, 1989.
- [270] Rischke D.H. “Fluid Dynamics for Relativistic Nuclear Collisions”, the proceedings of 11th Chris Engelbrecht Summer School in Theoretical Physics: Hadrons in Dense Matter and Hadrosynthesis, Cape Town, South Africa, 4-13 Feb 1998. In *Cape Town 1998, Hadrons in dense matter and hadrosynthesis* 21-70; arXiv: nucl-th/9809044.
- [271] Landau V, Lifshitz E.M. Fluid Mechanics. Pergamon, New York, 1979.
- [272] Очелков Ю.П., Прилуцкий О. Ф., Розенталь И.Л., Усов В.В. Релятивистская кинетика и гидродинамика // Атомиздат. Москва. 1979. 200с.
- [273] Милехин Г.А. Гидродинамическая теория множественного образования частиц при столкновении быстрых нуклонов с ядрами // Журн. эксперим. и теор. физ. 1959. Т. 35, N 5, с.1185-1197.

- [274] Милехин Г.А. Анализ возможных гидродинамических теорий множественного образования частиц при различных уравнениях состояния // В кн.: Труды Международной конференции по космическим лучам. Т. 1. М., Изд-во АН СССР, 1960, с. 223-229.
- [275] Cooper F., Frye G. Comment on the single particle distribution in the hydrodynamic and statistical thermodynamic models of multiparticle production // Phys. Rev. D. 1974. Vol. 10, N 1, P.186-189.
- [276] Sinyukov Yu.M. Direct conversion of mixed phase into free hadronic gas and transverse pion momenta in ultra-relativistic nuclear collisions // Sov. J. Nucl. Phys. 1989. Vol. 50, N 1(7), P.228-238.
- [277] Sinyukov Yu.M. Model of the mixed phase direct transition into free hadronic gas and transverse momenta of pions in ultrarelativistic nuclear collisions // Z. Phys. C. 1989. Vol. 43, N 3, P.401-409.
- [278] Muroya S., Nakamura H., Namiki M. Numerical analysis of CERN 200-GeV/A heavy ion collisions based on a hydrogen numerical model with phase transition. // Progr. Theor. Phys. Suppl. 1995. Vol. 120, P.209-216.
- [279] Rischke D.H., Bernard S., Maruhn J.A. Relativistic hydrodynamics for heavy ion collisions. 1. General aspects and expansion into vacuum // Nucl. Phys. A. 1995. Vol. 595, N 3, P.346-382.
- [280] Csernai L.P., Lazar Z., Molnar D. Idealized freezeout in relativistic fluid dynamical models. // Heavy Ion Phys. 1997. Vol. 5, P.467-474.
- [281] Anderlik Cs., Csernai L.P., Grassi F., Hama Y., Kodama T., Lazar Zs. Freeze-out in hydrodynamical models // Phys. Rev. C. 1999. Vol. 59, N 6, P.3309-3316.
- [282] Anderlik Cs., Lazar Zs., Magas V.K., Csernai L.P., Stöcker H., Greiner W. Nonideal particle distributions from kinetic freeze-out models // Phys. Rev. C. 1999. Vol. 59, N 1, P.388-394

- [283] Magas V. Freeze out in hydrodynamical models, Master of Science Thesis// University of Bergen, January, 1999.
- [284] Csernai L.P. et. al. Phase transitions in high-energy heavy ion collisions // “Camyuva-Kerner 2003. Structure and Dynamics of Elementary Matter”, Proceedings of the NATO Advanced Study Institute: Structure and Dynamics of Elementary Matter, Kerner, Turkey, 22 Sept. -2 Oct. 2003, P.127-142.
- [285] Neumann J.J., Lavrenchuk B., Fai G. Feedback from freezeout in hydrodynamics // Heavy Ion Phys. 1997. Vol. 5, N 1, P.27-40.
- [286] Grassi F. Particle emission in hydrodynamics: a problem needing a solution // Braz. J. Phys. 2005. Vol. 35, N 1, P. 52-69.
- [287] Sinyukov Yu.M., Akkelin S.V., Hama Y. On freezeout problem in hydro kinetic approach to $A + A$ collisions//Phys. Rev. Lett. 2002. Vol. 89, N 5, P.052301-1–052301-4.
- [288] Molnar D., Gyulassy M. New solutions to covariant nonequilibrium dynamics // Phys. Rev. C. 2000. Vol. 62, N 5, P.054907-1–054907-12.
- [289] Bravina L.V. et al. Microscopic study of freeze-out in relativistic heavy ion collisions at SPS energies// Phys. Rev. C. 1999. Vol. 60, N 4, P.044905-1–044905-9.
- [290] Gorenstein M.I., Sinyukov Yu.M. Local Anisotropy Effects In The Hydrodynamical Theory Of Multiparticle Production // Phys. Lett. B. 1984. Vol. 142, N 5-6, P.425-428.
- [291] Shuryak E.V. Can recent CERN experiments with 200 GeV/N O^{16} ions be explained by the independent NN collisions?// Phys. Lett. B. 1988. Vol. 207, N 3, P.345-348.
- [292] Holme A.K., Staubo E.F., Csernai L.P., Osnes E., Strottman D. Hadronization from supercooled baryon-rich quark-gluon plasma // Phys. Rev. D. 1989. Vol. 40, N 11, P.3735-3742 .
- [293] Gorenstein M.I., Miller H.G., Quick R.M., Ritchie R.A. Timelike shock hadronization of a supercooled quark-gluon plasma// Phys. Lett. B. Vol. 340, 1994, N 1-2, P.109-114.

- [294] Csernai L.P., Gong M. Shock phenomena in supercooled baryon-free strongly interacting matter // Phys. Rev. D. 1988. Vol. 37, N 11, P. 3231-3236.
- [295] Gorenstein M.I. Discontinuity-like freeze-out in the hydrodynamic approach // Preprint UFTP 251/1990 of the University of Frankfurt, 1990, 9p.
- [296] Russkikh V.N., Ivanov Yu.B. Dynamical Freeze-out in 3-Fluid Hydrodynamics / e-print archive nucl-th/0611094 2006. 13p.
- [297] Csörgő T., Csernai L.P. Quark - gluon plasma freezeout from a supercooled state? //Phys. Lett. B. 1994. Vol. 333, N 3-4, P.494-499.
- [298] Taub A.H. Relativistic Rankine-Hugoniot Equations // Phys. Rev. 1948. Vol. 74, N 3, P.328-334.
- [299] Bugaev K.A., Gorenstein M.I. Relativistic Shocks In Baryonic Matter//J. Phys. G. 1987. Vol. 13, N 10, P.1231-1238.
- [300] Rozhdestvensky B.L., Yanenko N.N. Systems of Quasi-Linear Equations// Nauka, Moscow (1978).
- [301] Bugaev K.A., Gorenstein M.I., Kämpfer B., Zhdanov V.I. Generalized shock adiabatics and relativistic nuclear collisions// Phys. Rev. D. 1989. Vol. 40, N 9, P.2903-2913.
- [302] Bugaev K.A., Gorenstein M.I., Kämpfer B., Zhdanov V.I. Generalized shock adiabates and relativistic nuclear collisions//Sov. J. Nucl. Phys. 1989. Vol. 50, N 4, P.1172-1182.
- [303] Bugaev K.A., Gorenstein M.I., Zhdanov V.I. Relativistic shocks in the systems containing domains with anomalous equation of state and quark baryonic matter hadronization // Z. Phys. C. 1988. Vol. 39, N 3, P.365-370.
- [304] de Groot S.R., van Leeuwen W.A., van Weert Ch.G. Relativistic Kinetic Theory, North-Holland Publishing Company, Amsterdam (1980).

- [305] N. N. Bogolyubov, *Problems of Dynamic Theory in Statistical Physics* (Gostekhizdat, Moscow 1946) (in Russian). [Reprinted in *Studies in Statistical Mechanics*, vol. 1 (J. de Boer and G. E. Uhlenbeck, eds., North-Holland Publishing, Amsterdam 1962).]
- [306] R. Balescu, *Equilibrium and Nonequilibrium Statistical Mechanics* (Krieger Publishing, Malabar, Florida 1991).
- [307] Csernai L.P. *Introduction to Relativistic Heavy Ion Collisions* // Willey (1994).
- [308] Hung C.M., Shuryak E.V. Hydrodynamics near the QCD phase transition: Looking for the longest lived fireball// *Phys. Rev. Lett.* 1995. Vol. 75, N 22, P.4003-4006.
- [309] Hung C.M., Shuryak E. Equation of state, radial flow and freezeout in high-energy heavy ion collisions// *Phys. Rev. C.* 1998. Vol. 57, N 4, P.1891-1906.
- [310] van Hove L. Two Problems Concerning Hot Hadronic Matter and High-Energy Collisions (Equilibrium Formation, Plasma Deflagration)//*Z. Phys. C.* 1983. Vol. 21, N 1-2, P.93-98.
- [311] Gyulassy M., Kajantie K., Kurki-Suonio H., McLerran L. Deflagrations and detonations as a mechanism of hadron bubble growth in supercooled quark gluon plasma. //*Nucl. Phys. B.* 1984. Vol. 237, N 3, P.477-501.
- [312] Anderson E. et al. Enhancement of central, and yields in Pb–Pb collisions at 158 A GeV/ c^2 (WA97 Collab.)//*Phys. Lett. B.* 1998. Vol.433, N 1-2, P.209-216.
- [313] Antinori F. et al. Strange baryon production in Pb–Pb collisions at 158-A-GeV/ c (WA97 Collab.)//*J. Phys. G.* 2001. Vol. 27, N 3, P.375-381.
- [314] Abreu M.C. et al. Transverse momentum distributions of J/Ψ , Ψ' , DrellYan and continuum dimuons produced in Pb-Pb interactions at the SPS (NA50 Collab.)//*Physl. Lett. B.* 2001. Vol. 499, N 1-2, P.85-96.
- [315] Afanasev S.V. et al. Production of φ -mesons in p+p, p+Pb and central Pb+Pb collisions at $E_{\text{beam}} = 158A$ GeV (NA49 Collab.)// *Phys. Lett. B.* 2000. Vol. 491, N 1-2, P.59-66.

- [316] Abreu M.C. et al. φ , ρ and ω production in Pb–Pb collisions at 158-GeV/ c^2 per nucleon (NA50 Collab.) // Nucl Phys. A. 1999. Vol. 661, N 1-4, P.534-537.
- [317] Csernai L.P., Lazar Z. and Molnar D. Idealized freezeout in relativistic fluid dynamical models//Heavy Ion Phys. 1997. Vol. 5, P.467-474.
- [318] Afanasiev S.V. et al. Energy dependence of pion and kaon production in central Pb+Pb collisions (NA49 Collab.)//Phys. Rev. C. 2002. Vol. 66, N 5, P.054902-1–054902-9.
- [319] Alt C. et al. Strangeness from 20 A GeV to 158 A GeV (NA49 Collab.), //J. Phys. G. 2004. Vol. 30, N 1, P.S119-S128.
- [320] Gazdzicki M., Gorenstein M.I., Mrowczynski St. Fluctuations and deconfinement phase transition in nucleus nucleus collisions // Phys. Lett. B. 2004. Vol. 585. N 1-2, P. 115-121.
- [321] Gorenstein M.I., Gazdzicki M., Zozulya O.S. Fluctuations of strangeness and deconfinement phase transition in nucleus nucleus collisions // Phys. Lett. B. 2004. Vol. 585. N 3-4, P. 237-242.
- [322] Letessier J., Rafelski J. and Tounsi A. Strangeness and particle freezeout in nuclear collisions at 14.6 GeV/A//Phys. Lett. B. 1994. Vol. 328, N 3-4, P.499-505.
- [323] Gazdzicki M. and Gorenstein M.I. Evidence for statistical production of J/Ψ mesons in nuclear collisions at 158-200 A GeV//Phys. Rev. Lett. 1999. Vol. 83, N 20, P.4009-4012.
- [324] Braun-Münzinger P. and Stachel J. (Non)thermal aspects of charmonium production and a new look at J/Ψ suppression //Phys. Lett. B. 2000. Vol. 490, N 3-4, P.196-202.
- [325] Appelshauser H. et all. Hadronic expansion dynamics in central Pb + Pb collisions at 158 GeV per nucleon (NA49 Collaboration)//Eur. Phys. J. C. 1998. Vol. 2, N 4, P.661-670.
- [326] Csorgo T., Lorstad B. and Zimanyi J. Quantum statistical correlations for slowly expanding systems //Phys. Lett. B. 1994. Vol. 338, N 2-3, 134-140.
- [327] Heiselberg H. and Levy A. Elliptic flow and Hanbury–Brown–Twiss correlations in noncentral nuclear collisions //Phys. Rev. C. 1999. Vol. 59, N 5, P.2716-2727.

- [328] Sinyukov Yu.M., Akkelin S.V. and Xu N. Final conditions in high energy heavy ion collisions //Phys. Rev. C. 1999. Vol. 59, N 6, P.3437-3440.
- [329] Bureau G.R.G., Blaschke D.B. and Kalinovsky Y.L. Mott effect at the chiral phase transition and anomalous J/Ψ suppression //Phys. Lett. B. 2001. Vol. 506, N 3-4, P.297.
- [330] Afanasev S.V. et al. Deuteron production in central Pb+Pb collisions at 158 A GeV (NA49 Collab.) //Phys. Lett. B. 2000. Vol. 486, N1-2, P.22-28.
- [331] Margetis S. et al. Strangeness measurements in NA49 experiment with Pb projectiles(NA49 Collab.) //J. Phys. G. 1999. Vol. 25, N 2, P.189-197.
- [332] Barton R.A. et al. Production of multi-strange hyperons and strange resonances in the NA49 experiment (NA49 Collab.)//J. Phys. G. 2001. Vol. 27, N 3, P.367-374.
- [333] Beusch W. et al. (WA97 Collab.) Strange baryon production in Pb–Pb collisions at 158 A GeV/c //J. Phys. G. 2001. Vol. 27, N 3, P.375-381.
- [334] Braun-Munzinger P. et al. Hadron production in Au-Au collisions at RHIC // Phys. Lett. B. 2001. Vol. 518, N 1-2, P.41-46.
- [335] Dumitru A. and Spieles C. Inverse slope systematics in high-energy p+p and Au+Au reactions //Phys. Lett. B. 2001. Vol. 446, N 3-4, P.326-331.
- [336] Afanasiev S.V. et al. Energy dependence of pion and kaon production in central Pb+Pb collisions (NA49 Collab.) //Phys. Rev. C. 2002. Vol. 66, N 5, P.054902-1–054902-9.
- [337] Kämpfer B. et al. Thermal open charm signals versus hard initial yields in ultrarelativistic heavy-ion collisions // J. Phys. G. 1997. Vol. 23, N 12, P.2001-2012.
- [338] Wiedemann U.A., Heinz U. Particle interferometry for relativistic heavy ion collisions // Phys. Rep. 1999. Vol. 319, N 4-5, P.145-230.
- [339] van Hecke H., Sorge H., Xu N. Evidence of early multistrange hadron freezeout in high-energy nuclear collisions // Nucl. Phys. A. 1999. Vol. 661, N 1-4, P. 493-496.

- [340] Stock R. The Parton to hadron phase transition observed in Pb + Pb collisions at 158-GeV per nucleon // Phys. Lett. B. 1999. Vol. 456, N 2-4, P. 277-282.
- [341] Schnedermann E., Sollfrank J., Heinz U. Thermal phenomenology of hadrons from 200A GeV S+S collisions // Phys. Rev. C. 1999. Vol. 48, N 5, P. 2462-2475
- [342] Gorenstein M. I. et al. Statistical coalescence model with exact charm conservation // Phys. Lett. B. 2001. Vol. 509, N. 3-4, P. 277-282.
- [343] Grandchamp L., Rapp R. Thermal versus direct J/Ψ production in ultrarelativistic heavy ion collisions// Phys. Lett. B. 2001. Vol. 523, N 1-2, P.60-66.
- [344] Gyulassy M. Theory of high-energy A+A at RHIC // Lect. Notes Phys. 2002. Vol. 583, P. 37-79.
- [345] Rafelski J. Strange anti-baryons from quark-gluon plasma // Phys. Lett. B. 1991. Vol. 262, N 2-3, P.333-340.
- [346] Broniowski W. and Florkowski W. Explanation of the RHIC p(T) spectra in a thermal model with expansion// Phys. Rev. Lett. 2001. Vol. 87, N 27, P.272302-1–272302-4.
- [347] Broniowski W. and Florkowski W. Description of strange particle production in Au+Au collisions of $\sqrt{s_{NN}} = 130$ GeV in a single-freeze-out model // Phys. Rev. C. 2002. Vol. 65, N 6, P.064905-1–064905-6.
- [348] Adler C. et al. (STAR Collaboration) d and ^3He production in $\sqrt{s_{NN}} = 130$ GeV Au+Au Collisions// Phys. Rev. Lett. 2001. Vol. 87, N 26, P.262301-1–262301-6.
- [349] Adler C. et al. (STAR Collaboration) Midrapidity Λ and $\bar{\Lambda}$ production in Au+Au collisions at $\sqrt{s_{NN}} = 130$ GeV // Phys. Rev. Lett. 2002. Vol. 89, N 9, P.092301-1–092301-6 .
- [350] Adcox K. et al. (PHENIX Collaboration) Centrality dependence of $\pi^{+/-}$, $K^{+/-}$, p and anti- p production from $\sqrt{s_{NN}} = 130$ GeV Au+Au collisions at RHIC // Phys. Rev Lett. 2002. Vol. 88, N 24, P.242301-1–242301-6.

- [351] Adcox K. et al. (PHENIX Collaboration) Measurement of Λ and $\bar{\Lambda}$ Particles in Au+Au Collisions at $\sqrt{s_{NN}} = 130$ GeV // Phys. Rev. Lett. 2002. Vol. 89, N 9, P.092302-1–092302-6.
- [352] P. Seyboth *et al.* [NA49 Collaboration]. Indications for the onset of deconfinement in Pb + Pb collisions at the CERN SPS from NA49 // Acta Phys. Polon. B. 2005. Vol. 36, N. 2, P. 565-573.
- [353] Gaździcki M. and Röhricht D. Pion multiplicity in nuclear collisions // Z. Phys. C. 1995. Vol. 65, N 2, P.215-223.
- [354] van Hove L. Multiplicity Dependence of p_t spectrum as a possible signal for a phase transition in hadronic collisions// Phys. Lett. B. 1982. Vol. 118, N 1-3, P.138-140.
- [355] Shuryak E.V. and Zhirov O.V. Vacuum pressure effects in low- p_{\perp} hadronic spectra // Phys. Lett. B. 1979. Vol. 89, N 2, P.253-255.
- [356] Ahle L. et al. An excitation function of K^{-} and K^{+} production in Au+Au reactions at the AGS (E866 and E917 Collab.)// Phys. Lett. B. 2000. Vol. 490, N 1-2, P.53-60.
- [357] Adler C. et al. Kaon production and kaon to pion ratio in Au+Au collisions at $\sqrt{s_{NN}} = 130$ GeV /(STAR Collab.)//Phys. Lett. B. 2004. Vol. 595, N 1-4, P.143-150.
- [358] Alessandro B. et al. φ production in Pb–Pb collisions at 158 GeV/c per nucleon incident momentum (NA50 Collab.)// Phys. Lett. B. 2003. Vol. 555, N 3-4, P.147-155.

